ADSORPTION, THERMODYNAMIC AND DENSITY FUNCTIONAL THEORY INVESTIGATION OF SOME SULPHONAMIDES AS CORROSION INHIBITORS FOR SOME SELECTED METALS IN ACIDIC MEDIUM

LUTENDO CHESTER MURULANA

B.Sc (UNIVEN), B.Sc (Hons) (NWU), M.Sc (NWU)

A thesis submitted in fulfillment of the requirements for the degree of Doctor of Philosophy in the

Department of Chemistry

Faculty of Agriculture, Science and Technology,

North-West University (Mafikeng Campus)

Supervisor: Prof Eno. E. Ebenso

Co-supervisor: Dr Mwadham. M. Kabanda

November 2015

DECLARATION

I declare that this project which is submitted in fulfillment of the requirements for the degree of Doctor of Philosophy in Chemistry (Ph.D) at the North West University (Mafikeng Campus) has not been previously submitted for a degree at this university or any other university.

The following research was compiled, collated and written by me. All the quotations are indicated by appropriate punctuation marks. Sources of my information are acknowledged in the reference pages.

…….

LUTENDO CHESTER MURULANA

TABLE OF CONTENTS

No	CONTENTS	PAGE
	Acknowledgements -	ii
	Abstract –	iii
	List of Abbreviations -	v
	List of figures -	x
	List of tables –	xxvi
1.	INTRODUCTION -	1
1.1	Background to the Study-	2
1.2	Justification/Significance-	2
1.3	Problem Statement-	3
1.4	Aims and Objectives of the Study-	4
2.	LITERATURE REVIEW-	6
2.1	Definition of Corrosion-	7
2.1.1	Basic Reaction during Metal Corrosion-	7
2.1.2	Corrosive Environments-	9
2.1.3	Corrosion in Different Media-	10
2.1.4	Kinetics and Thermodynamics of Corrosion-	11
2.1.5	The Rate of Corrosion-	13
2.1.6	Factors Affecting the Rate of Corrosion-	14
2.1.7	Types of Corrosion-	16
2.1.8	Classification of Corrosion Process-	20
2.1.9	Consequences of Corrosion-	21

2.2 Corrosion of Metals- 22
2.2.1 Mild Steel- 22
2.2.2 Aluminium- 22
2.2.3 Zinc- 24

2.3 Corrosion Control Measures- 26
2.4 Inhibitors and Inhibition- 27
2.4.1 Definition of Corrosion Inhibitors- 27
2.4.2 Types of Inhibitors- 27

2.5 Sulphonamides- 30
2.5.1 Development of Sulphonamides - 31
2.5.2 Preparations/Synthesis of Sulphonamides - 33
2.5.3 Sulphonamides as Corrosion Inhibitors- 34

2.6 Quantum Chemical Approaches- 38
2.6.1 Geometry of Molecules- 38
2.6.1.1 The Geometry Parameters- 38
2.6.1.2 Molecular Conformations - 40
2.6.1.3 Molecular Geometry and Potential Energy Surface- 40
2.6.2 Major Approaches to the Study of Molecules- 41
2.6.2.1 Molecular Mechanics Approaches- 42
2.6.2.2 Quantum Mechanics Approaches - 43

2.6.3 The Schrodinger Equation- 43
2.6.4 The Description of Molecules in Quantum Mechanics- 44
2.6.4.1 The Born Oppenheimer Approximation- 45
2.6.4.2 The Hatree Fork Method - 45
2.6.4.3 Molecular Orbitals and LCAO Method- 47
2.6.5 Semi-Empirical and *Ab Initio* Quantum Chemical Approaches- 48
2.6.5.1 Semi-Empirical Approaches- 48
2.6.5.2 *Ab Initio* Approaches- 50
2.6.5.3 Density Functional Theory (DFT)- 50

2.6.6 Molecular Surface Interactions- 51
2.6.6.1 Van der Waals Interactions- 52
2.6.7 Molecular Reactivity Parameters- 57

3. EXPERIMENTAL DETAILS- 61

3.1 Metal Specimens- 62
3.2 Solutions- 62
3.3 Corrosion Inhibitors- 62
3.4 Electrochemical Techniques- 63
3.4.1 Potentiodynamic Polarization (PDP) - 63
3.4.2 Electrochemical Impedance Spectroscopy (EIS) - 65
3.5 Fourier Transform Infrared Spectroscopy (FTIR) - 65
3.6 Scanning Electron Microscopy (SEM) - 65
3.7 Weight Loss Measurements- 65
3.8 Computational Methods- 66

4. RESULTS AND DISCUSSION- 68

4.1 Mild Steel- 69
4.1.1 Potentiodynamic Polarization (PDP) - 69
4.1.2 Electrochemical Impedance Spectroscopy (EIS) - 75
4.1.3 Adsorption Film Analysis (FTIR) - 87
4.1.4 Surface Analysis (SEM) - 93
4.1.5 Corrosion Rate and Inhibition Efficiency - 99
4.1.6 Kinetic Parameters: Effect of Temperature - 104
4.1.7 Thermodynamic Parameters: Adsorption Isotherms - 116

4.2 Aluminium - 126
4.2.1 Potentiodynamic Polarization (PDP) - 126
4.2.2 Electrochemical Impedance Spectroscopy (EIS) - 132
4.2.3 Fourier Transform Infrared Spectroscopy (FTIR) - 144
4.2.4 Surface Analysis (SEM) - 150
4.2.5 Corrosion Rate and Inhibition Efficiency - 156

4.2.6 Kinetic Parameters: Effect of Temperature - 160
4.2.7 Thermodynamic Parameters: Adsorption Isotherms - 172

4.3 Zinc - 179
4.3.1 Potentiodynamic Polarization (PDP) - 179
4.3.2 Electrochemical Impedance Spectroscopy (EIS) - 185
4.3.3 Fourier Transform Infrared Spectroscopy (FTIR) - 196
4.3.4 Surface Analysis (SEM) - 202
4.3.5 Corrosion Rate and Inhibition Efficiency - 206
4.3.6 Effect of Temperature and Kinetic Energy- 211
4.3.7 Adsorption Isotherms and Thermodynamic Parameters - 225
4.3.8 Comparison of the effects of the sulphonamides on the metals selected - 231

4.4 Quantum Chemical Calculations- 233
4.4.1 Results of the Calculations in vacuo - 233
4.4.2 Results of the Protonated Inhibitors in vacuo- 249
4.4.3 Quantitative Structure Activity Relationship (QSAR) - 256

5. CONCLUSIONS - 258
5.1 Conclusions - 259

RECOMMENDATIONS - 261

REFERENCES - 262

APPENDIX - 280

Presentation at Conferences - 281
Publications from the Study - 281

ACKNOWLEDGEMENTS

First and foremost I would like to extend my heartfelt and profound appreciation where it is due, to God. This is mostly because of the life that He freely gave to me as well as the wisdom that He has bestowed upon me to take this endeavour and succeeded.

I always run out of words that could suitably describe and express my sincere and deepest appreciation to my supervisor and mentor, Prof Eno E. Ebenso. You have successfully transformed and transposed the hopeless me into a hopeful creature regarding matters of both academia and life in general.

My profound gratitude is also directed towards my co-supervisor Dr Mwadham. M. Kabanda, due to the meticulous and scintillate work he has done as far as the quantum chemical work is concerned. You have managed to make the notorious theoretical chemistry palatable to me.

Some tremendous and enormous heartfelt gratitude is sent to my buddy and colleague, Lukman O. Olasunkanmi for all of the scientific discussions and his positive and unending constructive contributions that he has made into this work.

This whole work would have adopted a rather different shape than it is currently had it not been for Dr A.S. Adekunle. I gratefully acknowledge him for his immense assistance with regard to the electrochemical analysis.

ABSTRACT

In this thesis, nine sulphonamides derivatives namely, sulphanilamide (SNA), sulphamethoxazole (SMX), sulphadimethoxine (SDM), sulphisoxazole (SSZ), sulphamethazine (SMT), sulphachloropyridazine (SCP), sulphabenzamide (SBZ), sulphaquinoxaline (SQX) and sulphamethizole (SMZ) were investigated as corrosion inhibitors for three different metals namely, mild steel, aluminium and zinc in 1.0 M hydrochloric acid solutions at 30-50 °C. The corrosion inhibition characteristics including corrosion mechanism, corrosion inhibition efficiencies and inhibitor-metal adsorption/desorption behaviour were studied using electrochemical impedance spectroscopy, potentiodynamic polarization and gravimetric analysis. Fourier transform infrared spectroscopy (FTIR) was used to gain more insight into the functional groups that formed or disappeared during the adsorption/desorption of the inhibitor molecules on the alloy surfaces. The adsorption film that resulted on these metal surfaces were further investigated using scanning electron microscopy (SEM) coupled with energy dispersive spectroscopy (EDS). Density functional theory (DFT) was used to compute all theoretical studies. Quantum chemical calculations and quantitative structure activity relationship (QSAR) were also used to establish correlations between experimentally determined inhibition efficiencies and molecular quantum chemical descriptors.

All nine sulphonamide compounds inhibited the corrosion of mild steel, aluminium and zinc in 1.0 M hydrochloric acid at 30-50 °C through adsorption of the inhibitor molecules on the metal surfaces without altering the corrosion mechanism. The comparison on the effect of temperature on the corrosion of mild steel, aluminium and zinc showed that mild steel is affected the most with the lowest inhibition efficiencies at the highest temperature of 50 °C. Potentiodynamic polarization results indicated that the use of all nine sulphonamide compounds as corrosion inhibitors significantly reduced the corrosion current densities for both anodic and cathodic half-reactions which suggest that both anodic dissolution and cathodic reduction of the hydrogen ions were inhibited. The obtained potentiodynamic polarization parameters revealed that all nine inhibitors studied acted as mixed-type inhibitors that protected the mild steel, aluminium and zinc surfaces through spontaneous adsorption. The aluminium Tafel plots showed a more pronounced passive region (the elongated section) than both mild steel and zinc. Electrochemical impedance spectroscopy showed that all nine

inhibitors protected mild steel, aluminium and zinc surfaces through the adsorption at the metal/hydrochloric acid interface.

The adsorption process of all studied inhibitors on mild steel, aluminum and zinc in 1.0 M HCl solution followed the Langmuir adsorption isotherm and a mixed-type mechanism. Analysis of the SEM micrographs and their respective EDS spectra showed that the surfaces of the alloys prior immersion in 1.0 M HCl solution exhibit a smooth nature with minor damages that might have resulted due to the abrasion with various emery papers. After the immersion in 1.0 M HCl solutions, all these metals showed a more degraded nature.

Fourier transform infrared spectroscopy studies revealed that all sulphonamide compounds studied interacted with Fe (in mild steel), aluminium and zinc resulting in Fe – inhibitor, Al – inhibitor and Zn – inhibitor complexes.

Quantum chemical studies showed that all nine sulphonamide compounds were active inhibitors for mild steel surfaces in acidic medium. Analysis of the HOMO densities for the neutral species showed that the highest HOMO densities occurs at C2, C4, C5 and C6, the amino N1, O9 and O10 atoms for all the sulphonamides studied. The effect of the protonated sulphonamide species was also studied and some protonated species were found to be among the enhanced adsorbates. The best QSAR equation correlating theoretical inhibition efficiency with the experimental inhibition efficiency corresponded to the combination of ω, E_{LUMO}, μ, η and logP quantum chemical parameters. The results from the weight loss and electrochemical measurements show that the order of inhibition efficiency by the sulphonamides on mild steel followed the order: SDM > SMT > SBZ > SCP > SNA > SQX > SSZ > SMX > SMZ and SNA > SBZ > SMX > SMZ > SSZ > SMT > SQX > SDM > SCP for aluminum while the order SBZ > SMX > SNA > SSZ > SCP> SMT > SDM > SQX > SMZ was followed for zinc.

LIST OF ABBREVIATIONS

MS	Mild Steel
Zn	Zinc
Al	Aluminium
MINTEK	Council for Mineral Technology
GS	Green Solvents
HCl	Hydrochloric Acid
MIC	Microbial Corrosion
IE	Inhibition Efficiency
SCC	Stress Corrosion Cracking
CorriSA	Corrosion Institute of Southern Africa
SNA	Sulphanilamide
SBZ	Sulphabenzamide
SMX	Sulphamethoxazole
SCP	Sulphachloropyridazine
SDM	Sulphadimethoxine
SSZ	Sulphisoxazole
SMZ	Sulphamethizole
SMT	Sulphamethazine
SQX	Sulphaquinoxaline
CorriSA	Corrosion Institute of Southern Africa
FHWA	U.S Federal Highway Administration
NACE	National Association of Corrosion Engineers

GDP	Nation’s Gross Domestic Product
VCI	Volatile Corrosion Inhibitors
VPI	Vapour Phase Inhibitors
SEM	Scanning Electron Microscopy
UV	Ultraviolet Spectrometry
FTIR	Fourier Transform Infrared Spectroscopy
AFM	Atomic Force Microscopy
NMM	N-methyl morphine
TEA	Triehylamine
SAM	Sulphonamide
XPS	X-ray Photoelectron Spectroscopy
APAS	N-acetil p-aminobenzene sulphonamide
FSM	4-chloro-2-((furan-2-ylmethyl)amino))-5-sulfamoylbenzoic acid
TSM	N-(isopropylcarbomoyl)-4-(m-tolyamino) pyridine-3-sulphonamide
HF	Hartree Fock
PES	Potential Energy Surface
PCE	Platinum Counter Electrode
SCE	Saturated Calomel Electrode
WE	Working Electrode
PDP	Potentiodynamic Polarization
EIS	Electrochemical Impedance Spectroscopy
HOMO	Highest Occupied Molecular Orbital
LUMO	Lowest Unoccupied Molecular Orbital
EA	Electron Affinity
IP	Ionization Potential
QSAR	Quantitative Structure Activity Relationship
DFT	Density Functional Theory

B3LYP	The Becke's Three Parameter Hybrid Functional using the Lee-Yang-Parr Correlation Functional Theory
MV	Molecular Volume
RMSE	Root Mean Square Error
SSE	Sum of Squared Errors
EQCM	Electrochemical Quartz Crystal Microbalance
ICP-OES	Inductively Coupled Plasma Optical Emission Spectrometry
DNA	Deoxyribonucleic acid
LCAO	Linear Combination of Atomic Orbitals
AM1	Austin Model 1
PM3	Parametric Method
MNDO	Modified Neglect of Diatomic Overlap
NDDO	Neglect of Diatomic Differential Overlap
MP2	Moller-Plesset Method
FRA	Frequency Response Analyzer
PGSTAT302N	Metrohm Autolab Potentiostat/Galvanostat
AC	Alternating current
EDS	Energy Dispersive Spectroscopy
JOEL JSM-7500F	Field Emission Electron Microscope
B3LYP	Becke's Three Parameter and the Lee-Yang-Parr
HF	High Frequency
LF	Low Frequency
C_{dl}	Double Layer Capacitance
R_s	Resistor
R_{ct}	Resistance of Charge Transfer
CPE	Constant Phase Element
SNA-MS	Sulphanilamide-Mild Steel

SBZ-MS	Sulphabenzamide-Mild Steel
SMX-MS	Sulphamethoxazole-Mild Steel
SCP-MS	Sulphachloropyridazine-Mild Steel
SDM-MS	Sulphadimethoxine-Mild Steel
SSZ -MS	Sulphisoxazole-Mild Steel
SMZ-MS	Sulphamethizole-Mild Steel
SMT-MS	Sulphamethazine-Mild Steel
SQX-MS	Sulphaquinoxaline-Mild Steel
SNA-Al	Sulphanilamide-Aluminium
SBZ-Al	Sulphabenzamide-Aluminium
SMX-Al	Sulphamethoxazole-Aluminium
SCP-Al	Sulphachloropyridazine-Aluminium
SDM-Al	Sulphadimethoxine-Aluminium
SSZ-Al	Sulphisoxazole-Aluminium
SMZ-Al	Sulphamethizole-Aluminium
SMT-Al	Sulphamethazine-Aluminium
SQX-Al	Sulphaquinoxaline-Aluminium
SNA-Zn	Sulphanilamide-Zinc
SBZ-Zn	Sulphabenzamide-Zinc
SMX-Zn	Sulphamethoxazole-Zinc
SCP-Zn	Sulphachloropyridazine- Zinc
SDM-Zn	Sulphadimethoxine- Zinc
SSZ -Zn	Sulphisoxazole- Zinc
SMZ-Zn	Sulphamethizole- Zinc
SMT-Zn	Sulphamethazine- Zinc

SQX-Zn	Sulphaquinoxaline- Zinc

LIST OF FIGURES

No	DESCRIPTION	PAGE
2.1	Relationship between corrosion and extraction-	7
2.2	Schematic representation of the four sub-reactions (corrosion mechanism) which takes place when mild steel undergoes the corrosion process-	8
2.3	Schematic representation of aluminium pitting corrosion mechanism in acidic medium-	24
2.4	Schematic representation of the process of zinc corrosion in hydrochloric acid-	26
2.5	The functional group of the sulphonamides-	30
2.6	Some sulphonamides compounds: a) Hydrochlorothiazide and b) Furosemide-	30
2.7	Structures of prontosil and sulphanilamide-	31
2.8	Structures of some important derivatives of sulphanilamide-	32
2.9	Reactivity of PFP-Sulphonate in Aqueous Media-	33
2.10	Synthesis of Sulphathiazole-	34
2.11	Synthesis of Sulphonamide-	34
2.12	Bond lengths and bond angles in an ammonia molecule-	39
2.13	The torsion angles in a molecule containing atoms A-B-C-B-	39
2.14	Conformations of butane resulting from the 60° rotation around C-C single bond-	40
2.15	Potential Energy Surface plot of the water molecule-	41
2.16	Dipole-dipole interactions between two Iodine monochloride (ICl) molecules-	53
2.17	Dipole-induced-dipole interactions between two molecules-	54
2.18	Induced-dipole-induced-dipole interactions between two He atoms-	55
2.19	Hydrogen bonding between two water molecules-	55
2.20	Formation of a covalent bond between two hydrogen atoms-	56
3.1	Molecular structures of the sulphonamides corrosion inhibitors utilized in this study-	64

4.1 Tafel Plots for mild steel in 1 M HCl in the absence and presence of different concentrations of SNA inhibitor compound- 69
4.2 Tafel Plots for mild steel in 1 M HCl in the absence and presence of different concentrations of SBZ inhibitor compound- 70
4.3 Tafel Plots for mild steel in 1 M HCl in the absence and presence of different concentrations of SMX inhibitor compound- 70
4.4 Tafel Plots for mild steel in 1 M HCl in the absence and presence of different concentrations of SCP inhibitor compound- 71
4.5 Tafel Plots for mild steel in 1 M HCl in the absence and presence of different concentrations of SDM inhibitor compound- 71
4.6 Tafel Plots for mild steel in 1 M HCl in the absence and presence of different concentrations of SSZ inhibitor compound- 72
4.7 Tafel Plots for mild steel in 1 M HCl in the absence and presence of different concentrations of SMZ inhibitor compound- 72
4.8 Tafel Plots for mild steel in 1 M HCl in the absence and presence of different concentrations of SMT inhibitor compound- 73
4.9 Tafel Plots for mild steel in 1 M HCl in the absence and presence of different concentrations of SQX inhibitor compound- 73
4.10 Nyquist plot of mild steel in 1 M HCl in the absence and presence of different concentrations of SNA inhibitor compound- 76
4.11 Bode plots of mild steel in 1 M HCl in the absence and presence of different concentrations of SNA inhibitor compound- 76
4.12 Nyquist plot of mild steel in 1 M HCl in the absence and presence of different concentrations of SBZ inhibitor compound- 77
4.13 Bode plots of mild steel in 1 M HCl in the absence and presence of different concentrations of SBZ inhibitor compound- 77
4.14 Nyquist plot of mild steel in 1 M HCl in the absence and presence of different concentrations of SMX inhibitor compound- 78
4.15 Bode plots of mild steel in 1 M HCl in the absence and presence of different concentrations of SMX inhibitor compound- 78
4.16 Nyquist plot of mild steel in 1 M HCl in the absence and presence of different concentrations of SCP inhibitor compound- 79
4.17 Bode plots of mild steel in 1 M HCl in the absence and presence of different concentrations of SCP inhibitor compound- 79

4.18 Nyquist plot of mild steel in 1 M HCl in the absence and presence of different concentrations of SDM inhibitor compound- 80
4.19 Bode plots of mild steel in 1 M HCl in the absence and presence of different concentrations of SDM inhibitor compound- 80
4.20 Nyquist plot of mild steel in 1 M HCl in the absence and presence of different concentrations of SSZ inhibitor compound- 81
4.21 Bode plots of mild steel in 1 M HCl in the absence and presence of different concentrations of SSZ inhibitor compound- 81
4.22 Nyquist plot of mild steel in 1 M HCl in the absence and presence of different concentrations of SMZ inhibitor compound- 82
4.23 Bode plots of mild steel in 1 M HCl in the absence and presence of different concentrations of SSZ inhibitor compound- 82
4.24 Nyquist plot of mild steel in 1 M HCl in the absence and presence of different concentrations of SMT inhibitor compound- 83
4.25 Bode plots of mild steel in 1 M HCl in the absence and presence of different concentrations of SMT inhibitor compound- 83
4.26 Nyquist plot of mild steel in 1 M HCl in the absence and presence of different concentrations of SQX inhibitor compound- 84
4.27 Bode plots of mild steel in 1 M HCl in the absence and presence of different concentrations of SQX inhibitor compound- 84
4.28 Equivalent circuit used to fit the impedance spectra obtained for mild steel corrosion in 1.0 M HCl in the absence and presence of SNA, SBZ, SMX, SCP, SDM, SSZ, SMZ, SMT and SQX- 85
4.29 FT-IR spectra for the studied corrosion inhibitors and adsorption films formed on the mild steel in 1.0 M HCl using SNA corrosion inhibitor- 87
4.30 FT-IR spectra for the studied corrosion inhibitors and adsorption films formed on the mild steel in 1.0 M HCl using SBZ corrosion inhibitor- 88
5.31 FT-IR spectra for the studied corrosion inhibitors and adsorption films formed on the mild steel in 1.0 M HCl using SMX corrosion inhibitor- 88
4.32 FT-IR spectra for the studied corrosion inhibitors and adsorption films formed on the mild steel in 1.0 M HCl using SCP corrosion inhibitor- 89
4.33 FT-IR spectra for the studied corrosion inhibitors and adsorption films formed on the mild steel in 1.0 M HCl using SDM corrosion inhibitor- 89

4.34 FT-IR spectra for the studied corrosion inhibitors and adsorption films formed on the mild steel in 1.0 M HCl using SSZ corrosion inhibitor- 90
4.35 FT-IR spectra for the studied corrosion inhibitors and adsorption films formed on the mild steel in 1.0 M HCl using SMZ corrosion inhibitor- 90
4.36 FT-IR spectra for the studied corrosion inhibitors and adsorption films formed on the mild steel in 1.0 M HCl using SMT corrosion inhibitor- 91
4.37 FT-IR spectra for the studied corrosion inhibitors and adsorption films formed on the mild steel in 1.0 M HCl using SQX corrosion inhibitor- 91
4.38 SEM micrograph of the surface of mild steel and EDS spectrum of plain mild steel specimen used in this study- 93
4.39 SEM micrograph of the surface of mild steel and EDS spectrum of mild steel immersed in HCl uninhibited- 94
4.40 SEM micrograph of the surface of mild steel and EDS spectrum of mild steel immersed in HCl in the presence of SNA corrosion inhibitor- 94
4.41 SEM micrograph of the surface of mild steel and EDS spectrum of mild steel immersed in HCl in the presence of SBZ corrosion inhibitor- 95
4.42 SEM micrograph of the surface of mild steel and EDS spectrum of mild steel immersed in HCl in the presence of SMX corrosion inhibitor- 95
4.43 SEM micrograph of the surface of mild steel and EDS spectrum of mild steel immersed in HCl in the presence of SCP corrosion inhibitor- 96
4.44 SEM micrograph of the surface of mild steel and EDS spectrum of mild steel immersed in HCl in the presence of SDM corrosion inhibitor- 96
4.45 SEM micrograph of the surface of mild steel and EDS spectrum of mild steel immersed in HCl in the presence of SSZ corrosion inhibitor- 97
4.46 SEM micrograph of the surface of mild steel and EDS spectrum of mild steel immersed in HCl in the presence of SMZ corrosion inhibitor- 97
4.47 SEM micrograph of the surface of mild steel and EDS spectrum of mild steel immersed in HCl in the presence of SMT corrosion inhibitor- 98
4.48 SEM micrograph of the surface of mild steel and EDS spectrum of mild steel immersed in HCl in the presence of SQX corrosion inhibitor- 98
4.49 Variations of the percentage inhibition efficiencies with various concentrations of the utilized corrosion inhibitors at 30 °C- 100
4.50 Variations of the percentage inhibition efficiencies with various concentrations of the utilized corrosion inhibitors at 40 °C- 100

4.51 Variations of the percentage inhibition efficiencies with various concentrations of the utilized corrosion inhibitors at 50 °C- 101
4.52 Arrhenius plots for the corrosion of mild steel in 1.0 M HCl in the absence and presence of various concentrations of SNA corrosion inhibitor- 105
4.53 Arrhenius plots for the corrosion of mild steel in 1.0 M HCl in the absence and presence of various concentrations of SBZ corrosion inhibitor- 105
4.54 Arrhenius plots for the corrosion of mild steel in 1.0 M HCl in the absence and presence of various concentrations of SMX corrosion inhibitor- 106
4.55 Arrhenius plots for the corrosion of mild steel in 1.0 M HCl in the absence and presence of various concentrations of SCP corrosion inhibitor- 106
4.56 Arrhenius plots for the corrosion of mild steel in 1.0 M HCl in the absence and presence of various concentrations of SDM corrosion inhibitor- 107
4.57 Arrhenius plots for the corrosion of mild steel in 1.0 M HCl in the absence and presence of various concentrations of SSZ corrosion inhibitor- 107
4.58 Arrhenius plots for the corrosion of mild steel in 1.0 M HCl in the absence and presence of various concentrations of SMZ corrosion inhibitor- 108
4.59 Arrhenius plots for the corrosion of mild steel in 1.0 M HCl in the absence and presence of various concentrations of SMT corrosion inhibitor- 108
4.60 Arrhenius plots for the corrosion of mild steel in 1.0 M HCl in the absence and presence of various concentrations of SQX corrosion inhibitor- 109
4.61 Variation of the activation energy with the concentration of the utilized corrosion inhibitors- 109
4.62 Transition state plots for the corrosion of mild steel in 1.0 M HCl in the absence and presence of various concentrations of SNA corrosion inhibitor- 111
4.63 Transition state plots for the corrosion of mild steel in 1.0 M HCl in the absence and presence of various concentrations of SBZ corrosion inhibitor- 112
4.64 Transition state plots for the corrosion of mild steel in 1.0 M HCl in the absence and presence of various concentrations of SMX corrosion inhibitor- 112
4.65 Transition state plots for the corrosion of mild steel in 1.0 M HCl in the absence and presence of various concentrations of SCP corrosion inhibitor- 113
4.66 Transition state plots for the corrosion of mild steel in 1.0 M HCl in the absence and presence of various concentrations of SDM corrosion inhibitor- 113
4.67 Transition state plots for the corrosion of mild steel in 1.0 M HCl in the absence and presence of various concentrations of SSZ corrosion inhibitor- 114

4.68 Transition state plots for the corrosion of mild steel in 1.0 M HCl in the absence and presence of various concentrations of SMZ corrosion inhibitor- 114
4.69 Transition state plots for the corrosion of mild steel in 1.0 M HCl in the absence and presence of various concentrations of SMT corrosion inhibitor- 115
4.70 Transition state plots for the corrosion of mild steel in 1.0 M HCl in the absence and presence of various concentrations of SQX corrosion inhibitor- 115
4.71 Langmuir adsorption isotherms for the corrosion of mild steel in 1.0 M HCl at various temperatures for SNA corrosion inhibitor- 119
4.72 Langmuir adsorption isotherms for the corrosion of mild steel in 1.0 M HCl at various temperatures for SBZ corrosion inhibitor- 119
4.73 Langmuir adsorption isotherms for the corrosion of mild steel in 1.0 M HCl at various temperatures for SMX corrosion inhibitor- 120
4.74 Langmuir adsorption isotherms for the corrosion of mild steel in 1.0 M HCl at various temperatures for SCP corrosion inhibitor- 120
4.75 Langmuir adsorption isotherms for the corrosion of mild steel in 1.0 M HCl at various temperatures for SDM corrosion inhibitor- 121
4.76 Langmuir adsorption isotherms for the corrosion of mild steel in 1.0 M HCl at various temperatures for SSZ corrosion inhibitor- 121
4.77 Langmuir adsorption isotherms for the corrosion of mild steel in 1.0 M HCl at various temperatures for SMZ corrosion inhibitor- 122
4.78 Langmuir adsorption isotherms for the corrosion of mild steel in 1.0 M HCl at various temperatures for SMT corrosion inhibitor- 122
4.79 Langmuir adsorption isotherms for the corrosion of mild steel in 1.0 M HCl at various temperatures for SQX corrosion inhibitor- 123
4.80 Langmuir adsorption isotherms for the corrosion of mild steel in 1.0 M HCl obtained from the PDP results at 30° C for SNA, SBZ, SMX, SCP, SDM, SSZ, SMZ, SMT and SQX corrosion inhibitors- 124
4.81 Langmuir adsorption isotherms for the corrosion of mild steel in 1.0 M HCl obtained from the EIS results at 30° C for SNA, SBZ, SMX, SCP, SDM, SSZ, SMZ, SMT and SQX corrosion inhibitors- 124
4.82 Tafel Plots for aluminium in 1 M HCl in the absence and presence of different concentrations of SNA inhibitor compound- 126
4.83 Tafel Plots for aluminium in 1 M HCl in the absence and presence of different concentrations of SBZ inhibitor compound- 126

4.84 Tafel Plots for aluminium in 1 M HCl in the absence and presence of different concentrations of SMX inhibitor compound- 127
4.85 Tafel Plots for aluminium in 1 M HCl in the absence and presence of different concentrations of SCP inhibitor compound- 128
4.86 Tafel Plots for aluminium in 1 M HCl in the absence and presence of different concentrations of SDM inhibitor compound- 128
4.87 Tafel Plots for aluminium in 1 M HCl in the absence and presence of different concentrations of SSZ inhibitor compound- 129
4.88 Tafel Plots for aluminium in 1 M HCl in the absence and presence of different concentrations of SMZ inhibitor compound- 129
4.89 Tafel Plots for aluminium in 1 M HCl in the absence and presence of different concentrations of SMT inhibitor compound- 130
4.90 Tafel Plots for aluminium in 1 M HCl in the absence and presence of different concentrations of SQX inhibitor compound- 130
4.91 Nyquist plot of aluminium in 1 M HCl in the absence and presence of different concentrations of SNA inhibitor compound- 133
4.92 Bode plots of aluminium in 1 M HCl in the absence and presence of different concentrations of SNA inhibitor compound- 133
4.93 Nyquist plot of aluminium in 1 M HCl in the absence and presence of different concentrations of SBZ inhibitor compound- 134
4.94 Bode plots of aluminium in 1 M HCl in the absence and presence of different concentrations of SBZ inhibitor compound- 134
4.95 Nyquist plot of aluminium in 1 M HCl in the absence and presence of different concentrations of SMX inhibitor compound- 135
4.96 Bode plots of aluminium in 1 M HCl in the absence and presence of different concentrations of SMX inhibitor compound- 135
4.97 Nyquist plot of aluminium in 1 M HCl in the absence and presence of different concentrations of SCP inhibitor compound- 136
4.98 Bode plots of aluminium in 1 M HCl in the absence and presence of different concentrations of SCP inhibitor compound- 136
4.99 Nyquist plot of aluminium in 1 M HCl in the absence and presence of different concentrations of SDM inhibitor compound- 137
4.100 Bode plots of aluminium in 1 M HCl in the absence and presence of different concentrations of SDM inhibitor compound- 137

4.101 Nyquist plot of aluminium in 1 M HCl in the absence and presence of different concentrations of SSZ inhibitor compound- 138
4.102 Bode plots of aluminium in 1 M HCl in the absence and presence of different concentrations of SSZ inhibitor compound- 138
4.103 Nyquist plot of aluminium in 1 M HCl in the absence and presence of different concentrations of SMZ inhibitor compound- 139
4.104 Bode plots of aluminium in 1 M HCl in the absence and presence of different concentrations of SSZ inhibitor compound- 139
4.105 Nyquist plot of aluminium in 1 M HCl in the absence and presence of different concentrations of SMT inhibitor compound- 140
4.106 Bode plots of aluminium in 1 M HCl in the absence and presence of different concentrations of SMT inhibitor compound- 140
4.107 Nyquist plot of aluminium in 1 M HCl in the absence and presence of different concentrations of SQX inhibitor compound- 141
4.108 Bode plots of aluminium in 1 M HCl in the absence and presence of different concentrations of SQX inhibitor compound- 141
4.109 Equivalent circuit used to fit the impedance spectra obtained for aluminium corrosion in 1.0 M HCl in the absence and presence of SNA, SBZ, SMX, SCP, SDM, SSZ, SMZ, SMT and SQX- 142
4.110 FT-IR spectra for the studied corrosion inhibitors and adsorption films formed on the aluminium in 1.0 M HCl using SNA corrosion inhibitor- 144
4.111 FT-IR spectra for the studied corrosion inhibitors and adsorption films formed on the aluminium in 1.0 M HCl using SBZ corrosion inhibitor- 145
4.112 FT-IR spectra for the studied corrosion inhibitors and adsorption films formed on the aluminium in 1.0 M HCl using SMX corrosion inhibitor- 145
4.113 FT-IR spectra for the studied corrosion inhibitors and adsorption films formed on the aluminium in 1.0 M HCl using SCP corrosion inhibitor- 146
4.114 FT-IR spectra for the studied corrosion inhibitors and adsorption films formed on the aluminium in 1.0 M HCl using SDM corrosion inhibitor- 146
4.115 FT-IR spectra for the studied corrosion inhibitors and adsorption films formed on the aluminium in 1.0 M HCl using SSZ corrosion inhibitor- 147
4.116 FT-IR spectra for the studied corrosion inhibitors and adsorption films formed on the aluminium in 1.0 M HCl using SMZ corrosion inhibitor- 147

4.117 FT-IR spectra for the studied corrosion inhibitors and adsorption films formed on the aluminium in 1.0 M HCl using SMT corrosion inhibitor- 148
4.118 FT-IR spectra for the studied corrosion inhibitors and adsorption films formed on the aluminium in 1.0 M HCl using SQX corrosion inhibitor- 148
4.119 SEM micrograph of the surface of aluminium and EDS spectrum of plain mild steel specimen used in this study- 150
4.120 SEM micrograph of the surface of aluminium and EDS spectrum of mild steel immersed in HCl uninhibited- 151
4.121 SEM micrograph of the surface of aluminium and EDS spectrum of mild steel immersed in HCl in the presence of SNA corrosion inhibitor- 151
4.122 SEM micrograph of the surface of aluminium and EDS spectrum of mild steel immersed in HCl in the presence of SBZ corrosion inhibitor- 152
4.123 SEM micrograph of the surface of aluminium and EDS spectrum of mild steel immersed in HCl in the presence of SMX corrosion inhibitor- 152
4.124 SEM micrograph of the surface of aluminium and EDS spectrum of mild steel immersed in HCl in the presence of SCP corrosion inhibitor- 153
4.125 SEM micrograph of the surface of aluminium and EDS spectrum of mild steel immersed in HCl in the presence of SDM corrosion inhibitor- 153
4.126 SEM micrograph of the surface of aluminium and EDS spectrum of mild steel immersed in HCl in the presence of SSZ corrosion inhibitor- 154
4.127 SEM micrograph of the surface of aluminium and EDS spectrum of mild steel immersed in HCl in the presence of SMZ corrosion inhibitor- 154
4.128 SEM micrograph of the surface of aluminium and EDS spectrum of mild steel immersed in HCl in the presence of SMT corrosion inhibitor- 155
4.129 SEM micrograph of the surface of aluminium and EDS spectrum of mild steel immersed in HCl in the presence of SQX corrosion inhibitor- 155
4.130 Variations of the percentage inhibition efficiencies with various concentrations of the utilized corrosion inhibitors at 30 °C- 156
4.131 Variations of the percentage inhibition efficiencies with various concentrations of the utilized corrosion inhibitors at 40 °C- 157
4.132 Variations of the percentage inhibition efficiencies with various concentrations of the utilized corrosion inhibitors at 50 °C- 157
4.133 Arrhenius plots for the corrosion of aluminium in 1.0 M HCl in the absence and presence of various concentrations of SNA corrosion inhibitor- 160

4.134 Arrhenius plots for the corrosion of aluminium in 1.0 M HCl in the absence and presence of various concentrations of SBZ corrosion inhibitor- 161
4.135 Arrhenius plots for the corrosion of aluminium in 1.0 M HCl in the absence and presence of various concentrations of SMX corrosion inhibitor- 161
4.136 Arrhenius plots for the corrosion of aluminium in 1.0 M HCl in the absence and presence of various concentrations of SCP corrosion inhibitor- 162
4.137 Arrhenius plots for the corrosion of aluminium in 1.0 M HCl in the absence and presence of various concentrations of SDM corrosion inhibitor- 162
4.138 Arrhenius plots for the corrosion of aluminium in 1.0 M HCl in the absence and presence of various concentrations of SSZ corrosion inhibitor- 163
4.139 Arrhenius plots for the corrosion of aluminium in 1.0 M HCl in the absence and presence of various concentrations of SMZ corrosion inhibitor- 163
4.140 Arrhenius plots for the corrosion of aluminium in 1.0 M HCl in the absence and presence of various concentrations of SMT corrosion inhibitor- 164
4.141 Arrhenius plots for the corrosion of aluminium in 1.0 M HCl in the absence and presence of various concentrations of SQX corrosion inhibitor- 164
4.142 Variation of the activation energy with the concentration of the utilized corrosion inhibitors- 166
4.143 Transition state plots for the corrosion of aluminium in 1.0 M HCl in the absence and presence of various concentrations of SNA corrosion inhibitor- 167
4.144 Transition state plots for the corrosion of aluminium in 1.0 M HCl in the absence and presence of various concentrations of SBZ corrosion inhibitor- 167
4.145 Transition state plots for the corrosion of aluminium in 1.0 M HCl in the absence and presence of various concentrations of SMX corrosion inhibitor- 168
4.146 Transition state plots for the corrosion of aluminium in 1.0 M HCl in the absence and presence of various concentrations of SCP corrosion inhibitor- 168
4.147 Transition state plots for the corrosion of aluminium in 1.0 M HCl in the absence and presence of various concentrations of SDM corrosion inhibitor- 169
4.148 Transition state plots for the corrosion of aluminium in 1.0 M HCl in the absence and presence of various concentrations of SSZ corrosion inhibitor- 169
4.149 Transition state plots for the corrosion of aluminium in 1.0 M HCl in the absence and presence of various concentrations of SMZ corrosion inhibitor- 170
4.150 Transition state plots for the corrosion of aluminium in 1.0 M HCl in the absence and presence of various concentrations of SMT corrosion inhibitor- 170

4.151 Transition state plots for the corrosion of aluminium in 1.0 M HCl in the absence and presence of various concentrations of SQX corrosion inhibitor- 171
4.152 Langmuir adsorption isotherms for the corrosion of aluminium in 1.0 M HCl at various temperatures for SNA corrosion inhibitor- 172
4.153 Langmuir adsorption isotherms for the corrosion of aluminium in 1.0 M HCl at various temperatures for SBZ corrosion inhibitor- 173
4.154 Langmuir adsorption isotherms for the corrosion of aluminium in 1.0 M HCl at various temperatures for SMX corrosion inhibitor- 173
4.155 Langmuir adsorption isotherms for the corrosion of aluminium in 1.0 M HCl at various temperatures for SCP corrosion inhibitor- 174
4.156 Langmuir adsorption isotherms for the corrosion of aluminium in 1.0 M HCl at various temperatures for SDM corrosion inhibitor- 174
4.157 Langmuir adsorption isotherms for the corrosion of aluminium in 1.0 M HCl at various temperatures for SSZ corrosion inhibitor- 175
4.158 Langmuir adsorption isotherms for the corrosion of aluminium in 1.0 M HCl at various temperatures for SMZ corrosion inhibitor- 175
4.159 Langmuir adsorption isotherms for the corrosion of aluminium in 1.0 M HCl at various temperatures for SMT corrosion inhibitor- 176
4.160 Langmuir adsorption isotherms for the corrosion of aluminium in 1.0 M HCl at various temperatures for SQX corrosion inhibitor- 176
4.161 Tafel Plots for zinc in 1 M HCl in the absence and presence of different concentrations of SNA inhibitor compound- 179
4.162 Tafel Plots for zinc in 1 M HCl in the absence and presence of different concentrations of SBZ inhibitor compound- 180
4.163 Tafel Plots for zinc in 1 M HCl in the absence and presence of different concentrations of SMX inhibitor compound- 180
4.164 Tafel Plots for zinc in 1 M HCl in the absence and presence of different concentrations of SCP inhibitor compound- 181
4.165 Tafel Plots for zinc in 1 M HCl in the absence and presence of different concentrations of SDM inhibitor compound- 181
4.166 Tafel Plots for zinc in 1 M HCl in the absence and presence of different concentrations of SSZ inhibitor compound- 182
4.167 Tafel Plots for zinc in 1 M HCl in the absence and presence of different concentrations of SMZ inhibitor compound- 182

4.168 Tafel Plots for zinc in 1 M HCl in the absence and presence of different concentrations of SMT inhibitor compound- 183
4.169 Tafel Plots for zinc in 1 M HCl in the absence and presence of different concentrations of SQX inhibitor compound- 183
4.170 Nyquist plot of zinc in 1 M HCl in the absence and presence of different concentrations of SNA inhibitor compound- 185
4.171 Bode plots of zinc in 1 M HCl in the absence and presence of different concentrations of SNA inhibitor compound- 186
4.172 Nyquist plot of zinc in 1 M HCl in the absence and presence of different concentrations of SBZ inhibitor compound- 186
4.173 Bode plots of zinc in 1 M HCl in the absence and presence of different concentrations of SBZ inhibitor compound- 187
4.174 Nyquist plot of zinc in 1 M HCl in the absence and presence of different concentrations of SMX inhibitor compound- 187
4.175 Bode plots of zinc in 1 M HCl in the absence and presence of different concentrations of SMX inhibitor compound- 188
4.176 Nyquist plot of zinc in 1 M HCl in the absence and presence of different concentrations of SCP inhibitor compound- 188
4.177 Bode plots of zinc in 1 M HCl in the absence and presence of different concentrations of SCP inhibitor compound- 189
4.178 Nyquist plot of zinc in 1 M HCl in the absence and presence of different concentrations of SDM inhibitor compound- 189
4.179 Bode plots of zinc in 1 M HCl in the absence and presence of different concentrations of SDM inhibitor compound- 190
4.180 Nyquist plot of zinc in 1 M HCl in the absence and presence of different concentrations of SSZ inhibitor compound- 190
4.181 Bode plots of zinc in 1 M HCl in the absence and presence of different concentrations of SSZ inhibitor compound- 191
4.182 Nyquist plot of zinc in 1 M HCl in the absence and presence of different concentrations of SMZ inhibitor compound- 191
4.183 Bode plots of zinc in 1 M HCl in the absence and presence of different concentrations of SSZ inhibitor compound- 192
4.184 Nyquist plot of zinc in 1 M HCl in the absence and presence of different concentrations of SMT inhibitor compound- 192

4.185 Bode plots of zinc in 1 M HCl in the absence and presence of different concentrations of SMT inhibitor compound- 193
4.186 Nyquist plot of zinc in 1 M HCl in the absence and presence of different concentrations of SQX inhibitor compound- 193
4.187 Bode plots of zinc in 1 M HCl in the absence and presence of different concentrations of SQX inhibitor compound- 194
4.188 FT-IR spectra for the studied corrosion inhibitors and adsorption films formed on the zinc in 1.0 M HCl using SNA corrosion inhibitor- 196
4.189 FT-IR spectra for the studied corrosion inhibitors and adsorption films formed on the zinc in 1.0 M HCl using SBZ corrosion inhibitor- 197
4.190 FT-IR spectra for the studied corrosion inhibitors and adsorption films formed on the zinc in 1.0 M HCl using SMX corrosion inhibitor- 197
4.191 FT-IR spectra for the studied corrosion inhibitors and adsorption films formed on the zinc in 1.0 M HCl using SCP corrosion inhibitor- 198
4.192 FT-IR spectra for the studied corrosion inhibitors and adsorption films formed on the zinc in 1.0 M HCl using SDM corrosion inhibitor- 198
4.193 FT-IR spectra for the studied corrosion inhibitors and adsorption films formed on the zinc in 1.0 M HCl using SSZ corrosion inhibitor- 199
4.194 FT-IR spectra for the studied corrosion inhibitors and adsorption films formed on the zinc in 1.0 M HCl using SMZ corrosion inhibitor- 199
4.195 FT-IR spectra for the studied corrosion inhibitors and adsorption films formed on the zinc in 1.0 M HCl using SMT corrosion inhibitor- 200
4.196 FT-IR spectra for the studied corrosion inhibitors and adsorption films formed on the zinc in 1.0 M HCl using SQX corrosion inhibitor- 200
4.197 SEM micrographs of the surface of zinc: (a) plain zinc and (b) zinc immersed in HCl uninhibited- 202
4.198 SEM micrographs of the surface of zinc immersed in HCl in the presence of (a) SNA (b) SBZ- 203
4.199 SEM micrographs of the surface of zinc immersed in HCl in the presence of (a) SMX (b) SCP- 203
4.200 SEM micrographs of the surface of zinc immersed in HCl in the presence of (a) SDM (b) SSZ- 204
4.201 SEM micrographs of the surface of zinc immersed in HCl in the presence of (a) SMZ (b) SMT- 204

4.202 SEM micrographs of the surface of zinc immersed in HCl in the presence of SQX- 205
4.203 Variations of the percentage inhibition efficiencies with various concentrations of the utilized corrosion inhibitors at 30 °C- 206
4.204 Variations of the percentage inhibition efficiencies with various concentrations of the utilized corrosion inhibitors at 40 °C- 207
4.205 Variations of the percentage inhibition efficiencies with various concentrations of the utilized corrosion inhibitors at 50 °C- 207
4.206 Arrhenius plots for the corrosion of zinc in 1.0 M HCl in the absence and presence of various concentrations of SNA corrosion inhibitor- 211
4.207 Arrhenius plots for the corrosion of zinc in 1.0 M HCl in the absence and presence of various concentrations of SBZ corrosion inhibitor- 212
4.208 Arrhenius plots for the corrosion of zinc in 1.0 M HCl in the absence and presence of various concentrations of SMX corrosion inhibitor- 212
4.209 Arrhenius plots for the corrosion of zinc in 1.0 M HCl in the absence and presence of various concentrations of SCP corrosion inhibitor- 213
4.210 Arrhenius plots for the corrosion of zinc in 1.0 M HCl in the absence and presence of various concentrations of SDM corrosion inhibitor- 213
4.211 Arrhenius plots for the corrosion of zinc in 1.0 M HCl in the absence and presence of various concentrations of SSZ corrosion inhibitor- 214
4.212 Arrhenius plots for the corrosion of zinc in 1.0 M HCl in the absence and presence of various concentrations of SMZ corrosion inhibitor- 214
4.213 Arrhenius plots for the corrosion of zinc in 1.0 M HCl in the absence and presence of various concentrations of SMT corrosion inhibitor- 215
4.214 Arrhenius plots for the corrosion of zinc in 1.0 M HCl in the absence and presence of various concentrations of SQX corrosion inhibitor- 215
4.215 Variation of the activation energy with the concentration of the utilized corrosion inhibitors- 218
4.216 Transition state plots for the corrosion of zinc in 1.0 M HCl in the absence and presence of various concentrations of SNA corrosion inhibitor- 219
4.217 Transition state plots for the corrosion of zinc in 1.0 M HCl in the absence and presence of various concentrations of SBZ corrosion inhibitor- 219
4.218 Transition state plots for the corrosion of zinc in 1.0 M HCl in the absence and presence of various concentrations of SMX corrosion inhibitor- 220

4.219 Transition state plots for the corrosion of zinc in 1.0 M HCl in the absence and presence of various concentrations of SCP corrosion inhibitor- 220
4.220 Transition state plots for the corrosion of zinc in 1.0 M HCl in the absence and presence of various concentrations of SDM corrosion inhibitor- 221
4.221 Transition state plots for the corrosion of zinc in 1.0 M HCl in the absence and presence of various concentrations of SSZ corrosion inhibitor- 221
4.222 Transition state plots for the corrosion of zinc in 1.0 M HCl in the absence and presence of various concentrations of SMZ corrosion inhibitor- 222
4.223 Transition state plots for the corrosion of zinc in 1.0 M HCl in the absence and presence of various concentrations of SMT corrosion inhibitor- 222
4.224 Transition state plots for the corrosion of zinc in 1.0 M HCl in the absence and presence of various concentrations of SQX corrosion inhibitor- 223
4.225 Langmuir adsorption isotherms for the corrosion of zinc in 1.0 M HCl at various temperatures for SNA corrosion inhibitor- 225
4.226 Langmuir adsorption isotherms for the corrosion of zinc in 1.0 M HCl at various temperatures for SBZ corrosion inhibitor- 226
4.227 Langmuir adsorption isotherms for the corrosion of zinc in 1.0 M HCl at various temperatures for SMX corrosion inhibitor- 226
4.228 Langmuir adsorption isotherms for the corrosion of zinc in 1.0 M HCl at various temperatures for SCP corrosion inhibitor- 227
4.229 Langmuir adsorption isotherms for the corrosion of zinc in 1.0 M HCl at various temperatures for SDM corrosion inhibitor- 227
4.230 Langmuir adsorption isotherms for the corrosion of zinc in 1.0 M HCl at various temperatures for SSZ corrosion inhibitor- 228
4.231 Langmuir adsorption isotherms for the corrosion of zinc in 1.0 M HCl at various temperatures for SMZ corrosion inhibitor- 228
4.232 Langmuir adsorption isotherms for the corrosion of zinc in 1.0 M HCl at various temperatures for SMT corrosion inhibitor- 229
4.233 Langmuir adsorption isotherms for the corrosion of zinc in 1.0 M HCl at various temperatures for SQX corrosion inhibitor- 229
4.234 The optimized geometries of the studied sulphonamides compounds- 234
4.235 The HOMO for the studied sulphonamides obtained from (B3LYP/6-31G(d,p) results *in vacuo*)- 235

4.236 The LUMO for the studied sulphonamides obtained from (B3LYP/6-31G(d,p) results *in vacuo*) - 236
4.237 The HOMO densities for the studied sulphonamides obtained for neutral species- 237
4.238 The LUMO densities for the studied sulphonamides obtained for neutral species- 238
4.239 Illustration of Fukui f^- isodensity - 247
4.240 Illustration of Fukui f^+ isodensity - 248
4.241 The optimized protonated geometries of the studied sulphonamides- 252
4.242 The HOMO densities for the studied sulphonamides obtained for protonated species - 253
4.242 The LUMO densities for the studied sulphonamides obtained for protonated species - 254

LIST OF TABLES

No	DESCRIPTION	PAGE
4.1	Potentiodynamic polarization (PDP) parameters such as corrosion potential (E_{corr}), Corrosion current density (i_{corr}) and anodic and cathodic Tafel slopes (b_a and b_c) using different inhibitors-	74
4.2	Electrochemical impedance (EIS) parameters such as the resistance of charge transfer (R_{ct}), constant phase element (CPE) and the CPE exponent (n) using different inhibitors-	86
4.3	Peaks and their identification, from FT-IR spectra of the studied corrosion inhibitors and adsorption films formed (i.e. SQX-MX) on the mild steel in 1.0 M HCl using different corrosion inhibitors-	92
4.4	Percentage inhibition efficiencies and corrosion rates values obtained from the weight loss of mild steel in 1.0 M HCl in the absence and presence of various concentrations of inhibitors-	103
4.5	Kinetic and activation parameters (derived from the Arrhenius and transition-states plots) for mild steel in 1.0 M HCl in the absence and presence of various concentrations of inhibitors-	110
4.6	Thermodynamic and adsorption parameters (Langmuir adsorption isotherms) for mild steel in 1.0 M HCl at various temperatures for the utilized corrosion inhibitors-	117
4.7	Thermodynamic and adsorption parameters (Langmuir adsorption isotherms) for mild steel in 1.0 M HCl at 30 °C using PDP and EIS for the utilized corrosion inhibitors-	118
4.8	Potentiodynamic polarization (PDP) parameters such as corrosion potential (E_{corr}), corrosion current density (i_{corr}) and anodic and cathodic Tafel slopes (b_a and b_c) using different inhibitors-	131
4.9	Electrochemical impedance (EIS) parameters such as the resistance of charge transfer (R_{ct}), constant phase element (CPE) and the CPE exponent (n) using different inhibitors-	143

4.10 Peaks and their identification, from FT-IR spectra of the studied corrosion inhibitors and adsorption films formed (i.e. SQX-MX) on the mild steel in 1.0 M HCl using different corrosion inhibitors- 149
4.11 Percentage inhibition efficiencies and corrosion rates values obtained from the weight loss of aluminium in 1.0 M HCl in the absence and presence of various concentrations of inhibitors - 159
4.12 Kinetic and activation parameters (derived from the Arrhenius and transition-states plots) for aluminium in 1.0 M HCl in the absence and presence of various concentrations of inhibitors- 165
4.13 Thermodynamic and adsorption parameters (Langmuir adsorption isotherms) for mild steel in 1.0 M HCl at various temperatures for the utilized corrosion inhibitors- 177
4.14 Potentiodynamic polarization (PDP) parameters such as corrosion potential (E_{corr}), corrosion current density (i_{corr}) and anodic and cathodic Tafel slopes (b_a and b_c) using different inhibitors- 184
4.15 Electrochemical impedance (EIS) parameters such as the resistance of charge transfer (R_{ct}), constant phase element (CPE) and the CPE exponent (n) using different inhibitors- 195
4.16 Peaks and their identification, from FT-IR spectra of the studied corrosion inhibitors and adsorption films formed (i.e. SQX-MX) on zinc in 1.0 M HCl using different corrosion inhibitors- 201
4.17 Percentage inhibition efficiencies and corrosion rates values obtained from the weight loss of zinc in 1.0 M HCl in the absence and presence of various concentrations of inhibitors- 210
4.18 Kinetic and activation parameters (derived from the Arrhenius and transition-states plots) for zinc in 1.0 M HCl in the absence and presence of various concentrations of inhibitors- 217
4.19 Thermodynamic and adsorption parameters (Langmuir adsorption isotherms) for zinc in 1.0 M HCl at various temperatures for the utilized corrosion inhibitors- 230
4.20 Comparison of the effects of selected Sulphonamides as corrosion inhibitors on mild steel, aluminium and zinc in 1.0 M HCl- 232
4.21 The molecular properties for studied sulphonamides obtained from (B3LYP/6-31G(d,p) results *in vacuo*)- 240

4.22 Mulliken atomic charges and Fukui functions on the heavy atoms of the Sulphonamides used as corrosion inhibitors - 243
4.23 The molecular properties for protonated studied sulphonamides obtained from (B3LYP/6-31G(d,p) results *in vacuo*)- 255
4.24 Quantum chemical parameters utilized to derive the non-linear multiple regression equation that correlates the theoretically estimated and the experimentally determined inhibition efficiencies- 257

CHAPTER 1

INTRODUCTION

1.1 BACKGROUND TO THE STUDY

Corrosion of materials has been of a major concern for a long time to many industries due to its consequences on industrial equipments such as reaction vessels, engineering vehicles, mining equipment and packaging machineries. The other major problem of corrosion is the contamination of the industrial products [1].

Corrosion mostly involves the deterioration of the material and it is widely common in metals although it is not limited to them. Materials of different types such as plastics, ceramics and composites are also prone to corrosion. Metals that have been affected by corrosion normally yield the corrosion product commonly known by a layman as 'rust'. The type of rust formed depends strongly on the nature of the metal undergoing the corrosion process. The effects of corrosion are detrimental to humans. In addition to having negative effects on the economy of a particular nation, corrosion also have a tremendous negative impact on human health and safety.

Over the years, there have been many observations made as far as corrosion is concerned. Many scientists, writers and philosophers recorded a number of discoveries, developments and solutions regarding this undesired process [1, 2]. Such observations include, among others, the discovery by Austin in 1788 that when neutral water comes into contact and react with iron, it changes its state to alkaline. In 1819 another profound observation was made by Thernard when he discovered that the process of corrosion is an electrochemical one. The fact that iron does not rust in the absence of moisture was established in 1829 by Hall.

1.2 JUSTIFICATION/SIGNIFICANCE OF THE STUDY

The economy of nations depends highly on the industrial products which can be sold locally or exported. Nevertheless, most industrial equipments are prone to the effects of corrosion since they are made largely from metallic products. The corrosion of these equipments may results in the following:

- Contamination of the product. This can be experienced by a manufacturing company if the rust that developed as a corrosion product interferes with the desired product of the company. This will require a substantial amount of money to recover or at least decontaminate the product thereof.

- Loss of efficiency. When the machinery or instrument has been attacked by corrosion, its efficiency is also affected in one way or the other to some extent. The cost of remedying this problem is enormous.
- Plant shutdown as a consequence of poor equipment efficiency and therefore poor economic productivity.
- Warranty claims. This is perhaps one of the most disturbing problems that indirect cost of corrosion carries with it.

If the effects of corrosion are not attended to for a long time, they may result in the affected industries shutting down. Such an outcome may result in economic loss not only for the industry but also for the country at large. Countries worldwide spend a large financial expenditure to counteract the effects of corrosion. For instance, in South Africa, the research conducted by the council for mineral technology (MINTEK) group showed that the direct cost of corrosion to the South African economy was R130-billion per annum in 2004. This is further strengthened by the research conducted by the Corrosion Institute of Southern Africa in collaboration with the University of Witwatersrand which showed that a value of R154-billion per annum is spent on solving the effects of corrosion in industrial areas [3]. Intensive studies have been conducted regarding the prevention and repairing of corrosion and their findings show that prevention is the most cost effective method as opposed to repairing the damage caused thereafter [4 – 11].

1.3 PROBLEM STATEMENT

Metals and the products derived from them are very important in life and their importance towards human life can never be over emphasized. The products derived from metals include, among others, automobiles, computers and construction structures. We are mostly surrounded by industries that make use of metals in one way or the other. These industries contribute to human life in many forms. Petrochemical industries see to it that each human being has enough fuel for day to day survival. Plants that are utilized in the food industries are also constructed from metals.

The challenge is that most of these metals do not remain in their metallic form once subjected to the atmospheric environments. They cannot resist the attacks by acids and bases, as a direct consequence, they resort to their metal oxides [1].

There is a need to find ways of preserving these metals and hence protect them from degrading to their metal oxides. This act may prolong their lifespan so that they can offer us their optimum performance.

This project is important for many reasons, such as the contribution of corrosion towards the economy of South Africa and the effects of corrosion on human safety and health.

- Corrosion has a tremendous impact on the global economy. (The economy of every country has its share in the corrosion control). The reports of the Corrosion Institute of Southern Africa show that the estimated direct cost of corrosion to the South African economy is 5.2 % of the GNP [3]. Hence, the economy of South Africa can be improved by doing research on this topic. With corrosion monitoring, a tremendous amount between R10 billion and R30 billion can be saved per annum.
- The second aspect of significance of this research is the health of human beings. Materials which are corroded have an impact on the health of the surrounding inhabitants. Iron can release iron oxide (rust) which can be toxic and dangerous towards human beings. If materials are protected from rusting, human health can be improved.

1.4 AIM AND OBJECTIVES OF THE STUDY

The main aim of the present work therefore is to investigate the inhibition potential of some sulphonamides namely Sulphaquinoxaline (SQX), Sulphamethoxazole (SMX), Sulphamethazine (SMT), Sulphisoxazole (SSZ), Sulphanilamide (SNA), Sulphamethizole (SMZ), Sulphachloropyridazine (SCP), Sulphabenzamide (SBZ) and Sulphadimethoxine (SDM) on three different metals, namely; mild steel, aluminium and zinc in hydrochloric acid.

The research specific objectives are to;

- Apply thermodynamics, kinetics and adsorption principles in studying the inhibition potentials of sulphonamides compounds, effect of sulphonamides compounds concentration and temperature on the corrosion rate.
- Propose the possible mechanism, type of adsorption and adsorption isotherm for the corrosion inhibition.

- Use the electrochemical techniques (potentiodynamic polarization [PDP] and the electrochemical impendence spectroscopy [EIS]) to study the corrosion behavior of different metals and the influence of the corrosion inhibitors.
- Use Scanning Electron Microscopy (SEM), Fourier Transform Infrared spectrometry (FTIR) to study the surface morphology/ interface interactions between the sulphonamides compounds and the metal surfaces to determine the mode of interfacial reactions and to investigate the interaction between sulphonamides compounds and metals to see the functional groups that have interacted.
- Use quantitative structure activity relationship (QSAR) studies using some quantum chemical/theoretical techniques e.g. density functional theory (DFT). To calculate quantum chemical parameters of the selected inhibitors and correlate them with the experimentally obtained inhibition efficiency and to derive equations for computation of theoretical inhibition efficiencies using QSAR, nucleophilicity, electrophilicity, Fukui and global softwares indices.

CHAPTER 2

LITERATURE REVIEW

2.1 DEFINITION OF CORROSION

It is worthwhile to mention that corrosion is an electrochemical process and a chemical reaction. This is so because the corrosion process brings about a complete change in the properties of the material concerned. For example, when a hard and ductile mild steel metal is left exposed to moisture and oxygen for a lengthy period, it changes completely from that form to a powder or rust. The proper definition of corrosion takes into consideration both the material and the environment. Corrosion is therefore defined as the undesirable deterioration of a material through a reaction with its environment [1–3].

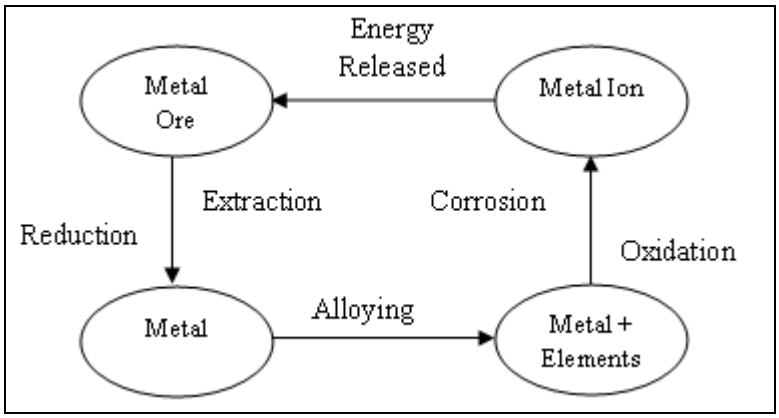

Figure 2.1: Relationship between corrosion and extraction

Figure 1.1 depicts the relationship between the process of corrosion and that of extraction. While during extraction of metals the metal ore is reduced through the addition of energy to obtain a pure metal, during corrosion the process is reversed. Energy is given off when the metal returns to its oxidized ore state (corrosion). This oxidized ore state differs depending on the metal used. If iron metal is used the oxidized ore state would be iron oxide which many understand as rust.

2.1.1 BASIC REACTIONS DURING METAL CORROSION

The general features of corrosion include the fact that corrosion is a chemical process, the rate of corrosion depends not only on the metal but also the environment concerned and the fact that in the absence of moisture corrosion does not take place.

There are four sub reactions of corrosion. The basis for corrosion prevention is based on these sub reactions. If one of these sub reactions is disturbed or altered, the rate of corrosion is also disturbed or reduced [3].

The *firs*t step marked as shown in figure 2 is the oxidation half reaction. In this step, the Fe metal changes to its charged specie which goes into the solution.

$$Fe_{(s)} \rightarrow Fe^{2+}_{(aq)} + 2e^{-} \quad (1)$$

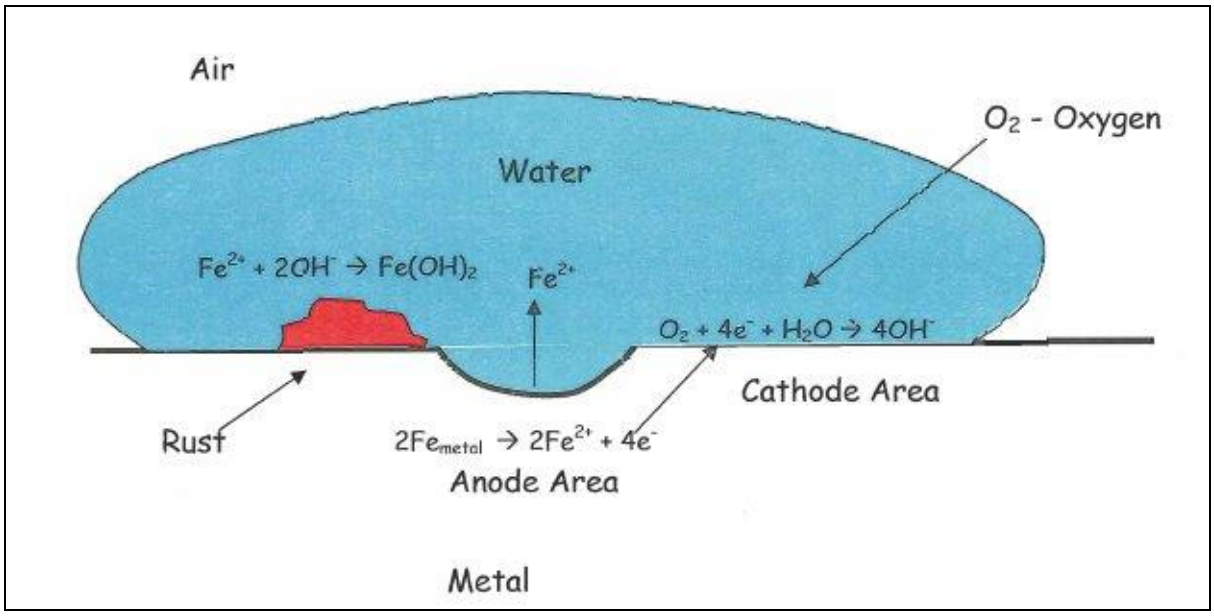

Figure 2.2: Schematic representation of the four sub-reactions (corrosion mechanism) which take place when mild steel undergoes the corrosion process.

Reaction 1 is also known as the anodic reaction, thus the Fe metal acts as the anode. From this step, it is clear that the metal has lost its identity and the electrons are lost or given away. A reaction such as the one above is known as an electrochemical half reaction. Electrochemical reactions are reactions that involve the exchange of electrons between species. The exchange of electrons refers to the giving away and accepting of electrons by species. In equation (1) the electrons are given away and are therefore going to be received by a species in the reduction reaction [2, 3].

The *second* step, involves the movement of electrons which were given off in the first step. They flow through the steel. This flow of electrons symbolizes the current (I). The only possible route for the movement of electrons is through the steel since the electrolyte can only allow the movement of ionic species (cations and anions).

The *third* step is known as the reduction half reaction. In this half reaction oxygen is reduced (the process of corrosion does not take place in the absence of oxygen), the reduction of the dissolved oxygen is written as;

$$O_{2\,(g)} + 2H_2O_{\,(l)} + 4e^- \rightarrow 4OH^-_{(aq)} \qquad (2)$$

From reaction 2, it is clear to see that the electrons given off in reaction 1 are accepted here.

The *fourth* step, to complete the corrosion of Fe involves the closing of the electrical circuit between the anodic and cathodic reactions. This requires the current to also pass through the electrolyte via ions which are dissolved in water such as Fe^{2+}, OH^- and H^+.
Reaction 3 illustrates this;

$$4Fe^{2+}_{\,(aq)} + O_{2\,(g)} + XH_2O_{\,(l)} \rightarrow 2Fe_2O_3.XH_2O_{\,(s)} + 8H^+_{\,(aq)} \qquad (3)$$

These four steps occur simultaneously during the process of corrosion of mild steel. In dry conditions (where there is less moisture), such as in a desert, corrosion is slower than in a moist area, where there is moisture carrying oxygen (O_2). There are many other factors that influence the rate of corrosion of mild steel, including the presence of salt. The molten salt increases the conductivity of the aqueous solution that is formed at the surface of the metal. The temperature of the system also affects the rate of corrosion of mild steel.

2.1.2 CORROSIVE ENVIRONMENTS

It is imperative to have a better understand regarding different types of environments during the studies of corrosion of metals. This is due to the fact that complete information about the corrosion of a metal can be gathered when both the metal surface being corroded and the environment are considered. The environments exist in three main groups, namely atmospheric environments (mining, marine, urban and rural), man-made environments (synthetic petrochemical, industrial, molten salts and metals) and outer space environments (vacuum). These different types of environments are dependent on factors such as temperatures, pressures, etc. For instance, a high temperature of the environment is associated with high corrosion rate of metals [4–6].

The environment also plays an important role in the type of corrosion a material undergoes. These types of corrosion include dry or wet corrosion. Wet corrosion occurs in aqueous or

electrolytic environments while dry corrosion occurs above the dew point of the environment such as in cases when the corrodents are gases and vapours [7]. Nevertheless, most literature reveals that all environments are corrosive to a certain degree [7].

2.1.3 CORROSION IN DIFFERENT MEDIA

The most common media in which corrosion takes place include acidic, neutral and alkaline. Metals which are utilized in various industrial applications such as acid pickling, oil and gas fields, coatings and industrial cooling water systems are often subjected to such different types of media [8]. There are certain media which possess a low pH value (i.e., acidic medium) and those with high pH values (i.e., basic medium).

Acidic medium: Studies have shown that concentrated acids are less corrosive in comparison with the diluted acids [1]. This is because the diluted acids contain more amount of water than when metals are subjected to dilute acid, hydrogen is given off and the result is the corrosion of the metal. For instance, when aluminium is subjected to dilute hydrochloric acid, the result is the aluminium trichloride and the hydrogen which is given off. The reaction equation is given below;

$$2\ Al + 6\ HCl \rightarrow \ 2\ AlCl_3 + 3\ H_2\uparrow \quad (4)$$

If dilute hydrochloric acid is replaced by dilute sulphuric acid, the result is the formation of aluminium sulphate according to the reaction equation given below;

$$2\ Al + 3\ H_2SO_4 \rightarrow \ 2\ Al_2(SO_4)_3 + 3\ H_2\uparrow \quad (5)$$

Alkaline and neutral media: Environments such as water, salt solutions and alkaline solutions (such as sodium hydroxide) can also be corrosive towards metal surfaces, especially in the presence of dissolved oxygen. Air carries oxygen which in most cases dissolves in water. This is normally the main cause of corrosion formation in the event when metal surfaces come into contact with water [9]. For instance, the reaction of water and aluminium in the presence of oxygen is given below;

$$4\ Al + 6\ H_2O + 3O_2 \rightarrow \ 4\ Al(OH)_3 \quad (6)$$

The aluminium hydroxide that is formed exists in aqueous solution as aluminate ion of the formula $[Al(OH)_4]^-$. This ion forms bauxite (an aluminium ore) of the formula $Al_2O_3.x\ H_2O$ when exposed to mild heat [9].

2.1.4 KINETICS AND THERMODYNAMICS OF CORROSION

Kinetics of Corrosion:

The kinetics of corrosion informs how fast corrosion occurs at a given time and environment. The reactions which are involved in corrosion produce and consume electrons. These electrons can further be quantified as current.

More information on the electrochemical behavior of metallic materials in aggressive media can be generated through the influence of temperature on the kinetic process of corrosion. Arrhenius law gives the relationship between the dependence of the rate constant of chemical reactions on the temperature [12, 13].

$$k = Ae^{-E_a / RT} \tag{7}$$

where;

k = the rate constant

A = the pre-exponential factor or the pre-factor

R = time gas constant

E_a = the activation energy

T = the absolute temperature

According to equation (7), the corrosion rate should increase when the temperature increases and E_a and A may vary with temperature.

The rate of corrosion can be measured differently depending on the method of analysis employed. If traditional gravimetric methods (weight loss) are employed, equations such as (8) below can be used directly.

$$\rho = \left(\frac{\Delta w}{St} \right) \tag{8}$$

where;

ρ = the corrosion rate

W = the average weight loss of the material

S = the total area of the of the material

t = the immersion time

Thermodynamics of Corrosion:

The corrosion phenomenon can best be explained in terms of the stability of chemical species and reactions associated therein. Therefore the thermodynamic control concept has significant importance in understanding the corrosion process. However, the rates of corrosion cannot be predicted through thermodynamics calculations. One of the great advantages of thermodynamics is that it can be used to calculate the theoretical activity of a given metal when the composition of the environment is known.

The concept of spontaneous and non-spontaneous reactions is also important in the study of corrosion processes. Corrosion processes are known to be spontaneous processes. For a reaction to occur spontaneously, the free energy of that particular reaction should have a negative value [12, 13]. Corrosion involves both oxidation and reduction half reactions. The overall free energy for the redox reaction is negative. The standard free energy of the cell reaction ΔG^0 under standard conditions can be calculated by the following equation;

$$\Delta G^0 = -nF\Delta E^0 \tag{9}$$

where ΔG^0 is the standard free energy change, n is the number of electrons exchanged, F is the Faraday constant and ΔE^0 is the standard energy change in the reaction. Studies indicate that the values of ΔG^0 of around –20 $kJ.mol^{-1}$ or lower imply physical adsorption (physisorption) and those around –40 $kJ.mol^{-1}$ or higher imply chemical adsorption (chemisorption) for a particular corrosion process [13]. Chemisorption is a process in which the interactions involved are covalent in nature and the type of layer that results is monolayer [13]. Physisorption is a process that involves weak Van der Waals intermolecular interactions that result in multilayer products [13]. The other distinction between these two is that chemisorption is irreversible while physisorption is reversible.

From the electrochemical measurements, other thermodynamics quantities such as the adsorptive enthalpy, ΔH^0_{ads} can be derived. The Van't Hoff equation can be utilized for this purpose.

$$\ln K = -\frac{\Delta H^{0}{}_{ads}}{RT} + Cons\tan t \tag{10}$$

where K is the adsorptive constant. The value of the ΔH^{0}_{ads} obtained from this equation can also be verified using the Gibbs-Helmholts equation.

$$\left[\frac{\partial\left(\Delta G^{0}{}_{ads}/T\right)}{\partial T}\right]_{P} = -\frac{\Delta H^{0}{}_{ads}}{T^{2}} \tag{11}$$

The other thermodynamic quantity that can be deduced is the standard entropy, ΔS^{0}_{ads} through the use of the thermodynamic basic equation (12).

$$\Delta G^{0}{}_{ads} = \Delta H^{0}{}_{ads} - T\Delta S^{0}{}_{ads} \tag{12}$$

The equilibrium constant (K_{eq}) for the reaction can be calculated using equation (13) below;

$$RT\ln K_{eq} = -\Delta G^{0} = nF\Delta E^{0} \tag{13}$$

2.1.5 THE RATE OF CORROSION

During the process of corrosion, the metal that is being corroded undergoes a decrease in its molecular mass, which is also known as weight loss. When the weight loss is considered per unit time, it is referred to as rate of corrosion. The environment in which the metal resides, the type of the metal and the total exposure time determines the rate of corrosion. Most metals possess various resistances to corrosion. Mild steel is mostly utilized since it is readily available due to its affordability. Consequently, mild steel serves most applications which require a bulk amount of steel. Zinc on the other hand finds its most applications in building construction as roofing means. During the corrosion of mild steel, the responsible component is iron as it is the most abundant [12]. Unlike aluminium that forms passive films; mild steel and zinc do not have as much ability to form such films and consequently their rates of corrosion is much enhanced than that of aluminium. A passive film is a thin film of oxidation products that prevent further corrosion of the metal surface. Depending on the aggressive environment, the life span of passive films varies. More aggressive environments cause

corrosion through the breakdown of the passive films and exposing fresh surface of the metal [14].

2.1.6 FACTORS AFFECTING THE RATE OF CORROSION

In addition to the type and nature of the corroding substance, there are a number of factors that affect the rate of corrosion. Those factors that are particularly interesting for this work are briefly discussed.

Fluid speed: The main causes of corrosion for fluids in motion are diffusion effects. Corrosion is strongly experienced by those metals that are protected by chemical coatings as soon as they subjected to fluid carrying particles which are moving very fast. These fast moving particles are likely to remove the chemical coatings and leave the metal exposed to corrosion. High corrosion rates are directly related to high fluid speeds [15].

Environment temperature: Literature reveals that the collision factor associated with the molecules has a direct relationship with the environment temperature. At lower temperatures the molecules move slowly with low collision speed while at higher temperatures they move at high speed and collide with each other with high collision speed [16]. Hydrogen molecules exhibit a similar behavioral trend. At higher temperatures hydrogen molecules possess greater collision energy and consequently the rate of corrosion increases since the metal surface is left exposed to the corrosive solutions [17].

Hydrogen ion concentration of the solution: Corrosion rates increases with the increase in concentration of hydrogen ions in a given environment (when the pH of the medium is decreased) [18]. Acidic environments are more aggressive than alkaline environments which have low concentrations of hydrogen ions and high pH values. The fact that in alkaline environments the metal ions leave the anode and move to the cathode leads to slower corrosion rates in alkaline environments as compared to acidic environments [18, 19].

Availability of corrosion inhibitors: Inhibitors are substances which when introduced (in minute concentrations) into the corrosive environment effects of corrosion from a given material. Several studies have shown that as the concentration of the inhibitor is increased the rate of corrosion is decreased [19–21].

Oxygen and metal ion concentrations: Corrosion rates of metals increases as concentrations of oxygen and the metal ions are increased in a given corrosion reaction. The excess availability of oxidizing agents such as Cl_2, Br_2, I_2 and H^+ in a given environment enhances the rate of corrosion. Metal oxides of specific metals often result as soon as a specific metal comes into contact with these oxidizing species [19].

Ratio of the cathode\anode size: Corrosion rate also depends on the ratio between the cathode and anode electrodes. The rate at which the electrons combine with oxygen and water leading to corrosion depends chiefly on the ratio of the cathode: anode size. The size of the cathode does not have to be excessively big. If it is excessively big, the demand for the electrons to satisfy it from the anode will be too much; hence the anode will be consumed quickly. On the other hand, if the anode is excessively large it is consumed far slower. In order to control the ratio of the cathode: anode size one has to reduce the size of the cathode or substitute the anode with the other source of electrons. If this ratio is correctly balanced, the rate of corrosion can be minimized to a reasonably acceptable level [22].

Galvanic effects: The resultant corrosion that arises as two different metals are joined together in the construction of the cooling system and are exposed to water is known as galvanic corrosion. In the galvanic series, lower metals have a high tendency to corrode while the upper metals have the least tendency to corrode. From this series, gold is the least active while magnesium metal is the most active. Galvanic series is based on measuring the potentials of metals as compared to a reference electrode. If one joins two metals which are very far apart in the galvanic series in the presence of an electrolyte, the rate of galvanic corrosion is much rapid. However, if the two joined metals are carefully selected from the galvanic series (that is, if the two metals are enough close to each other), the rate of corrosion maybe reduced [22].

Coating thickness/thinness: A thin metal coating decreases the time for the migration of reactants to the metal surface which in turn increases the corrosion rate. Nevertheless, if the coating that is applied on the metal surface is reasonably thick, the time that will be taken by the migration of the reactant will also be reasonably long, thus lengthening the time it will take for the material to be corroded [23].

Chemical deposits: Electrolysis and evaporation processes can be utilized to introduce chemical deposits in a form of coatings left on metal surfaces. Amongst all the factors that

affect the rate of corrosion this is one which is less researched upon. However, chemical deposits are the most disturbing when it comes to metal surfaces destruction. The deposits in the form of the chemical treatment used as a means of inhibiting corrosion can lead to a more serious corrosion on the material intended to be protected. Anodes may develop underneath the formed deposits. The next consequence is the development of localized pitting once the anode is developed [24, 25].

2.1.7 TYPES OF CORROSION

The effects of corrosion on metals are adverse and in most instances manifests as damages on the surfaces of these metals. In this view, the classification of corrosion by physical appearance is a proper, most reliable, less complex and convenient method of identification. Most types of corrosion are a result of what remains when a metal comes into contact with the aggressive or corrosive environments in the presence of oxygen [19]. Some of the possible types of corrosion which mostly affect all metals and alloys are briefly described.

General Corrosion: This type of corrosion is also referred to as uniform surface corrosion. It is caused by direct chemical attack on the substance or metal surface. During this type of corrosion only the surfaces of the metal are attacked. General corrosion is the most studied and common of all types of corrosion [1, 26].

Galvanic Corrosion: Galvanic corrosion occurs when two dissimilar metals are placed in contact under electrochemical action in the presence of an electrolyte. Normally the consequence of this type of corrosion is the rust at the joints between the metals [1, 26].

Pitting Corrosion: Pitting corrosion is a dangerous, much localized form of corrosion and takes place at microscopic defects on a metal surface [1]. Metals that form protective film, such as aluminium and magnesium, are the most attacked by pitting corrosion. White or gray powder often forms as a byproduct of this type of corrosion. Pitting corrosion can thus be noticed and recognized through the observation of this powder. Tiny pits or holes are then left on the metal surface as soon as the powder is cleaned away. A great amount of damage can be caused on the metal when these small surface openings penetrate deeply into the structural members. In cases where conditions that give rise to this type of corrosion cannot be altered, materials containing high alloy content often provide relief to the problem [1, 26].

Fretting Corrosion: This type of corrosion is also referred to as wear or friction corrosion. It can be defined as the attack that is accelerated by the relative motion of contacting surfaces. Two highly loaded surfaces which are not supposed to move against each other can be affected by this type of corrosion at their interfaces as soon as they start to move. This is mainly due to the fact that as they are moving against each other they create friction, leaving an abrasive wear called fretting. The friction process also removes the protective film on the metallic surface. With this rubbing action, the surface of the metal combines with the oxygen and the metal oxide forms [1]. While many types of corrosion are driven by an electrolyte, fretting corrosion is not. One way of reducing or minimizing fretting corrosion is through the application of a lubricant; nevertheless, the installation of a fretting-resistant material between the two surfaces can also contribute greatly in reducing this type of corrosion [1, 26].

Crevice Corrosion: Some authors refer to crevice corrosion as shielded corrosion [26]. This is due to the fact that this corrosion occurs where the surface is shielded thereby preventing the free and open interactions of oxygen and the surface of the metal. The passive films that results from some metals during the corrosion process often tend to break down in these areas [26].

Intergranular Corrosion: A type of corrosion that occurs with alloys when a difference in potential exists between the grain boundary and the grain is known as intergranular corrosion. The highlight of this type of corrosion is that the grain boundaries of a substance are attacked by the environment (perhaps strong acid or base). Any commercial alloy has a highly-magnified cross that shows granular structure of the metal. There are individual grains and all these grains possess a defined boundary which further possesses different chemical characteristics in comparison with that of the metal within the grain. The grain boundary can act as an anode while the grain centre can act as the cathode. As soon as these two come in contact with the electrolyte, they react. It is imperative that the alloys are properly heat-treated in order to avoid intergranular corrosion when they are exposed to acidic environment. Aluminium alloys such as 2014 and 7075 suffer the most from this type of corrosion. [1, 26].

Stress Corrosion Cracking: Under certain conditions both crevice and pitting corrosion can give rise to stress corrosion cracking. Identifying characteristics of this type of corrosion include a brittle fracture that occurs in a ductile material. In order for the stress corrosion cracking to take place the following three factors must be met:

- *A temperature range*: Under temperatures of 60°C stress corrosion cracking to does not take place [26].
- *The presence of ions*: The availability of aggressive ions such as Cl^- often initiates stress corrosion cracking.
- *The presence of tensile stress*: In order for a successful formation of stress corrosion cracking to form an applied or residual stress must be present. This stress may result from metal forming, fabrication and welding procedure.

Corrosion generally is a slow process and this type of corrosion is not exceptional. These three factors are to some extent complementary and synergistic. The pits that result during the initial stages of stress corrosion cracking act as a local stress riser which leads to pits opening. This opening gives way to the fresh electrolyte which eventually reaches the anodic portion located in the pit. A step such as this one gives rise to corrosion that is initially predominating at the tip of the pit. After some amount of time, this corrosion further branches to the other areas of the pit and subsequently the entire surface of the metal [26].

Corrosion Fatigue: This type of corrosion develops as consequence of a combination of the effects of cyclic stress and the corrosive environment. Each metal has the endurance limit of cyclic stress and once the limit has been exceeded the metal will crack and fail from metal fatigue. There are two main stages that are involved in the process of corrosion fatigue failure. First, the metal is damaged by pitting and crack formation which is caused by the combined action of corrosion and cyclic stress. This causes fracture by cyclic stress. The second stage involves the propagation of the crack. As a consequence the fatigue corrosion will result in the fracture of the metal [1, 26].

Filiform Corrosion: When moisture finds its way in the coating of the surface that is painted, the result is likely to be a filiform corrosion. This type of corrosion can be further categorized as a special form of oxygen concentration cell. Traces of corrosion products that have the characteristic worm-like develop beneath the paint as soon as the material has been attacked

by this type of corrosion. In order for the filiform corrosion to take place the following criteria apply:

- The surface should be slightly acidic.
- The relative humidity of the air should be between 78 and 90 %.
- The surfaces of substances must be painted.

Aluminium and steel suffer the most from this type of corrosion although these effects are experienced the most in cases of aluminium. This is because in aluminium the traces cross under one another. Normally one type of corrosion leads to another if it is not treated early enough. Two main actions as listed below can be applied in order to minimize filiform corrosion:

- The application of glass bead blasting material.
- The storage conditions such that the material is stored in a place where the relative humidity is less than 70 %.
- The removal of acidic contaminants from the surface.
- The usage of the type of coating that contains low rate of diffusion for oxygen and water vapour [1, 26].

Exfoliation Corrosion: The advanced form of Intergranular corrosion is known as exfoliation corrosion. It normally starts from below the surface when the force of expanding corrosion products starts to lift the surface grains [1].

Active-Passive Cells: This type of corrosion targets the metal that utilizes a tightly adhering passive film as protection shield corrosion. Metal oxides in most cases act as these adhering passive films. This type of corrosion is sometimes referred to as another form of concentration cell corrosion. There are two forms of corrosion which are working together in the active-passive cell corrosion. The corrosive action normally commences as an oxygen concentration cell. For instance, an oxygen cell can develop as a result of some salt deposits on the metal surface in the presence of water which has some oxygen in it. Beneath the salt crystals the passive film is broken. As a consequence, the active metal beneath the film is exposed to the wrath of corrosion. The second form of corrosion that is involved is pitting. After all, when the metal is exposed to the wrath of corrosion attack, the rapid pitting of the active metal occurs. The end result is normally deep pits that are formed in a short space of time and a greater rate of corrosion is normally experienced in these conditions [1, 26].

Dealloying: Just like many other corrosion types dealloying is problematic although it is not commonly experienced. This process occurs when the alloy loses its atomic component of the metal and retains its corrosion resistance component of the metal [1, 26].

Microbiologically induced corrosion: The attraction and binding of bacteria onto the surfaces of the metals often results into microbiological induced corrosion. Consequently, crevices develop. The extent of this type of corrosion also depends largely on the type and nature of bacteria. Some bacteria have the ability to produce aggressive metabolic products which are responsible for the increase in the state of corrosion [1].

2.1.8 CLASSIFICATION OF CORROSION PROCESS

The process of corrosion any metal can take place only if the metal comes into contact with a corrosive environment in the presence of oxygen and moisture. The products that normally results are oxides of the involved metals. The mechanistic pathways towards the production of these oxides depend entirely on the type, nature and class of the corrosion process. Three main processes, namely; electrochemical, chemical and physical are briefly discussed [25, 26].

Electrochemical corrosion: From the known corrosion processes, electrochemical corrosion is the most common and frequently encountered. The electrochemical reaction that is responsible for metal corrosion is composed of four factors, namely; anode, cathode, electrolyte and electronic circuit. The kinetics of electrochemical reactions are the most dominant governing factors behind electrochemical corrosion [25, 26].

Chemical corrosion: The law of ordinary heterogeneous chemical reactions is the most important factor that leads to the characteristic traits of chemical corrosion. Here the metal is destroyed at high temperatures by aggressive gases since these gases prevent the condensation of moisture on the surface of the metal [25, 26].

Physical corrosion: This type of corrosion process is not caused by any chemical reactions but through physical dissolution of the material. These dissolutions are not to be confused with chemical reactions. The dissolution of a material in liquid metals such as mercury is a good example of this phenomenon [25, 26].

2.1.9 CONSEQUENCES OF CORROSION

Corrosion results in consequences that are experienced negatively. Some of these effects are briefly discussed [25, 26].

Economic effects: Corrosion affects the economy of every nation. These effects maybe experienced indirectly or directly. Large industries such as petroleum companies utilize metals for the purposes of carrying and transportation of fluids. In cases where these metal containers are affected by corrosion, a large financial expenditure is required to remedy this problem. Thus the economy is negatively affected.

Safety effects: Human safety is always a high priority. Nevertheless, corrosion is predominantly problematic in this regard. Metals find numerous applications in transportation and construction industries which are mobility and dwelling-places solutions, respectively for human beings. In cases where these metals are corroded, human beings are at a large risk of injuries and to some extent losing their lives.

Health effects: Metals are useful in everyday life to such an extent that they are applicable in health sector. In recent times metal prosthetic devices (hip joints, pace makers, e.t.c.) are utilized on human bodies. Hence failure of the device due to corrosion may results in bad effects on human health.

Cultural effects: This consequence is observed on the precious and most historic statues of many nations that are severely deteriorated due to the effects of corrosion. These artifacts pass cultural beliefs from generation to generation. When corrosion attacks these metals, the line that connects generations is cut short.

Technological effects: Large industries utilize technology for a greater production such as the drilling of oil both in the sea and on land. When these technological systems are affected by corrosion the production is affected thereby affecting the cost of the company for the repairing of these systems.

2.2 CORROSION OF METALS

2.2.1 MILD STEEL

Mild steel is a type of steel that has low quantity of carbon and other elements as alloying constituents. It has some interesting mechanical properties for its low carbon content, such as ease shaping and softness because of its ductility. A greater amount of carbon makes steel stronger, harder and stiffer. Thus carbon is an alloying element that increases the hardness of mild steel [27]. Mild steel has various compositions depending on its applications. Nevertheless, in all compositions of mild steel the maximum limit of carbon content is acceptable at 0.29% while the proportions of manganese, copper and silicon are approximately fixed at 1.65%, 0.6% and 0.6%, respectively. The proportions of cobalt, chromium, niobium, molybdenum, titanium, nickel, tungsten, vanadium and zirconium are varied. Iron is always the predominant constituent with approximately 99% composition [28].

When materials such as metals corrode, an oxide is formed with certain characteristics which include the colour. The resultant colour depends on the amount of water present in the oxide. In environment that has low water content or humidity, the rate of corrosion is very slow in comparison with environments of high water content or acidic and alkaline conditions. When metals such as mild steel are subjected to harsh environments such as acidic media, corrosion takes place mainly on iron and rust is formed. Rust is a common name or term that is used to describe iron oxides and hydroxides. For instance, iron compounds such as $Fe(OH)_2$, $Fe(OH)_3$, $FeO(OH)$ and $Fe_2O_3.H_2O$ are all forms of rust that results from iron corrosion. Environments such as rain and dew also play major roles during the corrosion of materials [29].

The process of mild steel corrosion is always associated with two chemical half-reactions, namely reduction-oxidation half reactions which are also known as redox reactions. These reactions represented by iron as it is the main component in mild steel are similar to the ones reported in section 2.1.1 of this work.

2.2.2 ALUMINIUM

Aluminium is different from mild steel in the sense that the oxide that is formed by oxygen in mild steel does not stay or bond to the surface of the metal, whereas in aluminium, the oxide coating that is formed bonds with the surface of the metal. Consequently aluminium is not as

prone to corrosion as mild steel [30]. Aluminum is widely utilized worldwide because of its light-weightness (malleability and ductility). Examples of applications of aluminum include the automobile industries.

When aluminium is subjected to moist conditions, an oxide layer is formed. This layer assists in corrosion prevention. There are several factors that affect the thickness of this oxide layer. Amongst other factors, there is temperature, environment and the elements that are present in the alloy. At lower temperatures (such as room temperatures), the oxide layer is normally thicker than the one that may result at higher temperatures. One interesting trait of aluminium is that as soon the old oxide film is damaged due to corrosion, new one quickly forms [30].

Under environmental conditions with pH $\leq$ 4 (acidic) or $\geq$ 9 (alkaline), aluminium metal suffers from corrosion. Chloride and fluoride ions are known to possess the ability to attack the oxide layer thereby causing corrosion on aluminium metal. When chloride ions are present in the system, the type of corrosion that aluminium undergoes is known as pitting corrosion [14]. The chemical reactions that are involved during the process of pitting corrosion of aluminium metal are described below.

Firstly, aluminium metal is oxidized to Al^{3+} ion.

$$Al_{(s)} \rightarrow Al^{3+}_{(aq)} + 3e^- \quad (14)$$

This is followed by the reaction between the aluminium 3^+ ion and water to produce aluminium hydroxide.

$$Al^{3+}_{(aq)} + 3H_2O_{(l)} \rightarrow Al(OH)_{3\ (l)} + 3H^+_{(aq)} \quad (15)$$

The reaction involving hydrogen evolution takes place at the intermediate cathode as shown in reaction equation (16).

$$2H^+_{(aq)} + 2e^- \rightarrow H_{2\ (g)} \quad (16)$$

Lastly, the reaction involving oxygen reduction takes place according to reaction equation (17).

$$O_2\ (g) + 2H_2O_{(l)} + 4e^- \rightarrow 4OH^-_{(aq)} \quad (17)$$

The exact processes involved can be further elucidated schematically using Figure 2.3. This figure shows how reactions (14) to (17) take place.

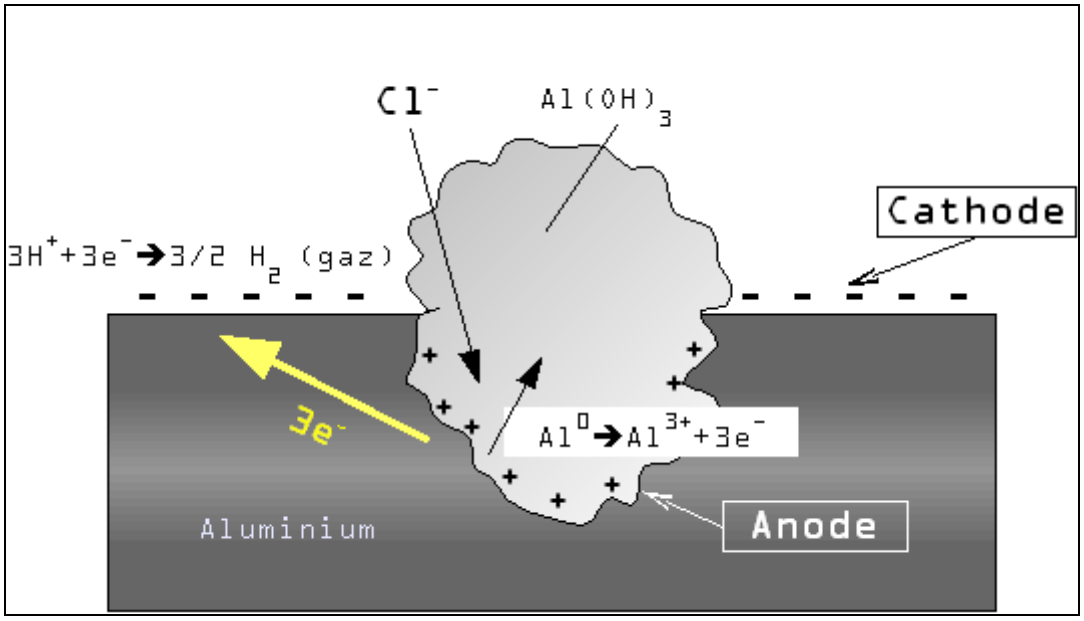

Figure 2.3: Schematic representation of aluminium pitting corrosion mechanism in acidic medium.

As clearly shown in Figure 2.3, chloride ions find their way into the pit and result in the formation HCl. This phenomenon increases the rate of pit propagation. Nevertheless, the reduction process give rise the alkaline environment. The aluminium metal cannot resist this kind of environment; consequently pits are formed in alkaline conditions.

2.2.3 ZINC

Zinc is one of the important metals extracted from the earth`s crust as an ore. It ranks the fourth most important among metals in worldwide production and consumption, behind iron, aluminium and copper. Zinc also finds important applications that can be divided into six categories such as coating, casting alloys, alloying elements in brass and other alloys, wrought zinc alloys, zinc oxide and zinc chemicals. Zinc finds most of its use in the production of alloys and in galvanizing to protect steel structures, present as a chemical additive in rubber and paints. This metal can also protect other metals connected to it by electrochemical series which is a good account for its usage in galvanizing industries. Galvanizing is mostly important in protection of building structures and machine elements [31].

The application of zinc coatings on steel structures for corrosion protection gave zinc the most important application in corrosion resistance in atmospheric environments. Zinc is similarly compared to aluminium in atmospheric environments since it also has the ability to produce a protective oxide layer of zinc carbonate which retards the rate of corrosion in the same manner in which aluminium does. Zinc has a range of compounds that are applicable and beneficiary [32]. Zinc compounds such as zinc oxide (ZnO, useful in rubber industry, ceramics and ink production), zinc sulfate ($ZnSO_4$, useful in treatment of zinc deficiency in soil and textile industries) and zinc chloride ($ZnCl_2$, useful as deodorant in many fluids) are in high demand in every country. In comparison to other metals such as cadmium and lead, zinc is not toxic and it is an essential trace element for human and plant growth [31, 33].

Zinc suffers corrosion the least compared to mild steel due to the fact that it has the ability of forming insoluble basic carbonate films that possess the ability to hold firm to its surfaces thereby reducing the rate of corrosion. The corrosion of zinc is dependent upon the type of environment. Environments with a pH of 6.5 - 12 have been found to have the lowest corrosion rates of zinc. Acidic, alkaline as well as marine conditions accelerate corrosion of zinc beyond the limits of usefulness and thus zinc is not a useful candidate in such environments, therefore the need for protection of zinc [32]. Zinc suffers pitting corrosion in the environment of aggressive ions such as chloride ions. Its corrosion behaviour follows the following half-reactions [34].

Firstly, zinc is oxidized to zinc 2^+ ions as shown in reaction equation (18).

$$Zn_{(s)} \rightarrow Zn^{2+}_{(aq)} + 2e^- \quad (18)$$

This is followed by the reduction of hydrogen ion to hydrogen gas by taking up the two electrons of the oxidized zinc.

$$2H^+_{(aq)} + 2e^- \rightarrow H_{2\,(g)} \quad (19)$$

The two reactions can be combined to form the final reaction as indicated in reaction equation (20).

$$Zn_{(s)} + 2HCl_{(l)} \rightarrow ZnCl_{(s)} + H_2\,(g) \quad (20)$$

The corrosion processes happening on zinc surface can be further elaborated schematically using Figure 2.4.

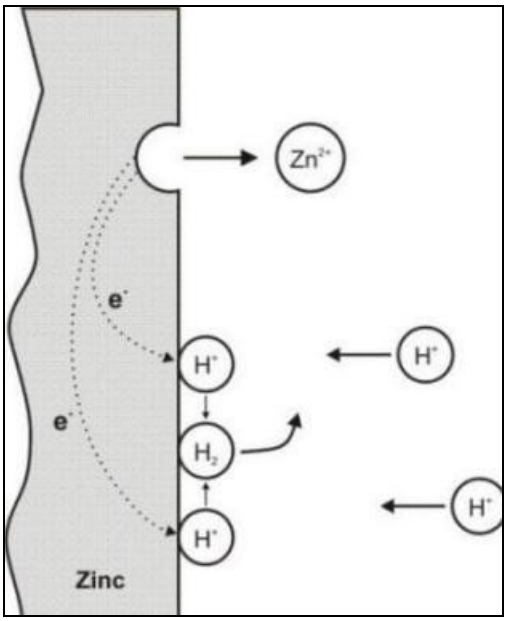

Figure 2.4: Schematic representation of the process of zinc corrosion in hydrochloric acid.

2.3 CORROSION CONTROL MEASURES

Although metals such as mild steel, aluminium and zinc are prone to corrosion, some alterations are applicable that may result in corrosion effects minimized. Once this is done, a substantial amount of money can be saved annually. There are a number of ways to control corrosion. These include protective coats (painting), surface cleaning and preparation, cathodic protection, planned maintenance, corrosion allowance, plating, bluing, dehumidity, data logging, inspection and inhibitors.

The work presented in this research involves the investigation of the use of sulphonamides compounds as corrosion inhibitors for the protection of mild steel, aluminium and zinc in hydrochloric acid environments. More detailed information is provided in the next section on the use of corrosion inhibitors in the protection of metal surfaces against corrosion.

2.4 INHIBITORS AND INHIBITION

2.4.1 DEFINITION OF CORROSION INHIBITORS

The attempt to minimizing or protect the metal from corrosion of is known as corrosion inhibition. The chemical substances utilized in minimizing or impeding the corrosion process of a certain material are known as corrosion inhibitors [35, 36]. The inhibitor is introduced to the system in small concentration. Various substances have shown the potential to inhibit metal corrosion and these include organic compounds, salts and some gases. Substances that act as a corrosion inhibitors need to have centers or functional groups in their molecules, with higher electron density from which electrons could be donated to the metal surface to result in the coordination (adsorption) of the inhibitor to the metal surface. For instance, organic compounds containing electronegative functional groups and π-electrons in triple or conjugated double bonds are usually good corrosion inhibitors. Heteroatoms such as sulphur, phosphorus, nitrogen and oxygen as well as aromatic rings in their structure are the major adsorption centers because they have high electron density. There are other factors influencing the adsorption of the inhibitors onto the metal surface such as the environment in which the inhibitor acts, the nature of the metal and the electrochemical potential at the interface [35, 36]. Most importantly, the efficiency of the inhibitor depends on the structure of the inhibitor, which includes the number of adsorption active centers in the molecule, their charge density, the mode of adsorption, the formation of metallic complexes and the projected area of the inhibitor on the metallic surface [35]. The formula weight of the molecule also plays a role in the efficiency of the inhibitor. Usually, the compound that has a high molecular weight tends to show high inhibition efficiency [35, 36].

2.4.2 TYPES OF INHIBITORS

Inhibitors can be classified into six main classes according to their chemical functionalities. The effect of a certain inhibitor depends on factors such as the nature of inhibitor, type of environment and the nature of the metal under investigation. Some classes of inhibitors are briefly described below.

Organic/inorganic inhibitors: These inhibitors alter the entire surface of the metal as soon as they are available in reasonable amount. Studies have indicated that organic/inorganic inhibitors that normally contain at least one functional group of the type =CO, -CHO and -NH_2 or one element from groups VA and VIA within their structures are active corrosion

inhibitors. Most researchers in the field of corrosion inhibition have reported the mechanism of adsorption [37, 38]. During adsorption the inhibitor is adsorbed on the entire surface of the metal thereby reducing the corrosion rate and consequently leaving the metal protected from the attack of the corrodents. The chemical composition is a very crucial factor towards the effectiveness of these types of inhibitors. Chain length and molecular structures are important factors as well. Examples of organic inhibitors comprise of cationic, anionic and mixed type. Cationic organic inhibitors include amines while anionic organic inhibitors include sulfonates. In cases where the metal is charged negatively, the cationic organic inhibitors are the best option while in cases where the metal is charged positively, the anionic organic inhibitors are preferable.

Cathodic inhibitors: As soon as these types of inhibitors are introduced into the system, one of the two cases can take place. That is, some precipitation on selected cathodic areas maybe formed so as to limit the diffusion of the cathodic species or the rate of the cathodic reaction maybe slowed down. Cathodic inhibitors normally function through either one of the mechanisms as oxygen scavengers, cathodic poisons or cathodic precipitates [39].

- *Oxygen scavengers*: These have the ability to react with dissolved oxygen. Oxygen scavengers may present themselves in the form of sulfites and bisulfates ions. As soon as these ions combine with dissolved oxygen some sulfates of the concerned metals maybe formed.
- *Cathodic poisons*: These are substances that have the ability to reduce the rates of cathodic reactions. Most compounds of antimony and bismuth shows the traits of cathodic poisons. The drawback of cathodic poisons is the fact that the exposure of a metal to hydrogen induced cracking is increased due to the fact that during the process of cathodic charging some hydrogen gets absorbed.
- *Cathodic precipitates*: These substances results in some precipitates on the surfaces of metals as soon as they are utilized. Most carbonates exhibits the traits of cathodic precipitates, such as calcium carbonate and magnesium carbonate. The adjustment of the pH of the environment allows for this inhibition to take effect.

Anodic inhibitors: These inhibitors are sometimes referred to as chromate inhibitors because chromates are used as the major anodic inhibitors. The formation of the protective film on the surface of the metal results in a large anodic shift and consequently the metallic surface is

forced into the passivation region. Because of this reason, terms such as passivators instead of anodic inhibitors are also used [40].

Mixed-type inhibitors: Those inhibitors that exhibit both the traits of anodic and cathodic inhibitors are known as mixed-type inhibitors. In this case the metal of concern is protected from corrosion through the processes from both anodic and cathodic reactions. These inhibitors typically form the precipitates which are able to act as protective films on the surfaces of the materials and in the process block the cathodic and anodic sites. For instance, a steam which passes through the boilers and drive turbines can protect the pipes that are involved therein. Another good example concerns hard and soft water. Hard water contains more concentration of calcium and magnesium as compared to soft water. This high concentration of calcium and magnesium in hard water tends to precipitate on the surface of the metal and form a protective layer which makes hard water less corrosive than soft water.

Ohmic inhibitors: Just like the organic/inorganic inhibitors, Ohmic inhibitors are also film forming inhibitors. The application of these corrosion inhibitors causes the Ohmic resistance of the electrolyte circuit to increase. If the film is deposited on cathodic areas, the corrosion potential shifts to the more negative values, while the corrosion potential will shift towards the more positive values provided the film is deposited on the anodic areas. This observation is due to the fact that the potential shift is dependent on the areas of film deposition.
Volatile corrosion inhibitors (VCI): These inhibitors involve the process of volatilization in which the compounds are transported, in a closed environment, to the site of corrosion. The principle behind VCI involves the vapours of the salts used as inhibitors. These vapours are condensed and hydrolyzed by the moisture and consequently liberate protective ions. Therefore, the volatility of the compounds used plays an important role in the corrosion inhibition mechanism. Some good examples of volatile corrosion inhibitors include ammonium benzoate and substituted ammonium nitrates [36, 41].

Sulphonamide compounds are known to possess corrosion resistant behavior on metals such as mild steel, aluminium and zinc. It is found that the action of such inhibitors depends on the specific interaction between the functional groups and the metal surface due to the presence of the $–NH_2–$ group, $–SO_2$ and –NH group, electronegative nitrogen (N) and oxygen (O) in the molecule and the aromatic rings [42–45]. The literature available on sulphonamide

compounds as corrosion inhibitors in acidic environments is fragmentary and more work needs to be investigated.

2.5 SULPHONAMIDES

Sulphonamides are a group of compounds of a tremendous medicinal importance [46, 47]. It is known that the gram-positive and negative microorganisms and some selected fungi have a measurable ability to cause some infections on human beings. These infections are treatable with the applications of sulfanoamides drugs.

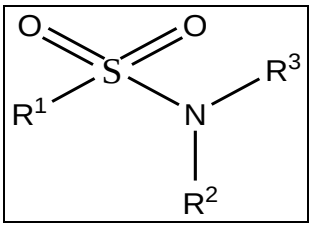

Figure 2.5: The functional group of the sulphonamides.

As indicated in Figure 2.5 above, the sulphanoamides compounds possess some useful functional groups, such as the $–SO_2–NR$ group, $–NR_2–$ group, electronegative nitrogen (N) and oxygen (O) in the molecule. R can be a hydrogen atom, a methyl, ethyl, propyl, e.t.c. or an aromatic ring. These are the key functional groups as they are the main sites of adsorption during the metal/ sulphonamides adsorption process. Aromatic rings such as benzenes, furans, thiophenes, pyridines, pyrroles, azulenes, naphthalenes and anthracenes, depending on the chemical nature of a certain sulphonamides, may form part of the structure in addition to the above-mentioned functional groups. In some cases, a certain sulphonamides will be constituted with more than one aromatic ring.

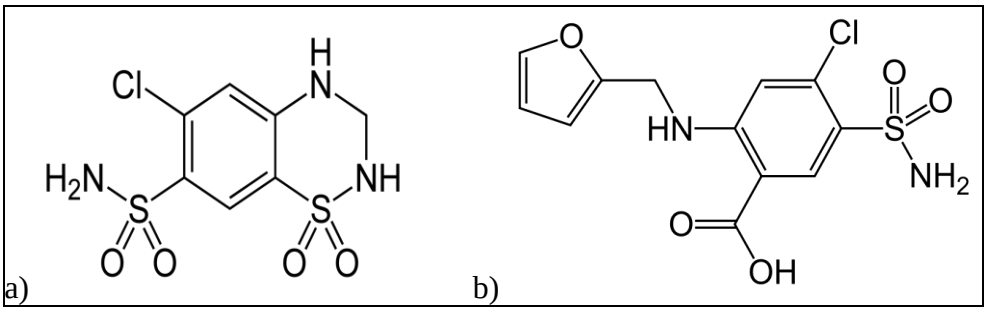

Figure 2.6: Some sulphonamides compounds: a) Hydrochlorothiazide and b) Furosemide.

As shown above, the structure in Figure 2.6 a) has only one aromatic ring while the one in Figure 2.6 b) contains two aromatic rings. This variation is common with sulphonamides compounds. The variations in atoms are also noticeable here, wherein the other structure contains a chlorine atom while the other one does not.

Sulphonamides play an important role in chemotherapy. This approach was discovered after the relationship between p-aminobenzoic acid and sulphanilamide was illustrated [48]. The variety of these sulphonamides as elucidated in Figure 2.6 also means, as they are applied in medicine, that they differ in their rates of absorption and excretion. This observation has increased their value in therapeutics. Other important characteristic of these compounds are their ease of administration and a wide spectrum of antimicrobial activity. In addition, they are able to resist the interference with the host defense mechanisms within their medicinal applications [48].

2.5.1 DEVELOPMENT OF SULPHONAMIDES

Sulphonamides have been of significant importance since 1934, when two compounds, namely prontosil and sulphanilamide were synthesized [48]. Mietzsch and Klarer synthesized prontosil in 1934, and its antibacterial activity compound was investigated using infected mice by Domagk in 1935. In the same year Trefouel suggested that this activity may have been because of the sulphanilamide that was formed in vivo. The year 1937 saw the isolation of sulphanilamide from samples of urine obtained from patients who had been treated with prontosil. This isolation process was experimented by Fuller [48]. After this experimentation with the structure of sulphanilamide, a number of sulphanilamide derivatives were successfully synthesized. This act of synthesizing these compounds was done with the main aim of improving their activity. These improved compounds or sulphanilamide derivatives were later tried-on against many infections that were direct consequences of many bacteria, viruses and protozoa.

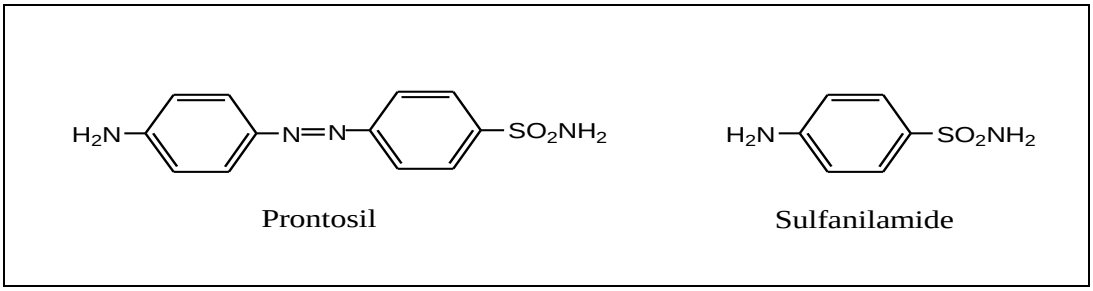

Figure 2.7: Structures of prontosil and sulphanilamide

May and Baker were the first to synthesize a derivative of a sulphanilamide called sulphapyridine in the year 1938 [48]. This derivative found its major applications in the treatment of pneumonia. As previously mentioned, the activity of these sulphonamides can be enhanced through tempering with their functional groups. In line with this, sulphapyridine was later replaced with another sulphanilamide derivative, sulphathiazole, due to its higher therapeutic index in comparison with sulphapyridine. The replacement of these compounds by a much enhanced one continued for some time. Sulphadiazine, a mildly structurally different sulphonamide came to replace sulphathiazole. The latter compound possessed some strong properties which qualified it as an alternative for generations. Later as the developments in this fraternity proceeded, two derivatives of sulphadiazine were discovered and also found their applications in therapeutic. These methylated derivatives were called sulphamerazine and sulphamethazine as indicated in Figure 2.8.

In the year 1939, a major development transpired, where a much better precision was possible during the determination of absorption, excretion, deposition and conjugation of sulphonamides. This act was made possible by the development of a standardization procedure for a method that was used for the quantitative determination of these compounds from the fluids and tissues of the human body [47, 48].

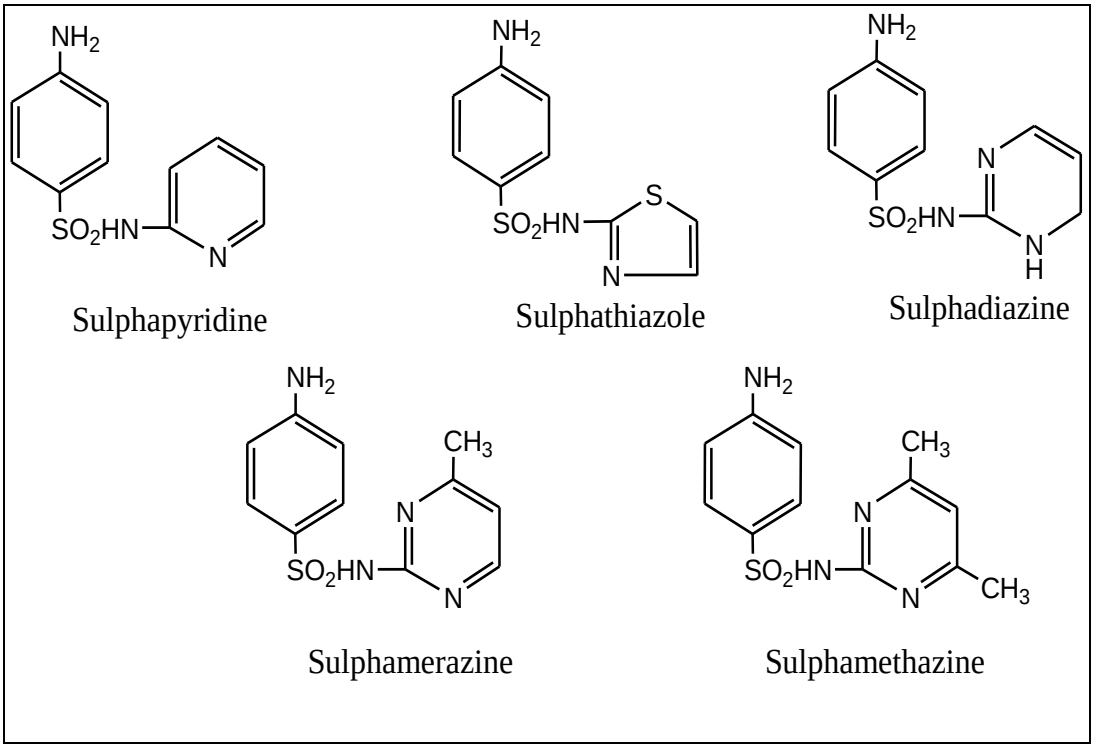

Figure 2.8: Structures of some important derivatives of sulphanilamide

2.5.2 PREPARATION/SYNTHESIS OF SULPHONAMIDES

A successful synthesis of sulphonamides is possible from the reaction of sulphonyl chloride and ammonia or an amine as starting materials. Nevertheless, this is not the only way of synthesizing these compounds as many researchers have successfully produced a variety of sulphonamides using more greener and innovative methods.

Shi et al., [49] have reported a green and efficient synthesis of sulphonamides which were catalyzed by Nano-Ru/Fe_3O_4. In their study, a domino dehydrogenation-condensation-hydrogenation sequence of alcohol and sulphonamides with the aid of a nano-structured catalyst was achieved. A convincing isolation of the product as well as maximum recyclability of the catalyst was achieved due to the magnetic property of the catalyst system. Some convincing and satisfactory percentage yields such as 80 % were successfully isolated from a number of coupling reactions involving benzylic alcohols and sulphonamides. It was also discovered that during this process, only one equivalent of primary alcohols was consumed. Their further investigations showed that the rate determining step was the dehydrogenation of the alcohol.

A direct synthesis of sulphonamides was done reported by Caddick et al., [50]. These authors commented on the fact that the synthesis of sulphonamides has been from the synthesis of sulphonyl chlorides that then get subjected to reactions with nucleophiles such as amines. It has also been noted that one of the disadvantages of sulphonyl chlorides is that they can be very difficult to handle and exhibit some challenges related to long time storage. In order to combat this challenge, Caddick together with his colleagues established the PFP-Sulphonate as a shelf-stable alternative to sulphonyl chloride. Some high yields of sulphonamides were possible as shown in Figure 2.9. High yields can be attributed to the fact that PFP-Sulphonate species go through many reactions with amines under various conditions, including aqueous environment.

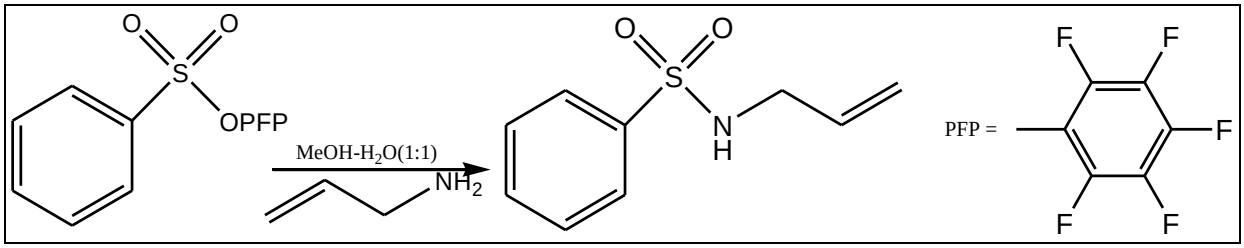

Figure 2.9: Reactivity of PFP-Sulphonate in aqueous media

Boyle et al., [51] reported a safer and convenient method for the synthesis of sulphathiazole. In their work they have successfully reported a method that eliminates the usage of hazardous pyridine for the synthesis of sulphathiazole. Instead some organic and inorganic bases, including N-methyl morphine (NMM), triethylamine (TEA) and anhydrous potassium carbonate were utilized as shown in Figure 2.10.

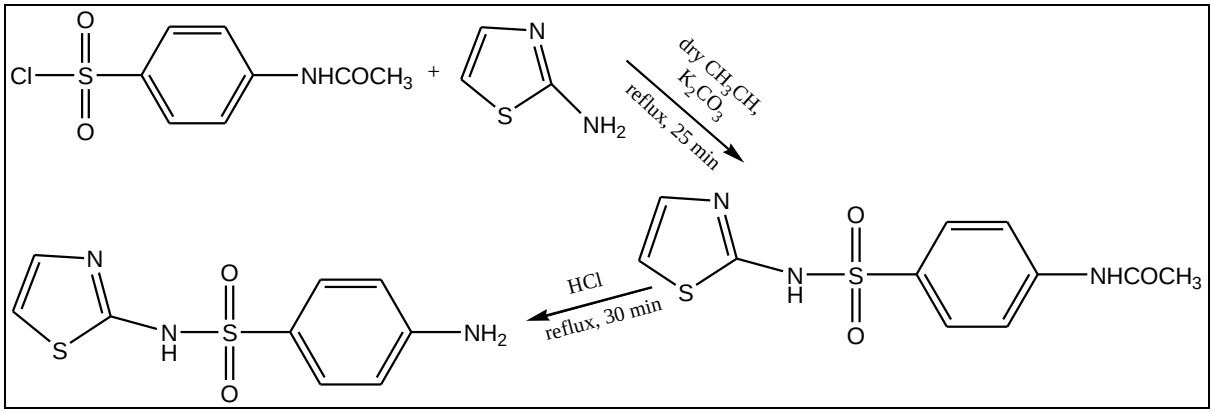

Figure 2.10: Synthesis of Sulphathiazole

Another greener sulfonamide synthesis was reported by Deng and Mani [52]. Their synthesis was done in water. In their synthesis, some equimolar amounts of amino compounds and arylsulphonyl chlorides were utilized. Organic bases were avoided as shown in Figure 2.11. Their isolation process involved two steps, namely filtration and acidification. They have also realized that their percentage yields for the products were good without any further purification necessary due to the fact that the purity thereof was excellent.

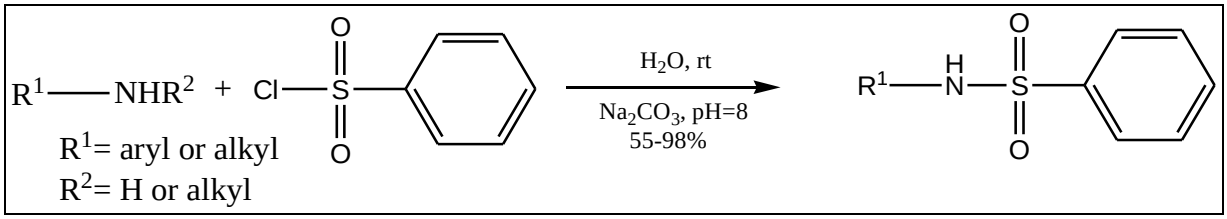

Figure 2.11: Synthesis of Sulphonamide

Raju and Kogan [53] successfully prepared sulphonamides in solid phase using a carbamate linker.

2.5.3 SULPHONAMIDES AS CORROSION INHIBITORS

A tremendous amount of effort has been expanded over a long period with the main objective of finding more environmentally friendly corrosion inhibitors. Sulphonamides possess properties that make them to be classified as green corrosion inhibitors for different metals in

acid and basic media. Their greenness not only grants them applications in this field but also in the medicinal fraternity [46-48, 52].

The observations that have been made by different corrosion scientists led them to profound conclusions concerning the events that take place during the process of corrosion. One such conclusion is that during the process of corrosion, a material breaks down into its own constituent atoms due to the chemical reactions with its surroundings. Sulphonamides compounds contain some active functional groups that play an important role of blocking the active sites of the metal during the corrosion process. This takes place through the adsorption or sometimes desorption mechanism [48].

A typical illustration of the adsorption process between the inhibitor and the metal adopts the pattern that is depicted in reaction equation (21) wherein the efficiency of the sulphonamide (SAM) shows the ability to be adsorbed on the metal surface by displacing the water molecule from the interface which is affected by corrosion.

$$SAM_{(sol)} + nH_2O_{(ads)} \rightarrow SAM_{(ads)} + nH_2O_{(sol)} \quad (21)$$

where $H_2O_{(sol)}$ is the water molecule in aqueous phase and $H_2O_{(ads)}$ is the water molecule on the metallic surface. $SAM_{(sol)}$ and $SAM_{(ads)}$ are the sulphonamide molecules in aqueous phase and adsorbed on the metallic surface, respectively, and n represent the number of water molecules replaced by one molecule of sulphonamides adsorbate. The adsorption of the sulphonamides on the surface of the metal during the process of corrosion is further influenced by factors such as the steric, electron density at the donor atoms and the nature of the electronic structure [48, 54].

The phenomenon that is observed during the process of corrosion, when the inhibitors are being adsorbed on the metal surface can be easily elucidated through comparison with the event that transpires when two compartments are being made to separate through a door that is in-between them. In such conditions it is very difficult if not impossible for one to traverse from one compartment to the other if the door is locked. Likewise, the aggressive ions resulting from either the acidic or basic medium find it very irksome to come into contact with the surface of the metal due to the presence of the sulphonamides compounds as corrosion inhibitors. This act often results in corrosion being minimized; consequently the metal lasts longer than previously.

Obot et.al., [54] studied the thermodynamic and density functional theory of sulphathiazole as a green corrosion inhibitor at mild steel/hydrochloric acid interface. From their studies the inhibition efficiency of this sulphonamide, that is, sulphathiazole on mild steel in 0.5 M HCl was investigated. Their investigations involved methods such as experimental gravimetric analysis and some theoretical quantum chemical calculations. Experimental methods were done at a temperature range of 303-333K. Their results were very interesting in that they have managed to prove that even at very low concentrations, sulphathiazole showed some inhibition ability thereby protecting mild steel from corrosion. The type of an adsorption isotherm that was proposed was Temkin due to the numerical thermodynamic and kinetic parameters that were obtained. This adsorption was further classified as chemisorption after the authors have meticulously examined the calculated values of Gibbs free energy and activation energy. Chemisorption means that the sulphathiazole inhibitor adsorbs on the mild steel surface thorough charge transfer or sharing between itself and charged mild steel surfaces. These experimental results and observations were further compared with the results from the theoretical studies. From theoretical quantum calculations, molecular properties such as E_{HOMO}, E_{LUMO}, energy gap, Mulliken charges, HOMO and LUMO orbitals were calculated and successful correlation was made between structure and reactivity traits of sulphathiazole. Density functional theory (DFT) using BLYP/6-31G(d) was utilized to calculate these molecular properties.

Arslan et.al., [55] studied the corrosion inhibition ability of some sulphonamides (Sulphaguanidine, Sulphamethazine, Sulphamethoxazole and Sulphadiazine) on mild steel in acidic medium. The relationship between molecular structures and inhibition efficiencies of these inhibitor compounds were established from the quantum chemical calculations using DFT and other semi-empirical methods. Some correlation analysis was performed in order to compare the results obtained from the quantum chemical calculations and the experimental ones. Their findings showed that the inhibition efficiencies of these compounds were comparable with the molecular property parameters such as E_{HOMO}, E_{LUMO}, energy gap, hardness, polarizability, dipole moment and Mulliken charges. Their results proved that as the values of E_{HOMO} and (E_{HOMO} - E_{LUMO}) were increased and decreased; respectively, the inhibition efficiencies of these inhibitor compounds were increased. A mechanism of physisorption was proposed from the sign of E_{HOMO} values and other thermodynamic and kinetic parameters.

Samide et.al., [56] published a paper entitled "Surface analysis of inhibitor film formed by 4-Amino-N-(1,3- thiazol-2-yl) benzene sulphonamide on carbon steel surface in acidic media". This is a comprehensive report on one of the sulphonamide compounds as corrosion inhibitors. The common name for this IUPAC named sulphonamide is sulphathiazole. These researchers have investigated the corrosion inhibition ability of sulphathiazole on carbon steel in 1.0 M HCl solution using weight loss measurements, electrochemical impedance spectroscopy (EIS), scanning electron microscopy (SEM) and X-ray photoelectron spectroscopy (XPS). Their results proved that this compound act as a good corrosion inhibitor for carbon steel under studied conditions. As the inhibitor concentration was increased the inhibition efficiency also increased. It was also revealed that the adsorption process followed Temkin adsorption isotherm spontaneously. The corrosion product was analyzed using XPS analysis where some interesting observations showed that the product was actually a non-stoichiometric Fe^{3+} oxide/oxyhydoxide which was mostly composed of Fe_2O_3, α and γ-FeO(OH) and/or $Fe(OH)_3$. Here α and γ-FeO(OH) was the main phase component.

Samide et.al., [57] investigated N-acetil p-aminobenzene sulphonamide (APAS) as an active corrosion inhibitor for carbon steel in 2.0 M HCl solution. In this study, weight loss, electrochemical impedance spectroscopy, scanning electron microscopy and Mossbauer spectroscopy techniques were utilized. From the results, APAS was found to be a good corrosion inhibitor for carbon steel in this high concentrated HCl solution. The inhibition efficiency increased with an increase in concentration of APAS. Their experimental results proved that the availability of this inhibitor in solution increased the surface coverage which indicated the adsorption process of APAS on the surfaces of carbon steel. Langmuir adsorption isotherm model/mechanism was further concluded. Results from Mossbauer spectroscopy indicated that the main product of corrosion was a non-stoichiometric Fe^{3+} oxyhydoxide which was composed mainly of α, β and γ-FeOOH. Here α and γ-FeOOH was the main phase component.

Sappani and Karthikeyan [58] reported studies on 4-chloro-2-((furan-2-ylmethyl)amino))-5-sulfamoylbenzoic acid (FSM) and N-(isopropylcarbomoyl)-4-(m-tolyamino) pyridine-3-sulphonamide (TSM) as potential inhibitors for mild steel corrosion in 1 N H_2SO_4 medium. In this investigation, these two sulphonamide drugs were tested for their corrosion inhibition ability using weight loss studies, electrochemical impedance spectroscopy (EIS), Fourier Transform Infrared spectroscopy (FTIR), Ultraviolet–visible absorption spectroscopy (UV)

and scanning electron microscopy (SEM). The results proved that both FSM and TSM are good corrosion inhibitors for mild steel in sulfuric acid and their inhibition efficiencies increased with an increase in their concentration. Nevertheless, the inhibition efficiencies decreased with an increase in temperature as all weight loss measurements were done at a temperature range of 303-333K. A mixed-type adsorption mechanism was proposed from the results of the potentiodynamic polarization. Thermodynamic and activation parameters showed that a Langmuir adsorption isotherm model was obeyed by the two inhibitors. The mode of inhibition reaction that resulted in the complex formation between mild steel and FSM/TSM was analyzed by using FTIR and UV. The protective layer that resulted as a consequence of adsorption between mild steel and FSM/TSM was confirmed using SEM images and their respective EDS spectra.

Zor and Sagdinc [59] reported the experimental and theoretical study of sulphathiazole as environmentally friendly inhibitor on aluminium corrosion in NaCl. In this investigation, the inhibitive ability of sulphathiazole was studied on aluminium in 1.0 M NaCl at various temperatures. This was achieved using potentiodynamic polarization method, scanning electron microscopy and quantum chemical calculations. A mixed-type adsorption was concluded from the polarization curves. The type of adsorption mechanism that sulphathiazole followed was Langmuir. The kinetic theory including Arrhenius equations and plots were used to explain the effect of temperature on aluminium corrosion. Quantum chemical molecular parameters were calculated using density functional theory (DFT) and Hartree Fock (HF) methods. Consequently these parameters were correlated to the structure and reactivity traits of sulphathiazole.

2.6 QUANTUM CHEMICAL APPROACHES

2.6.1 GEOMETRY OF MOLECULES

2.6.1.1 THE GEOMETRY PARAMETERS

The theoretical study of molecules requires the understanding of the nature of molecules, molecular geometry. Molecules are a stable system of electrons and nuclei composed of atoms that are bonded to each other. The arrangement of these atoms, which is due to bonding, is specific for different molecules. Depending on the arrangement of atoms, molecules can have different shapes. The term “geometry of molecules” is often used to express the shape of the molecules. Molecular geometry not only assist in describing the

shape of the molecule but the three dimensional arrangement of atoms within the molecule as well. This is elucidated in terms of three parameters, namely, bond length, bond angles and torsion angle [60]. These parameters are defined as below;

Bond length: it is defined as the average distance between the nuclei of two bonded atoms in a molecule.

Bond angle: it is the angle formed between three atoms across at least two bonds. Different bonds have different bond angles.

Torsion angle: it is the angle between two planes within a molecule formed by interconnected bonds. For example, consider a molecule containing a chain of atoms A-B-C-D, the torsion angle is the angle between the plane containing the atoms A, B, C and the atoms B, C, D. Figure 2.12 shows the bond angle and bond length while torsion angle is illustrated in figure 2.13.

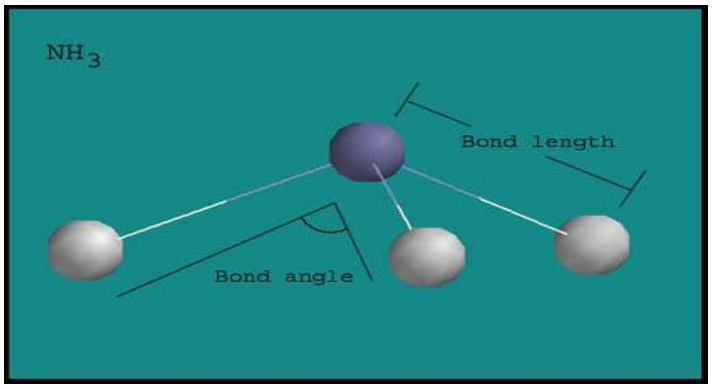

Figure 2.12: Bond lengths and bond angles in an ammonia molecule.

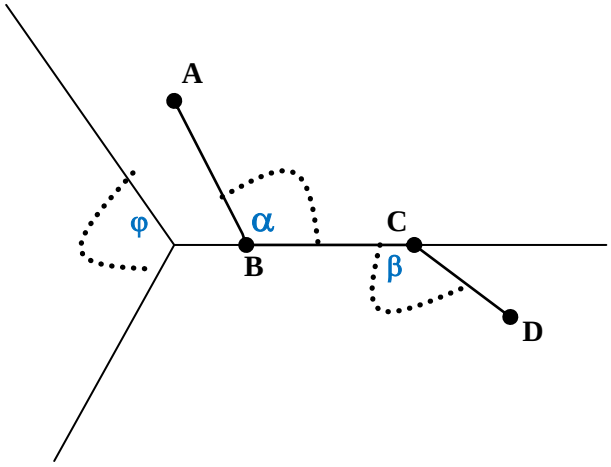

Figure 2.13: The torsion angles in a molecule containing atoms A-B-C-B.

2.6.1.2 MOLECULAR CONFORMATIONS

Once the geometry of a molecule is defined, it is interesting to determine the conformation which corresponds to the lowest energy geometry. This is because a particular geometry of a molecule may have different conformations.

Two molecules which are different only when they are rotated about a single bond are otherwise known as different conformations of that molecule. These molecules possess different nuclear arrangements. Through the change of one or more of their torsion angles, they can be transformed into each other [61]. A good example of molecular conformation is the rotation of ethane molecule. The rotation around the C-C single bond in this molecule brings about two different ethane conformations, namely, eclipsed and staggered as shown in Figure 2.14.

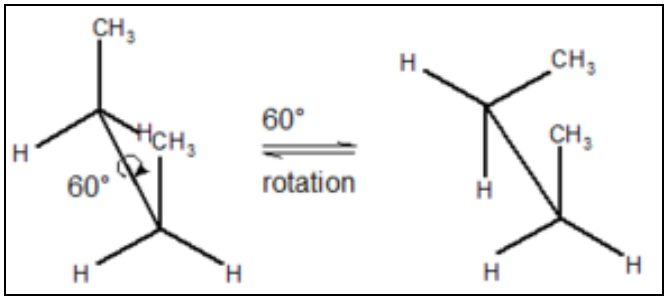

Figure 2.14: Conformations of butane resulting from the 60° rotation around C-C single bond.

2.6.1.3 MOLECULAR GEOMETRY AND POTENTIAL ENERGY SURFACE

Molecular conformations are very important because they are related to different activities of molecules. Usually the most interesting conformation is the one corresponding to the lowest energy geometry. The low-energy conformers of the molecule are the most dominant ones. Due to these dominant conformers, there is a continuous need to perform conformational analysis (that is, the search to find and identify the stable conformations of a molecule). Studies reveal that molecules are found to be stable when their energy is low [62, 63]. When a molecule has two or more conformations, each conformation will have different energy. This is because each conformer has its specific geometry. One way of testing various ways to see conformer possesses the lowest energy value is to study its Potential Energy Surface (PES). This is a mathematical relationship that compares different molecular geometries and

their corresponding single point energies. This is accomplished through plotting of a three-dimensional graph as indicated below.

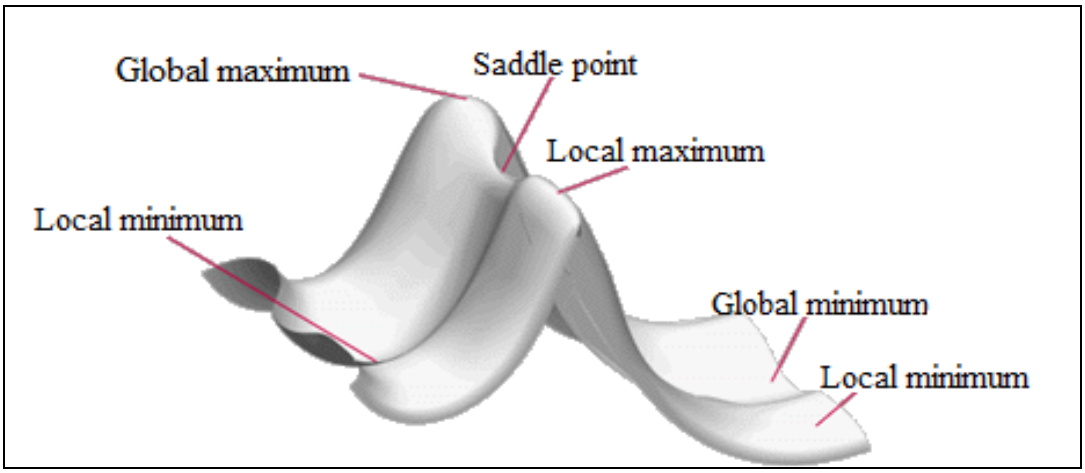

Figure 2.15: Potential Energy Surface plot of the water molecule.

There are five significant points that characterize the potential energy surface plots, namely, local maximum, global maximum, local minimum, global minimum and saddle point. From the PES, a minimum position is the bottom of a valley. These five significant points can be distinguished from each other as defined below [64].

Local minimum- it is the lowest possible point in a region of focus on the potential surface.

Local maximum- it is the highest possible point in a region of focus on the potential surface.

Global minimum- it is the lowest energy point anywhere on the potential surface.

Global maximum- it is the highest energy point anywhere on the potential surface.

Saddle point- it is the point that is somewhat neutral, in a sense that it is a maximum in one direction and simultaneously a minimum when observed from the other direction.

2.6.2 MAJOR APPROACHES TO THE STUDY OF MOLECULES

Once we have defined and described the geometry of a molecule, it is of vital importance to know the different approaches utilised in the study of the properties of the molecule. Among the different approaches utilised are molecular mechanics and electronic structure methods. The descriptions of these methods are given below.

2.6.2.1 MOLECULAR MECHANICS APPROACHES

In this approach, classical mechanics laws are utilized to model molecular systems [65]. According to classical mechanics, a molecule is composed of atoms that are interconnected through springs. The force fields, which are the force constants related to each spring, are used to calculate the potential energy of the molecules. A range of small molecules such as H_2O to large complex molecules such as DNA can be studied using molecular mechanics [65, 66].

This method is also solely based on the following assumptions;

- Each atom in a molecule is manipulated as an individual single particle.
- Each particle has its own radius, polarizability and a constant net charge.
- Bonded interactions are treated as "springs" that carries an equilibrium distance. This distance is assumed to be of the same magnitude with the experimental or calculated bond length of such bonding atoms [67].

The energy of the molecule can be estimated through the mechanics force field as shown in equation (22) below;

$$E_{steric} = \sum_{bonds} K_r \left(r - r_{eq}\right)^2 + \sum_{angles} K_\theta \left(\theta - \theta_{eq}\right)^2 + \sum_{dihedrals} \frac{V_n}{2}\left[1 + \cos\left(n\phi - \gamma\right)\right] + \sum_{non-bonding}\left[\frac{A_{ij}}{R_{ij}^{12}} - \frac{B_{ij}}{R_{ij}^{6}} + \frac{q_i q_j}{\varepsilon R_{ij}}\right]$$

$$+ \sum_{H-bonding}\left[\frac{C_{ij}}{R_{ij}^{12}} - \frac{D_{ij}}{R_{ij}^{10}}\right] \qquad (22)$$

The first term contains the force constant, K_r, and it is used to compensate for the bond length. It is also important to note that this constant is specific to every atom-type pair.

The second term also contains K_θ which accounts for the bond angles between the atoms in the molecule.

The third term accounts for the dihedral or torsion angles, where ϕ is the dihedral angle, γ is a phase factor depending on whether $\phi = 0$ is maximum or minimum and *n* represents the number of symmetry.

The fourth term in this equation is corresponding to the non-bonding interactions. The dispersion of energy is accounted for by the second part of this term. The last portion of term four is the electrostatic portion and it requires charges on each atom pair.

The fifth term is related to the hydrogen bonding or π-configuration.

Molecular mechanics has several advantages and disadvantages. The advantages of this approach include [64];

- It is applicable for large molecules.
- The output involving simple energy functions are obtained rapidly.
- It produces very accurate and precise results as long as the models used to produce the force field are very close to the systems calculated.

The disadvantages of Molecular mechanics include [64];

- The quality of the parameters to be calculated depends entirely on the experimental data that is used.
- The background knowledge about the atom/bond type for all molecules is a complete requirement.
- The second derivatives (output such as entropy) are not computable with most mechanics implementations.
- Unpredicted bonding or interactions are difficult to deal with when using mechanical approaches.
- Mechanical approaches cannot be employed for bond-breaking transition states and therefore they cannot be useful for the reactions.

2.6.2.2 QUANTUM MECHANICS APPROACHES

The quantum mechanical approach differs from the molecular mechanics approach in that it assumes that the chemistry of a molecule can be fully explained in terms of the interactions between electronic charges within molecules. Here a molecule is considered to be composed of electrons and nuclei [68]. The knowledge about the system is defined through the Schrödinger Equation.

2.6.3 THE SCHRODINGER EQUATION

The Schrödinger equation was proposed by Erwin Schrödinger, the Austrian physicist in 1926. This equation is the basis for finding the wavefunction of any system. Equation (24) below shows the time-independent Schrödinger equation. This equation is suitable for a

particle of mass m that is moving in one dimension with energy E in a system that is time independent [69].

$$-\frac{\hbar^2}{2m}\frac{d^2\psi}{dx^2}+V(x)\psi=E\psi \tag{23}$$

where V(x) is the potential energy of the particle at the point x, E is the total energy of the system. It is well known that the total energy E, is the sum of the potential energy and kinetic energy, therefore we can rightfully say that the first term in equation (23) is related to the kinetic energy[10]. $\hbar=\frac{h}{2\pi}$ is a modified Planck's constant and has the value of 1.055×10^{-34} Js.

For three dimensional systems, equation (23) can be expressed as;

$$-\frac{\hbar^2}{2m}\nabla^2\psi+V(x)\psi=E\psi \tag{24}$$

In this equation, V depends on the position and the right side part of the first term in equation (24) can be expressed as below;

$$\nabla^2=\left(\frac{\partial}{\partial x^2}+\frac{\partial}{\partial y^2}+\frac{\partial}{\partial z^2}\right) \tag{25}$$

According to Schrödinger equation, the Hamiltonian operator and the wave function depend entirely on the coordinates of all the particles making up a system or molecule. Therefore all the coordinates of all electrons and nuclei for a particular system or molecule are extremely important [69, 70]. Solving the Schrödinger equation brings about important outcomes such as the expression for the wave function and the corresponding energy values of the system. When this equation is applied to chemical systems such as atoms, the solutions obtained are known as atomic orbitals and likewise molecular orbitals if it is applied to molecules.

2.6.4 THE DESCRIPTION OF MOLECULES IN QUANTUM MECHANICS

According to quantum mechanics, a molecule is composed of electrons and nuclei [71]. Due to the lack of mathematical procedures, it is very difficult to solve the Schrödinger equation exactly for moving and interacting nuclei and electrons in a way that is completely satisfactory. For this reason, theoretical chemists resorted to approximation approaches [71].

2.6.4.1 THE BORN OPPENHEIMER APPROXIMATION

One such approximation is the Born Oppenheimer Approximation. This approximation assumes that it is possible to separate the two motions in molecules, namely the electronic motions and the nuclear motions [71].

Thereafter, this approximation leads to a molecular wavefunction in terms of two positions, $\vec{r}_i$ and $\vec{R}_j$, where $\vec{r}_i$ and $\vec{R}_j$ are the electron and nuclear positions, respectively. The Born Oppenheimer approximation is represented by the equation (26) below;

$$\psi_{molecule}\left(\vec{r}_i, \vec{R}_j\right) = \psi_{electrons}\left(\vec{r}_i, \vec{R}_j\right) + \psi_{nuclei}\left(\vec{r}_i, \vec{R}_j\right) \tag{26}$$

where $\psi_{molecule}$ is the total wavefunction of the molecule, $\psi_{electrons}$ is the wave function of the electrons and ψ_{nuclei} is the wave function of the nuclei.

It follows that the total energy of the system or molecule is the sum of the corresponding contributions as shown in equation (27) below;

$$E_{total} = E_{electrons} + E_{nuclei} \tag{27}$$

where E_{total} is representing the total energy of the system, $E_{electrons}$ is representing the energy of the electrons and E_{nuclei} is representing the energy of the nuclei.

Equation (28) works in association with the following two assumptions;

- Since the nuclear motion is significantly slower than that of the electrons, the electronic wave function is dependent only on the nuclear motions.
- Motions such as vibrations and rotation of molecules are nuclear motions and experience a potential from the speedy electrons.

2.6.4.2 THE HARTREE FORK METHOD

One of the quantum chemical methods that implement the Born-Oppenheimer approximations is the Hartree Fork method. This method considers electrons as independent in a multi-electron system. In this way, the motion of one electron does not influence the other electron motions and it is not influenced by the motion of other electrons. In these conditions, the total wavefunction can be expressed as a product of functions. For a system

possessing n number of electrons,, the wavefunction can be expresses as in equation (28) below;

$$\psi_{total} = (R_{1,} R_2 ......R_n) = \psi(R_1)\psi(R_2).....\psi_n(R_n) \tag{28}$$

where ψ_{total} is the total wavefunction, $\psi_{1,}$ ψ_2 ... ψ_n are the wavefunction for electrons 1, 2 … n, respectively. R_1, R_2, ….R_n is the space and spin coordinates for electron 1, 2, …n, respectively.

The drawback of equation (28) is that the wavefunction expressed in this manner does not satisfy the antisymmetry principle [72]. The antisymmetry principle states that a wavefunction describing a particle (such as an electron, proton or neutron) that has half-integral spin, should be antisymmetric with respect to the interchange of any set of space-spin coordinates. These particles with half-integral spin are known as bosons. The antisymmetry principle problem can be satisfied by writing the linear combination for a system of n number of electrons as indicated in the equation below;

$$\psi_{total}(1,2,...n) = \frac{1}{\sqrt{n!}} \sum (-1)^p \psi_1(k_1), \psi_2(k_2)....\psi_n(k_n) \tag{29}$$

where $\frac{1}{\sqrt{n!}}$ is the normalization factor and p represent the number of transpositions that were done in order to obtain the given term in the linear combination. The sign for the wavefunction is taken care of by the factor $(-1)^p$. This factor makes sure that the sign of the wavefunction remains unchanged for the even number of transposition and changes for the odd number of transpositions [15].

The Slater determinant is a determinant of spin orbitals and is often used to express the linear combination in equation (29) as indicated below;

$$\begin{vmatrix} \psi_1(R_1) & \psi_1(R_2) & \psi_1(R_3) & ... & ... & ... \psi_1(R_n) \\ \psi_2(R_1) & \psi_2(R_2) & \psi_2(R_3) & ... & ... & ... \psi_2(R_n) \\ \psi_3(R_1) & \psi_3(R_2) & \psi_3(R_3) & ... & ... & ... \psi_3(R_n) \\ \ldots & & & & & \\ \psi_1(R_1) & \psi_1(R_2) & \psi_1(R_3) & ... & ... & ... \psi_1(R_n) \end{vmatrix}$$

2.6.4.3 MOLECULAR ORBITALS AND LCAO METHOD

The mathematical function that is used to describe this electronic behaviour is called a molecular orbital. The regions within the molecule where electrons have the highest probability of being located are known as the electronic molecular orbitals. The significance of the molecular orbitals (MO) is that they assist in the calculations of chemical and physical properties including the chances of locating an electron in any specific region within a given molecule.

The drawback that is associated with the Hartree-Fork equations is that it practically impossible to obtain the exact solutions for molecules. One way of addressing this problem is to express each orbital as a linear combination of atomic orbitals (LCAO) [73]. According to molecular orbital theory, electrons are spread throughout the whole molecule and they do not necessarily belong to a particular bond [70]. If two different atoms A and B contain a similar electron within their atomic orbitals, the overall wavefunction is expressed in terms of the two atomic orbitals as in equation (30) below;

$$\psi_{\pm} = N\left(A \mp B\right) \tag{30}$$

This equation is known as a linear combination of atomic orbitals (LCAO).

where;

Ψ is the wavefunction,

A and B are the atomic orbitals of atoms A and B, respectively, and

N is a normalization factor.

The molecular orbital that result from the linear combination of atomic orbitals is known as a Linear Combination of Atomic Orbitals-Molecular Orbital (LCAO-MO). The wavefunction also depend on the type of the orbitals, such as bonding and antibonding orbitals. In cases of bonding orbitals, the probability density is expressed as;

$$\psi_{+}^{2} = N^{2}\left(A^{2} + B^{2} + 2AB\right) \tag{31}$$

In this case both atomic orbitals have similar amplitudes. From equation (31), A^2 is the probability density if electrons were confined to atomic orbital A, B^2 is the probability density if electrons were confined to atomic orbital B and 2AB is the contribution to the density from atomic orbitals A and B. This contribution is also known as the overlap density and it assist in finding the electron in the internuclear region.

In cases of antibonding orbitals, the probability density is expressed as in equation (32) below;

$$\psi_{-}^{2} = N^{2}\left(A^{2} + B^{2} - 2AB\right) \tag{32}$$

The symbols in equation (32) are described in the same way as in equation (31). The linear combination of atomic orbitals corresponds to different energies depending on the nature of bonding of atomic orbitals. The wavefunction of the antibonding orbitals corresponds to a higher energy than that of the bonding orbitals.

In the case of antibonding orbitals, the two atomic orbitals overlap and bring about the destructive interference. As it can be observed from equation (32), the term -2AB causes the probability density to decrease.

2.6.5 SEMI-EMPIRICAL AND *Ab Initio* QUANTUM CHEMICAL APPROACHES

The calculations associated with quantum mechanics can be classified into two major classes; namely, semi empirical and *ab initio*. The major discrepancy between these two classes is solely in the way in which the integrals from the Hartree-Fork-Roothaan equations are solved.

2.6.5.1 SEMI-EMPIRICAL APPROACHES

Semi-empirical methods simplify the solutions of the equations of Hartree-Fork-Roothaan through the reduction of the number of integrals to be calculated [75]. These methods in most cases omit some parts of the information and integrals such as the three-and-four-centre integrals from the two-electron integrals. Approximations also play an important part as far as the semi-empirical methods are concerned. This, for an example, is seen in the case of electrons in the calculations. One of the approximations or exclusions revolves around electrons. Semi-empirical methods calculations consider only the valence electrons and

exclude the core electrons. There are some advantages associated with these approximations and exclusions, such as the speed of computational calculations. Semi-empirical calculations are normally faster than the *ab initio* calculations. However, there are some disadvantages associated with the semi-empirical methods. These include the accuracy of the results obtained. In order for the results to be of outmost accuracy with these methods, the molecules on the database used to parameterize the method should be similar to the molecule under study [76]. Some examples of semi-empirical methods are AM1, PM3 and MNDO. These models are briefly described below;

Austin Model 1 (AM1) – these approach make use of approximations in that it approximates the two-electron integrals although it utilizes a different expression for nuclear-nuclear core repulsions. This expression takes care of the van der Waals interactions since it brings about non-physical attractive forces. Austin Model 1 is a good tool for the description of the hydrogen bonds. Perhaps one disadvantage associated with AM1 could be that the basicities of substances or molecules are systematically over-estimated [64].

Parametric Method 3 (PM3) – this model make use of a functional group-specific modification of the core repulsion function. The van der Waals attraction between atoms is explained with the aid of the Pairwize Distance Directed Gaussian (PDDG) modification. PM3 with this modification is very good for the molecules that have forces of attractions and repulsions between their atoms. The other strength of PM3 lies in the estimation of heats of formation. Some disadvantages associated with PM3 include the fact that molecular conformational energies are not accurate, the over-estimation of the activation barriers and the fact that the explanations for radicals are not very accurate [64].

Modified Neglect of Diatomic Overlap (MNDO) – this method is a modified version of the old version of the Neglect of Diatomic Differential Overlap (NDDO). In this model one-centre-two-centre integrals are parameterized using the spectroscopic data that is generated for all isolated atoms. The most recent MNDO/d model uses an additional d orbital basis sets in addition to the only s and p orbital basis sets from the MNDO. This addition of the d-orbital basis set enables for the description of the hypervalent sulphur species as well as all the d-block elements. The disadvantages of MNDO include its inability to describe the hydrogen bond because of the strong intermolecular repulsions and the poor accuracy of the heats of formation results [64].

2.6.5.2 *Ab Initio* APPROACHES

The principle behind *ab initio* approaches is that the quantum mechanical calculations are solved using mathematical procedures only. This means that, unlike in semi-empirical approaches, the Schrödinger equation is solved without introducing any parameters or by ignoring some integrals in the equations [77]. There are many advantages these approaches carry along with, including;

- The accuracy of the result obtained is higher than that of semi-empirical methods since the results do not depend on the molecules on the database.
- It is possible to study excited states due to the fact that they are very good in the study of electronic configurations.

However, there are some disadvantages associated with the *Ab initio* approaches. These include the expense in terms of computational time. *Ab initio* calculations take longer time to complete due to all terms and integrals that are considered. Molecules that contain a large number of atoms are costly to compute with these approaches. Some *Ab initio* calculations also fail to take into consideration the effects of the correlation of electrons [78].

Some examples of ab initio methods include the Hartree-Fork method (HF), Moller-Plesset method (MP2) and to some extent the Density Functional Theory (DFT), although the later is not a wavefunction method. In the next section we provide more information on the DFT method because it is the one that has been extensively utilized for the study of the molecules in the work reported in this thesis

2.6.5.3 DENSITY FUNCTIONAL THEORY (DFT)

In DFT, the energy of the molecule is expressed as a function of the electron density and it is denoted as $E[\rho]$, where E is the energy of the molecules and ρ is the electron density. The electron density is also a function of position and denoted as $\rho(r)$. A functional is a function of a function. In DFT a functional is the electronic density which is a function of space and time. The electron density is used in DFT as the fundamental property unlike Hartree-Fork theory which deals directly with the many-electron wavefunction. Using electron density significantly speeds up the calculations. Most importantly, the density of any system determines all ground state properties of the system [64, 70]. In this case the total ground state energy of a many-electron system is a functional of the density. So, if we know the

electron density functional, we know the total energy of the system. The electron density is constructed from the occupied orbitals according to the relation in equation (33) below [70];

$$\rho(r) = \sum_m |\psi_m(r)|^2 \tag{33}$$

where ρ(r) is the electron density as a function of position and ψ is the wavefunction.
These occupied orbitals that are utilized to construct the electron density are evaluated from the Kohn-Sham equations as in equation (34) below;

$$\left\{ h_1 + j_0 \int \frac{\rho(2)}{r_{12}} d\tau_2 + V_{xc}(1) \right\} \psi_m(1) = \varepsilon_m \psi_m(1) \tag{34}$$

The Kohn-Sham equations are the extended or modified version of the Hartree-Fork equations. The modification involves the term V_{xc} which is known as the exchange-correlation potential. In equation (34), the one-electron kinetic and potential energy is represented by the term on the left while the potential energy of repulsion between electrons 1 and 2 is represented by the second term [70]. Many expressions of V_{xc} are utilised in DFT to construct the exchange-correlation potential. The superposition of atomic electron densities is used to guess the electron density, which is followed by solving the resulting equations from which the initial sets of orbitals are obtained. Afterwards, a better approximation to the electron density is obtained through making use of this set of orbitals. DFT requires the repetition of this last step up until such point when the density and exchange-correlation energy are constant.
DFT is in most cases the preferred *Ab initio* electronic structure method which computational chemists utilize to study a wide range of molecular properties and it is capable of studying large systems [79 – 82].

2.6.6 MOLECULAR SURFACE INTERACTIONS

As discussed previously, molecular properties are obtained by solving the Schrödinger equation from which the geometry and the energy of the system are obtained. Other properties such as electronic and magnetic are then derived from the first and second derivatives of the geometry or energy with respect to the desired parameter. In this section we

focus our attention on the molecular surface interactions. These forces may also be explained through properties derived from the Schrödinger equation.

This study focuses on studying the possible types of interactions between molecules of interest and the metal surfaces. The interaction between metal and corrosion inhibitor fall in the category of molecular surface interactions. For this reason, it is important to give a brief description of different types of molecular interactions.

2.6.6.1 VAN DER WAALS INTERACTIONS

The van der Waals interactions were named after Dutch scientist Johannes Diderik van der Waals. These interactions are the combined attractive or repulsive forces that take place between molecules [70]. The potential energy associated with this type of interactions is dependent on the intermolecular distance. The interaction that may be experienced between the ions and the partial charges of polar molecules may be classified as van der Waals interactions. These interactions may include a force that exist in between two dipoles (known as the Keesom force), a force that exist between a dipole and a corresponding induced dipole (known as Debye force) and a force that exist between two instantaneously induced dipoles (known as London dispersion force). A brief description of these interactions is outlaid below, starting with the potential energy of interaction as this plays an important role during the interaction between two dipoles.

- **The Potential Energy of Interaction:**

Dipoles or molecular dipoles take place in the event when there is an unbalanced sharing of electrons between atoms within a molecule. This normally is a consequence when the atoms that are more electronegative within a molecule pull the bonded electrons closer to their directions. Molecular dipoles in which one portion of the molecule is characterized by a partially positive charge normally result from the build-up of electron density around a certain region of the molecule. A molecular dipole that is characterized by a much smaller separation between the charges than the distance at which the dipole is being observed is called a point dipole [70].

The energy of interaction between a point dipole ($\mu_1 = Q_1 l$) and a point charge (Q_2) is given by the relation in equation (35) below;

$$V = \frac{\mu_1 Q_2}{4\pi\varepsilon_0 r^2} \tag{35}$$

where ε_0 is the permeability of space and r is the distance. The units of a point dipole are in Coulomb meters, while those of a point charge and distance are in Coulombs and meters, respectively. The overall units for this potential energy in equation (35) are expressed in Joules [70].

- **Dipole-Dipole Interactions**

The event involving two polar molecules approaching in the direction of each other result in what is known as dipole-dipole interactions. During this type of interaction, the partially charged sites of the two molecules interact. That is, the partially negative site of one molecule is attracted to the partially positive site of the other molecule as indicated in Figure 2.16 below.

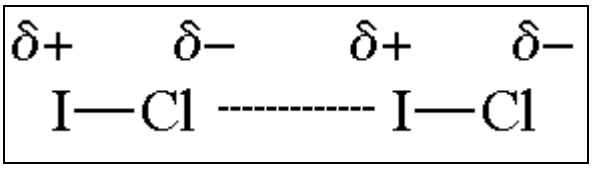

Figure 2.16: Dipole-dipole interactions between two Iodine monochloride (ICl) molecules.

The energy of interaction between two fixed parallel dipoles is given by the expression in equation (36) below;

$$V = \frac{\mu_1 \mu_2 f(\theta)}{4\pi\varepsilon_0 r^3} \qquad f(\theta) = 1 - 3\cos^2\theta \tag{36}$$

where ($\mu_1 = Q_1 l$) and ($\mu_2 = Q_2 l$) are permanent dipoles for molecules 1 and 2, respectively, and are expressed in Coulomb meters. The symbol ε_0, is the permeability of space and r is the distance in meters.

The average potential energy of interaction between two rotating polar molecules is a kind of van der Waals interaction known as the Keesom interaction. This interaction is expressed as in equation (37) below [70];

$$\langle V \rangle = -\frac{C}{r^6} \qquad C = \frac{2\mu_1^2 \mu_2^2}{3(4\pi\varepsilon_0)^2 kT} \tag{37}$$

where k is a constant which is equivalent to 1.38×10^{-23} J.K^{-1} and T is temperature in Kelvins. All other symbols in equation (37) are explained in the same way as in equation (36). From equation (37), the significance of the negative sign is its association with the mode of interaction. Here a negative sign means that there is an attractive interaction [70]. The van der Waal interaction trait is indicated by the dependence of the average interaction energy on the inverse sixth power of the separation as indicated in equation (37). This equation is also significant in a way that it shows, through the inverse dependence on the temperature, the manner in which the greater thermal motion overcomes the mutual orientating effects of the dipoles at higher temperatures.

- **Dipole-Induced-Dipole Interactions**

Unlike a dipole-dipole interaction, the dipole-induced-dipole interactions occur when a polar molecule and a non-polar molecule come close to each other. Here, a non-polar molecule experiences an induced dipole from a polar molecule; the resulting action is a weak attraction between the two molecules, as illustrated below.

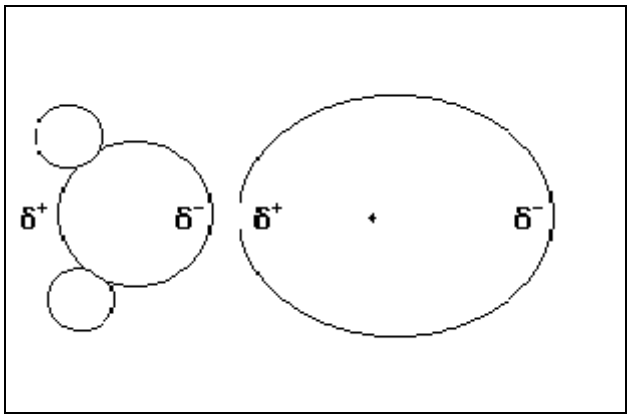

Figure 2.17: Dipole-induced-dipole interactions between two molecules.

The average energy of interaction between a polar molecule and a polarisable molecule is given by the expression in equation (38) below;

$$V = -\frac{C}{r^6} \qquad C = \frac{\mu_1^2 \alpha_2'}{4\pi\varepsilon_0} \tag{38}$$

where μ_1 is the dipole moment for molecule 1 and α_2 is the polarizability volume for molecule 2. The other symbols in this equation are explained in the same manner as in equations (36 and 37). The thermal motion has no effect on the averaging process; hence the

dipole-induced-dipole interaction energy does not depend on temperature [70]. Nevertheless, the potential energy depends on $1/r^6$ just like the dipole-dipole interaction.

- **Induced-Dipole-Induced-Dipole Interactions**

Induced-Dipole-Induced-Dipole Interactions takes place between two non-polar molecules. These molecules attract each other despite the fact that they do not possess any permanent dipole moment [70]. The fluctuations by the positions of electrons give rise to the transient dipoles to molecules, thus the interactions between non-polar molecules. Figure 2.14 below illustrate the induced-dipole-induced-dipole interactions between two helium atoms.

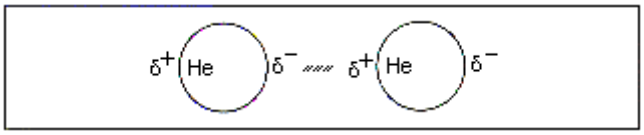

Figure 2.18: Induced-dipole-induced-dipole interactions between two He atoms.

Induced-dipole-induced interactions also manifest themselves as dispersion interaction wherein one non-polar molecule induces a dipole on another non-polar molecule; hence the two dipoles interact to lower the energy. Dispersion interactions are also known as London interactions since they were first described by Fritz London. The polarizability of the first molecule during this interaction influences the strength of the dispersion interaction due to the fact that the instantaneous dipole moment has its influence from the looseness of the control that the nuclear charge subjects on the electrons that lie on the outside of the sphere [70]. Since the polarizability is a factor that determines the extent by which a dipole can be induced by another molecule, it is then realized that the polarizability of the second molecule during this type of interaction also has an influence on the strength of this interaction. The London formula as shown in equation (39) below is used in the estimation of the dispersion interaction and the interaction energy between two non-polar molecules.

$$V = -\frac{C}{r^6} \qquad C = \frac{3}{2}\alpha_1'\alpha_2'\frac{I_1 I_2}{I_1 + I_2} \tag{39}$$

where α_1 and α_2 are the polarizability volumes of molecules 1 and 2, respectively. I_1 and I_2 are the ionization energies for molecules 1 and 2, respectively. From this equation, the contribution to the van der Waals interaction is contributed by the proportionality to the inverse sixth power of the separation of the molecules to the interaction energy.

- **Hydrogen Bonding**

Hydrogen bonds are generally stronger than the van der Waals interactions (hydrogen bond is about 20 kJ mol^{-1} and van der Waals interactions is about 0.6 – 2 kJ mol^{-1}). Hydrogen bonding is defined as the electromagnetic attractive interaction that takes place between polar molecules wherein hydrogen makes a bond with a highly electronegative site of the other molecule or atom such as oxygen. This type of bonding can take place intermolecularly or intramolecularly. Intermolecularly means that these attractions occur between two different or similar molecules while intramolecularly means that these attractions take place within a single molecule through different parts of that molecule. Figure 2.19 below illustrates hydrogen bonding in a system of two water molecules.

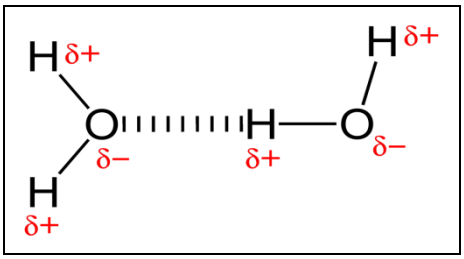

Figure 2.19: Hydrogen bonding between two water molecules.

Hydrogen bonding normally involves heteroatoms such as nitrogen and oxygen. Nonetheless, some ionic species such as chlorine ion and fluorine ions may also take part in this process [70, 84]. A molecular orbital model can be developed in the quest of understanding the electrostatic interaction during the formation of a bond of the A – H nature. In this model, this bond is assumed to result from the overlap of an orbital on A, Ψ_A, and a 1s orbital from hydrogen, Ψ_H, and an orbital on B, Ψ_B. Three molecular orbitals can be built from three basis orbitals as the two molecules come close together;

$$\psi = c_1\psi_A + c_2\psi_H + c_3\psi_B \tag{40}$$

From this equation, the first molecular orbital is a bonding, the second is almost a nonbonding and the third one is an antibonding molecular orbital. All four electrons from the above scenario are accommodated within these three molecular orbitals. These four electrons are all together coming from the original A – H bond and the lone pair of an orbital on B. The net effect of lowering the energy may result due to the fact that the anti-bonding orbital

remain unfilled. These net effects depend entirely on the position of the almost nonbonding molecular orbital [70, 84, 85].

- **Covalent Bonding**

Covalent bonding involves the sharing of electron pairs between atoms; this requires that the forces of attraction and repulsion be balanced during the sharing of these electrons. Figure 2.20 below illustrates the formation of a covalent bond between two hydrogen atoms.

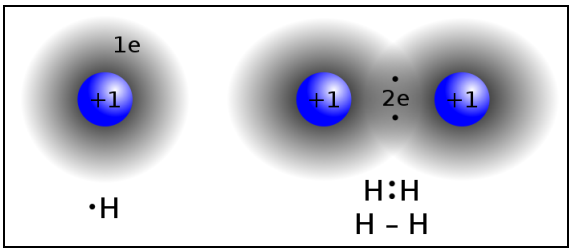

Figure 2.20: Formation of a covalent bond between two hydrogen atoms.

There are many kinds of possible interactions between atoms as far as covalent bonding is concerned, such as sigma bonding (σ-bonding), pi bonding (π-bonding), metal-to-metal bonding, agnostic interactions and three-centre two-electrons bond [69, 85 – 87]. Sigma bonds are the type of bonds that are formed when the atomic orbitals experience a head-on overlapping. They are the strongest of all covalent bond types. Pi-bonds are the type of bonds that are formed when two lobes of one involved atomic orbital overlap two lobes of the other involved atomic orbital.

Electronegativity plays a major role in covalent bonding. The tendency for two concerned atoms to form a covalent bond is higher when the two atoms have similar electronegativities. This type of bond is not limited to two atoms only, in some cases it can happen between three or more atoms, wherein the electrons are shared among all involved atoms. When such is the case, the covalent bonding is referred to as a delocalized covalent bonding [86 – 88].

2.6.7 MOLECULAR REACTIVITY PARAMETERS

Molecular reactivity parameters are important because they provide information on the ability/tendency of a given system to interact with other systems [64, 70]. In our case the interaction is between the inhibitor and the metal surface. Molecular reactivity parameters of a series of inhibitor molecules would provide information on which inhibitor molecule has the highest tendency to interact with the metal surface. Some of these molecular reactivity

parameters are the Highest Occupied Molecular Orbital (HOMO), Lowest Unoccupied Molecular Orbitals (LUMO), energy gap ($\Delta E_{LUMO-HOMO}$), electronegativity (χ), global hardness (η), global electrophilicity index (ω), global softness (σ), electron affinity (A) and ionization potential (I). These molecular reactivity parameters are used to determine the regions on the molecules that have the tendency to interact with the metal surface. A brief description of each of these parameters is given below;

- **Highest Occupied Molecular Orbital (HOMO) and Lowest Unoccupied Molecular Orbital (LUMO);**

The mathematical function that is utilized to describe the wave-like behaviour of electrons within a given molecule is called a molecular orbital. Sometimes a molecular orbital is simply defined as a wavefunction of a molecule's electron. The most important molecular orbitals are the Highest Occupied Molecular Orbital (HOMO) and Lowest Unoccupied Molecular Orbital (LUMO). These orbitals are also referred to as frontier orbitals and are used to predict the reactivity of molecules. The energy of the Lowest Unoccupied Molecular Orbital (E_{LUMO}) indicates the ability of the molecule to accept electrons. The lower the (E_{LUMO}) values, the easier it is for that molecule to accept electrons during the reaction. In the same light, the energy of the Highest Occupied Molecular Orbital (E_{HOMO}) provides the information on the electron donating ability by the molecule. The lower the (E_{HOMO}), the easier it would be for that molecule to donate electrons during the reaction.

- **The Energy Gap ($\Delta E_{HOMO - LUMO}$)**

This is the difference in the energy between the energy of the Highest Occupied Molecular Orbital (E_{HOMO}) and energy of the Lowest Unoccupied Molecular Orbital (E_{LUMO}), denoted by equation (41) below;

$$\Delta E = E_{LUMO} - E_{HOMO} \tag{41}$$

This molecular reactivity parameter is very important in that it gives further information about the reactivity of a molecule towards other chemical species. Molecules with small values of ΔE have a higher reactivity, whereas those with high values are normally associated with poor reactivity.

- **Electronegativity (χ);**

The frontier molecular orbitals (HOMO and LUMO) are related to the electronegativity of the molecules according to the relation in equation (42) below;

$$\chi \cong -\tfrac{1}{2}\,(E_{HOMO} + E_{LUMO}) \tag{42}$$

The significance of this molecular reactivity parameter is that is measures the power of an electron or group of atoms to attract electrons towards itself [86].

- **Global Hardness (η);**

The HOMO and LUMO orbitals are also related to another important molecular reactivity parameter called the global hardness of the molecule. This parameter helps to measure the resistance of an atom to a charge transfer [88]. The global hardness of the molecule is defined as in equation (43) below;

$$\eta \cong -\tfrac{1}{2}\,(E_{HOMO} - E_{LUMO}) \tag{43}$$

- **Global Electrophilicity Index (ω);**

This molecular reactivity parameter provides information regarding the electrophilicity of the molecule, or the ability to act as an electrophile by the molecule. Higher values of the global electrophilicity index are associated with a good electrophile whereas molecules with small or lower values are associated with being good nucleophiles. The global electrophilicity index of the molecule is related to the electronegativity and the global hardness according to equation (44) below;

$$\omega = \chi^2/2\eta \tag{44}$$

- **Global Softness (σ);**

The global softness is a molecular reactivity parameter that is used to describe the capacity of an atom or group of atoms to accept electrons. It is related to the global hardness and the frontier orbitals (HOMO and LUMO) as in the equation below;

$$\sigma = 1/\eta \cong -2/(E_{HOMO} - E_{LUMO}) \tag{45}$$

- **Electron Affinity (A);**

The energy that is released during a process that involves the addition of an electron to a neutral molecule is known as the electron affinity (A). This parameter provides us with an idea regarding the energy that is released by a molecule of concern should it accept any electron in the chemical reaction with other chemical species. The electron affinity is related to the energy of the Lowest Unoccupied Molecular Orbital by the expression in equation (46) below;

$$A \cong - E_{LUMO} \tag{46}$$

- **Ionization Potential (I);**

The other molecular reactivity parameter of note is the ionization potential (I). it is significant due to the fact that it is related to the amount of energy that is required in order to remove an electron from the molecule. This parameter gives us an idea regarding the energy that is released by a molecule during its chemical reaction with other chemical species when an electron is lost. It is related to the energy of the Highest Occupied Molecular Orbital through the expression given below in equation (47);

$$I \cong - E_{HOMO} \tag{47}$$

CHAPTER 3

EXPERIMENTAL DETAILS

3.1 METAL SPECIMENS

All experimental procedures involving mild steel were executed using mild steel specimens of a chemical composition (wt %): (P = 0.02), (Mn = 0.37), (S = 0.03), (Mo = 0.01), (Ni = 0.039), (C = 0.21) and (Fe = 99.32). These specimens were meticulously prepared prior all experimental procedures. They were abraded utilizing emery papers (from 100, 600 and 1200 grit sizes) washed with doubly distilled water followed by acetone and consequently air-dried overnight before their storage in desiccators until such time when they were utilized for all experimental procedures.

All experimental procedures involving zinc were executed using zinc specimens of a 99.90 (wt %) purity and approximately 99 (wt %) aluminium sheets were used for all experimental procedures involving aluminum metals.

3.2 SOLUTIONS

All of the working solutions were prepared as reported elsewhere [90]. Aggressive solutions of 1.0 M HCl were carefully prepared by diluting Analytical grade 32% Hydrochloric acid from Merck Chemicals through addition of appropriate amounts of doubly distilled water. A stock solution of 10.0×10^{-5} M corrosion inhibitors was carefully prepared through the addition of appropriate amount of doubly distilled water. To ensure complete dissolution of the sulphonamides compounds, a 1:100 of ethanol and doubly distilled water was utilized. From the stock solution, a series of concentrations as indicated in the results section were prepared through the usage of appropriate amounts of doubly distilled water.

3.3 CORROSION INHIBITORS

Sulphonamides corrosion inhibitors, namely, Sulphanilamide, Sulphabenzamide, Sulphachloropyridazine, Sulphadimethoxine, Sulphamethoxazole, Sulphamethazine, Sulphaquinoxaline, Sulphisoxazole and Sulphamethazine were purchased from SIGMA-ALDRICH CHEMICALS and were used without any further purification. The working solutions in the concentration range of 1.0×10^{-5} M – 5.0×10^{-5} M were prepared for each sulphonamide from the stock solution of 10.0×10^{-5} M. The names and structures of the sulphonamides used in this study are shown in Figure 3.1.

3.4 ELECTROCHEMICAL TECHNIQUES

All electrochemical measurements were performed using a Metrohm Autolab Potentiostat/Galvanostat (PGSTAT302N) which employed a three-electrode cell, namely a platinum counter electrode (CE), saturated calomel with Ag/AgCl reference electrode (RE) and mild steel working electrode (WE). Prior to all electrochemical measurements, a 30 min period was allowed as a period of stabilization, since it was proved to be an appropriate period to attain a stable value of E_{corr}. Tafel curves were measured at the potential range of −250 to +250 mV (SCE) and scan rate of 1 $mV.s^{-1}$. Electrochemical Impedance curves were measured using a frequency response analyser (FRA) connected to the Potentiostat/Galvanostat at the frequency range of 100 kHz to 0.00001 kHz under potentiodynamic conditions with amplitude of 10 mV peak-to-peak, using AC signal at E_{corr}. The mild steel specimens utilized had a 1 cm^2 surface area exposed to the corrosive solution. All these measurements were done at atmospheric conditions without any stirring.

3.4.1 POTENTIODYNAMIC POLARIZATION (PDP)

The PDP method was utilized to obtain the relevant electrochemical parameters such as the corrosion potential, corrosion density, anodic and cathodic Tafel slopes. The measured corrosion current densities values were used to calculate the inhibition efficiency by making use of the equation given below:

$$\%IE_{PDP} = \left(\frac{i^{0}{}_{corr} - i^{i}{}_{corr}}{i^{0}{}_{corr}} \right) \times 100 \tag{48}$$

where i^{0}_{corr} and i^{i}_{corr} are values of corrosion current density in absence and in presence of inhibitor, respectively.

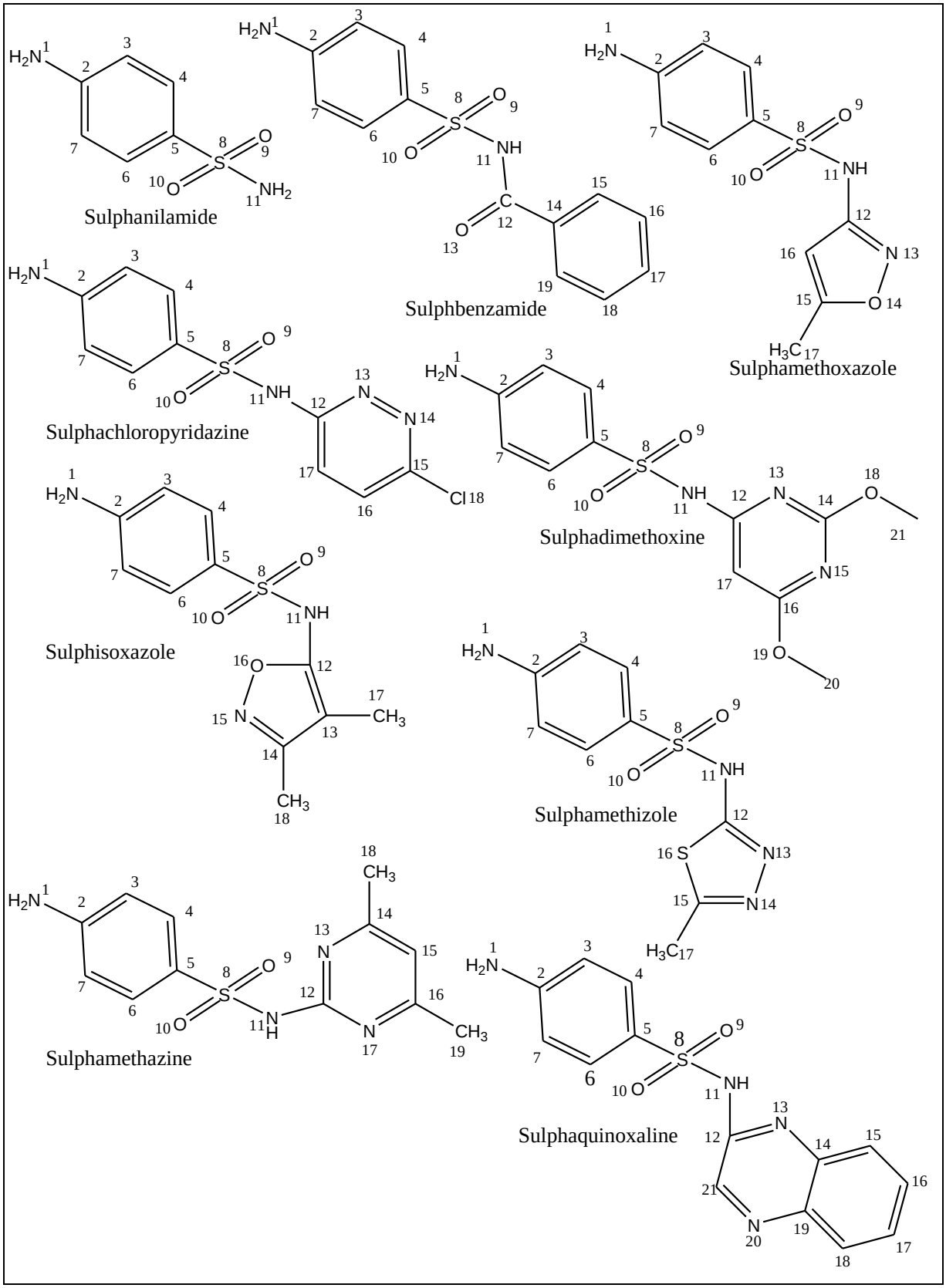

Figure 3.1: Molecular structures of the sulphonamides used as corrosion inhibitors in this study.

3.4.2 ELECTROCHEMICAL IMPEDANCE SPECTROSCOPY (EIS)

EIS was also used to study the corrosion of mild steel in 1 M hydrochloric acid. The electrochemical parameters such as the resistance of charge transfer, capacity of double layer, the constant phase element constant and exponents were obtained and used to calculate the inhibition efficiency from the equation given below:

$$\%IE_{EIS} = \left(1 - \frac{R^{0}{}_{ct}}{R_{ct}}\right) \times 100 \tag{49}$$

where, $R^{0}{}_{ct\ is}$ the charge transfer resistance in the absence of the inhibitor and R_{ct} is the charge transfer resistance in the presence of the inhibitor.

3.5 FOURIER TRANSFORM INFRARED SPECTROMETER (FTIR)

Adsorption films that were formed during the corrosion of mild steel, aluminum and zinc specimens in 1.0 M HCl in the absence and presence of all studied corrosion inhibitors at 30 °C were carefully scratched off the specimens surfaces with a sharp scissors and the resultant powders were investigated using Nicolet iS5 Fourier Transform Infrared Spectrometer.

3.6 SCANNING ELECTRON MICROSCOPE (SEM)

Mild steel, aluminum and zinc specimens with a surface area of 1 cm^2 were treated with 1.0 M HCl in the absence and presence of all studied corrosion inhibitors at 30 °C. Their surface morphology and Energy Dispersive Spectroscopy (EDS) analysis were performed using JOEL JSM-7500F Field Emission Scanning Electron Microscope.

3.7 WEIGHT LOSS MEASUREMENTS

Most studies indicate that weight loss method is the most preferred method for the corrosion studies because it is simple, accurate, precise and reliable [90–93]. Weight loss measurements were carried out as previously reported in our works [90]. Mild steel, aluminium and zinc specimens were totally immersed in corrosive solutions of 1.0 M HCl in the absence and presence of various concentrations of all studied corrosion inhibitors at 30-50

°C for a total immersion time of 15 h. The percent inhibition was calculated using the equation:

$$\%IE_{WL} = \left(1 - \frac{w_1}{w_0}\right) \times 100 \tag{50}$$

where w_0 is the weight loss of mild steel in the absence of corrosion inhibitors and w_1 is the weight loss of mild steel in the presence of corrosion inhibitors.

3.8 COMPUTATIONAL METHODS

All geometry optimizations and quantum chemical calculations were performed using density functional theory (DFT) utilizing the Becke's Three Parameter and the Lee-Yang-Parr correlation functional theory (B3LYP) [93]. The 6-31+G(d,p) basis set was also selected for the study. Density functional theory (DFT) has found wide applicability in the analysis of the characteristics of the inhibitor/metal surface mechanisms and in the description of the structure nature of the inhibitor on the corrosion process [93, 94]. Moreover, there is a good agreement between experimental results and the quantum chemical parameters computed using DFT [95]. Some of the chemical parameters calculated include chemical hardness, chemical softness, electron affinity and polarization potential. Chemical hardness (η) measures the resistance of an atom to a charge transfer [96] , it is estimated by using the equation:

$$\eta \cong -\tfrac{1}{2}\,(E_{HOMO} - E_{LUMO}) \tag{51}$$

Chemical softness (σ) describes the capacity of an atom or group of atoms to receive electrons [96] and is estimated by using the equation:

$$\sigma = 1/\eta \cong -2/(E_{HOMO} - E_{LUMO}) \tag{52}$$

Electron affinity (A) related to E_{LUMO} through the equation:

$$A \cong - E_{LUMO} \tag{53}$$

Ionization potential (I) is related to the energy of the E_{HOMO} through the equation:

$$I \cong - E_{HOMO} \tag{54}$$

All calculations were done by using the Gaussian09 program [97]. Schematic structures were drawn using the ChemOffice package in the UltraChem 2010 version while optimized structures were drawn using the gaussView5 program.

CHAPTER 4

RESULTS AND DISCUSSION

4.1 MILD STEEL

4.1.1 POTENTIODYNAMIC POLARIZATION (PDP)

Mild steel corrosion comprises a simultaneous anodic dissolution of mild steel and the cathodic reduction of hydrogen ions [98]. Potentiodynamic polarization measurements were carried out in order to fully understand this process. To facilitate this objective, the current-potential curves for mild steel in hydrochloric acid solutions were obtained in the absence and presence of various concentrations of the nine (9) compounds namely sulphanilamide (SNA), sulphamethoxazole (SMX), sulphadimethoxine (SDM), sulphisoxazole (SSZ), sulphamethazine (SMT), sulphachloropyridazine (SCP), sulphabenzamide (SBZ), sulphaquinoxaline (SQX) and sulphamethizole (SMZ) used as corrosion inhibitors at 30 °C, as shown in Figures 4.1 – 4.9.

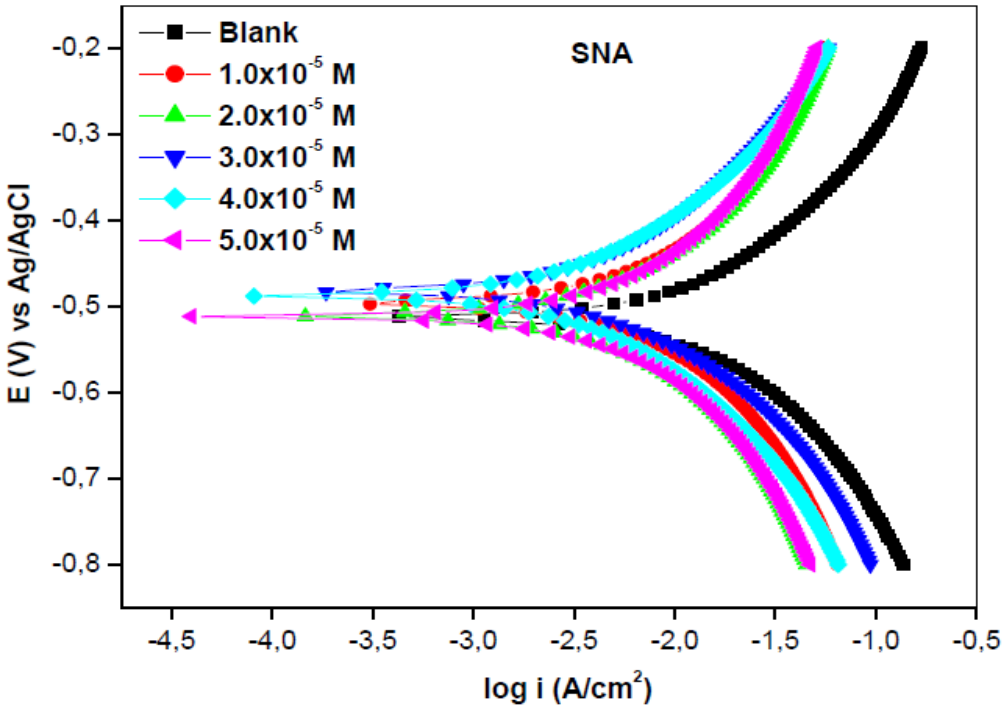

Figure 4.1: Tafel plots for mild steel in 1 M HCl in the absence and presence of different concentrations of SNA inhibitor compound.

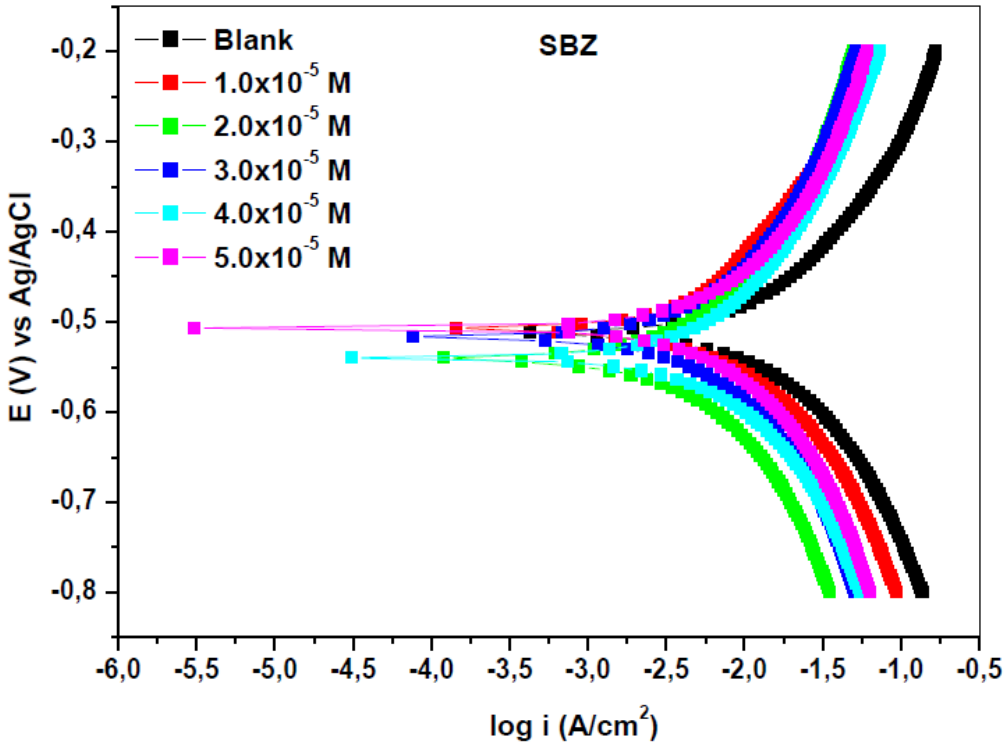

Figure 4.2: Tafel plots for mild steel in 1 M HCl in the absence and presence of different concentrations of SBZ inhibitor compound.

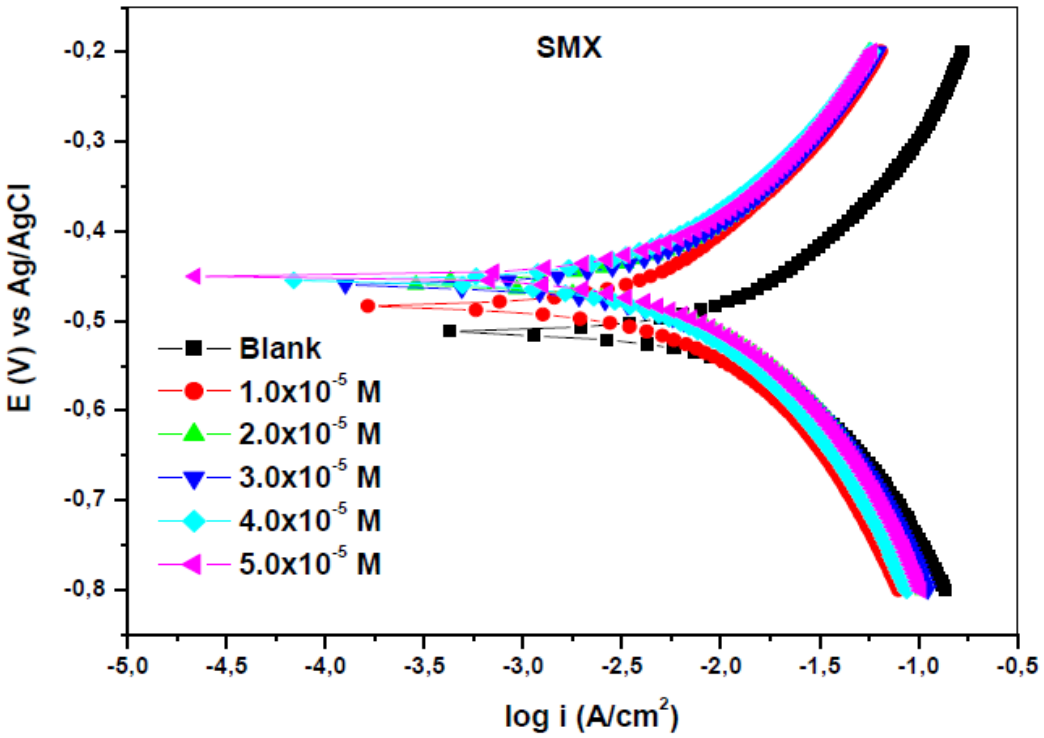

Figure 4.3: Tafel plots for mild steel in 1 M HCl in the absence and presence of different concentrations of SMX inhibitor compound.

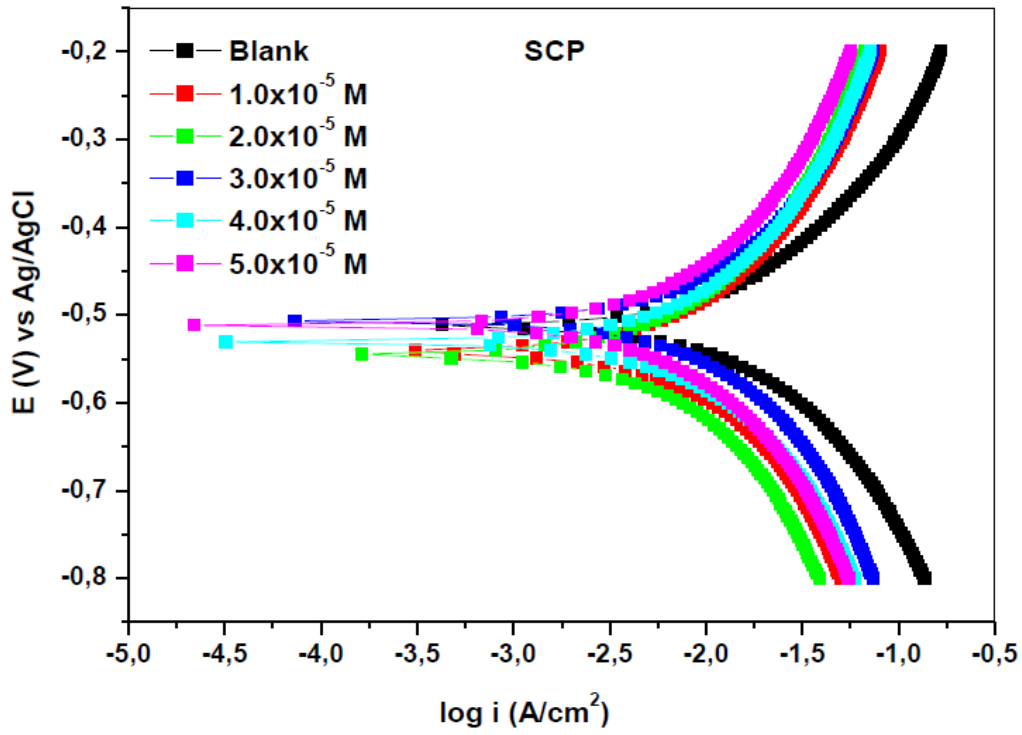

Figure 4.4: Tafel plots for mild steel in 1 M HCl in the absence and presence of different concentrations of SCP inhibitor compound.

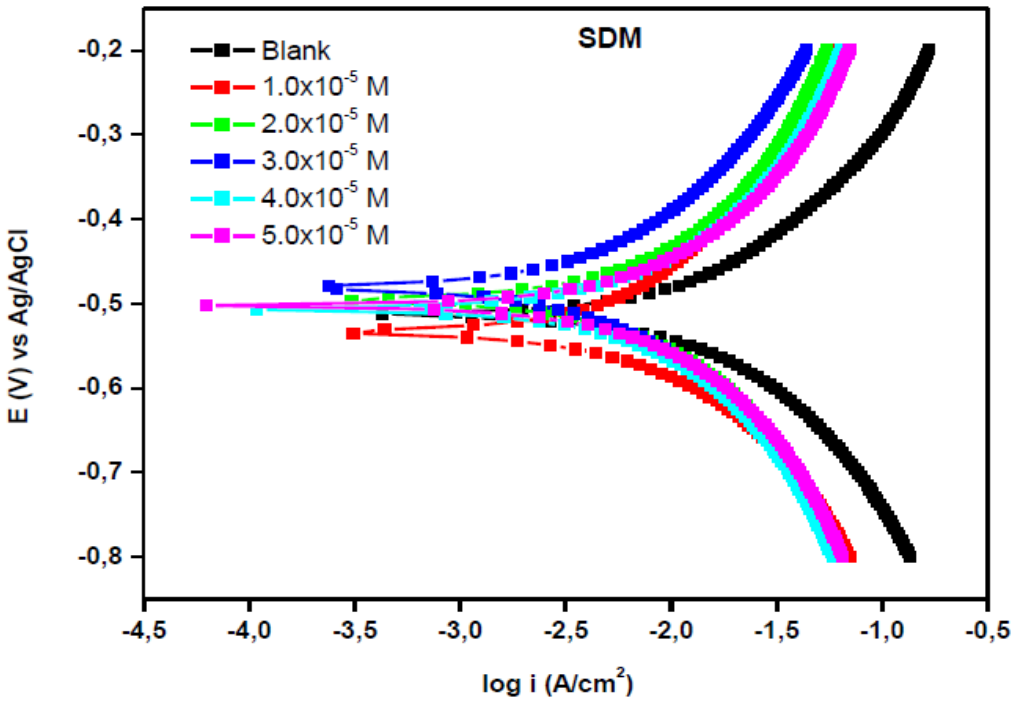

Figure 4.5: Tafel plots for mild steel in 1 M HCl in the absence and presence of different concentrations of SDM inhibitor compound.

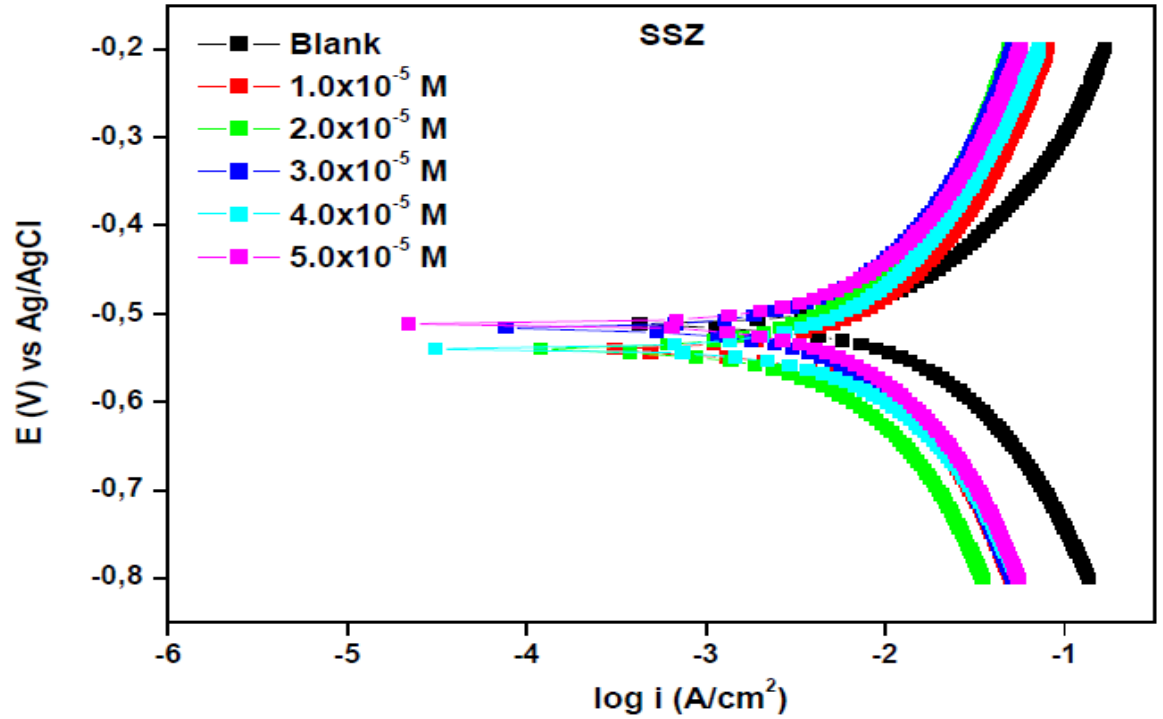

Figure 4.6: Tafel plots for mild steel in 1 M HCl in the absence and presence of different concentrations of SSZ inhibitor compound.

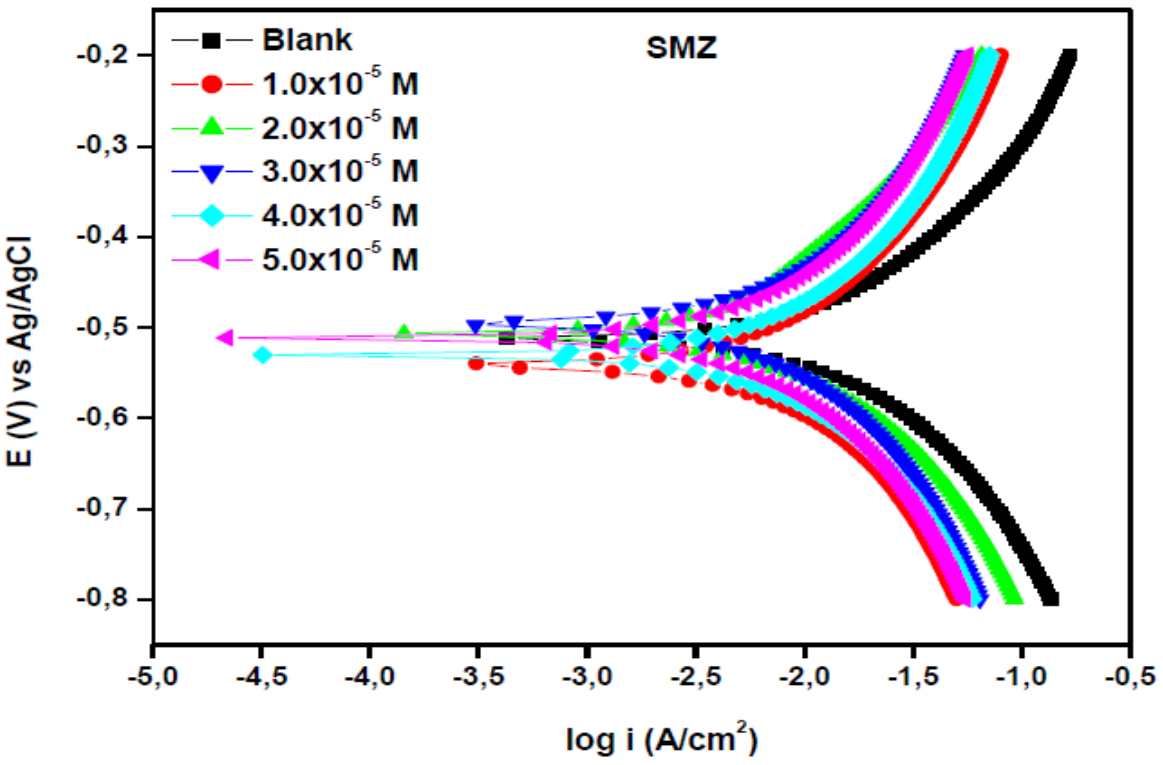

Figure 4.7: Tafel plots for mild steel in 1 M HCl in the absence and presence of different concentrations of SMZ inhibitor compound.

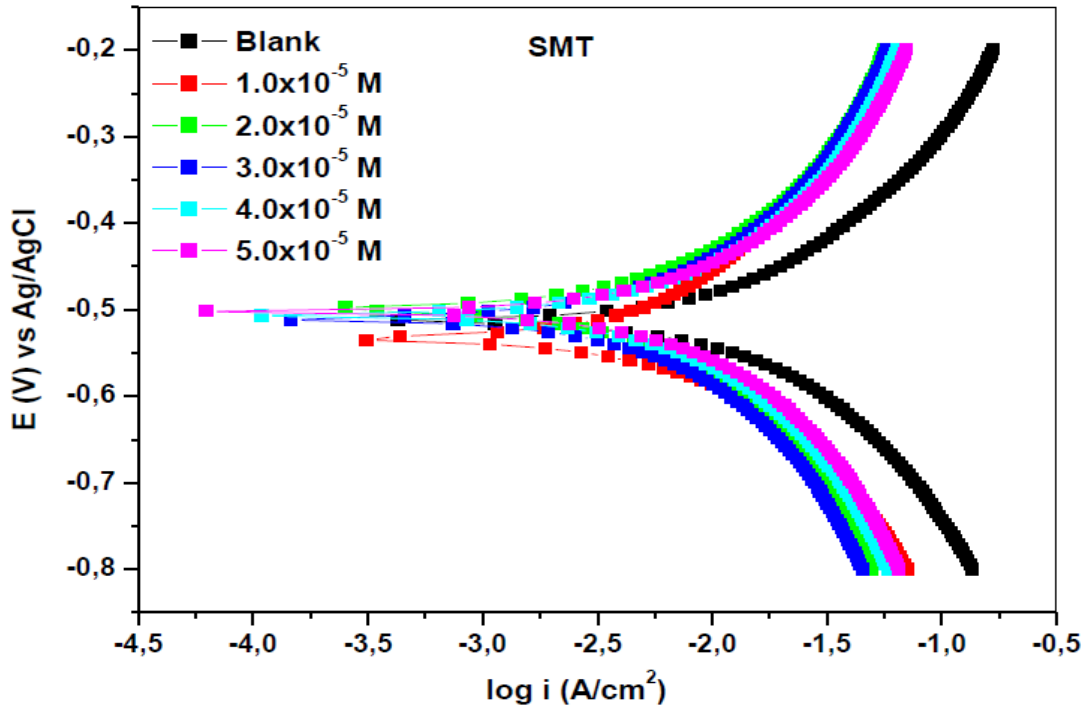

Figure 4.8: Tafel plots for mild steel in 1 M HCl in the absence and presence of different concentrations of SMT inhibitor compound.

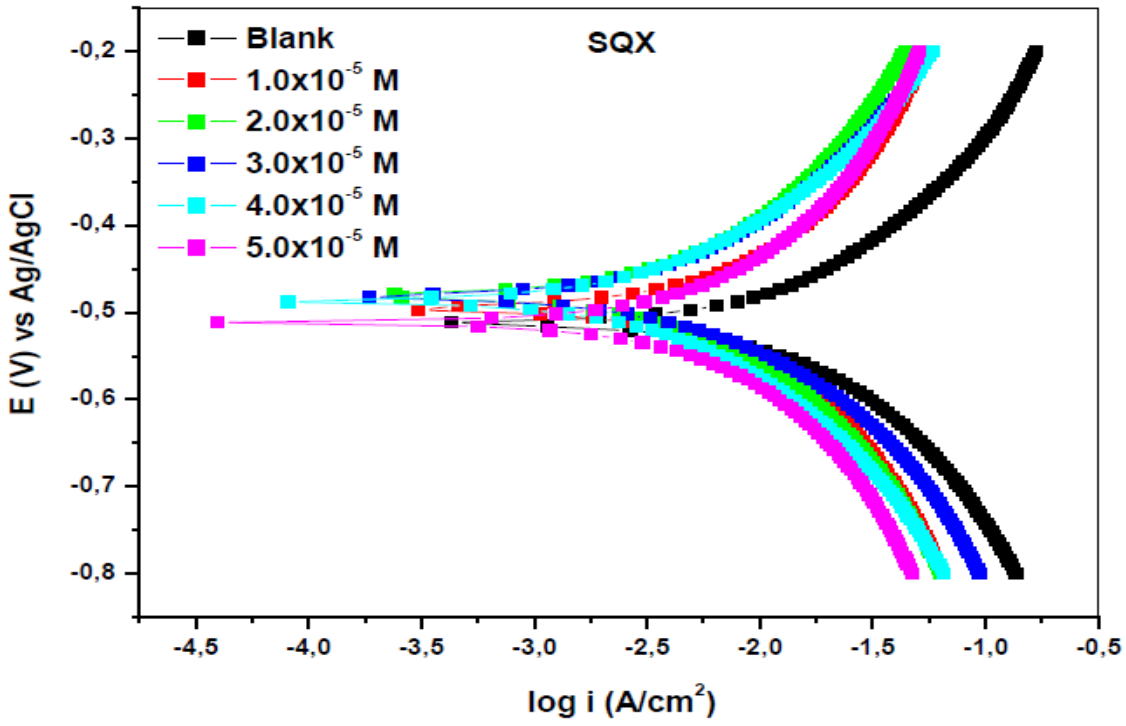

Figure 4.9: Tafel plots for mild steel in 1 M HCl in the absence and presence of different concentrations of SQX inhibitor compound.

The figures show both anodic and cathodic half-reactions of the mild steel corrosion in hydrochloric acid. It is also observed that both half-reactions are affected by the introduction of all nine inhibitors. From these curves, a successful extrapolation of their linear Tafel segments produced some valuable potentiodynamic parameters such as corrosion current density (i_{corr}), corrosion potential (E_{corr}), anodic Tafel slope (b_a) and cathodic Tafel slope (b_c). These parameters are recorded in Table 4.1. The potentiodynamic polarization inhibition efficiency ($\%IE_{PDP}$) was then calculated from equation (48).

Table 4.1: Potentiodynamic polarization (PDP) parameters such as corrosion potential (E_{corr}), corrosion current density (i_{corr}) and anodic and cathodic Tafel slopes (b_a and b_c) using different inhibitors

Inhibitor	Inhibitor Conc. (M)	$-E_{corr}$(mV) with Ag/AgCl	i_{corr}(mA.cm^{-2})	R_p(10^{-1}) (Ohm)	b_a (mV.dec^{-1})	b_c (mV.dec^{-1})	$\%IE_{PDP}$	$\%IE_{WL}$
Blank		513	3.63	1.62	66	75	-	-
SNA	1.0×10^{-5}	481	0.90	4.81	36	49	75.21	81.47
	2.0×10^{-5}	463	0.75	5.29	33	48	79.33	80.05
	3.0×10^{-5}	460	0.70	5.41	35	38	80.71	82.42
	4.0×10^{-5}	459	0.48	4.77	18	25	86.77	88.36
	5.0×10^{-5}	452	0.45	5.69	14	20	87.60	89.55
SBZ	1.0×10^{-5}	505	0.88	3.18	21	44	75.75	75.81
	2.0×10^{-5}	502	0.64	7.25	24	50	86.22	82.34
	3.0×10^{-5}	503	0.37	3.90	14	17	87.17	89.86
	4.0×10^{-5}	503	0.35	3.87	16	15	88.36	90.24
	5.0×10^{-5}	507	0.29	1.27	02	20	90.49	92.06
SMX	1.0×10^{-5}	499	1.30	7.91	39	51	64.19	79.67
	2.0×10^{-5}	485	0.91	7.80	35	51	74.93	67.02
	3.0×10^{-5}	488	0.41	4.21	29	47	88.70	84.79
	4.0×10^{-5}	476	0.40	3.50	10	34	88.98	81.63
	5.0×10^{-5}	461	0.37	3.25	07	21	89.81	86.59
SCP	1.0×10^{-5}	501	1.03	8.12	33	42	71.63	74.55
	2.0×10^{-5}	504	0.81	8.12	35	40	77.60	82.08
	3.0×10^{-5}	506	0.53	3.33	21	15	85.51	87.65
	4.0×10^{-5}	504	0.39	2.67	15	16	89.09	90.21
	5.0×10^{-5}	505	0.33	3.20	15	16	90.88	91.72
SDM	1.0×10^{-5}	506	1.25	4.86	48	51	65.56	71.97
	2.0×10^{-5}	491	0.93	4.69	33	45	74.38	85.99
	3.0×10^{-5}	497	0.71	5.41	30	32	80.44	89.31
	4.0×10^{-5}	499	0.65	4.53	15	38	82.09	89.79
	5.0×10^{-5}	478	0.58	5.11	09	15	84.02	93.83
SSZ	1.0×10^{-5}	473	1.28	7.15	38	48	64.74	56.76
	2.0×10^{-5}	469	1.20	6.09	36	44	66.94	76.24
	3.0×10^{-5}	462	0.85	4.73	22	28	76.58	72.44
	4.0×10^{-5}	455	0.51	2.98	18	22	85.95	81.95
	5.0×10^{-5}	435	0.28	3.25	19	11	92.29	88.36
SMZ	1.0×10^{-5}	503	1.01	6.16	31	51	72.18	65.21
	2.0×10^{-5}	500	0.76	7.00	35	58	79.06	74.25
	3.0×10^{-5}	501	0.56	4.50	36	49	84.57	79.67
	4.0×10^{-5}	489	0.55	3.22	14	45	84.84	82.38
	5.0×10^{-5}	465	0.40	1.09	04	28	88.98	85.97
SMT	1.0×10^{-5}	506	1.08	7.91	40	47	70.25	75.75
	2.0×10^{-5}	499	0.86	4.21	44	41	76.22	84.49
	3.0×10^{-5}	499	0.65	5.93	50	45	82.23	87.20
	4.0×10^{-5}	506	0.38	2.12	17	14	89.64	88.55
	5.0×10^{-5}	502	0.30	1.08	04	17	91.71	92.77
SQX	1.0×10^{-5}	495	1.11	6.56	31	54	69.42	65.32
	2.0×10^{-5}	481	0.91	5.17	36	69	74.93	78.62
	3.0×10^{-5}	482	0.77	6.04	19	58	78.62	82.19
	4.0×10^{-5}	487	0.49	3.80	37	34	86.39	88.36
	5.0×10^{-5}	503	0.48	5.71	26	25	86.72	89.07

Figures 4.1–4.9 and Table 4.1 show that the introduction of all nine inhibitors has significantly reduced the corrosion current densities for both anodic and cathodic half-reactions, (that is, the corrosion current densities the anodic and cathodic half-reactions for the uninhibited process are 66 $mV.dec^{-1}$ and 75 $mV.dec^{-1}$, respectively while those for the inhibited processes are ranging between 02 – 50 $mV.dec^{-1}$ for the anodic half reactions and between 11 – 58 $mV.dec^{-1}$ for the cathodic half reactions) which suggests that both anodic dissolution of mild steel and cathodic reduction of the hydrogen ions were inhibited. The trend of the values of E_{corr} shows consistency and a minimal change. This type of behaviour from the E_{corr} values is attributed to mixed-type inhibitors [99, 100]. The values of anodic and cathodic Tafel slopes for inhibited processes show some variations as compared to those of their blank counterparts. This indicates that both anodic and cathodic half-reactions are affected by the presence of the inhibitor molecules. The inhibition efficiency values obtained from PDP increase with the increase in the concentration of the inhibitors utilized in the study. It is reasonable to infer that the inhibition process could be caused by the formation of the adsorption film resulting from the interaction between mild steel surface and the sulphonamide inhibitor molecules.

4.1.2 ELECTROCHEMICAL IMPEDANCE SPECTROSCOPY (EIS)

Further information regarding the characteristics and kinetics of mild steel corrosion in acidic solutions and the inhibition by sulphonamide compounds was obtained using electrochemical impedance spectroscopy. The main advantage of electrochemical impedance spectroscopy is to follow the corrosion behaviour of the metal with time. Nyquist plots, represented by the imperfect semicircles and their corresponding bode plots are shown in Figures 4.10 – 4.27. The imperfect semicircles on Nyquist plots show the impedance spectra for mild steel corrosion in 1.0 M HCl solution in the absence and presence of various concentrations of the nine inhibitor compounds utilized at 30 °C. These imperfect semicircles increase in diameter with the increase in inhibitor concentrations, and this imperfection is an indication of a charge transfer process which governs the corrosion of mild steel in acidic solutions [101].

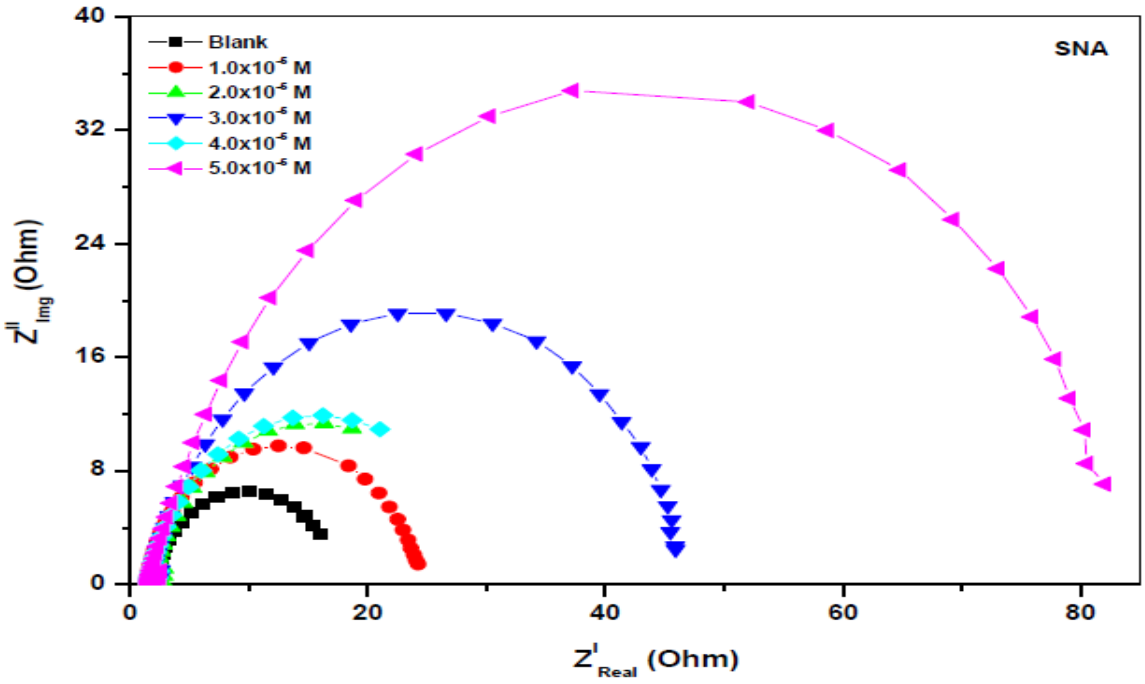

Figure 4.10: Nyquist plot of mild steel in 1 M HCl in the absence and presence of different concentrations of SNA inhibitor compound.

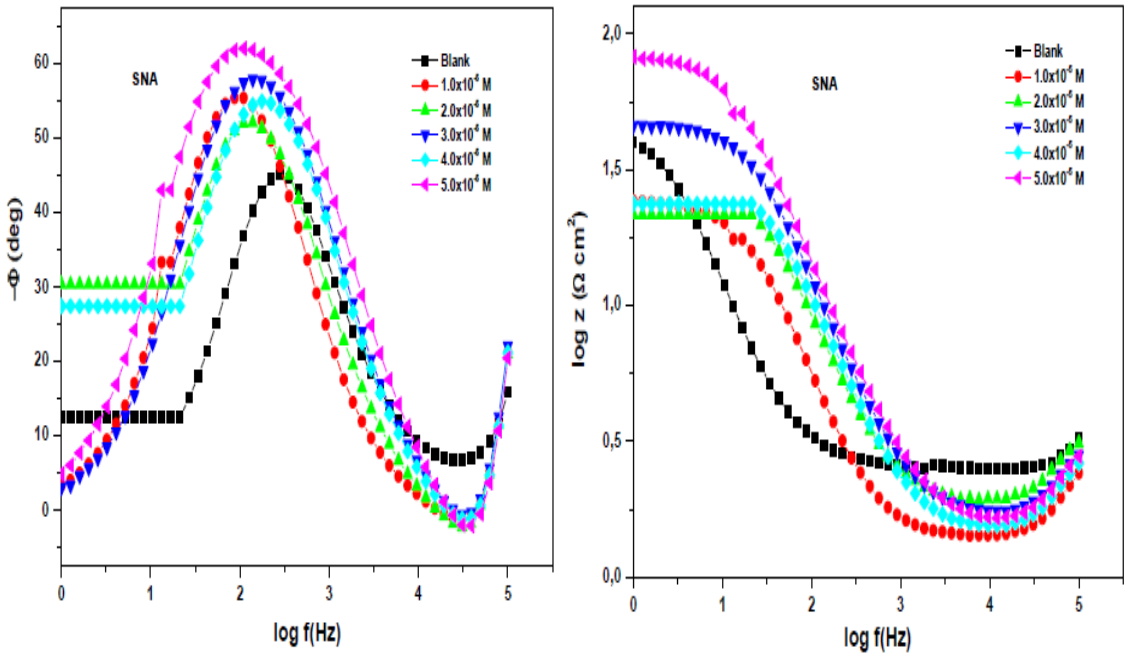

Figure 4.11: Bode plots of mild steel in 1 M HCl in the absence and presence of different concentrations of SNA inhibitor compound.

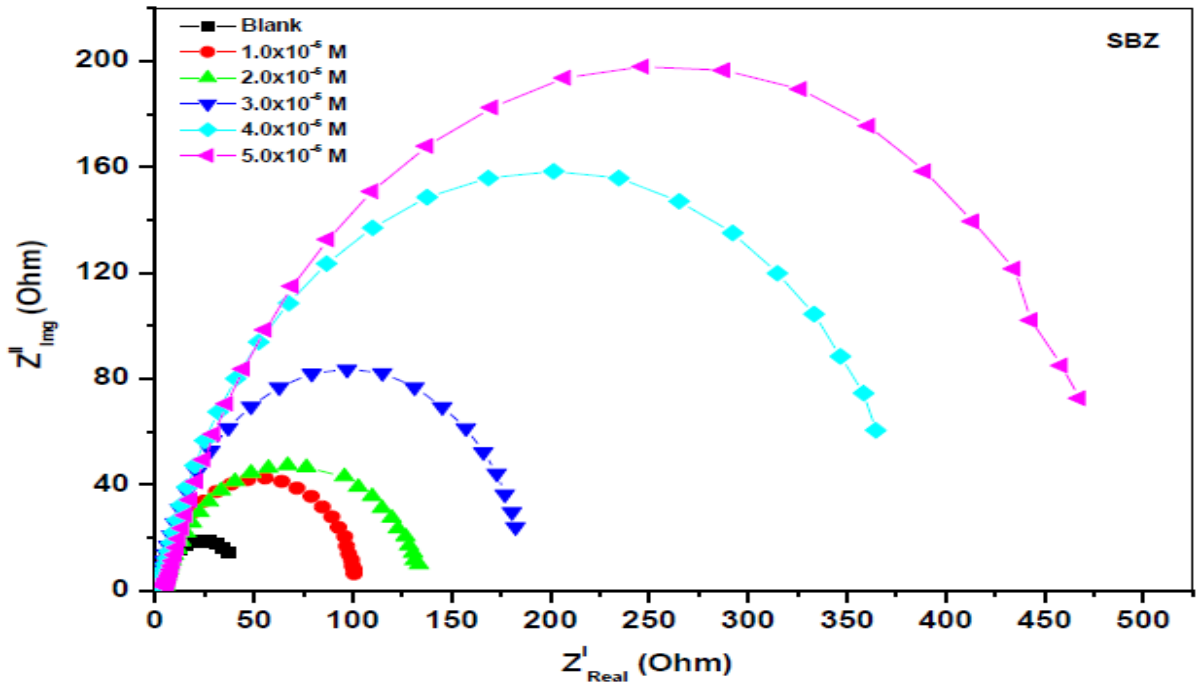

Figure 4.12: Nyquist plot of mild steel in 1 M HCl in the absence and presence of different concentrations of SBZ inhibitor compound.

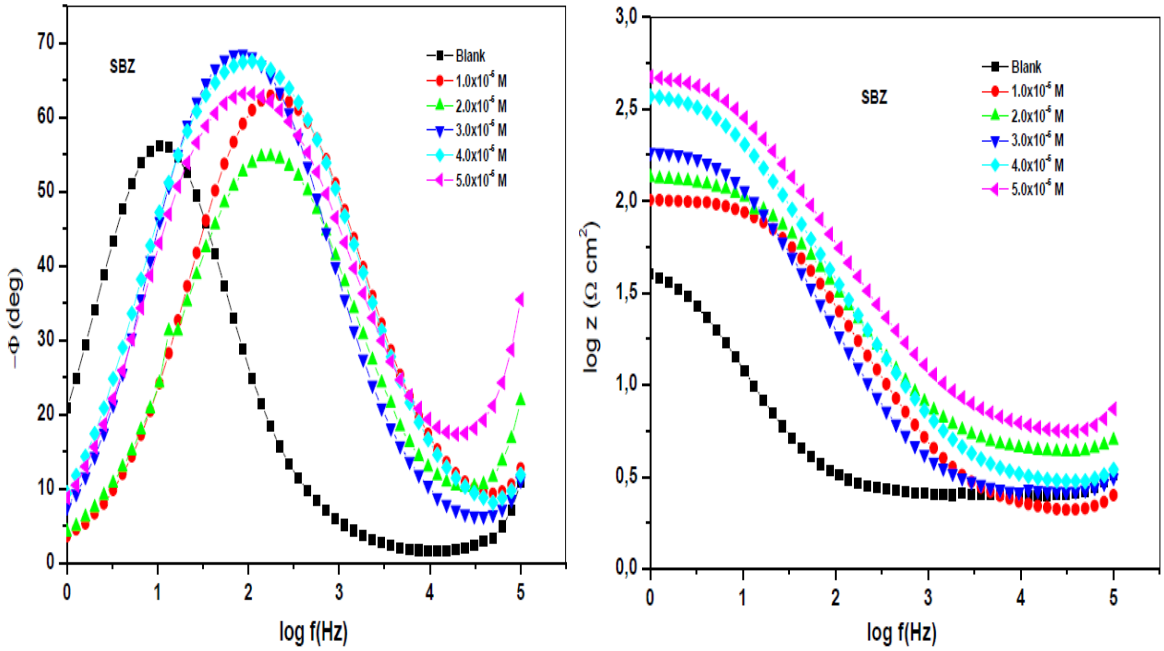

Figure 4.13: Bode plots of mild steel in 1 M HCl in the absence and presence of different concentrations of SBZ inhibitor compound.

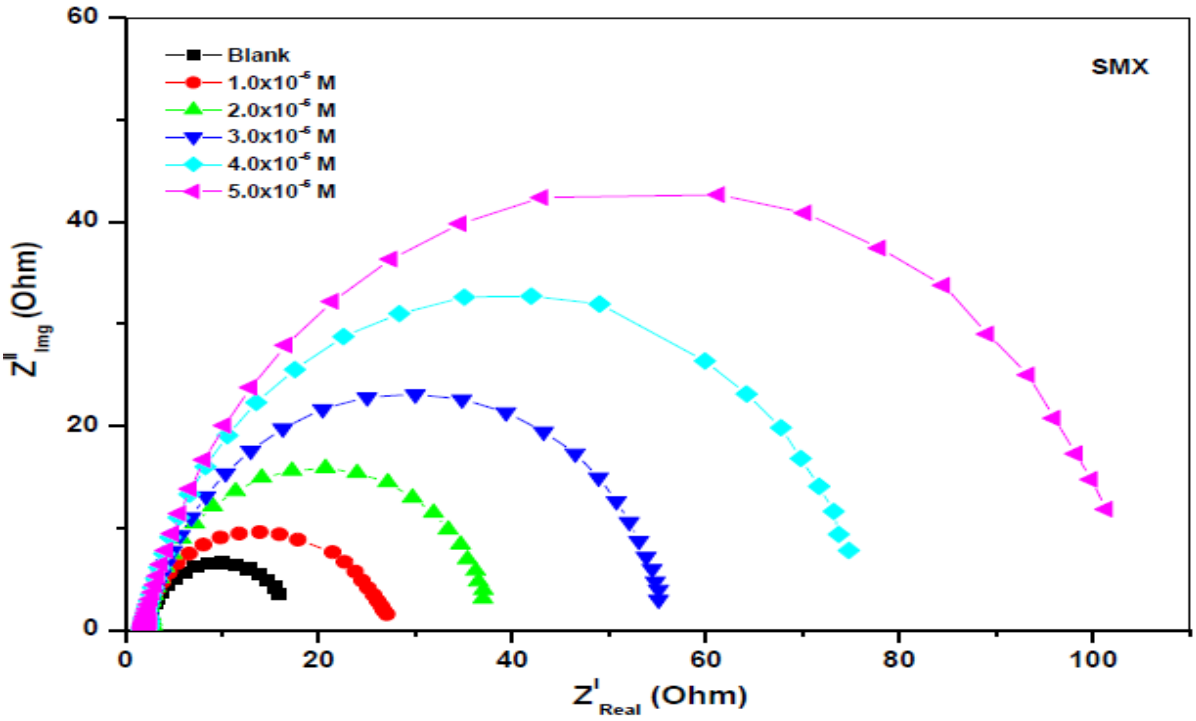

Figure 4.14: Nyquist plot of mild steel in 1 M HCl in the absence and presence of different concentrations of SMX inhibitor compound.

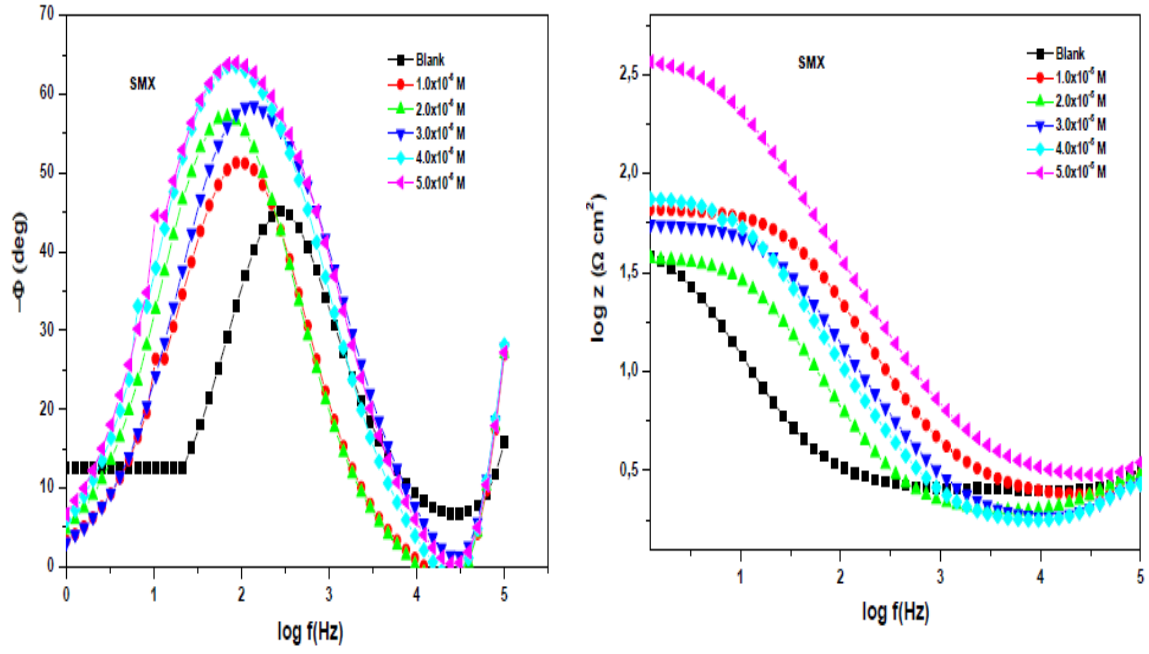

Figure 4.15: Bode plots of mild steel in 1 M HCl in the absence and presence of different concentrations of SMX inhibitor compound.

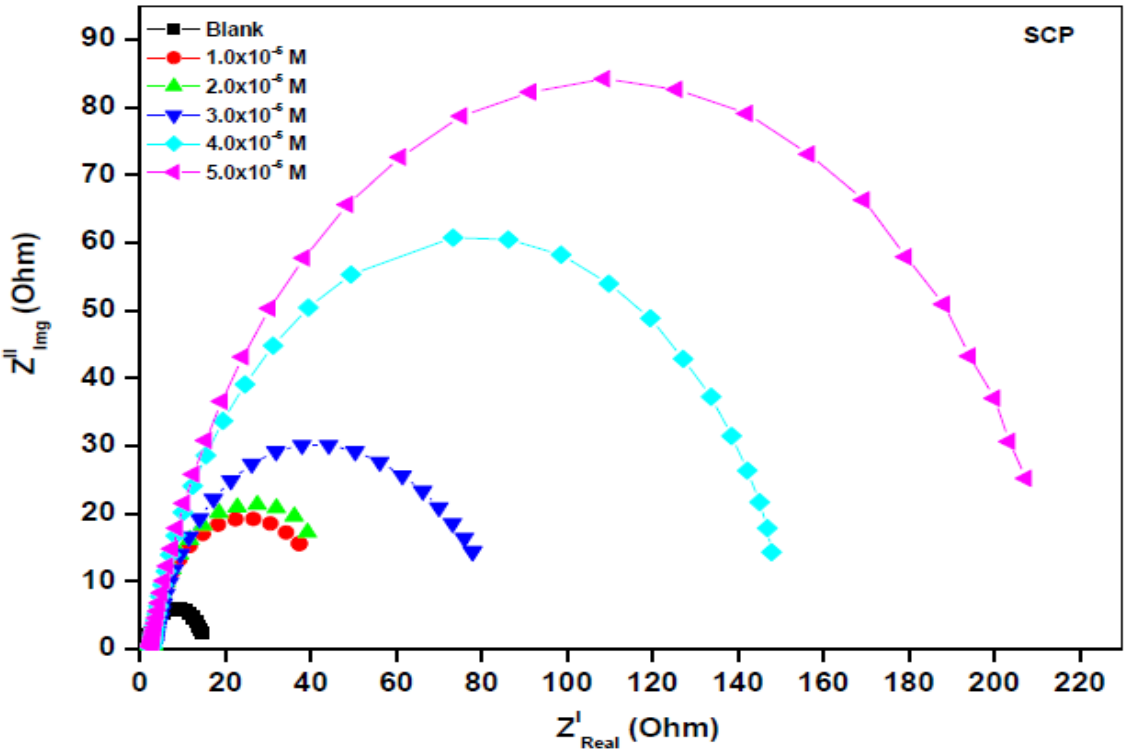

Figure 4.16: Nyquist plot of mild steel in 1 M HCl in the absence and presence of different concentrations of SCP inhibitor compound.

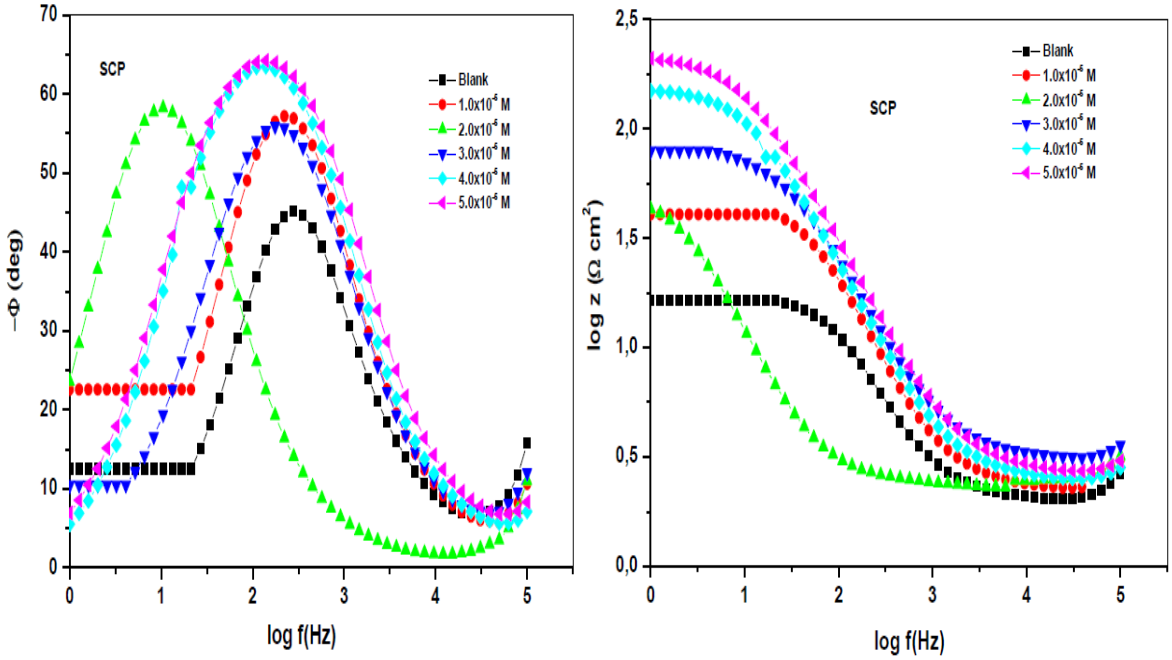

Figure 4.17: Bode plots of mild steel in 1 M HCl in the absence and presence of different concentrations of SCP inhibitor compound.

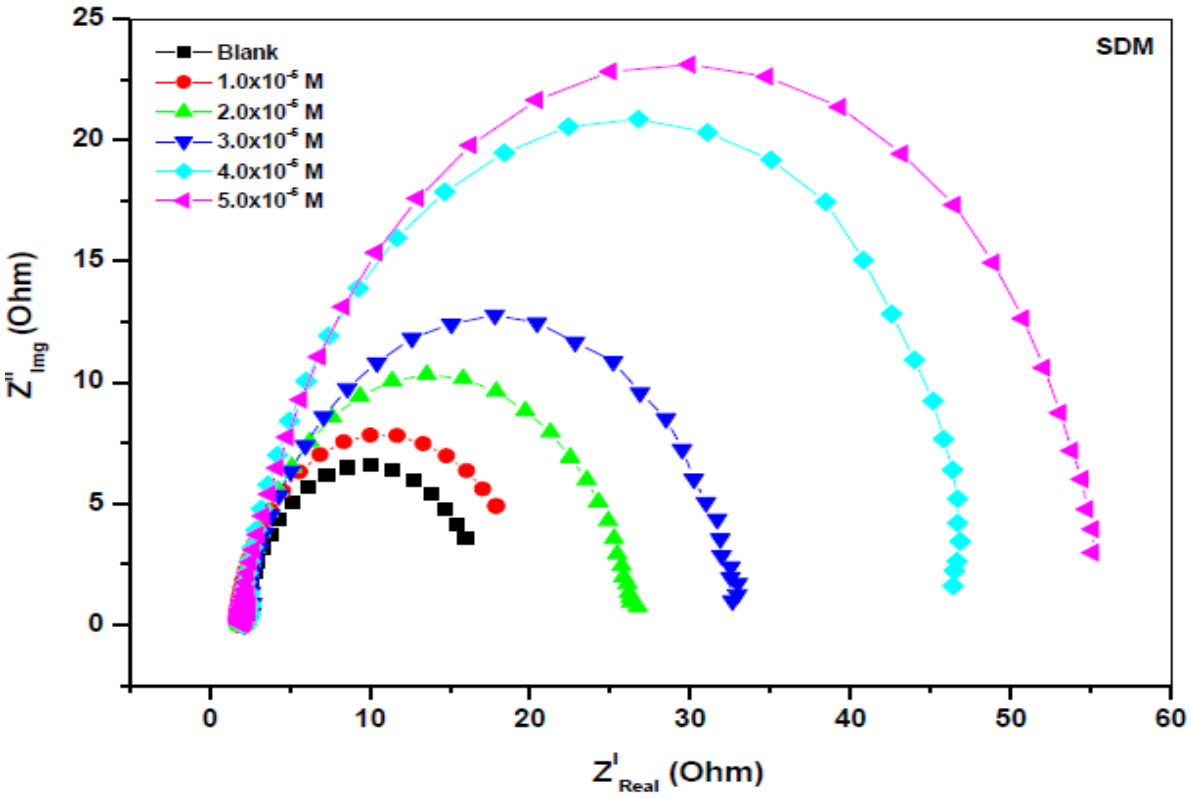

Figure 4.18: Nyquist plot of mild steel in 1 M HCl in the absence and presence of different concentrations of SDM inhibitor compound.

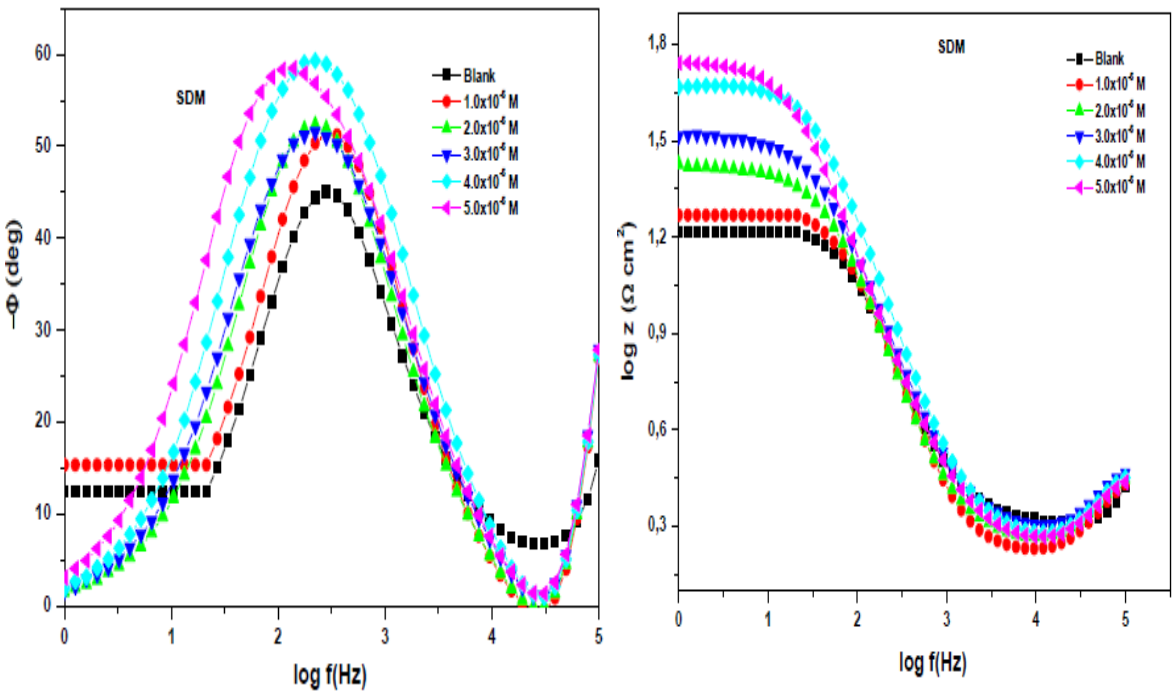

Figure 4.19: Bode plots of mild steel in 1 M HCl in the absence and presence of different concentrations of SDM inhibitor compound.

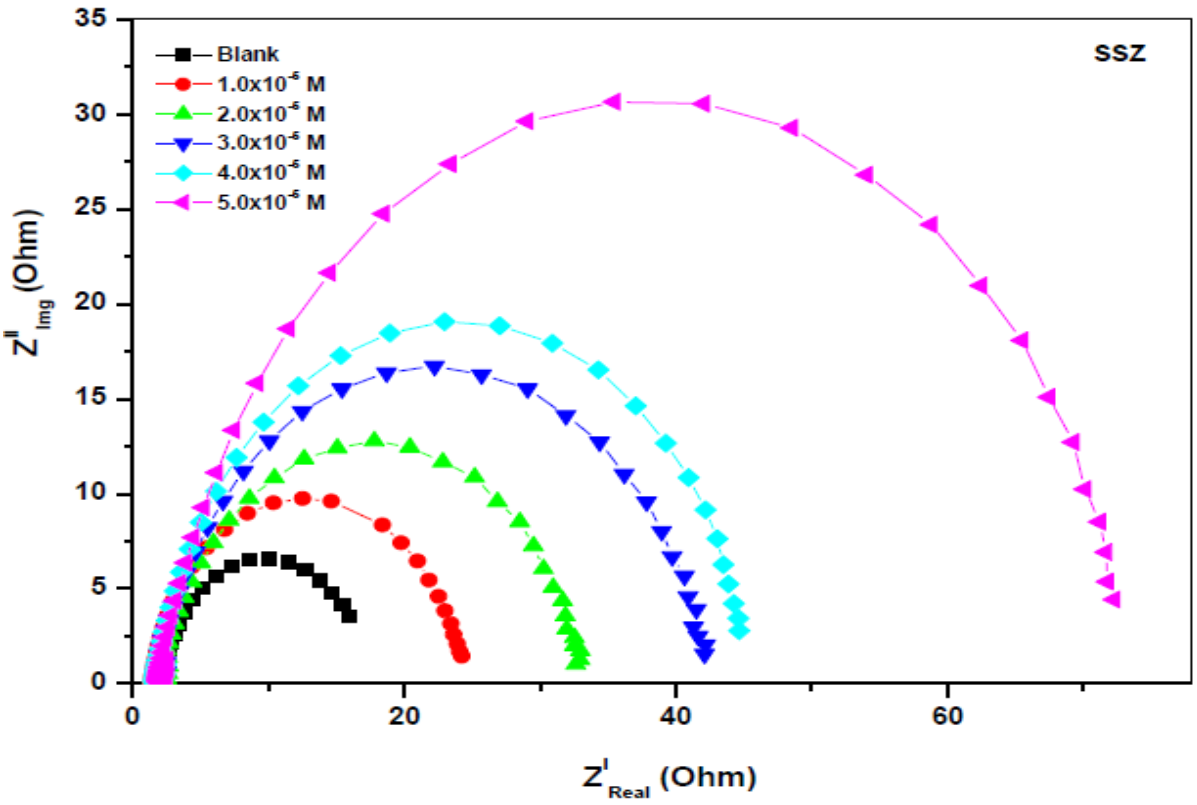

Figure 4.20: Nyquist plot of mild steel in 1 M HCl in the absence and presence of different concentrations of SSZ inhibitor compound.

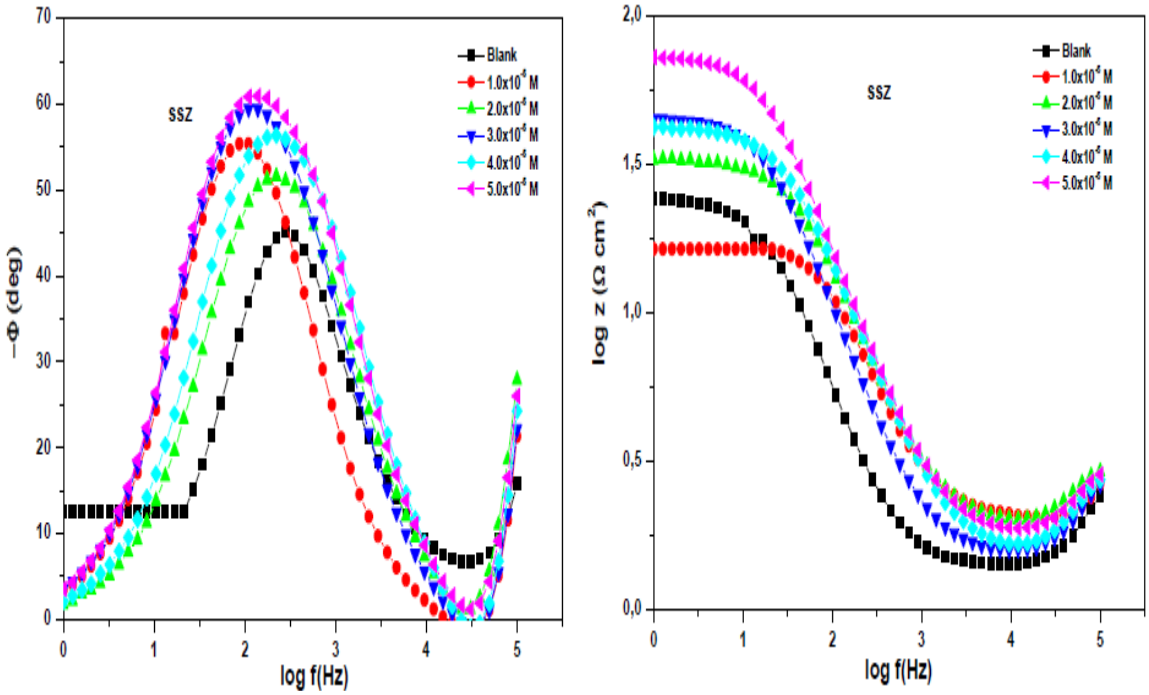

Figure 4.21: Bode plots of mild steel in 1 M HCl in the absence and presence of different concentrations of SSZ inhibitor compound.

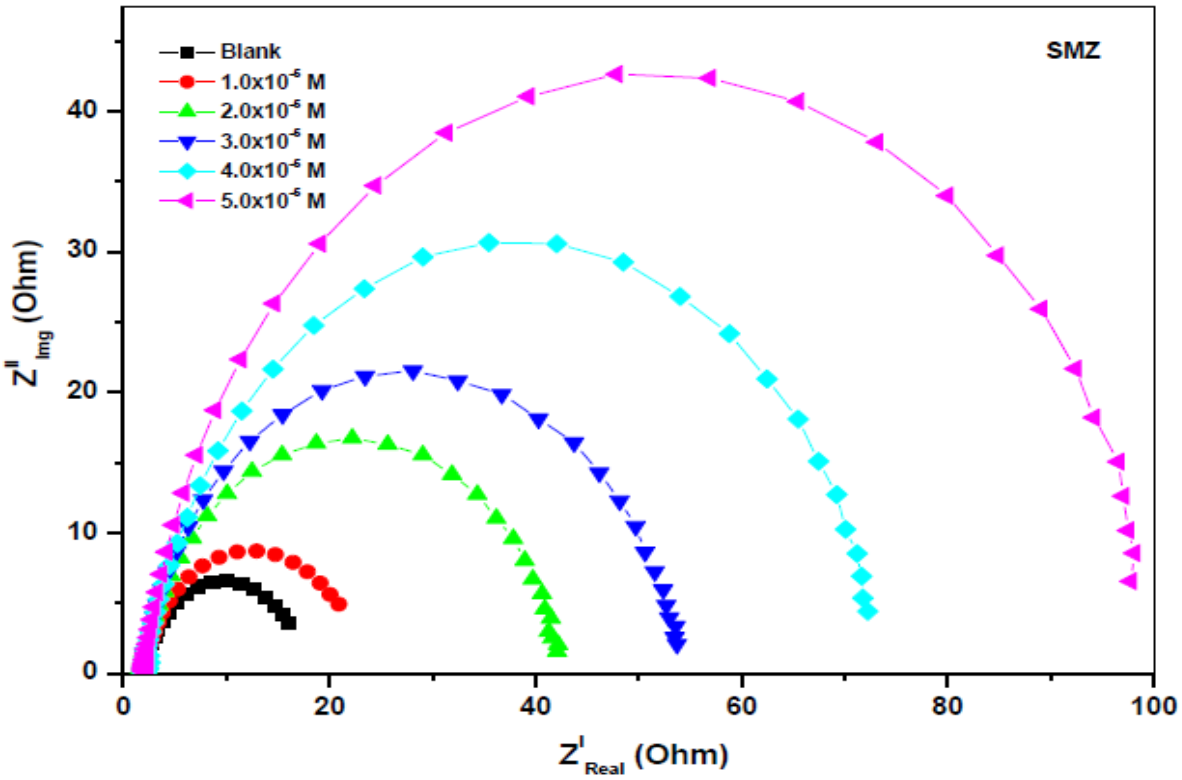

Figure 4.22: Nyquist plot of mild steel in 1 M HCl in the absence and presence of different concentrations of SMZ inhibitor compound.

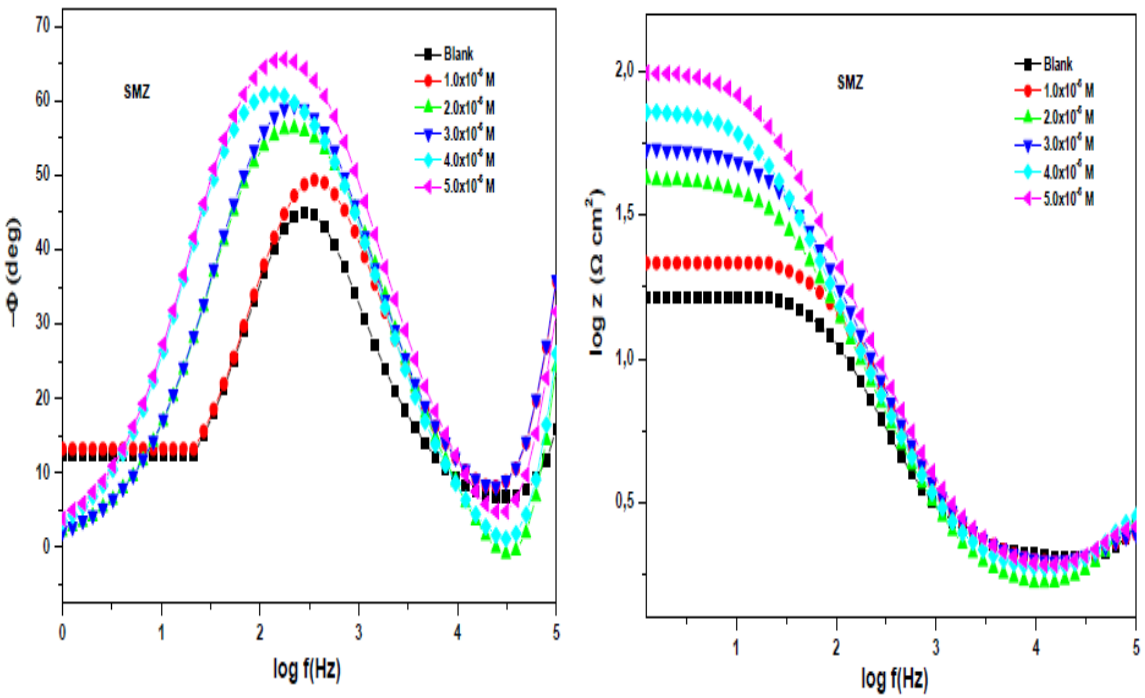

Figure 4.23: Bode plots of mild steel in 1 M HCl in the absence and presence of different concentrations of SMZ inhibitor compound.

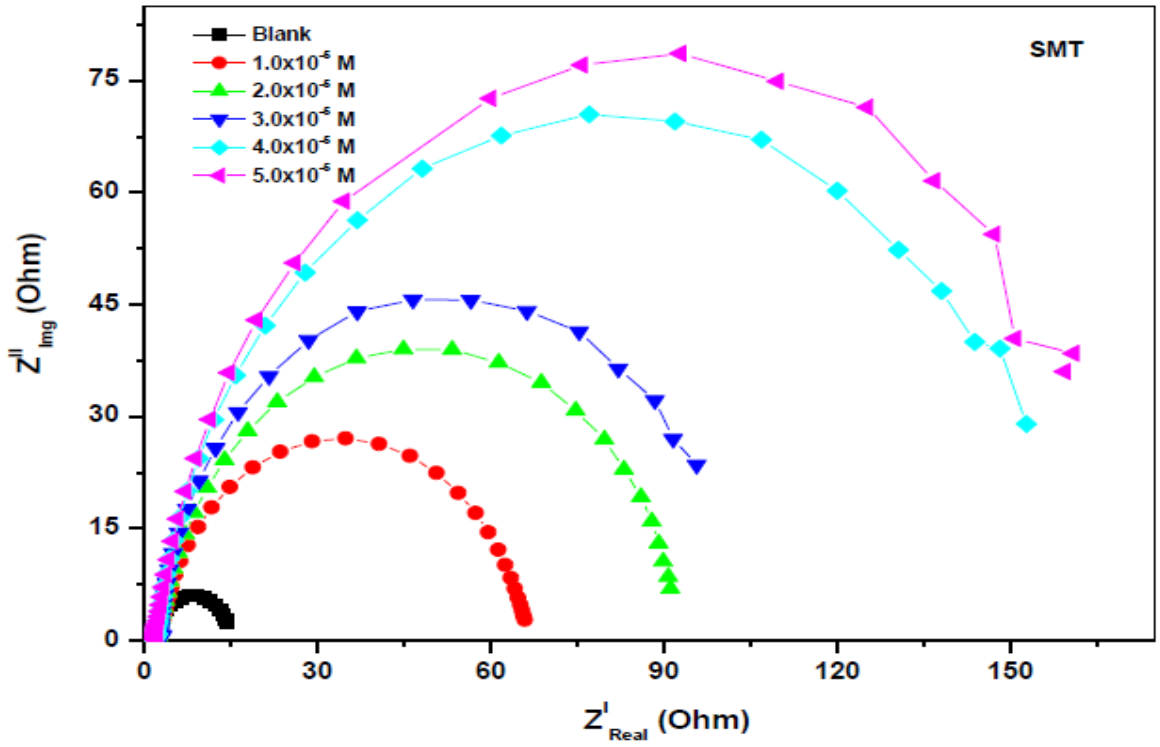

Figure 4.24: Nyquist plot of mild steel in 1 M HCl in the absence and presence of different concentrations of SMT inhibitor compound.

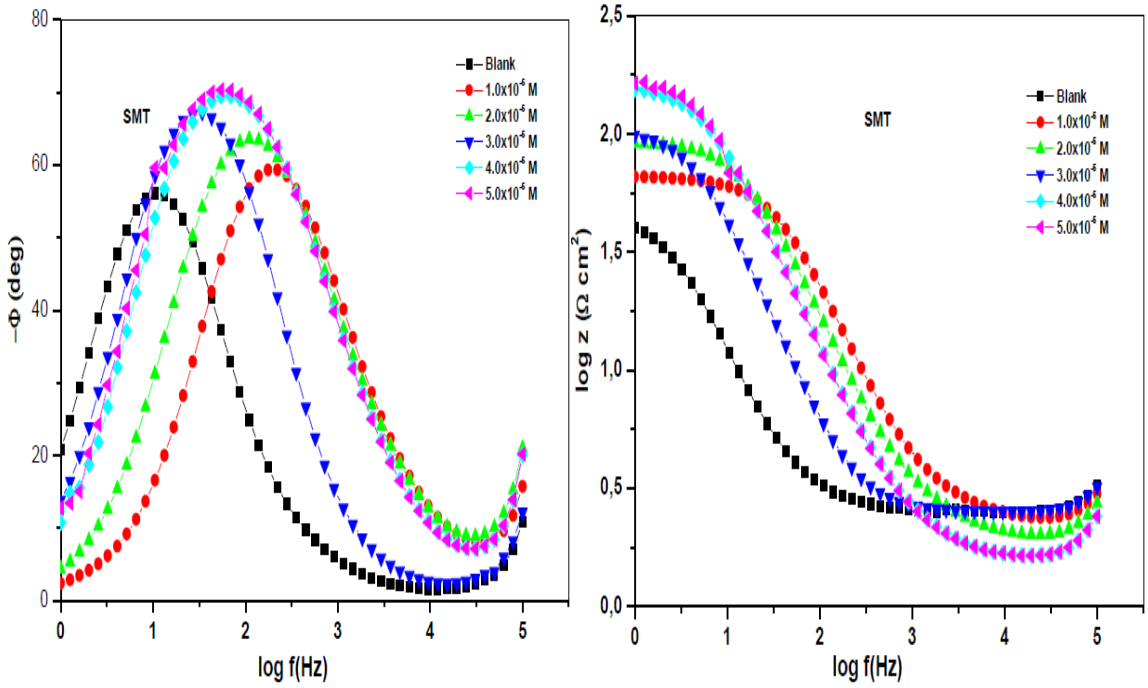

Figure 4.25: Bode plots of mild steel in 1 M HCl in the absence and presence of different concentrations of SMT inhibitor compound.

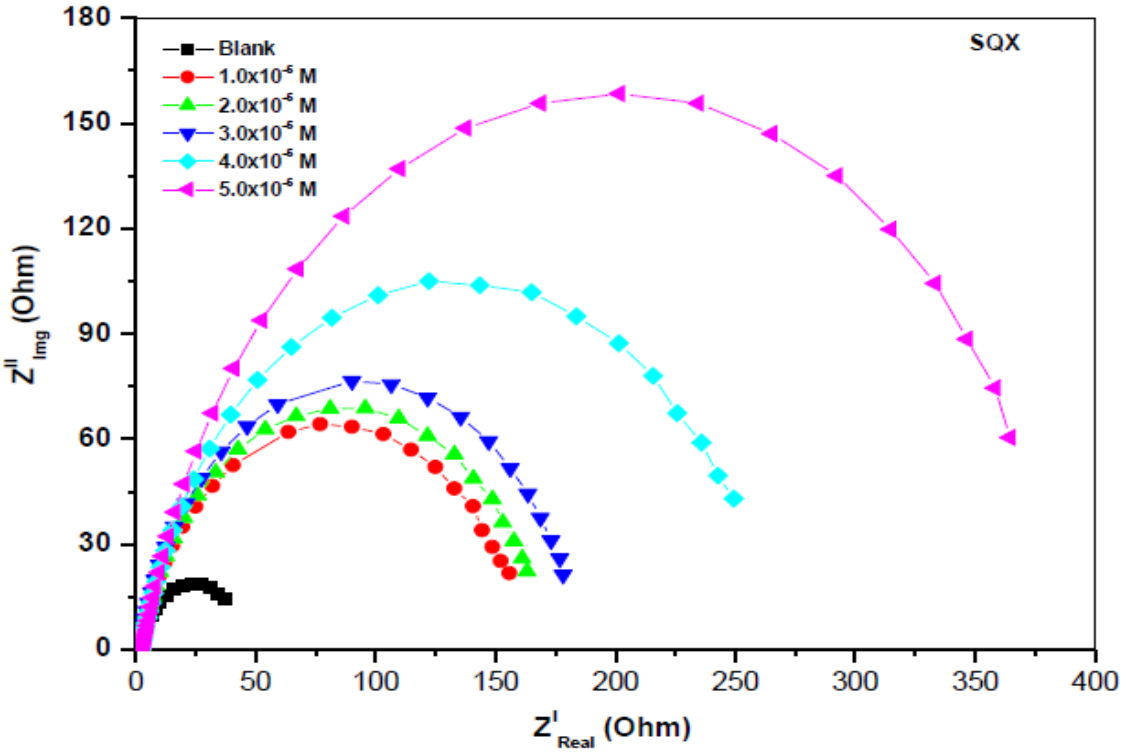

Figure 4.26: Nyquist plot of mild steel in 1 M HCl in the absence and presence of different concentrations of SQX inhibitor compound.

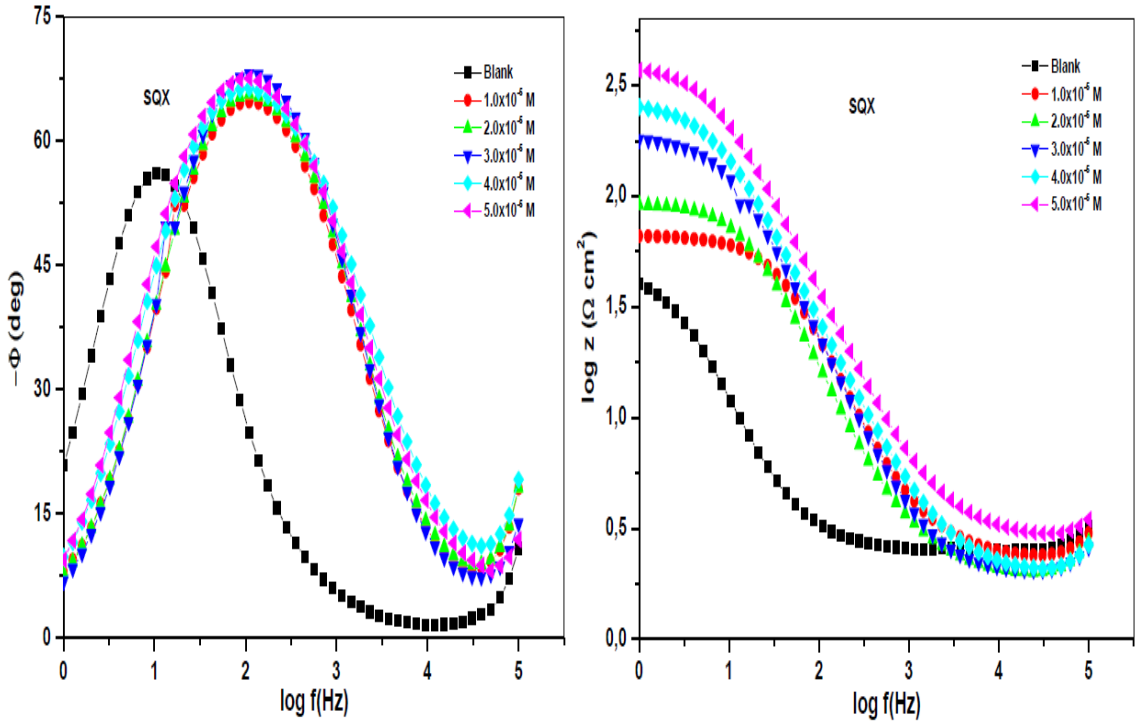

Figure 4.27: Bode plots of mild steel in 1 M HCl in the absence and presence of different concentrations of SQX inhibitor compound.

Observation of Nyquist plots in these figures show depressed capacitive at high-frequency (HF). Previous studies have shown that the low-frequency inductive loop is attributed to bulk relaxation process due to the adsorption of charged species onto the charged metal surfaces while the high-frequency capacitive loop is attributed to the charge transfer and double layer capacitance (C_{dl}) [102, 103].

The impedance nature of the corrosion reactions was explained utilizing a simple electrical equivalent circuit comprising the resistor (R_s), resistance of charge transfer (R_{ct}) and a double layer capacitance [104 − 106]. In order to obtain a more accurate and representative fit, the double layer capacitance was replaced by the constant phase element (CPE) as shown in Figure 4.28.

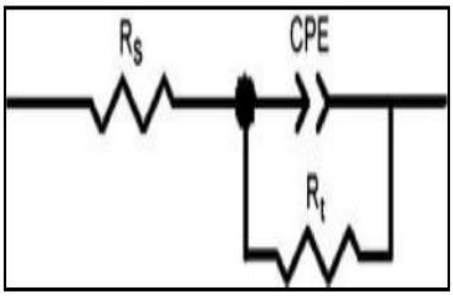

Figure 4.28: Equivalent circuit used to fit the impedance spectra obtained for mild steel corrosion in 1.0 M HCl in the absence and presence of SNA, SBZ, SMX, SCP, SDM, SSZ, SMZ, SMT and SQX.

The CPE is defined by the expression:

$$Z_{CPE} = \frac{1}{Y_0 (j\omega)^n} \tag{55}$$

where Y_0 is the CPE constant, ω is the angular frequency, j is the imaginary number and n is the phase shift (exponent) which is related to the degree of surface inhomogeneity [107]. Depending on the value of n, CPE can represent resistance (n=0, Y_0 = R), capacitance (n=1, Y_0 = C), inductance (n =−1, $Y_0 = L$) or Warburg impedance (n = 0.5, $Y_0 = W$).

The electrochemical impedance parameters such as R_s, R_{ct}, CPE, n and $\%IE_{EIS}$ were equation (49). The results of the calculations of these parameters are reported in Table 4.2.

Table 4.2: Electrochemical impedance (EIS) parameters such as the resistance of charge transfer (R_{ct}), constant phase element (CPE) and the CPE exponent (n) using different inhibitors.

Inhibitor	Inhibitor Conc. (M)	R_s (Ω cm^2)	R_{ct} (Ω cm^2)	n	CPE (μF cm^{-2})	%IE$_{EIS}$	%IE$_{WL}$
Blank		2.05	15.00	0.87	265.1	-	-
SNA	1.0×10^{-5}	1.49	49.90	0.91	157.8	69.94	81.47
	2.0×10^{-5}	1.98	58.20	0.85	147.6	74.23	80.05
	3.0×10^{-5}	1.83	72.60	0.88	125.3	79.33	82.42
	4.0×10^{-5}	1.73	75.80	0.88	114.5	80.21	88.36
	5.0×10^{-5}	1.73	83.70	0.86	101.3	82.08	89.55
SBZ	1.0×10^{-5}	2.09	103.8	0.85	146.2	85.54	75.81
	2.0×10^{-5}	4.19	132.5	0.80	134.6	88.67	82.34
	3.0×10^{-5}	2.65	192.5	0.89	136.5	92.20	89.86
	4.0×10^{-5}	2.99	401.0	0.84	112.4	96.25	90.24
	5.0×10^{-5}	5.35	529.0	0.79	94.60	97.16	92.06
SMX	1.0×10^{-5}	1.92	55.00	0.90	150.0	72.73	79.67
	2.0×10^{-5}	2.11	75.80	0.92	143.9	80.21	67.02
	3.0×10^{-5}	1.93	84.60	0.87	124.6	82.27	84.79
	4.0×10^{-5}	1.87	102.1	0.89	99.80	85.31	81.63
	5.0×10^{-5}	1.99	110.3	0.87	92.30	86.40	86.59
SCP	1.0×10^{-5}	2.36	40.70	0.88	159.4	63.14	74.55
	2.0×10^{-5}	2.47	49.30	0.90	144.0	69.57	82.08
	3.0×10^{-5}	3.30	79.30	0.85	147.6	81.08	87.65
	4.0×10^{-5}	2.65	140.0	0.92	106.4	89.28	90.21
	5.0×10^{-5}	2.59	232.5	0.79	105.7	93.54	91.72
SDM	1.0×10^{-5}	1.79	56.80	0.98	138.9	73.59	71.97
	2.0×10^{-5}	1.95	131.6	0.91	129.3	88.60	85.99
	3.0×10^{-5}	2.08	135.2	0.87	101.9	88.90	89.31
	4.0×10^{-5}	1.99	167.6	0.90	89.60	91.05	89.79
	5.0×10^{-5}	1.92	189.3	0.89	78.70	92.08	93.83
SSZ	1.0×10^{-5}	2.05	43.00	0.88	144.4	65.11	56.76
	2.0×10^{-5}	1.85	72.30	0.88	141.3	79.25	76.24
	3.0×10^{-5}	1.79	112.6	0.83	122.5	86.68	72.44
	4.0×10^{-5}	1.92	120.8	0.81	121.2	87.58	81.95
	5.0×10^{-5}	1.95	129.9	0.88	119.3	88.45	88.36
SMZ	1.0×10^{-5}	1.92	40.40	0.86	134.2	62.87	65.21
	2.0×10^{-5}	1.75	52.30	0.88	108.2	71.32	74.25
	3.0×10^{-5}	1.96	72.30	0.87	102.4	79.25	79.67
	4.0×10^{-5}	195	99.60	0.88	99.3	84.94	82.38
	5.0×10^{-5}	1.97	101.6	0.89	98.7	85.24	85.97
SMT	1.0×10^{-5}	2.42	64.7	0.87	145.8	76.81	75.75
	2.0×10^{-5}	2.06	94.1	0.86	136.8	84.05	84.49
	3.0×10^{-5}	2.57	101.8	0.93	134.7	85.25	87.20
	4.0×10^{-5}	1.70	166.5	0.88	111.2	90.99	88.55
	5.0×10^{-5}	1.69	181.4	0.88	107.8	91.73	92.77
SQX	1.0×10^{-5}	1.97	162.6	0.85	205.7	90.77	65.32
	2.0×10^{-5}	1.96	176.1	0.83	187.6	91.48	78.62
	3.0×10^{-5}	1.98	196.1	0.83	166.8	92.38	82.19
	4.0×10^{-5}	1.99	287.6	0.80	136.5	94.78	88.36
	5.0×10^{-5}	2.76	466.0	0.76	99.3	96.78	89.07

The values of R_{ct} provides details on the magnitude of the electron transfer over the mild steel surface and are directly proportional to the inhibition efficiency [101]. A close examination of the values in Table 4.2 shows that as the concentration of all nine inhibitors is increased, R_{ct} also increases while CPE decreases. This behaviour is a direct result of the increased

surface coverage on mild steel by the inhibitor molecules as a result of their increased concentration. Furthermore, the reduction in CPE indicates the decrease in dielectric constant and an enhancement of the thickness of the electrical double layer. This is a consequence of the adsorption of sulphonamides compounds on the mild steel/ hydrochloric acid interface which brings about the prevention of further corrosion of mild steel [108 − 110]. The values of n are very constant and close to unity which signifies that the interface is of a capacitive nature. The results from EIS correspond very well with those obtained from PDP.

4.1.3 ADSORPTION FILM ANALYSIS (FTIR)

The FT-IR technique is useful in studying the adsorption film resulting during the adsorption process [111]. The FT-IR spectra of the studied corrosion inhibitors as well as the adsorption films formed on the mild steel surface using different corrosion inhibitors are shown in Figures 4.29 − 4.37.

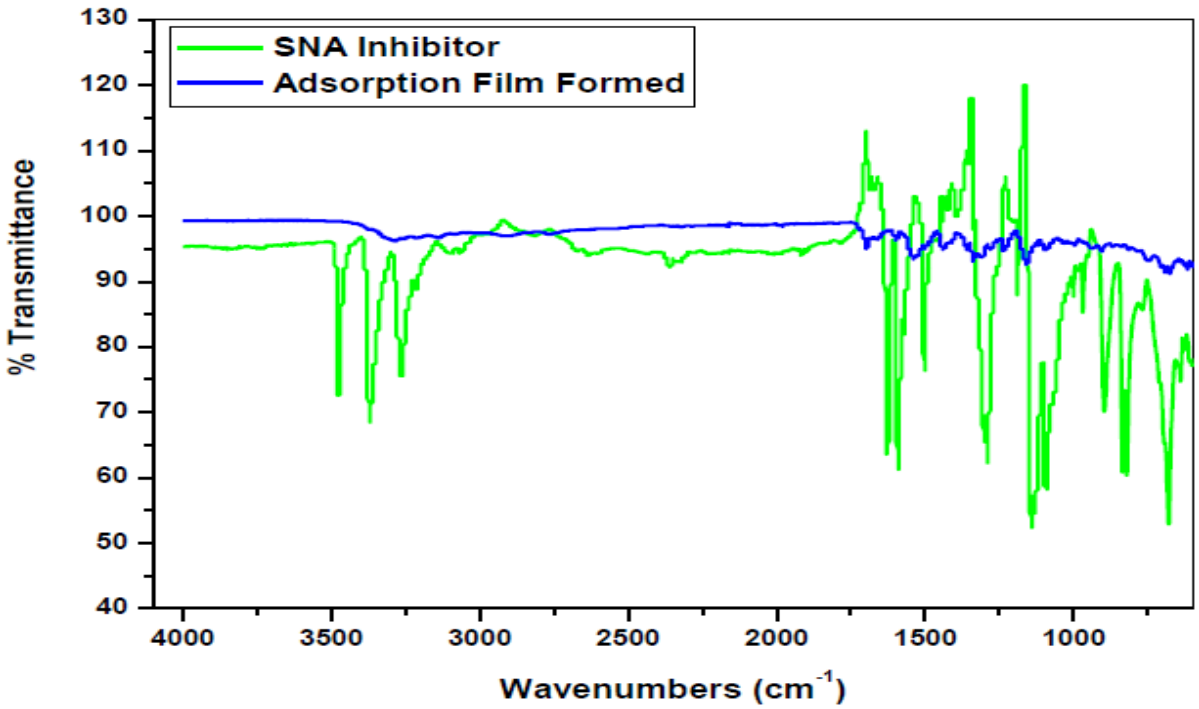

Figure 4.29: FT-IR spectra for the studied corrosion inhibitors and adsorption films formed on the mild steel in 1.0 M HCl using SNA corrosion inhibitor.

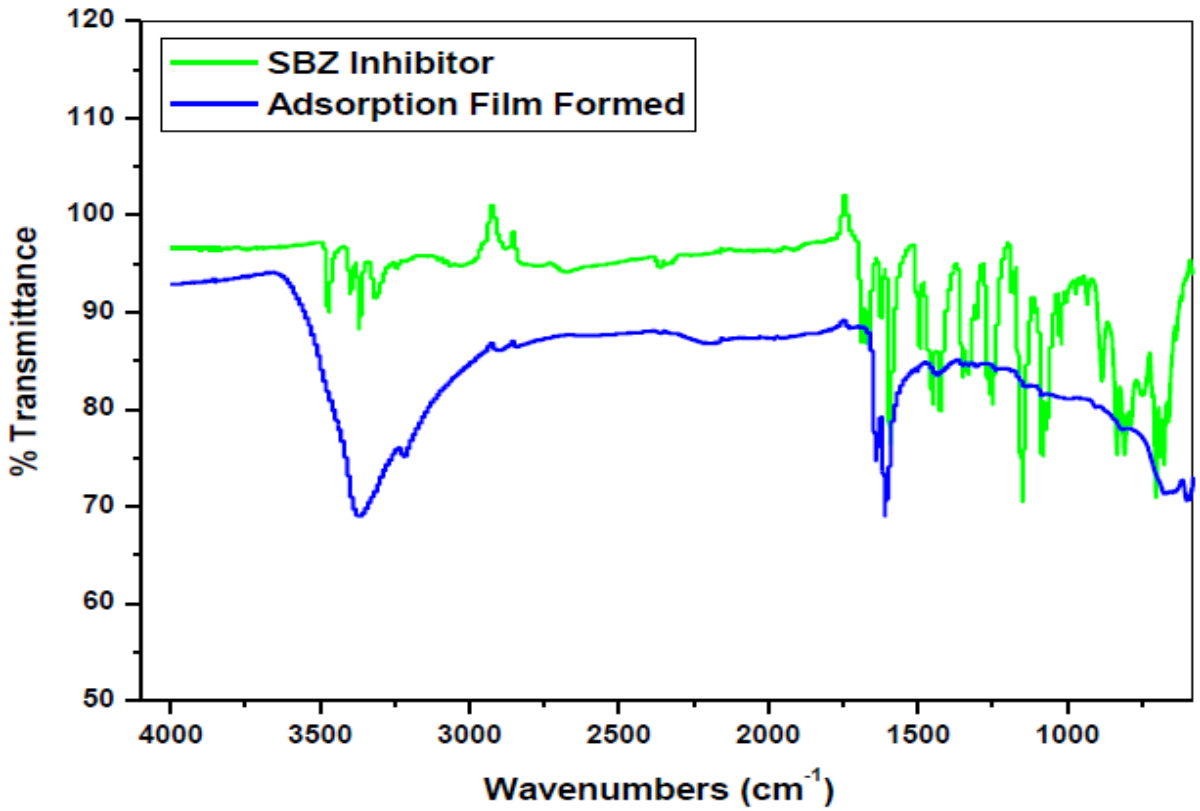

Figure 4.30: FT-IR spectra for the studied corrosion inhibitors and adsorption films formed on the mild steel in 1.0 M HCl using SBZ corrosion inhibitor.

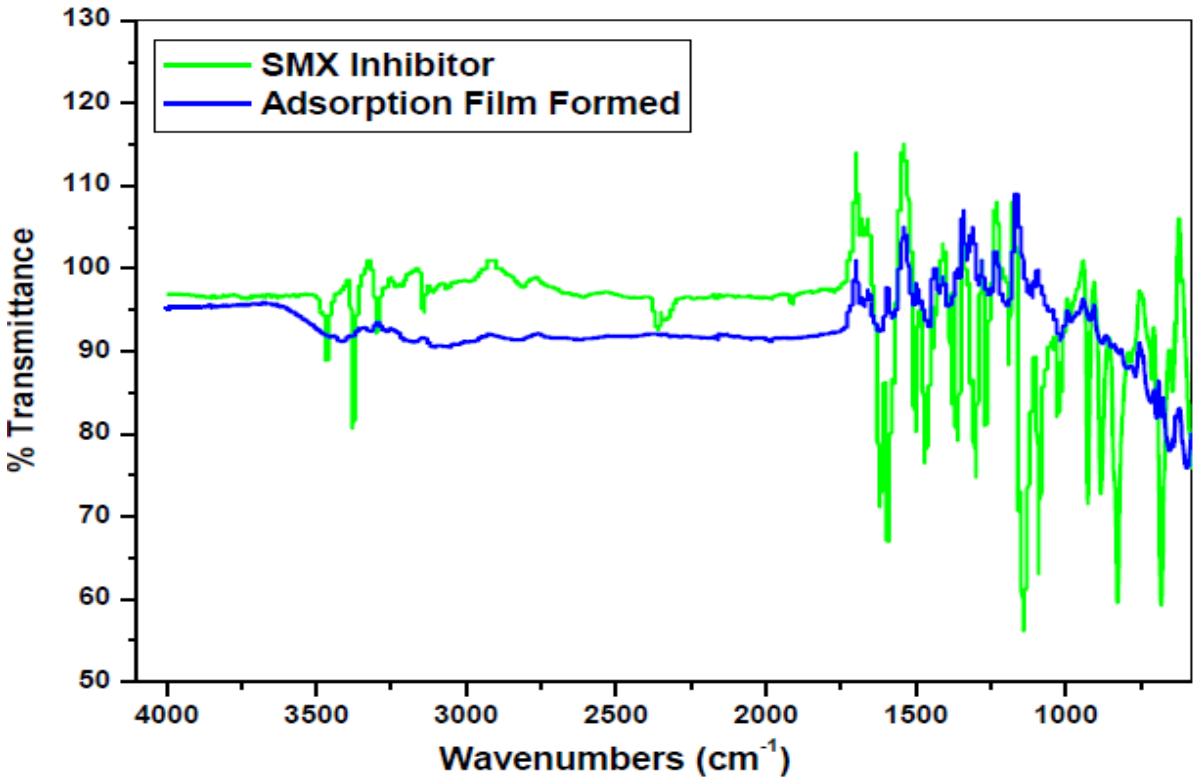

Figure 4.31: FT-IR spectra for the studied corrosion inhibitors and adsorption films formed on the mild steel in 1.0 M HCl using SMX corrosion inhibitor.

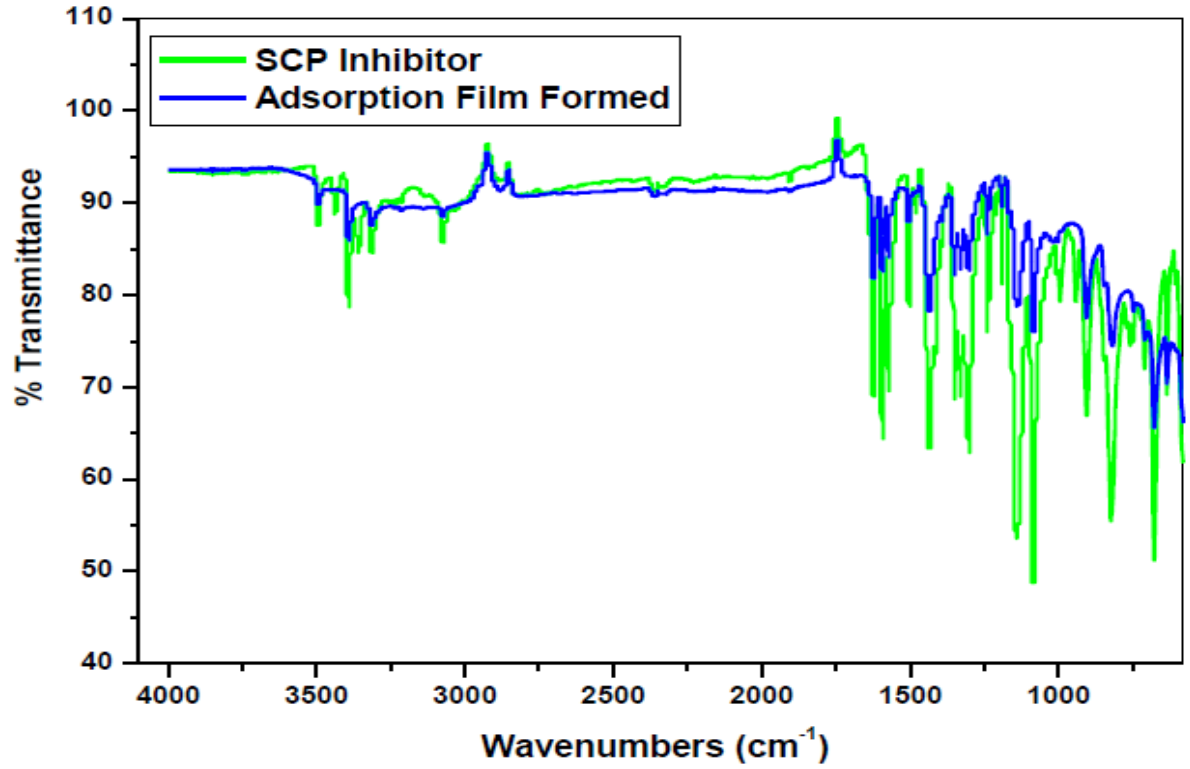

Figure 4.32: FT-IR spectra for the studied corrosion inhibitors and adsorption films formed on the mild steel in 1.0 M HCl using SCP corrosion inhibitor.

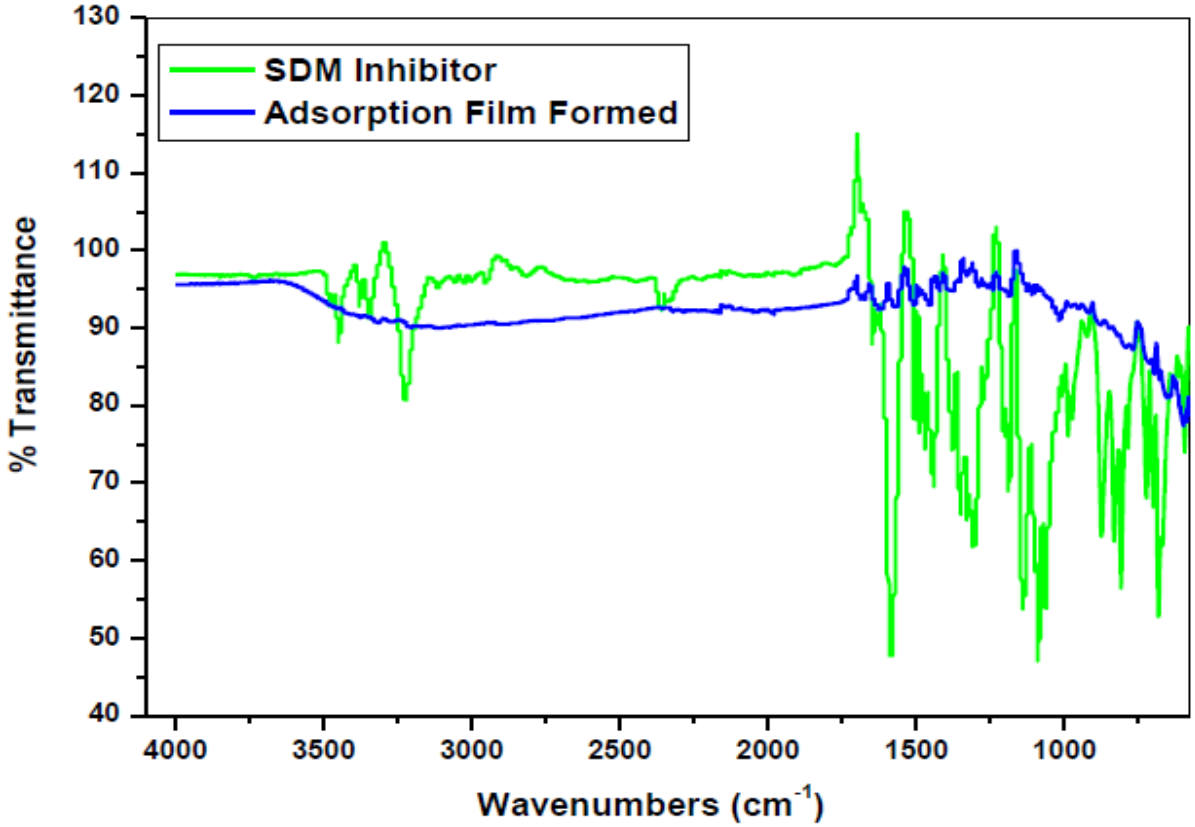

Figure 4.33: FT-IR spectra for the studied corrosion inhibitors and adsorption films formed on the mild steel in 1.0 M HCl using SDM corrosion inhibitor.

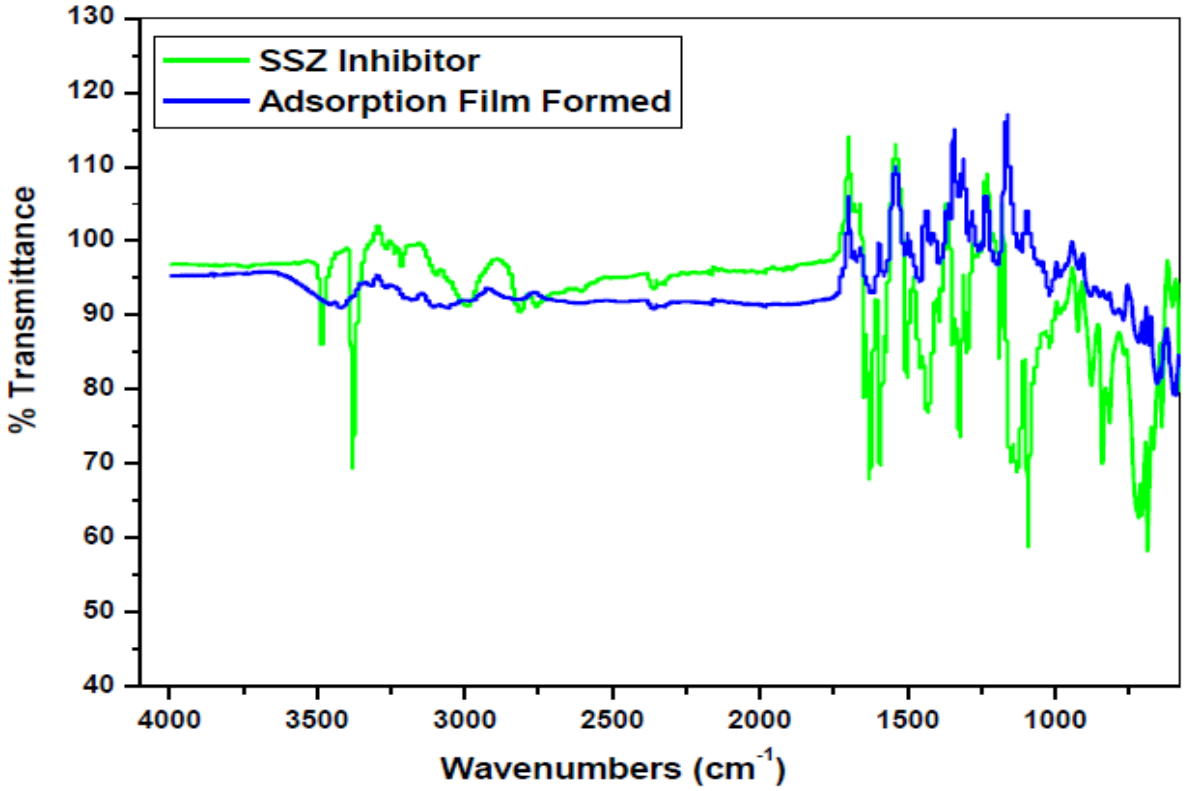

Figure 4.34: FT-IR spectra for the studied corrosion inhibitors and adsorption films formed on the mild steel in 1.0 M HCl using SSZ corrosion inhibitor.

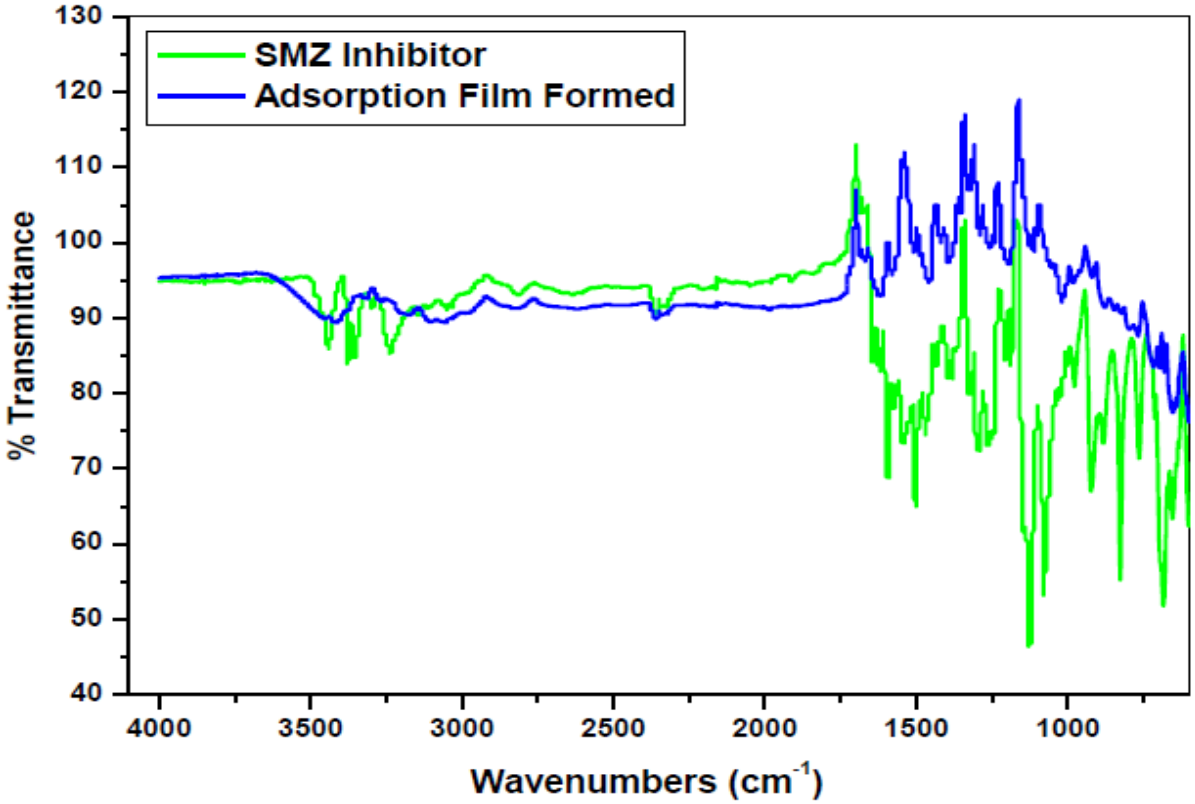

Figure 4.35: FT-IR spectra for the studied corrosion inhibitors and adsorption films formed on the mild steel in 1.0 M HCl using SMZ corrosion inhibitor.

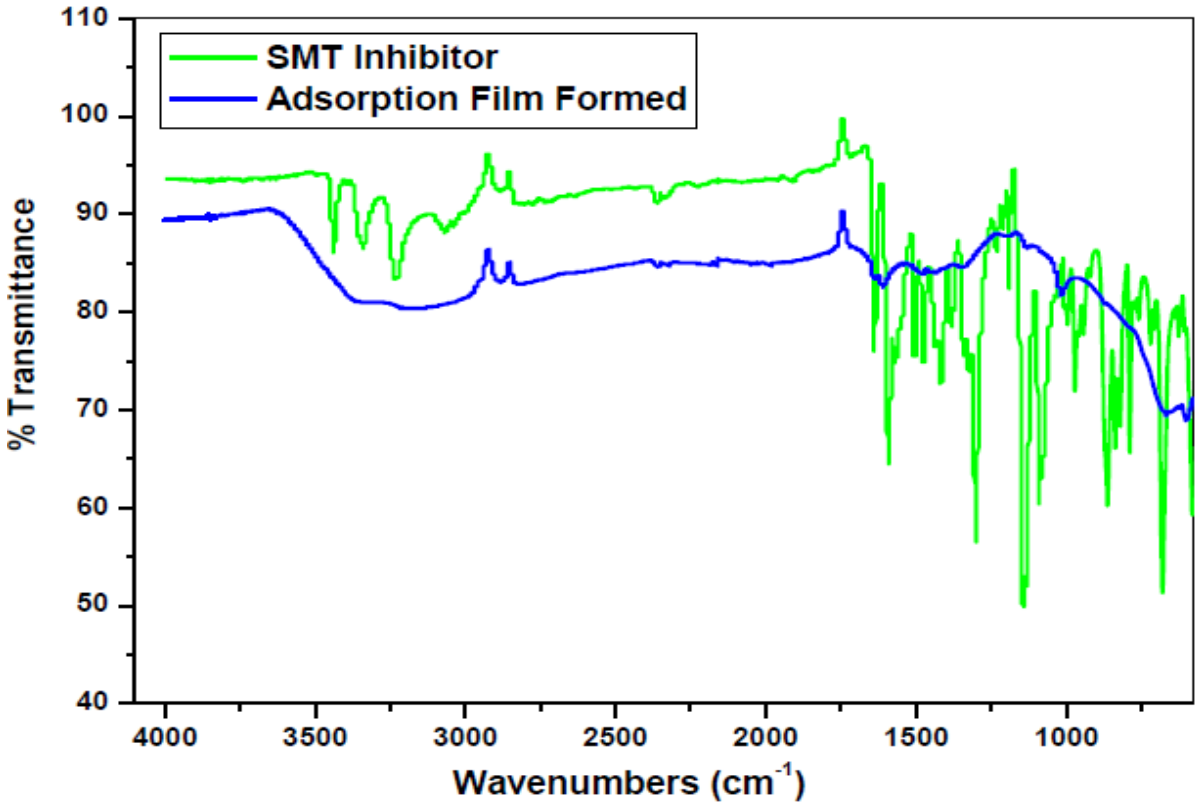

Figure 4.36: FT-IR spectra for the studied corrosion inhibitors and adsorption films formed on the mild steel in 1.0 M HCl using SMT corrosion inhibitor.

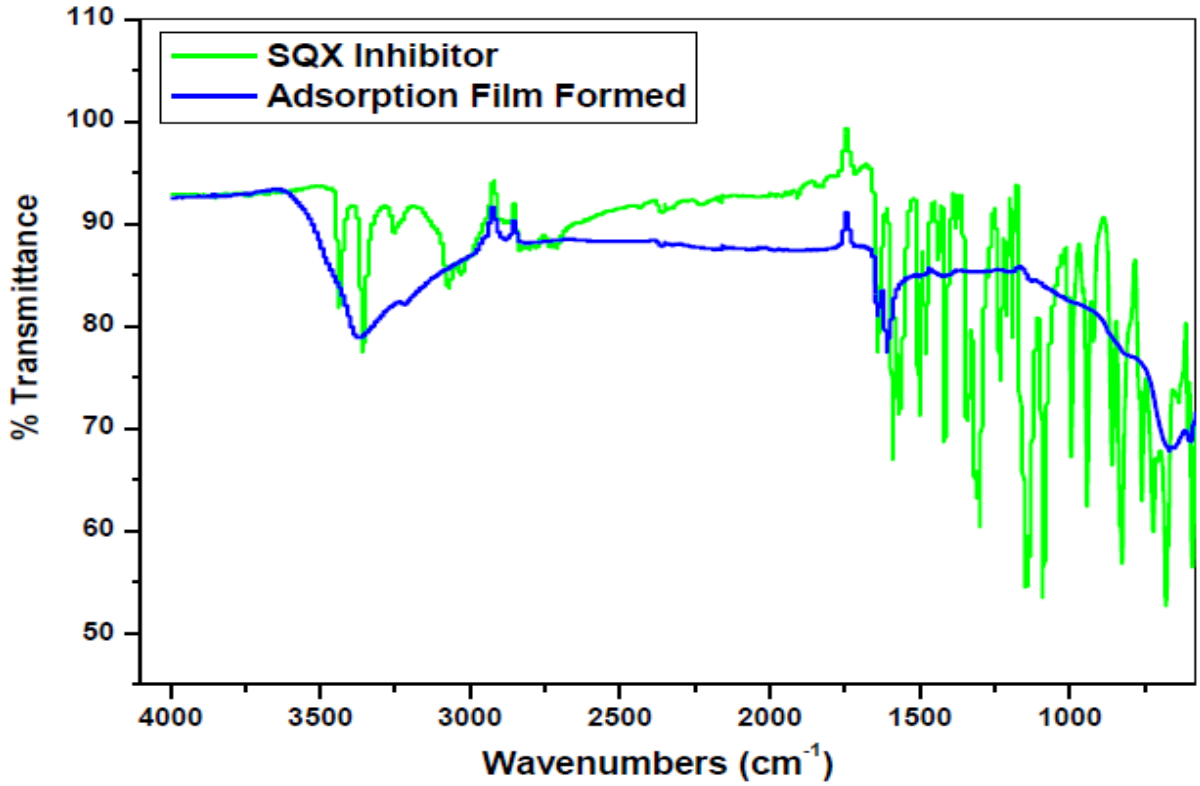

Figure 4.37: FT-IR spectra for the studied corrosion inhibitors and adsorption films formed on the mild steel in 1.0 M HCl using SQX corrosion inhibitor.

Sulphonamides possess several functional groups that have high electron density. This implies that the adsorption film between vacant *d*-orbitals of the metal and the sulphonamides is most likely to take place within these functional groups.

Table 4.3: Peaks and their identification, from FT-IR spectra of the studied corrosion inhibitors and adsorption films formed (i.e. SQX-MS) on the mild steel in 1.0 M HCl using different corrosion inhibitors.

Inhibitor-Mild Steel	**Functional Groups Peaks from FT-IR Spectra (cm^{-1})**					
	N-H	**NH_2**	**C=C**	**O=S=O**	**C-N**	**γ-Fe_2O_3**
SNA	3371.17	1592.89	1503.33	–	1142.70	–
SNA-MS	–	1538.98	1439.75	1339.05	1157.81	666.35
SBZ	3365.41	1592.88	1452.55	1331.61	1151.12	–
SBZ-MS	3366.31	1639.77	1609.25	–	1139.67	667.05
SMX	3376.52	1617.33	1501.78	1302.24	1141.39	–
SMX-MS	–	1622.89	–	–	–	597.64
SCP	3399.99	1624.57	1593.11	1330.51	1141.92	–
SCP-MS	3393.62	1622.06	1596.67	–	1137.30	667.25
SDM	–	1584.77	1504.74	1305.64	1139.74	–
SDM-MS	–	–	–	–	–	653.82
SSZ	3379.05	1627.48	1594.26	1322.81	1131.67	–
SSZ-MS	–	1622.98	1456.68	–	–	–
SMZ	–	–	1503.36	–	1126.18	–
SMZ-MS	–	1622.74	1456.35	–	1196.19	–
SMT	3342.84	1570.68	1591.80	1300.96	1143.93	–
SMT-MS	–	1641.80	1605.13	–	1134.03	667.60
SQX	3356.94	1590.11	1502.34	1343.94	1146.34	–
SQX-MS	3371.95	1638.98	1607.95	–	1136.85	667.21

Table 4.3 shows the characteristic absorption bands corresponding to the main electron source groups within the studied compounds and compares them with those that are obtained from the adsorption film of the inhibited process. Characteristic absorption bands within the wavenumber range of 1190-1130 cm^{-1} corresponds to the C-N stretch for secondary amine [109], 3490-3430 cm^{-1} and 3360-3310 cm^{-1} to heterocyclic amine N-H stretch and aliphatic secondary amine N-H stretch, respectively [110, 112], 1650-1590 cm^{-1} to NH_2 primary amine N-H bend [109], 1350-1325 cm^{-1} to O=S=O [108] and 1600, 1500 cm^{-1} to aromatic, conjugated C=C [109, 110]. The presence of bands at 3371.95 cm^{-1}, 1638.98 cm^{-1}, 1607.95 cm^{-1}, 1136.85 cm^{-1} and 667.21 cm^{-1} corresponding to N-H stretch, NH_2 group, aromatic conjugated C=C, C-N stretch and γ-Fe_2O_3, respectively for SQX signifies the formation of SQX-Fe^{2+} complex. Similar discussion was used for SNA, SBZ, SMX, SCP, SDM, SSZ, SMZ and SMT as reported in Table 4.3 and shown in Figures 4.29 − 4.38.

Nevertheless, a meticulous examination of all FT-IR spectra of inhibitor-Fe^{2+} complex in the absorption range between 1700-500 cm^{-1} shows that most of the characteristic absorption bands have disappeared. The disappearance of O=S=O, which is one of the possible electron donor, is more pronounced with respect to all four inhibitors. Another interesting observation is made with regard to SMT which shows the disappearance of a band corresponding to N-H, which is another possible electron donor. Therefore, the O=S=O functional group is the most preferred site for interaction with the mild steel surface. The lone pair of electrons on the O atoms in this functional group could donate electrons to the vacant or partially filled d orbitals of the Fe metal atoms and thereby result in the formation of a chemical bond and in the eventual protection of the metal surface. The N-H functional group from SMT also shows reactivity to some extent. The last column in Table 4.3 shows the characteristic absorption bands in the region of 450-700 cm^{-1} for all inhibitors. Literature indicates that these bands correspond to the passivating iron oxide layers (γ-Fe_2O_3) [112]. These layers are formed during the corrosion of mild steel in acidic medium. Studies have shown that passivating layers of iron oxide can also aid protection of mild steel from further destructions by the aggressive ions in acidic solutions [113, 114].

4.1.4 SURFACE ANALYSIS (SEM)

SEM micrographs and their corresponding EDS spectra for various mild steel specimens were taken in order to gain more insight into the adsorption process taking place during the corrosion process.

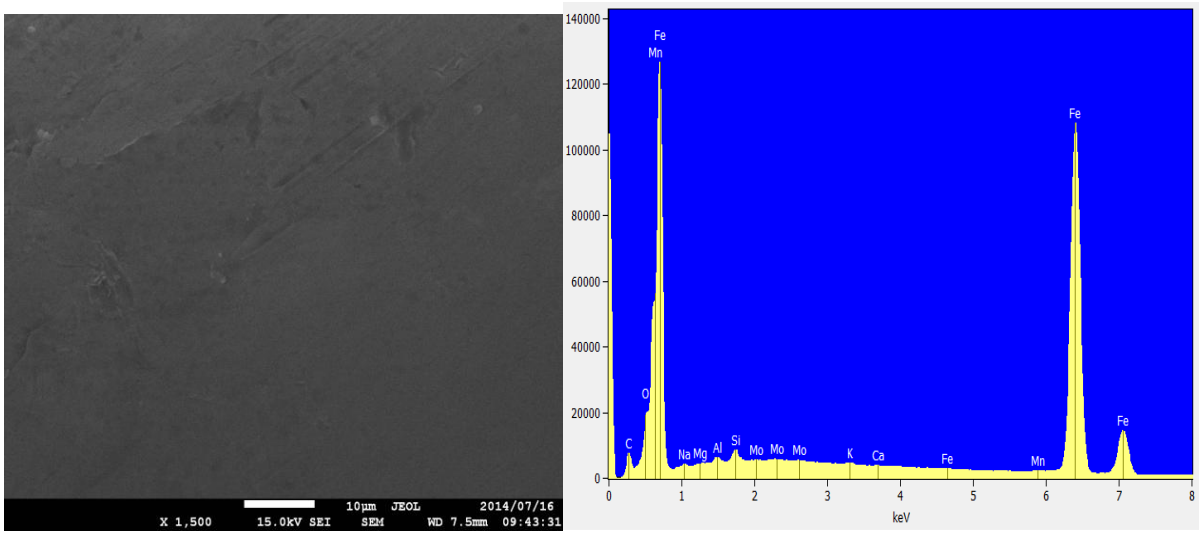

Figure 4.38: SEM micrograph of the surface of mild steel and EDS spectrum of plain mild steel specimen used in this study.

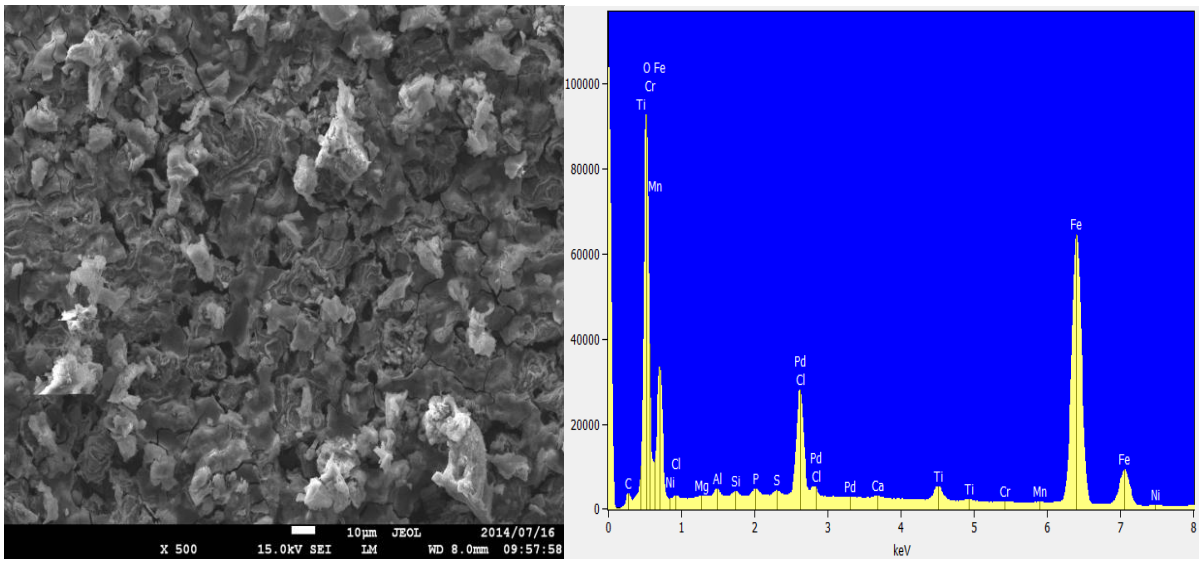

Figure 4.39: SEM micrograph of the surface of mild steel and EDS spectrum of mild steel immersed in HCl uninhibited.

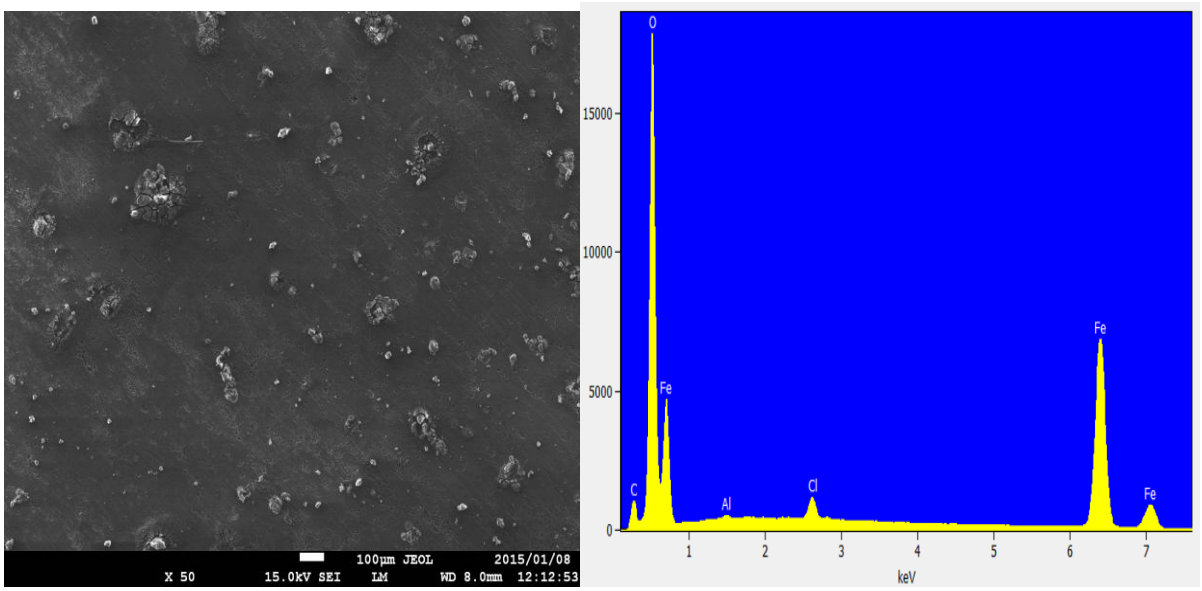

Figure 4.40: SEM micrograph of the surface of mild steel and EDS spectrum of mild steel immersed in HCl in the presence of SNA corrosion inhibitor.

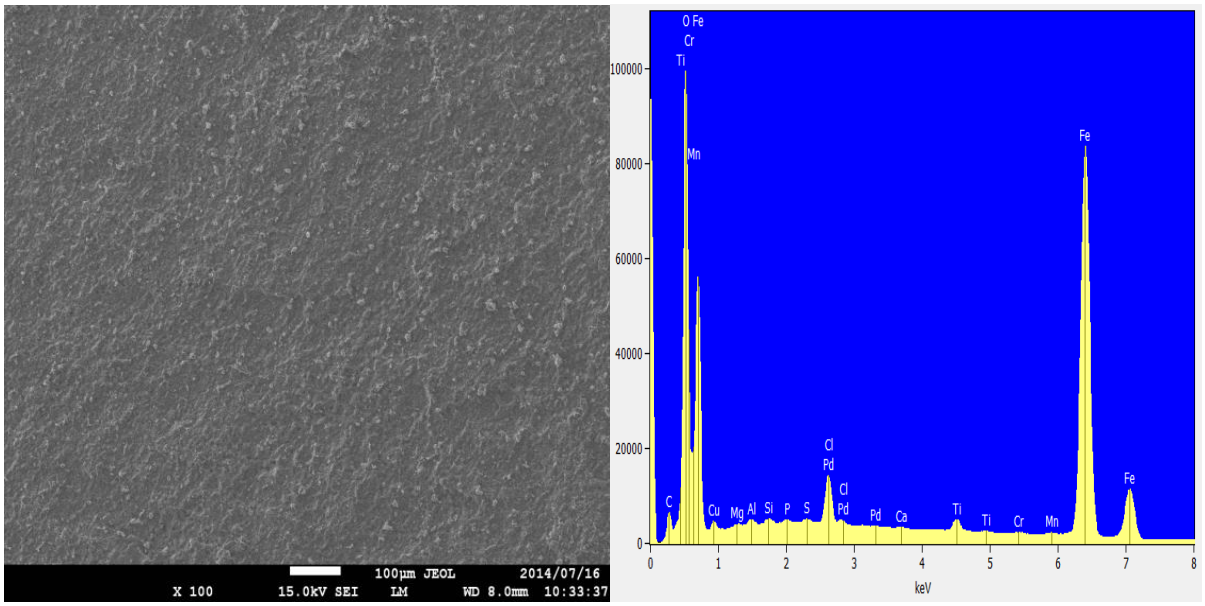

Figure 4.41: SEM micrograph of the surface of mild steel and EDS spectrum of mild steel immersed in HCl in the presence of SBZ corrosion inhibitor.

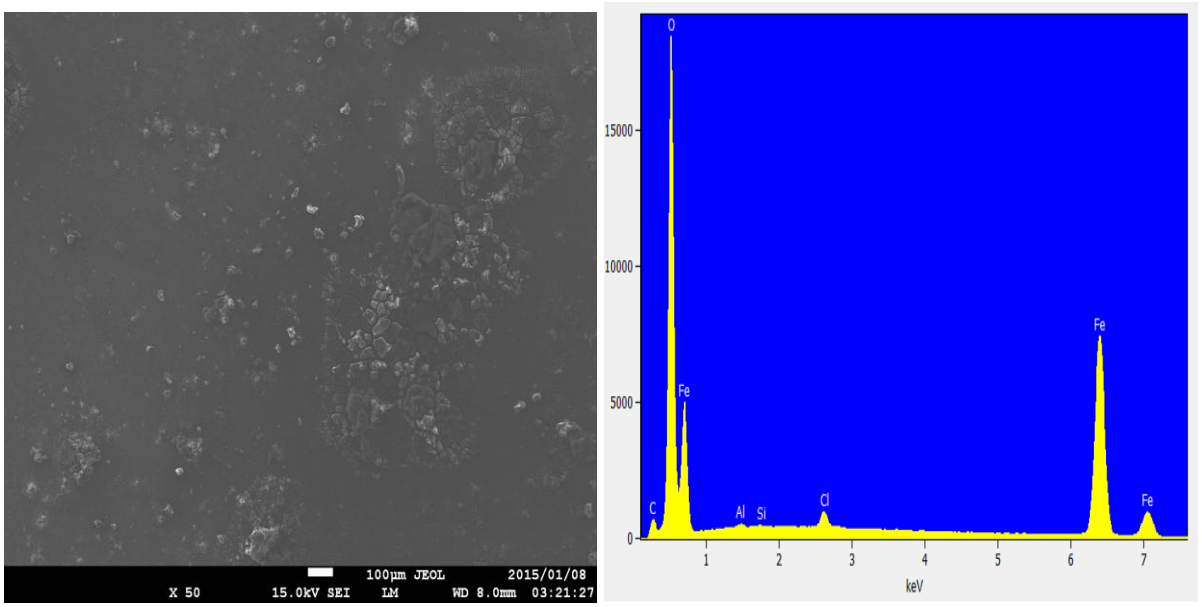

Figure 4.42: SEM micrograph of the surface of mild steel and EDS spectrum of mild steel immersed in HCl in the presence of SMX corrosion inhibitor.

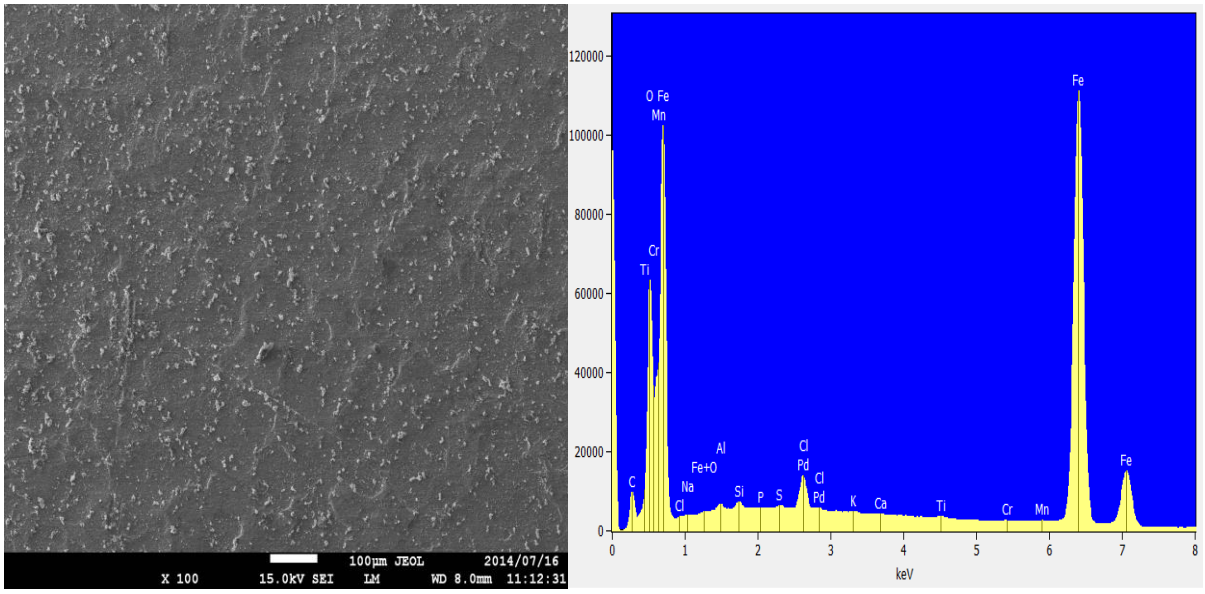

Figure 4.43: SEM micrograph of the surface of mild steel and EDS spectrum of mild steel immersed in HCl in the presence of SCP corrosion inhibitor.

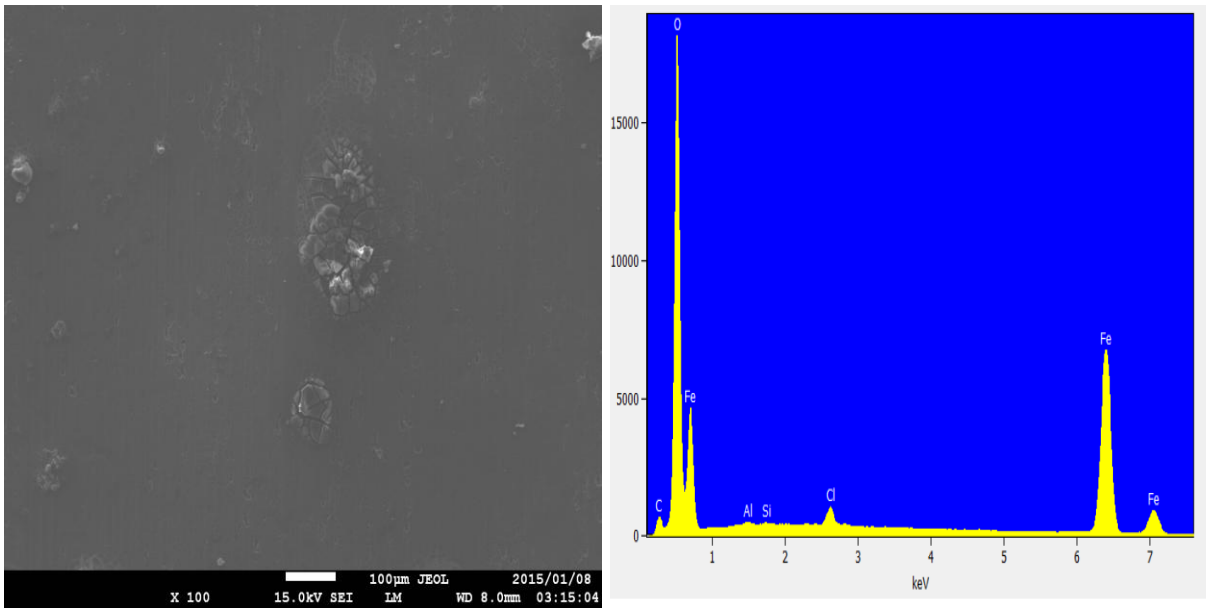

Figure 4.44: SEM micrograph of the surface of mild steel and EDS spectrum of mild steel immersed in HCl in the presence of SDM corrosion inhibitor.

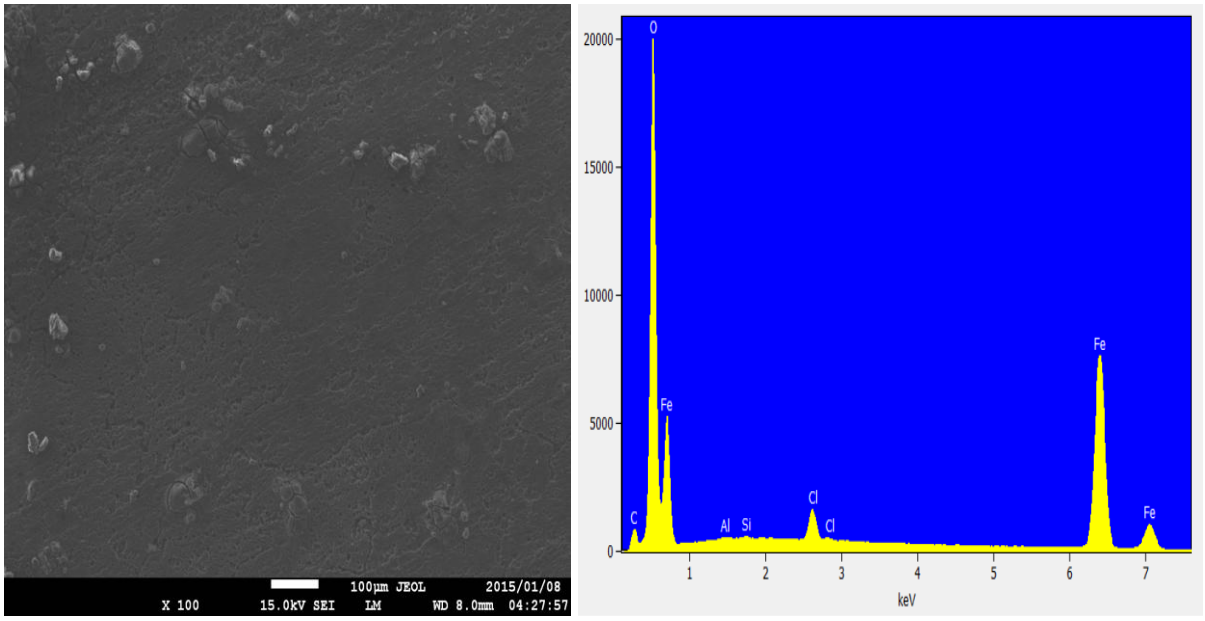

Figure 4.45: SEM micrograph of the surface of mild steel and EDS spectrum of mild steel immersed in HCl in the presence of SSZ corrosion inhibitor.

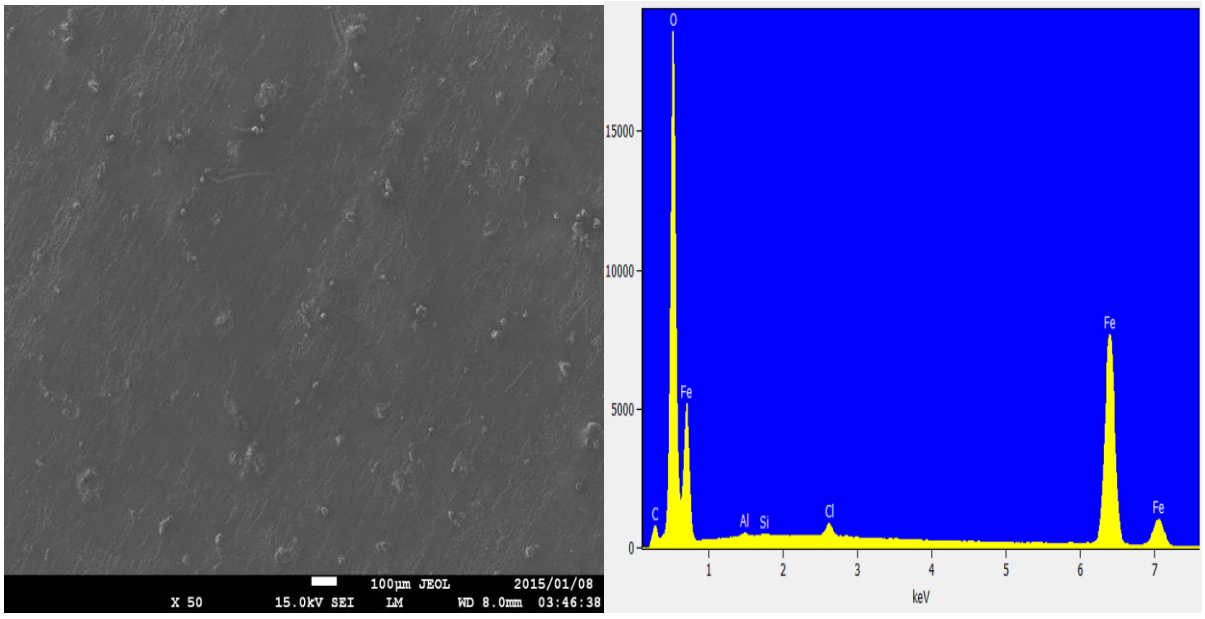

Figure 4.46: SEM micrograph of the surface of mild steel and EDS spectrum of mild steel immersed in HCl in the presence of SMZ corrosion inhibitor.

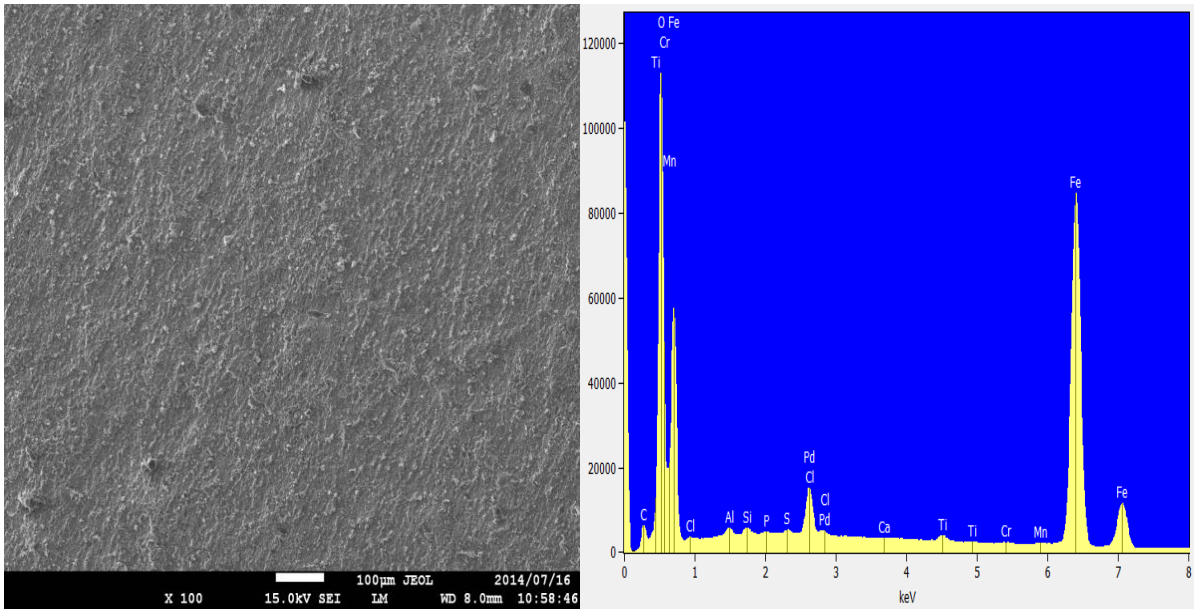

Figure 4.47: SEM micrograph of the surface of mild steel and EDS spectrum of mild steel immersed in HCl in the presence of SMT corrosion inhibitor.

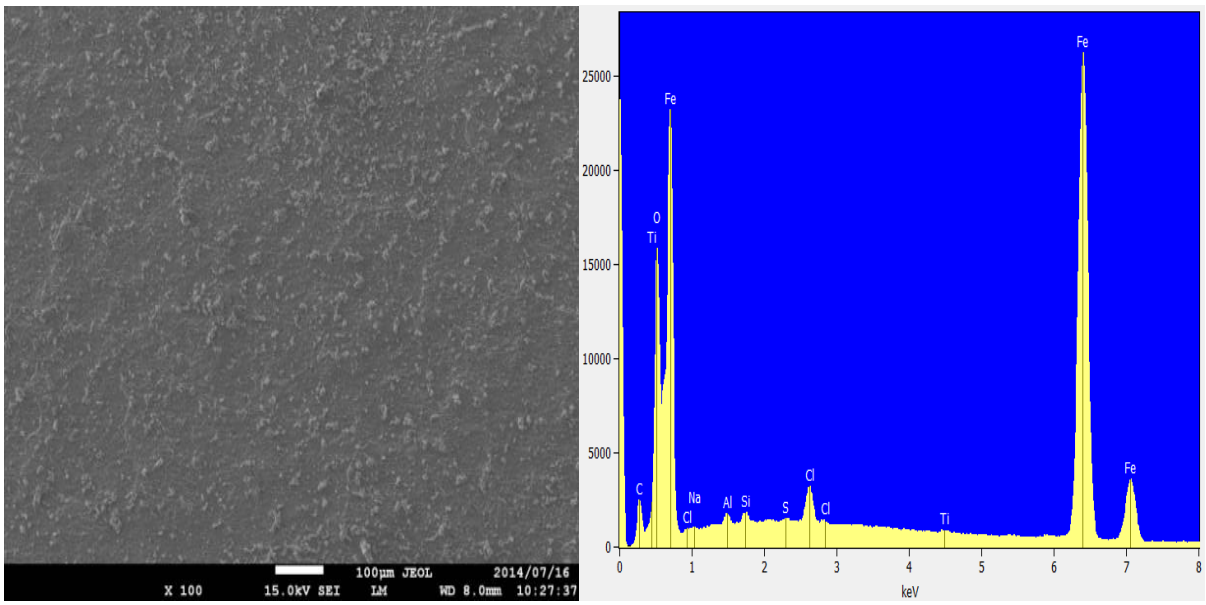

Figure 4.48: SEM micrograph of the surface of mild steel and EDS spectrum of mild steel immersed in HCl in the presence of SQX corrosion inhibitor.

The results are shown in Figures 4.39 − 4.49, respectively. From Figure 4.39 it is evident that the surfaces of mild steel prior immersion in hydrochloric acid solutions exhibit a smooth nature with minor damages that might be due to the abrasion with various emery papers. Nevertheless, these surfaces exhibit a more rough nature after their immersion in hydrochloric acid solutions as shown in Figure 4.40. A consideration of the corresponding EDS spectra in Figures 4.39 and 4.40 show the absence and presence of aggressive Cl^- ions, respectively which are responsible for the destruction of the smooth surfaces of mild steel [111, 115 − 117]. A comparison of SEM micrographs of mild steel in the presence of all nine corrosion inhibitors utilized in this study with those of the uninhibited surfaces shows that the availability of inhibitor compounds prevents the surfaces of mild steel from corrosion. This is evident from the smooth surfaces shown in Figures 4.41 − 4.49. The corresponding EDS spectra for these images are also shown in Figures 4.41 − 4.49. From these spectra it is easy to see that the absence of Cl^- ions is pronounced. It can be inferred that the sulphonamides compounds utilized exhibit better inhibition efficiency through the formation of the adsorption film on the mild steel surface. Similar observations were reported by Tang et al., [118] and Thiraviyam et al., [119], who concluded that protective adsorption films reduces corrosion rate and enhances inhibition efficiency due to the fact that they reduce the contact between mild steel surfaces and the acidic solutions.

4.1.5 CORROSION RATE AND INHIBITION EFFICIENCY

The variation of percentage inhibition efficiency from the weight loss measurements (%IE) with inhibitor concentration at 30 − 50 °C are shown in Figures 4.50 − 4.52.

The trend of the %IE versus inhibitor concentration is almost similar for all the nine inhibitors utilized at 30 − 50 °C. All nine inhibitors exhibit the highest %IE at their highest concentration of 5.0×10^{-5} M. The main reason behind this is the fact that at 5.0×10^{-5} M there is a greater availability of inhibitor molecules than at 1.0×10^{-5} M. The presence of more inhibitor molecules leads to a greater tendency of adsorption of inhibitor molecules on the surface of the metal, thus higher %IE.

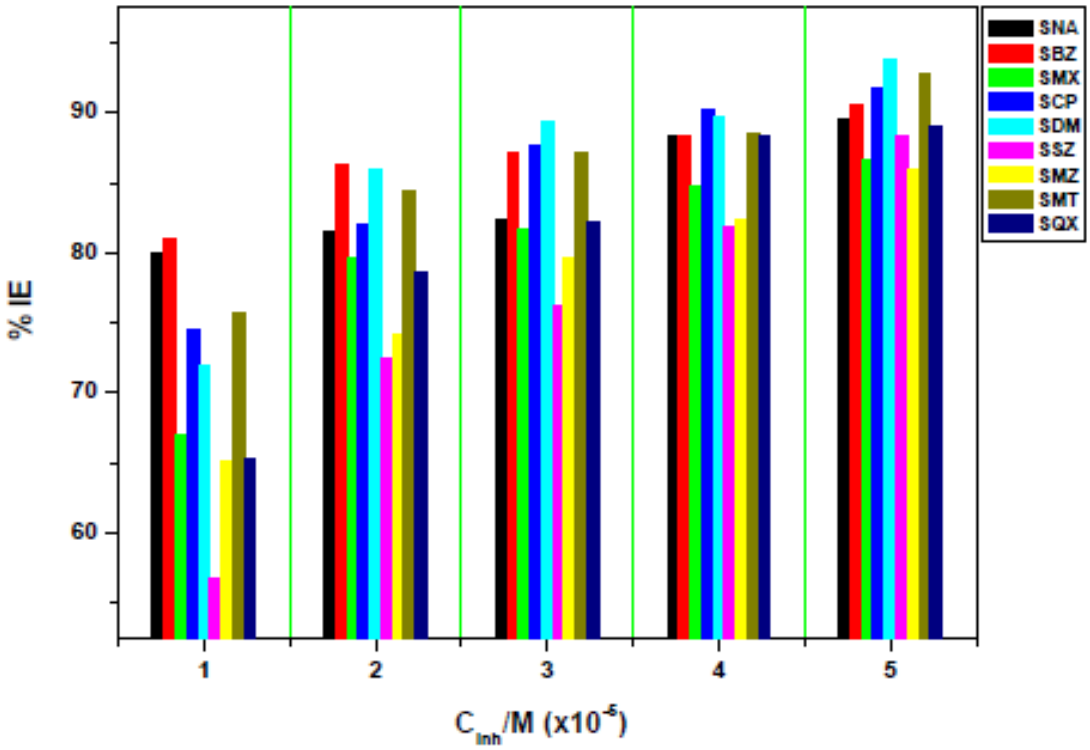

Figure 4.49: Variations of the percentage inhibition efficiencies (%IE) with various concentrations of the utilized corrosion inhibitors at 30 °C.

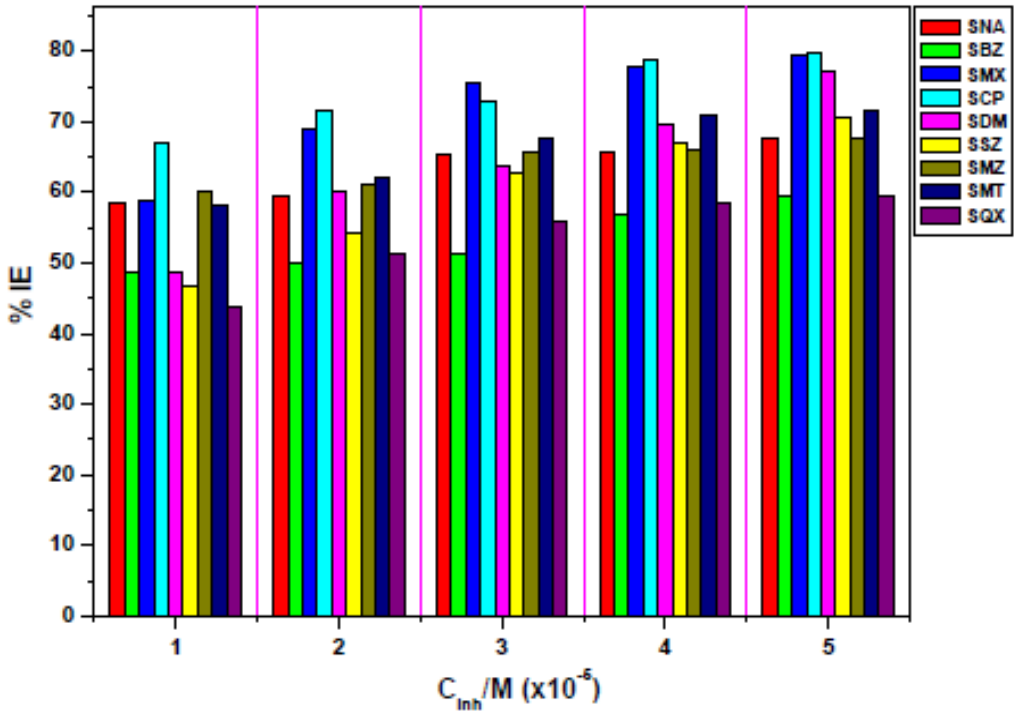

Figure 4.50: Variations of the percentage inhibition efficiencies (%IE) with various concentrations of the utilized corrosion inhibitors at 40 °C.

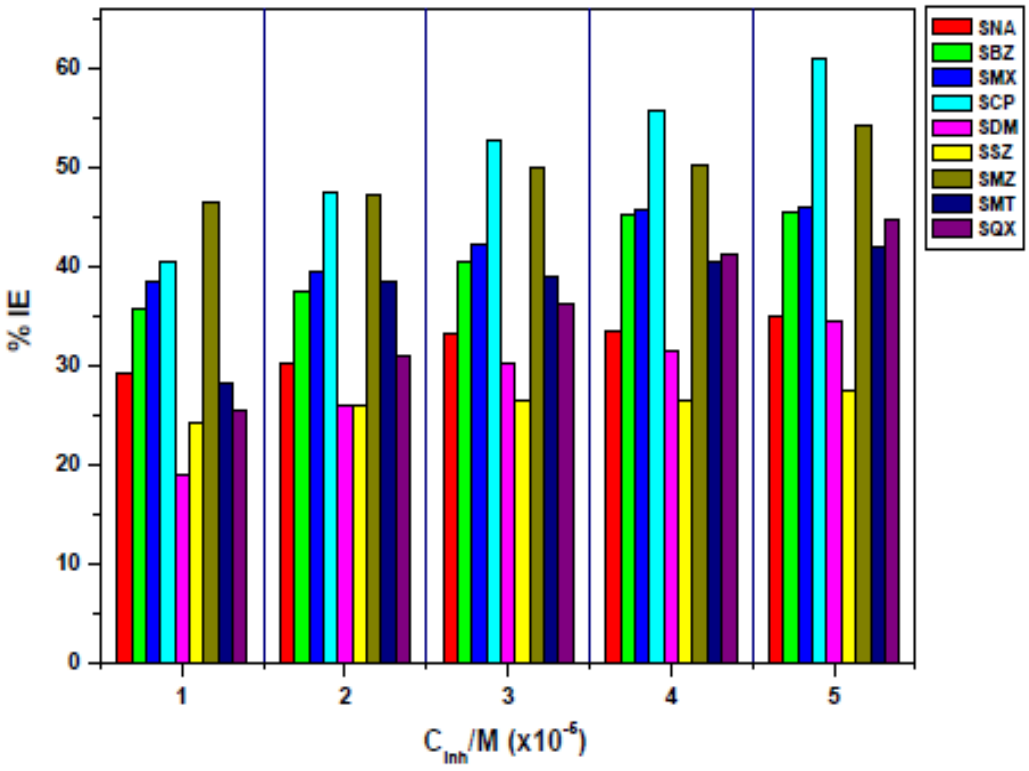

Figure 4.51: Variations of the percentage inhibition efficiencies (%IE) with various concentrations of the utilized corrosion inhibitors at 50 °C.

These results show that the inhibition efficiency increases as the concentration of the inhibitor is increased for all the sulphonamides studied. For instance, at the concentration of 1.0 x 10^{-5} M SNA the inhibition efficiency is 80.05 % and increases to 89.55 % at 5.0 x 10^{-5} M at 30 °C. The same trend is shown in the case of SBZ wherein the obtained inhibition efficiency at 1.0 x 10^{-5} M is 80.99 % and at 5.0 x 10^{-5} M is 90.49 % at the same temperature.

Figure 4.49 shows the relationship between the inhibition efficiencies and the concentrations of the nine inhibitors, namely SNA, SBZ, SMX, SCP, SDM, SSZ, SMZ, SMT and SQX at 30° C. The inhibition efficiency increased with the increase in the concentration of the inhibitor in all cases involving these nine sulphonamides with the maximum efficiency achieved at the highest concentration of 5.0 x 10^{-5} M. The fact that the weight loss is decreased with the increase in the inhibitor concentration implies that the corrosion rate is reduced. This may be due to the adsorption process between the inhibitor and the mild steel surface.

Figure 4.50 shows the relationship between the inhibition efficiencies and the concentrations of the nine inhibitors, SNA, SBZ, SMX, SCP, SDM, SSZ, SMZ, SMT and SQX at 40° C. The effect of the surrounding temperature is clearly shown by the comparing Figures 4.49 and 4.50. Interesting observations indicate that at 30° C, the least performing inhibitor is SSZ with the inhibition efficiency of 56.76 % and SDM being the best performing with inhibition efficiency of 93.83 % at the highest concentration of 5.0 x 10^{-5} M. Nevertheless, as the temperature is increased to 40° C, the performance of the inhibitor compounds also changed with the least performing inhibitor being SQX with the inhibition efficiency of 43.84 % and SCP being the best performing with inhibition efficiency of 79.79 % at the highest concentration of 5.0 x 10^{-5} M. As the temperature was further increased to 40° C, the least performing inhibitor was SDM with the inhibition efficiency of 18.97 % and SCP was the best performing with inhibition efficiency of 61.23 % at the highest concentration of 5.0 x 10^{-5} M.

Table 4.4 shows the corrosion rates and %IE for mild steel corrosion in 1.0 M HCl in the absence and presence of various concentrations of the utilized inhibitors at 30-50 °C. The results of the study suggests that the corrosion rate increases with an increase in temperature of the surrounding environment but decreases with an increase in inhibitor concentration for all four inhibitors. The corrosion rate for mild steel in 1.0 M HCl in the absence of the corrosion inhibitors was found to increase from 0.0023 $g.cm^{-2}.h^{-1}$ to 0.0039 $g.cm^{-2}.h^{-1}$ and then 0.0075 $g.cm^{-2}.h^{-1}$ at 30 °C, 40 °C and 50 °C, respectively. However, in the presence of corrosion inhibitors, these values are greatly reduced. For instance, as shown in this table, the corrosion rate for mild steel in 1.0 M HCl in the presence of SNA, SBZ, SMX, SCP, SDM, SSZ, SMZ, SMT and SQX corrosion inhibitors was found to be 0.00021, 0.00022, 0.00049, 0.00021, 0.00014, 0.00027, 0.00052, 0.000017 and 0.00026 $g.cm^{-2}.h^{-1,}$ respectively at 30° C and highest concentration of 5.0 x 10^{-5} M . At at 40° C and highest concentration of 5.0 x 10^{-5} M the corrosion rates were found to be 0.0012, 0.0016, 0.0012, 0.0007, 0.0009, 0.0011, 0.0019, 0.0011 and 0.0015 $g.cm^{-2}.h^{-1}$ in the presence of SNA, SBZ, SMX, SCP, SDM, SSZ, SMZ, SMT and SQX corrosion inhibitors, respectively at their highest concentration of 5.0 x 10^{-5} M. Furthermore, as the temperature was increased to 50° C, the corrosion rates were found to be 0.0048, 0.0041, 0.0062, 0.0033, 0.0048, 0.0053, 0.0055, 0.0044 and 0.0041 $g.cm^{-2}.h^{-1}$ in the presence of SNA, SBZ, SMX, SCP, SDM, SSZ, SMZ, SMT and SQX corrosion inhibitors, respectively at their highest concentration of 5.0 x 10^{-5} M.

Table 4.4: Percentage inhibition efficiencies and corrosion rates values obtained from the weight loss of mild steel in 1.0 M HCl in the absence and presence of various concentrations of inhibitors.

Inhibitor	**Inhibitor Conc. (M)**	**Temperature**					
		30 °C		40 °C		50 °C	
		$\%IE_{WL}$	$C_R(g.cm^{-2}.h^{-1})$	$\%IE_{WL}$	$C_R(g.cm^{-2}.h^{-1})$	$\%IE_{WL}$	$C_R(g.cm^{-2}.h^{-1})$
Blank	0.0	-	0.00230	-	0.0039	-	0.0075
SNA	1.0×10^{-5}	80.05	0.00046	58.56	0.0016	29.24	0.0052
	2.0×10^{-5}	81.47	0.00043	59.59	0.0015	30.36	0.0050
	3.0×10^{-5}	82.42	0.00041	65.47	0.0013	33.40	0.0049
	4.0×10^{-5}	88.36	0.00027	65.76	0.0013	33.63	0.0049
	5.0×10^{-5}	89.55	0.00021	67.76	0.0012	34.97	0.0048
SBZ	1.0×10^{-5}	80.99	0.00044	48.71	0.0020	35.50	0.0048
	2.0×10^{-5}	86.22	0.00032	50.14	0.0019	37.50	0.0047
	3.0×10^{-5}	87.17	0.00030	51.15	0.0018	40.48	0.0044
	4.0×10^{-5}	88.36	0.00027	56.88	0.0017	45.38	0.0041
	5.0×10^{-5}	90.49	0.00022	59.60	0.0016	45.46	0.0040
SMX	1.0×10^{-5}	67.02	0.00122	58.63	0.0024	38.42	0.0071
	2.0×10^{-5}	79.67	0.00075	68.77	0.0018	39.53	0.0069
	3.0×10^{-5}	81.63	0.00067	75.56	0.0014	42.22	0.0066
	4.0×10^{-5}	84.79	0.00056	77.64	0.0013	45.73	0.0062
	5.0×10^{-5}	86.59	0.00049	79.34	0.0012	46.06	0.0062
SCP	1.0×10^{-5}	74.55	0.00060	67.05	0.0013	40.48	0.0044
	2.0×10^{-5}	82.08	0.00042	71.49	0.0011	47.54	0.0039
	3.0×10^{-5}	87.65	0.00029	72.78	0.0010	52.82	0.0035
	4.0×10^{-5}	90.21	0.00023	78.65	0.0008	55.87	0.0033
	5.0×10^{-5}	91.72	0.00021	79.79	0.0007	61.23	0.0029
SDM	1.0×10^{-5}	71.97	0.00065	48.71	0.0019	18.97	0.0060
	2.0×10^{-5}	85.99	0.00033	60.17	0.0015	25.97	0.0055
	3.0×10^{-5}	89.31	0.00025	63.75	0.0014	30.21	0.0052
	4.0×10^{-5}	89.31	0.00024	69.48	0.0011	31.55	0.0051
	5.0×10^{-5}	93.83	0.00014	76.93	0.0009	34.60	0.0048
SSZ	1.0×10^{-5}	56.76	0.00101	46.84	0.0020	24.33	0.0056
	2.0×10^{-5}	72.44	0.00064	54.29	0.0017	25.97	0.0055
	3.0×10^{-5}	76.24	0.00055	62.60	0.0014	26.41	0.0054
	4.0×10^{-5}	81.95	0.00042	66.90	0.0012	26.64	0.0054
	5.0×10^{-5}	88.36	0.00027	70.63	0.0011	27.45	0.0053
SMZ	1.0×10^{-5}	65.21	0.00128	60.13	0.0024	46.68	0.0061
	2.0×10^{-5}	74.25	0.00095	61.16	0.0023	47.45	0.0060
	3.0×10^{-5}	79.67	0.00075	65.57	0.0020	50.00	0.0058
	4.0×10^{-5}	82.38	0.00065	66.04	0.0020	50.28	0.0057
	5.0×10^{-5}	85.97	0.00052	67.64	0.0019	54.25	0.0055
SMT	1.0×10^{-5}	75.75	0.00058	58.07	0.0016	28.34	0.0054
	2.0×10^{-5}	84.49	0.00037	62.10	0.0015	38.47	0.0047
	3.0×10^{-5}	87.20	0.00031	67.73	0.0013	38.95	0.0046
	4.0×10^{-5}	88.55	0.00028	70.73	0.0011	40.59	0.0045
	5.0×10^{-5}	92.77	0.00017	71.38	0.0011	41.93	0.0044
SQX	1.0×10^{-5}	65.32	0.00081	43.84	0.0022	25.44	0.0056
	2.0×10^{-5}	78.62	0.00050	51.43	0.0019	30.95	0.0052
	3.0×10^{-5}	82.19	0.00042	55.87	0.0017	36.31	0.0048
	4.0×10^{-5}	88.36	0.00027	58.59	0.0016	41.36	0.0044
	5.0×10^{-5}	89.07	0.00026	59.43	0.0015	44.72	0.0041

This observation is due to the fact that at higher temperatures molecules within the system have more energy and thus move with higher average kinetic speeds leading to higher corrosion rate. Nevertheless, as the inhibitor concentration is increased, the presence of inhibitor molecules within the system is increased and thus improves the adsorption of the inhibitor molecules on the surface of the metal thereby lowering the corrosion rate.

4.1.6 KINETIC PARAMETERS: EFFECT OF TEMPERATURE

An increase in temperature of the surrounding environment leads to an increase in mild steel corrosion rate [90]. There are numerous parameters that are directly or indirectly related to this behaviour, amongst them is the activation energy. The activation energy (E_a) of mild steel corrosion is the minimum amount of energy that mild steel components (mainly Fe), acidic medium components, oxygen and moisture would require in order to produce the corrosion products, such as rust. High mild steel dissolutions are associated with low E_a values while low dissolutions are associated with higher values. Arrhenius equations can be highly useful in terms of evaluating the effect of temperature on the adsorption tendencies and determination of activation parameters for mild steel corrosion [90, 91]. Equation 56 shows the type of Arrhenius equation to calculate E_a for mild steel corrosion [120, 121]:

$$\log C_R = \log A - \frac{E_a}{2.303RT} \tag{56}$$

where C_R is the corrosion rate in $g.cm^{-2}.h^{-1}$, A is the Arrhenius pre-exponential factor, R is the gas constant and T is the absolute temperature. The values of E_a are recorded in Table 4.5 and were calculated from the slopes and intercepts of the Arrhenius plots shown in Figures 4.52 − 4.60. The E_a values increase with the increase in the concentrations of inhibitor molecules. It is also noticed that E_a corresponding to the uninhibited mild steel corrosion is always less than that of the inhibited process. This implies that mild steel dissolution in 1.0 M HCl is reduced through the formation of inhibitor-Fe complex.

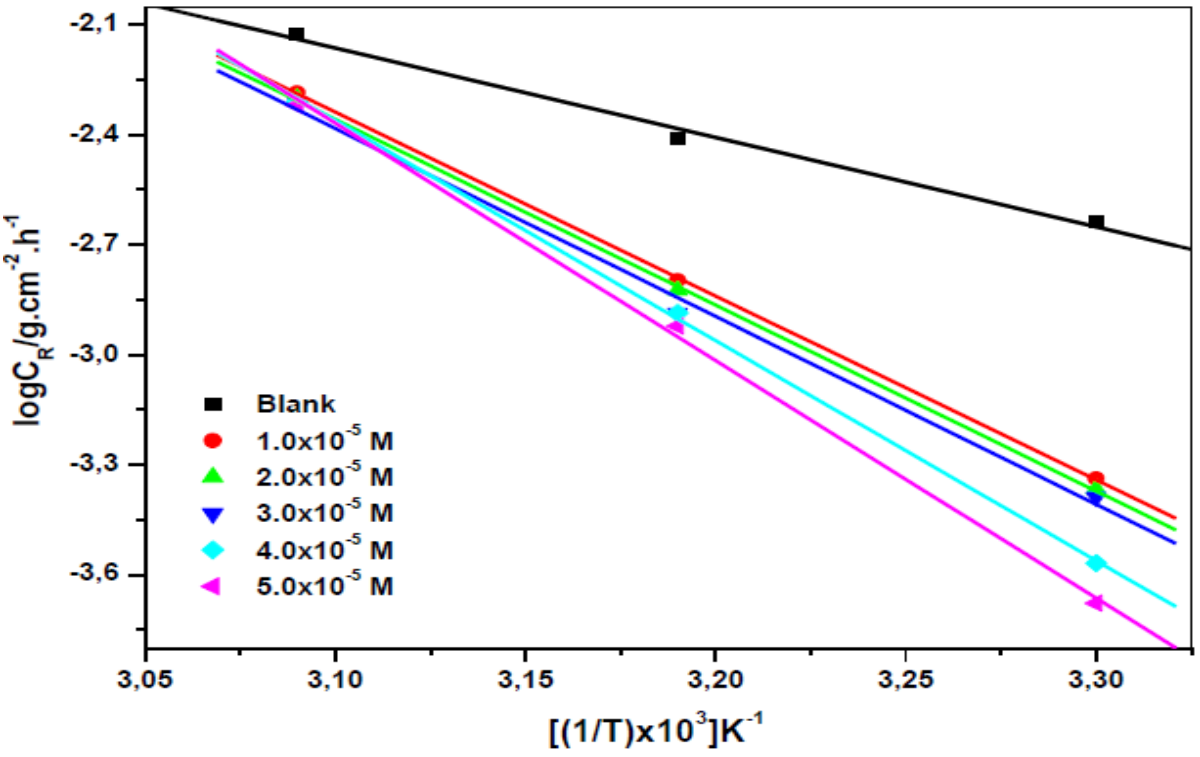

Figure 4.52: Arrhenius plots for the corrosion of mild steel in 1.0 M HCl in the absence and presence of various concentrations of SNA corrosion inhibitor.

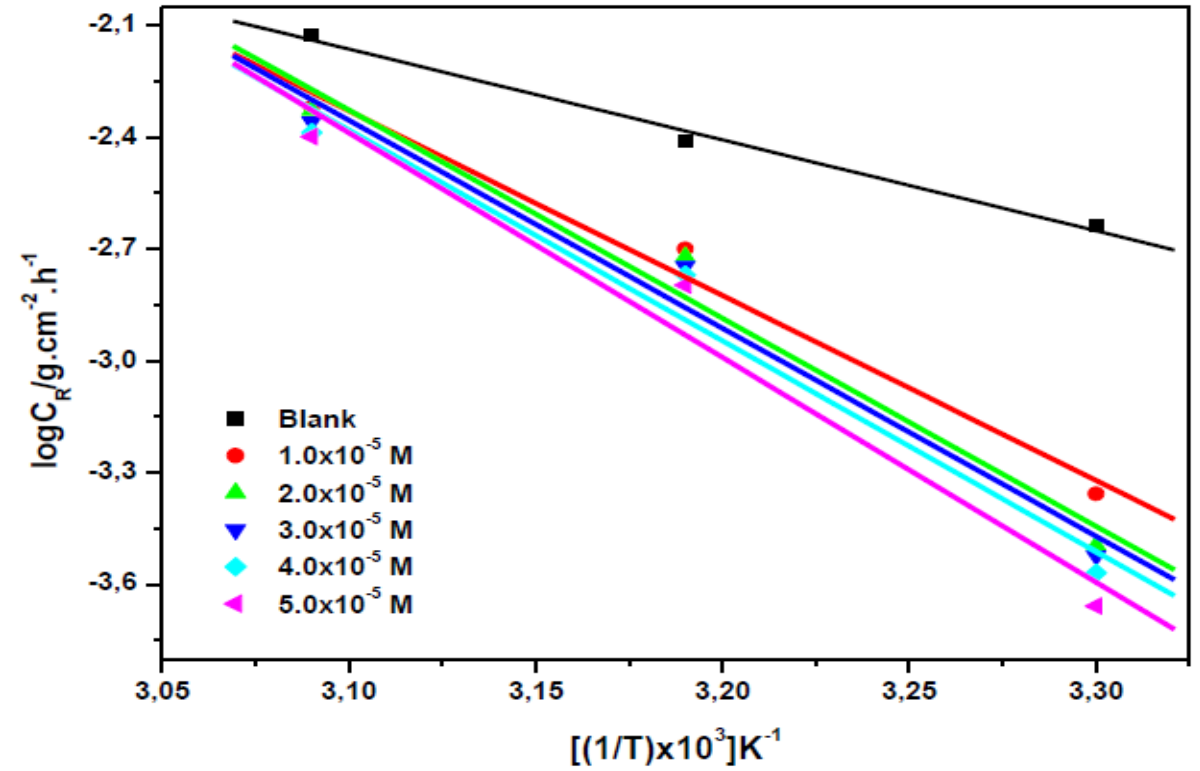

Figure 4.53: Arrhenius plots for the corrosion of mild steel in 1.0 M HCl in the absence and presence of various concentrations of SBZ corrosion inhibitor.

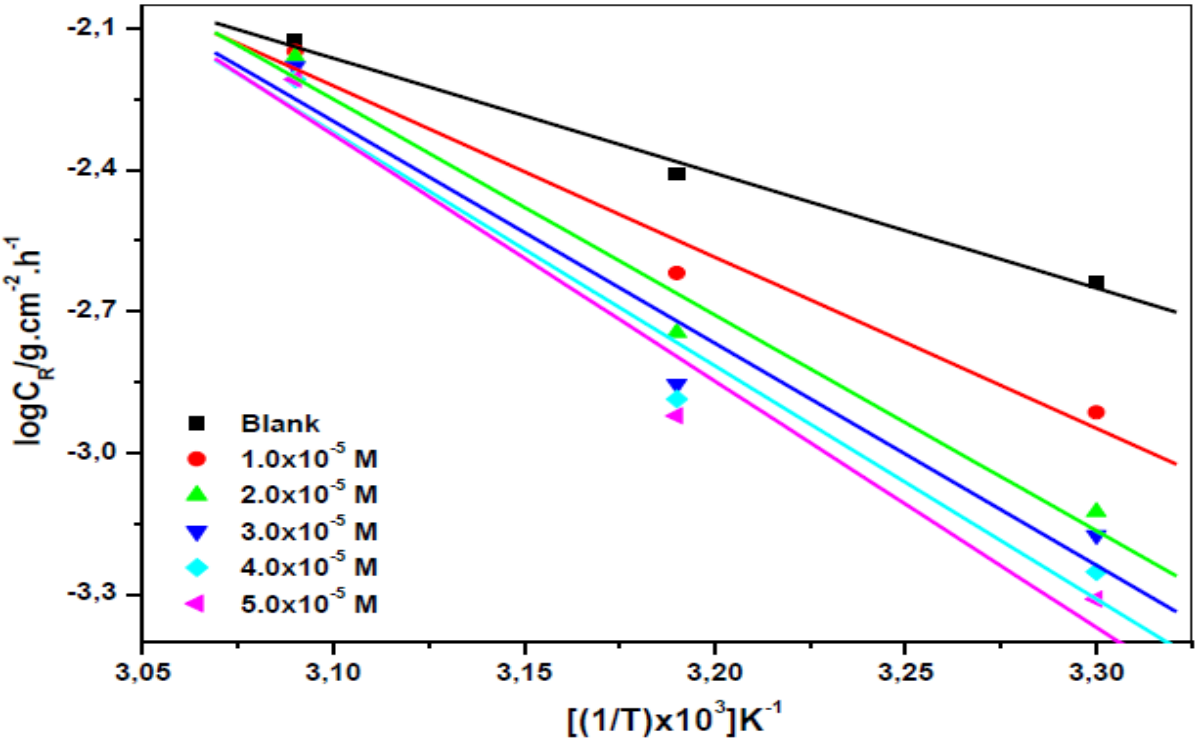

Figure 4.54: Arrhenius plots for the corrosion of mild steel in 1.0 M HCl in the absence and presence of various concentrations of SMX corrosion inhibitor.

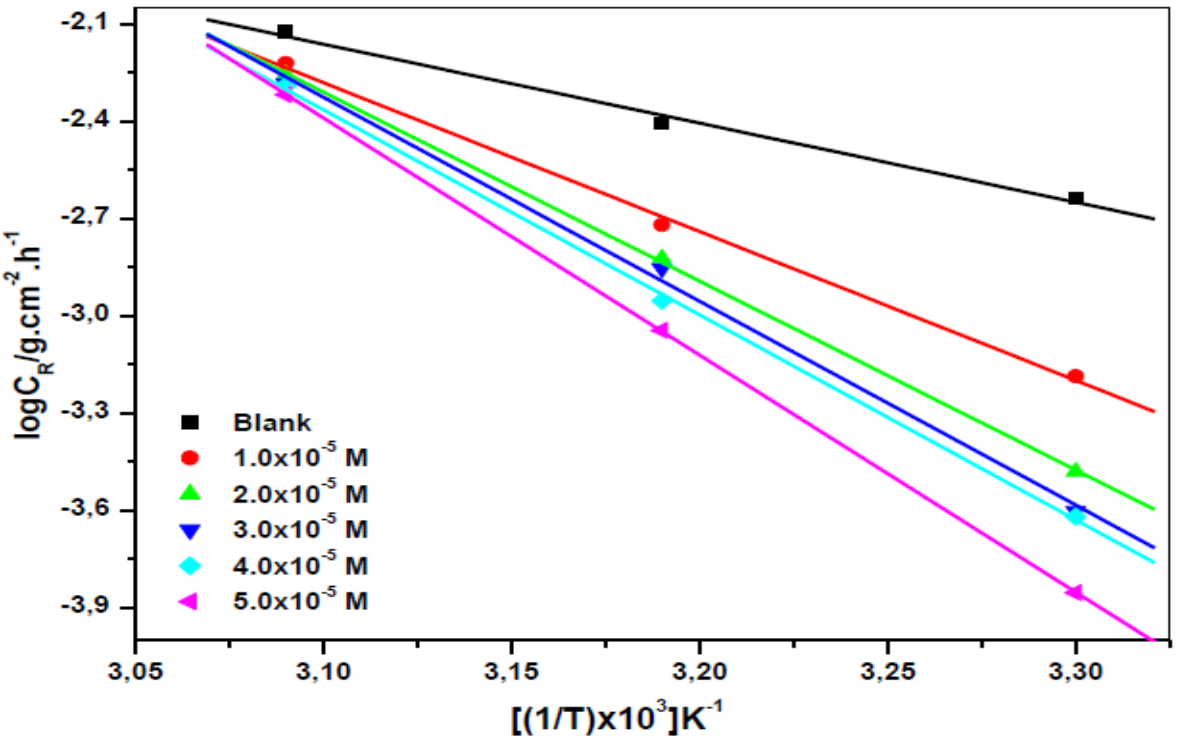

Figure 4.55: Arrhenius plots for the corrosion of mild steel in 1.0 M HCl in the absence and presence of various concentrations of SCP corrosion inhibitor.

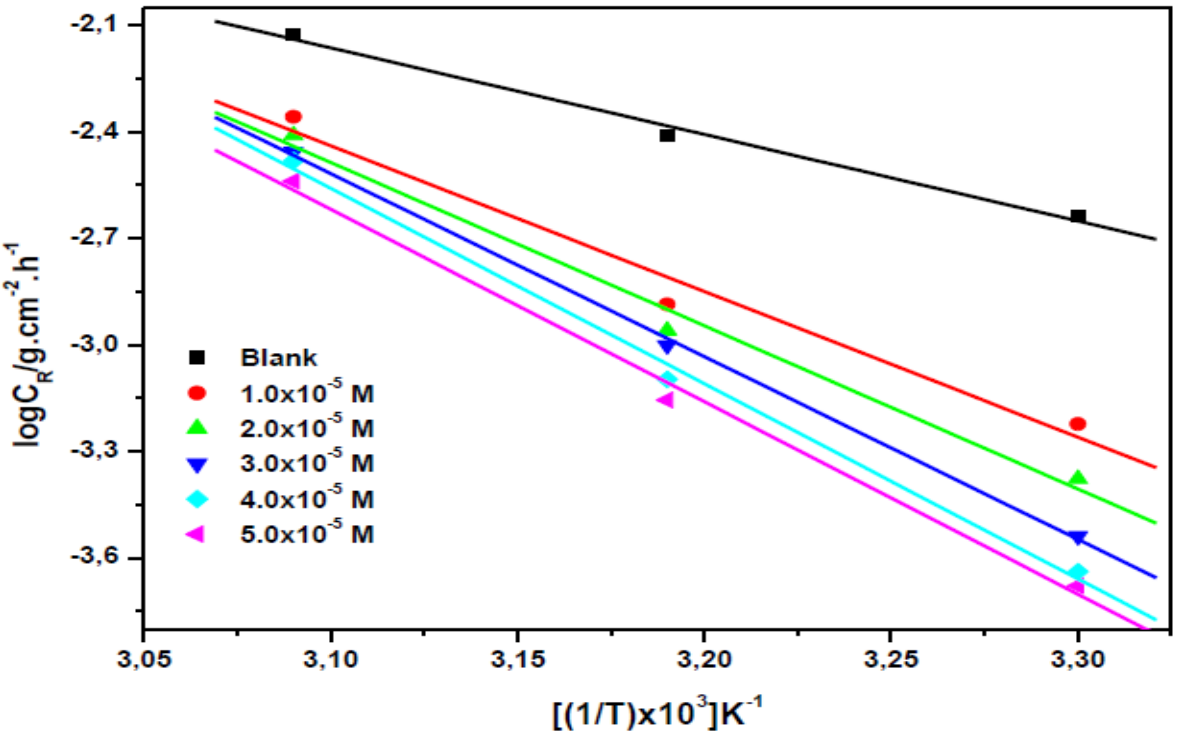

Figure 4.56: Arrhenius plots for the corrosion of mild steel in 1.0 M HCl in the absence and presence of various concentrations of SDM corrosion inhibitor.

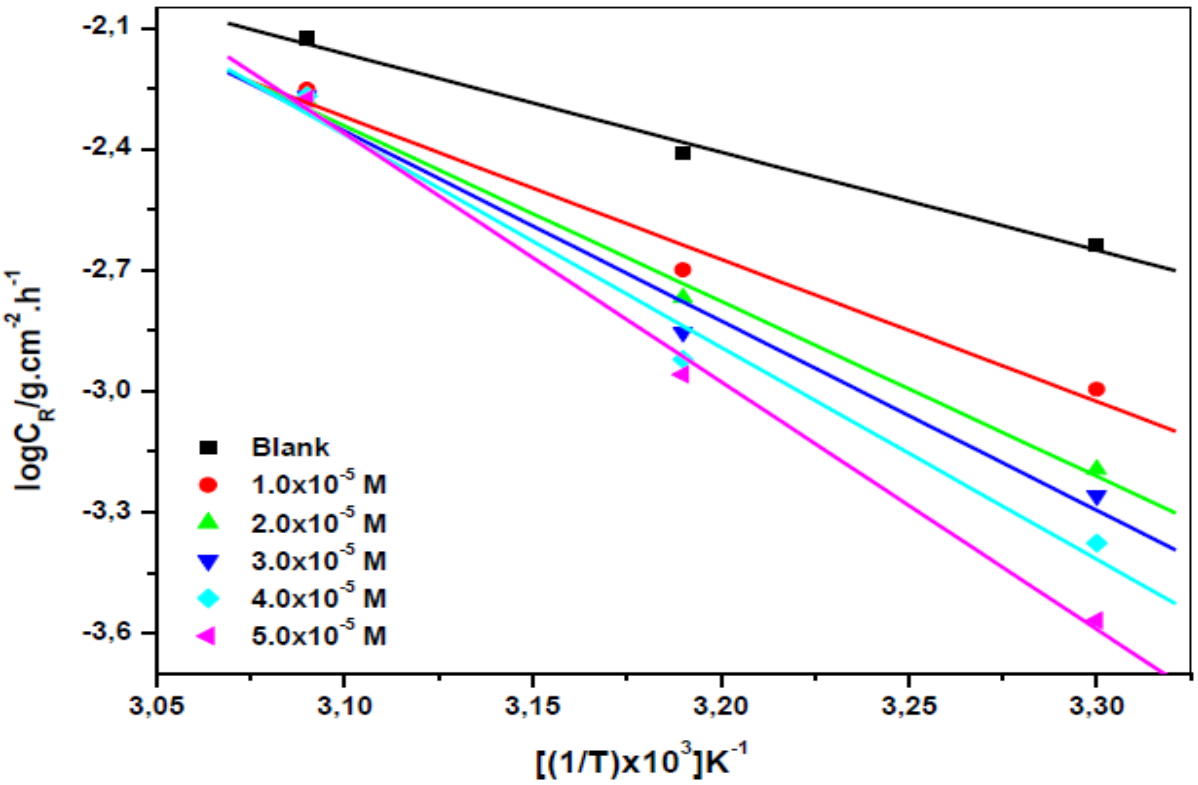

Figure 4.57: Arrhenius plots for the corrosion of mild steel in 1.0 M HCl in the absence and presence of various concentrations of SSZ corrosion inhibitor.

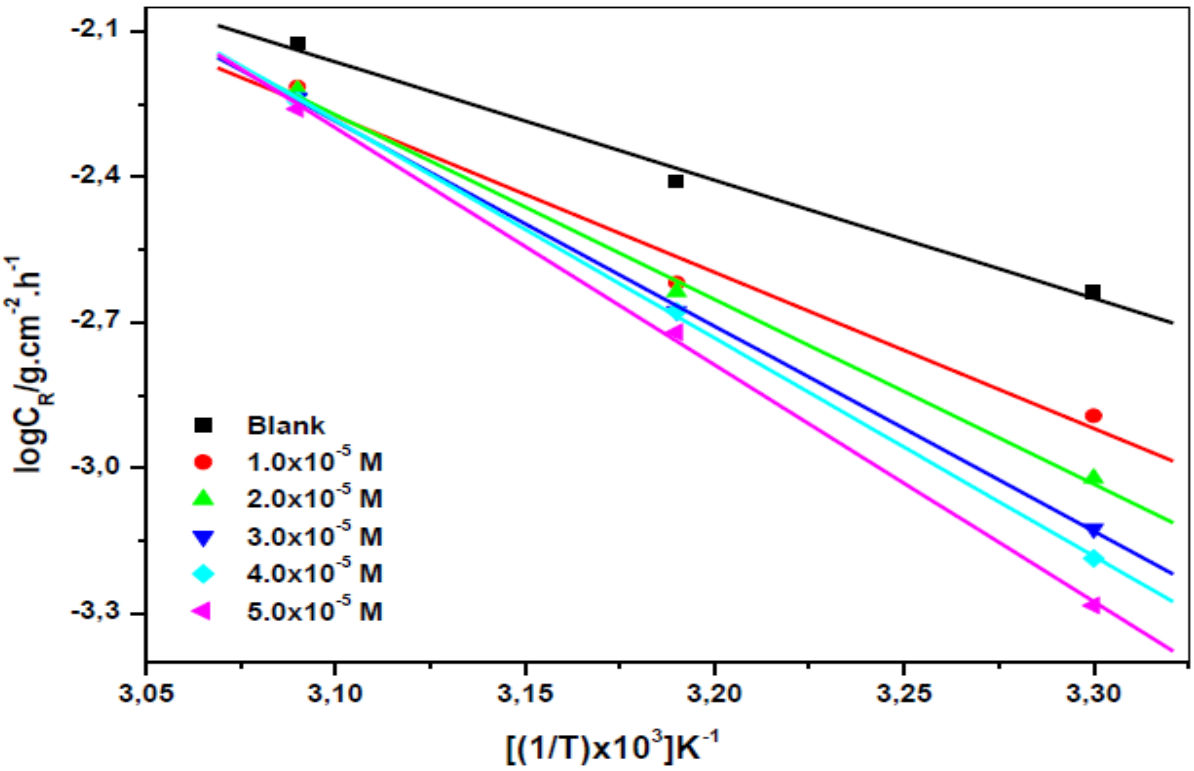

Figure 4.58: Arrhenius plots for the corrosion of mild steel in 1.0 M HCl in the absence and presence of various concentrations of SMZ corrosion inhibitor.

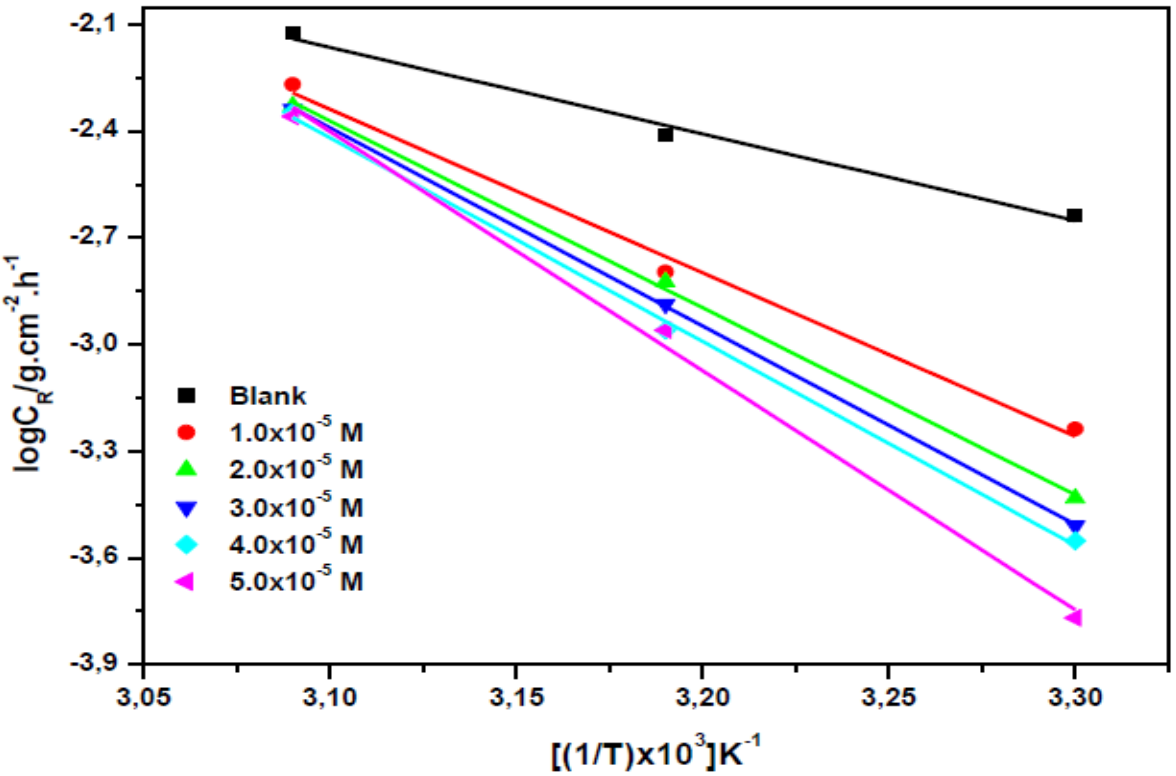

Figure 4.59: Arrhenius plots for the corrosion of mild steel in 1.0 M HCl in the absence and presence of various concentrations of SMT corrosion inhibitor.

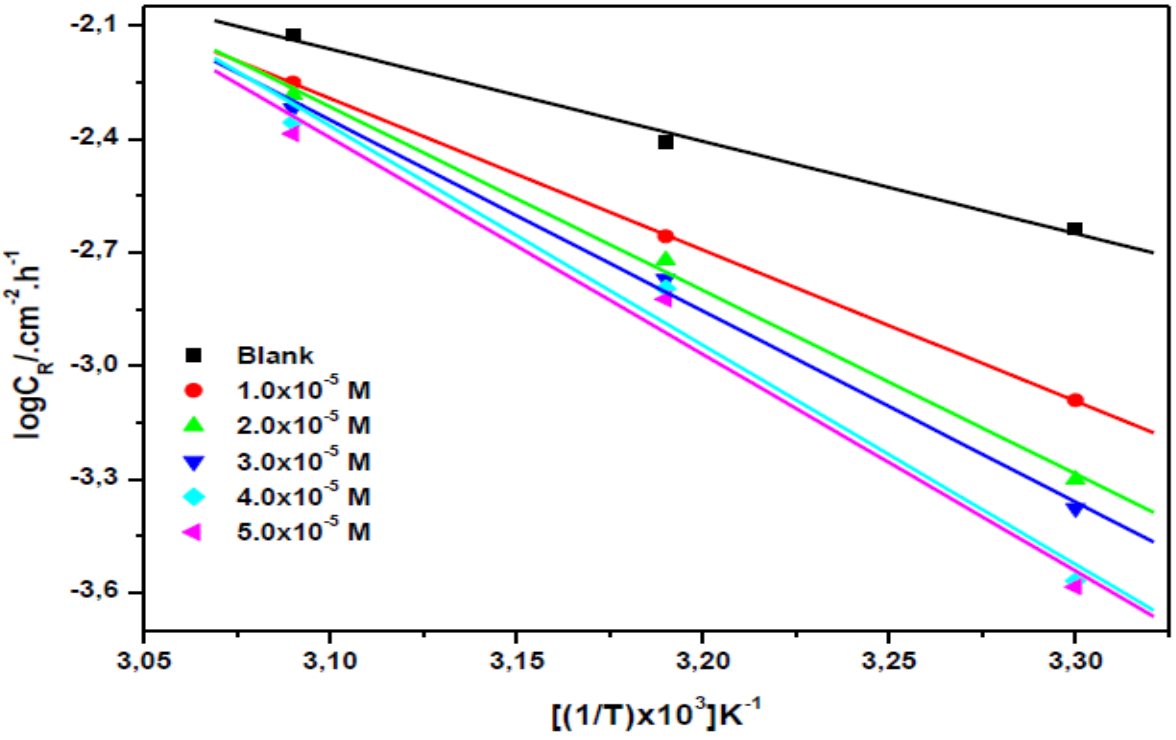

Figure 4.60: Arrhenius plots for the corrosion of mild steel in 1.0 M HCl in the absence and presence of various concentrations of SQX corrosion inhibitor.

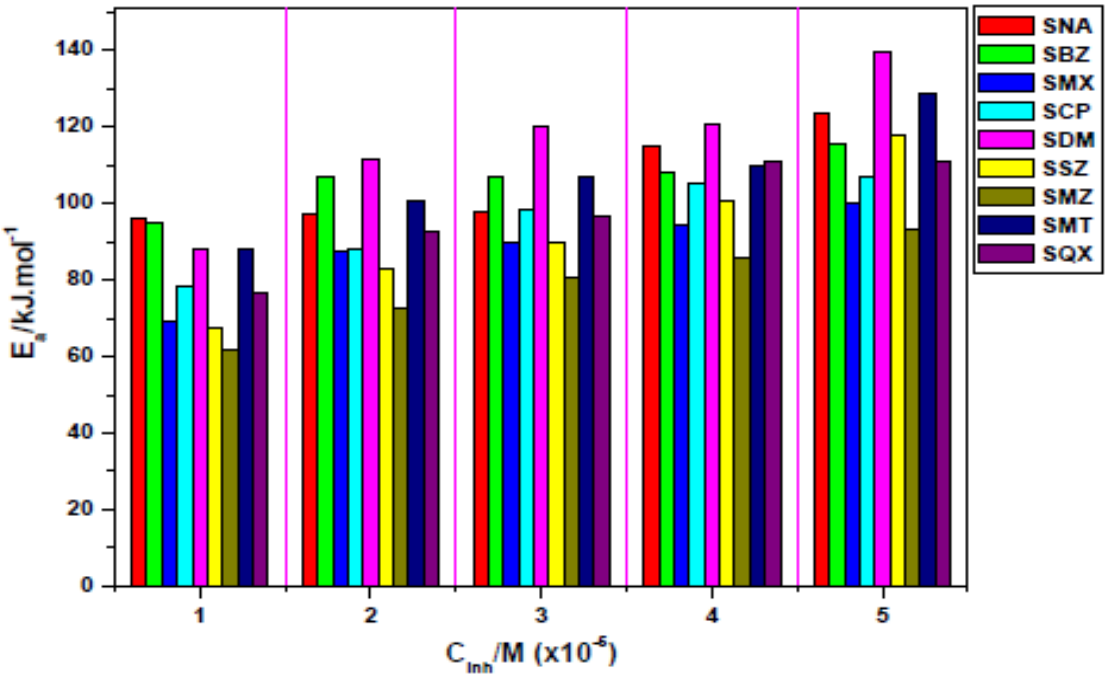

Figure 4.61: Variation of the activation energy with the concentration of the utilized corrosion inhibitors.

Table 4.5: Kinetic and activation parameters (derived from the Arrhenius and transition-states plots) for mild steel in 1.0 M HCl in the absence and presence of various concentrations of inhibitors.

Inhibitor	Inhibitor Conc. (M)	Activation Energy (E_a/kJ.mol^{-1})	Enthalpy of Activation (ΔH^*/ kJ.mol^{-1})	Entropy of Activation (ΔS^*/ J.mol^{-1}.K^{-1})
Blank	0.0	46.64	44.09	–150.29
SNA	1.0×10^{-5}	95.99	93.51	19.12
	2.0×10^{-5}	97.06	94.61	2.51
	3.0×10^{-5}	98.12	95.57	4.97
	4.0×10^{-5}	114.87	112.32	67.88
	5.0×10^{-5}	123.96	121.51	85.66
SBZ	1.0×10^{-5}	94.94	92.38	–3.71
	2.0×10^{-5}	106.83	104.29	33.24
	3.0×10^{-5}	106.76	104.27	32.54
	4.0×10^{-5}	108.25	105.66	36.47
	5.0×10^{-5}	115.42	112.87	58.65
SMX	1.0×10^{-5}	69.44	66.90	–80.83
	2.0×10^{-5}	87.55	84.99	–25.25
	3.0×10^{-5}	90.06	87.51	–18.35
	4.0×10^{-5}	94.68	92.22	–4.21
	5.0×10^{-5}	99.95	97.49	12.03
SCP	1.0×10^{-5}	78.50	76.00	–56.63
	2.0×10^{-5}	87.97	85.43	–28.27
	3.0×10^{-5}	98.53	95.97	3.81
	4.0×10^{-5}	105.26	102.72	23.94
	5.0×10^{-5}	107.03	101.15	17.95
SDM	1.0×10^{-5}	87.88	85.33	–24.82
	2.0×10^{-5}	111.48	109.02	48.07
	3.0×10^{-5}	120.36	117.89	75.28
	4.0×10^{-5}	121.02	118.55	75.92
	5.0×10^{-5}	139.99	137.71	135.51
SSZ	1.0×10^{-5}	67.58	65.02	–88.50
	2.0×10^{-5}	83.19	82.52	–34.38
	3.0×10^{-5}	90.04	87.58	–19.24
	4.0×10^{-5}	100.77	98.22	13.55
	5.0×10^{-5}	117.71	115.16	66.15
SMZ	1.0×10^{-5}	61.59	59.13	–105.91
	2.0×10^{-5}	72.85	70.39	–70.94
	3.0×10^{-5}	80.93	78.40	–46.49
	4.0×10^{-5}	86.04	83.42	–30.90
	5.0×10^{-5}	93.46	90.99	–7.58
SMT	1.0×10^{-5}	88.04	85.60	–24.92
	2.0×10^{-5}	100.67	98.17	13.43
	3.0×10^{-5}	106.80	104.26	31.94
	4.0×10^{-5}	109.86	107.27	40.87
	5.0×10^{-5}	128.81	126.45	100.57
SQX	1.0×10^{-5}	76.54	73.90	–60.36
	2.0×10^{-5}	92.83	90.28	–9.98
	3.0×10^{-5}	96.58	94.12	1.28
	4.0×10^{-5}	110.86	108.40	45.27
	5.0×10^{-5}	111.07	107.02	40.37

Further information regarding the effect of temperature on the inhibition efficiency was obtained from activation parameters such as enthalpy of activation (ΔH*) and entropy of activation (ΔS*). The corrosion rate and temperature is related to these parameters through transition-state equation of the form [120, 121]:

$$\log\frac{C_R}{T} = \left[\log\left(\frac{R}{hN}\right) + \left(\frac{\Delta S^*}{2.303R}\right)\right] - \frac{\Delta H^*}{2.303RT} \qquad (57)$$

where h is the Plank`s constant ($6.63\times10^{-34}$ Js) and N is the Avogadro`s number (6.023×10^{23} mol^{-1}). Plots of $\log(C_R/T)$ against (1/T), shown in Figures 4.63−4.71, enabled the calculation of ΔH* and ΔS* from the slopes and intercepts of the regression lines. These values are also recorded in Table 4.5.

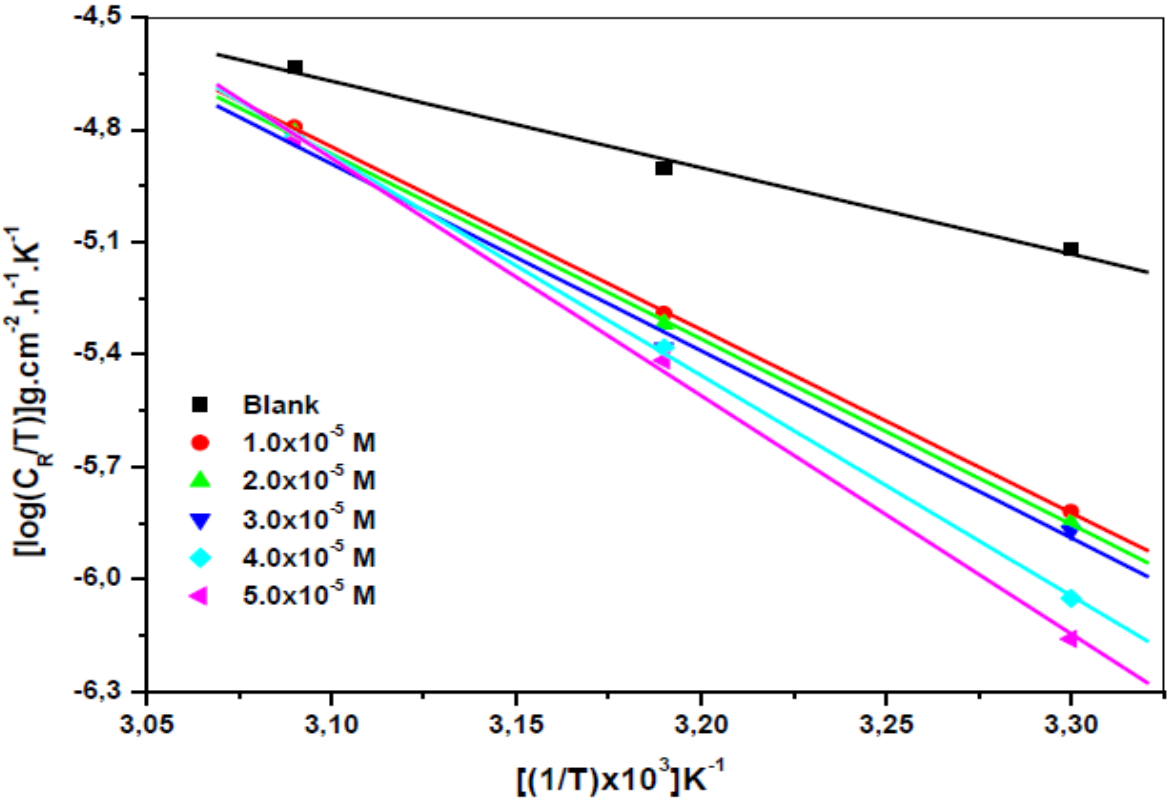

Figure 4.62: Transition state plots for the corrosion of mild steel in 1.0 M HCl in the absence and presence of various concentrations of SNA corrosion inhibitor.

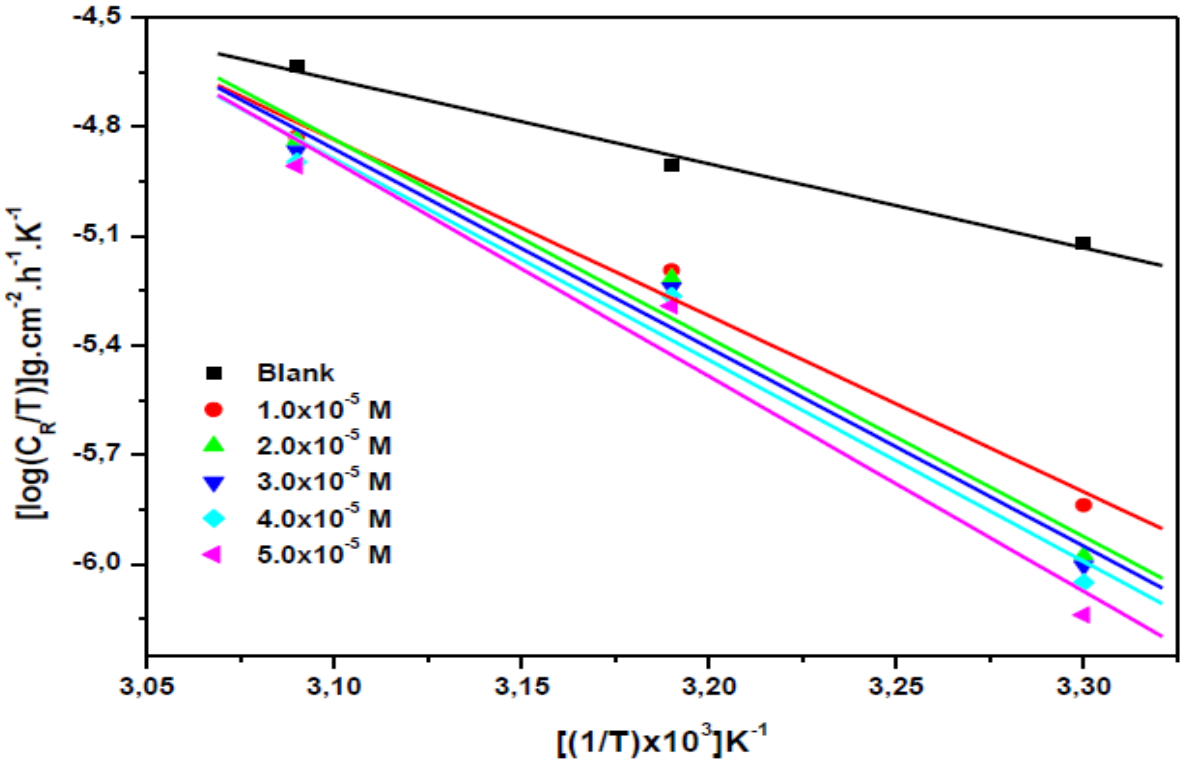

Figure 4.63: Transition state plots for the corrosion of mild steel in 1.0 M HCl in the absence and presence of various concentrations of SBZ corrosion inhibitor.

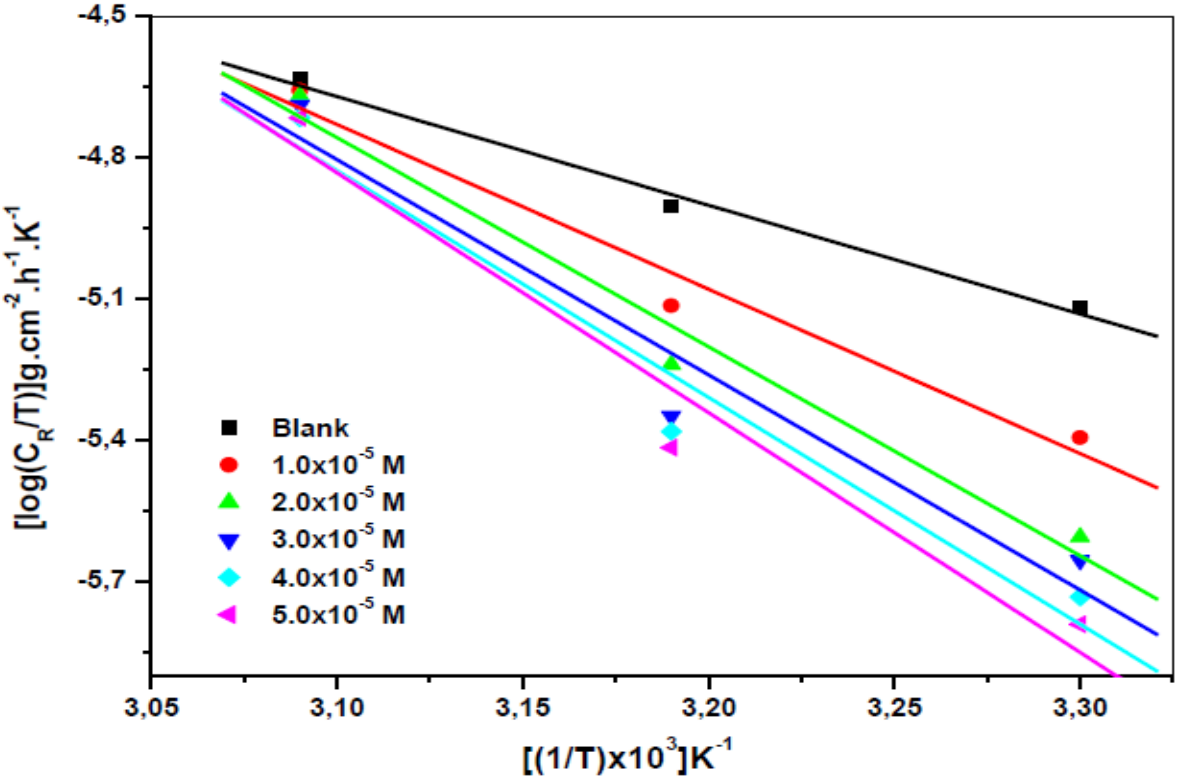

Figure 4.64: Transition state plots for the corrosion of mild steel in 1.0 M HCl in the absence and presence of various concentrations of SMX corrosion inhibitor.

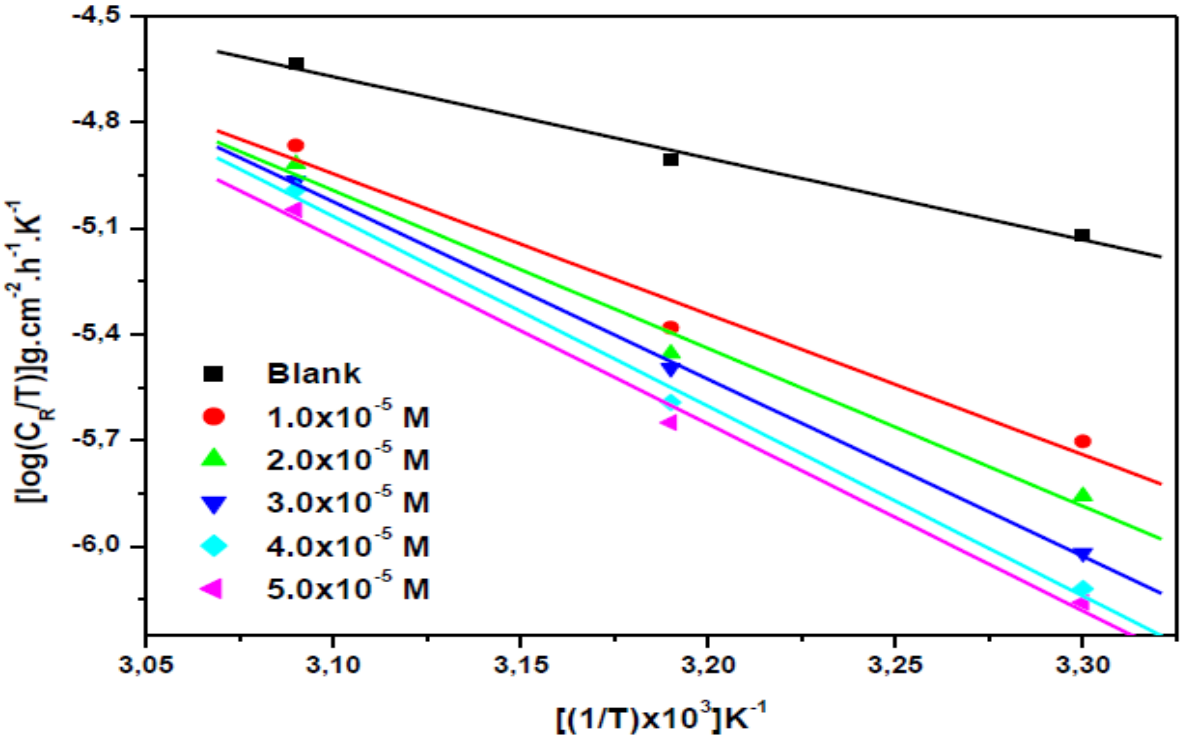

Figure 4.65: Transition state plots for the corrosion of mild steel in 1.0 M HCl in the absence and presence of various concentrations of SCP corrosion inhibitor.

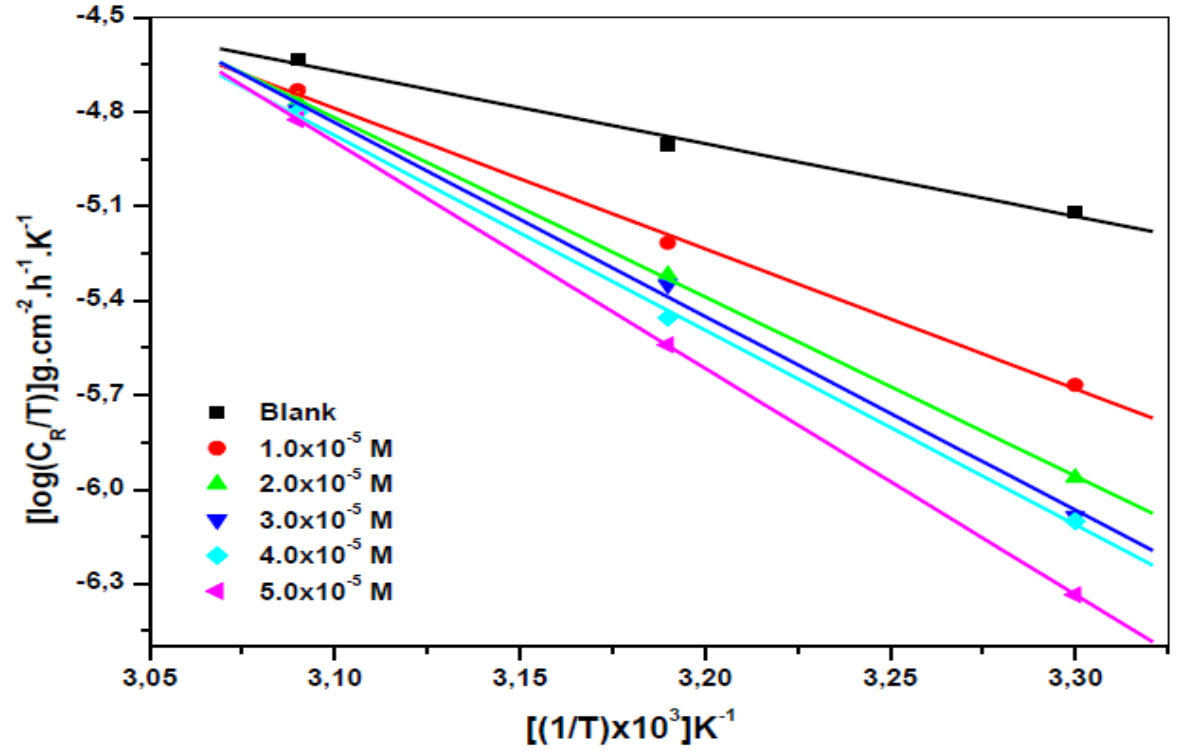

Figure 4.66: Transition state plots for the corrosion of mild steel in 1.0 M HCl in the absence and presence of various concentrations of SDM corrosion inhibitor.

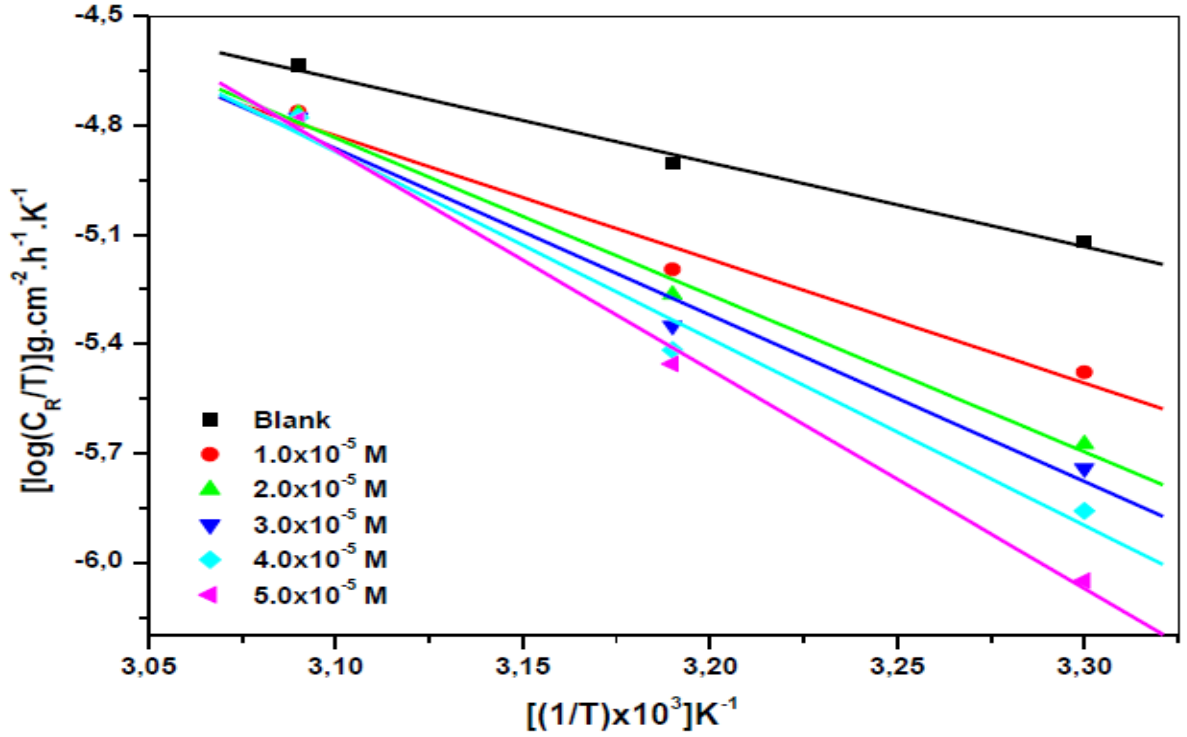

Figure 4.67: Transition state plots for the corrosion of mild steel in 1.0 M HCl in the absence and presence of various concentrations of SSZ corrosion inhibitor.

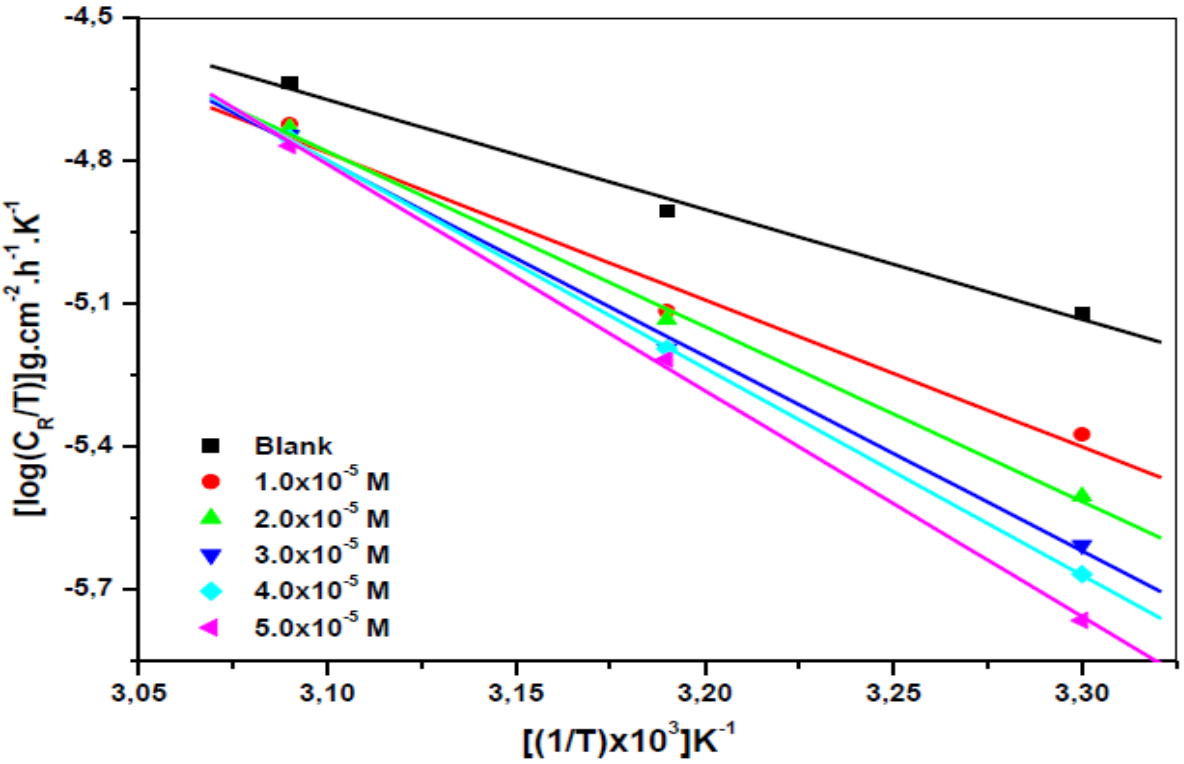

Figure 4.68: Transition state plots for the corrosion of mild steel in 1.0 M HCl in the absence and presence of various concentrations of SMZ corrosion inhibitor.

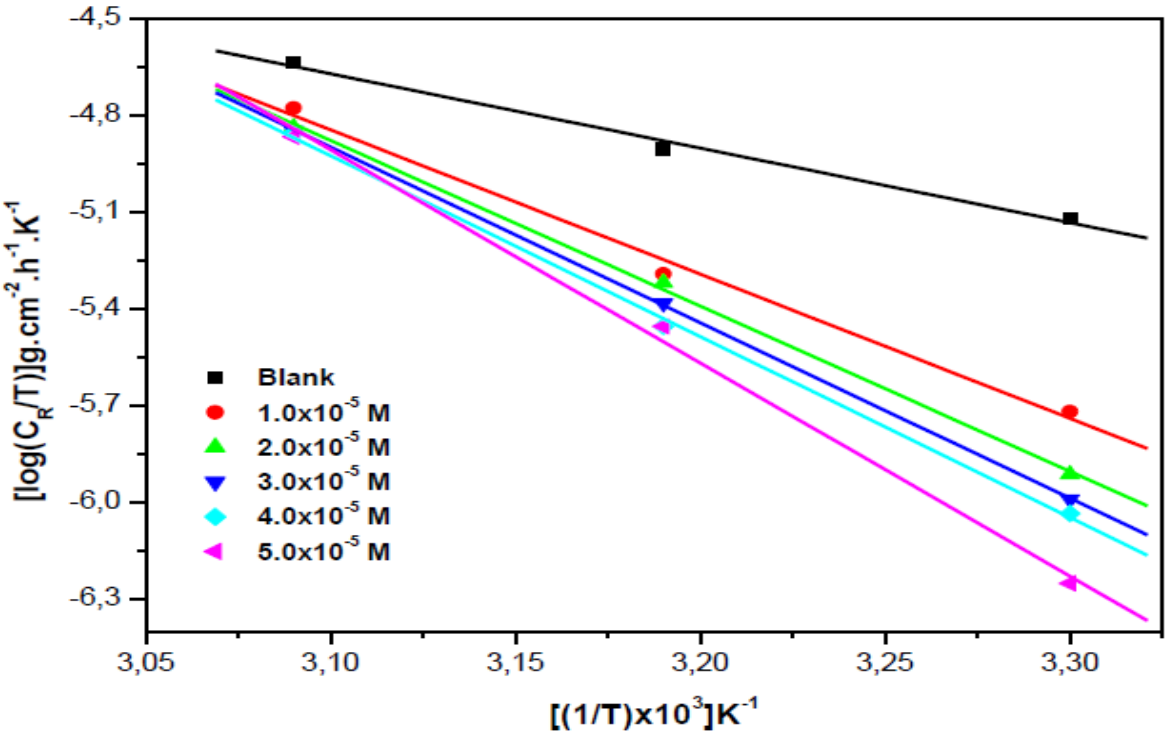

Figure 4.69: Transition state plots for the corrosion of mild steel in 1.0 M HCl in the absence and presence of various concentrations of SMT corrosion inhibitor.

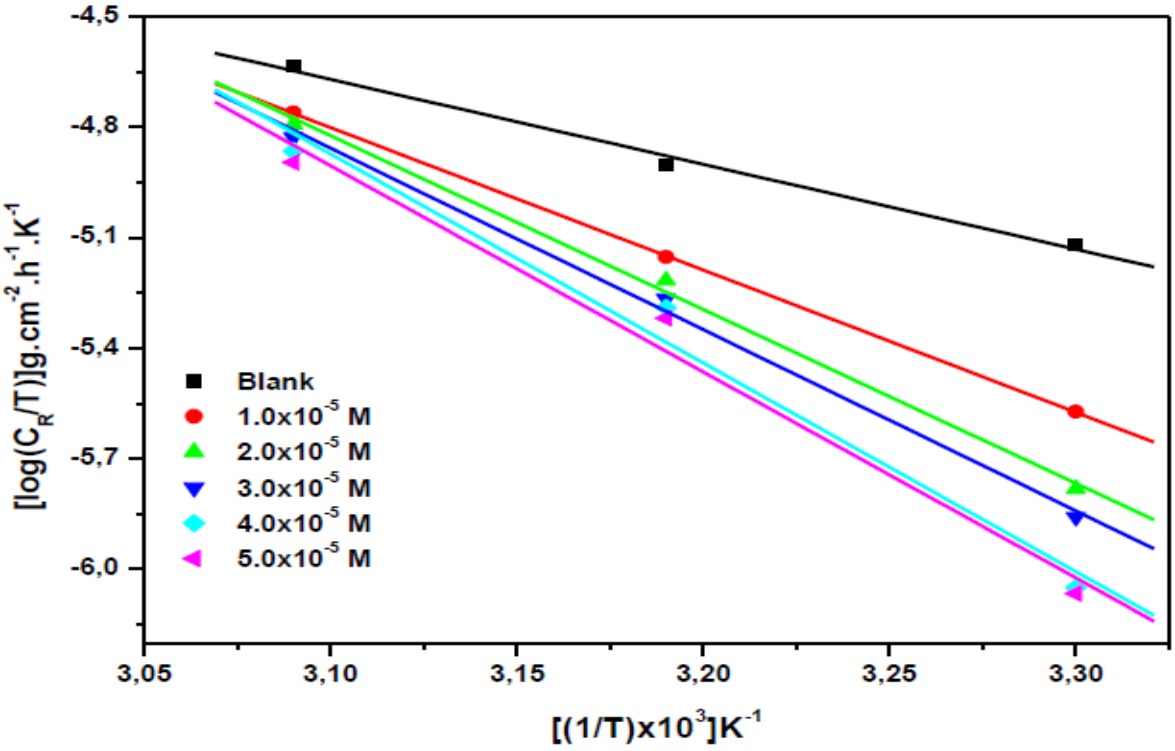

Figure 4.70: Transition state plots for the corrosion of mild steel in 1.0 M HCl in the absence and presence of various concentrations of SQX corrosion inhibitor.

The adsorption process between mild steel surface and inhibitor molecules can be classified as either exothermic or endothermic. In general terms, exothermic process gives off heat and may suggest either chemisorption or physisorption whereas endothermic process entirely suggests chemisorption [120, 122]. Chemisorption involves the sharing of electron pairs with the vacant *d*-orbitals of Fe in mild steel while physisorption involves the electrostatic interactions between charged mild steel surfaces and charged inhibitor molecules [122]. Positive values of the enthalpy of activation in the present study signifies the fact that mild steel dissolution process is of endothermic nature, comparison of the values of enthalpy of activation for the uninhibited process to that of inhibited shows that the inhibited process has higher values. This observation pronounces the fact that there is an adsorption process that took place between the inhibitor molecules and surfaces of mild steel. Studies show that numerical values of enthalpy of activation ranging up to 41.86 $kJ.mol^{-1}$ are associated with physisorption type of adsorption whereas those around 100 $kJ.mol^{-1}$ or higher are associated chemisorption [123]. Table 4.5 shows that the values of enthalpy of activation are slightly less than those of their respective activation energies and are above 41.86 $kJ.mol^{-1}$ yet slightly less than 100 $kJ.mol^{-1}$. This kind of behaviour may be attributed to a mixed-type of adsorption of mild steel adsorption and the type of adsorption correlates very well with the correlation predicted by the electrochemical measurements.

Entropy of activation provides some further insight into the mild steel adsorption process. This parameter assists with information regarding the extent of disorder of the adsorption/desorption process between mild steel and inhibitor compounds. The values of entropy of activation, reported in Table 5.5, shows that as the concentration of the inhibitor molecules is increased, the entropy is also increased. Similar trend in entropy of activation values against inhibitor concentrations was reported by Singh and Quraishi [122], who attributed this behaviour to the fact that there is an increase in disorder during the adsorption process on going from reactants to activated complex [122].

4.1.7 THERMODYNAMIC PARAMETERS: ADSORPTION ISOTHERMS

Corrosion inhibitors normally protect mild steel through adsorbing onto its surface. This process may adopt a chemisorption, physisorption or mixed-type mode. A typical adsorption phenomenon between the corrosion inhibitor and metal surface involves the replacement of water molecule at a corroding interface according to the pattern represented in equation (58) [124]:

$$SFA_{(sol)} + nH_2O_{(ads)} \Leftrightarrow SFA_{(ads)} + nH_2O_{(sol)} \quad (58)$$

where SFA is the sulfanoamide corrosion inhibitor and n is the size ratio of the number of molecules replaced by adsorbed molecules. The efficiency of the corrosion inhibitor shows the ability to be adsorbed on the metal surface by displacing the water molecule from the interface which is attacked by corrosion. In order for us to completely understand the adsorption mechanism, it is important to assume a quasi-equilibrium adsorption through application of a suitable adsorption isotherm. This assumption is considered reasonable due to the fact that the adsorption phenomenon on the corroding mild steel surface never achieves a complete equilibrium but instead achieves an adsorption steady-state [124]. Various adsorption isotherms were fitted in the current investigation namely Langmuir, Freundlich, Flory-Huggins, BET, Temkin and Frumkin. Nevertheless, the maximum values of regression coefficients (r^2) from the linear relationship showed that Langmuir adsorption isotherm was the most appropriate isotherm. The numerical values of (r^2) and slopes are recorded in Tables 4.6 and 4.7.

Table 4.6: Thermodynamic and adsorption parameters (Langmuir adsorption isotherms) for mild steel in 1.0 M HCl at various temperatures for the utilized corrosion inhibitors.

Inhibitor	Temperature (°C)	r^2	Slope	K_{ads} (M^{-1})	ΔG^0_{ads} ($kJ.mol^{-1}$)	ΔH^0_{ads} ($kJ.mol^{-1}$)	ΔS^0_{ads} ($J.mol^{-1}.K^{-1}$)
SNA	30	0.997	1.095	6.110	–14.67	–66.52	–150
	40	0.999	1.407	2.495	–12.83		
	50	0.998	2.707	1.090	–11.02		
SBZ	30	0.999	1.081	5.988	–14.63	–77.51	–208
	40	0.993	1.732	1.893	–12.11		
	50	0.996	1.126	0.888	–10.47		
SMX	30	0.999	1.077	2.488	–12.41	–55.63	–135
	40	0.999	1.144	1.734	–11.85		
	50	0.998	2.019	1.225	–11.33		
SCP	30	0.999	1.021	2.833	–12.74	–51.38	–126
	40	0.998	1.186	2.538	–12.87		
	50	0.996	1.435	0.811	–10.22		
SDM	30	0.999	1.003	2.726	–12.64	–63.19	–189
	40	0.996	1.324	1.257	–11.01		
	50	0.998	2.334	0.333	–07.83		
SSZ	30	0.999	3.552	1.605	–12.06	–54.74	–128
	40	0.998	0.991	1.213	–10.60		
	50	0.998	1.218	0.927	–10.22		
SMZ	30	0.999	1.424	3.144	–25.33	–85.41	–211
	40	0.999	1.073	1.942	–11.79		
	50	0.997	1.789	1.855	–12.44		
SMT	30	0.999	1.030	3.164	–13.02	–55.64	–140
	40	0.999	1.299	1.972	–12.22		
	50	0.998	2.144	0.829	–10.28		
SQX	30	0.999	1.015	1.898	–11.73	–65.12	–175
	40	0.999	1.152	1.264	–11.06		
	50	0.992	1.771	0.387	–08.23		

Table 4.7: Thermodynamic and adsorption parameters (Langmuir adsorption isotherms) for mild steel in 1.0 M HCl at 30 °C using PDP and EIS for the utilized corrosion inhibitors.

Inhibitor	Method	r^2	Slope	K_{ads} (M^{-1})	ΔG^0_{ads} ($kJ.mol^{-1}$)
SNA	PDP	0.998	1.074	3.663	-13.38
	EIS	0.999	1.162	3.206	-13.05
SBZ	PDP	0.999	1.081	5.988	-14.63
	EIS	0.999	0.986	4.170	-13.72
SMX	PDP	0.998	1.145	3.494	-13.27
	EIS	0.999	1.102	3.430	-13.22
SCP	PDP	0.999	1.011	2.159	-12.06
	EIS	0.995	0.918	1.180	-10.54
SDM	PDP	0.999	1.001	2.711	-12.63
	EIS	0.999	1.028	3.581	-13.33
SSZ	PDP	0.997	1.005	1.355	-10.88
	EIS	0.999	1.028	2.151	-12.05
SMZ	PDP	0.999	1.073	1.943	-11.79
	EIS	0.999	1.043	1.628	-11.35
SMT	PDP	0.997	0.989	1.801	-11.60
	EIS	0.999	1.032	3.184	-13.04
SQX	PDP	0.997	1.063	2.105	-11.99
	EIS	0.999	1.017	7.410	-15.16

A direct relationship between the surface coverage of the sulphanoamides corrosion inhibitors on the mild steel surface and the concentration of these inhibitors is best given by the Langmuir adsorption isotherm according to the following equation [125 − 127].

$$\frac{\theta}{1-\theta} = K_{ads} C_{inh} \tag{59}$$

where K_{ads} is the equilibrium constant for the adsorption of inhibitor molecules on the mild steel surface, C_{inh} is the molar concentration of inhibitor molecules and θ is the degree of surface coverage of inhibitor molecules on the mild steel surface. Rearrangement of this equation produces a much simpler relationship of the form:

$$\frac{C_{inh}}{\theta} = \frac{1}{K_{ads}} + C_{inh} \tag{60}$$

Langmuir plots are shown in Figures 4.72−4.80 (as obtained from the weight loss methods) at 30 °C and Figure 4.81−4.82 (as obtained from the electrochemical methods) at 30 °C.

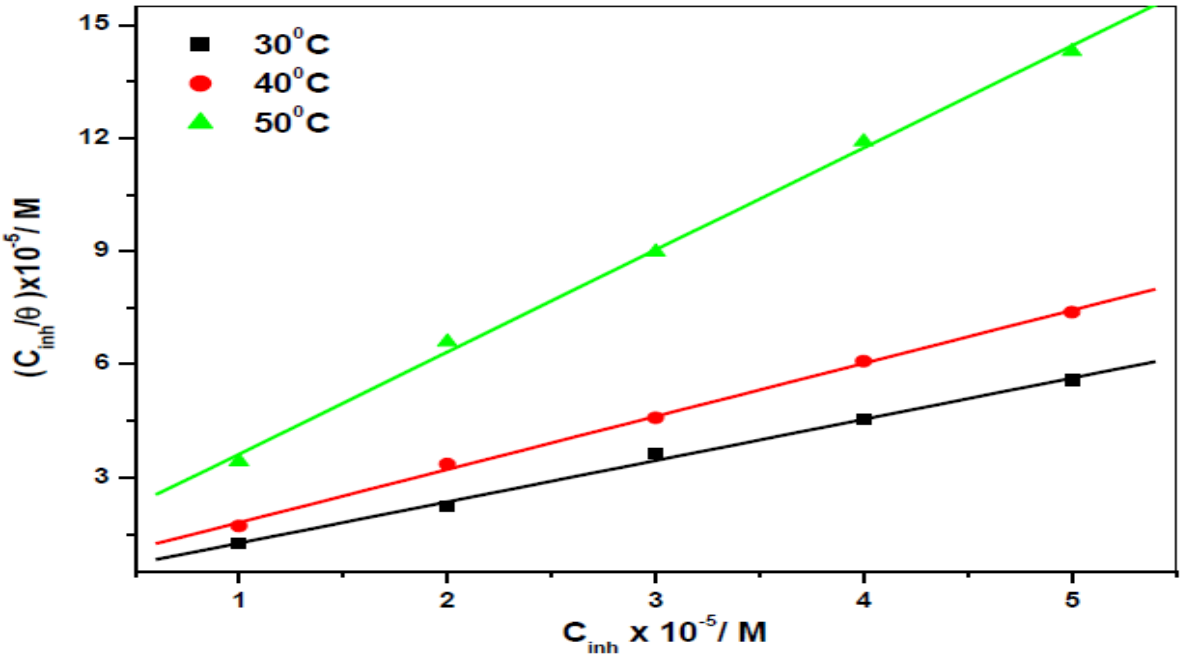

Figure 4.71: Langmuir adsorption isotherms for the corrosion of mild steel in 1.0 M HCl at various temperatures for SNA corrosion inhibitor.

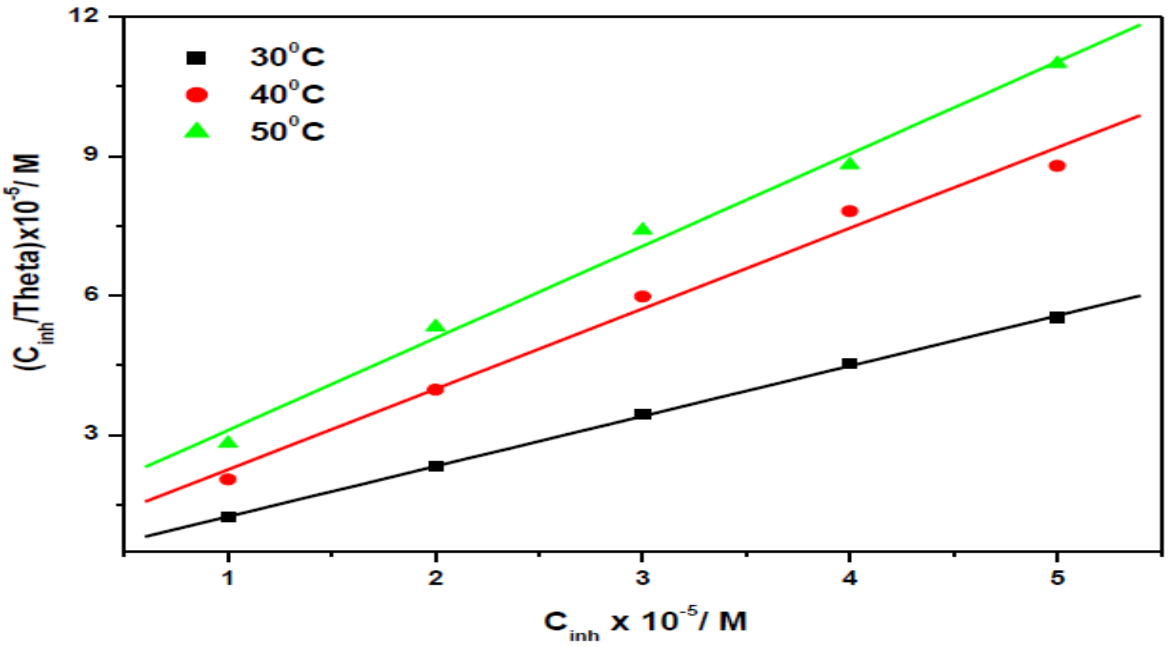

Figure 4.72: Langmuir adsorption isotherms for the corrosion of mild steel in 1.0 M HCl at various temperatures for SBZ corrosion inhibitor.

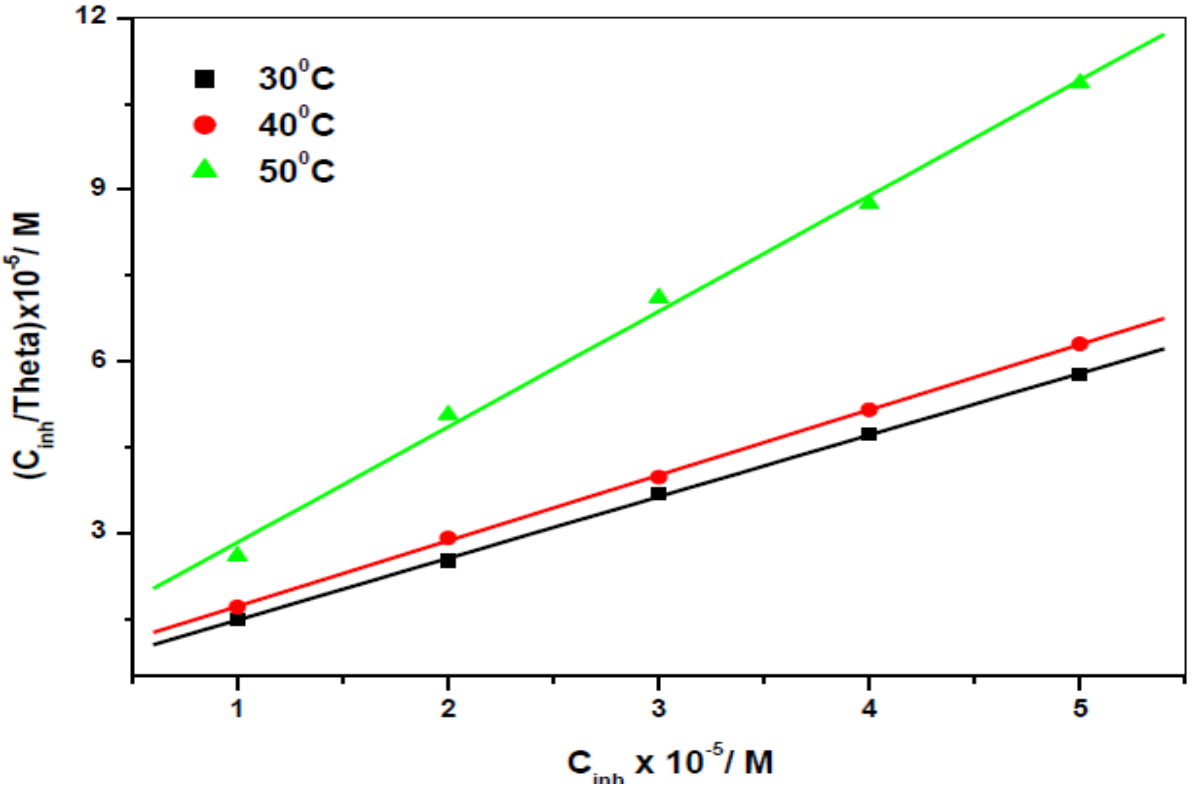

Figure 4.73: Langmuir adsorption isotherms for the corrosion of mild steel in 1.0 M HCl at various temperatures for SMX corrosion inhibitor.

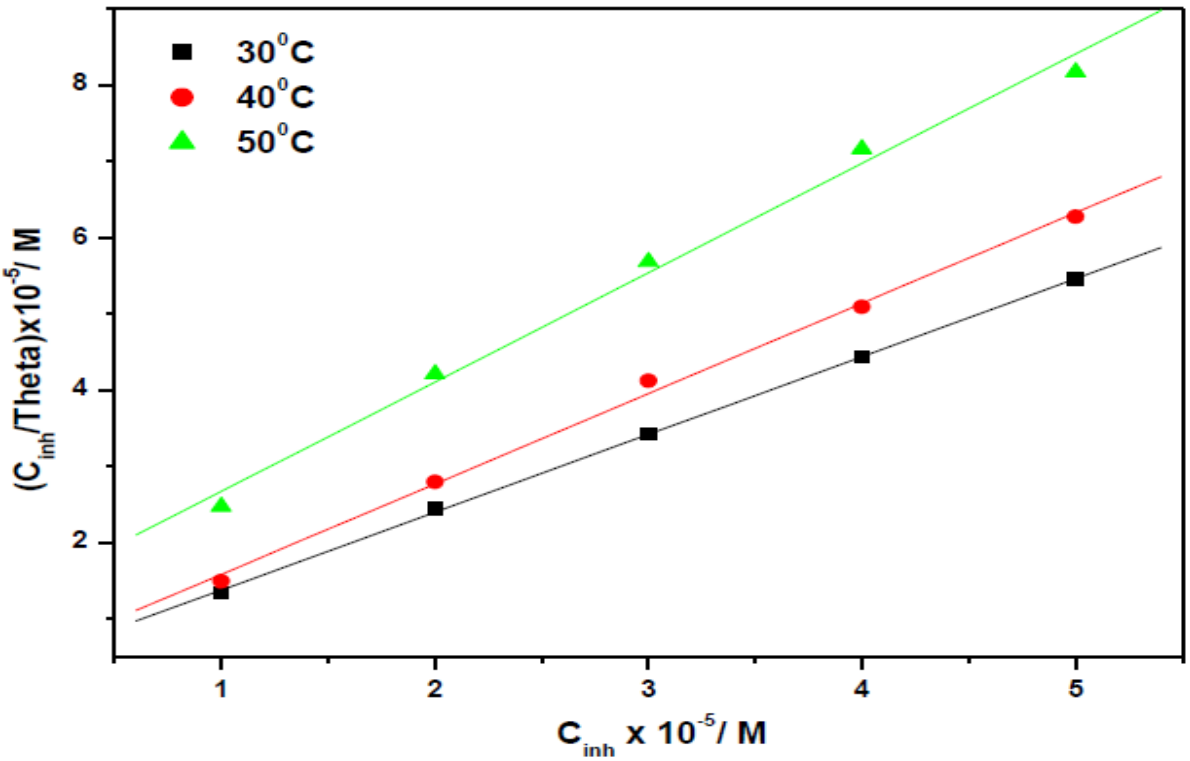

Figure 4.74: Langmuir adsorption isotherms for the corrosion of mild steel in 1.0 M HCl at various temperatures for SCP corrosion inhibitor.

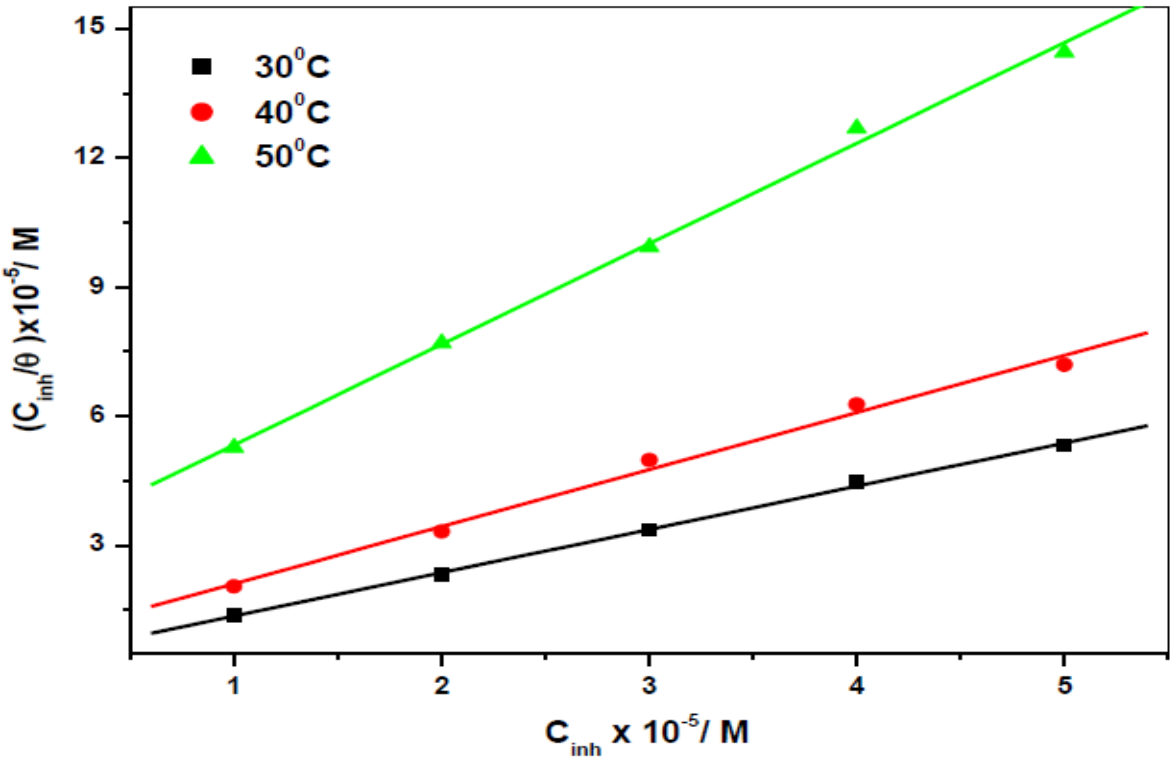

Figure 4.75: Langmuir adsorption isotherms for the corrosion of mild steel in 1.0 M HCl at various temperatures for SDM corrosion inhibitor.

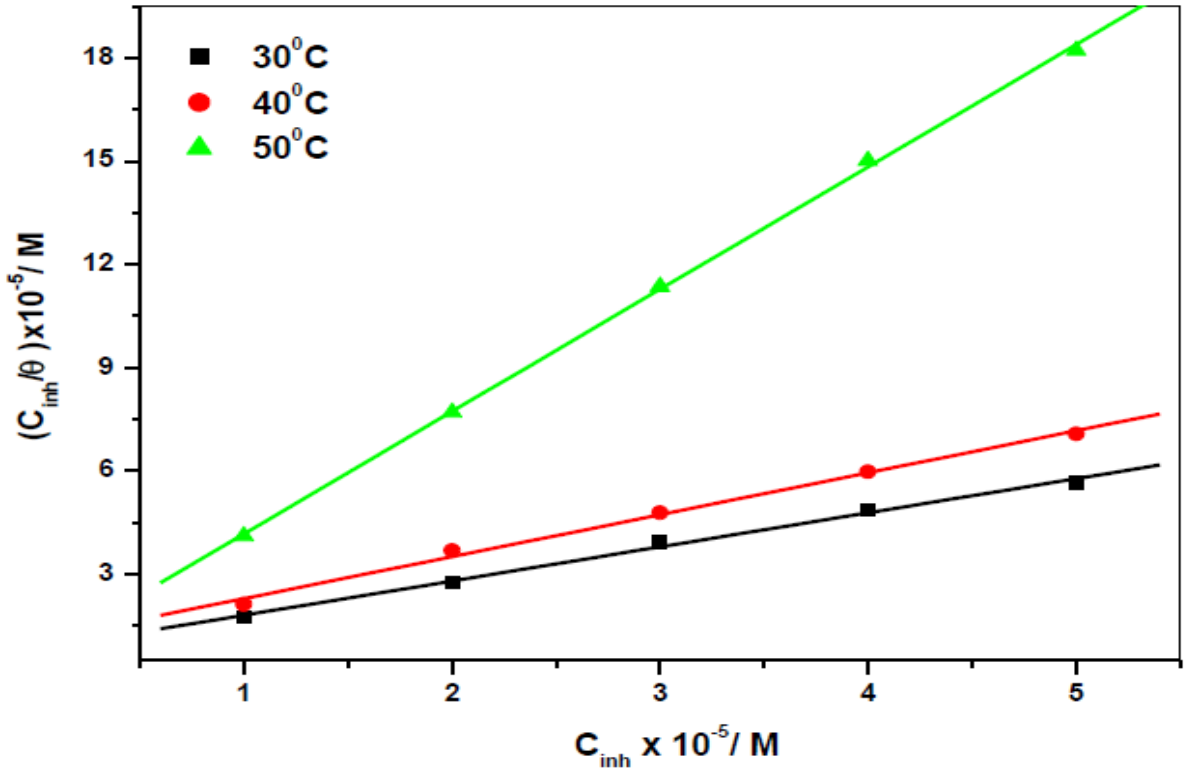

Figure 4.76: Langmuir adsorption isotherms for the corrosion of mild steel in 1.0 M HCl at various temperatures for SSZ corrosion inhibitor.

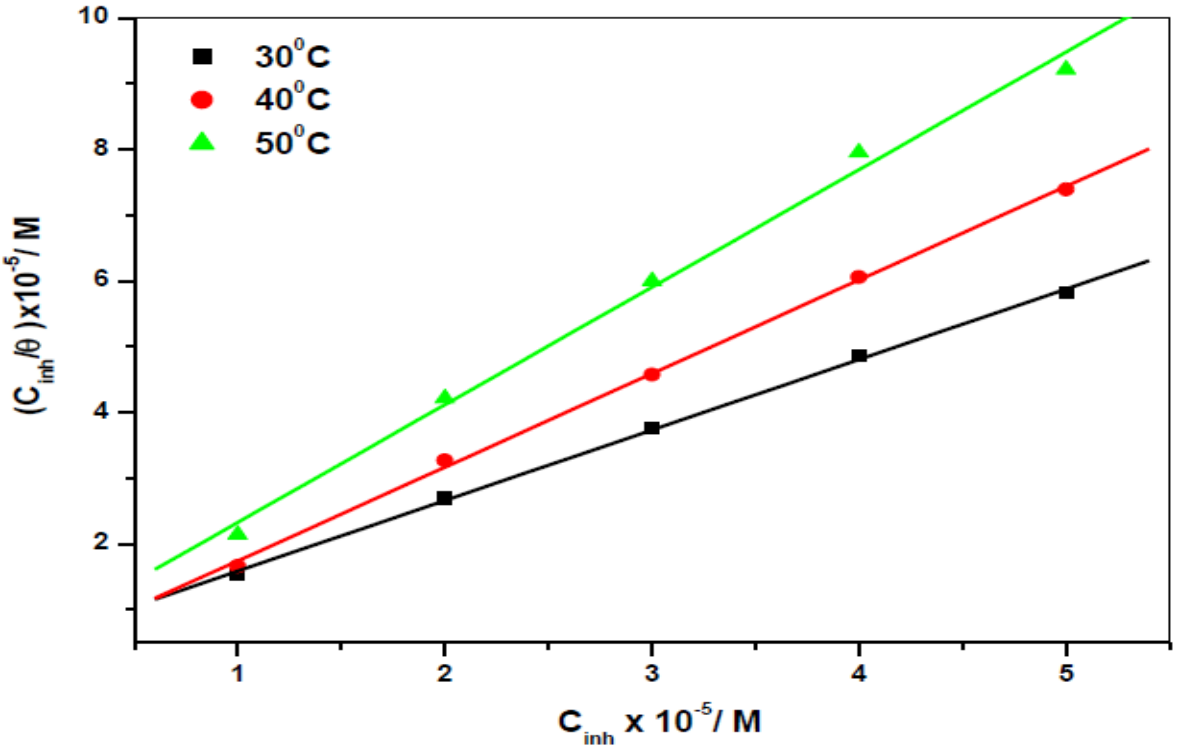

Figure 4.77: Langmuir adsorption isotherms for the corrosion of mild steel in 1.0 M HCl at various temperatures for SMZ corrosion inhibitor.

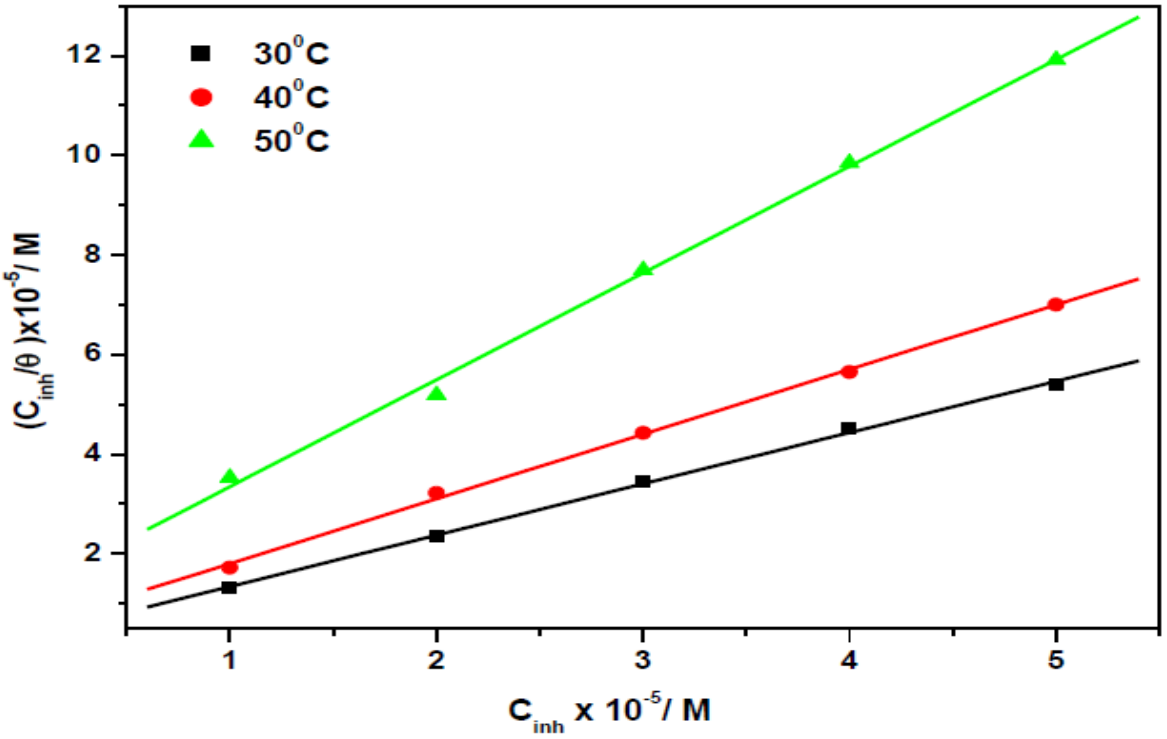

Figure 4.78: Langmuir adsorption isotherms for the corrosion of mild steel in 1.0 M HCl at various temperatures for SMT corrosion inhibitor.

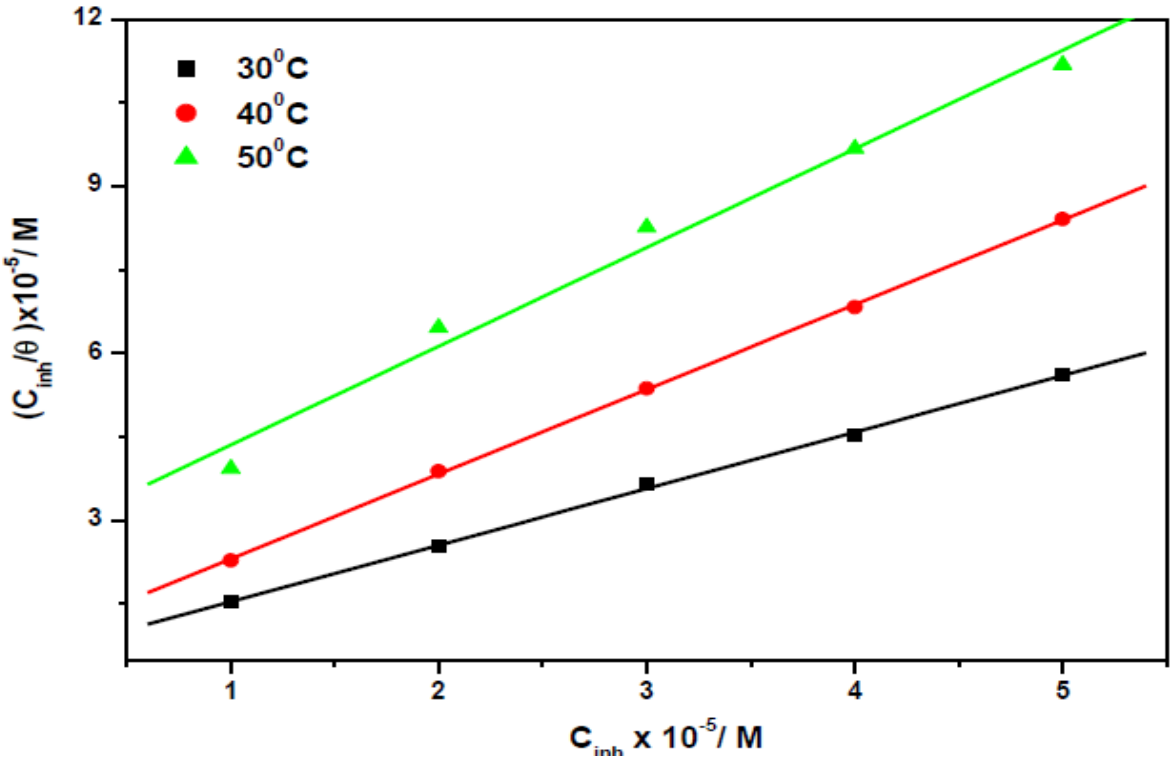

Figure 4.79: Langmuir adsorption isotherms for the corrosion of mild steel in 1.0 M HCl at various temperatures for SQX corrosion inhibitor.

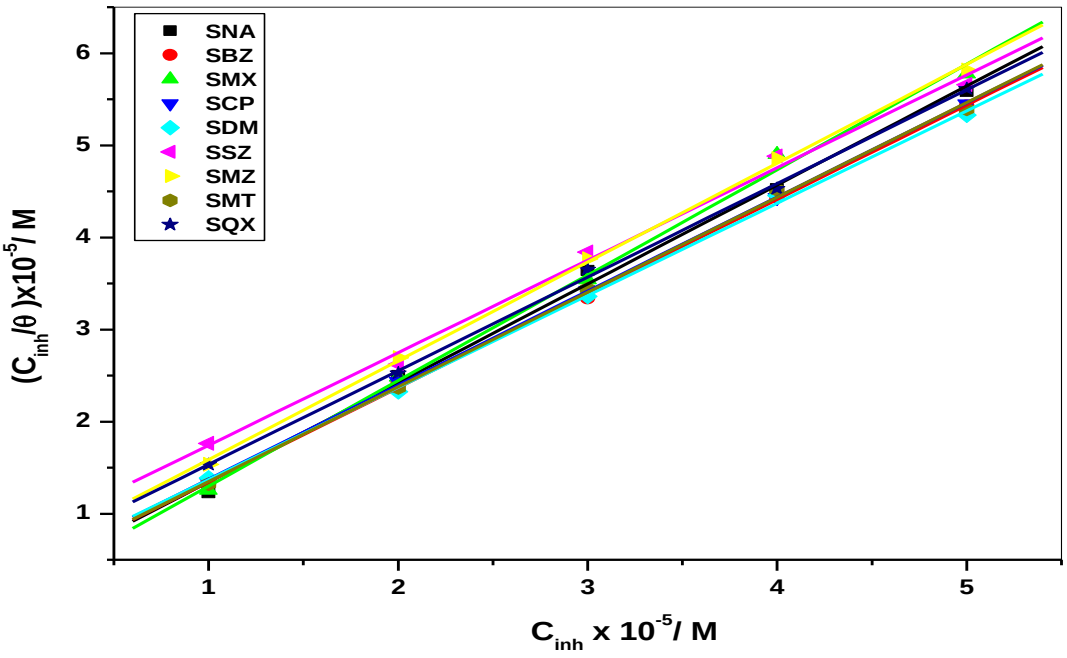

Figure 4.80: Langmuir adsorption isotherms for the corrosion of mild steel in 1.0 M HCl obtained from the PDP results at 30° C for SNA, SBZ, SMX, SCP, SDM, SSZ, SMZ, SMT and SQX corrosion inhibitors.

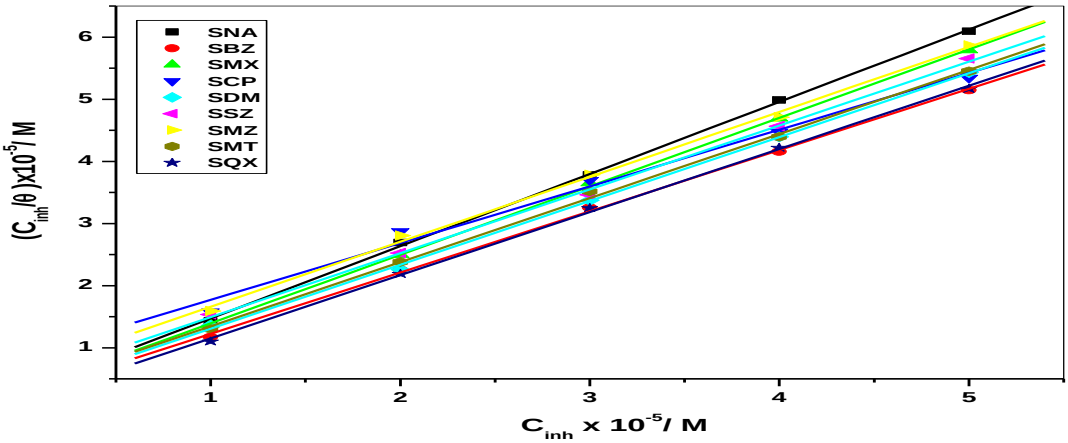

Figure 4.81: Langmuir adsorption isotherms for the corrosion of mild steel in 1.0 M HCl obtained from the EIS results at 30° C for SNA, SBZ, SMX, SCP, SDM, SSZ, SMZ, SMT and SQX corrosion inhibitors.

These figures enabled the calculation of the values of adsorption equilibrium constants. The significance of these values lies in the fact that they can be interpreted to provide information regarding the strength between the adsorbate molecules and the adsorbate surfaces; an efficient adsorption process that leads to better inhibition efficiency is often obtained when the adsorption equilibrium constants have large values. From values of adsorption equilibrium constants, standard free energy of adsorption can be calculated as:

$$\Delta G^{\circ}_{ads} = -RT \ln(55.5K_{ads}) \quad (61)$$

where ΔG° is the standard free energy of adsorption and the value 55.5 represents the molar concentration of water in solution. Studies indicates that values of $\Delta G°_{ads}$ varying between -40 kJ.mol^{-1} and above are symbolic of the sharing or transfer of an electron from the adsorbate molecules to the substrate surfaces resulting into a coordinate type of bond (chemisorption) while those around -20 kJ.mol^{-1} and lower are symbolic of an electrostatic interaction between the charged adsorbate and charged surfaces of the substrate (physisorption) [127, 128]. The values of $\Delta G°_{ads}$ reported in Tables 5.6 and 5.7 show a negative nature which is an indication of spontaneity of the adsorption process and the stability of the adsorbed film on the surface of mild steel [129]. The trend in these values is utilized to further explain the nature of adsorption between mild steel and corrosion inhibitors. In cases where $\Delta G°_{ads}$ increases with increase in temperature, an exothermic adsorption is predominant whereas in cases where $\Delta G°_{ads}$ decreases with increase in temperature indicates the occurrence of an endothermic adsorption [119]. The values of $\Delta G°_{ads}$ are increasing with increase in temperature, thus the adsorption between mild steel surface and sulfonamides inhibitors is of an exothermic nature which signifies either chemisorption or physisorption. This inhibitor behaviour correlates very well with the one predicted by the electrochemical measurements. The results from the weight loss and electrochemical measurements show that the order of inhibition efficiency by the sulphonamides follows the order: SDM > SMT > SBZ > SCP > SNA > SQX > SSZ > SMX > SMZ.

4.2 ALUMINIUM

4.2.1 POTENTIODYNAMIC POLARIZATION (PDP)

The corrosion of aluminium is an electrochemical process involving both the cathodic reduction of H^+ ions and anodic dissolution of aluminium [130, 131]. In order to understand the mechanism of corrosion and inhibition processes, potentiodynamic polarization measurements were carried out for aluminium in hydrochloric acid solutions in the absence and presence of sulphonamide inhibitors of different concentrations at 30°C, and Figures 4.83 – 4.91 show the current-potential curves (Tafel plots) that were obtained.

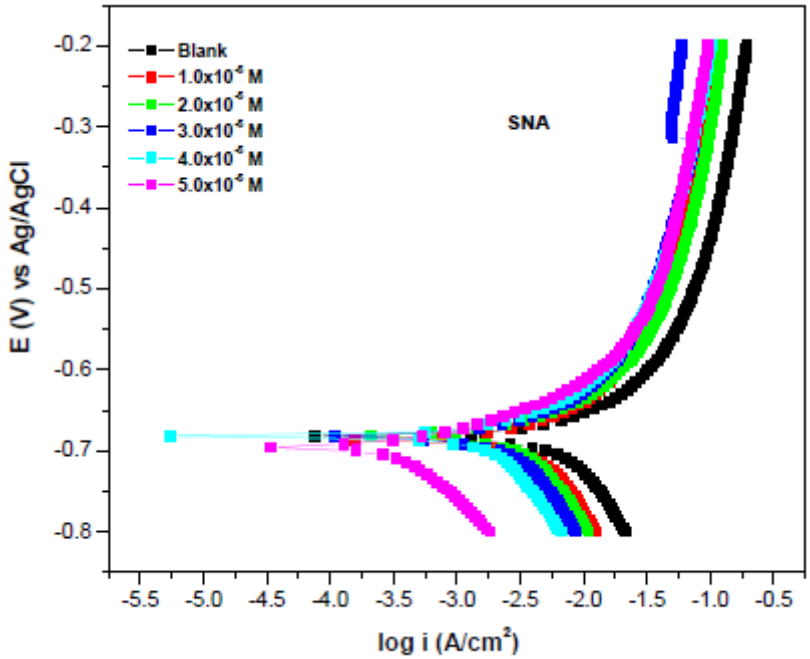

Figure 4.82: Tafel plots for aluminum in 1 M HCl in the absence and presence of different concentrations of SNA inhibitor compound.

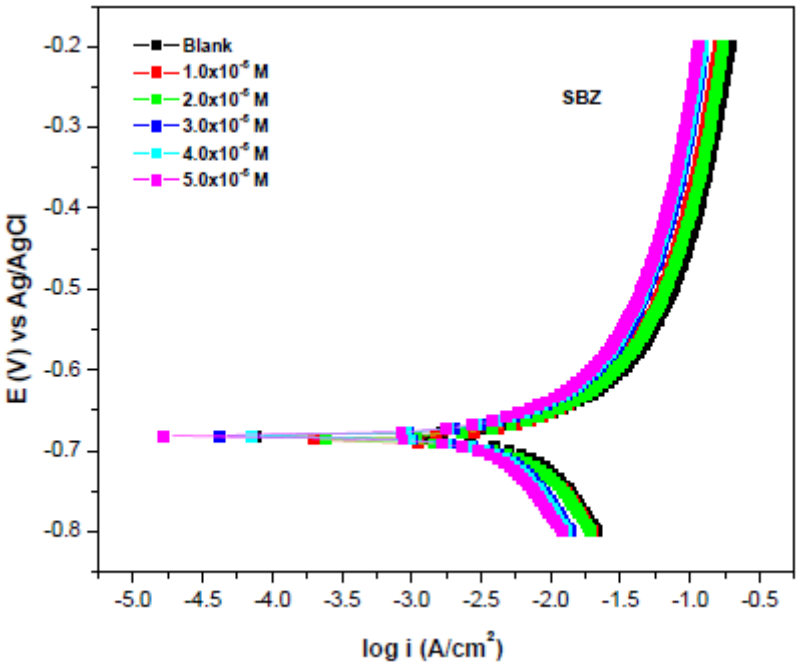

Figure 4.83: Tafel plots for aluminum in 1 M HCl in the absence and presence of different concentrations of SBZ inhibitor compound.

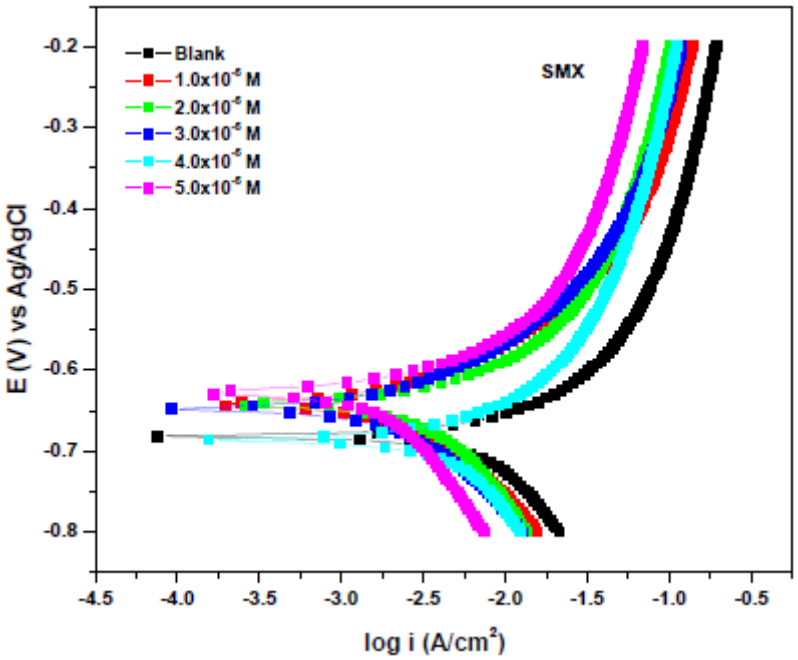

Figure 4.84: Tafel plots for aluminum in 1 M HCl in the absence and presence of different concentrations of SMX inhibitor compound.

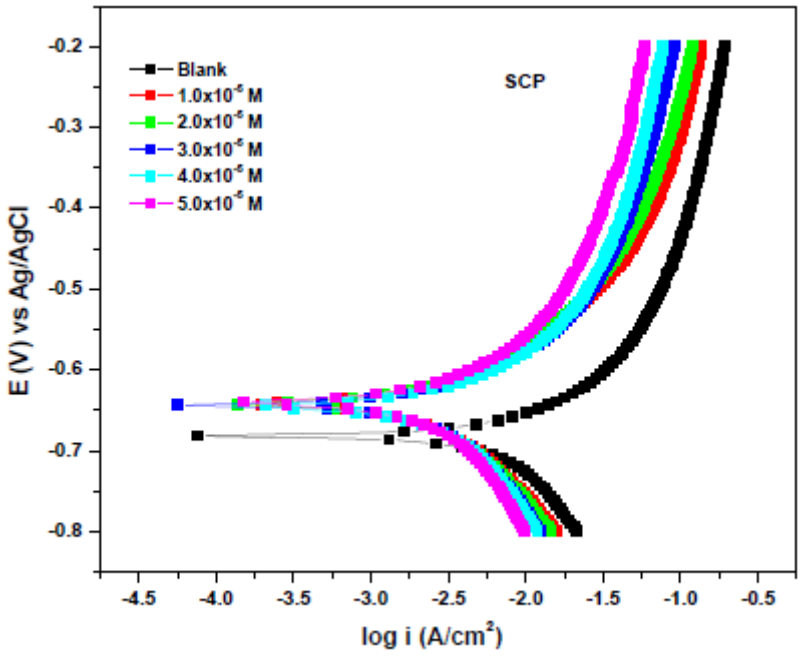

Figure 4.85: Tafel plots for aluminum in 1 M HCl in the absence and presence of different concentrations of SCP inhibitor compound.

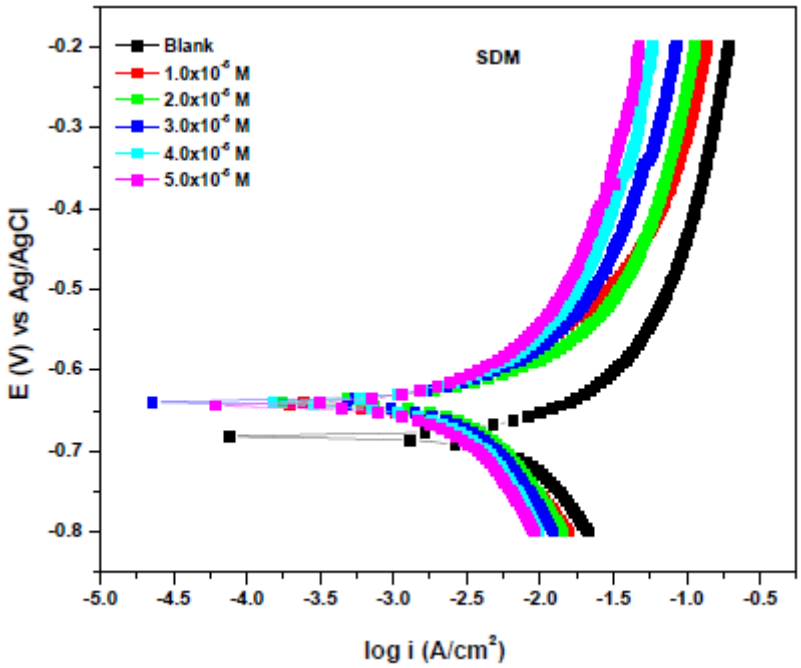

Figure 4.86: Tafel plots for aluminum in 1 M HCl in the absence and presence of different concentrations of SDM inhibitor compound.

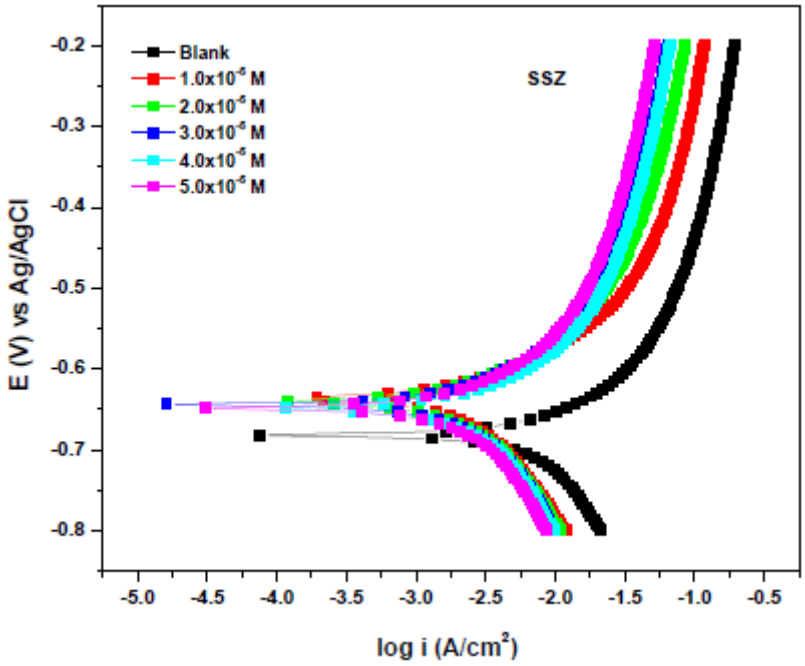

Figure 4.87: Tafel plots for aluminum in 1 M HCl in the absence and presence of different concentrations of SSZ inhibitor compound.

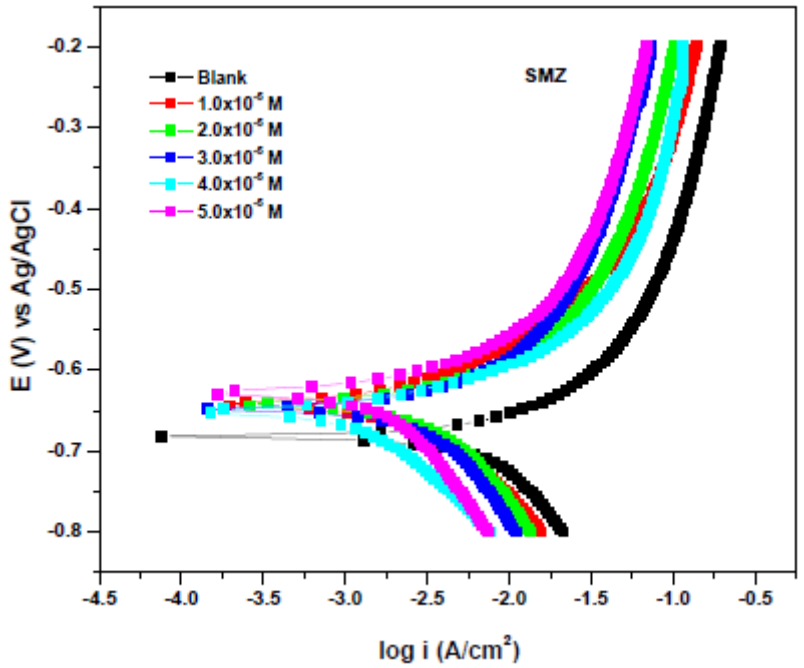

Figure 4.88: Tafel plots for aluminum in 1 M HCl in the absence and presence of different concentrations of SMZ inhibitor compound.

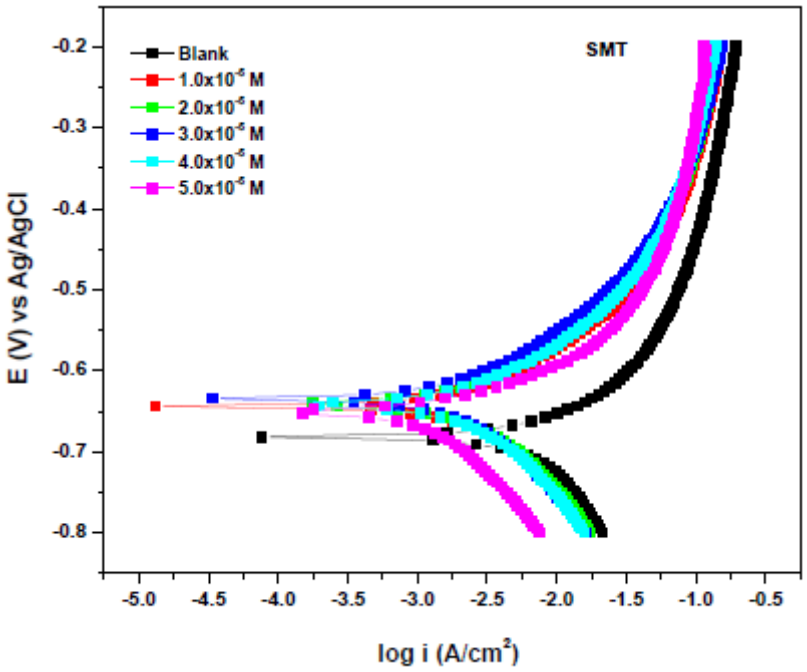

Figure 4.89: Tafel plots for aluminum in 1 M HCl in the absence and presence of different concentrations of SMT inhibitor compound.

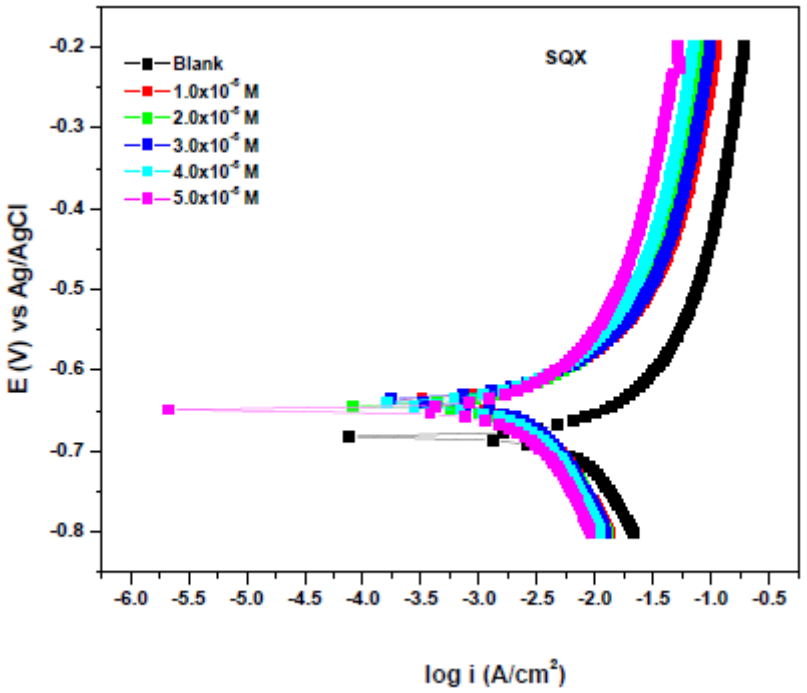

Figure 4.90: Tafel plots for aluminum in 1 M HCl in the absence and presence of different concentrations of SQX inhibitor compound.

These plots show the same trend for both the absent and presence of inhibitors cases, indicating that the mechanism of corrosion of aluminium is the same as that of the inhibition process. It can also be observed from these figures that both anodic and cathodic half-reactions are altered through the introduction of all inhibitors used. That is, the cathodic reduction of H^+ ions is hindered while the anodic dissolution of aluminium is minimized.

Table 4.8: Potentiodynamic polarization (PDP) parameters such as corrosion potential (E_{corr}), corrosion current density (i_{corr}) and anodic and cathodic Tafel slopes (b_a and b_c) using different inhibitors

Inhibitor	Inhibitor Conc. (M)	$-E_{corr}$(mV) with Ag/AgCl	i_{corr}(mA.cm^{-2})	R_p(10^{-1}) (Ohm)	b_a (V.dec^{-1})	b_c (V.dec^{-1})	%IE_{PDP}	%IE_{WL}
Blank		712	8.63	4.99	9.82	8.95	-	-
SNA	1.0×10^{-5}	650	2.53	3.18	1.52	0.69	70.68	95.92
	2.0×10^{-5}	648	1.85	2.53	0.21	0.05	78.56	96.31
	3.0×10^{-5}	637	1.47	3.29	0.11	0.14	82.96	96.83
	4.0×10^{-5}	641	1.43	3.14	0.10	0.10	83.42	98.16
	5.0×10^{-5}	644	1.27	3.22	0.09	0.09	85.28	99.60
SBZ	1.0×10^{-5}	621	1.99	3.65	1.13	0.66	76.94	96.57
	2.0×10^{-5}	599	1.61	3.22	1.52	0.56	81.34	96.57
	3.0×10^{-5}	666	1.13	3.12	1.51	0.88	86.90	96.84
	4.0×10^{-5}	614	1.10	2.56	0.99	0.95	87.25	97.89
	5.0×10^{-5}	621	1.01	3.68	0.41	0.65	88.29	99.47
SMX	1.0×10^{-5}	588	1.78	3.69	1.88	0.98	79.37	90.95
	2.0×10^{-5}	548	1.68	2.56	1.78	0.97	80.53	97.82
	3.0×10^{-5}	622	1.44	4.78	1.47	1.08	83.31	98.18
	4.0×10^{-5}	615	1.05	2.58	1.99	2.82	87.83	99.06
	5.0×10^{-5}	589	0.94	2.22	2.58	2.15	89.11	99.13
SCP	1.0×10^{-5}	631	2.64	1.98	2.14	1.45	69.40	60.74
	2.0×10^{-5}	645	2.81	2.01	1.99	0.98	67.43	64.56
	3.0×10^{-5}	615	2.60	2.14	1.84	1.02	69.87	65.74
	4.0×10^{-5}	608	2.51	2.56	1.95	0.78	70.91	68.51
	5.0×10^{-5}	645	2.43	2.41	2.54	1.44	71.84	70.09
SDM	1.0×10^{-5}	566	2.99	2.98	1.98	1.54	65.35	63.24
	2.0×10^{-5}	614	2.85	2.36	1.97	1.56	66.97	66.00
	3.0×10^{-5}	598	2.61	3.12	1.69	2.08	69.75	70.88
	4.0×10^{-5}	601	2.60	3.01	1.65	0.96	69.87	76.94
	5.0×10^{-5}	613	2.51	3.11	2.05	1.55	70.91	79.71
SSZ	1.0×10^{-5}	589	0.91	3.61	2.01	1.66	89.45	89.85
	2.0×10^{-5}	601	0.87	2.98	1.99	1.54	89.91	91.96
	3.0×10^{-5}	578	0.78	2.52	1.85	1.21	90.96	92.62
	4.0×10^{-5}	612	0.74	3.12	1.84	1.81	91.42	93.14
	5.0×10^{-5}	613	0.69	3.14	1.47	1.68	92.00	94.07
SMZ	1.0×10^{-5}	618	1.69	2.96	1.99	1.87	80.41	83.85
	2.0×10^{-5}	598	1.45	2.87	1.67	1.85	83.19	91.89
	3.0×10^{-5}	612	1.11	2.55	1.55	1.99	87.13	93.77
	4.0×10^{-5}	615	0.98	3.10	1.41	1.84	88.64	94.42
	5.0×10^{-5}	599	0.81	3.12	1.58	1.78	90.61	94.71
SMT	1.0×10^{-5}	598	1.78	2.96	1.99	1.87	79.37	81.61
	2.0×10^{-5}	498	1.65	2.87	1.67	1.85	80.88	87.32
	3.0×10^{-5}	444	1.62	2.55	1.55	1.99	81.22	87.40
	4.0×10^{-5}	415	1.11	3.10	1.41	1.84	87.13	92.54
	5.0×10^{-5}	555	0.41	3.12	1.58	1.78	95.24	93.92
SQX	1.0×10^{-5}	614	1.18	6.56	31	54	86.32	80.23
	2.0×10^{-5}	661	1.10	5.17	36	69	87.25	80.89
	3.0×10^{-5}	541	0.84	6.04	19	58	90.26	81.68
	4.0×10^{-5}	584	0.55	3.80	37	34	93.62	83.00
	5.0×10^{-5}	514	0.40	5.71	26	25	95.36	84.84

These plots were extrapolated through their Tafel segments and some important potentiodynamic parameters including the Tafel anodic and cathodic slopes (b_a and b_c), corrosion potential (E_{corr}) and corrosion current density (i_{corr}) were obtained and recorded in Table 4.8. The corrosion current densities of the blank and inhibited experiments were used to calculate the potentiodynamic polarization inhibition efficiency using the equation 41.

A careful examination of Table 4.8 shows that both anodic and cathodic current densities were decreased by the introduction of all sulphonamide compounds, signifying that the anodic dissolution of aluminium was minimized and the cathodic reduction of H^+ ions was hindered. The values of E_{corr} using all inhibitors show no particular trend. This observation means that these sulphonamides inhibitors are of a mixed-type nature [132 – 134]. The values of both anodic and cathodic Tafel slopes for the blank processes are very different from those for the inhibited processes. This observation further informs that the presence of the inhibitors had some effect on the anodic and cathodic half-reactions. The maximum inhibition efficiency of 95.36 % was achieved using SQX at 30°C.

4.2.2 ELECTROCHEMICAL IMPEDANCE SPECTROSCOPY (EIS)

Research has shown that it is necessary to follow the behaviour of the corrosion of metal against time [135, 136]. Electrochemical impedance spectroscopy has various advantages, including providing insights into the behaviour of the corrosion of metal against time as well as the surface properties of the metal and inhibitors. The characteristic nature of the impedance from the Nyquist plots which are obtained from EIS provide some insights regarding the mechanism of the process of corrosion inhibition. Nyquist plots, represented by the imperfect semicircles and their corresponding bode plots are shown in Figures 4.91 – 5.108. Careful comparison of the blank imperfect circles with those of the inhibited process shows that the diameter of the blank is much smaller than that of the inhibited processes. Further comparison reveals that the least concentration of the inhibitor (1.0×10^{-5} M) produced the least diameter size of these semicircles as compared to the highest concentration (5.0×10^{-5} M). The imperfect character is a result of the formation of the adsorption film on the mild steel surface as well as a transfer of charge. The larger diameter size of the semicircles resulting from the highest inhibitor concentration shows that as there are more inhibitor molecules available in the corrosive medium, the rate of formation of the adsorption film increases and consequently the inhibition efficiency increases.

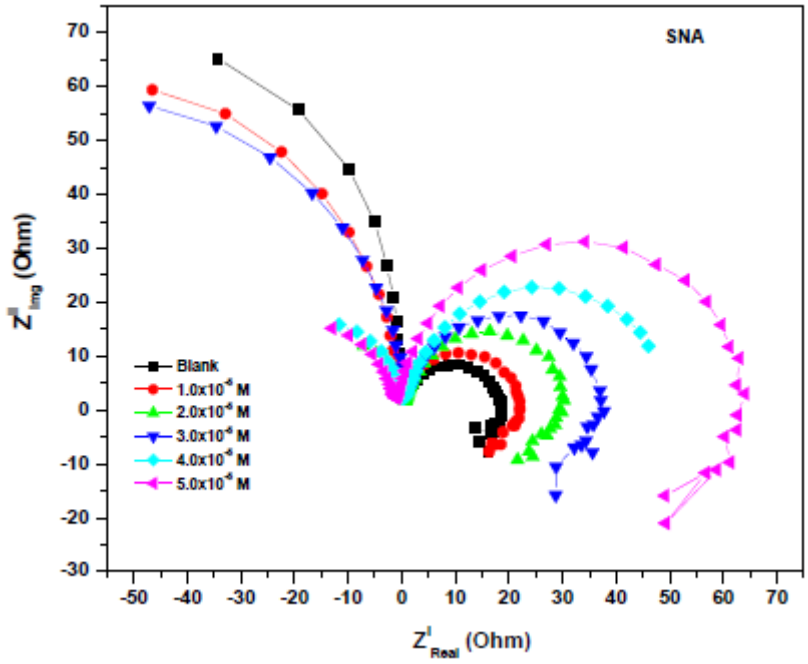

Figure 4.91: Nyquist plot of aluminium in 1 M HCl in the absence and presence of different concentrations of SNA inhibitor compound.

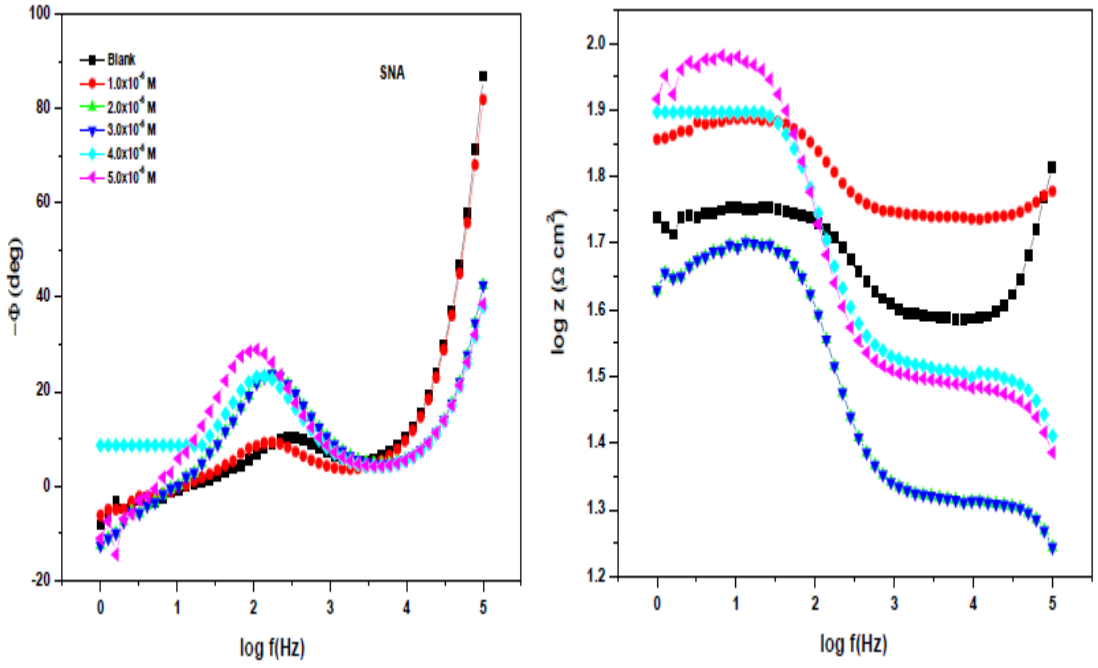

Figure 4.92: Bode plots of mild steel in 1 M HCl in the absence and presence of different concentrations of SNA inhibitor compound.

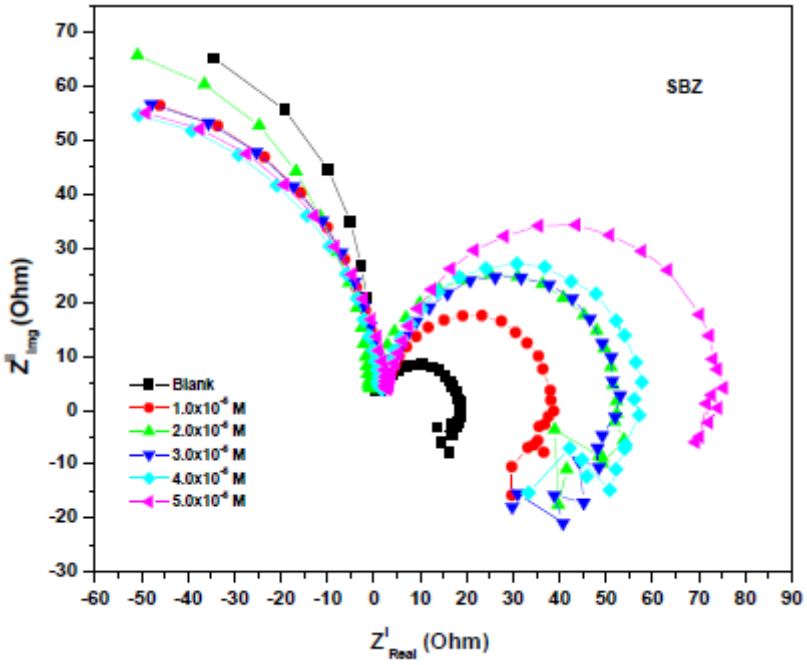

Figure 4.93: Nyquist plot of aluminium in 1 M HCl in the absence and presence of different concentrations of SBZ inhibitor compound.

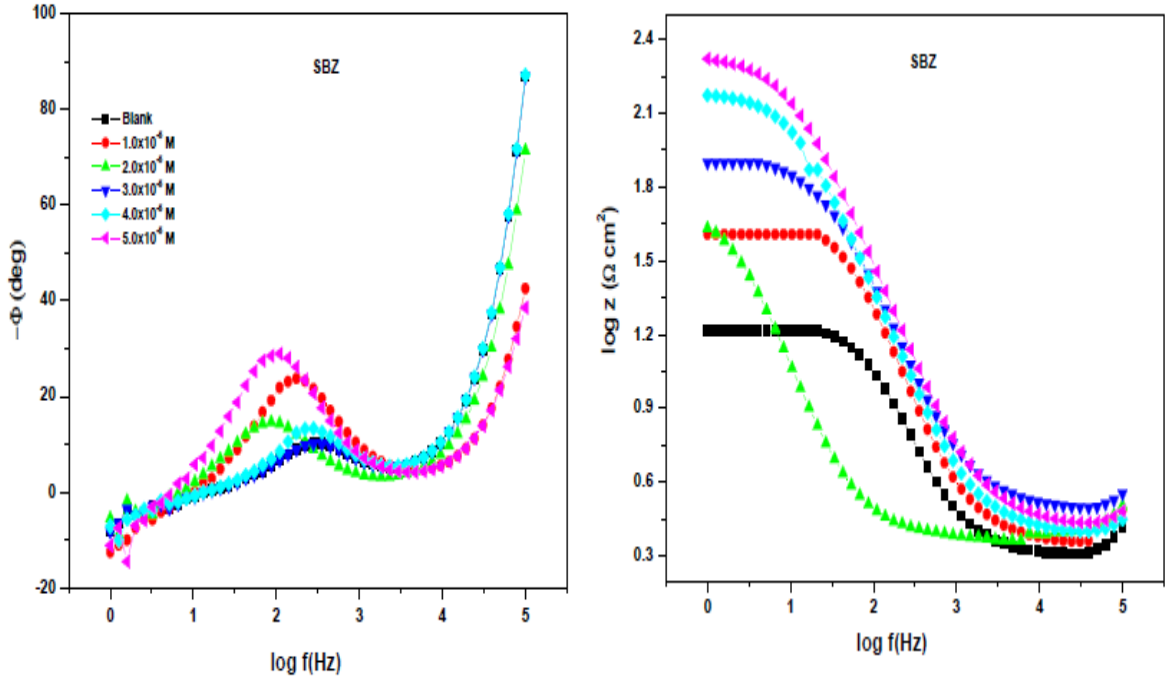

Figure 4.94: Bode plots of mild steel in 1 M HCl in the absence and presence of different concentrations of SBZ inhibitor compound.

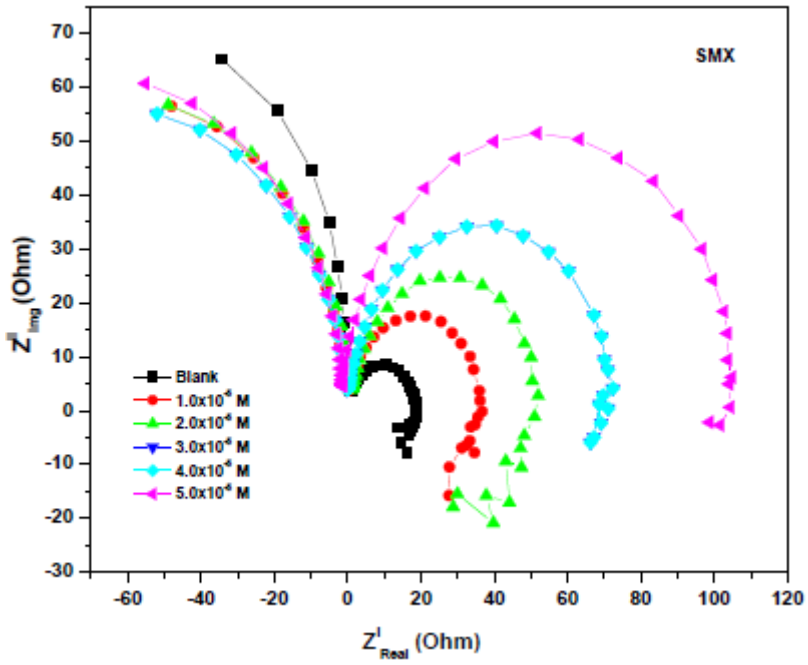

Figure 4.95: Nyquist plot of aluminium in 1 M HCl in the absence and presence of different concentrations of SMX inhibitor compound.

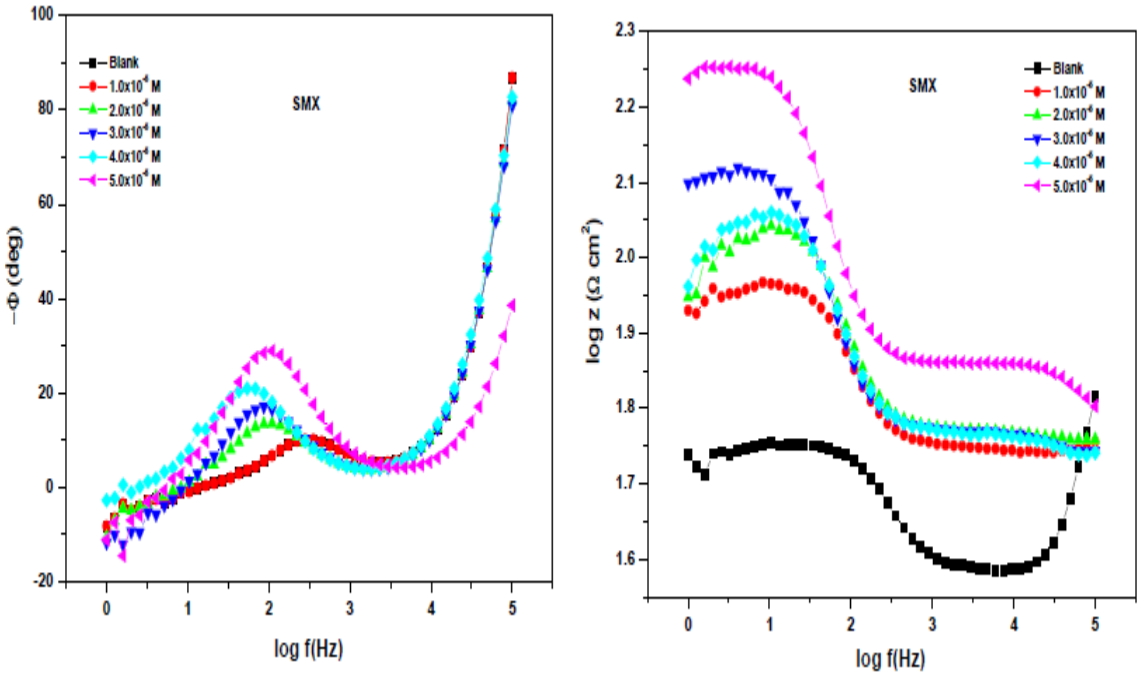

Figure 4.96: Bode plots of mild steel in 1 M HCl in the absence and presence of different concentrations of SMX inhibitor compound.

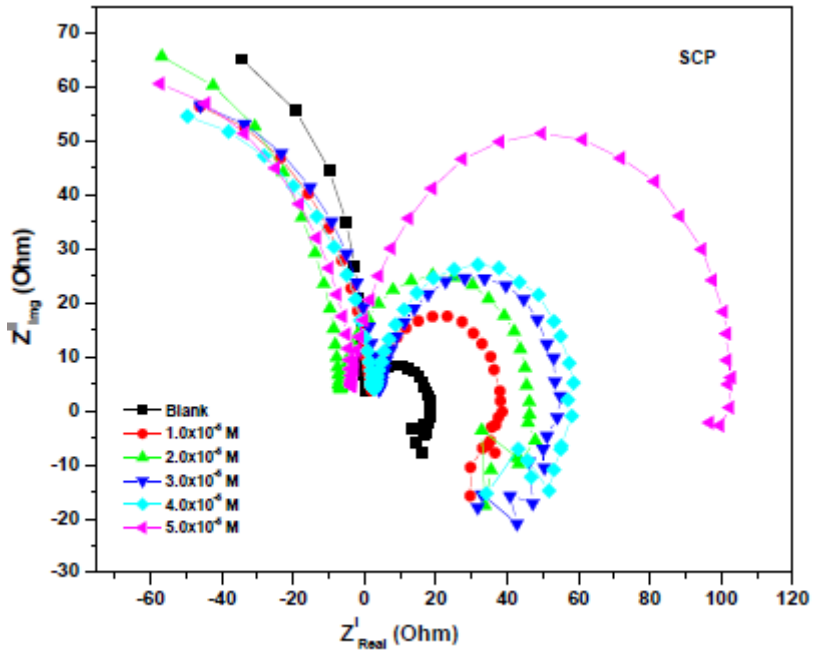

Figure 4.97: Nyquist plot of aluminum, in 1 M HCl in the absence and presence of different concentrations of SCP inhibitor compound.

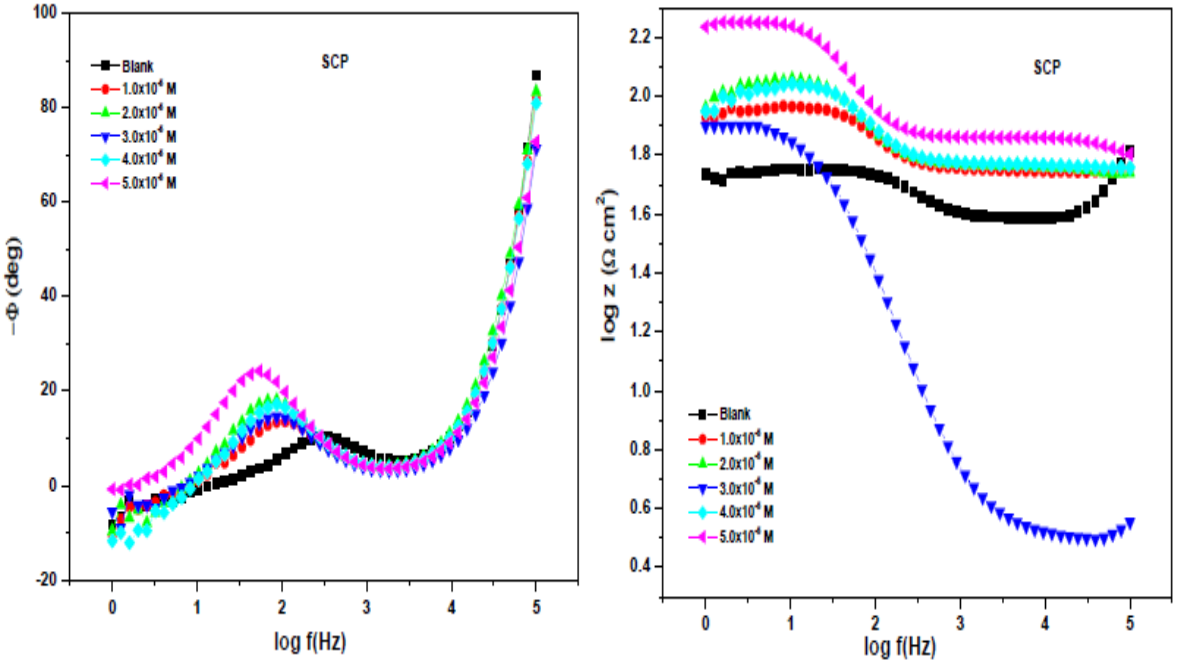

Figure 4.98: Bode plots of mild steel in 1 M HCl in the absence and presence of different concentrations of SCP inhibitor compound.

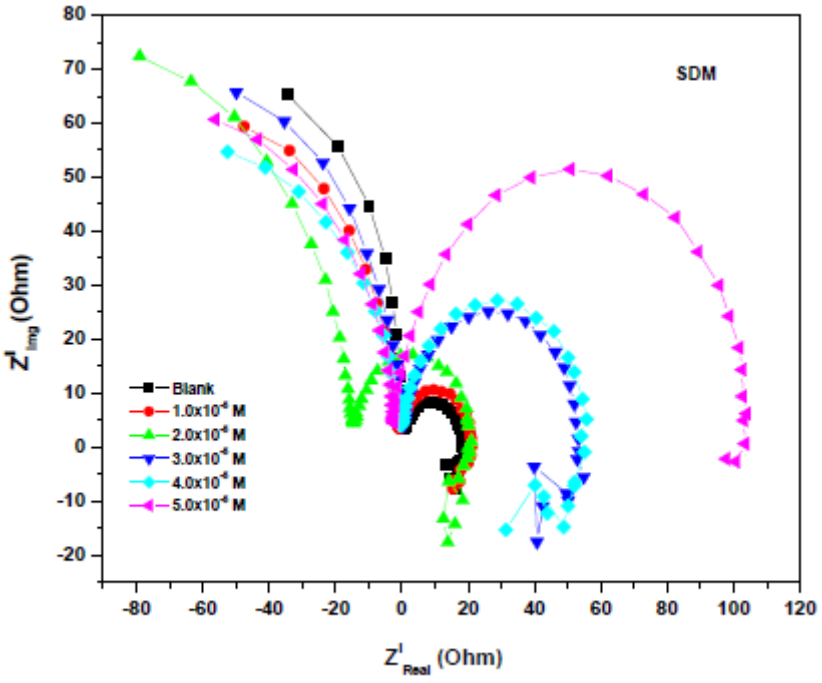

Figure 4.99: Nyquist plot of aluminium in 1 M HCl in the absence and presence of different concentrations of SDM inhibitor compound.

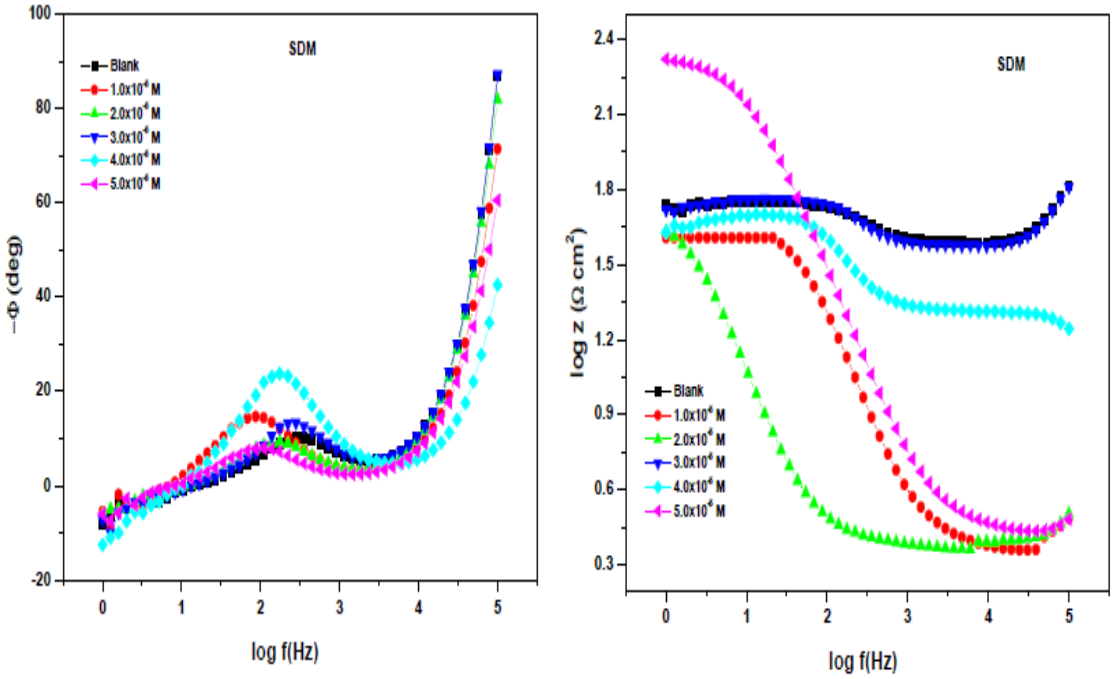

Figure 4.100: Bode plots of mild steel in 1 M HCl in the absence and presence of different concentrations of SDM inhibitor compound.

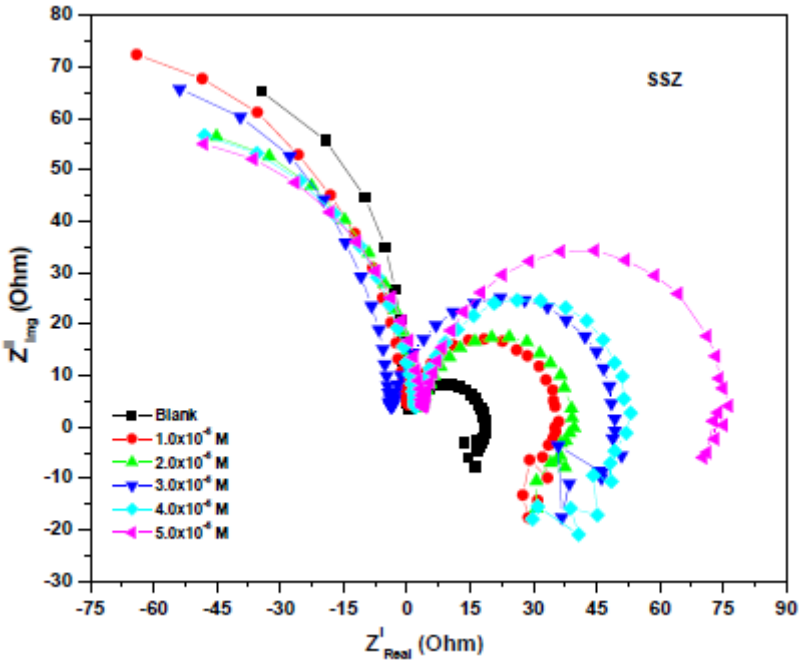

Figure 4.101: Nyquist plot of aluminium in 1 M HCl in the absence and presence of different concentrations of SSZ inhibitor compound.

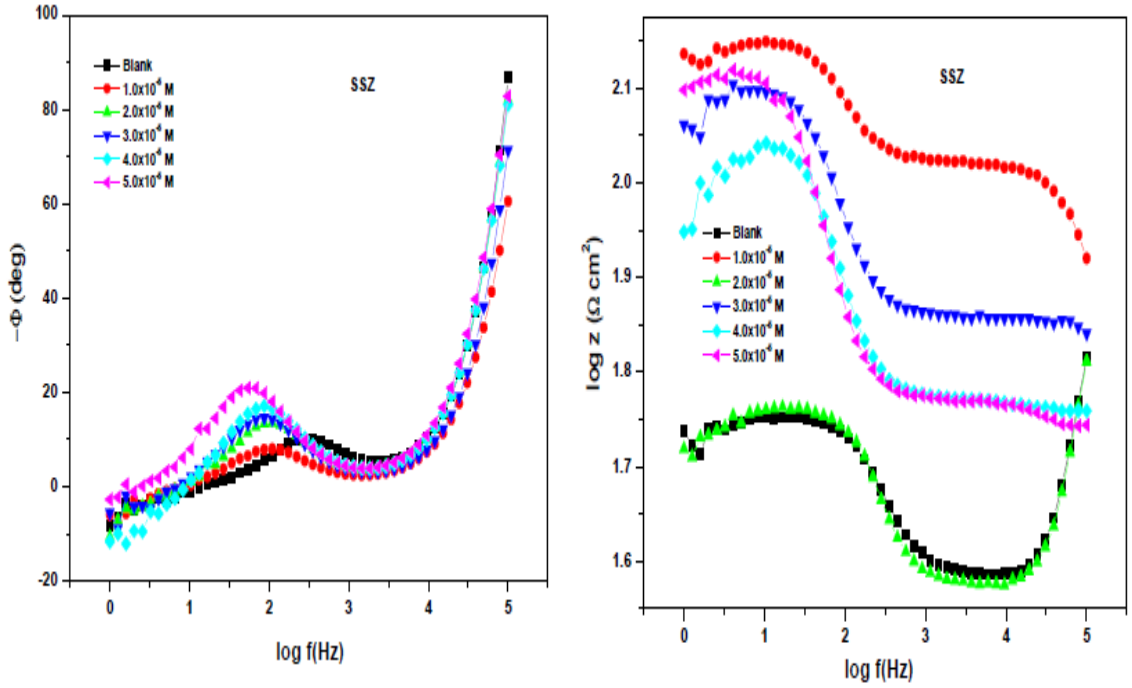

Figure 4.102: Bode plots of mild steel in 1 M HCl in the absence and presence of different concentrations of SSZ inhibitor compound.

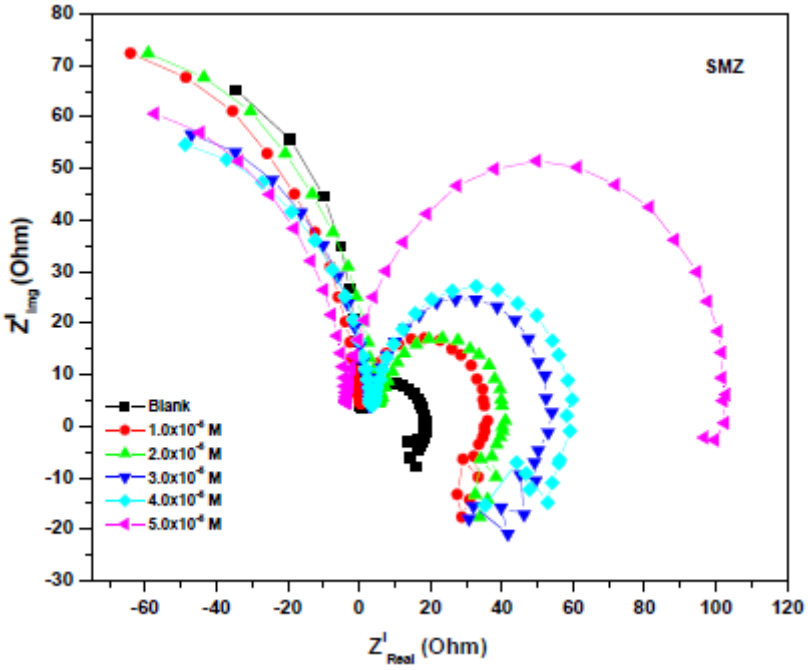

Figure 4.103: Nyquist plot of aluminium in 1 M HCl in the absence and presence of different concentrations of SMZ inhibitor compound.

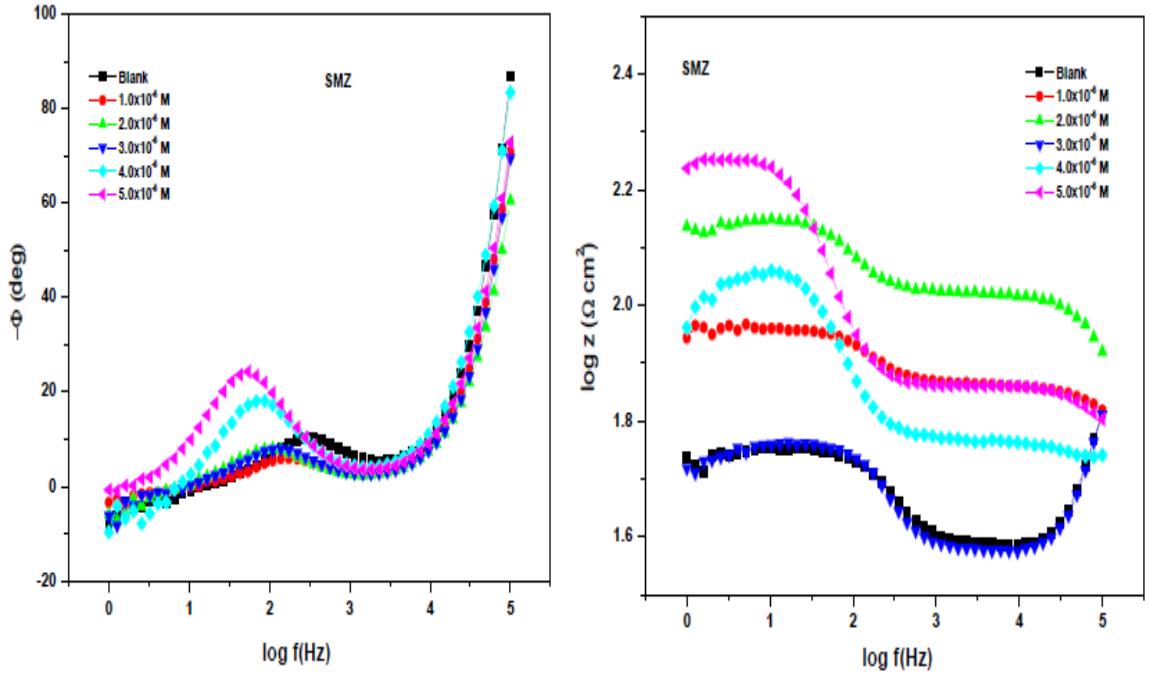

Figure 4.104: Bode plots of mild steel in 1 M HCl in the absence and presence of different concentrations of SMZ inhibitor compound.

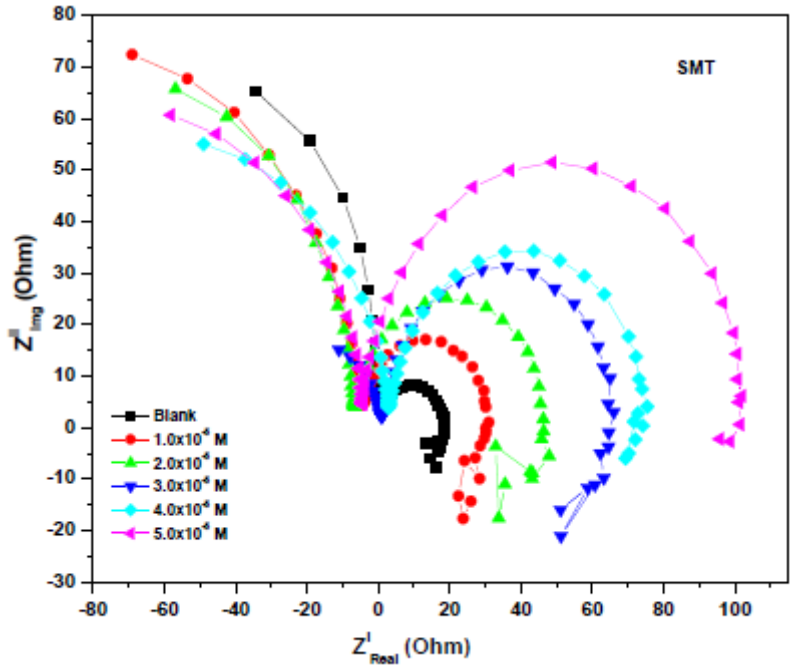

Figure 4.105: Nyquist plot of aluminium in 1 M HCl in the absence and presence of different concentrations of SMT inhibitor compound.

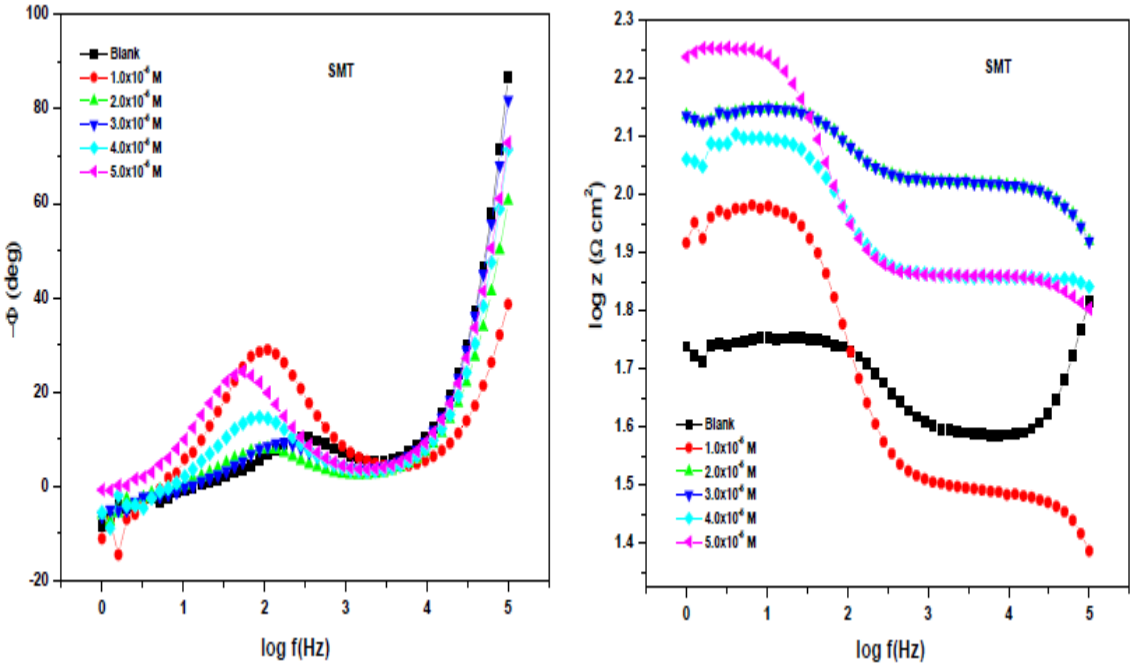

Figure 4.106: Bode plots of mild steel in 1 M HCl in the absence and presence of different concentrations of SMT inhibitor compound.

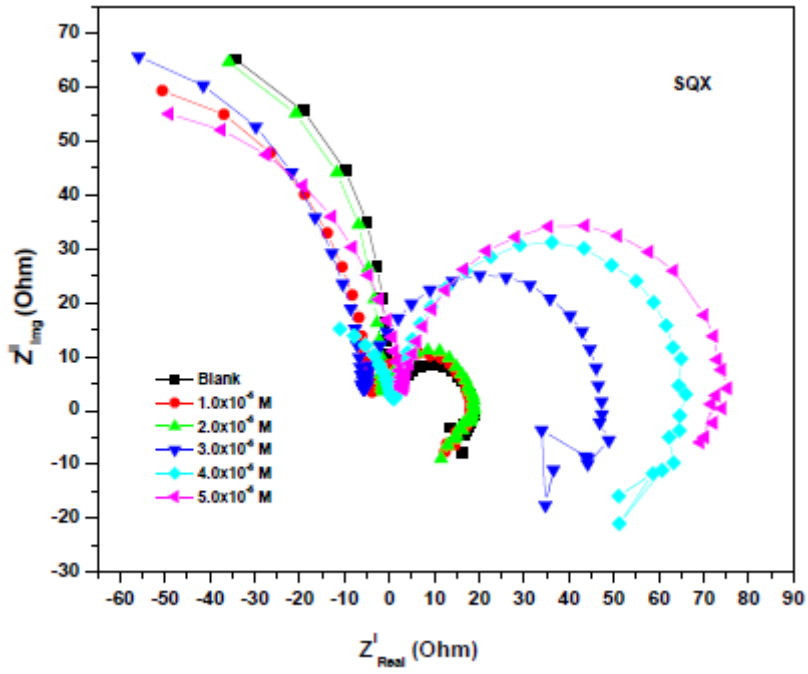

Figure 4.107: Nyquist plot of aluminium in 1 M HCl in the absence and presence of different concentrations of SQX inhibitor compound.

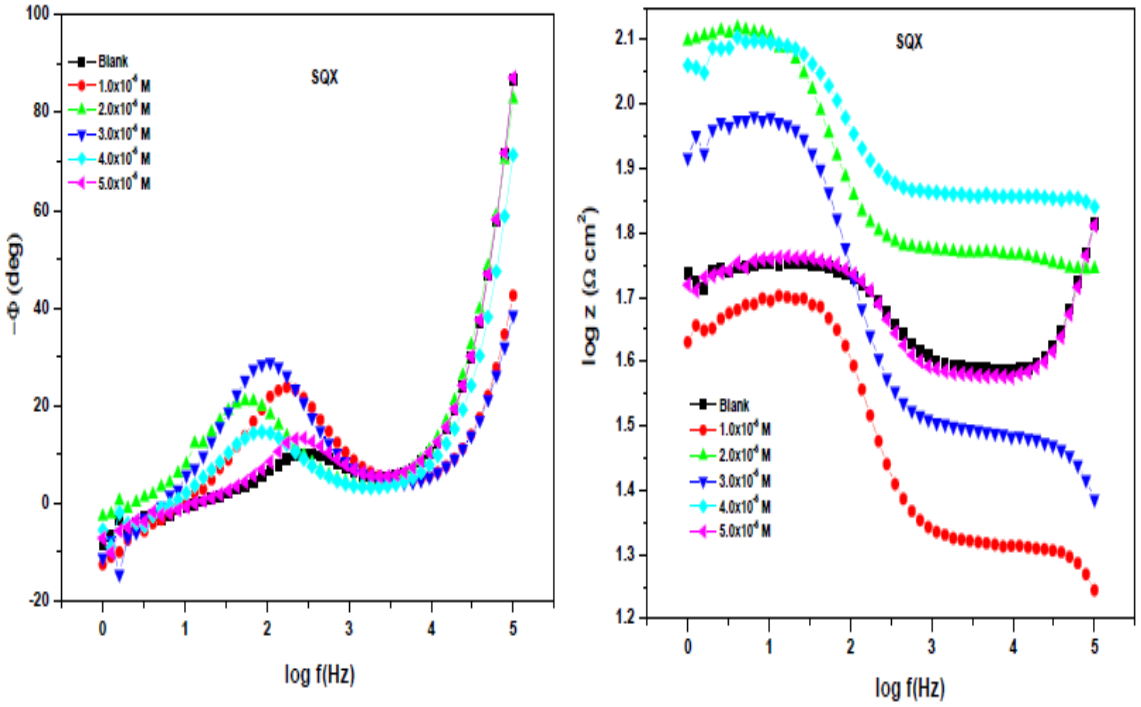

Figure 4.108: Bode plots of mild steel in 1 M HCl in the absence and presence of different concentrations of SQX inhibitor compound.

The impedance spectra in Figures 4.91 – 4.108 are characterized by the depressed capacitive loop at high-frequency. This loop is related to the process of transfer of charges and double layer capacitance (C_{dl}) [137-139]. The electrical equivalent model circuit as shown in Figure 4.109 was used for the simulation of Nyquist and Bode plots as well as the fitting of the curves resulting into the electrochemical impedance kinetic parameters as recorded in Table 4.9.

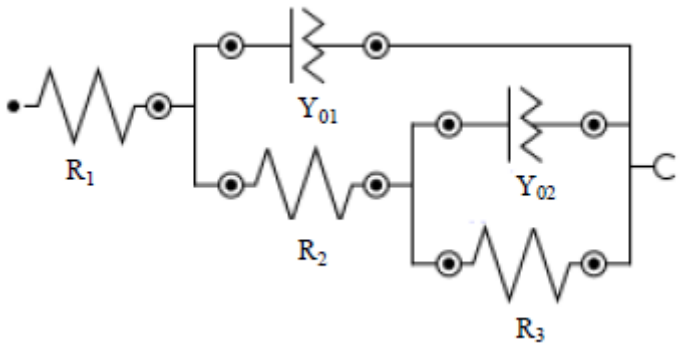

Figure 4.109: Equivalent circuit used to fit the impedance spectra obtained for aluminium corrosion in 1.0 M HCl in the absence and presence of SNA, SBZ, SMX, SCP, SDM, SSZ, SMZ, SMT and SQX.

The definition of the impedance (Z) of the CPE is shown by the expression in equation 48 and the electrochemical impedance spectroscopy inhibition efficiency ($\%IE_{EIS}$) was calculated from the values of R_s and R^0_{ct} using the expression in equation 42.

The values of R_s as shown in Table 4.9 do not follow a particular trend with the increase in concentration of the inhibitors. Normally this behaviour is accounted for by the variation of the geometry of the area which assists in the transportation of the current in the systems [140]. The significance of the R_{ct} values is that they are related to the magnitude of the electron transfer between the metal and inhibitors, and consequently related to the inhibition efficiency [141].

Table 4.9: Electrochemical impedance (EIS) parameters such as the resistance of charge transfer (R_{ct}) and the CPE exponent (n) using different inhibitors.

Inhibitor	Inhibitor Conc. (M)	R_s (Ω cm^2)	R_{ct1} (Ω cm^2)	R_{ct2} (Ω cm^2)	$Y_{01}\times10^{-8}$ (μF cm-2)	$Y_{02}\times10^{-5}$ (μF cm^{-2})	n_1	n_2	$\%IE_{EIS}$
Blank		-63.70	06.64	08.54	1.91	2.50	1.100	0.955	-
SNA	1.0×10^{-5}	-8.199	29.29	26.38	6.50	3.33	0.944	1.044	77.33
	2.0×10^{-5}	-9.661	31.56	26.59	3.72	7.07	0.94	1.045	78.96
	3.0×10^{-5}	-1.392	33.54	48.90	6.52	3.31	0.993	0.912	80.20
	4.0×10^{-5}	-66.34	121.4	20.08	9.52	3.56	1.000	1.052	94.53
	5.0×10^{-5}	-90.12	256.9	57.83	1.45	3.12	0.561	1.082	97.41
SBZ	1.0×10^{-5}	-8.199	29.29	26.38	6.51	3.31	0.945	1.041	77.33
	2.0×10^{-5}	-7.577	39.26	59.60	1.11	3.56	0.880	1.023	80.06
	3.0×10^{-5}	-7.895	40.80	56.70	1.12	3.62	0.981	1.036	83.72
	4.0×10^{-5}	-84.41	122.2	17.65	2.28	3.75	1.096	0.978	94.56
	5.0×10^{-5}	-64.57	137.2	48.30	9.11	3.34	0.999	1.044	95.16
SMX	1.0×10^{-5}	-7.986	39.26	59.60	1.12	3.65	0.886	1.063	83.08
	2.0×10^{-5}	-61.68	121.0	69.79	2.45	5.97	0.948	0.996	94.51
	3.0×10^{-5}	-65.64	122.2	32.81	1.68	3.78	0.965	1.065	94.56
	4.0×10^{-5}	-64.78	124.7	41.49	1.95	2.58	0.986	1.110	94.67
	5.0×10^{-5}	-56.99	129.9	105.2	1.63	4.61	0.963	0.985	94.88
SCP	1.0×10^{-5}	-65.62	123.6	32.81	1.96	3.54	0.995	1.063	94.62
	2.0×10^{-5}	-64.80	123.8	41.49	1.98	2.54	0.956	1.123	94.63
	3.0×10^{-5}	-64.09	124.7	47.14	2.91	2.88	0.925	1.095	94.88
	4.0×10^{-5}	-56.99	129.9	105.2	1.63	4.62	0.963	0.987	95.16
	5.0×10^{-5}	-64.51	137.2	48.30	9.12	3.26	0.999	1.056	94.53
SDM	1.0×10^{-5}	-66.34	121.4	20.08	9.51	3.56	1.000	1.056	94.64
	2.0×10^{-5}	-87.07	124.1	18.94	9.52	3.56	1.088	1.056	94.88
	3.0×10^{-5}	-56.99	129.9	105.2	1.63	4.61	0.963	0.985	95.73
	4.0×10^{-5}	-73.65	155.6	37.80	1.32	4.36	0.785	1.000	95.83
	5.0×10^{-5}	-53.46	159.3	31.83	1.56	3.45	0.985	1.042	94.51
SSZ	1.0×10^{-5}	-61.64	121.0	69.79	2.40	5.91	0.945	0.995	94.56
	2.0×10^{-5}	-65.64	122.2	32.81	1.65	3.75	0.963	1.056	95.33
	3.0×10^{-5}	-64.76	142.2	41.49	1.95	2.48	0.951	1.120	95.16
	4.0×10^{-5}	-64.51	137.2	48.30	9.12	3.26	0.999	1.012	95.83
	5.0×10^{-5}	-53.44	159.4	31.02	1.46	3.56	0.956	1.046	94.63
SMZ	1.0×10^{-5}	-64.09	123.8	47.14	2.96	2.88	0.925	1.096	94.88
	2.0×10^{-5}	-56.99	129.9	105.2	1.62	4.62	0.965	0.958	94.93
	3.0×10^{-5}	-57.76	131.0	17.43	1.27	5.61	0.978	1.000	95.72
	4.0×10^{-5}	-73.44	155.5	37.80	1.30	4.32	0.789	1.026	95.83
	5.0×10^{-5}	-57.76	159.3	31.83	1.56	3.28	0.958	1.098	83.94
SMT	1.0×10^{-5}	-08.97	41.36	59.65	1.11	3.56	0.996	1.025	94.52
	2.0×10^{-5}	-61.68	121.3	69.79	2.51	5.92	0.945	0.999	94.88
	3.0×10^{-5}	-56.99	129.9	105.2	1.62	4.61	0.965	0.987	95.16
	4.0×10^{-5}	-64.51	137.2	48.30	9.12	3.56	0.999	1.089	95.83
	5.0×10^{-5}	-53.44	159.3	31.83	1.58	3.24	0.941	1.063	83.08
SQX	1.0×10^{-5}	-07.57	39.26	59.60	1.12	3.25	0.885	1.032	94.53
	2.0×10^{-5}	-61.68	121.5	69.79	2.41	5.62	0.954	0.999	94.53
	3.0×10^{-5}	-84.84	122.2	17.65	2.26	3.54	1.091	0.954	94.56
	4.0×10^{-5}	-87.07	124.1	18.96	2.54	2.16	1.056	1.041	94.64
	5.0×10^{-5}	-64.51	137.2	48.30	9.23	3.65	0.994	1.078	95.16

From Table 4.9, it can be observed that as the concentration of the inhibitors is increased, the values of R_{ct} also increase. This signifies that increasing the inhibitor molecules in the corrosive medium also increases the surface coverage on aluminium by inhibitors. The decrease in dielectric constant is shown by the decrease in the values of Y_0 which ensures the improvement of the thickness of the electrical double layer, signifying the adsorption of

inhibitor compounds on the mild steel surface. The nature of the interface is directly related to the CPE exponent (n). Results in Table 4.9 show the values of CPE exponent that are almost constant and close to unity showing the interface of a capacitive nature.

4.2.3 FOURIER TRANSFORM INFRARED SPECTROMETER (FTIR)

The functional groups present within the adsorption film that result during the adsorption process were investigated using FTIR technique. The FTIR spectra of the studied sulphonamides and aluminium surfaces after corrosion in the presence of various sulphonamides are shown in Figures 4.110 – 4.118. The characteristic absorption bands corresponding to sulphonamides functional groups that are believed to be responsible for the adsorption on to the metal surfaces are recorded in Table 4.10. Literature review reveals that C-N stretch for secondary amine is associated with characteristic absorption bands within the wavenumber range of 1190-1130 cm^{-1} while heterocyclic amine N-H stretch is associated with 3490-3430 cm^{-1} and and aliphatic secondary amine N-H stretch is associated with 3360-3310 cm^{-1} [109, 110]. NH_2 primary amine N-H bend is associated with 1650-1590 cm^{-1}, aromatic, conjugated C=C is associated with 1600, 1500 cm^{-1} and SO_2 is associated with 1350-1325 cm^{-1} [112, 113].

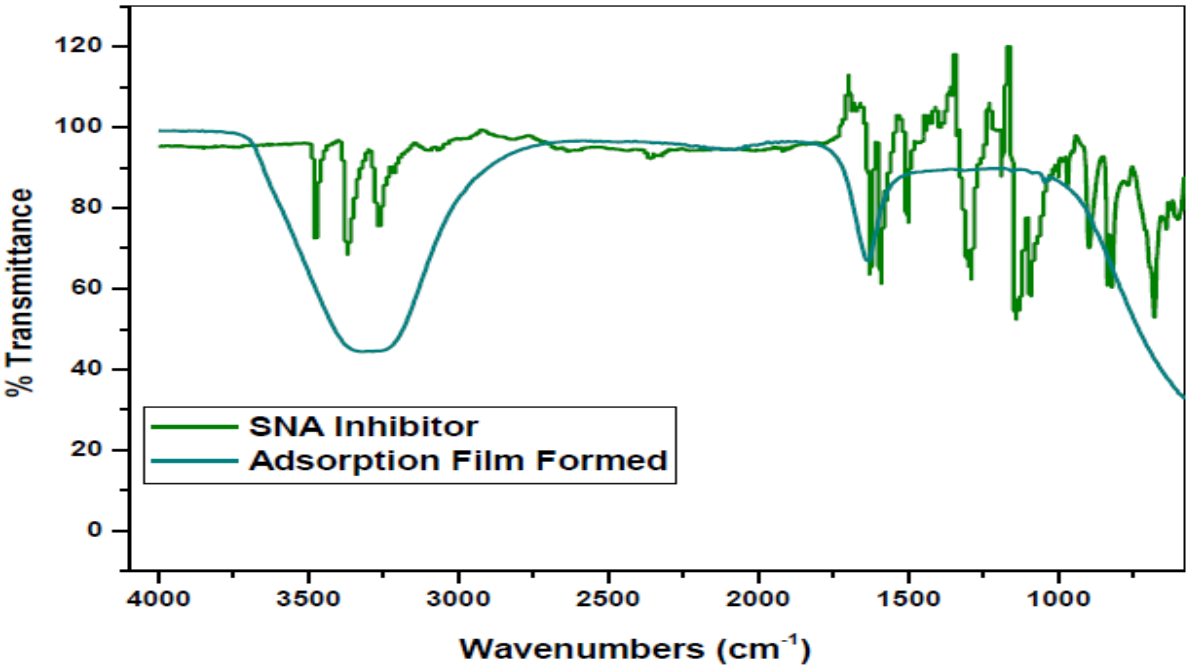

Figure 4.110: FT-IR spectra for the studied corrosion inhibitors and adsorption films formed on the aluminium in 1.0 M HCl using SNA corrosion inhibitor.

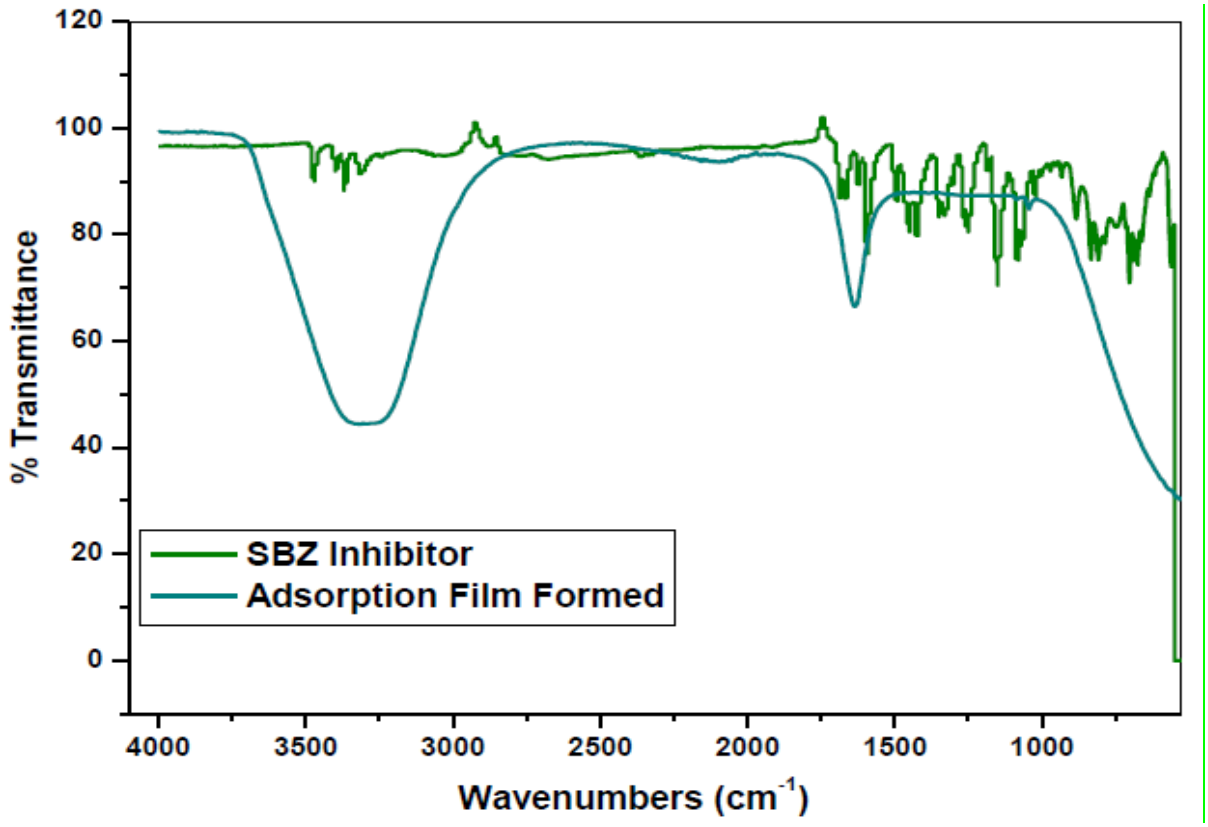

Figure 4.111: FT-IR spectra for the studied corrosion inhibitors and adsorption films formed on the aluminium in 1.0 M HCl using SBZ corrosion inhibitor.

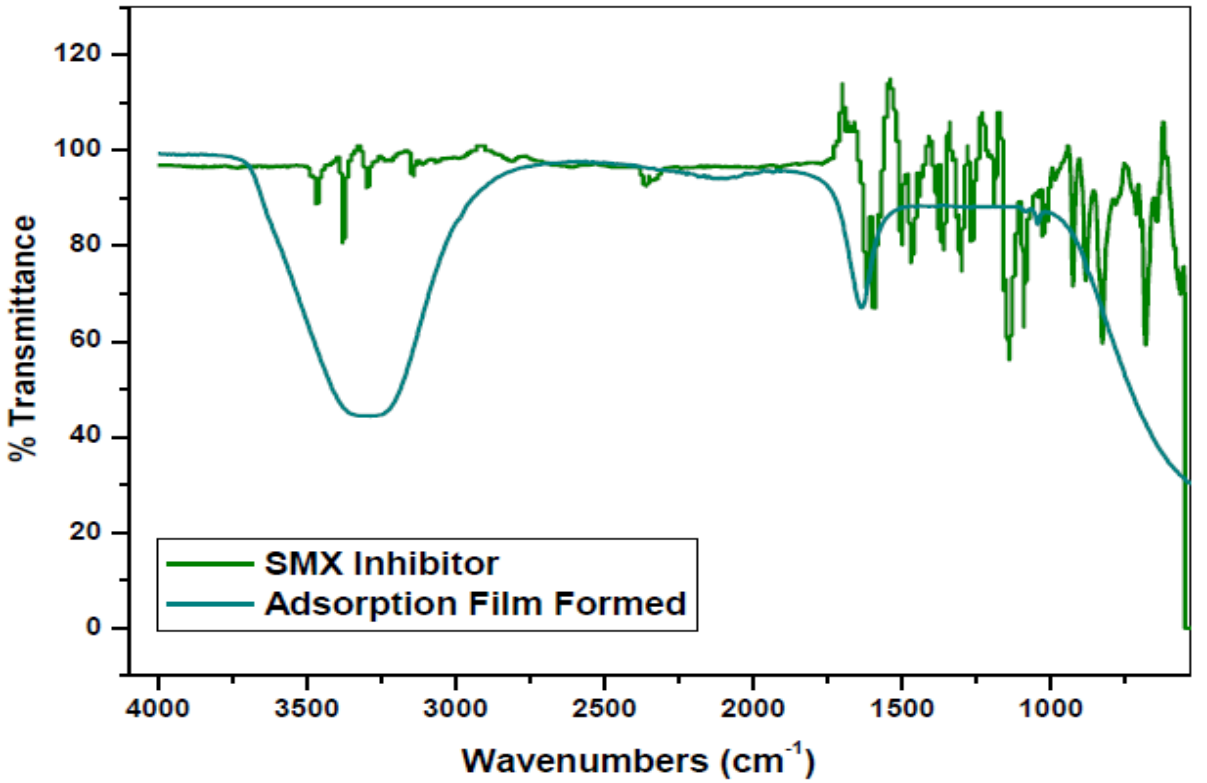

Figure 4.112: FT-IR spectra for the studied corrosion inhibitors and adsorption films formed on the aluminium in 1.0 M HCl using SMX corrosion inhibitor.

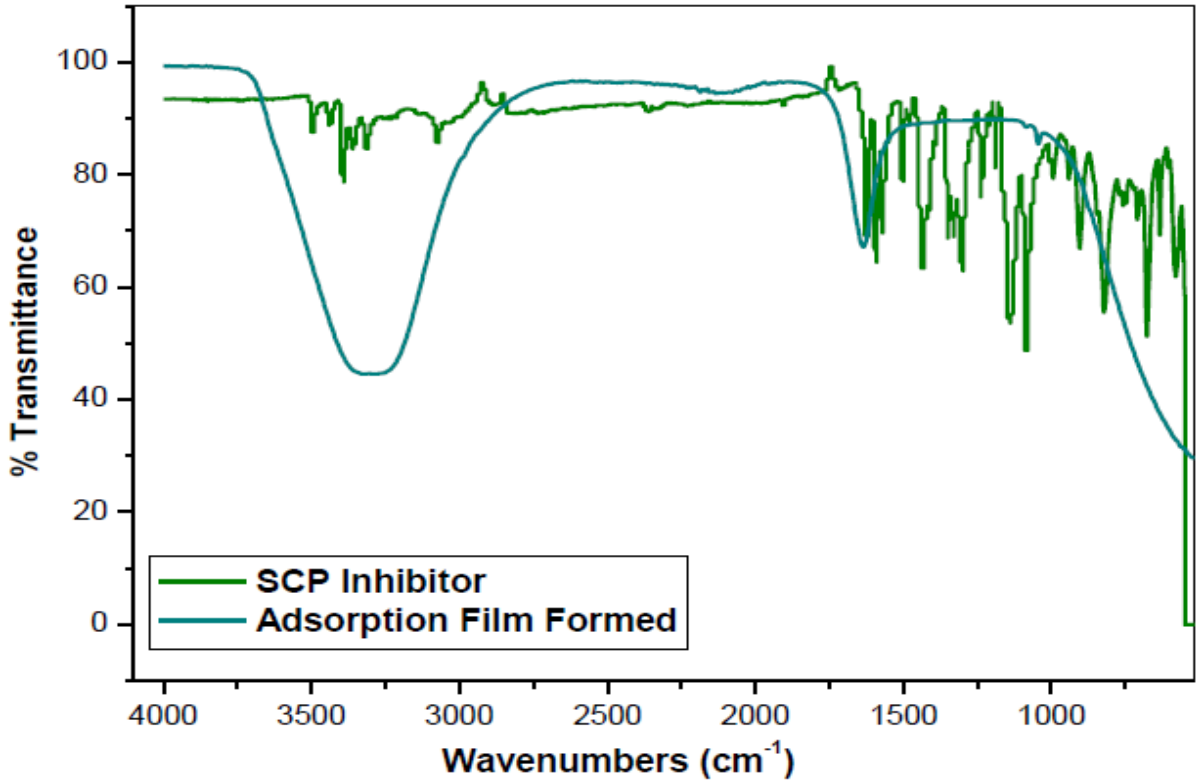

Figure 4.113: FT-IR spectra for the studied corrosion inhibitors and adsorption films formed on the aluminium in 1.0 M HCl using SCP corrosion inhibitor.

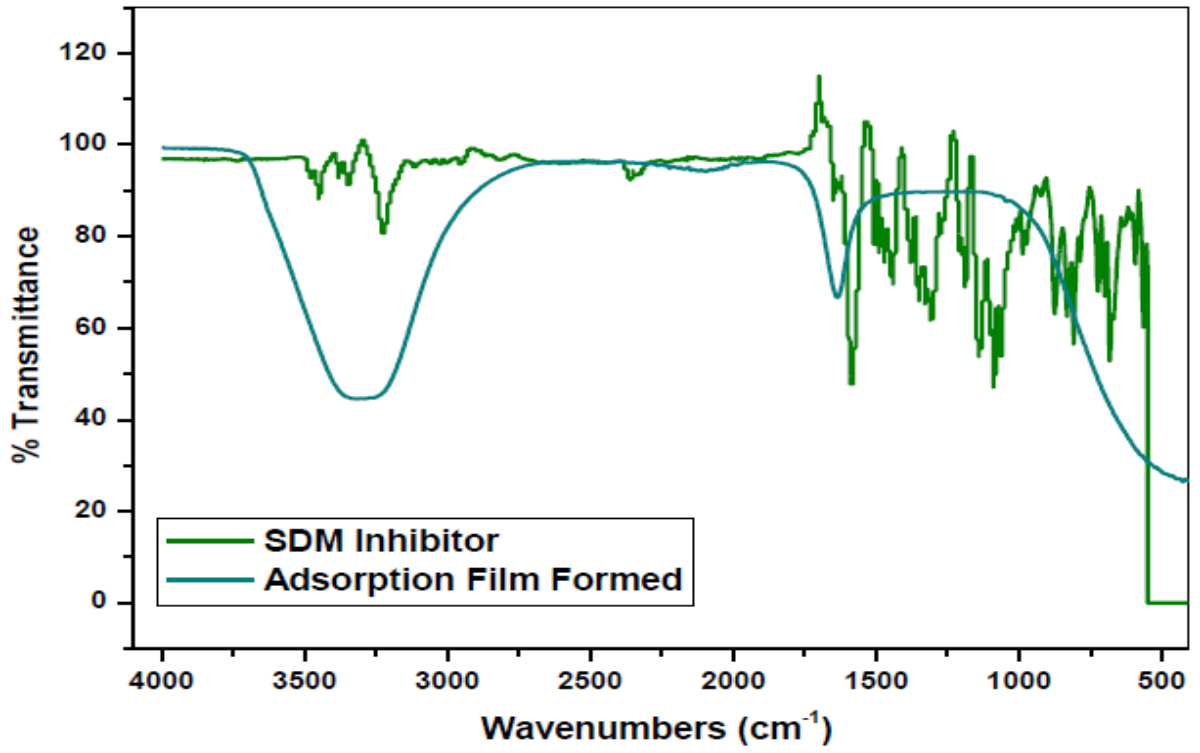

Figure 4.114: FT-IR spectra for the studied corrosion inhibitors and adsorption films formed on the aluminium in 1.0 M HCl using SDM corrosion inhibitor.

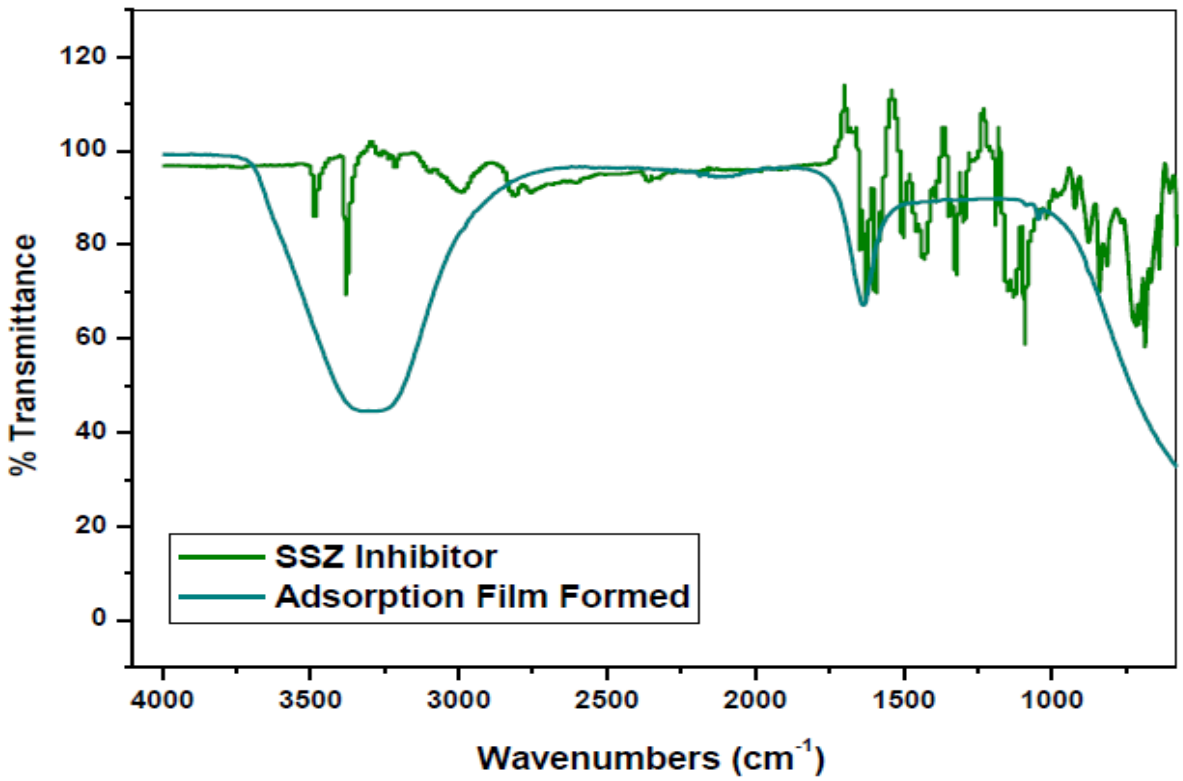

Figure 4.115: FT-IR spectra for the studied corrosion inhibitors and adsorption films formed on the aluminium in 1.0 M HCl using SSZ corrosion inhibitor.

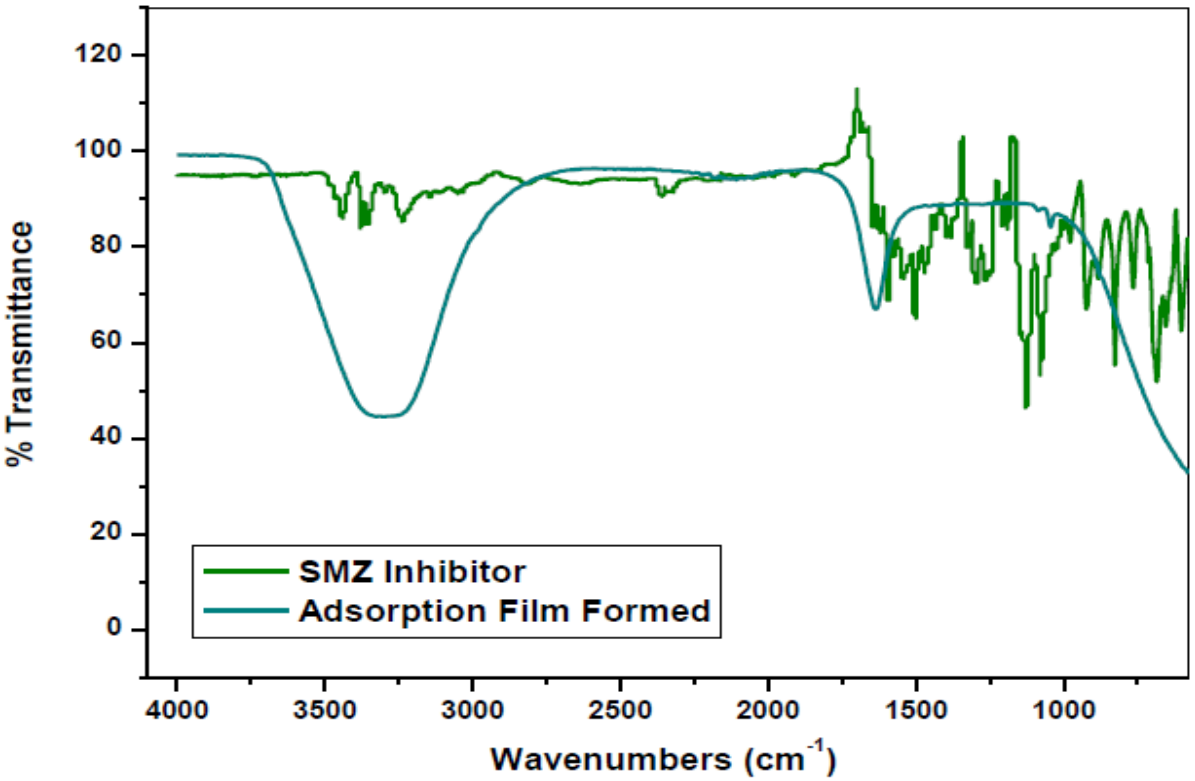

Figure 4.116: FT-IR spectra for the studied corrosion inhibitors and adsorption films formed on the aluminium in 1.0 M HCl using SMZ corrosion inhibitor.

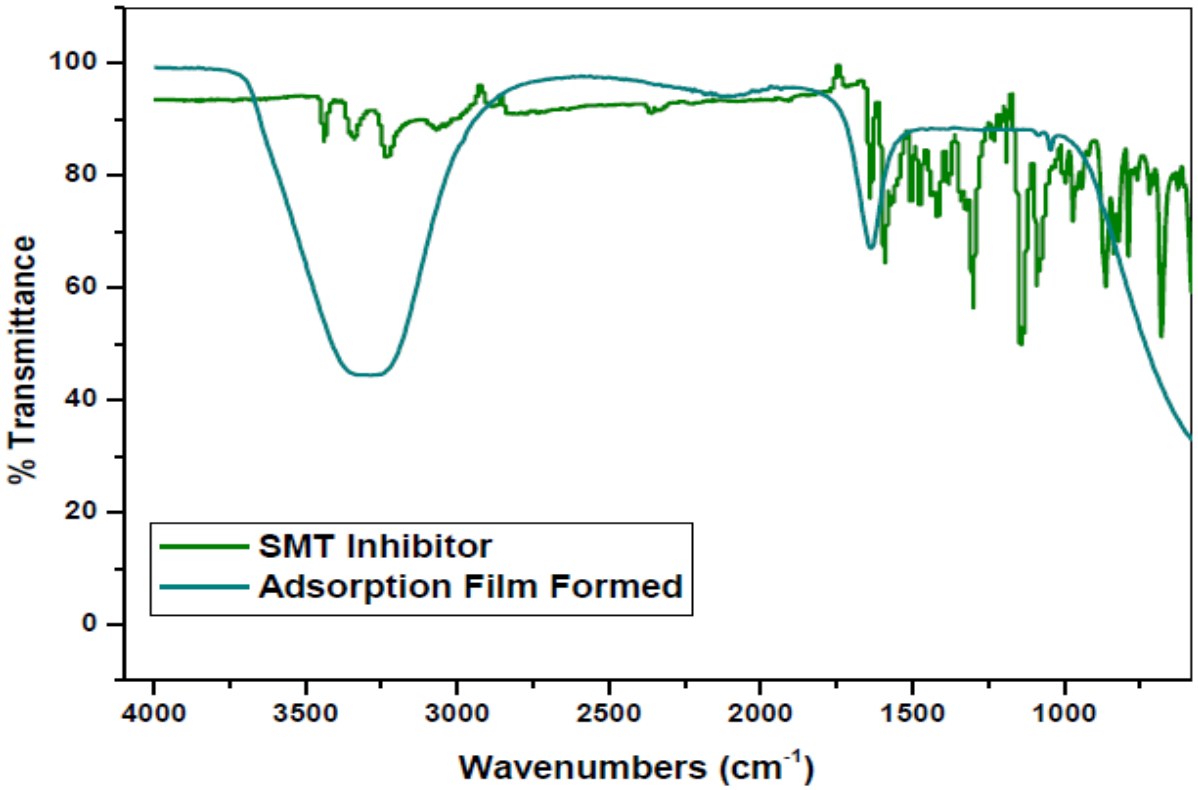

Figure 4.117: FT-IR spectra for the studied corrosion inhibitors and adsorption films formed on the aluminium in 1.0 M HCl using SMT corrosion inhibitor.

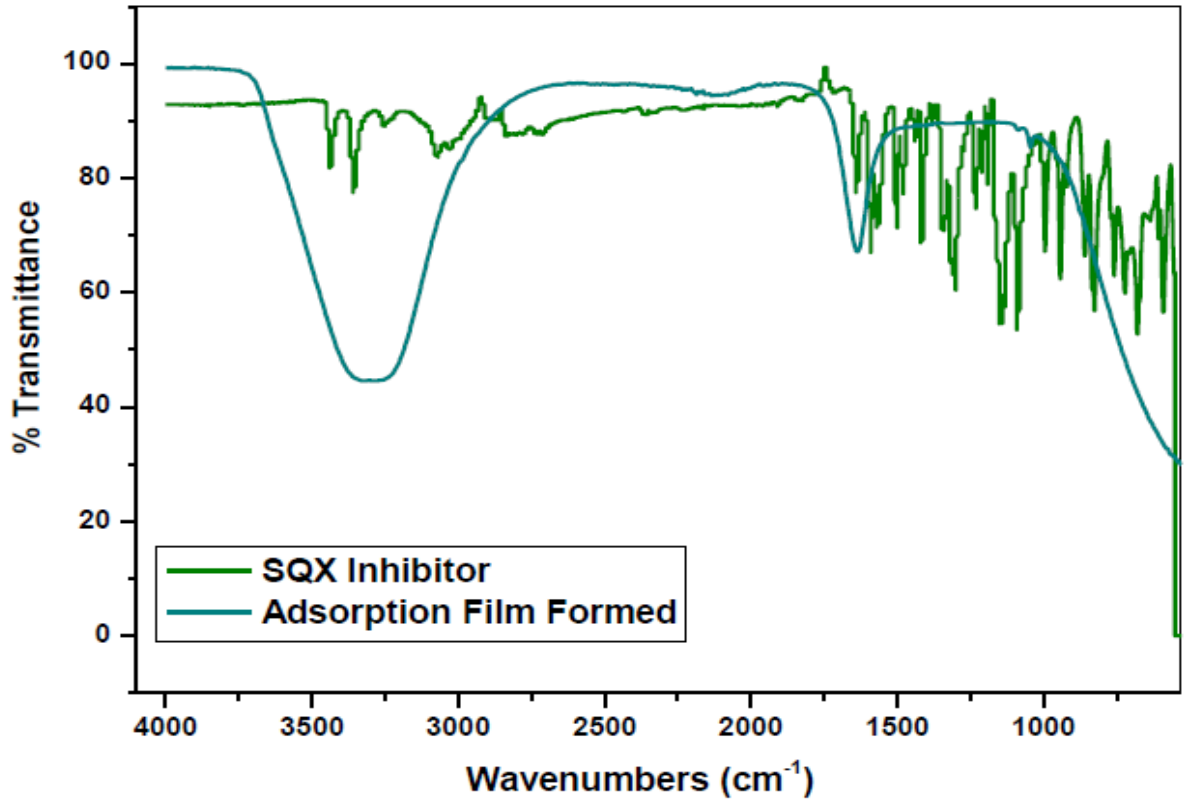

Figure 4.118: FT-IR spectra for the studied corrosion inhibitors and adsorption films formed on the aluminium in 1.0 M HCl using SQX corrosion inhibitor.

Table 4.10 shows the functional groups, N-H, NH_2, aromatic conjugated C=C and C-N stretch and their corresponding bands at 3371.17 cm^{-1}, 15928.89 cm^{-1}, 1503.33 cm^{-1} and 1142.70 cm^{-1} respectively for SNA while SNA-Al shows only functional groups between 3500 – 3000 cm^{-1} and 1600 – 1500 cm^{-1}. This signifies the formation of SNA-Al^{3+} complex. Similar discussions can be used regarding, SBZ, SMX, SCP, SDM, SSZ, SMZ, SMT and SQX shown in Figures 4.110 – 4.118.

Table 4.10: Peaks and their identification, from FT-IR spectra of the studied corrosion inhibitors and adsorption films formed (i.e. SQX-Al) on the mild steel in 1.0 M HCl using different corrosion inhibitors.

Inhibitor-Aluminium	**Functional Groups Peaks from FT-IR Spectra (cm^{-1})**				
	N-H	**NH_2**	**C=C**	**O=S=O**	**C-N**
SNA	3371.17	1592.89	1503.33	–	1142.70
SNA-Al	3251.21	1622.89	–	–	–
SBZ	3365.41	1592.88	1452.55	1331.61	1151.12
SBZ-Al	3251.21	1622.89	–	–	–
SMX	3376.52	1617.33	1501.78	1302.24	1141.39
SMX-Al	3251.21	1622.89	–	–	–
SCP	3399.99	1624.57	1593.11	1330.51	1141.92
SCP-Al	3393.62	1622.06	–	–	–
SDM	–	1584.77	1504.74	1305.64	1139.74
SDM-Al	3342.84	1622.89	–	–	–
SSZ	3379.05	1627.48	1594.26	1322.81	1131.67
SSZ-Al	3251.21	1622.98	–	–	–
SMZ	–	–	1503.36	–	1126.18
SMZ-Al	3251.21	1622.74	–	–	–
SMT	3342.84	1570.68	1591.80	1300.96	1143.93
SMT-Al	3251.21	1624.57	–	–	–
SQX	3356.94	1590.11	1502.34	1343.94	1146.34
SQX-Al	3251.21	1622.89	–	–	–

Careful observation of all FTIR spectra of sulphonamide-Al^{3+} complex in the absorption range between 1700-500 cm^{-1} shows that most of the characteristic absorption bands have disappeared. Some of the possible electron donors within the sulphonamides compounds include the aromatic ring (C=C) and SO_2. From Table 4.10, it is interesting to note that both C=C and SO_2 disappeared with respect to the results of all sulphonamides used. It can be deduced that C=C and SO_2 functional groups might be the most preferred site for the interaction between aluminium and sulphonamides. The partially filled orbitals in Al may accept electron pairs from the aromatic ring through C=C and SO_2 through O atom thereby

giving rise to the adsorption bond between aluminium and sulphonamide inhibitor, and consequently leaving aluminium prevented from further exposure to the aggressive ions.

4.2.4 SURFACE ANALYSIS (SEM)

The morphology of the aluminium surfaces in hydrochloric acid solution in the absence and presence of 5.0×10^{-5} M of SNA, SBZ, SMX, SCP, SDM, SSZ, SMZ, SMT and SQX was investigated using scanning electron microscope while the elements of these compounds on the aluminium surface were determined using energy dispersive spectroscopy. SEM micrographs with their respective EDS spectra for mild steel and all inhibitors are shown in Figures 4.119−4.129. From Figure 4.119 it is observed that the surface of aluminium is smooth with perhaps some negligible rough nature which may be attributed to the sample preparation procedure that involved abrasion with emery papers. It is also noted that the treatment aluminium with hydrochloric acid resulted in a tremendous roughness on its surface as shown in Figure 4.120. The corresponding EDS spectra in Figures 4.119 and 4.120 show the absence and presence of Cl^- ions, respectively, which are aggressive and the main cause for these damages on the surfaces of mild steel [116, 117]. The introduction of sulphonamide inhibitors somehow improved the smoothness on the surfaces of samples in Figures 4.121−4.127. A close observation of the corresponding EDS spectra in images Figures 4.121−4.127 clearly shows that there is an absence of the aggressive Cl^- ions. From this observation, it can be deduced that the presence of the inhibitor compounds reduces the effects of corrosion through adsorption on to the metal surfaces [115−117].

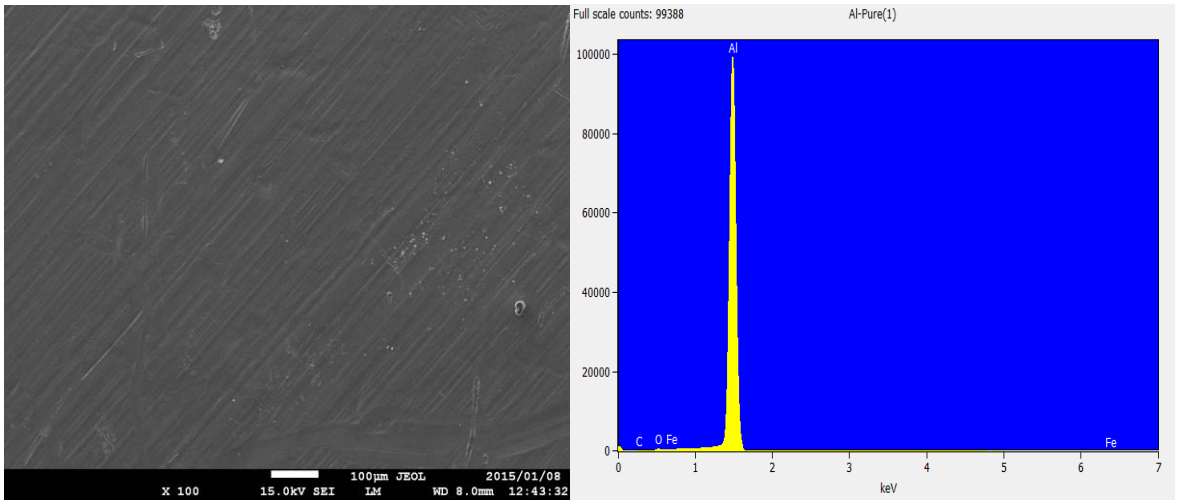

Figure 4.119: SEM micrograph of the surface of aluminium and EDS spectrum of aluminium before immersed in HCl uninhibited.

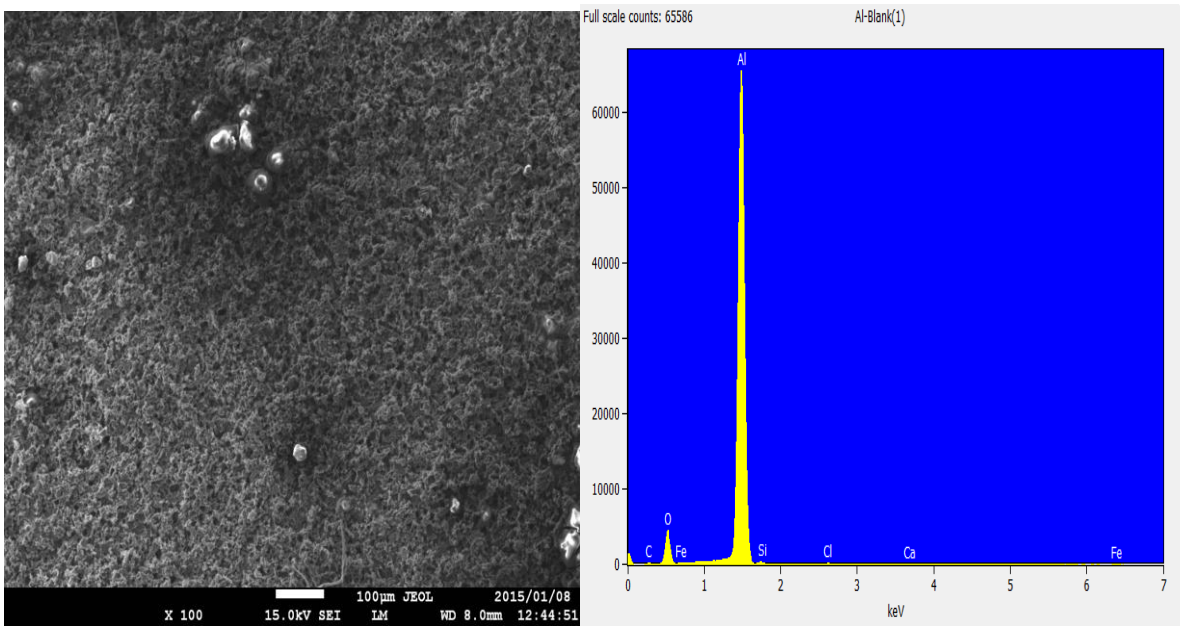

Figure 4.120: SEM micrograph of the surface of aluminium and EDS spectrum of aluminium immersed in HCl uninhibited.

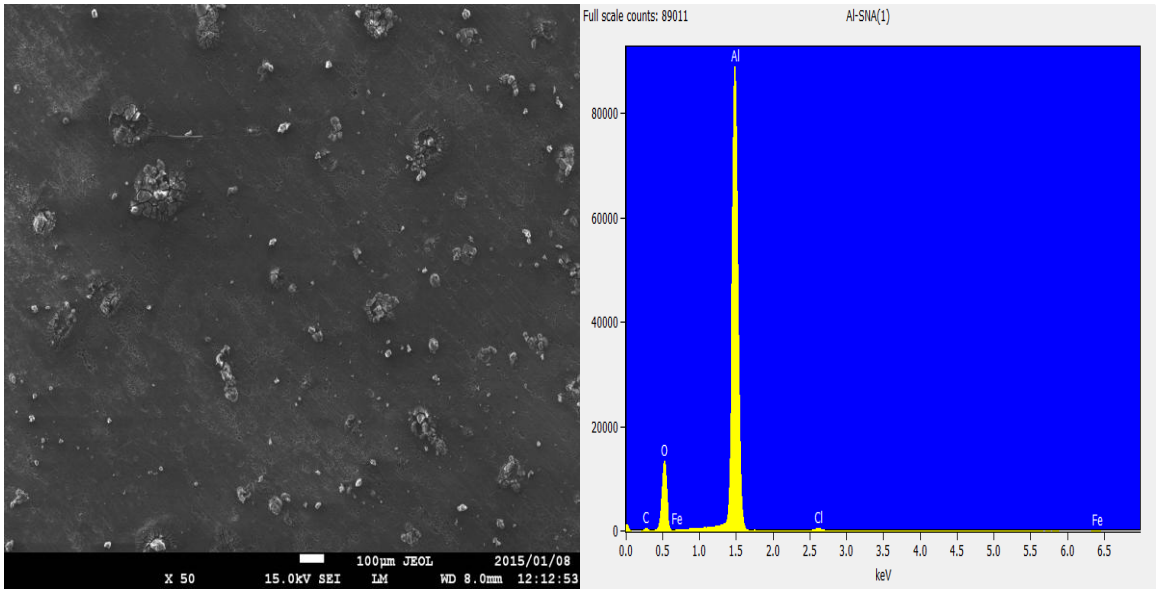

Figure 4.121: SEM micrograph of the surface of aluminium and EDS spectrum of aluminium in HCl in the presence of SNA corrosion inhibitor.

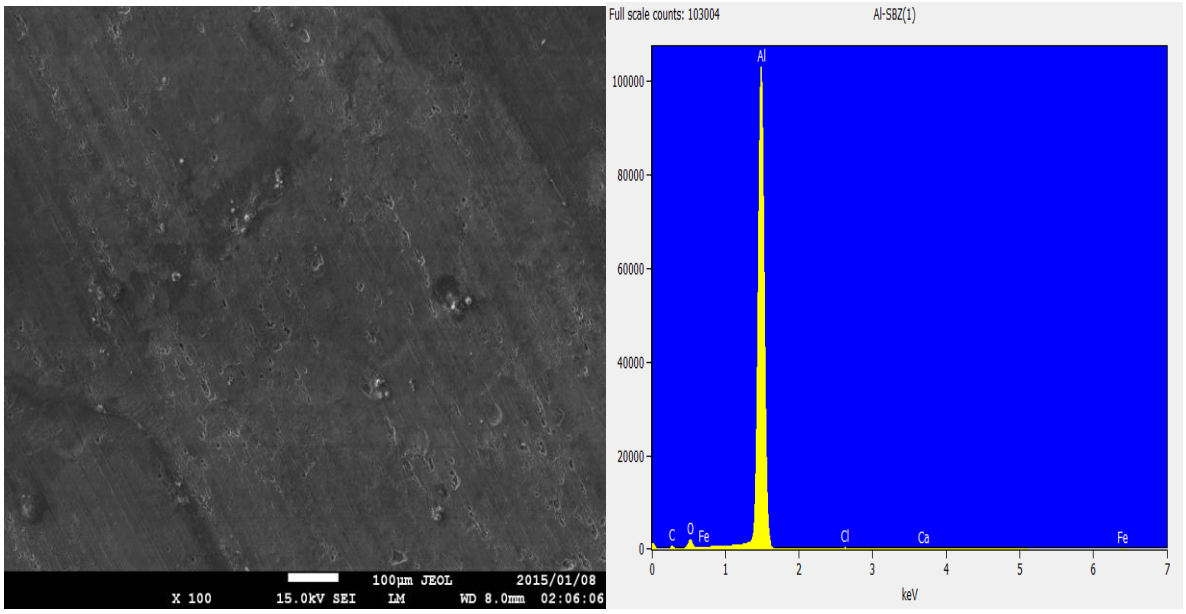

Figure 4.122: SEM micrograph of the surface of aluminium and EDS spectrum of aluminium immersed in HCl in the presence of SBZ corrosion inhibitor.

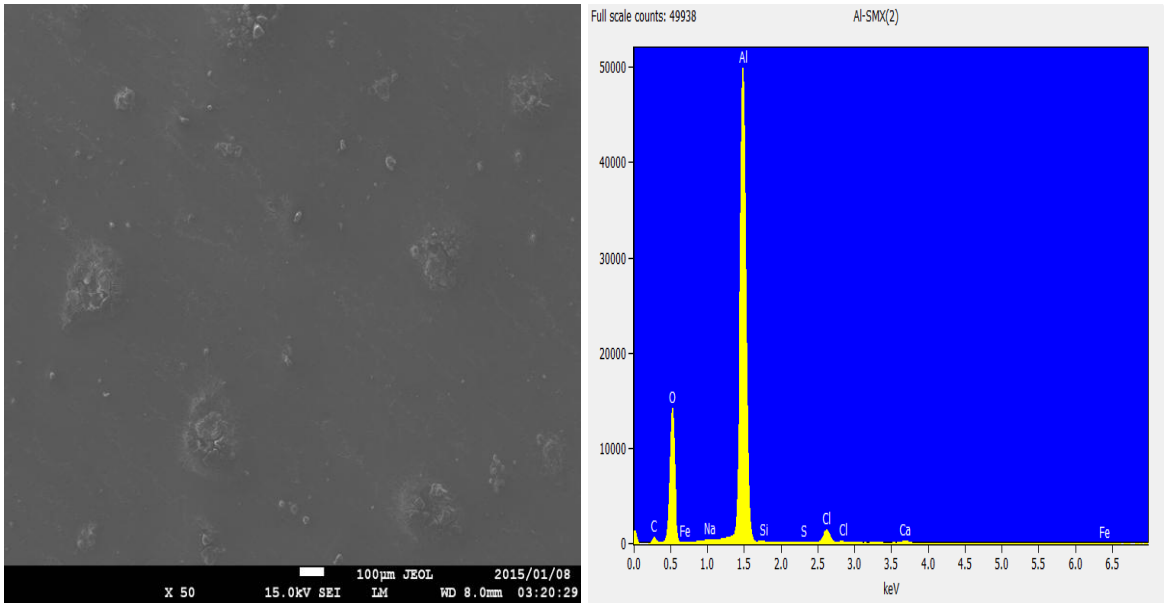

Figure 4.123: SEM micrograph of the surface of aluminium and EDS spectrum of aluminium immersed in HCl in the presence of SMX corrosion inhibitor.

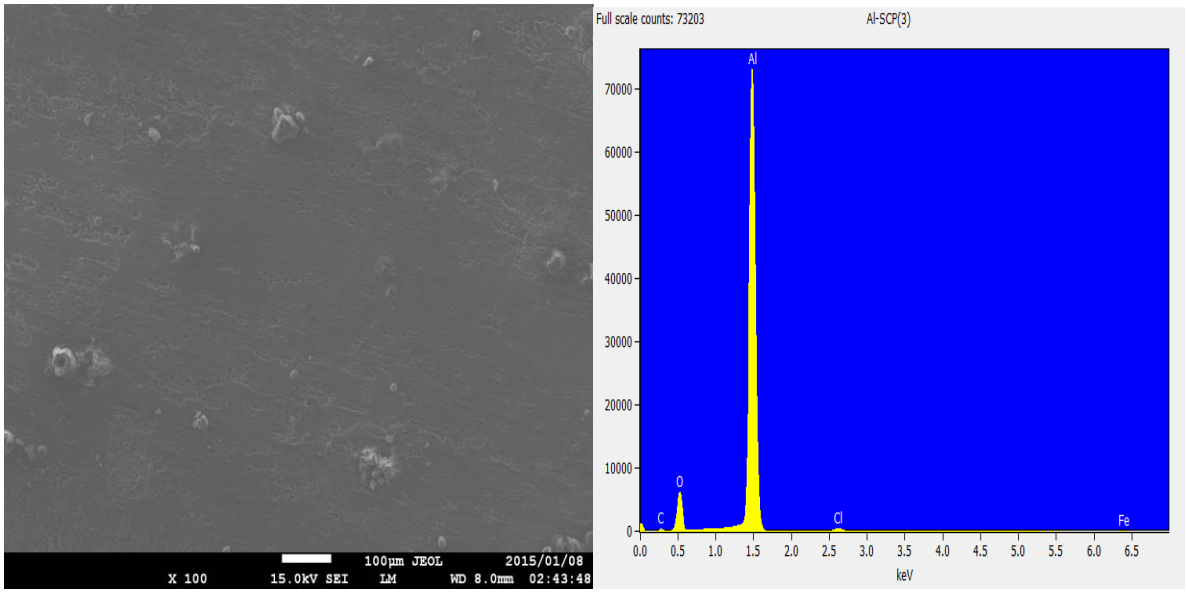

Figure 4.124: SEM micrograph of the surface of aluminium and EDS spectrum of aluminium immersed in HCl in the presence of SCP corrosion inhibitor.

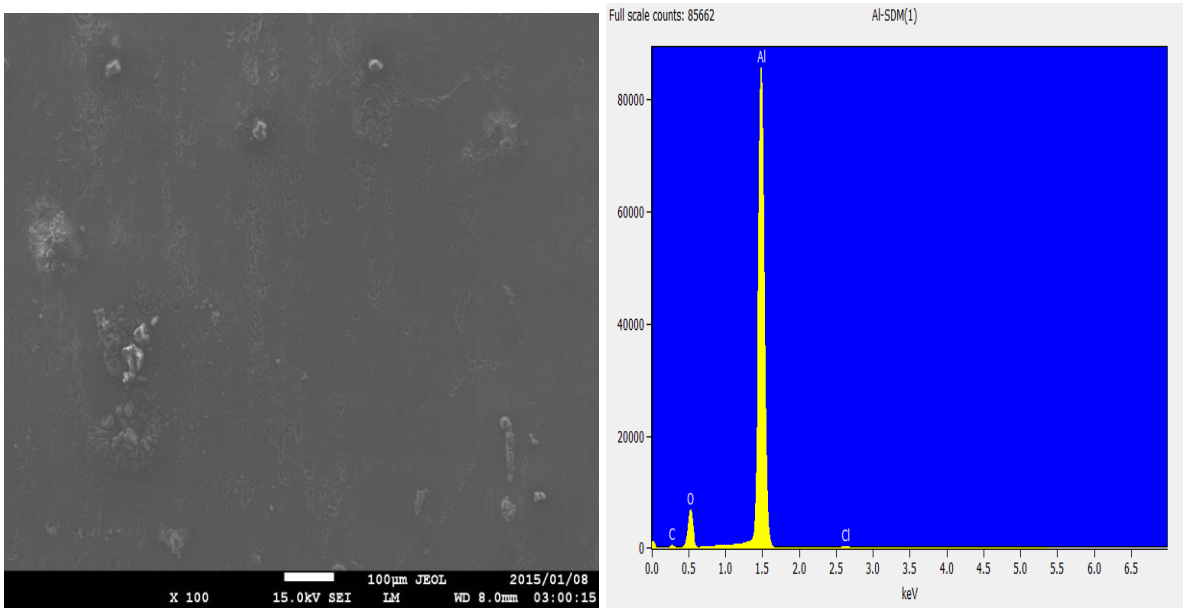

Figure 4.125: SEM micrograph of the surface of aluminium and EDS spectrum of aluminium immersed in HCl in the presence of SDM corrosion inhibitor.

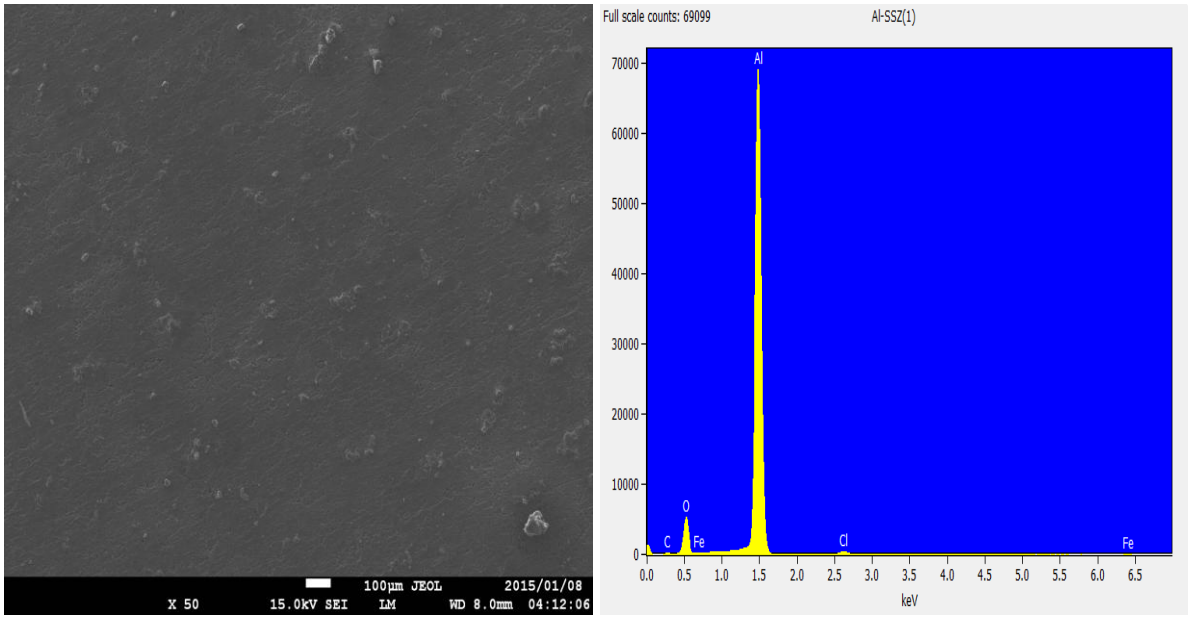

Figure 4.126: SEM micrograph of the surface of aluminium and EDS spectrum of aluminium immersed in HCl in the presence of SSZ corrosion inhibitor.

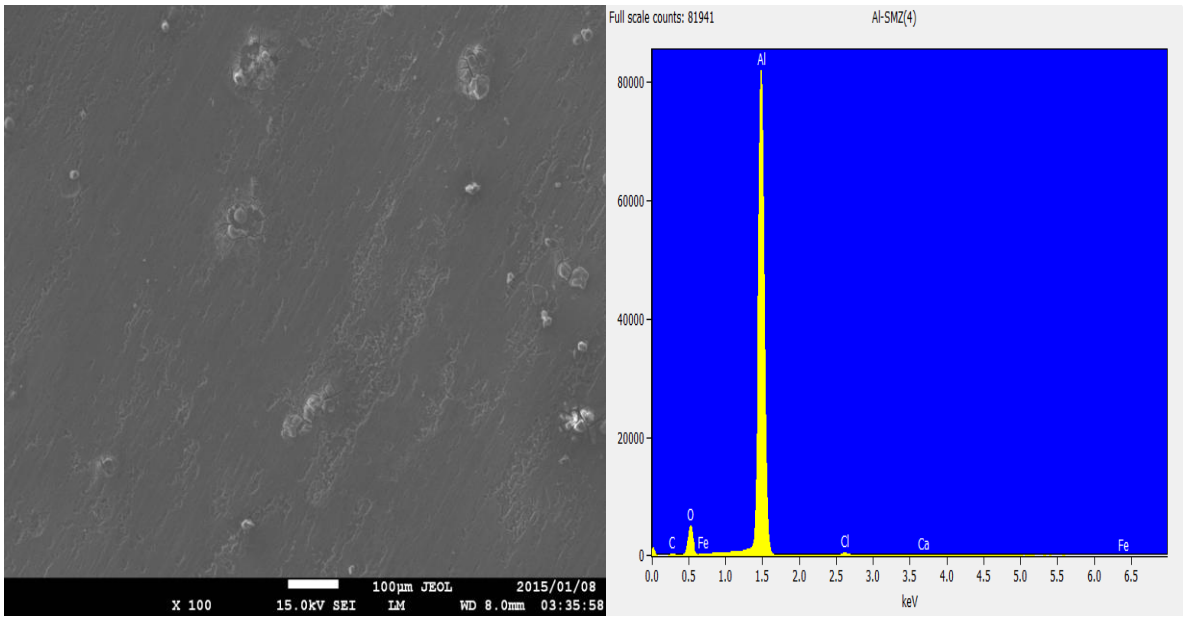

Figure 4.127: SEM micrograph of the surface of aluminium and EDS spectrum of aluminium immersed in HCl in the presence of SMZ corrosion inhibitor.

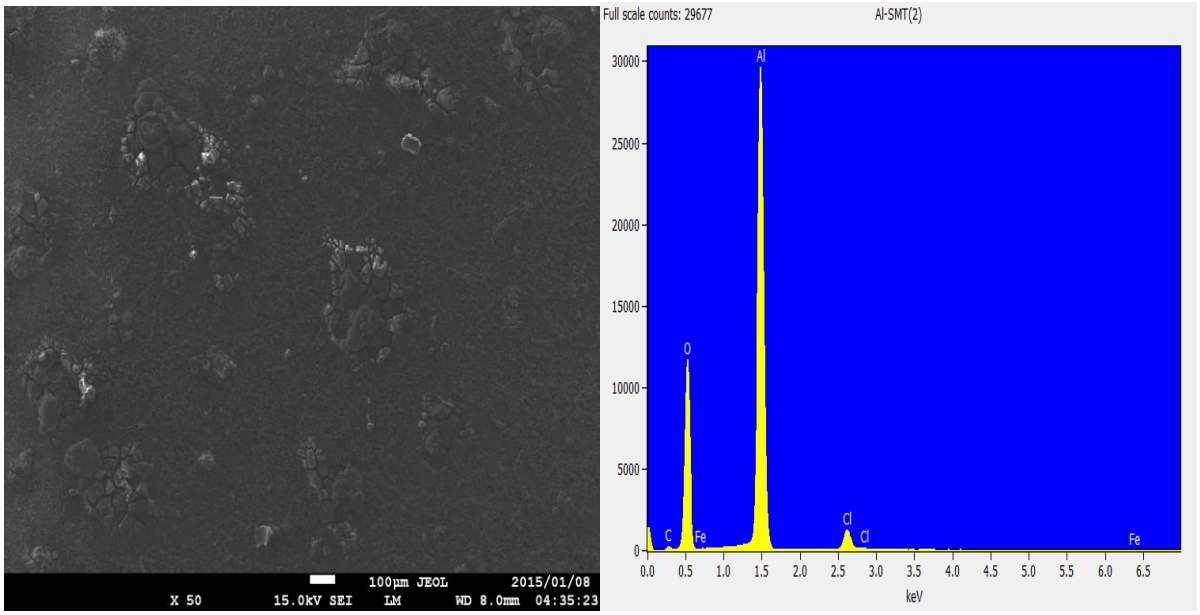

Figure 4.128: SEM micrograph of the surface of aluminium and EDS spectrum of aluminium immersed in HCl in the presence of SMT corrosion inhibitor.

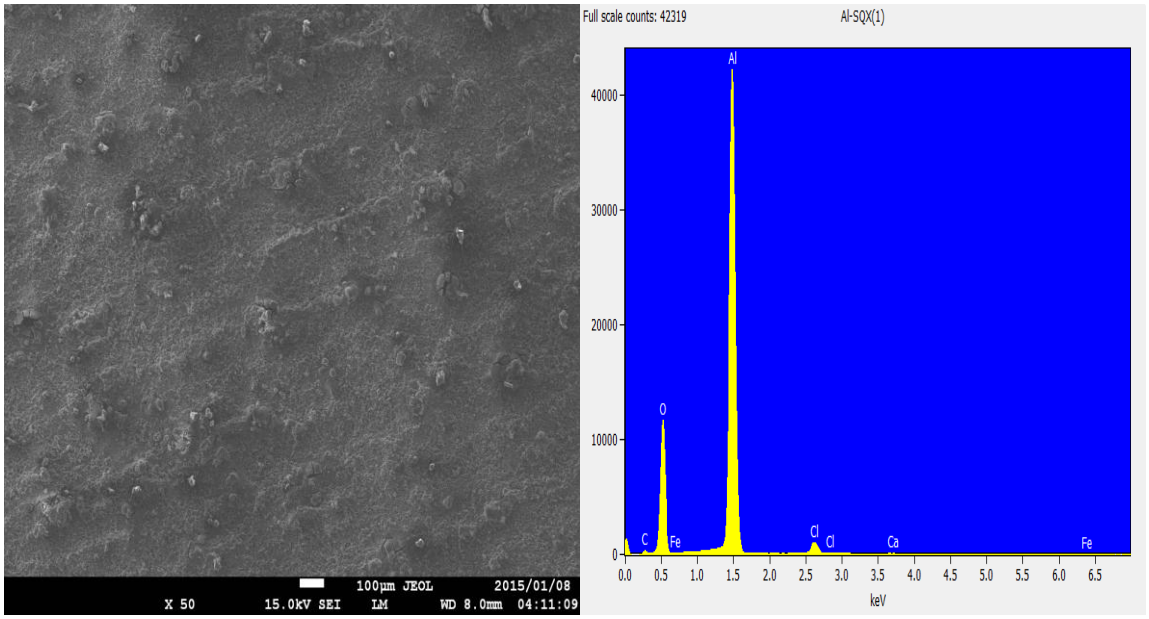

Figure 4.129: SEM micrograph of the surface of aluminium and EDS spectrum of aluminium immersed in HCl in the presence of SQX corrosion inhibitor.

4.2.5 CORROSION RATE AND INHIBITION EFFICIENCY

The percentage inhibition efficiencies from the weight loss measurements (%IE) were obtained and plots of %IE versus the inhibitor concentration at 30 − 50 °C are shown in Figures 4.130 − 4.132. The increase of concentration from 1.0 x 10^{-5} M to 5.0 x 10^{-5} M shows an increasing trend in efficiency of each sulphonamide. The inhibition efficiency of these compounds is observed to decrease as the temperature is increased. The effect of temperature can be demonstrated by the values of inhibition efficiency at 5.0 x 10^{-5} M for the three temperatures. For SNA at 30°C, 99.60% inhibition efficiency was attained while at 40 and 50°C, 87.74 and 78.34% inhibition efficiencies were attained respectively. Increasing temperature increases the rate corrosion density severely. SBZ has similar trend with increased inhibition efficiencies compared to SNA. At 30°C, 99.47% inhibition efficiency was obtained and at 40 and 50°C, 88.00% and 78.84% inhibition efficiencies were obtained respectively. Increasing the temperature to 40 and 50°C decreased the efficiency to 98.18 and 94.95% inhibition efficiency.

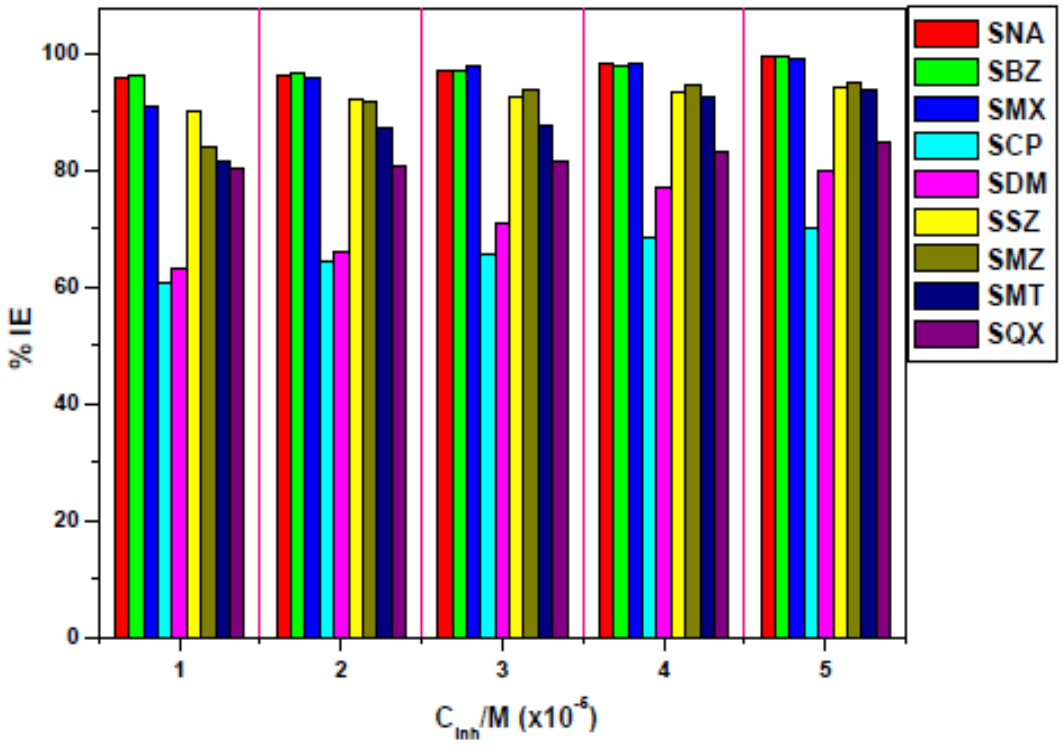

Figure 4.130: Variations of the percentage inhibition efficiencies with various concentrations of the utilized corrosion inhibitors aluminium for at 30 °C.

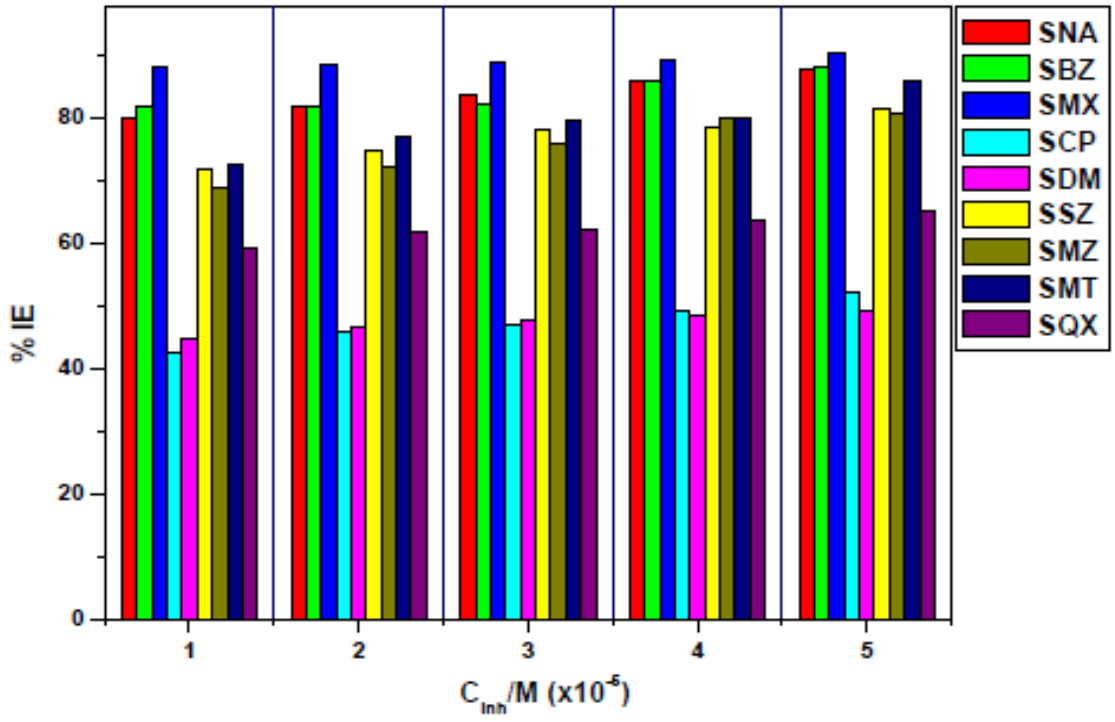

Figure 4.131: Variations of the percentage inhibition efficiencies with various concentrations of the utilized corrosion inhibitors aluminium for at 40 °C.

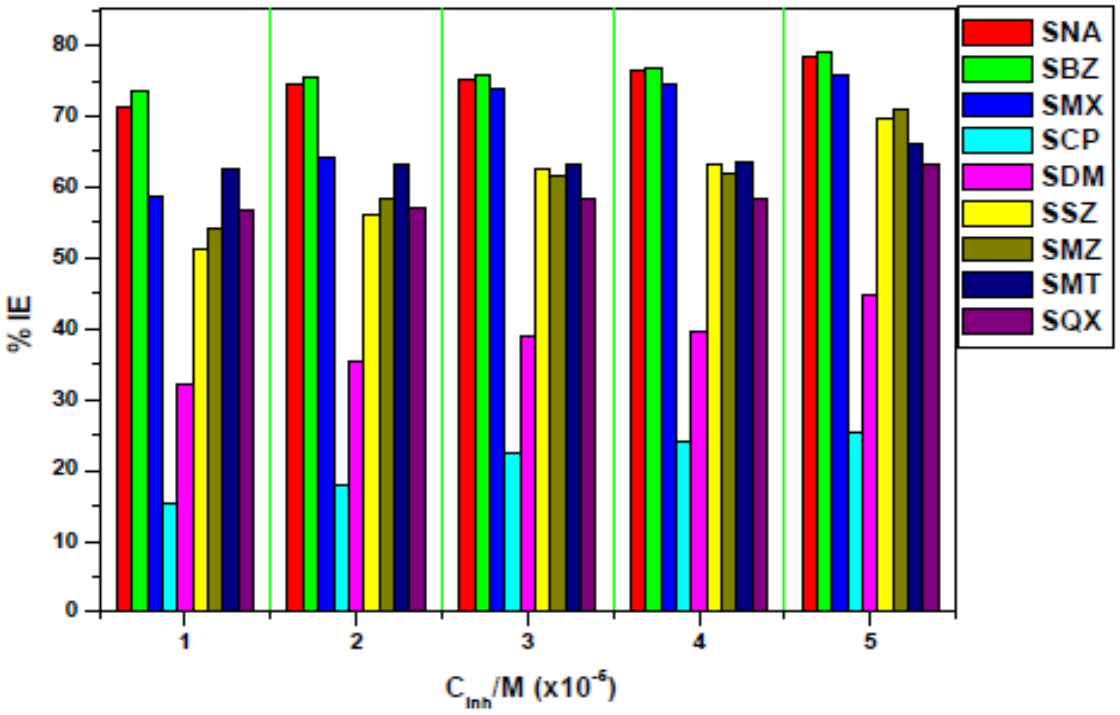

Figure 4.132: Variations of the percentage inhibition efficiencies with various concentrations of the utilized corrosion inhibitors aluminium for at 50 °C.

The effect of temperature on the inhibition efficiency is of the same trend with all nine sulphonamides used as shown in these plots.

Studies have shown that the rate of metal dissolution is opposed by increasing concentration of inhibitor [142, 143]. The same outcome was observed with aluminium whereby the corrosion rate was decreased as the inhibitor concentration is increased. When there was no inhibitor added in the solution the rate of corrosion was found to be high at all temperatures. At 30, 40 and 50°C, the rates of corrosion obtained are 0.00422, 0.00431 and 0.00438 g.cm^{-2}.hr^{-1}, respectively. It is clear for one to observe what temperature brings to the rate of corrosion. When the inhibitor is introduced in the solution rate of corrosion was observed to decrease. This was also documented by other authors [144, 145]. The rate of corrosion was found to be 0.00002 g.cm^{-2}.hr^{-1} when 5.0×10^{-5} M of SNA was added at 30°C. Increasing the temperature 40 and 50°C gave an increased corrosion rate of 0.00055 g.cm^{-2}.hr^{-1} and 0.00095 g.cm^{-2}.hr^{-1}, respectively. When 5.0×10^{-5} M of SBZ was added at 30°C, rate of metal dissolution was found to decrease to a value of 0.00002 g.cm^{-2}.hr^{-1} which is much lower relative to the uninhibited system. At 40 and 50°C, rate of corrosion increased to 0.00052 g.cm^{-2}.hr^{-1} and 0.00092 g.cm^{-2}.hr^{-1}, respectively. SMX inhibitor also presents very low corrosion rates when 5.0×10^{-5} M is used at the three temperatures under the study. At 30°C, corrosion rate was found to be 0.00007 g.cm^{-2}.hr^{-1} whereas at 40°C, 0.00076 g.cm^{-2}.hr^{-1} was attained and 50°C gave corrosion rate value of 0.00195 g.cm^{-2}.hr^{-1}. A corrosion rate of 0.00007 g.cm^{-2}.hr^{-1} shows that the inhibitor performs sufficiently at lower temperatures as compared to the ones at 40°C and 50°C. The trend of the effect of temperature on the corrosion rate is very similar even with all the other sulphonamides used in this study. Hence, it is clear that increasing the concentration of the sulphonamide inhibitor reduces the rate of corrosion and consequently increases the inhibition efficiency.

Table 4.11: Percentage inhibition efficiencies and corrosion rates values obtained from the weight loss of aluminium in 1.0 M HCl in the absence and presence of various concentrations of inhibitors.

Inhibitor	**Inhibitor Conc. (M)**	**Temperature**					
		30 °C		40 °C		50 °C	
		$\%IE_{WL}$	$C_R(g.cm^{-2}.h^{-1})$	$\%IE_{WL}$	$C_R(g.cm^{-2}.h^{-1})$	$\%IE_{WL}$	$C_R(g.cm^{-2}.h^{-1})$
Blank	0.0	-	0.00422	-	0.00431	-	0.00438
SNA	1.0×10^{-5}	95.92	0.00017	79.87	0.00088	71.14	0.00126
	2.0×10^{-5}	96.31	0.00015	81.77	0.00080	74.56	0.00112
	3.0×10^{-5}	96.83	0.00013	83.42	0.00073	75.12	0.00108
	4.0×10^{-5}	98.16	0.00007	85.95	0.00062	76.58	0.00103
	5.0×10^{-5}	99.60	0.00002	87.95	0.00055	78.34	0.00095
SBZ	1.0×10^{-5}	96.57	0.00016	81.81	0.00078	73.42	0.00116
	2.0×10^{-5}	96.57	0.00014	81.68	0.00078	75.44	0.00107
	3.0×10^{-5}	96.84	0.00013	82.19	0.00073	75.95	0.00105
	4.0×10^{-5}	97.89	0.00009	85.95	0.00061	76.84	0.00102
	5.0×10^{-5}	99.47	0.00002	88.00	0.00052	78.99	0.00092
SMX	1.0×10^{-5}	90.95	0.00069	87.94	0.00094	58.72	0.00332
	2.0×10^{-5}	97.82	0.00017	88.37	0.00091	64.23	0.00288
	3.0×10^{-5}	98.18	0.00014	88.79	0.00087	73.95	0.00207
	4.0×10^{-5}	99.06	0.00007	89.79	0.00085	74.56	0.00205
	5.0×10^{-5}	99.13	0.00007	90.35	0.00076	75.74	0.00195
SCP	1.0×10^{-5}	60.74	0.00167	42.58	0.00247	15.32	0.00370
	2.0×10^{-5}	64.56	0.00149	45.81	0.00233	17.97	0.00360
	3.0×10^{-5}	65.74	0.00144	46.84	0.00228	22.53	0.00340
	4.0×10^{-5}	68.51	0.00133	46.97	0.00228	24.17	0.00332
	5.0×10^{-5}	70.09	0.00126	52.13	0.00206	25.44	0.00327
SDM	1.0×10^{-5}	63.24	0.00155	44.65	0.00238	32.03	0.00298
	2.0×10^{-5}	66.00	0.00143	46.45	0.00230	35.32	0.00283
	3.0×10^{-5}	70.88	0.00123	47.74	0.00225	39.11	0.00228
	4.0×10^{-5}	76.94	0.00097	48.52	0.00221	39.62	0.00268
	5.0×10^{-5}	79.71	0.00086	49.03	0.00219	44.81	0.00242
SSZ	1.0×10^{-5}	89.85	0.00043	71.52	0.00123	51.14	0.00214
	2.0×10^{-5}	91.96	0.00034	74.70	0.00108	55.95	0.00193
	3.0×10^{-5}	92.62	0.00031	77.95	0.00095	62.66	0.00163
	4.0×10^{-5}	93.14	0.00029	78.19	0.00093	63.16	0.00161
	5.0×10^{-5}	94.07	0.00025	81.29	0.00081	69.75	0.00132
SMZ	1.0×10^{-5}	83.85	0.00123	68.65	0.00245	54.23	0.00368
	2.0×10^{-5}	91.89	0.00062	72.19	0.00217	58.25	0.00336
	3.0×10^{-5}	93.77	0.00047	75.82	0.00189	61.68	0.00308
	4.0×10^{-5}	94.42	0.00043	79.92	0.00157	61.88	0.00307
	5.0×10^{-5}	94.71	0.00041	80.49	0.00152	70.91	0.00245
SMT	1.0×10^{-5}	81.61	0.00141	72.48	0.00187	62.44	0.00302
	2.0×10^{-5}	87.32	0.00097	76.74	0.00182	63.06	0.00297
	3.0×10^{-5}	87.40	0.00096	79.54	0.00160	63.20	0.00296
	4.0×10^{-5}	92.54	0.00057	79.65	0.00159	63.40	0.00295
	5.0×10^{-5}	93.92	0.00046	85.89	0.00110	66.10	0.00273
SQX	1.0×10^{-5}	80.23	0.00083	60.77	0.00168	56.84	0.00189
	2.0×10^{-5}	80.89	0.00080	61.81	0.00164	57.08	0.00188
	3.0×10^{-5}	81.68	0.00077	62.19	0.00162	58.35	0.00182
	4.0×10^{-5}	83.00	0.00071	63.74	0.00156	58.48	0.00182
	5.0×10^{-5}	84.84	0.00063	65.03	0.00150	63.16	0.00162

4.2.6 EFFECT OF TEMPERATURE AND KINETIC PARAMETERS

Temperature is known to effectively increase the rate of metal dissolution and this effect results to lower activation energy barrier [146, 147]. The effect of temperature on the adsorption of sulphonamides onto the surfaces of aluminium is evaluated by a means of Arrhenius equations (equation 49) and plots. The plots of $\log C_R$ versus 1/T as shown in Figures 4.133 − 4.141 gave rise to the calculated values of activation energy for the corrosion process. Calculated activation parameters are recorded in Table 4.12. It is noted from this Table that the E_a for the uninhibited process is less than those of the inhibited processes. This means that the rate of corrosion for the inhibited mild steel is prolonged as compared to that of the uninhibited process due to the formation of sulphonamide–Al complex. Furthermore it is also observed that E_a increases with the increase of inhibitor concentration for all of the studied inhibitors as shown in Figure 4.142. This observation maybe attributed to the fact that as the concentration of the sulphonamide is increased, the stability of sulphonamide–Al complex also increases.

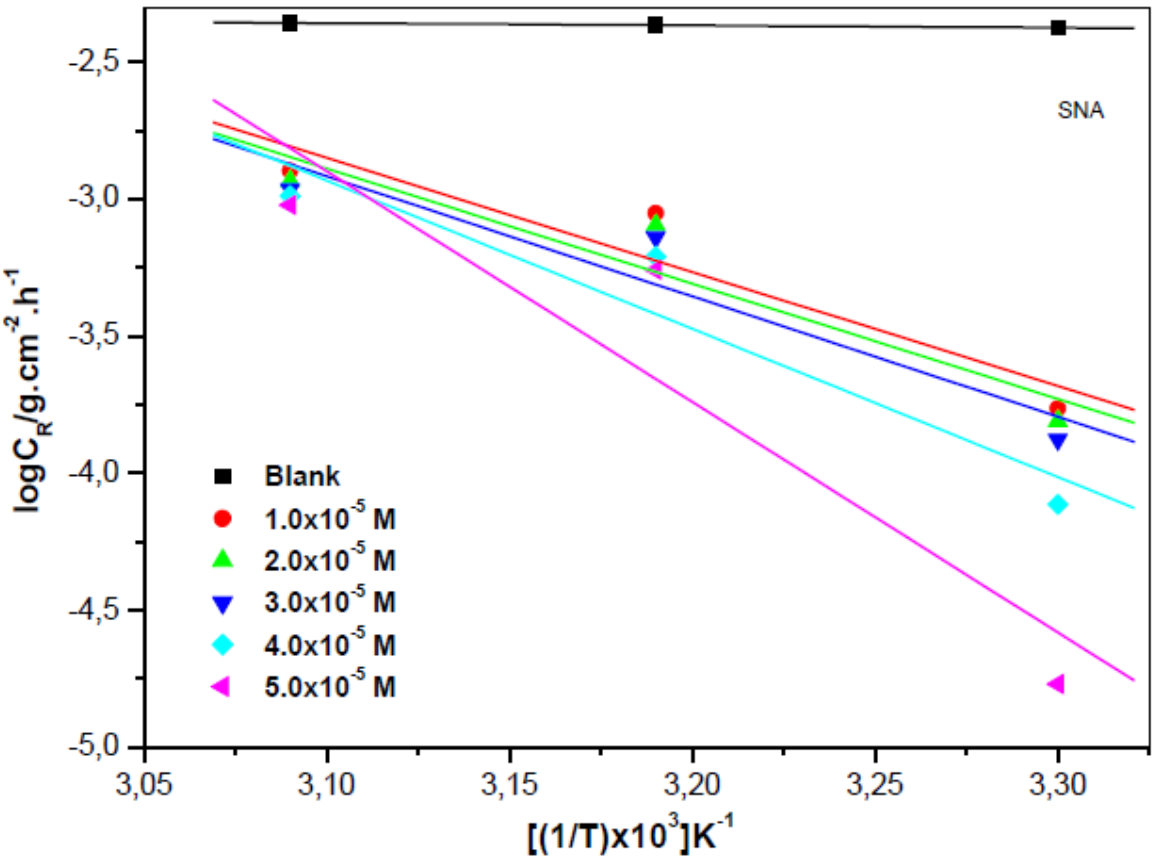

Figure 4.133: Arrhenius plots for the corrosion of aluminium in 1.0 M HCl in the absence and presence of various concentrations of SNA corrosion inhibitor.

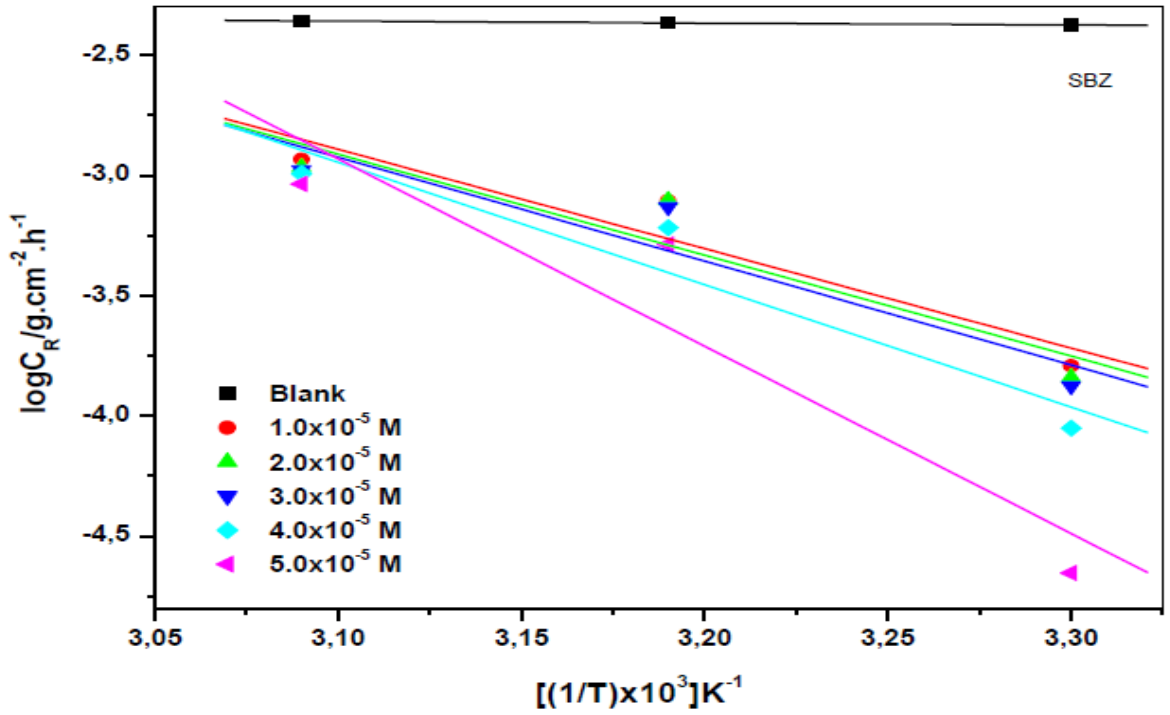

Figure 4.134: Arrhenius plots for the corrosion of aluminium in 1.0 M HCl in the absence and presence of various concentrations of SBZ corrosion inhibitor.

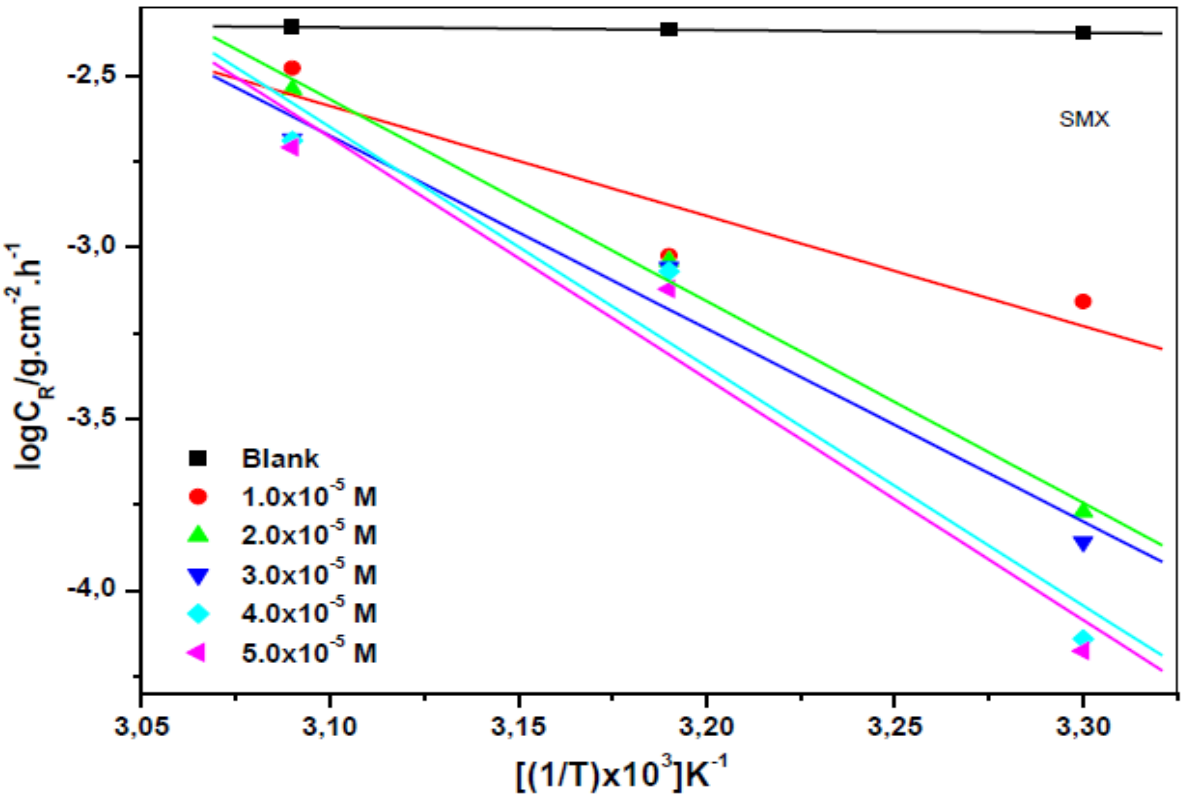

Figure 4.135: Arrhenius plots for the corrosion of aluminium in 1.0 M HCl in the absence and presence of various concentrations of SMX corrosion inhibitor.

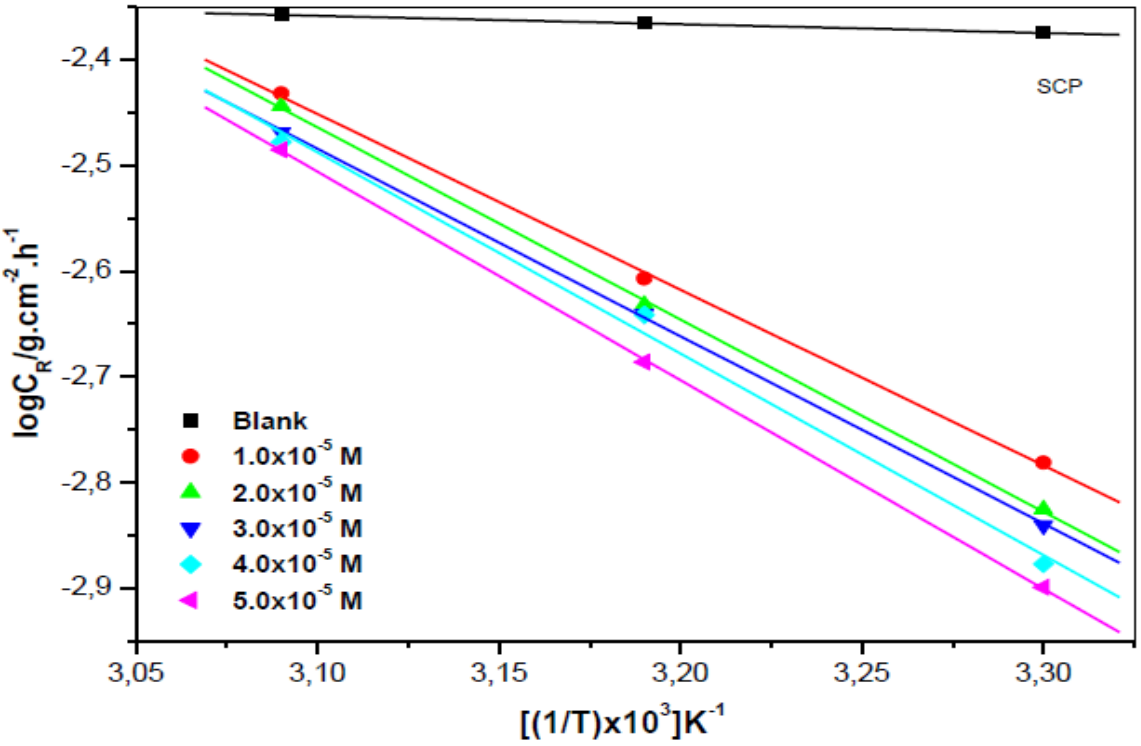

Figure 4.136: Arrhenius plots for the corrosion of aluminium in 1.0 M HCl in the absence and presence of various concentrations of SCP corrosion inhibitor.

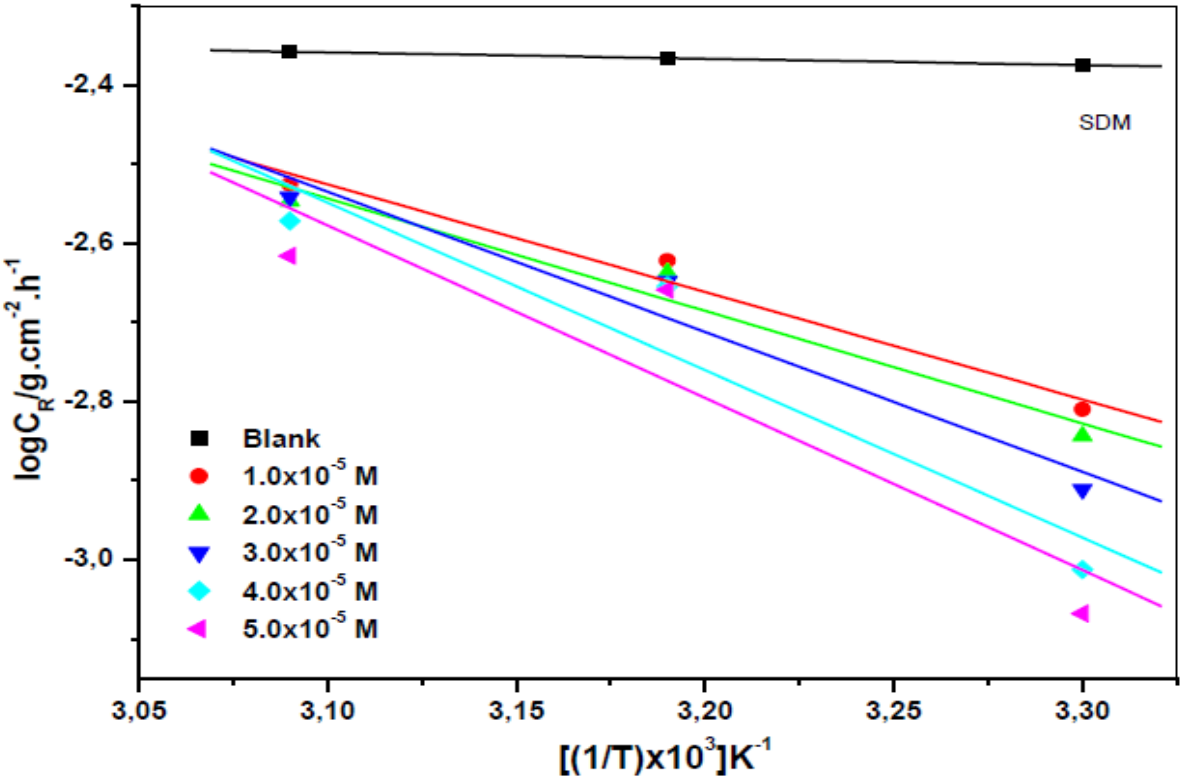

Figure 4.137: Arrhenius plots for the corrosion of aluminium in 1.0 M HCl in the absence and presence of various concentrations of SDM corrosion inhibitor.

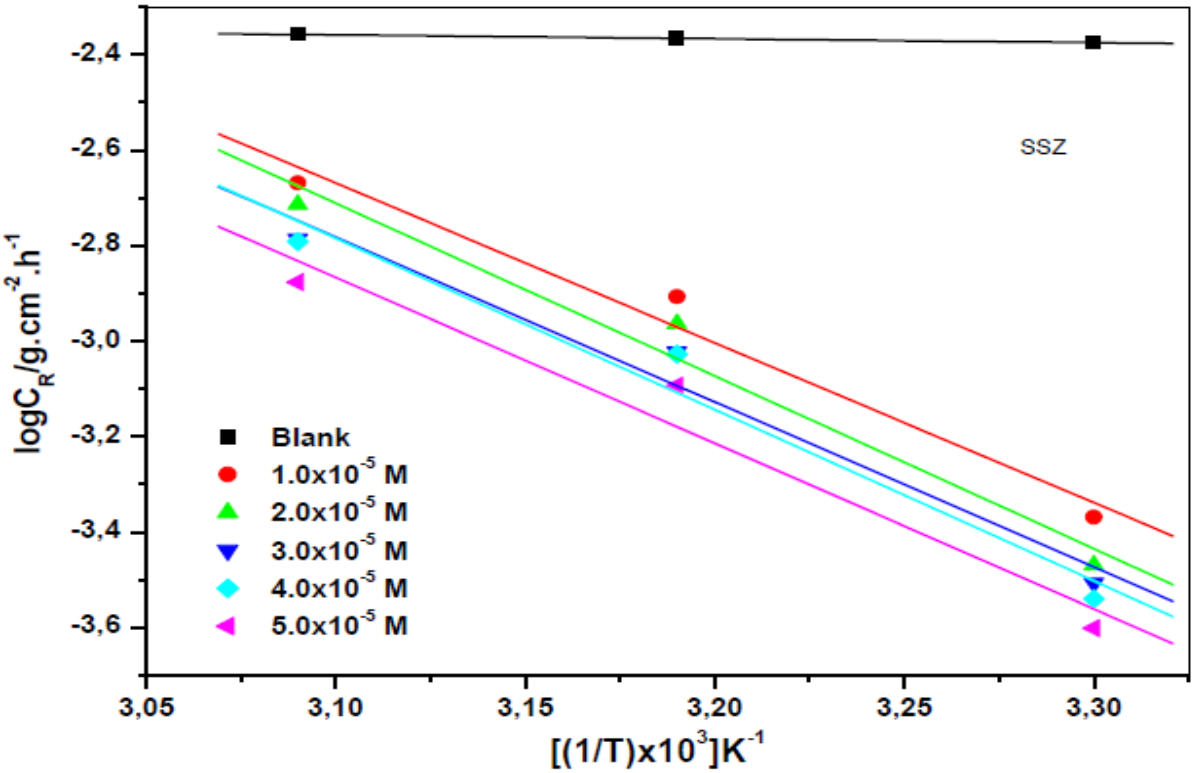

Figure 4.138: Arrhenius plots for the corrosion of aluminium in 1.0 M HCl in the absence and presence of various concentrations of SSZ corrosion inhibitor.

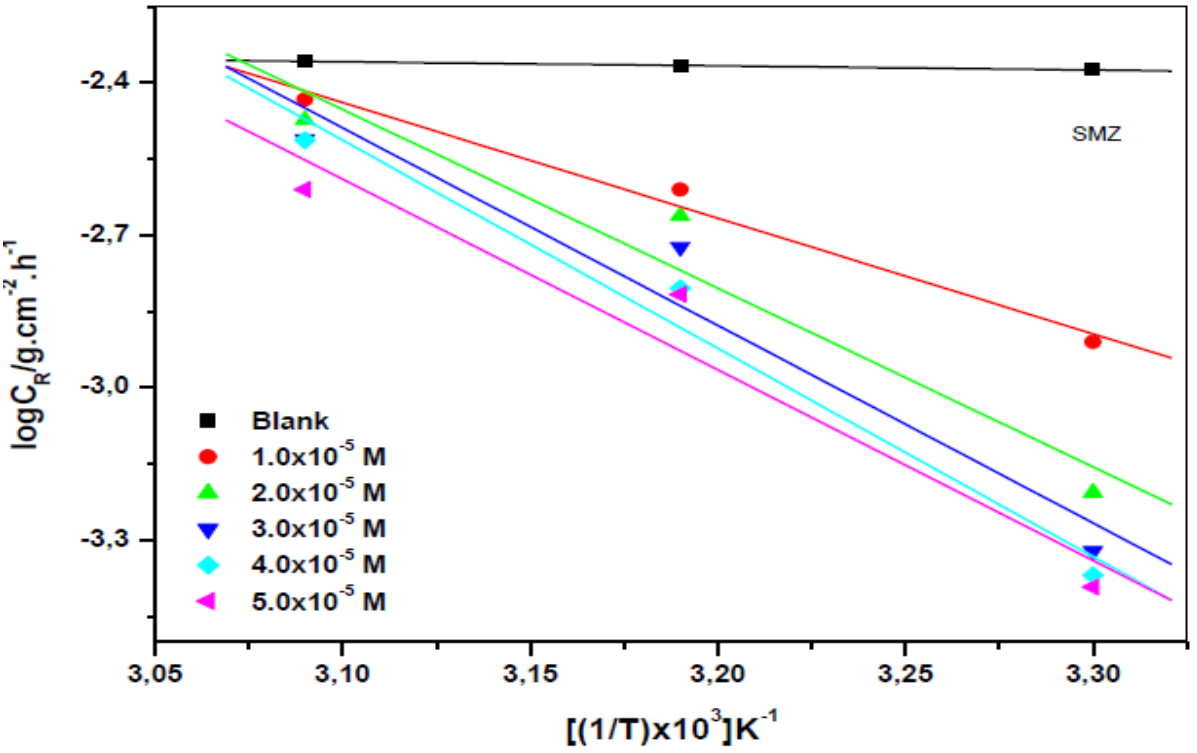

Figure 4.139: Arrhenius plots for the corrosion of aluminium in 1.0 M HCl in the absence and presence of various concentrations of SMZ corrosion inhibitor.

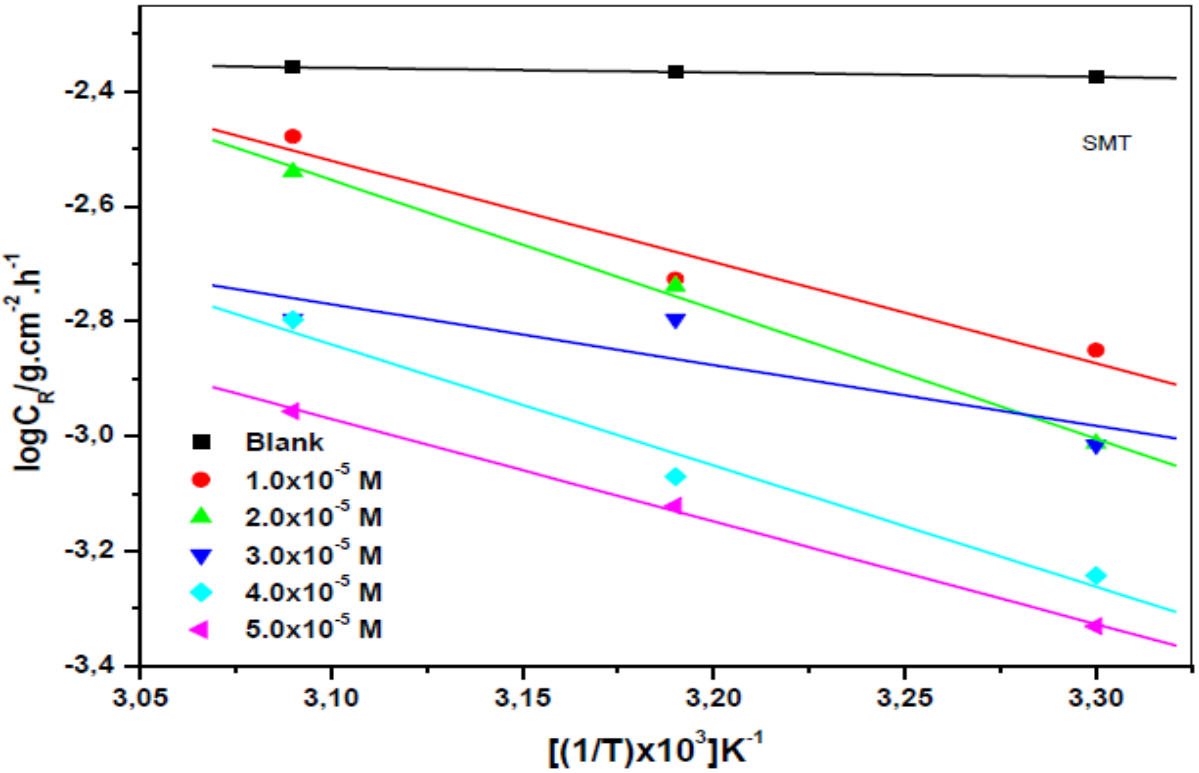

Figure 4.140: Arrhenius plots for the corrosion of aluminium in 1.0 M HCl in the absence and presence of various concentrations of SMT corrosion inhibitor.

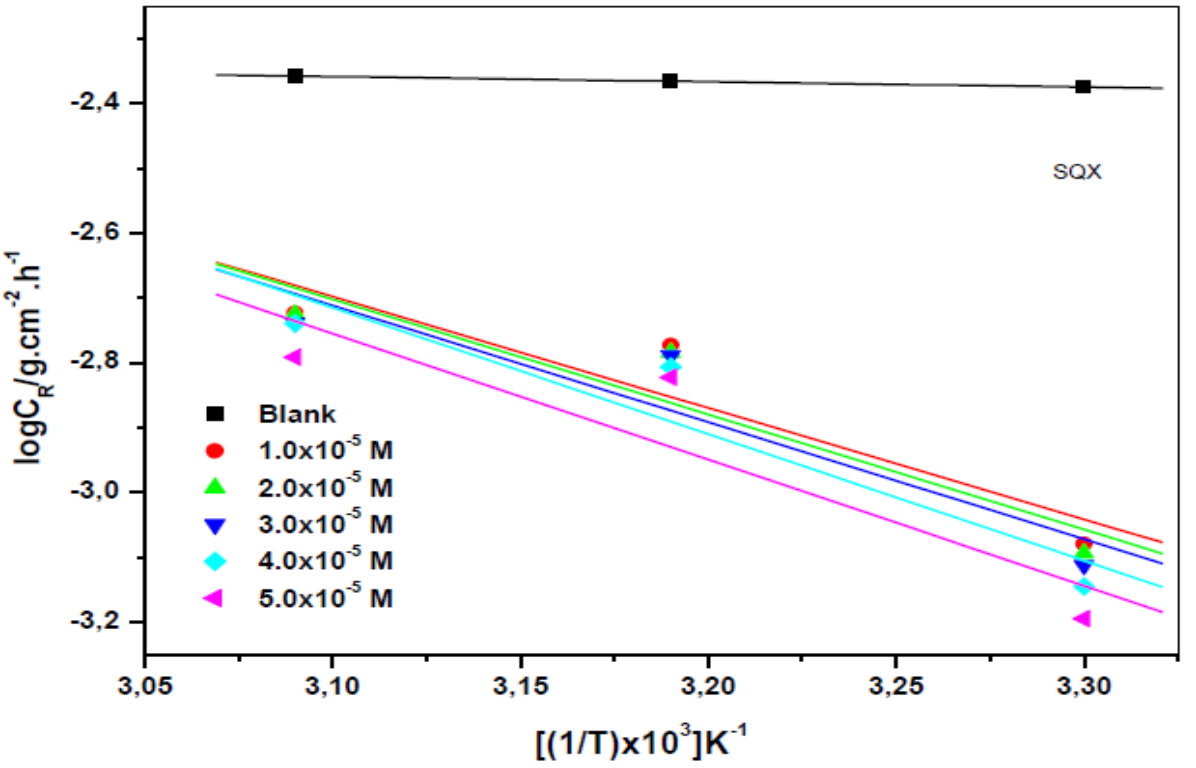

Figure 4.141: Arrhenius plots for the corrosion of aluminium in 1.0 M HCl in the absence and presence of various concentrations of SQX corrosion inhibitor.

Table 4.12: Kinetic and activation parameters (derived from the Arrhenius and transition-states plots) for aluminium in 1.0 M HCl in the absence and presence of various concentrations of inhibitors.

Inhibitor	Inhibitor Conc. (M)	Activation Energy (E_a/kJ.mol^{-1})	Enthalpy of Activation (ΔH^*/ kJ.mol^{-1})	Entropy of Activation (ΔS^*/ J.mol^{-1}.K^{-1})
Blank	0.0	1.540	0.9096	–293.60
SNA	1.0×10^{-5}	79.80	77.17	– 60.70
	2.0×10^{-5}	80.44	76.40	– 64.34
	3.0×10^{-5}	83.98	81.38	– 49.02
	4.0×10^{-5}	103.50	100.92	11.10
	5.0×10^{-5}	160.86	158.37	189.96
SBZ	1.0×10^{-5}	79.08	76.40	–63.76
	2.0×10^{-5}	80.39	77.74	– 60.13
	3.0×10^{-5}	82.71	80.23	– 52.85
	4.0×10^{-5}	97.32	94.79	– 8.234
	5.0×10^{-5}	149.09	146.30	152.24
SMX	1.0×10^{-5}	61.41	58.80	–112.98
	2.0×10^{-5}	112.55	110.49	47.87
	3.0×10^{-5}	107.60	105.13	28.91
	4.0×10^{-5}	133.40	130.60	109.15
	5.0×10^{-5}	134.66	131.94	112.21
SCP	1.0×10^{-5}	31.78	29.10	–193.33
	2.0×10^{-5}	34.79	32.17	–192.53
	3.0×10^{-5}	33.89	31.21	–195.94
	4.0×10^{-5}	36.38	33.70	–188.62
	5.0×10^{-5}	37.72	35.23	–184.41
SDM	1.0×10^{-5}	26.02	23.36	–174.26
	2.0×10^{-5}	27.19	24.51	–217.73
	3.0×10^{-5}	33.89	28.53	–205.86
	4.0×10^{-5}	40.40	33.89	–189.77
	5.0×10^{-5}	41.55	31.40	–197.97
SSZ	1.0×10^{-5}	63.96	61.47	–105.70
	2.0×10^{-5}	69.13	66.64	–90.57
	3.0×10^{-5}	66.06	63.57	–101.87
	4.0×10^{-5}	68.55	65.87	–94.40
	5.0×10^{-5}	66.45	63.76	–102.45
SMZ	1.0×10^{-5}	43.47	40.98	–65.07
	2.0×10^{-5}	67.21	64.72	–91.92
	3.0×10^{-5}	74.30	71.81	–70.47
	4.0×10^{-5}	78.32	75.81	–58.40
	5.0×10^{-5}	71.62	69.13	–80.62
SMT	1.0×10^{-5}	33.70	27.38	–209.30
	2.0×10^{-5}	43.08	41.55	–165.07
	3.0×10^{-5}	20.10	41.74	–165.45
	4.0×10^{-5}	40.21	62.42	–100.34
	5.0×10^{-5}	34.08	105.70	–86.55
SQX	1.0×10^{-5}	32.74	30.25	–203.37
	2.0×10^{-5}	33.89	31.40	–199.92
	3.0×10^{-5}	34.47	31.78	–198.58
	4.0×10^{-5}	37.15	34.66	–189.96
	5.0×10^{-5}	37.34	34.85	–190.73

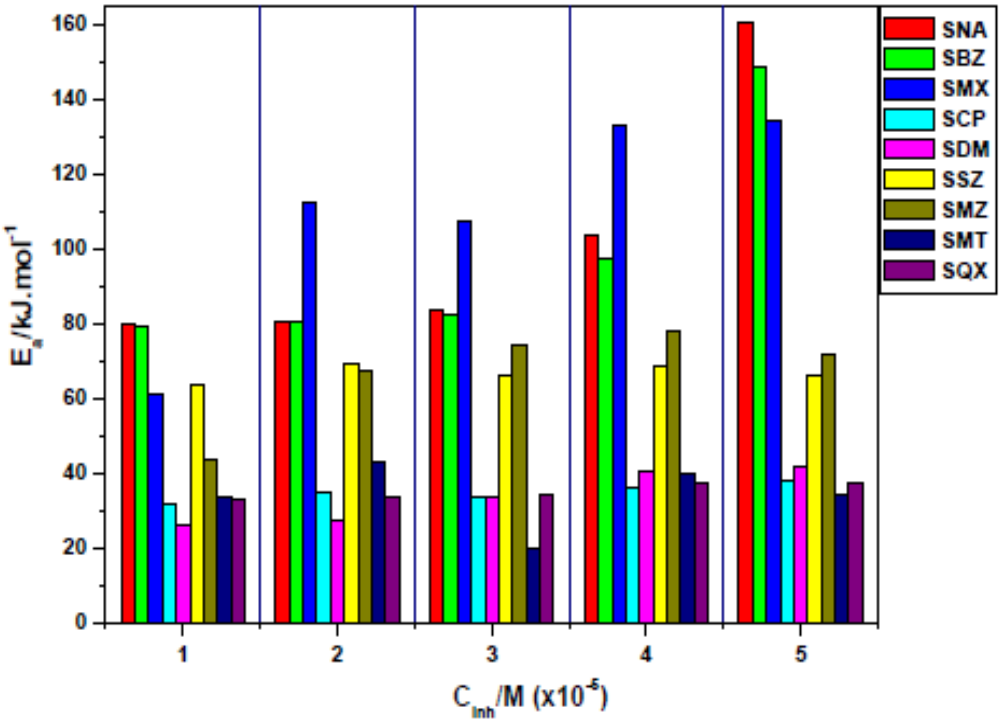

Figure 4.142: Variation of the activation energy with the concentration of the utilized corrosion inhibitors for aluminum.

Further investigation of inhibition efficiency on the aluminium surface can be determined by the values of entropy and enthalpy of activation. The negative values of entropy show that the destruction on the metal surface has been lowered and the positive once shows that the disordering of the system has increased [148, 149]. Enthalpy values can present both the endothermic or exothermic reaction depending on the sign of the value. Moreover endothermic processes are related to chemical adsorption while exothermic processes are related to either chemical or physical adsorption [150, 151]. Chemical adsorption is the most preferred over physical if prolonged results are desired. This is due to the fact that chemical adsorption is related to the sharing of electron pairs between the inhibitors and the empty of unpaired orbitals of the metals whereas physical adsorption is related to the electrostatic interactions between charged inhibitor molecules and the charged surfaces of the metals.

Transition state plots as shown in Figures 4.143 − 4.151 are constructed from equation 50. Kinetic and thermodynamic parameters obtained from the Transition state plots are also recorded in Table 4.12.

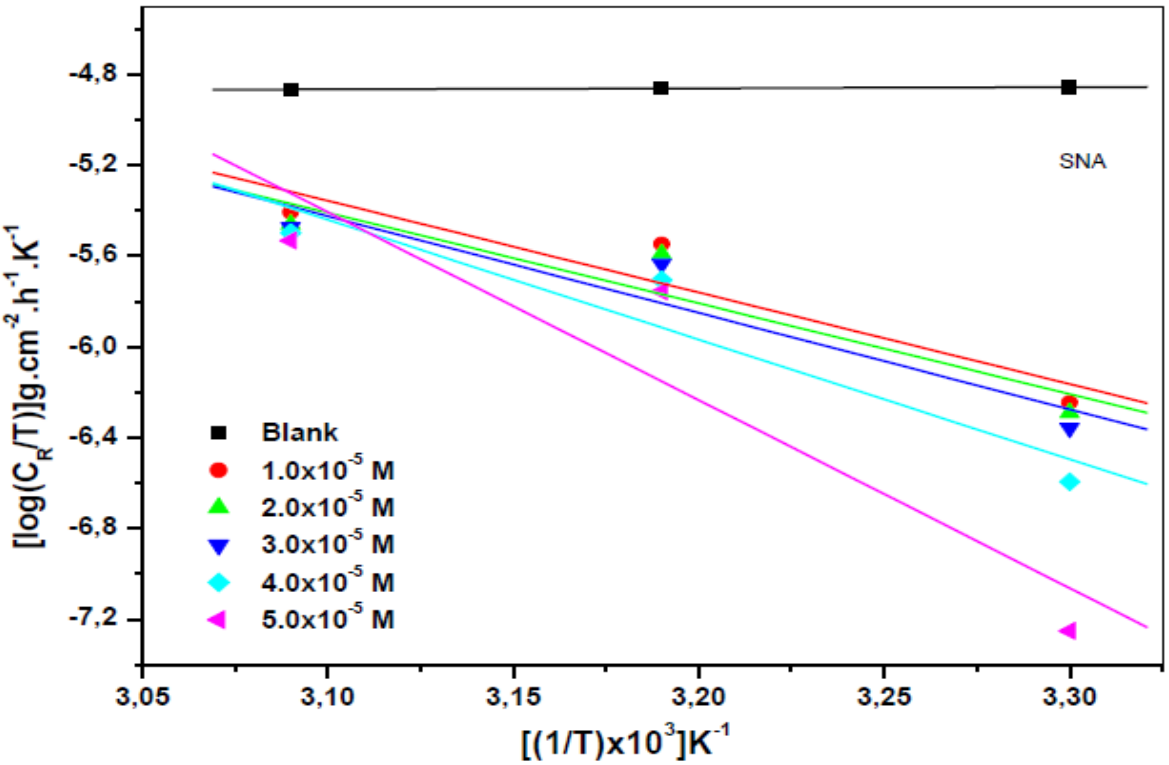

Figure 4.143: Transition state plots for the corrosion of aluminium in 1.0 M HCl in the absence and presence of various concentrations of SNA corrosion inhibitor.

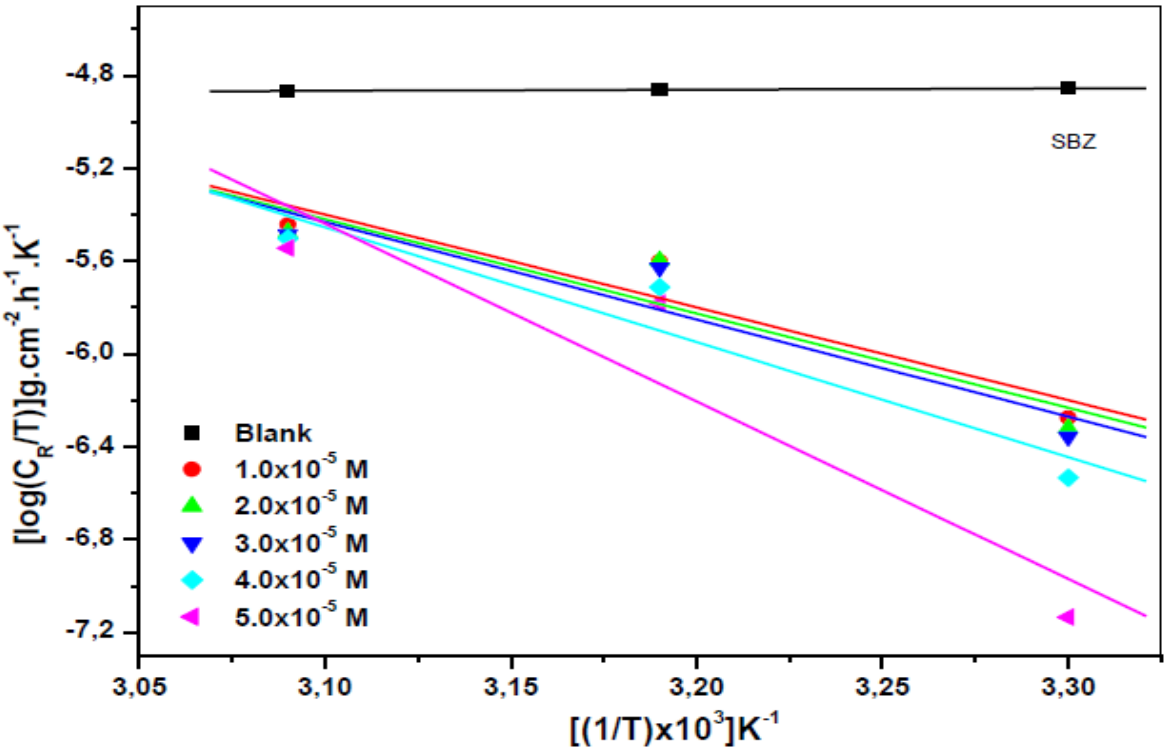

Figure 4.144: Transition state plots for the corrosion of aluminium in 1.0 M HCl in the absence and presence of various concentrations of SBZ corrosion inhibitor.

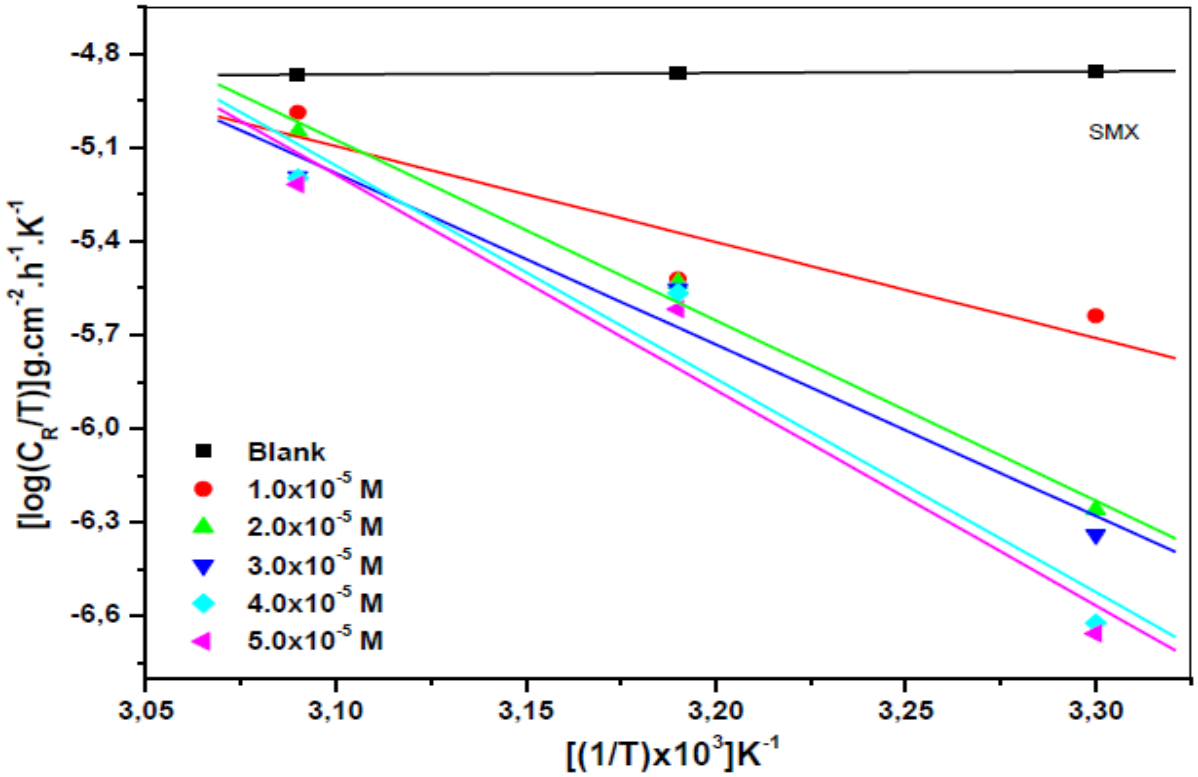

Figure 4.145: Transition state plots for the corrosion of aluminium in 1.0 M HCl in the absence and presence of various concentrations of SMX corrosion inhibitor.

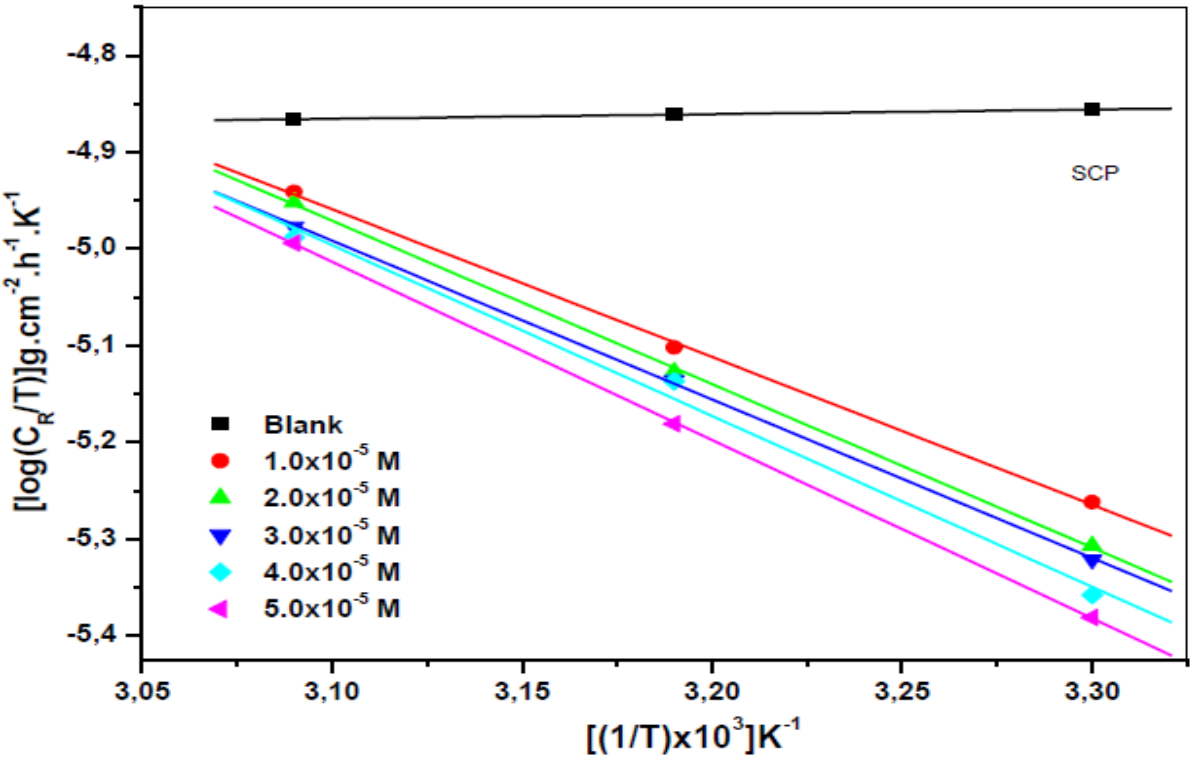

Figure 4.146: Transition state plots for the corrosion of aluminium in 1.0 M HCl in the absence and presence of various concentrations of SCP corrosion inhibitor.

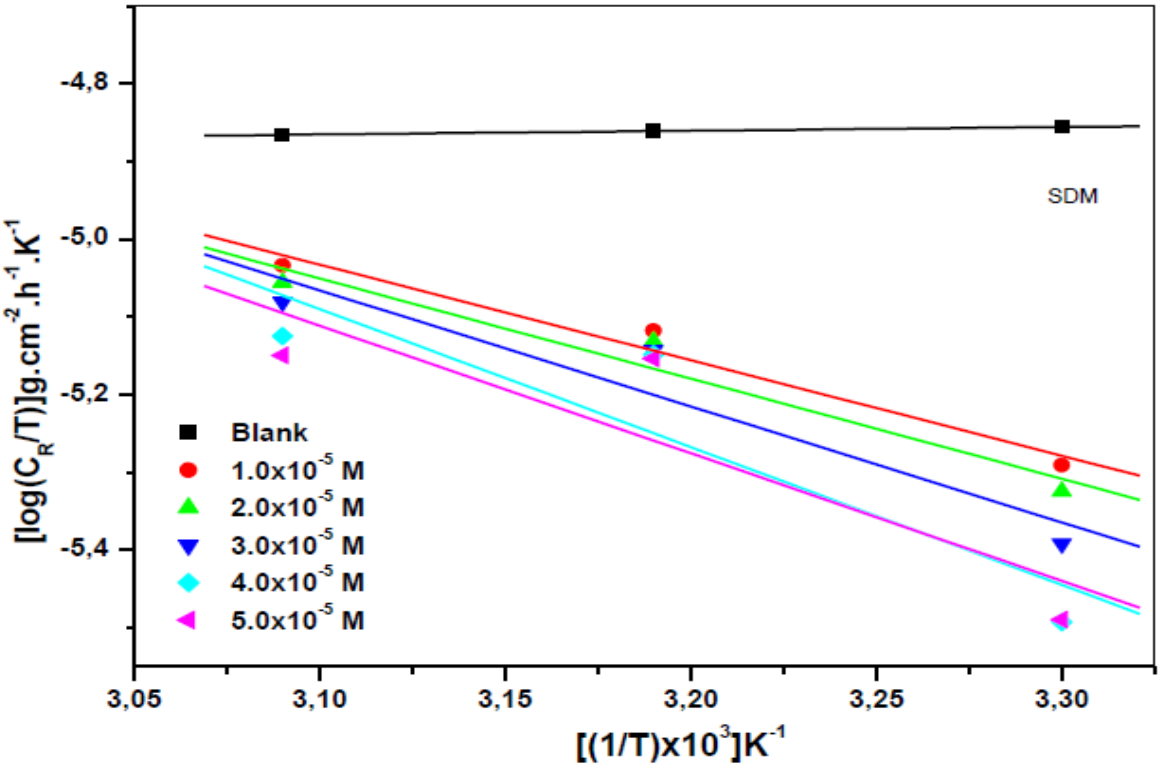

Figure 4.147: Transition state plots for the corrosion of aluminium in 1.0 M HCl in the absence and presence of various concentrations of SDM corrosion inhibitor.

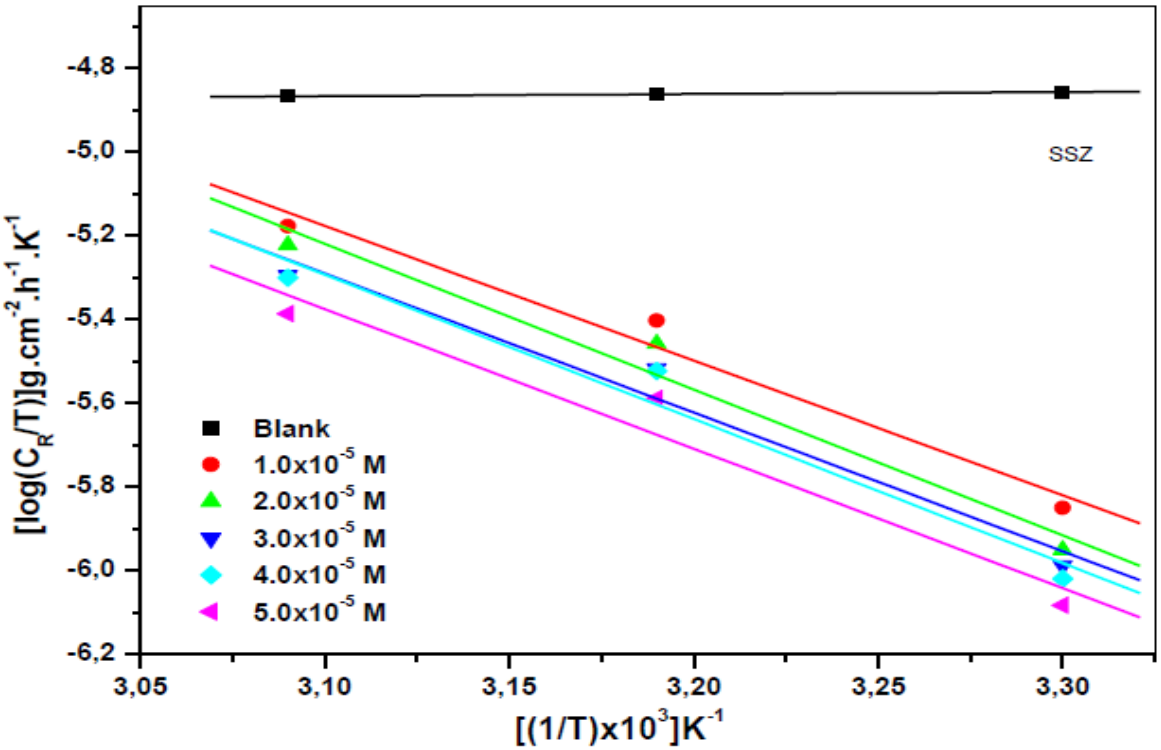

Figure 4.148: Transition state plots for the corrosion of aluminium in 1.0 M HCl in the absence and presence of various concentrations of SSZ corrosion inhibitor.

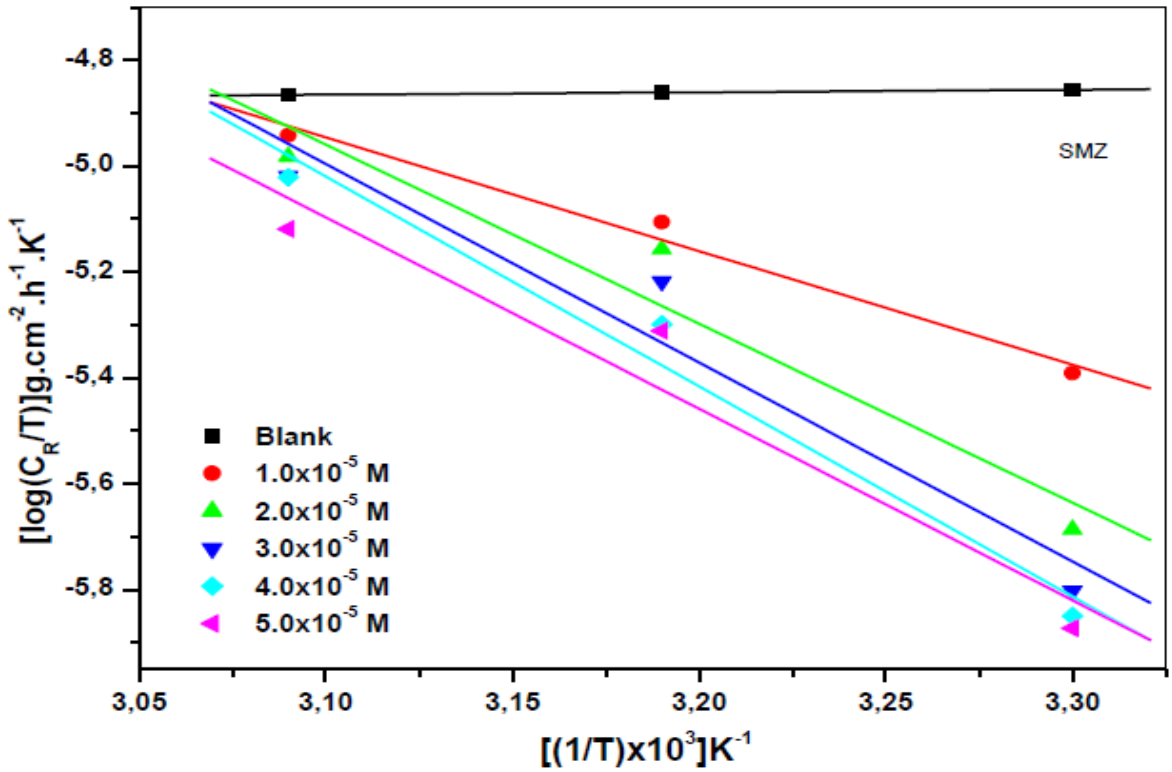

Figure 4.149: Transition state plots for the corrosion of aluminium in 1.0 M HCl in the absence and presence of various concentrations of SMZ corrosion inhibitor.

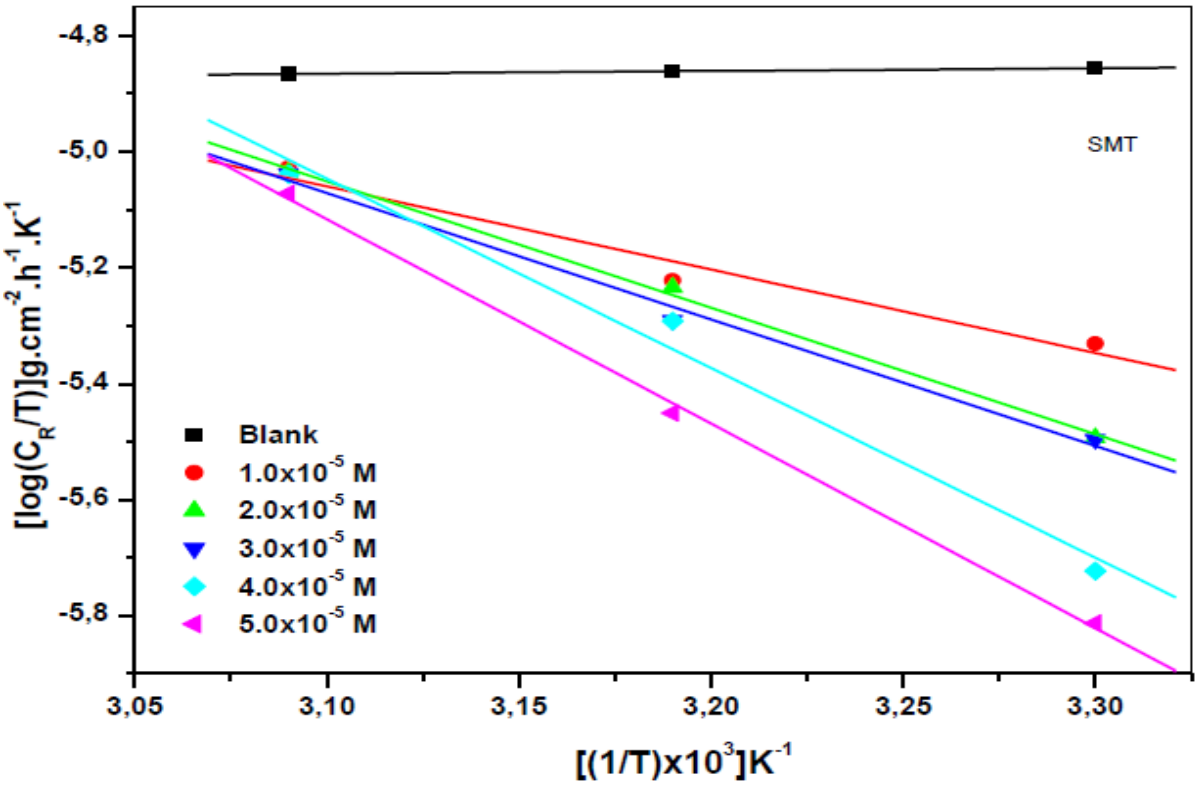

Figure 4.150: Transition state plots for the corrosion of aluminium in 1.0 M HCl in the absence and presence of various concentrations of SMT corrosion inhibitor.

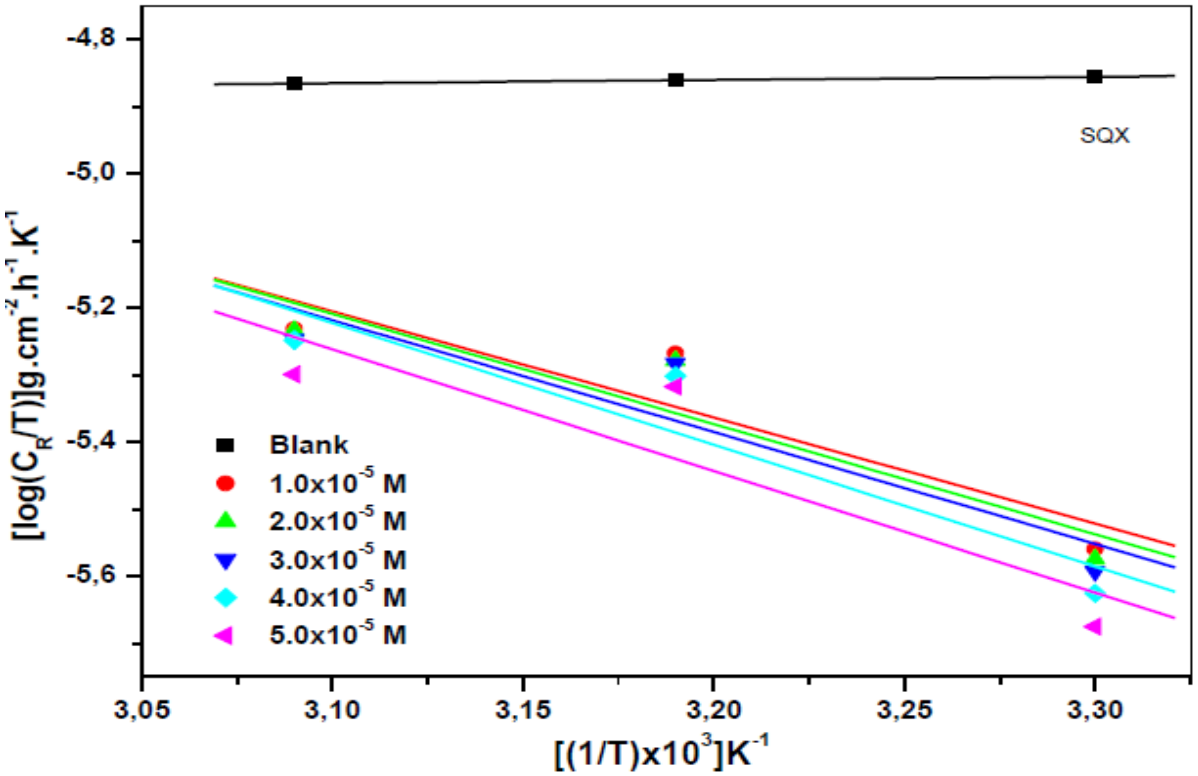

Figure 4.151: Transition state plots for the corrosion of aluminium in 1.0 M HCl in the absence and presence of various concentrations of SQX corrosion inhibitor.

Literature show that the values of ΔH* within a range of up to 41.86 kJmol^{-1} are characterized with physical adsorption while those around 100 kJmol^{-1} or more are characterized with chemical adsorption [152, 153]. Careful inspection of Table 4.12 shows that ΔH* values are slightly less than those of their E_a counterparts. Furthermore, uninhibited process has much less ΔH* values in comparison with the inhibited processes. The values of ΔH* for SNA, SBZ, SMX, SSZ and SMZ are all above the 100 kJmol^{-1} threshold signifying a chemical adsorption nature. It is noted the values of ΔH* for SCP, SDM and SQX are all below the 41.86 kJmol^{-1} threshold signifying a physical adsorption nature. It is interesting to observe that for SMT, the values of ΔH* are lower at the lowest concentration and higher at higher concentrations signifying a mixed-type adsorption. The values of ΔS* for the uninhibited process are much higher than those of the inhibited processes. This means that as the inhibitor molecules are introduced into the system, destruction on the metal surface has been lowered because of the disorder increase from reactant species to the activated complex during the adsorption process [154].

4.2.7 ADSORPTION ISOTHERMS AND THERMODYNAMIC PARAMETERS

A crucial way to determine the type of mechanism followed during adsorption processes between the inhibitor and the metal is to fit various adsorption isotherms and then select the best regression line and r^2 value that is close to unity. The attempted adsorption isotherms included Langmuir, Temkin, Freundlich, Frumkin, and Flory-Huggins. The relationship between the surface coverage and the concentrations of the sulphonamides adhered to the Langmuir adsorption isotherm which can be expressed by equation 53.

The Langmuir adsorption isotherms are plotted as shown in Figures 4.152 − 4.160. The confidence of Langmuir plots is supported by the values r^2 that are close to unity. The values of r^2, slope, calculated adsorption equilibrium constant (K_{ads}) and the standard free energy of adsorption (ΔG^o_{ads}) are recorded in Table 4.13. The slope values indicate the amount of layers adsorbed on surface of the metal. The values of r^2 for all studied sulphonamides, as recorded in Table 4.13 are close to unity, signifying that a monolayer type of layer was formed between metal surface and inhibitor.

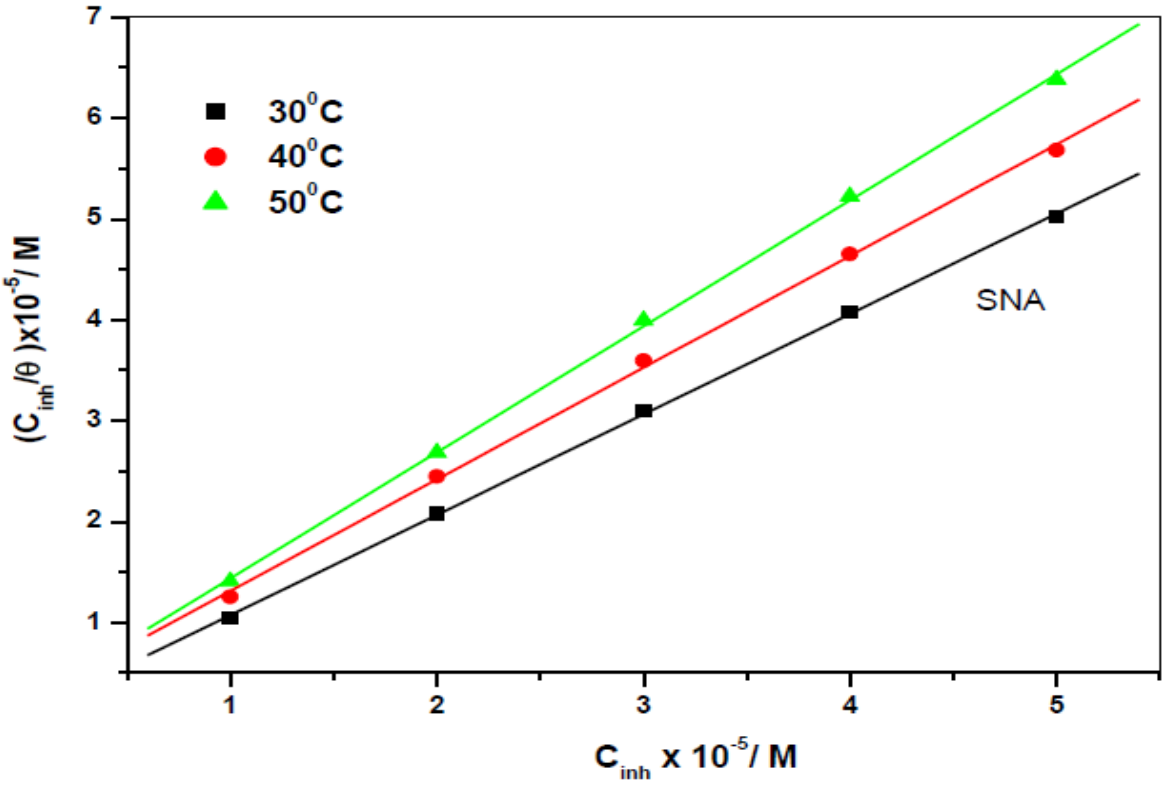

Figure 4.152: Langmuir adsorption isotherms for the corrosion of aluminium in 1.0 M HCl at various temperatures for SNA corrosion inhibitor.

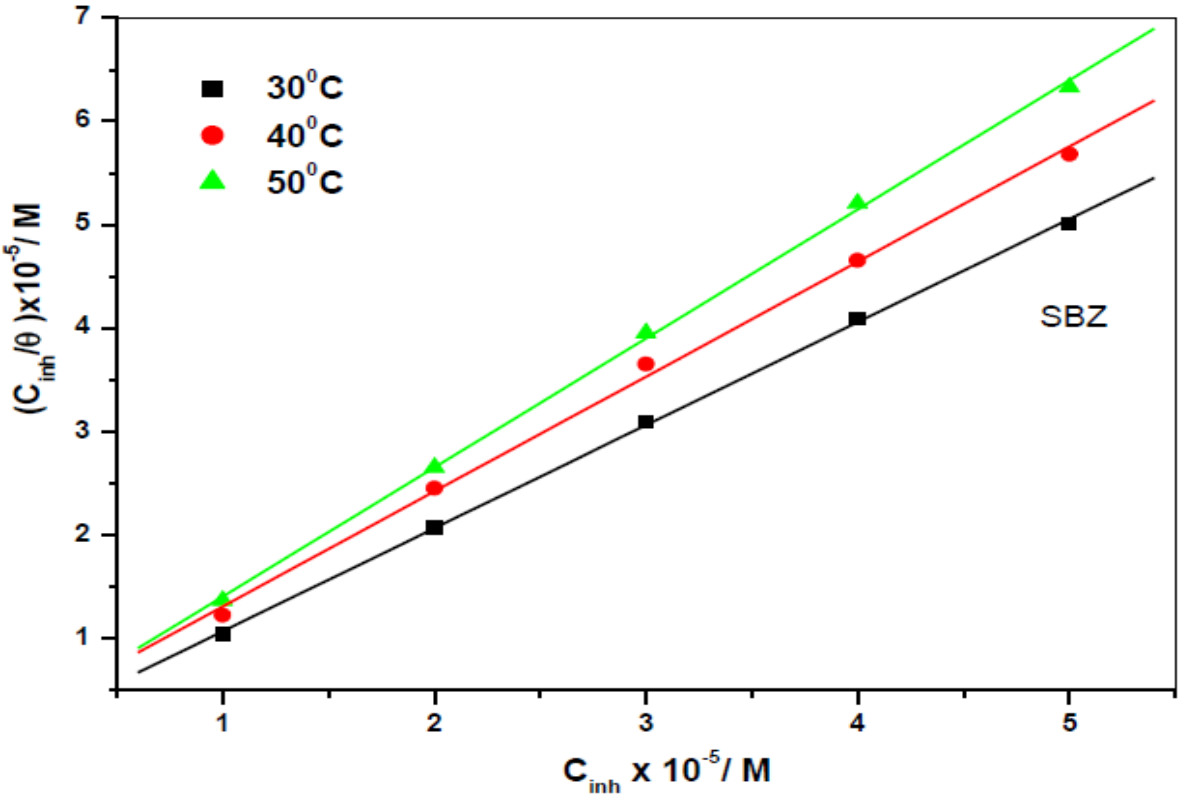

Figure 4.153: Langmuir adsorption isotherms for the corrosion of aluminium in 1.0 M HCl at various temperatures for SBZ corrosion inhibitor.

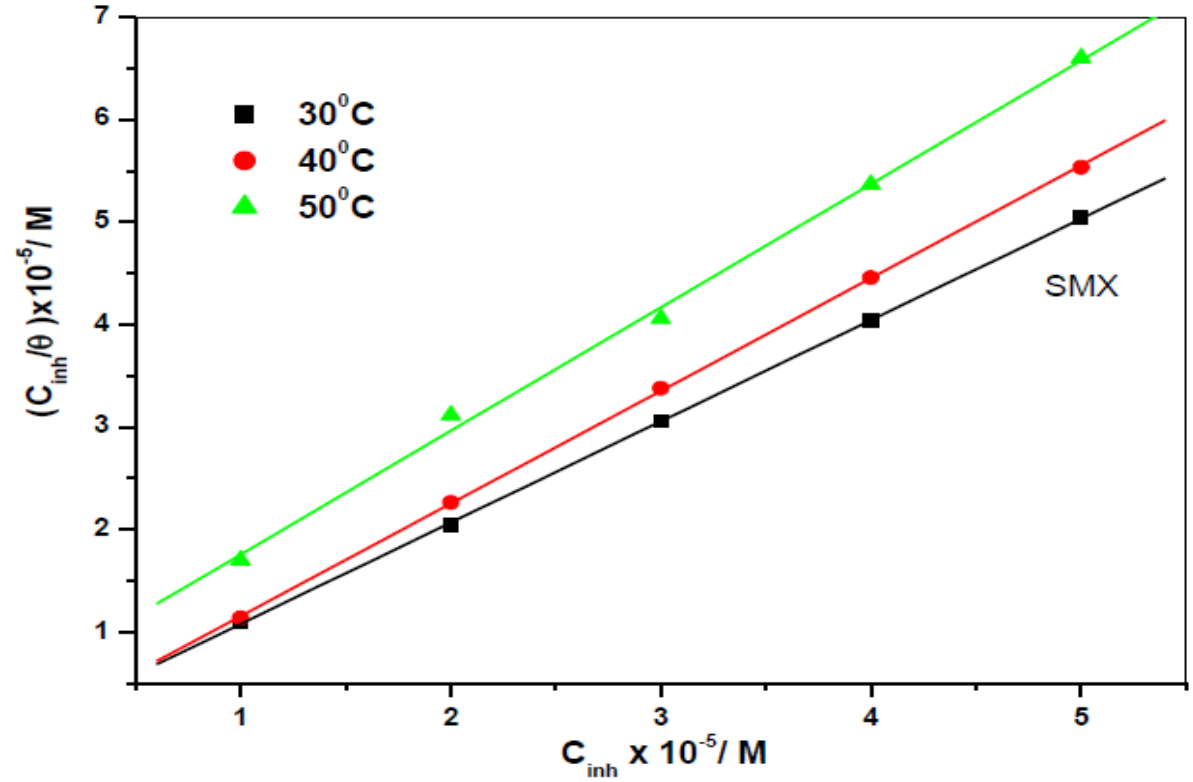

Figure 4.154: Langmuir adsorption isotherms for the corrosion of aluminium in 1.0 M HCl at various temperatures for SMX corrosion inhibitor.

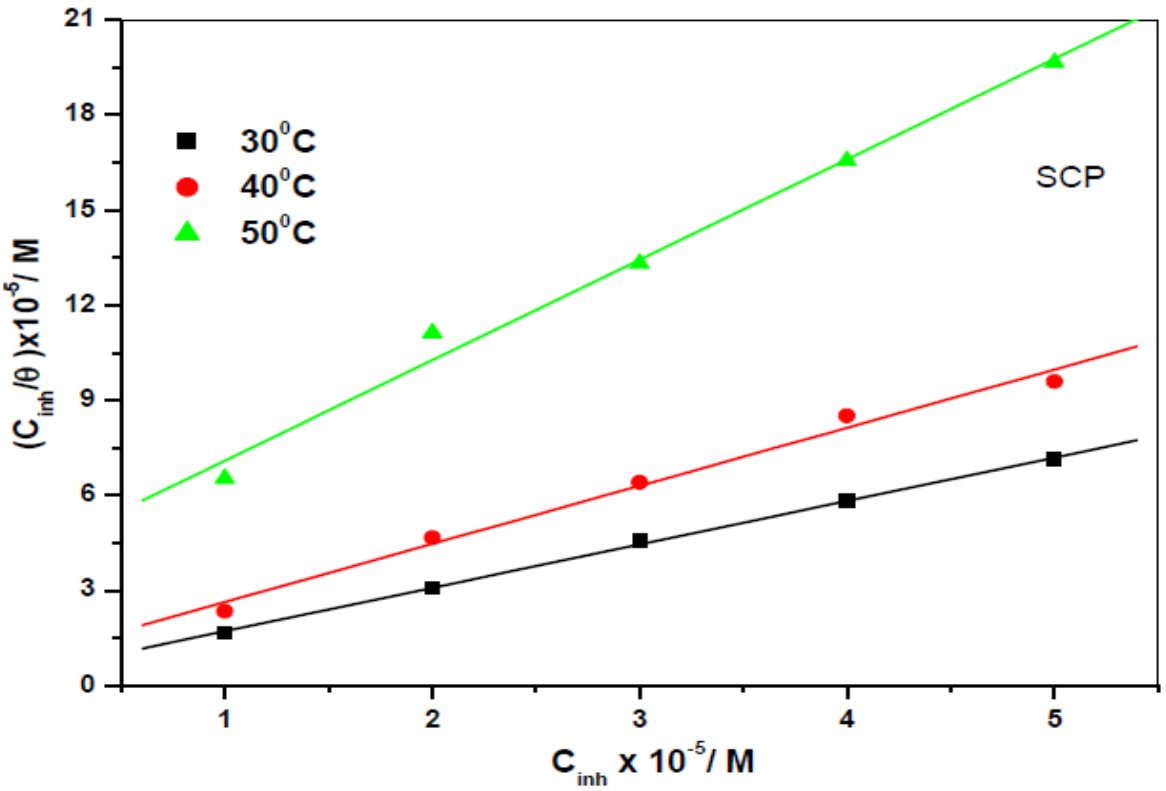

Figure 4.155: Langmuir adsorption isotherms for the corrosion of aluminium in 1.0 M HCl at various temperatures for SCP corrosion inhibitor.

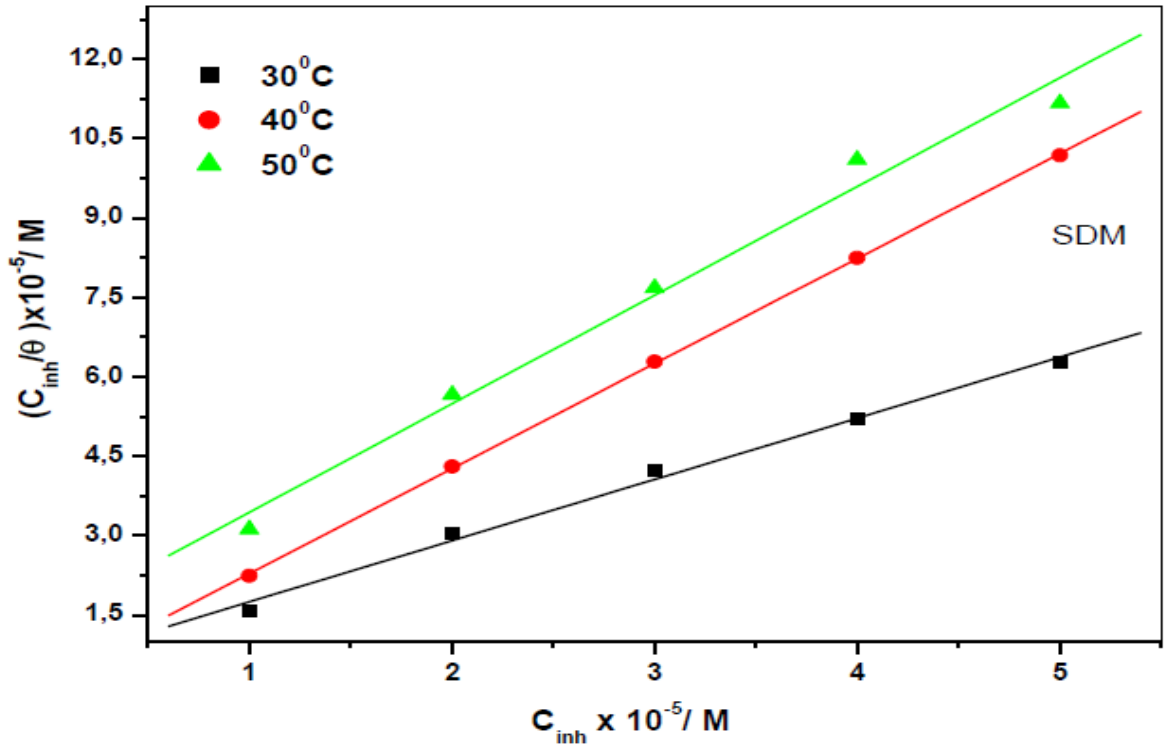

Figure 4.156: Langmuir adsorption isotherms for the corrosion of aluminium in 1.0 M HCl at various temperatures for SDM corrosion inhibitor.

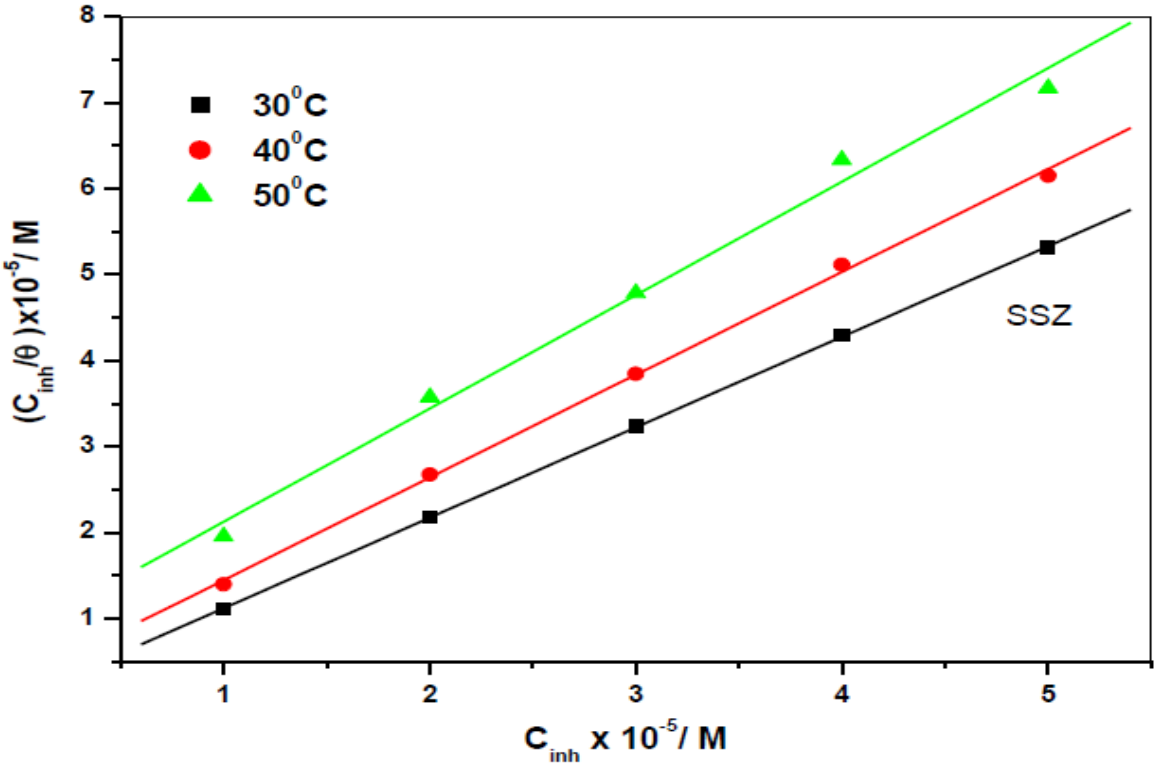

Figure 4.157: Langmuir adsorption isotherms for the corrosion of aluminium in 1.0 M HCl at various temperatures for SSZ corrosion inhibitor.

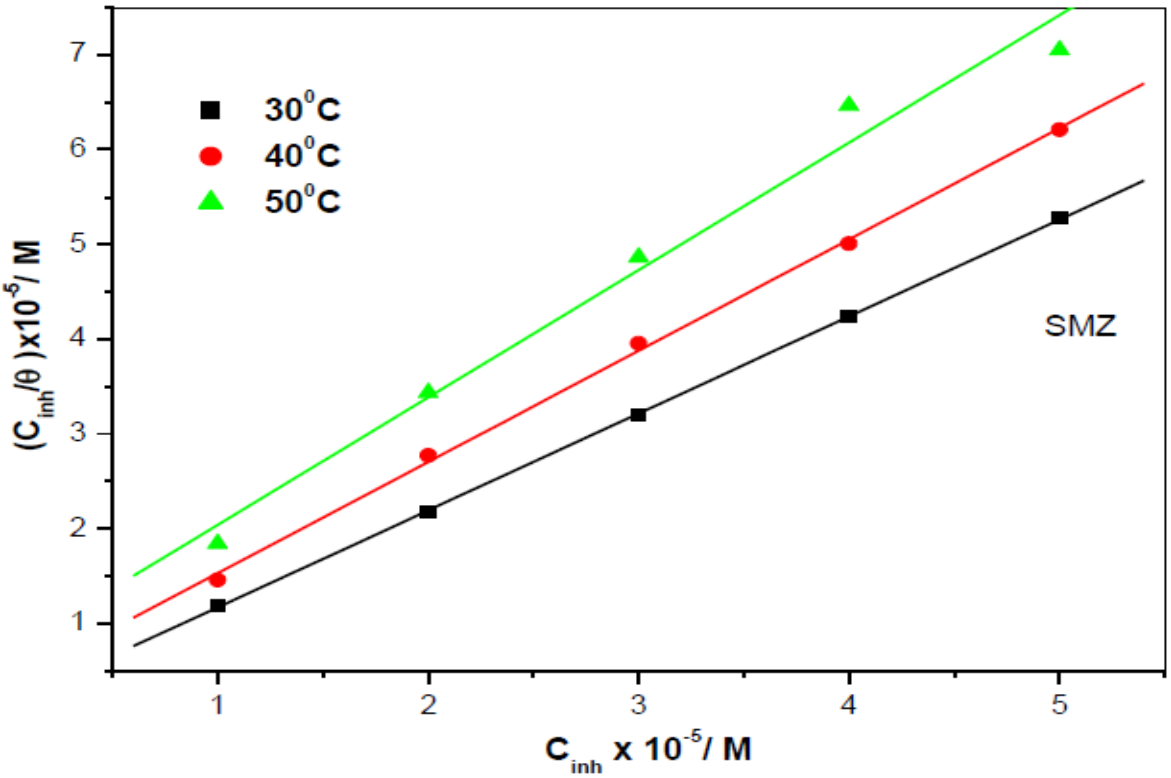

Figure 4.158: Langmuir adsorption isotherms for the corrosion of aluminium in 1.0 M HCl at various temperatures for SMZ corrosion inhibitor.

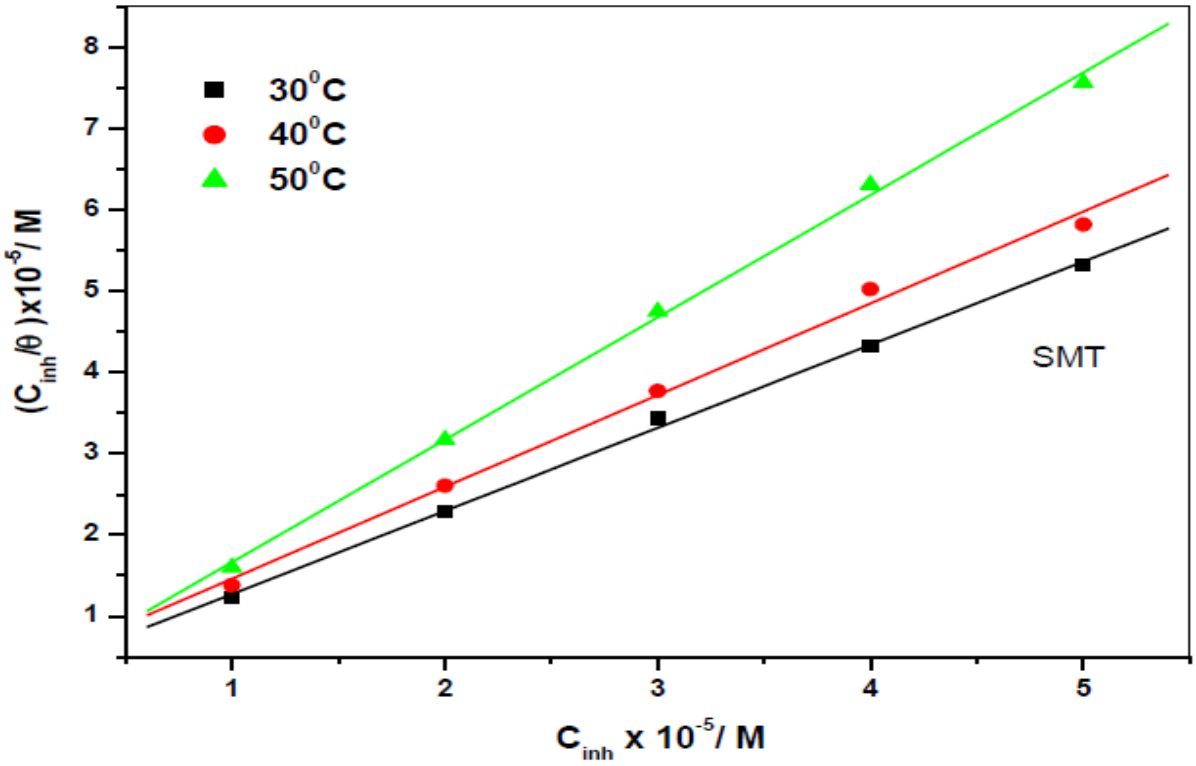

Figure 4.159: Langmuir adsorption isotherms for the corrosion of aluminium in 1.0 M HCl at various temperatures for SMT corrosion inhibitor.

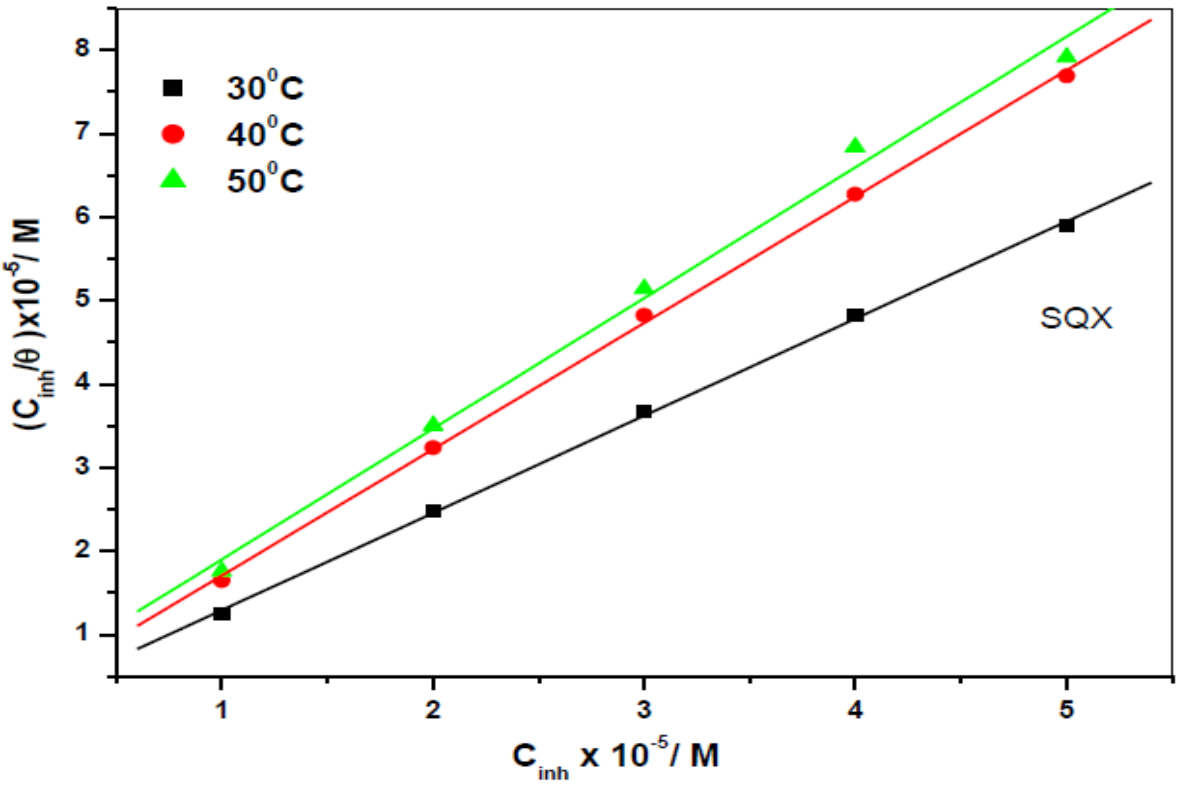

Figure 4.160: Langmuir adsorption isotherms for the corrosion of aluminium in 1.0 M HCl at various temperatures for SQX corrosion inhibitor.

Table 4.13: Thermodynamic and adsorption parameters (Langmuir adsorption isotherms) for mild steel in 1.0 M HCl at various temperatures for the utilized corrosion inhibitors.

Inhibitor	Temperature (°C)	r^2	Slope	K_{ads} (M^{-1})	ΔG^0_{ads} ($kJ.mol^{-1}$)
SNA	30	0.999	0.995	13.15	–16.60
	40	0.999	1.107	4.890	–14.54
	50	0.998	1.249	5.285	–15.25
SBZ	30	0.999	0.997	14.35	–16.82
	40	0.999	1.112	5.154	–15.18
	50	0.998	1.249	6.553	–15.83
SMX	30	0.999	0.988	10.91	–16.13
	40	0.999	1.098	17.29	–17.86
	50	0.998	1.204	1.806	–12.37
SCP	30	0.999	1.369	2.861	–12.76
	40	0.998	1.833	1.239	–11.01
	50	0.998	3.167	0.254	–07.15
SDM	30	0.999	1.155	1.672	–11.79
	40	0.999	1.981	3.279	–13.97
	50	0.999	2.050	0.719	–09.01
SSZ	30	0.999	1.052	14.24	–16.80
	40	0.999	1.194	3.921	–14.01
	50	0.998	1.318	1.237	–11.35
SMZ	30	0.999	1.023	6.808	–14.94
	40	0.996	1.174	2.807	–13.55
	50	0.999	1.344	1.433	–11.75
SMT	30	0.999	1.022	3.997	–13.61
	40	0.998	1.130	3.033	–13.34
	50	0.999	1.506	6.264	–15.71
SQX	30	0.999	1.164	7.776	–15.28
	40	0.999	1.512	5.101	–14.69
	50	0.999	1.565	2.966	–13.71

The standard free energy of adsorption provides more insights regarding the spontaneity of the inhibition process as well as the stability of the adsorption [127, 128]. The values of ΔG° were calculated using equation 54.

It has been reported that the negative values of ΔG^o_{ads} imply a spontaneous occurrence of a reaction [127, 128]. It is important to mention that ΔG^o_{ads} values of -20 $kJmol^{-1}$ and below signify physisorption while those that are -40 $kJmol^{-1}$ and above represent chemisorption. The values of ΔG^o_{ads} in Tables 4.13 show the spontaneity of reaction and the stability of the adsorption since they are of a negative nature. It is observable from Table 4.13 that ΔG^o_{ads} increases with the temperature of the surrounding environment. This observation is attributed

to an exothermic adsorption [119]. From the exothermic nature it can be deduced that the studied sulphonamides adsorb onto the metal surface through either physisorption or chemisorption. The results from the weight loss and electrochemical measurements show that the order of inhibition efficiency by the sulphonamides follows the order: SNA > SBZ > SMX > SMZ > SSZ > SMT > SQX > SDM > SCP.

.

4.3 ZINC

4.3.1 POTENTIODYNAMIC POLARIZATION (PDP)

Tafel plots can be utilized as a reliable tool to measure the corrosion potential (E_{corr}), corrosion current density (i_{corr}) and anodic and cathodic Tafel slopes (b_a and b_c). The linear Tafel segments of anodic and cathodic curves were extrapolated to corrosion potential to obtain corrosion current densities (i_{corr}). The measured i_{corr} values are related to the inhibition efficiency through equation (48).

The plots which are given in Figures 4.161−4.170 represent the Tafel plots for zinc in 1 M HCl which were obtained in the absence and presence of different concentrations of SNA, SBZ, SMX, SCP, SDM, SSZ, SMZ, SMT and SQX. It shows that in the presence of the inhibitor, the curves are shifted to the lower current regions. This trend confirms the inhibition ability of the sulphonamide corrosion inhibitors utilized in this study.

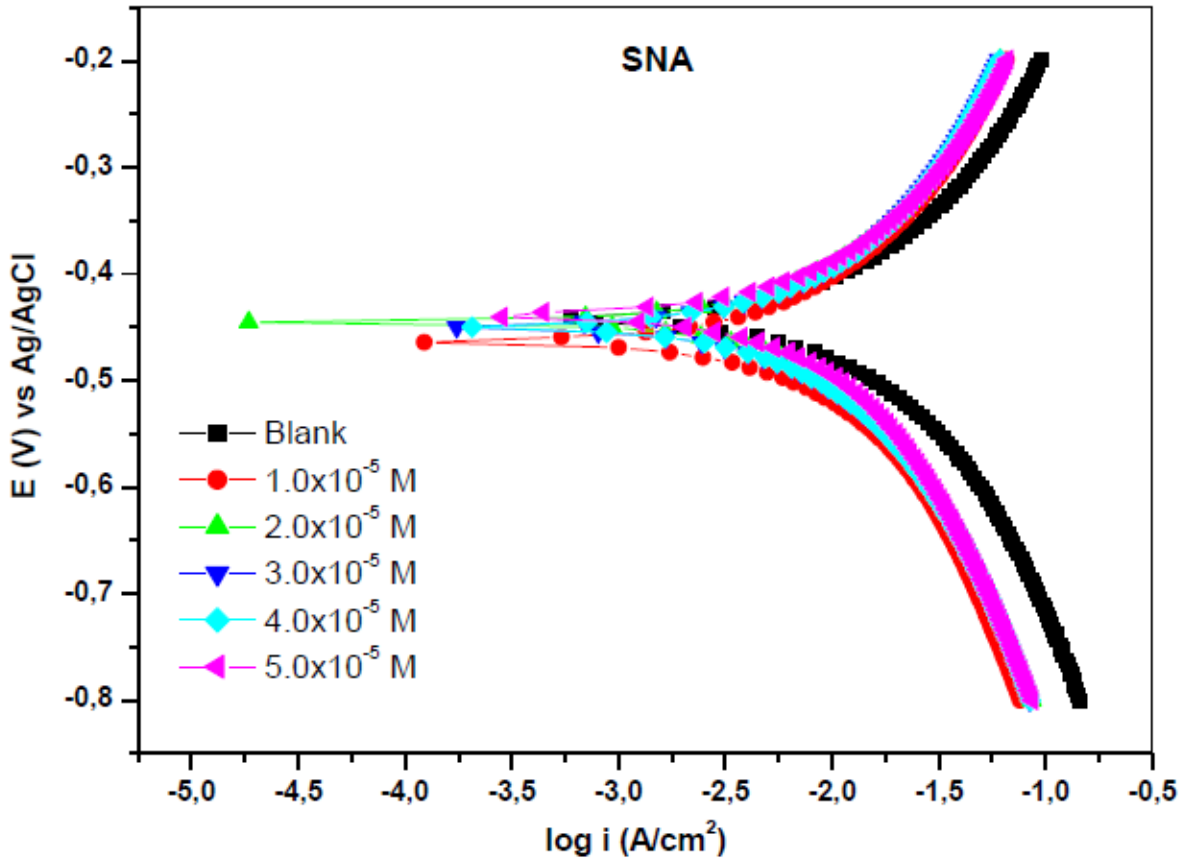

Figure 4.161: Tafel plots for zinc in 1 M HCl in the absence and presence of different concentrations of SNA inhibitor compound.

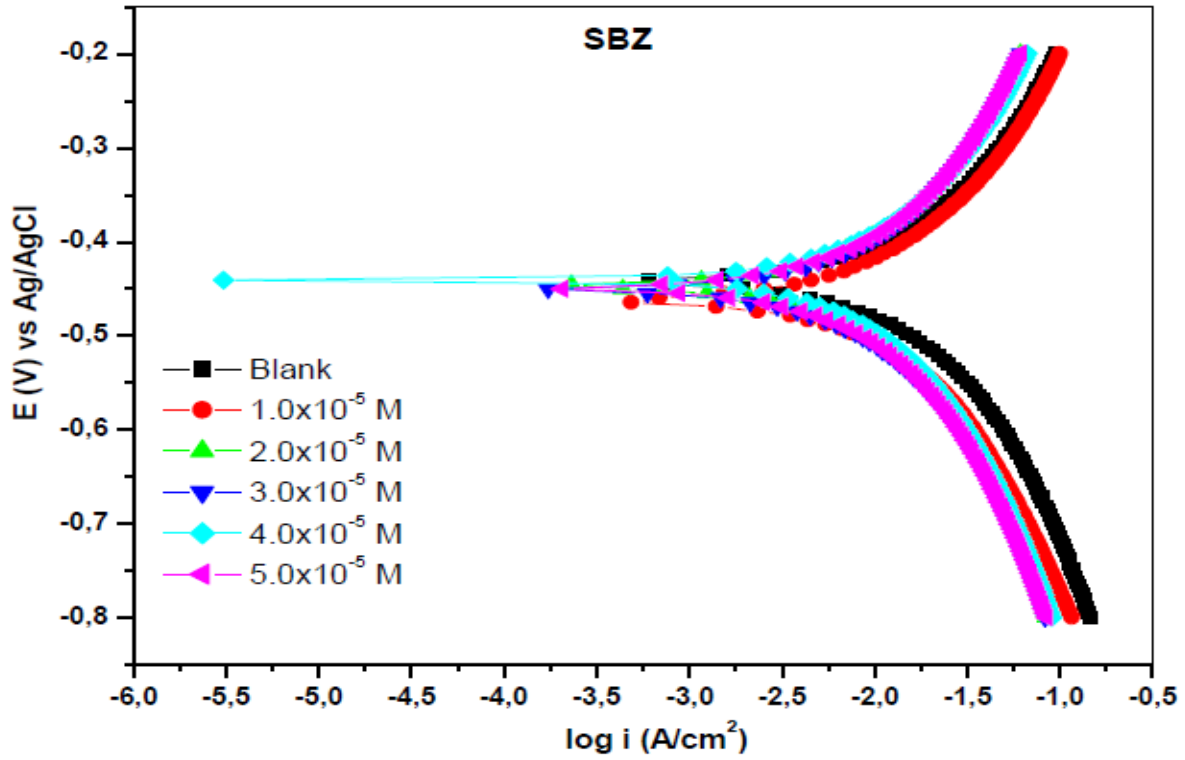

Figure 4.162: Tafel plots for zinc in 1 M HCl in the absence and presence of different concentrations of SBZ inhibitor compound.

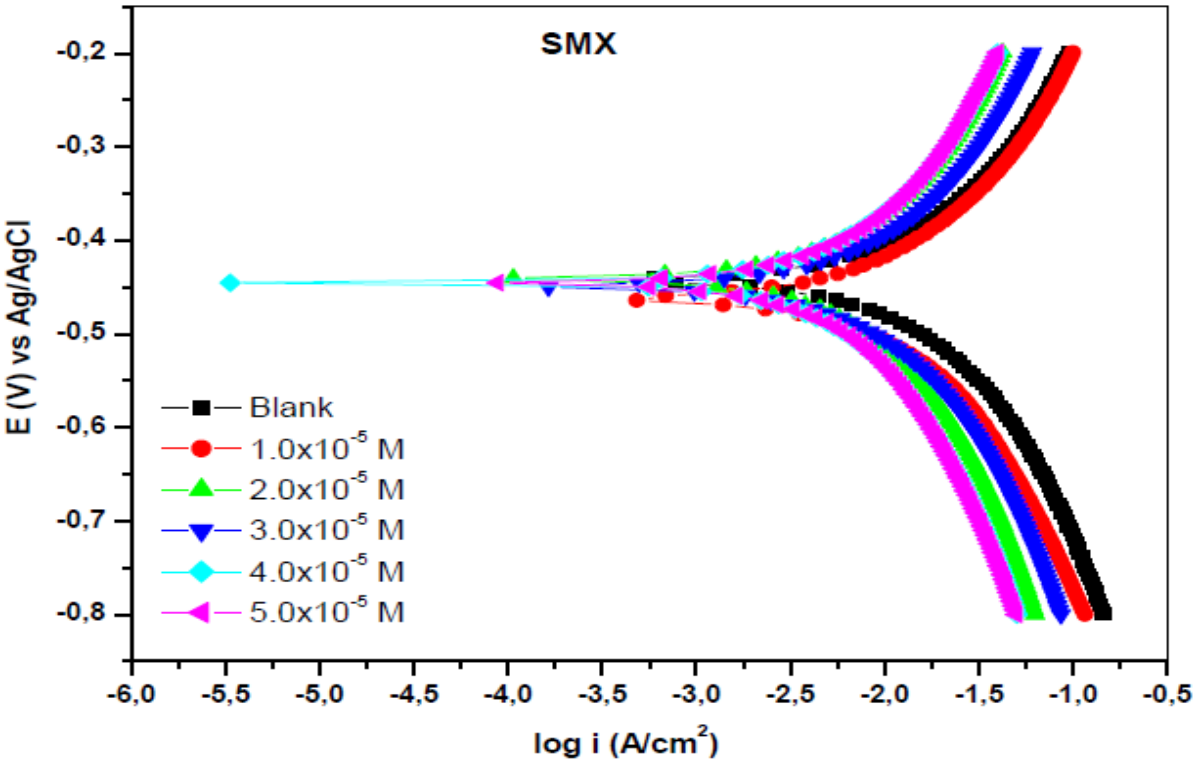

Figure 4.163: Tafel plots for zinc in 1 M HCl in the absence and presence of different concentrations of SMX inhibitor compound.

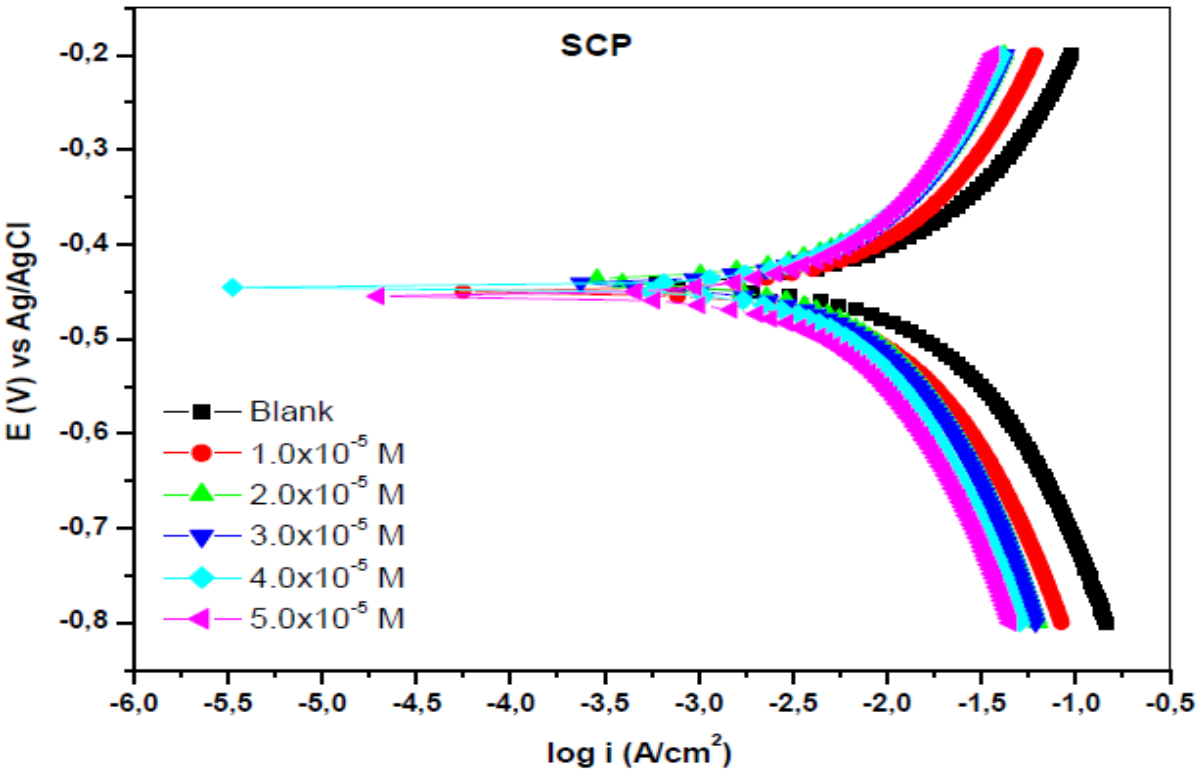

Figure 4.164: Tafel plots for zinc in 1 M HCl in the absence and presence of different concentrations of SCP inhibitor compound.

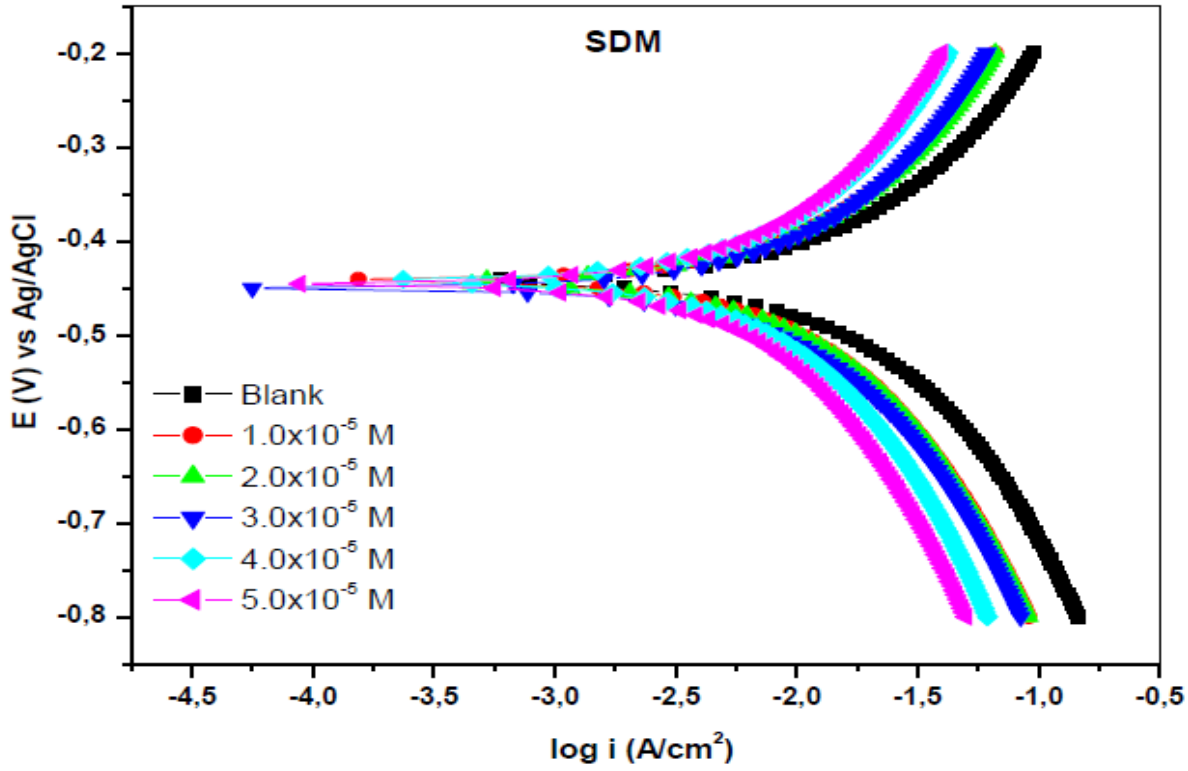

Figure 4.165: Tafel plots for zinc in 1 M HCl in the absence and presence of different concentrations of SDM inhibitor compound.

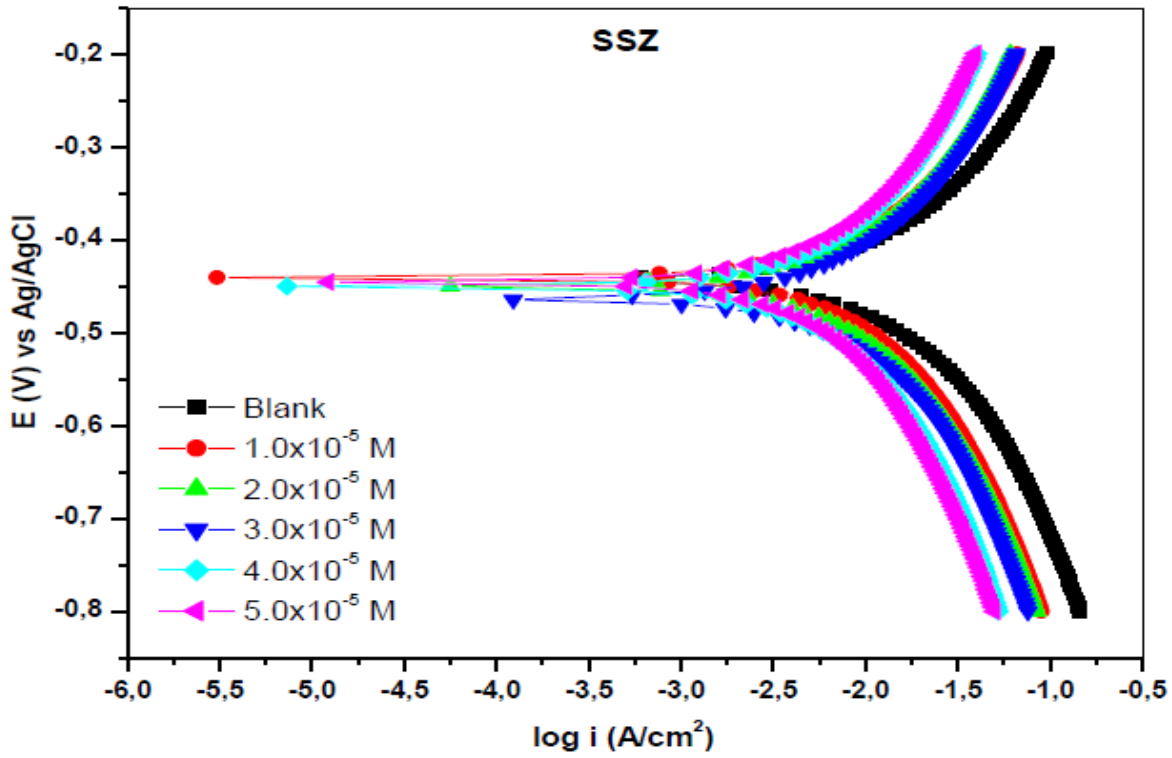

Figure 4.166: Tafel plots for zinc in 1 M HCl in the absence and presence of different concentrations of SSZ inhibitor compound.

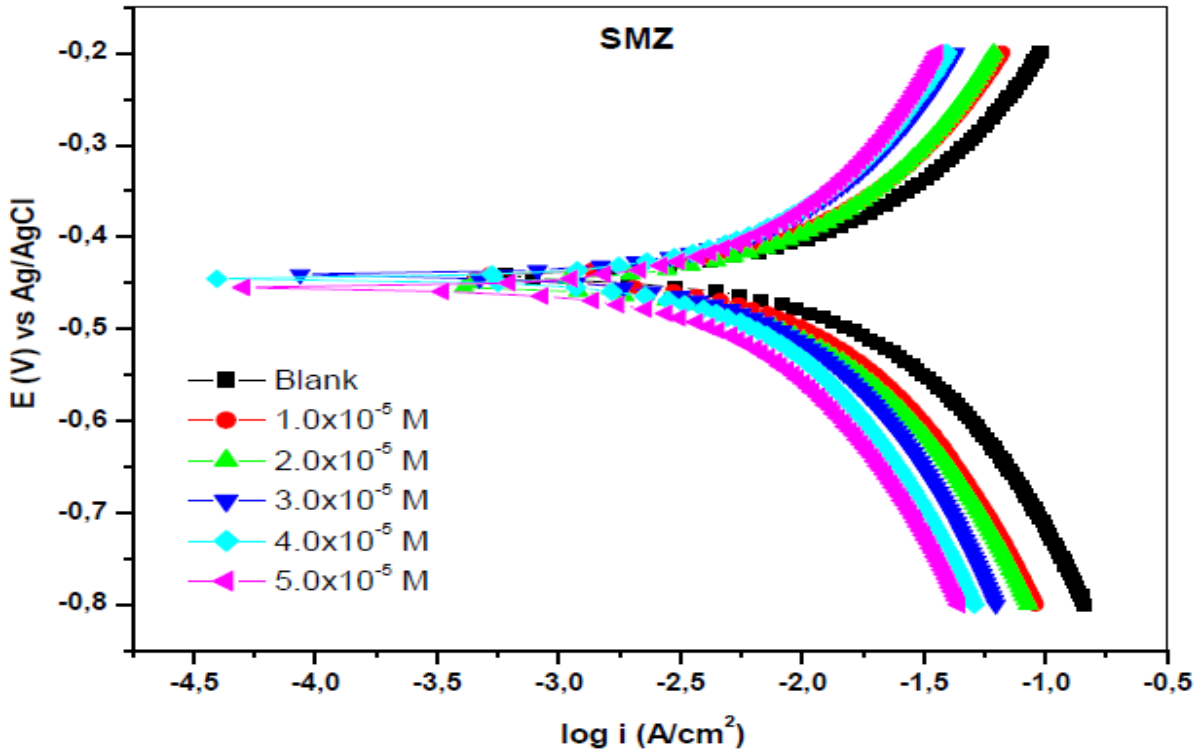

Figure 4.167: Tafel plots for zinc in 1 M HCl in the absence and presence of different concentrations of SMZ inhibitor compound.

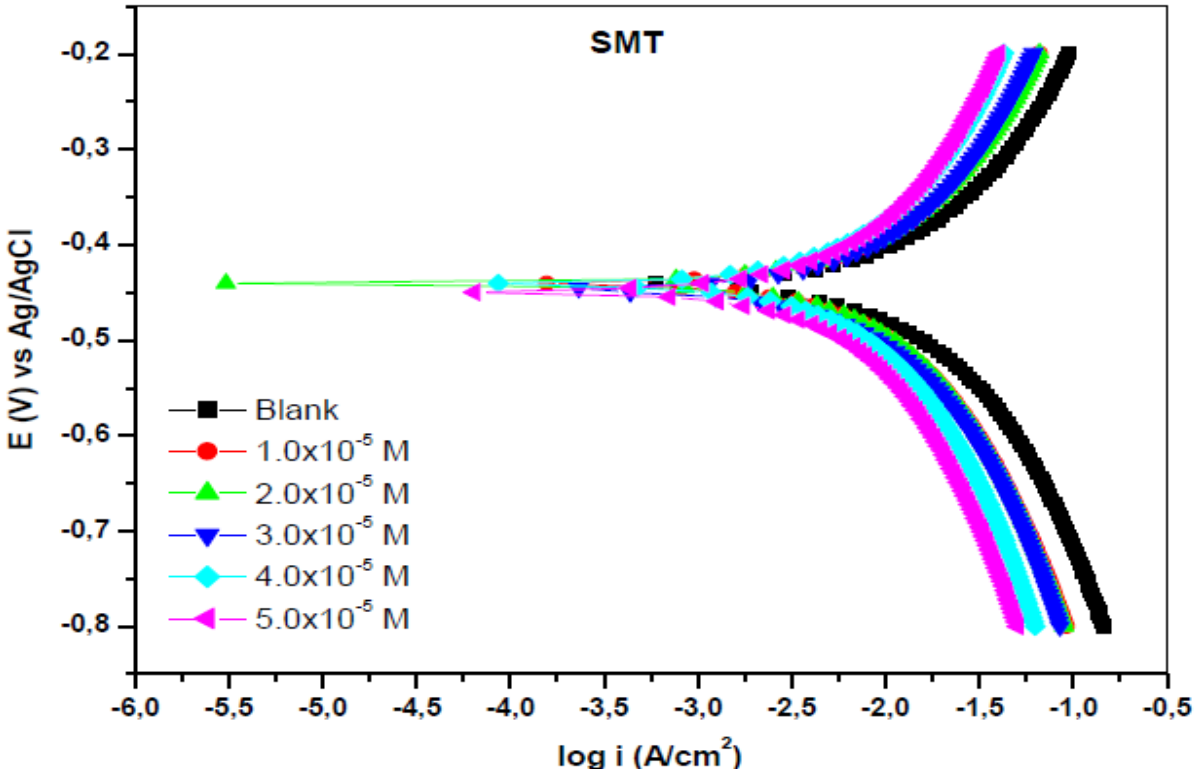

Figure 4.168: Tafel plots for zinc in 1 M HCl in the absence and presence of different concentrations of SMT inhibitor compound.

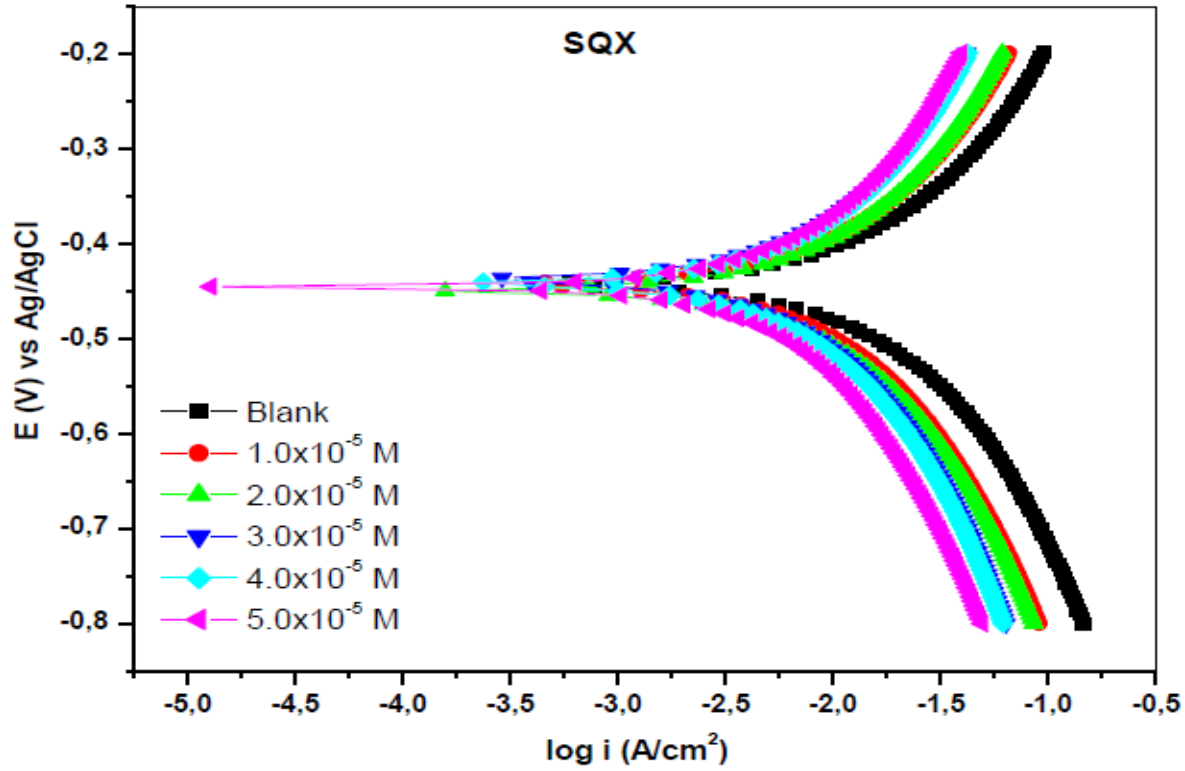

Figure 4.169: Tafel plots for zinc in 1 M HCl in the absence and presence of different concentrations of SQX inhibitor compound.

Table 4.14: Potentiodynamic polarization (PDP) parameters such as corrosion potential (E_{corr}), corrosion current density (i_{corr}) and anodic and cathodic Tafel slopes (b_a and b_c) using different inhibitors

Inhibitor	Inhibitor Conc. (M)	$-E_{corr}$(mV) with Ag/AgCl	i_{corr}(mA.cm^{-2})	R_p(10^{-1}) (Ohm)	b_a (mV.dec^{-1})	b_c (mV.dec^{-1})	%IE$_{PDP}$	%IE$_{WL}$
Blank		443	1.66	3.61	53	26	-	-
SNA	1.0×10^{-5}	463	0.38	5.90	36	19	77.10	74.81
	2.0×10^{-5}	446	0.39	9.16	33	15	76.50	76.40
	3.0×10^{-5}	451	0.35	6.85	28	09	78.92	79.41
	4.0×10^{-5}	439	0.36	5.09	15	02	78.31	79.83
	5.0×10^{-5}	450	0.36	9.04	09	25	78.31	80.67
SBZ	1.0×10^{-5}	463	0.40	9.42	29	16	75.90	66.61
	2.0×10^{-5}	445	0.38	6.06	26	11	77.10	74.23
	3.0×10^{-5}	449	0.36	8.75	12	08	78.31	75.82
	4.0×10^{-5}	450	0.33	9.28	09	07	80.12	78.99
	5.0×10^{-5}	438	0.28	5.71	03	03	83.13	81.58
SMX	1.0×10^{-5}	441	0.37	9.83	33	17	77.71	70.88
	2.0×10^{-5}	448	0.37	3.94	26	14	77.71	73.56
	3.0×10^{-5}	446	0.32	12.3	26	08	80.72	75.82
	4.0×10^{-5}	447	0.29	9.41	11	06	82.53	78.66
	5.0×10^{-5}	463	0.26	9.29	09	01	84.33	81.51
SCP	1.0×10^{-5}	449	0.69	5.25	36	20	58.43	70.71
	2.0×10^{-5}	449	0.66	8.75	35	21	60.24	72.30
	3.0×10^{-5}	438	0.50	15.3	23	17	69.87	74.73
	4.0×10^{-5}	442	0.45	14.8	11	11	72.89	75.82
	5.0×10^{-5}	455	0.40	5.40	08	05	75.90	77.32
SDM	1.0×10^{-5}	447	0.68	8.08	35	19	59.04	63.68
	2.0×10^{-5}	449	0.69	8.25	26	17	58.43	64.68
	3.0×10^{-5}	441	0.55	13.0	21	12	66.86	65.69
	4.0×10^{-5}	442	0.48	15.5	08	09	71.08	67.45
	5.0×10^{-5}	446	0.42	10.4	04	06	74.69	70.46
SSZ	1.0×10^{-5}	439	0.43	4.15	38	24	74.09	64.28
	2.0×10^{-5}	449	0.39	8.70	31	21	76.50	67.03
	3.0×10^{-5}	463	0.34	4.39	23	19	79.51	71.21
	4.0×10^{-5}	450	0.35	4.12	14	15	78.92	74.48
	5.0×10^{-5}	445	0.29	8.43	06	07	82.53	77.49
SMZ	1.0×10^{-5}	441	0.67	10.4	35	21	59.63	50.79
	2.0×10^{-5}	443	0.67	10.4	35	14	59.63	54.47
	3.0×10^{-5}	446	0.61	9.12	25	11	63.25	57.57
	4.0×10^{-5}	455	0.55	9.24	13	10	66.86	61.84
	5.0×10^{-5}	453	0.51	12.0	07	03	69.27	67.36
SMT	1.0×10^{-5}	446	0.66	7.59	36	23	60.24	61.84
	2.0×10^{-5}	439	0.45	7.90	29	20	72.89	65.52
	3.0×10^{-5}	441	0.42	1.66	23	14	74.69	69.96
	4.0×10^{-5}	456	0.30	9.15	19	11	81.93	73.05
	5.0×10^{-5}	436	0.29	4.88	08	10	82.53	76.65
SQX	1.0×10^{-5}	451	0.58	6.43	37	24	65.06	60.75
	2.0×10^{-5}	445	0.51	11.0	35	18	69.27	64.35
	3.0×10^{-5}	442	0.48	10.7	25	10	71.08	66.53
	4.0×10^{-5}	443	0.44	7.60	19	08	73.49	68.03
	5.0×10^{-5}	438	0.32	8.16	08	03	80.72	70.46

The E_{corr} values in the presence of all the nine sulphonamides do not exhibit a significant change in trend. Literature studies show that values of this trend confirm a mixed type mechanism by the inhibitors [155, 156].

Valuable information can be derived from Tafel polarization plots including the different electrochemical parameter such as percentage inhibition efficiency of the inhibitors,

corrosion potential (E_{corr}), corrosion current density (i_{corr}) and anodic and cathodic Tafel slopes (b_a and b_c). These parameters are documented in Table 4.14.

The results presented in this table show that the both values of b_a and b_c exhibit some discrepancies in the presence of all the sulphonamides utilized. This trend within the values of anodic and cathodic Tafel slopes (b_a and b_c) confirms that both the anodic and cathodic reactions are affected by the inhibitors even though the effect on the cathodic reactions is more rigorous than the effect on the anodic reactions. All the nine sulphonamides utilized are therefore mixed type inhibitors. Just as in the case of the gravimetric measurements, the inhibition efficiencies are increased with the increase in the concentration of the nine sulphonamides. This trend may be due to the adsorption of sulphonamides on zinc surface.

4.3.2 ELECTROCHEMICAL IMPEDANCE SPECTROSCOPY (EIS)

Electrochemical impedance spectroscopy was employed to study the corrosion behaviour of zinc in 1M HCl in the absence and presence of SNA, SBZ, SMX, SCP, SDM, SSZ, SMZ, SMT and SQX inhibitors after a total immersion time of 30 minutes at 30 ° C. The Nyquist plots and their respective Bode plots of zinc in uninhibited and inhibited acid solutions containing various concentrations of studied sulphonamides are presented in Figures 4.170 – 4.187.

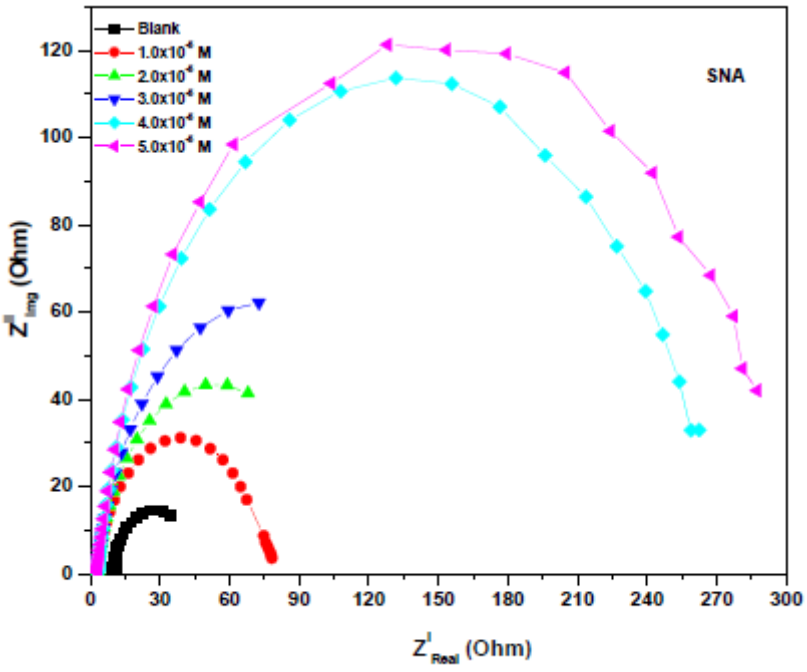

Figure 4.170: Nyquist plot of zinc in 1 M HCl in the absence and presence of different concentrations of SNA inhibitor compound.

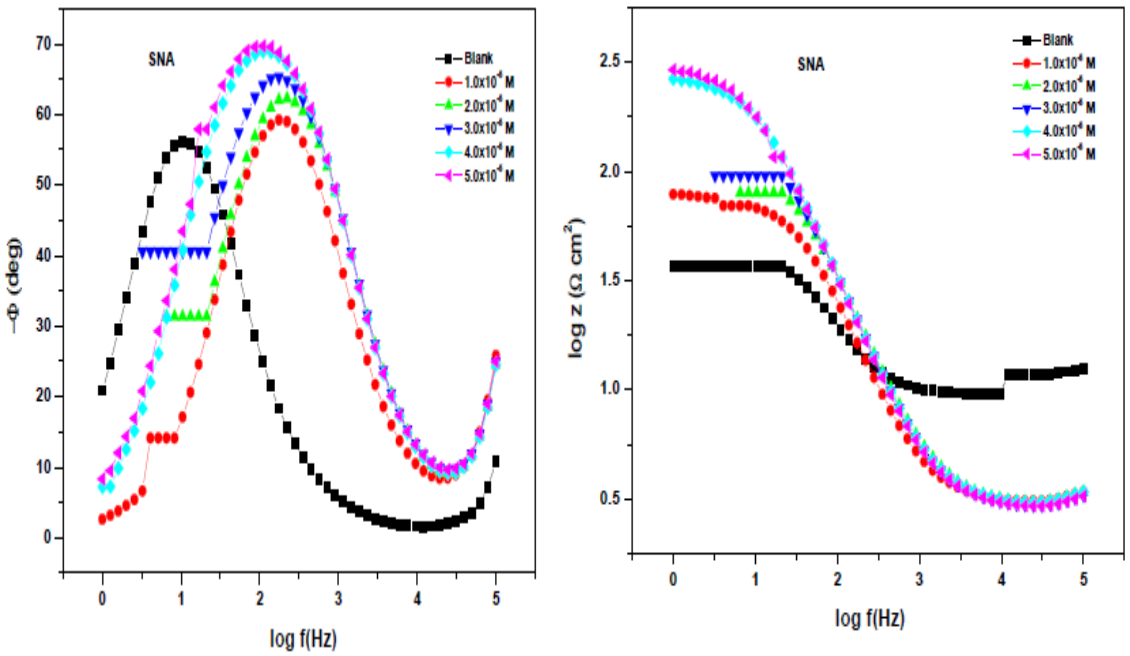

Figure 4.171: Bode plots of zinc in 1 M HCl in the absence and presence of different concentrations of SNA inhibitor compound.

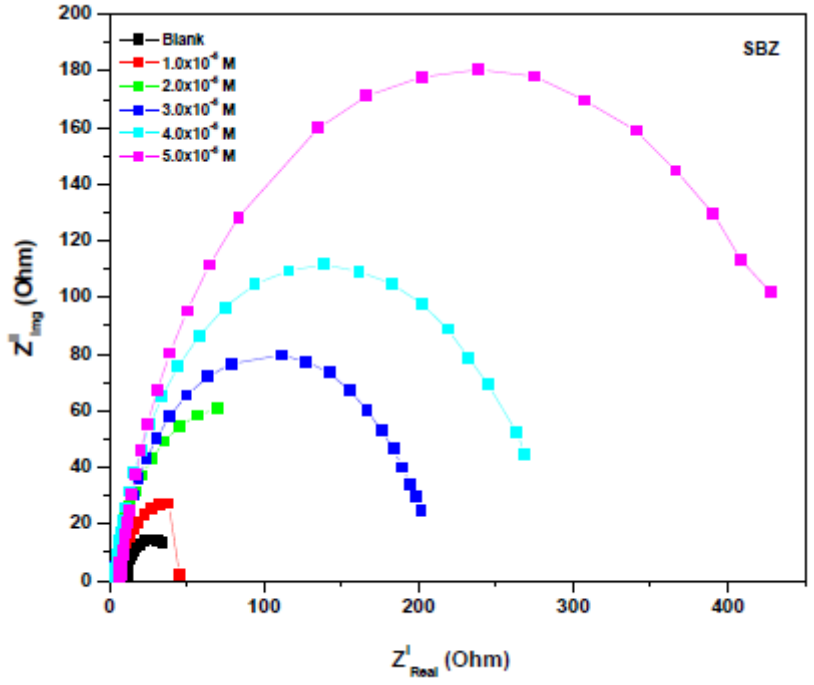

Figure 4.172: Nyquist plot of zinc in 1 M HCl in the absence and presence of different concentrations of SBZ inhibitor compound.

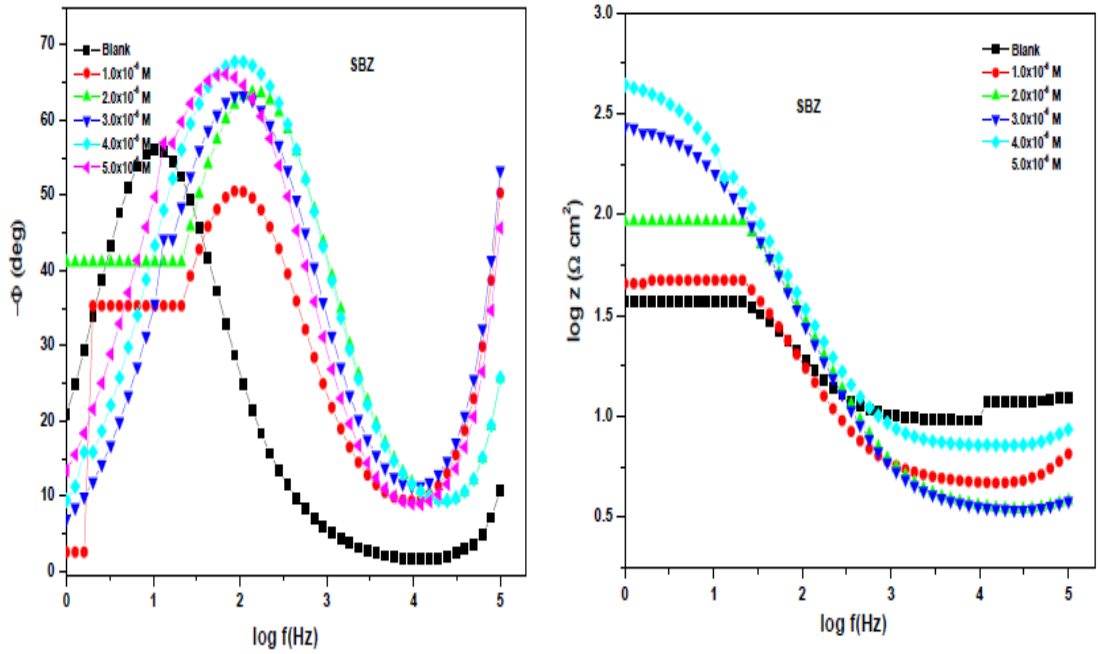

Figure 4.173: Bode plots of zinc in 1 M HCl in the absence and presence of different concentrations of SBZ inhibitor compound.

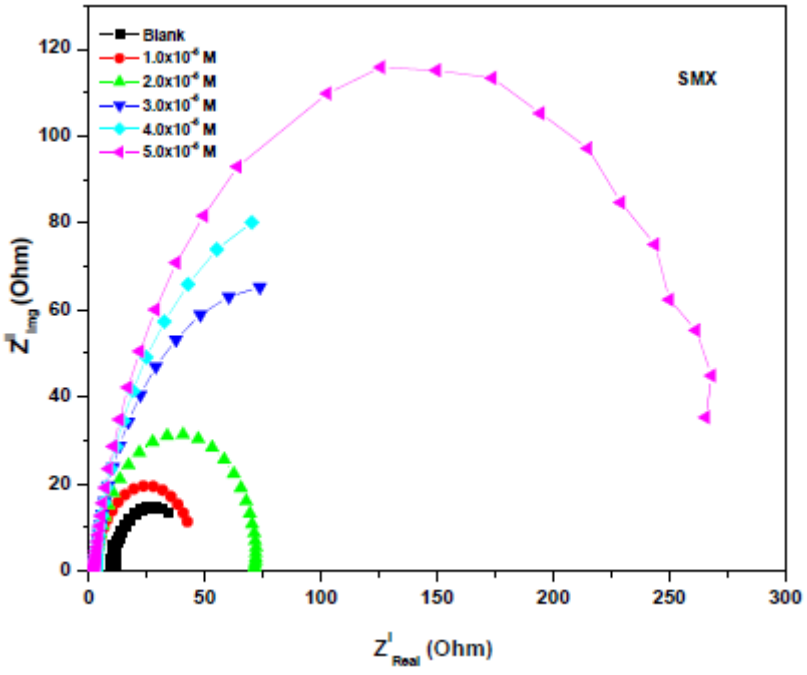

Figure 4.174: Nyquist plot of zinc in 1 M HCl in the absence and presence of different concentrations of SMX inhibitor compound.

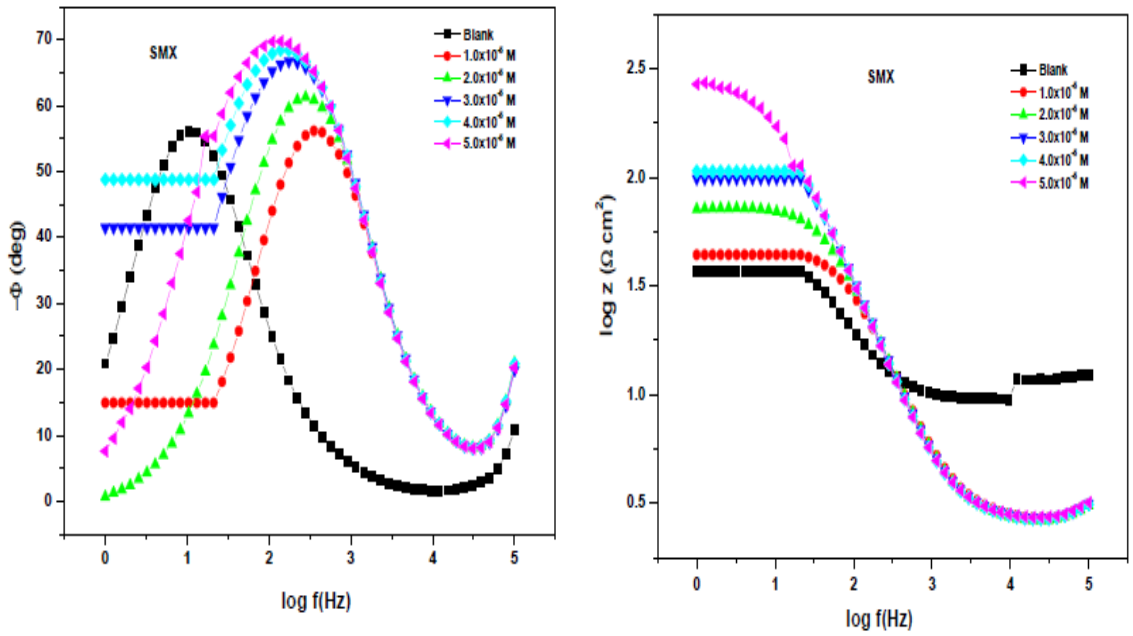

Figure 4.175: Bode plots of zinc in 1 M HCl in the absence and presence of different concentrations of SMX inhibitor compound.

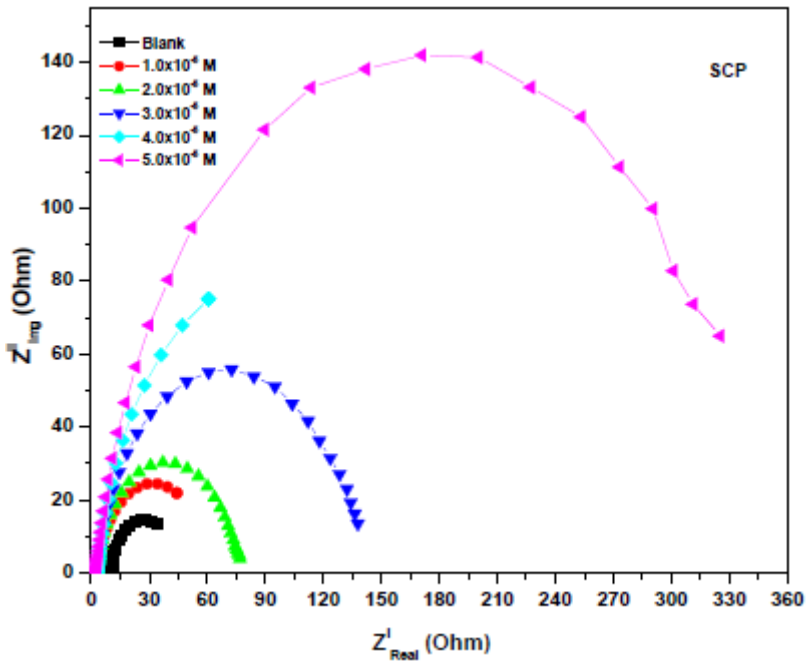

Figure 4.176: Nyquist plot of zinc in 1 M HCl in the absence and presence of different concentrations of SCP inhibitor compound.

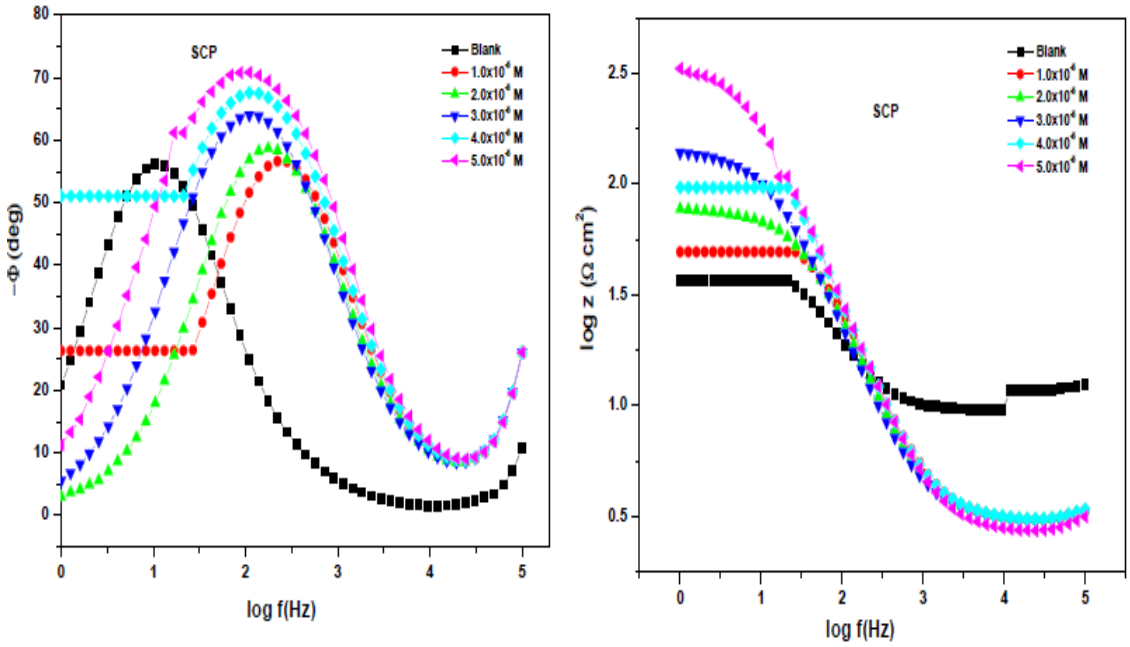

Figure 4.177: Bode plots of zinc in 1 M HCl in the absence and presence of different concentrations of SCP inhibitor compound.

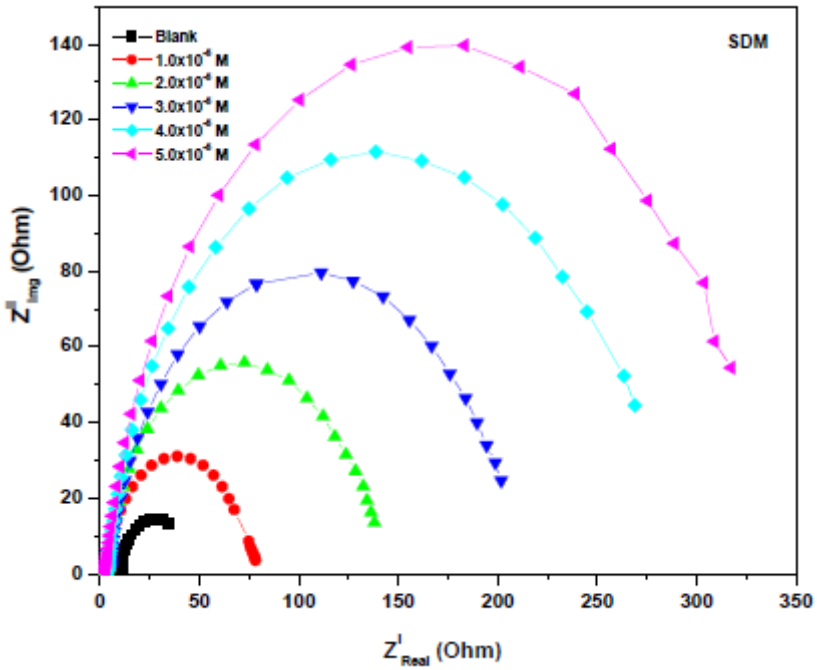

Figure 4.178: Nyquist plot of zinc in 1 M HCl in the absence and presence of different concentrations of SDM inhibitor compound.

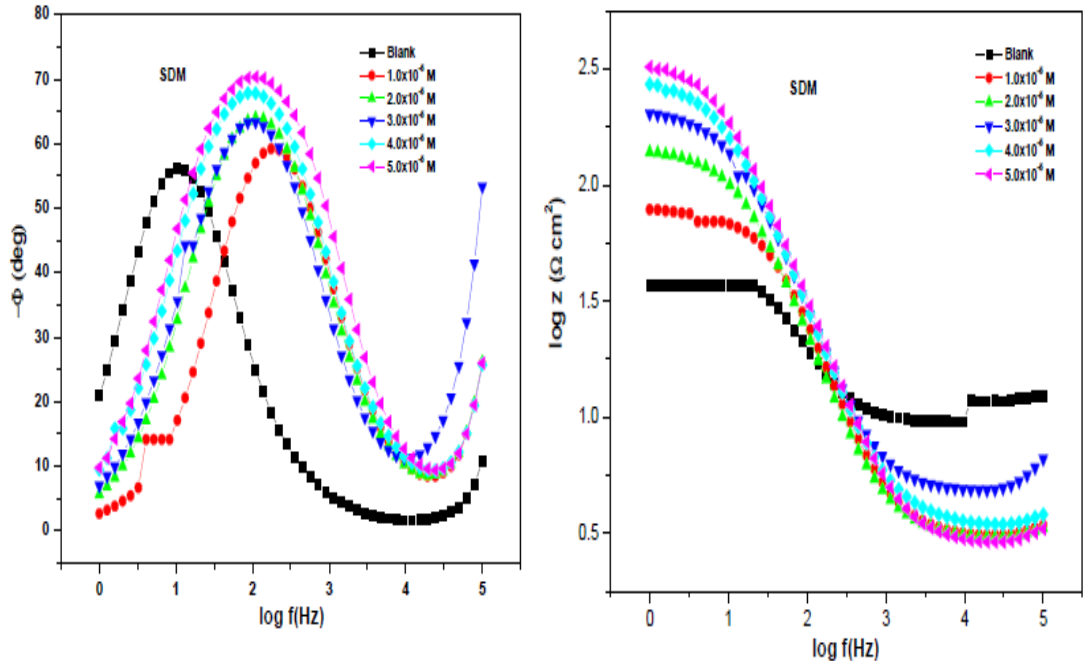

Figure 4.179: Bode plots of zinc in 1 M HCl in the absence and presence of different concentrations of SDM inhibitor compound.

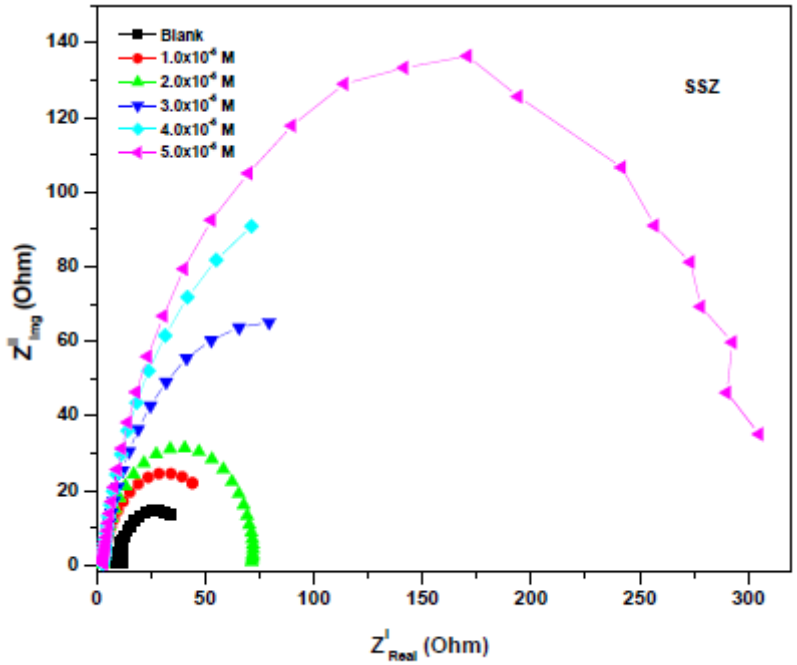

Figure 4.180: Nyquist plot of zinc in 1 M HCl in the absence and presence of different concentrations of SSZ inhibitor compound.

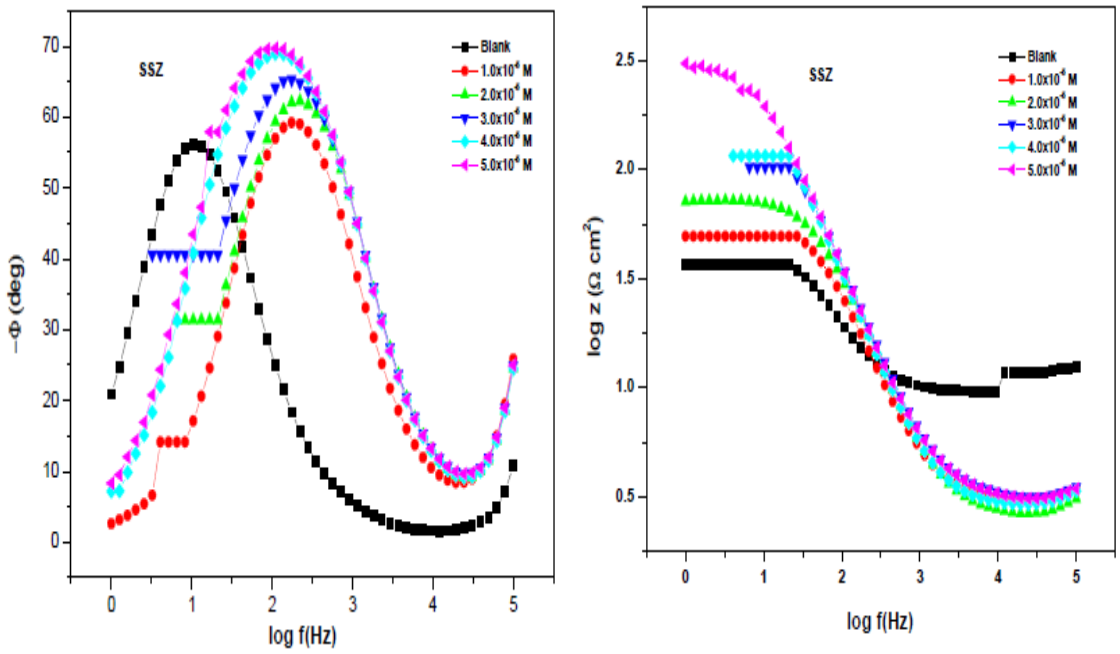

Figure 4.181: Bode plots of zinc in 1 M HCl in the absence and presence of different concentrations of SSZ inhibitor compound.

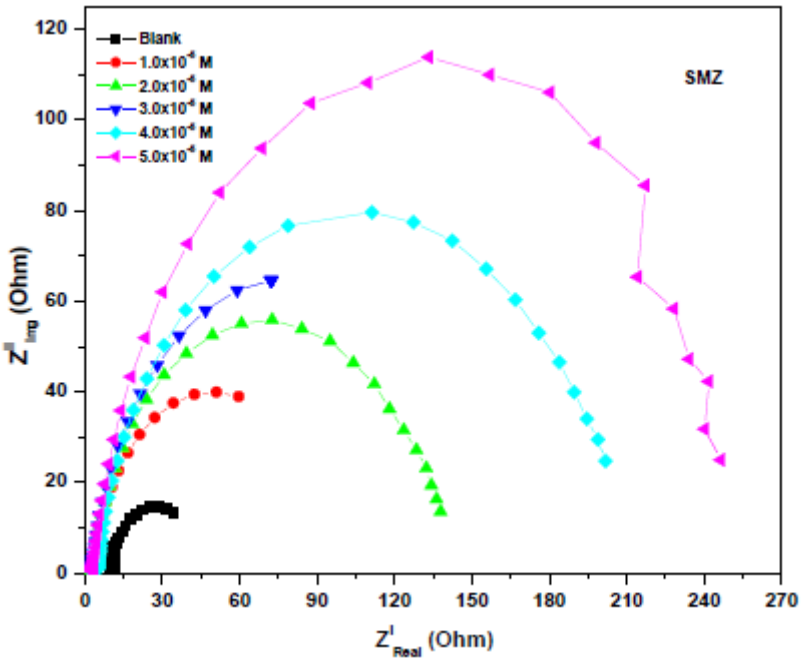

Figure 4.182: Nyquist plot of zinc in 1 M HCl in the absence and presence of different concentrations of SMZ inhibitor compound.

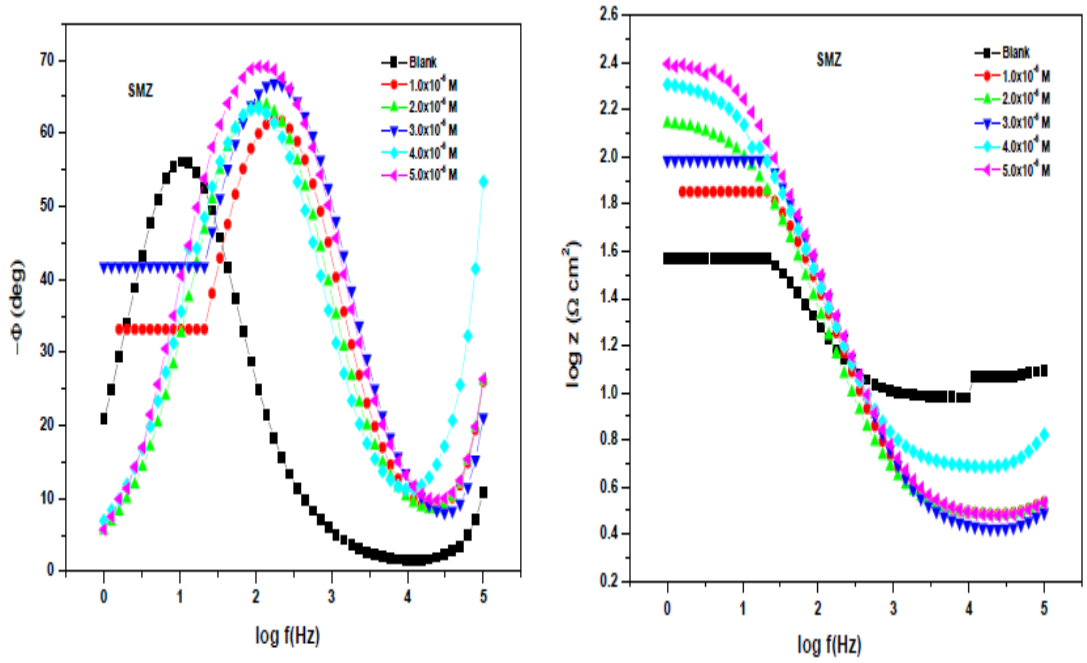

Figure 4.183: Bode plots of zinc in 1 M HCl in the absence and presence of different concentrations of SMZ inhibitor compound.

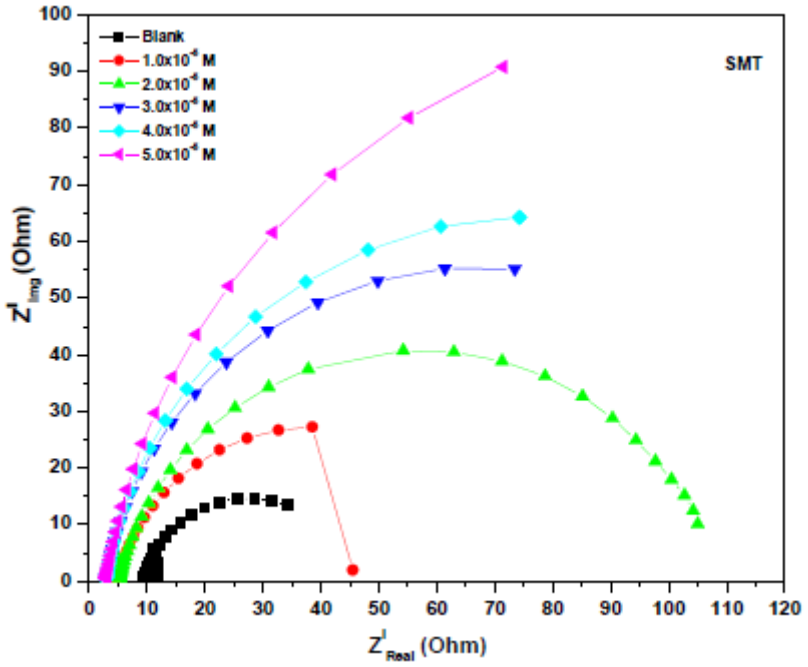

Figure 4.184: Nyquist plot of zinc in 1 M HCl in the absence and presence of different concentrations of SMT inhibitor compound.

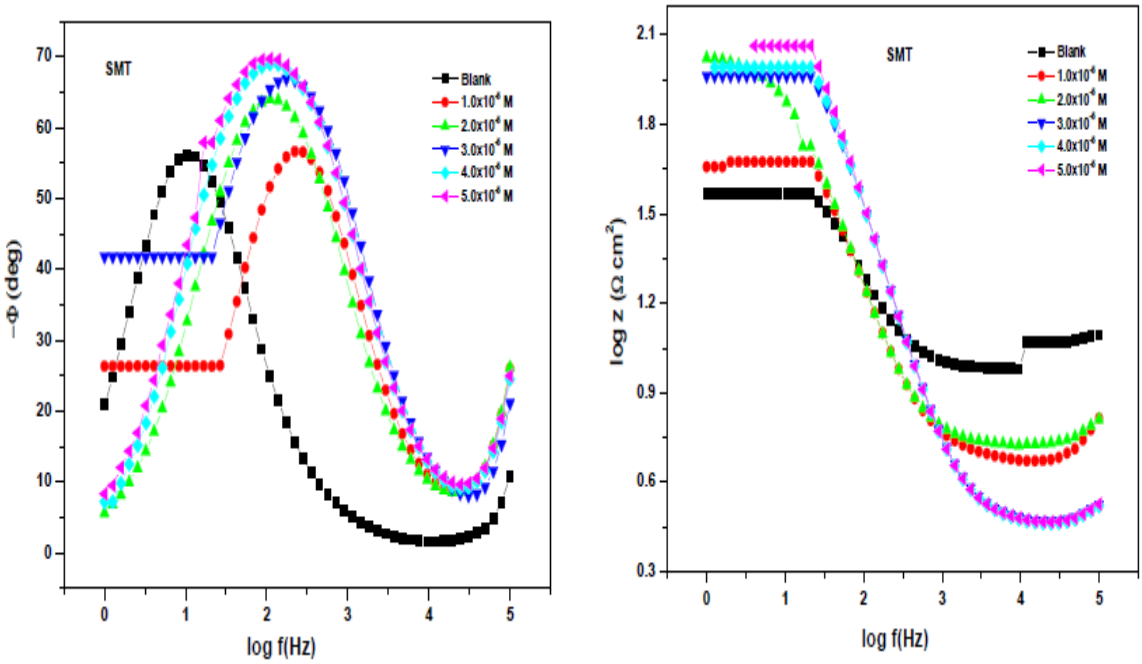

Figure 4.185: Bode plots of zinc in 1 M HCl in the absence and presence of different concentrations of SMT inhibitor compound.

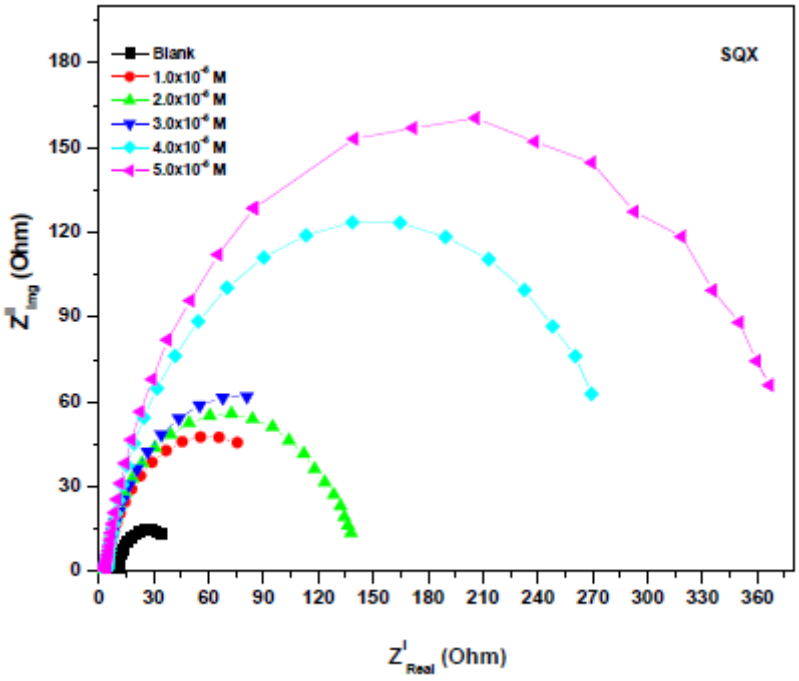

Figure 4.186: Nyquist plot of zinc in 1 M HCl in the absence and presence of different concentrations of SQX inhibitor compound.

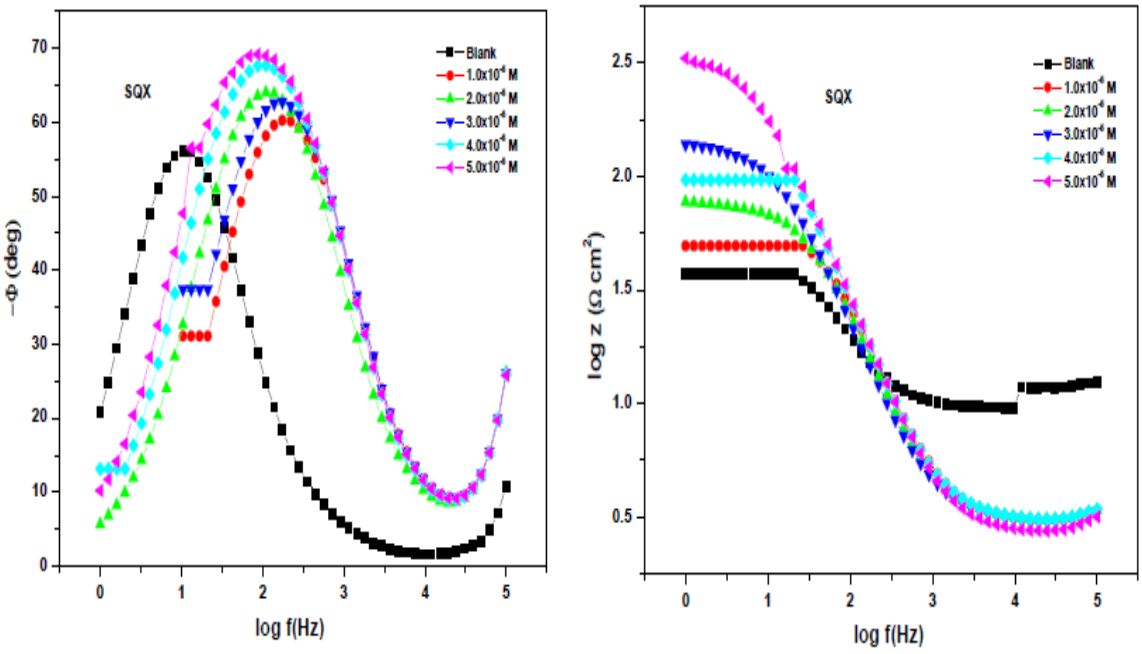

Figure 4.187: Bode plots of zinc in 1 M HCl in the absence and presence of different concentrations of SQX inhibitor compound.

The frequency dispersion which results from the roughness and other inhomogenities of the electrode surface often result in the Nyquist impedance diagrams to exhibit imperfect semicircles. The figures show that each impedance diagram is made up of a large capacitive loop with low frequencies dispersion (inductive arc). Normally the anodic adsorbed intermediates that control the anodic reactions are the main factor behind the inductive arc [157, 158]. Table 4.15 shows the electrochemical impedance data obtained. The presence of low frequency inductive loop may be attributed to the relaxation process obtained by adsorption species like Cl^-_{ads} and H^+_{ads} on the electrode surface [159, 160]. It may also be attributed to the re-dissolution of the passivated surface at low frequencies [161].

Table 4.15 shows that the impedance of the inhibited system amplified with increasing the inhibitor concentration and the CPE values decreased with increasing inhibitor concentration. This decrease in CPE results from a decrease in local dielectric constant and/or an increase in the thickness of the double layer, suggesting that the inhibitor molecules inhibit the mild steel corrosion by adsorption at the metal/acid interface [162]. The depression in Nyquist semicircles is a feature for solid electrodes and often referred to as frequency dispersion and attributed to the roughness and other inhomogenities of the solid electrode [163,164].

Table 4.15: Electrochemical impedance (EIS) parameters such as the resistance of charge transfer (R_{ct}), constant phase element (CPE) and the CPE exponent (n) using different inhibitors.

Inhibitor	Inhibitor Conc. (M)	R_s (Ω cm^2)	R_{ct} (Ω cm^2)	n	CPE (μF cm^{-2})	%IE_{EIS}	%IE_{WL}
Blank		9.00	25.5	0.74	59.00	-	-
SNA	1.0×10^{-5}	5.50	46.9	0.87	237.0	45.62	74.81
	2.0×10^{-5}	5.62	87.4	0.97	647.1	70.82	76.40
	3.0×10^{-5}	5.81	194.7	0.90	1021	86.90	79.41
	4.0×10^{-5}	5.92	251.1	0.95	775.3	89.84	79.83
	5.0×10^{-5}	5.96	485.0	0.89	1319	94.74	80.67
SBZ	1.0×10^{-5}	5.96	67.10	1.00	6101	61.99	66.61
	2.0×10^{-5}	5.62	80.80	1.00	4294	68.44	74.23
	3.0×10^{-5}	5.98	97.00	1.00	4703	73.71	75.82
	4.0×10^{-5}	6.10	243.4	0.97	5605	89.52	78.99
	5.0×10^{-5}	6.32	266.8	0.98	5990	90.44	81.58
SMX	1.0×10^{-5}	5.12	59.10	1.00	4282	56.85	70.88
	2.0×10^{-5}	5.63	65.90	1.00	4300	61.30	73.56
	3.0×10^{-5}	5.63	91.42	1.00	4715	72.10	75.82
	4.0×10^{-5}	6.14	93.66	1.00	4304	72.77	78.66
	5.0×10^{-5}	6.66	246.7	0.98	5561	89.66	81.51
SCP	1.0×10^{-5}	5.50	44.40	1.00	5569	42.56	70.71
	2.0×10^{-5}	5.96	63.25	1.00	4979	59.68	72.30
	3.0×10^{-5}	6.32	86.32	1.00	6048	70.45	74.73
	4.0×10^{-5}	6.25	121.7	0.99	7533	79.04	75.82
	5.0×10^{-5}	6.99	300.2	0.98	6379	91.50	77.32
SDM	1.0×10^{-5}	5.44	67.10	1.00	6093	61.99	63.68
	2.0×10^{-5}	6.32	121.7	0.99	7553	79.04	64.68
	3.0×10^{-5}	6.95	194.7	0.90	1051	86.90	65.69
	4.0×10^{-5}	7.10	251.1	0.95	7550	89.84	67.45
	5.0×10^{-5}	8.23	296.5	0.99	5778	91.39	70.46
SSZ	1.0×10^{-5}	4.88	44.60	1.00	5723	42.82	64.28
	2.0×10^{-5}	5.26	65.95	1.00	4300	61.33	67.03
	3.0×10^{-5}	5.66	115.0	0.98	4772	77.82	71.21
	4.0×10^{-5}	6.15	129.8	0.99	5218	80.35	74.48
	5.0×10^{-5}	6.89	285.5	0.96	5664	91.06	77.49
SMZ	1.0×10^{-5}	5.56	62.80	1.00	4048	59.39	50.79
	2.0×10^{-5}	5.68	90.70	0.99	7653	71.88	54.47
	3.0×10^{-5}	6.32	121.7	1.00	4890	79.04	57.57
	4.0×10^{-5}	6.99	194.7	0.90	1051	86.90	61.84
	5.0×10^{-5}	7.56	233.4	0.98	5268	89.07	67.36
SMT	1.0×10^{-5}	5.55	46.90	0.87	2372	45.62	61.84
	2.0×10^{-5}	5.66	86.10	1.00	4105	70.38	65.52
	3.0×10^{-5}	5.96	92.90	1.00	4770	72.55	69.96
	4.0×10^{-5}	6.99	101.8	0.87	2388	74.95	73.05
	5.0×10^{-5}	7.56	129.8	0.99	5218	80.35	76.65
SQX	1.0×10^{-5}	5.55	99.21	0.95	5550	74.29	60.75
	2.0×10^{-5}	5.69	121.7	0.99	7554	79.04	64.35
	3.0×10^{-5}	5.65	125.9	0.95	5845	79.74	66.53
	4.0×10^{-5}	5.78	278.0	0.93	6988	90.82	68.03
	5.0×10^{-5}	6.99	364.5	0.92	7295	93.00	70.46

It is observed that the values of double-layer capacitance, CPE, decreased with increasing sulphonamide concentration. This behaviour is possibly due to a decrease in local dielectric constant and/or an increase in the thickness of a protective layer at electrode surface, enhancing therefore the corrosion resistance of the studied steel.

The inhibition efficiency ($\%E_{EIS}$) was calculated from the data obtained from the electrochemical impedance according to equation 42.

4.3.3 FOURIER TRANSFORM INFRARED SPECTROMETER (FTIR)

The FT-IR technique is useful in studying the adsorption film resulting during the adsorption process [111]. The FT-IR spectra of the studied corrosion inhibitors as well as the adsorption films formed on the mild steel surface using different corrosion inhibitors are shown in Figures 4.188 − 4.196.

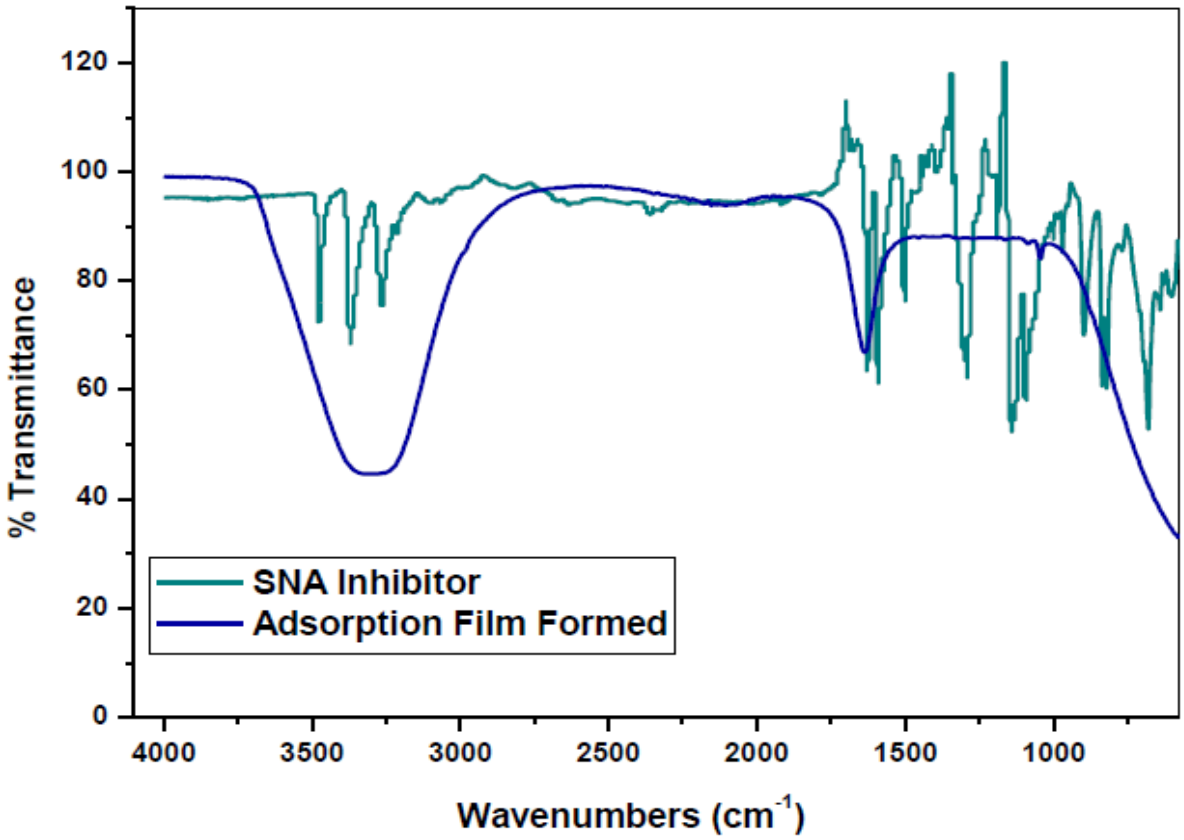

Figure 4.188: FT-IR spectra for the studied corrosion inhibitors and adsorption films formed on zinc in 1.0 M HCl using SNA corrosion inhibitor.

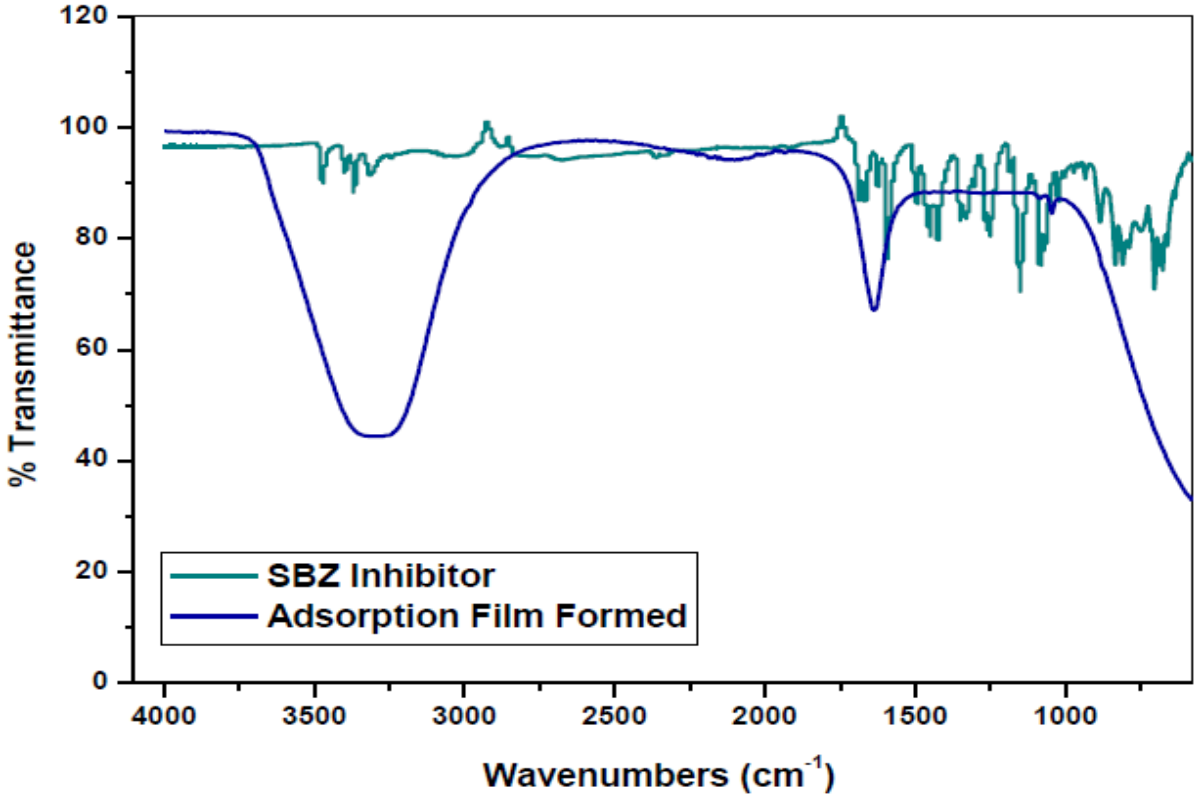

Figure 4.189: FT-IR spectra for the studied corrosion inhibitors and adsorption films formed on zinc in 1.0 M HCl using SBZ corrosion inhibitor.

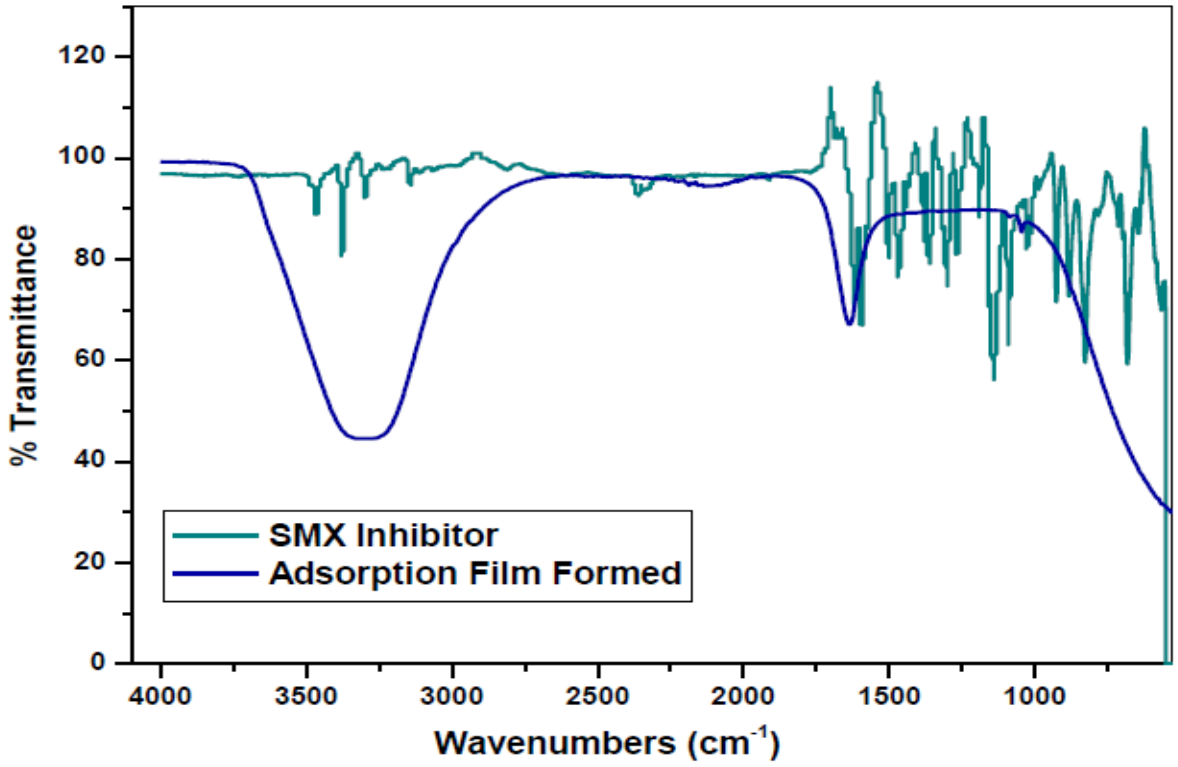

Figure 4.190: FT-IR spectra for the studied corrosion inhibitors and adsorption films formed on zinc in 1.0 M HCl using SMX corrosion inhibitor.

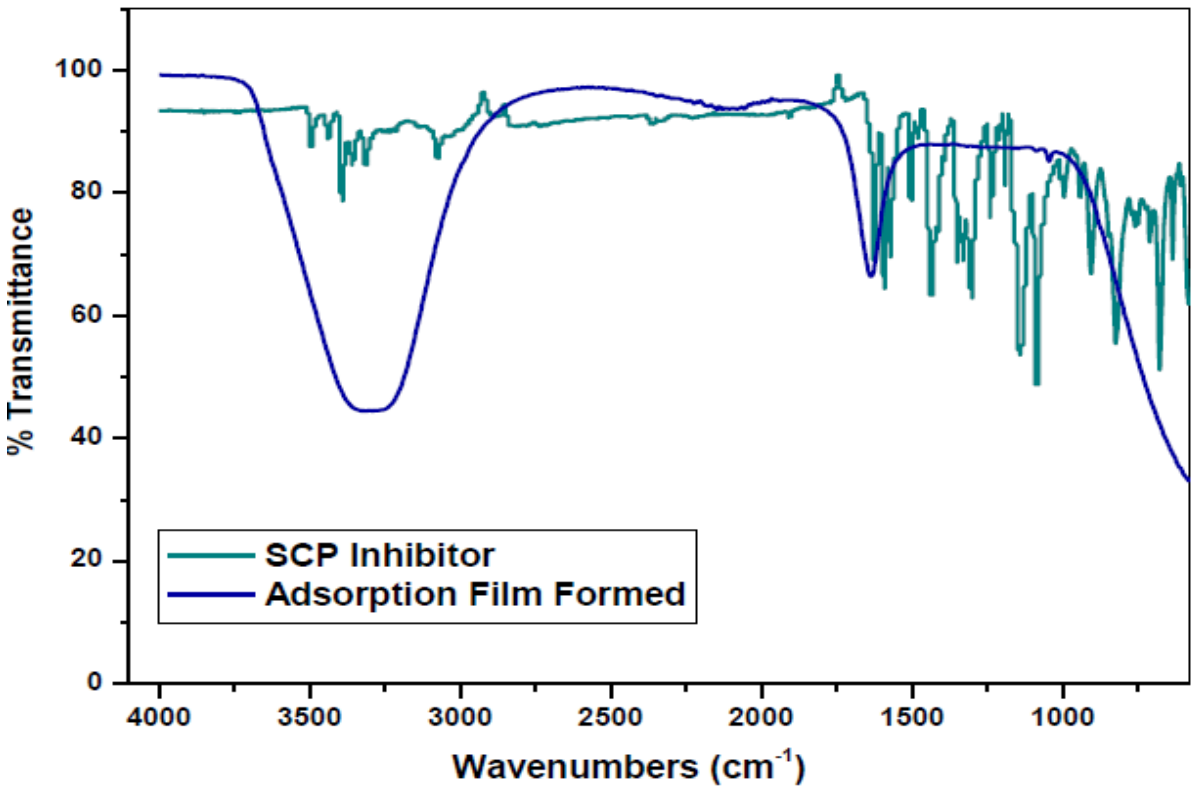

Figure 4.191: FT-IR spectra for the studied corrosion inhibitors and adsorption films formed on zinc in 1.0 M HCl using SCP corrosion inhibitor.

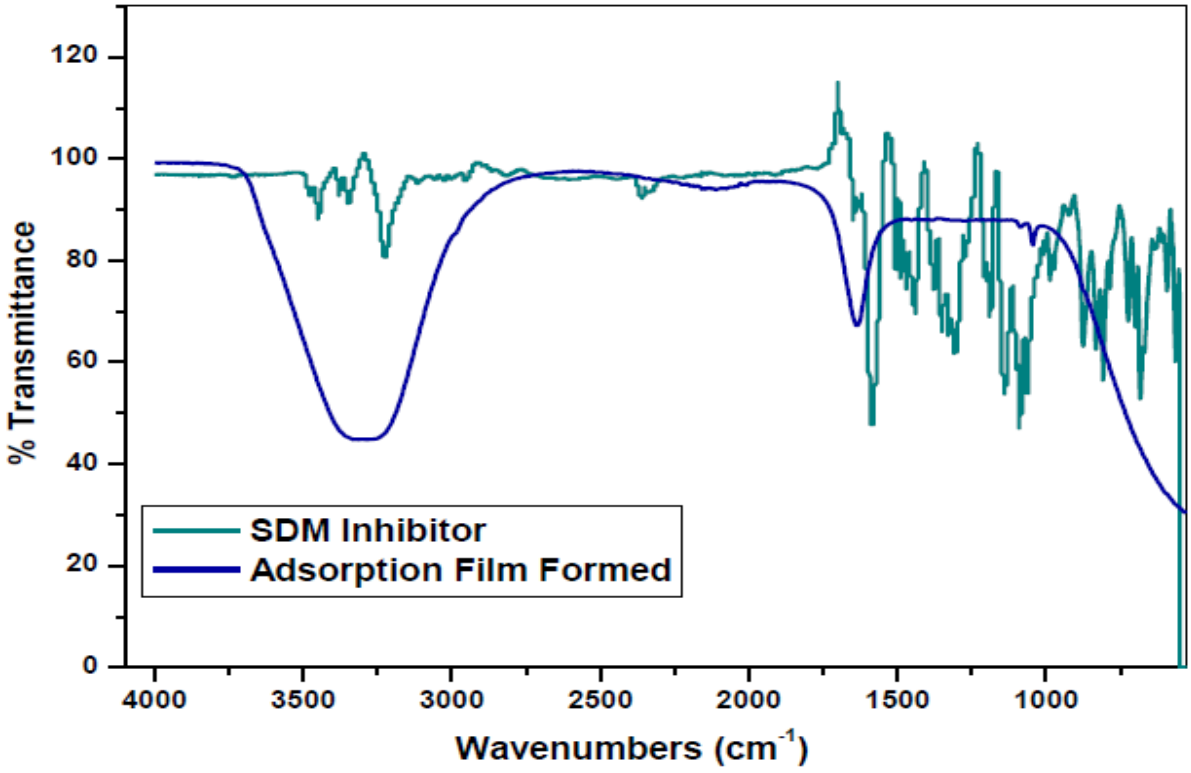

Figure 4.192: FT-IR spectra for the studied corrosion inhibitors and adsorption films formed on zinc in 1.0 M HCl using SDM corrosion inhibitor.

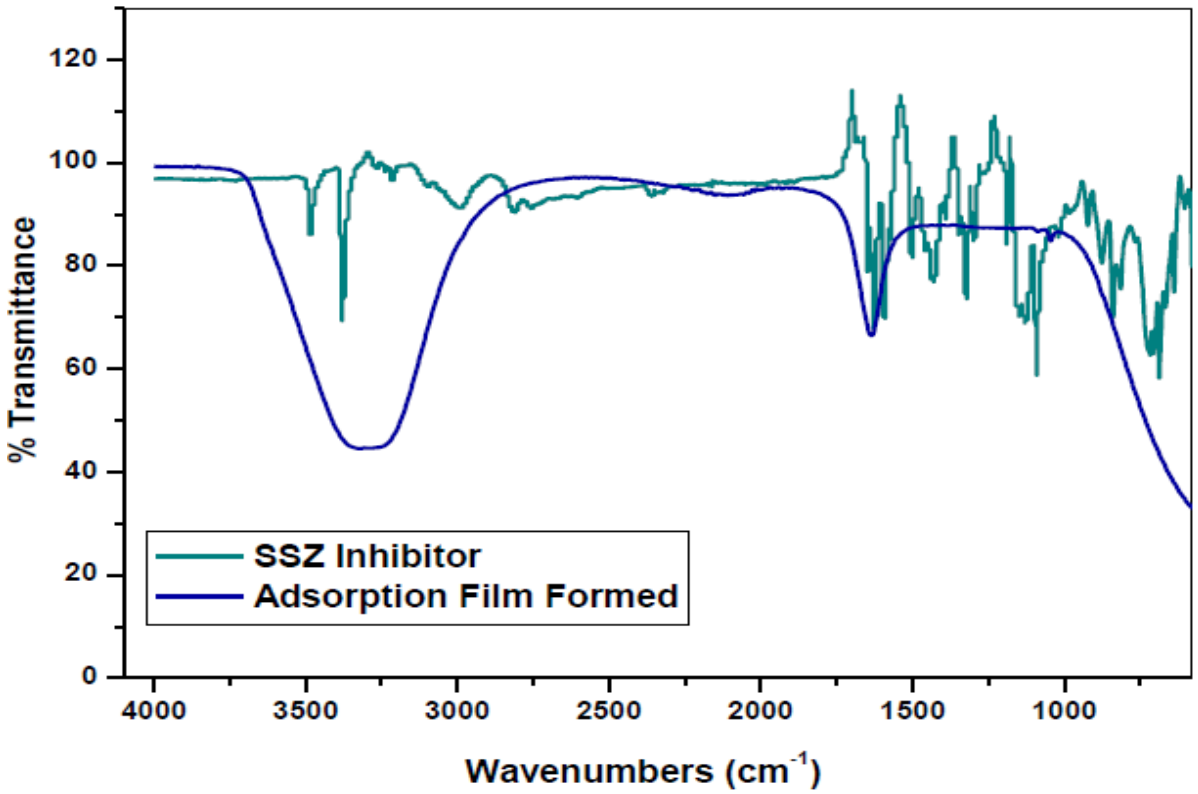

Figure 4.193: FT-IR spectra for the studied corrosion inhibitors and adsorption films formed on zinc in 1.0 M HCl using SSZ corrosion inhibitor.

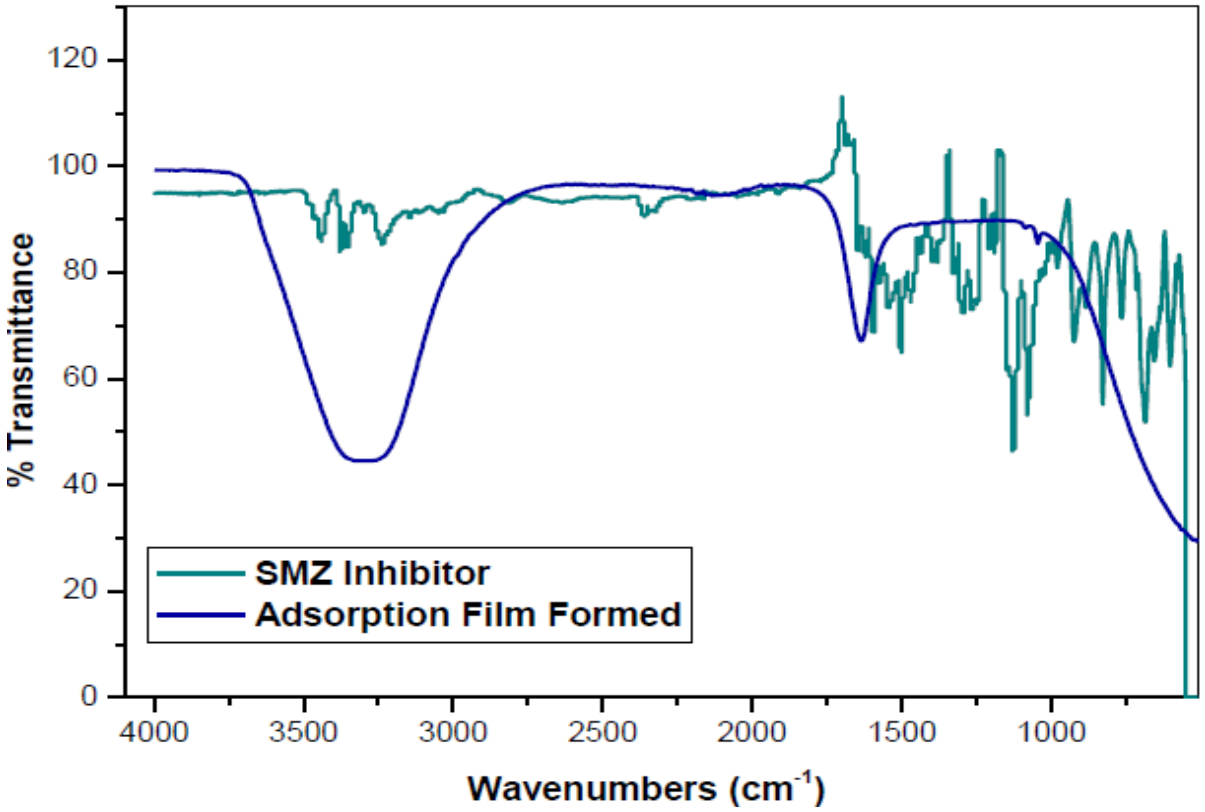

Figure 4.194: FT-IR spectra for the studied corrosion inhibitors and adsorption films formed on zinc in 1.0 M HCl using SMZ corrosion inhibitor.

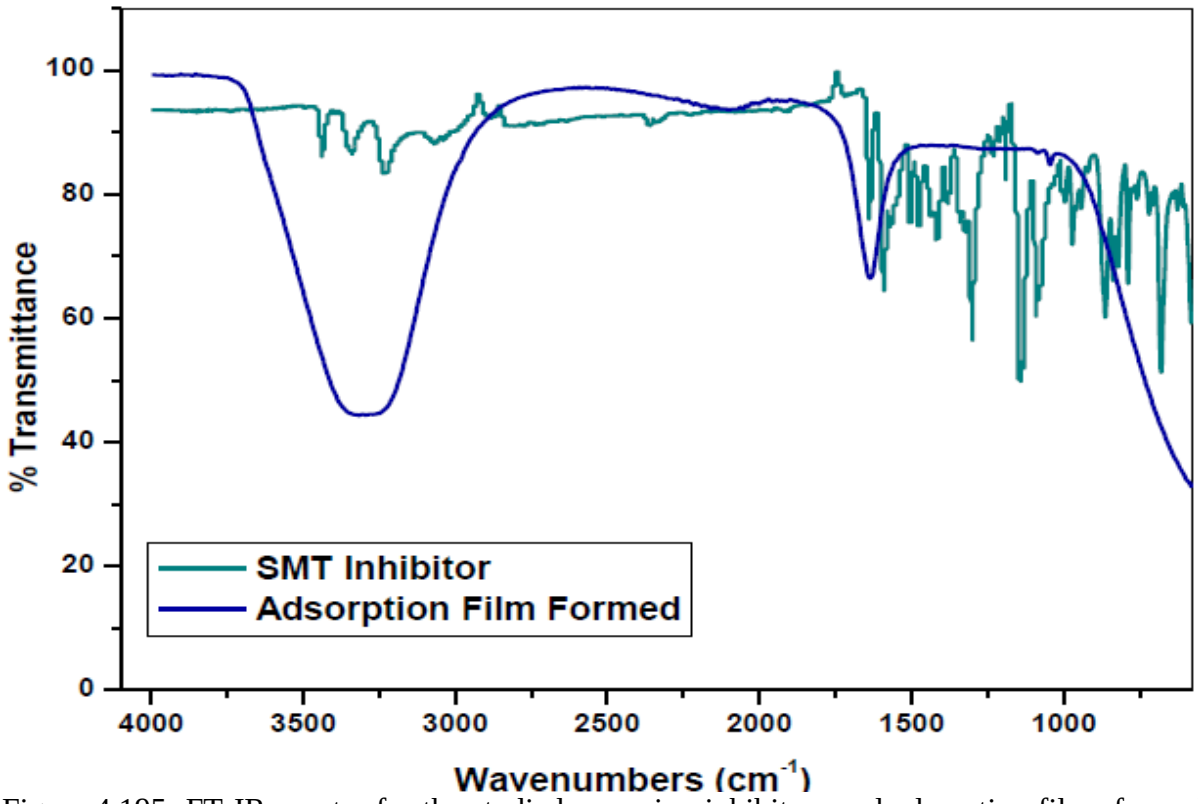

Figure 4.195: FT-IR spectra for the studied corrosion inhibitors and adsorption films formed on zinc in 1.0 M HCl using SMT corrosion inhibitor.

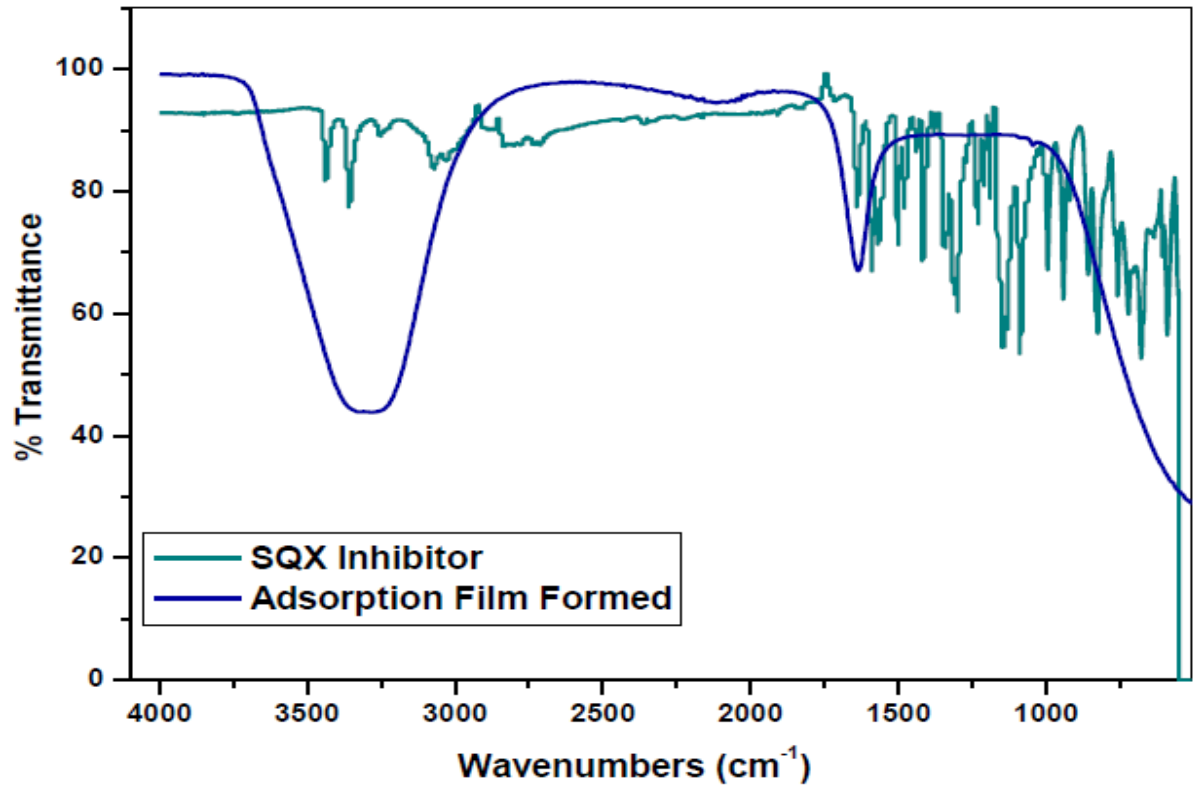

Figure 4.196: FT-IR spectra for the studied corrosion inhibitors and adsorption films formed on zinc in 1.0 M HCl using SQX corrosion inhibitor.

Sulphonamides possess several functional groups that have high electron density. This implies that the adsorption film between vacant *d*-orbitals of the metal and the sulfonamides is most likely to take place within these functional groups.

Table 4.16: Peaks and their identification, from FT-IR spectra of the studied corrosion inhibitors and adsorption films formed (i.e. SQX-Zn) on zinc in 1.0 M HCl using different corrosion inhibitors.

Inhibitor-Zinc	**Functional Groups Peaks from FT-IR Spectra (cm^{-1})**				
	N-H	**NH_2**	**C=C**	**O=S=O**	**C-N**
SNA	3371.17	1592.89	1503.33	–	1142.70
SNA-Zn	3251.21	1622.89	–	–	–
SBZ	3365.41	1592.88	1452.55	1331.61	1151.12
SBZ-Zn	3251.21	1622.89	–	–	–
SMX	3376.52	1617.33	1501.78	1302.24	1141.39
SMX-Zn	3251.21	1622.89	–	–	–
SCP	3399.99	1624.57	1593.11	1330.51	1141.92
SCP-Zn	3393.62	1622.06	–	–	–
SDM	–	1584.77	1504.74	1305.64	1139.74
SDM-Zn	3342.84	1622.89	–	–	–
SSZ	3379.05	1627.48	1594.26	1322.81	1131.67
SSZ-Zn	3251.21	1622.98	–	–	–
SMZ	–	–	1503.36	–	1126.18
SMZ-Zn	3251.21	1622.74	–	–	–
SMT	3342.84	1570.68	1591.80	1300.96	1143.93
SMT-Zn	3251.21	1624.57	–	–	–
SQX	3356.94	1590.11	1502.34	1343.94	1146.34
SQX-Zn	3251.21	1622.89	–	–	–

Table 4.16 shows the characteristic absorption bands corresponding to the main electron source groups within the studied compounds and compares them with those that are obtained from the adsorption film of the inhibited process. Characteristic absorption bands within the wavenumber range of 1190-1130 cm^{-1} corresponds to the C-N stretch for secondary amine [109], 3490-3430 cm^{-1} and 3360-3310 cm^{-1} to heterocyclic amine N-H stretch and aliphatic secondary amine N-H stretch, respectively [110, 112], 1650-1590 cm^{-1} to NH_2 primary amine N-H bend [109], 1350-1325 cm^{-1} to O=S=O [107] and 1600, 1500 cm^{-1} to aromatic, conjugated C=C [109, 110]. The presence of bands at 3351.21 cm^{-1} and 1624.57 cm^{-1}, corresponding to N-H stretch and NH_2 group, respectively as well as the absence of bands corresponding to aromatic rings (C=C), O=S=O, and C-N for SMT signifies the formation of SMT-Zn complex. Similar discussions can be used regarding SNA, SBZ, SMX, SCP, SDM, SSZ, SMZ and SQX as reported in Table 5.16 and shown in Figures 4.187 − 4.195.

4.3.4 SURFACE ANALYSIS (SEM)

The morphology of the zinc surfaces in hydrochloric acid solution in the absence and presence of 5.0×10^{-5} M of SNA, SBZ, SMX, SCP, SDM, SSZ, SMZ, SMT and SQX was investigated using scanning electron microscope. SEM micrographs for zinc and all inhibitors are shown in Figures 4.197−4.202. From Figure 4.197 it is observed that the surface of zinc is smooth with perhaps some negligible rough nature which may be attributed to the sample preparation procedure that involved abrasion with emery papers. It is also noted that the treatment zinc with hydrochloric acid resulted in a tremendous roughness on its surface as shown in Figure 4.198. The introduction of sulphonamide inhibitors somehow improved the smoothness on the surfaces of samples in Figures 4.199−4.202. From this observation, it can be deduced that the presence of the inhibitor compounds reduces the effects of corrosion through adsorption on to the metal surfaces [115−117].

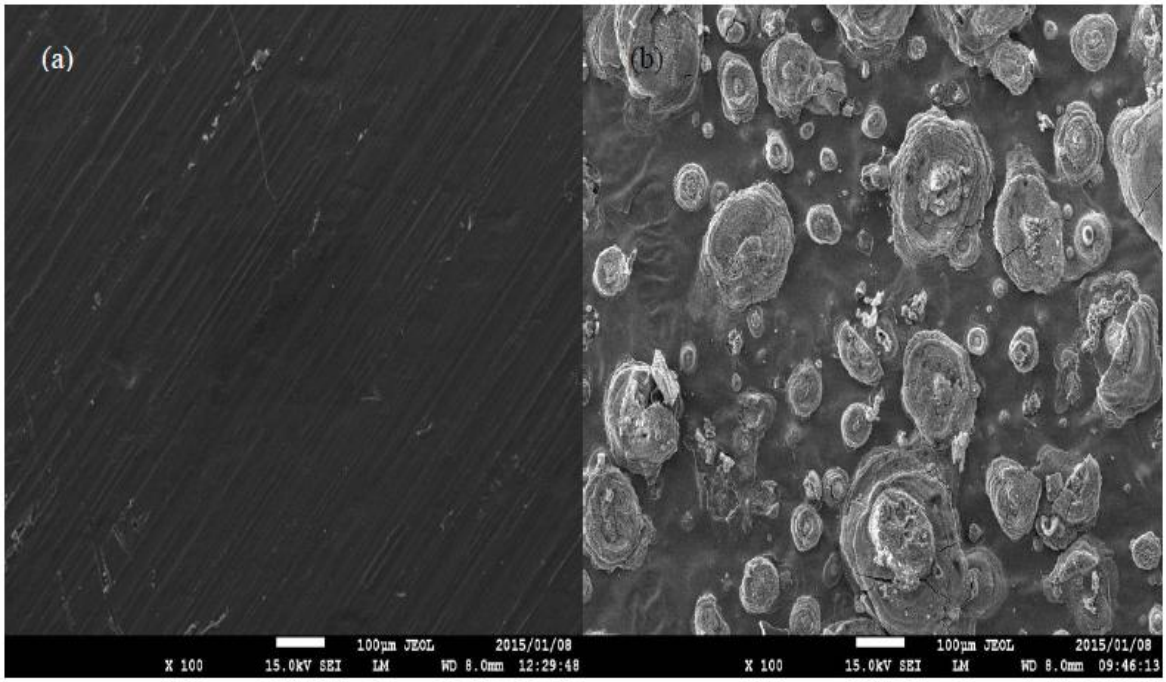

Figure 4.197: SEM micrographs of the surface of zinc: (a) plain zinc and (b) zinc immersed in HCl uninhibited.

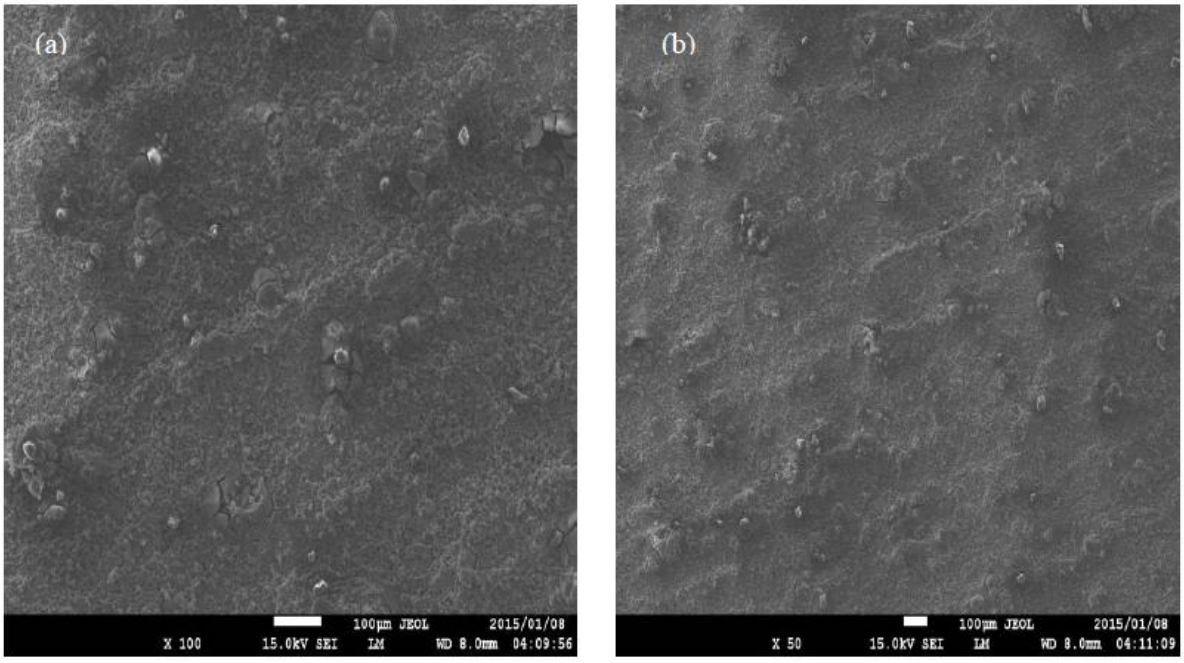

Figure 4.198: SEM micrographs of the surface of zinc immersed in HCl in the presence of (a) SNA (b) SBZ

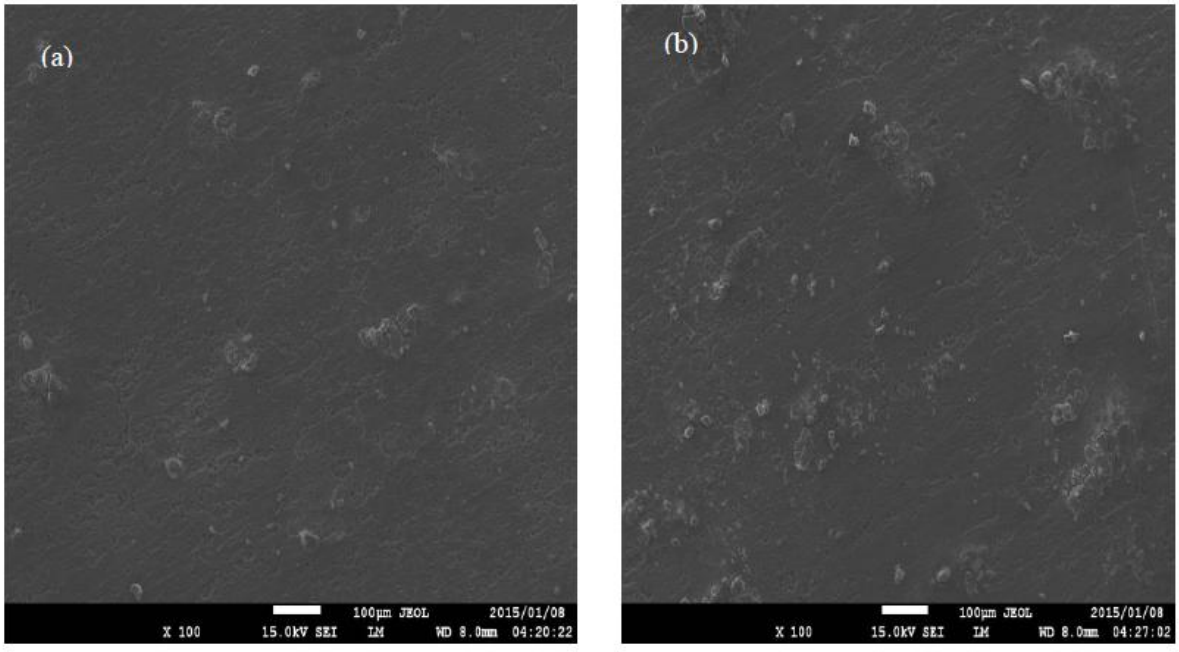

Figure 4.199: SEM micrographs of the surface of zinc immersed in HCl in the presence of (a) SMX (b) SCP

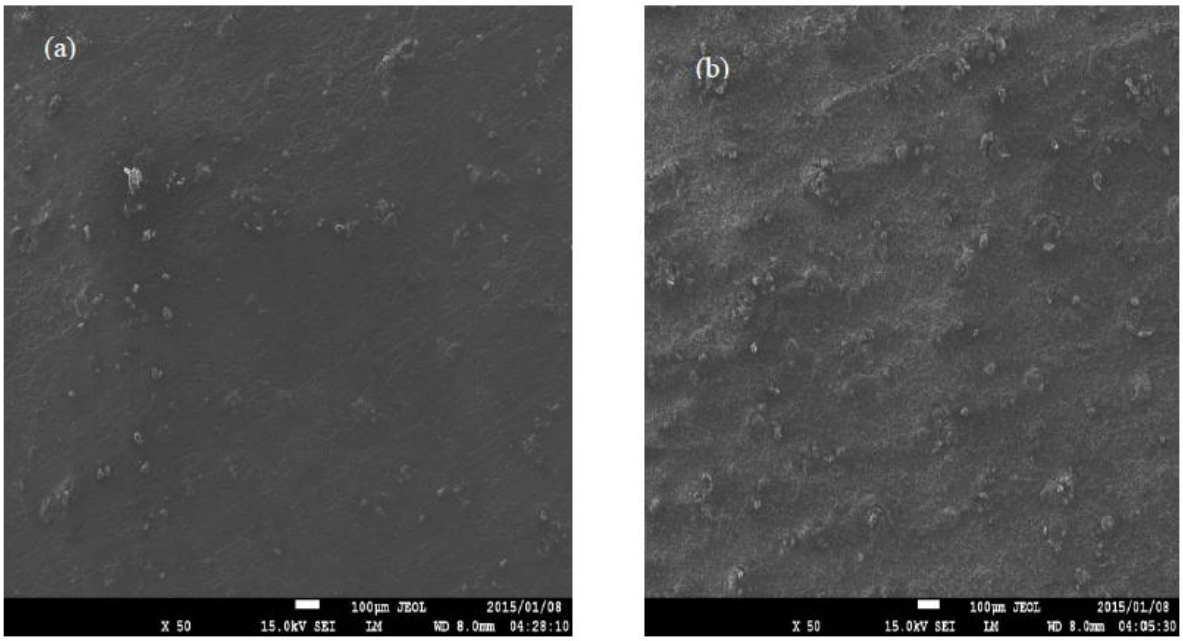

Figure 4.200: SEM micrographs of the surface of zinc immersed in HCl in the presence of (a) SDM (b) SSZ

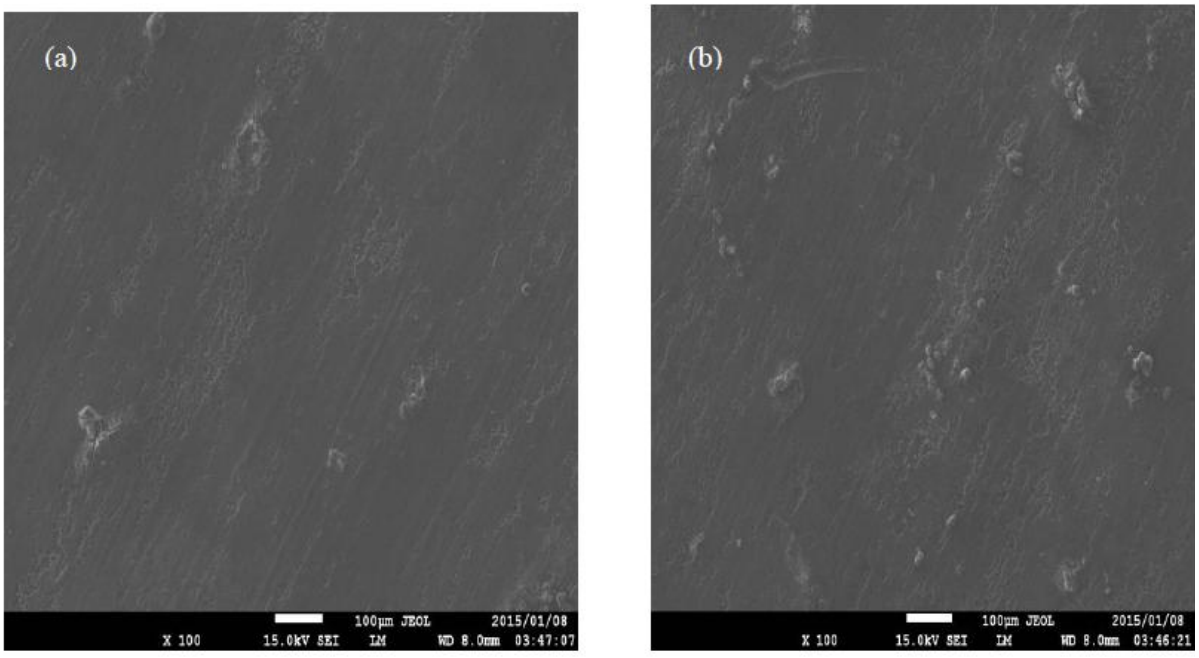

Figure 4.201: SEM micrographs of the surface of zinc immersed in HCl in the presence of (a) SMZ (b) SMT

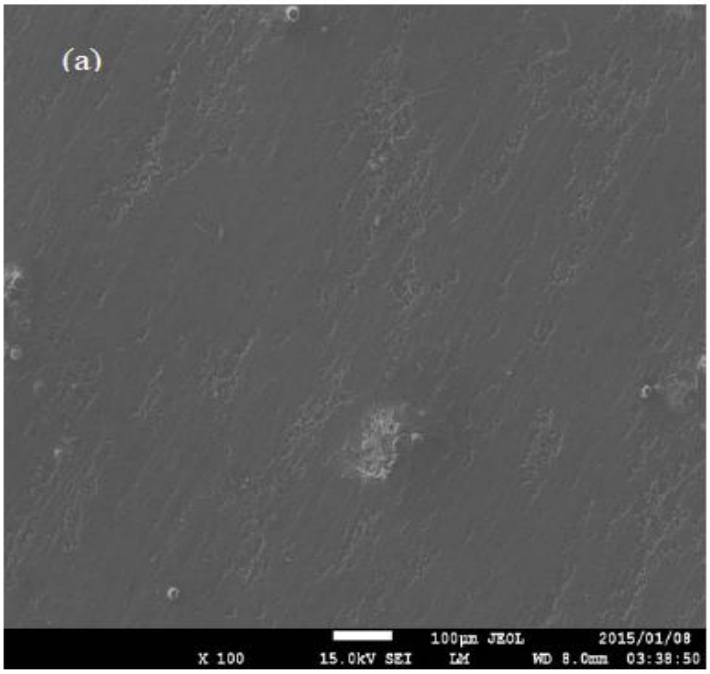

Figure 4.202: SEM micrographs of the surface of zinc immersed in HCl in the presence of SQX

4.3.5 CORROSION RATE AND INHIBITION EFFICIENCY

Figures 4.202−4.204 show the plot of the inhibition efficiency against concentration of the inhibitors at different temperatures. These results show that the inhibition efficiency increases as the concentration of the inhibitor is increased for all sulphonamides studied. For instance, at the concentration of 1.0×10^{-5} M SNA the inhibition efficiency is 74.81 % and increases to a maximum of 80.67 % at 5.0×10^{-5} M. The same trend is shown in the case of SBZ wherein the obtained inhibition efficiency at 1.0×10^{-5} M is 66.61 % and that at 5.0×10^{-5} M is 81.58 %. This trend of results is also observed with all other sulphonamides, that is, SMX, SCP, SDM, SSZ, SMZ, SMT and SQX. The results also show that inhibition efficiency decreases with an increase in temperature of the environment.

Figure 4.203 shows the relationship between the inhibition efficiencies and the concentrations of the nine inhibitors, namely SNA, SBZ, SMX, SCP, SDM, SSZ, SMZ, SMT and SQX at 30° C. The fact that the weight loss is decreased with the increase in the inhibitor concentration implies that the corrosion rate is hindered or slowed down. This may be due to the adsorption process between the inhibitor and the mild steel surface.

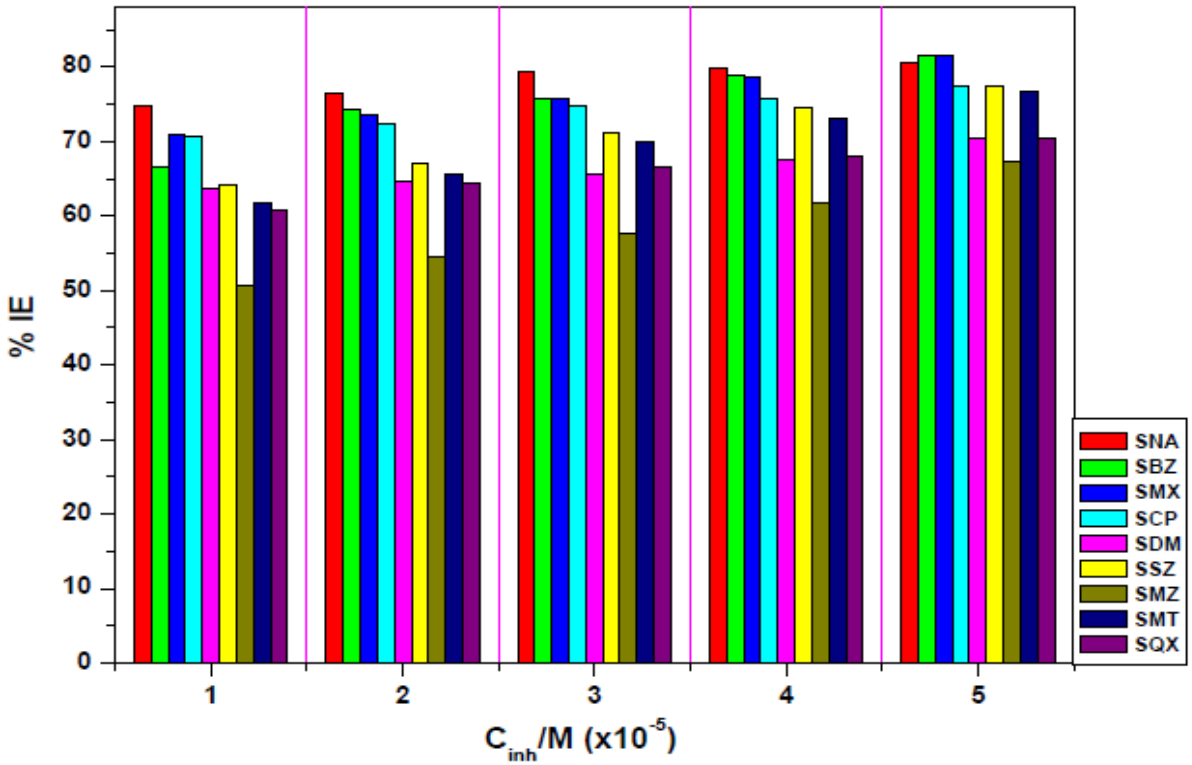

Figure 4.203: Variations of the percentage inhibition efficiencies with various concentrations of the utilized corrosion inhibitors at 30°C.

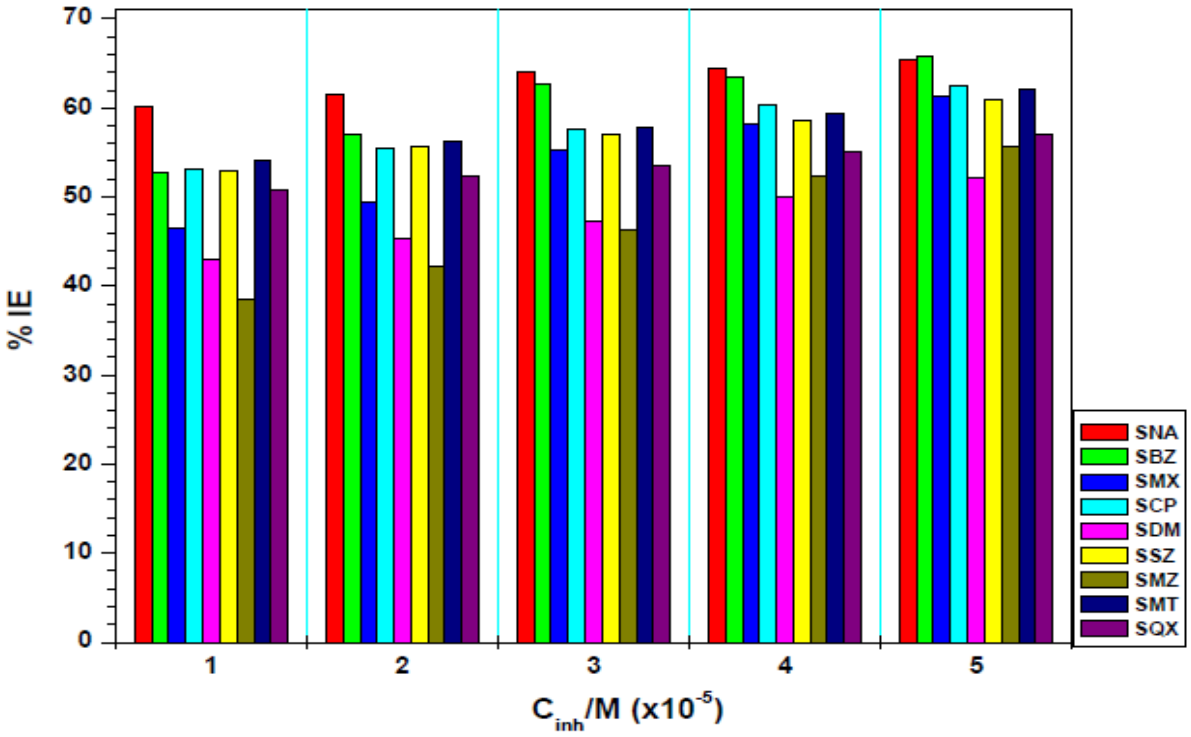

Figure 4.204: Variations of the percentage inhibition efficiencies with various concentrations of the utilized corrosion inhibitors at 40 °C.

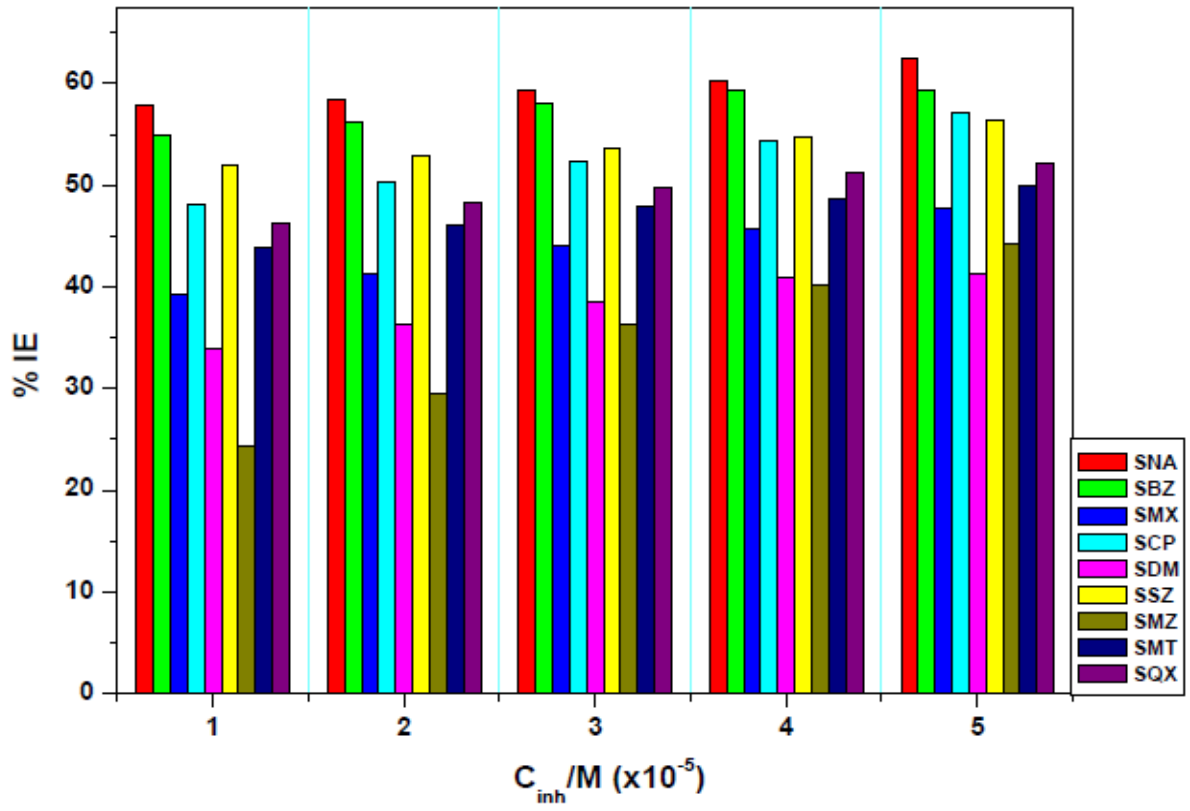

Figure 4.205: Variations of the percentage inhibition efficiencies with various concentrations of the utilized corrosion inhibitors at 50 °C.

Figure 5.204 shows the relationship between the inhibition efficiencies and the concentrations of the four inhibitors, namely SNA, SBZ, SMX, SCP, SDM, SSZ, SMZ, SMT and SQX at 40° C. The effect of the surrounding temperature is clearly shown by the comparison between Figures 4.203 and 4.204. The values of inhibition efficiencies and corrosion rates are recorded in table 5.18. The least performing inhibitor, SMZ, produced the inhibition efficiencies of 50.79 % and 67.36 % at 1.0×10^{-5} M and 5.0×10^{-5} M, respectively while the best performing inhibitor, SMX, produced the inhibition efficiencies of 70.71 % and 81.51 % using 1.0×10^{-5} M and 5.0×10^{-5} M, respectively at 30° C. As the temperature increased to 40° C the inhibition efficiencies decreased. For instance, SMZ decreased its efficiency to 43.06 % and 52.15 % using 1.0×10^{-5} M and 5.0×10^{-5} M, respectively while SMX decreased its efficiency to 46.49 % and 61.30 % using 1.0×10^{-5} M and 5.0×10^{-5} M, respectively. This behavior is better explained through the adsorption principles with the aid of the adsorption isotherms which will be described shortly in the subsections that follow. As the temperature is further increased to 50° C, the decrease in inhibition efficiency is pronounced with all inhibitors used as shown in Figure 4.205.

For instance, [PMIM][NTf_2], SMZ further decreased its efficiency to 24.28 % and 44.20 % using 1.0×10^{-5} M and 5.0×10^{-5} M, respectively while SMX further decreased its efficiency to 39.19 % and 47.67 % using 1.0×10^{-5} M and 5.0×10^{-5} M, respectively.

Studies have shown that the rate of metal dissolution decreases by increasing amount (concentration) of inhibitor [165]. The same outcome was observed with zinc whereby the corrosion rate was decreased as the inhibitor concentration is increased. When there was no inhibitor added in the solution the rate of corrosion was found to be high at all temperatures. Table 4.17 shows that at 30, 40 and 50°C, the rates of corrosion obtained are 0.00664, 0.00776 and 0.001230 $g.cm^{-2}.hr^{-1}$ indicating effects of temperature on corrosion rate. When the inhibitor is introduced in the solution rate of corrosion was observed to decrease. This was also documented by other authors [166−171]. The rate of corrosion was found to be 0.00128 $g.cm^{-2}.hr^{-1}$ when 5.0×10^{-5} M of SNA was added at 30°C. Increasing the temperature 40 and 50°C gave an increased corrosion rate of 0.00264 $g.cm^{-2}.hr^{-1}$ and 0.00462 $g.cm^{-2}.hr^{-1}$. When 5.0×10^{-5} M of SBZ was added at 30°C, rate of metal dissolution was found to decrease to a value of 0.00122 $g.cm^{-2}.hr^{-1}$, which is much lower relative to the uninhibited system. At 40 and 50°C, rate of corrosion increased to 0.00261 $g.cm^{-2}.hr^{-1}$ and 0.00499 $g.cm^{-2}.hr^{-1}$. SMX inhibitor also presents very low corrosion rates in comparison to the ones obtained for blank

experiments. For example, when 5.0×10^{-5} M is used at the three temperatures (30, 40 and 50°C) under the study the corrosion rates was found to be 0.00122, 0.00300 and 0.00643 $g.cm^{-2}.hr^{-1}$. The same trend in corrosion rates was observed with all other six inhibitors, SCP, SDM, SSZ, SMZ, SMT and SQX as shown in Table 4.17. It is clear that increasing the concentration reduces the rate of corrosion hence increasing the inhibition efficiency. This observation as explained in the mild steel section is due to the fact that at higher temperatures molecules within the system have more energy and thus move with higher average kinetic speeds leading to higher corrosion rate. Nevertheless, as the inhibitor concentration is increased, the presence of inhibitor molecules within the system is increased and thus improves the adsorption of the inhibitor molecules on the surface of the metal thereby lowering the corrosion rate.

Table 4.17: Percentage inhibition efficiencies and corrosion rates values obtained from the weight loss of zinc in 1.0 M HCl in the absence and presence of various concentrations of inhibitors.

Inhibitor	**Inhibitor Conc. (M)**	**Temperature**					
		30 °C		40 °C		50 °C	
		$\%IE_{WL}$	$C_R(g.cm^{-2}.h^{-1})$	$\%IE_{WL}$	$C_R(g.cm^{-2}.h^{-1})$	$\%IE_{WL}$	$C_R(g.cm^{-2}.h^{-1})$
Blank	0.0	-	0.00664	-	0.00776	-	0.01230
SNA	1.0×10^{-5}	74.81	0.00167	60.08	0.00310	57.92	0.00517
	2.0×10^{-5}	76.40	0.00156	61.52	0.00298	58.42	0.00511
	3.0×10^{-5}	79.41	0.00136	64.09	0.00278	59.32	0.00500
	4.0×10^{-5}	79.83	0.00134	64.37	0.00276	60.18	0.00490
	5.0×10^{-5}	80.67	0.00128	65.31	0.00264	62.44	0.00462
SBZ	1.0×10^{-5}	66.61	0.00226	52.72	0.00367	54.89	0.00555
	2.0×10^{-5}	74.23	0.00171	57.01	0.00333	56.16	0.00539
	3.0×10^{-5}	75.82	0.00160	62.73	0.00289	57.96	0.00517
	4.0×10^{-5}	78.99	0.00139	63.51	0.00283	59.32	0.00500
	5.0×10^{-5}	81.58	0.00122	65.74	0.00261	59.41	0.00499
SMX	1.0×10^{-5}	70.88	0.00193	46.49	0.00415	39.19	0.00748
	2.0×10^{-5}	73.56	0.00175	49.36	0.00393	41.35	0.00721
	3.0×10^{-5}	75.82	0.00160	55.29	0.00347	43.97	0.00689
	4.0×10^{-5}	78.66	0.00141	58.30	0.00323	45.78	0.00667
	5.0×10^{-5}	81.51	0.00122	61.30	0.00300	47.67	0.00643
SCP	1.0×10^{-5}	70.71	0.00194	53.08	0.00364	48.17	0.00637
	2.0×10^{-5}	72.30	0.00183	55.51	0.00345	50.34	0.00611
	3.0×10^{-5}	74.73	0.00167	57.62	0.00328	52.37	0.00586
	4.0×10^{-5}	75.82	0.00160	60.23	0.00308	54.81	0.00556
	5.0×10^{-5}	77.32	0.00150	62.58	0.00290	57.11	0.00527
SDM	1.0×10^{-5}	63.68	0.00241	43.06	0.00442	33.99	0.00812
	2.0×10^{-5}	64.68	0.00234	45.42	0.00423	36.34	0.00783
	3.0×10^{-5}	65.69	0.00227	47.35	0.00408	38.42	0.00757
	4.0×10^{-5}	67.45	0.00216	49.93	0.00388	40.90	0.00727
	5.0×10^{-5}	70.46	0.00196	52.15	0.00371	41.35	0.00721
SSZ	1.0×10^{-5}	64.28	0.00237	52.86	0.00366	51.92	0.00591
	2.0×10^{-5}	67.03	0.00218	55.72	0.00343	52.92	0.00579
	3.0×10^{-5}	71.21	0.00191	57.08	0.00333	53.59	0.00571
	4.0×10^{-5}	74.48	0.00169	58.58	0.00321	54.81	0.00556
	5.0×10^{-5}	77.49	0.00025	60.94	0.00303	56.43	0.00536
SMZ	1.0×10^{-5}	50.79	0.00326	38.48	0.00477	24.28	0.00931
	2.0×10^{-5}	54.47	0.00302	42.20	0.00448	29.53	0.00642
	3.0×10^{-5}	57.57	0.00281	46.28	0.00417	36.29	0.00783
	4.0×10^{-5}	61.84	0.00253	52.36	0.00370	40.23	0.00735
	5.0×10^{-5}	67.36	0.00216	55.72	0.00343	44.20	0.00686
SMT	1.0×10^{-5}	61.84	0.00253	54.07	0.00356	43.79	0.00691
	2.0×10^{-5}	65.52	0.00228	56.29	0.00339	46.15	0.00660
	3.0×10^{-5}	69.96	0.00199	57.87	0.00327	47.81	0.00642
	4.0×10^{-5}	73.05	0.00178	59.30	0.00316	48.71	0.00631
	5.0×10^{-5}	76.65	0.00155	62.16	0.00293	49.93	0.00616
SQX	1.0×10^{-5}	60.75	0.00260	50.72	0.00382	46.32	0.00660
	2.0×10^{-5}	64.35	0.00236	52.36	0.00370	48.26	0.00636
	3.0×10^{-5}	66.53	0.00222	53.57	0.00360	49.84	0.00617
	4.0×10^{-5}	68.03	0.00212	55.01	0.00349	51.27	0.00599
	5.0×10^{-5}	70.46	0.00196	56.94	0.00334	52.23	0.00587

4.3.6 EFFECT OF TEMPERATURE AND KINETIC ENERGY

As already explained in detail in the mild steel and aluminium sections, corrosion rate is influenced greatly by the temperature of the environment. This is particularly important because the mode of the inhibitor adsorption on zinc surface can be determined through temperature variation [172, 173]. The effect of temperature on the inhibition efficiency of zinc metal was investigated using the concentration range from 1.0×10^{-5} M − 5.0×10^{-5} M for SNA, SBZ, SMX, SCP, SDM, SSZ, SMZ, SMT and SQX at temperature range from 30°C − 50°C for 15 hours immersion time. The Arrhenius equation and the transition-state equation are often used to express the relationship between the corrosion rate (ρ) of mild steel in acidic medium and temperature (T). The Arrhenius equation (Eq. 49) and transition-state equation (Eq. 50) were used to produce the Arrhenius and transition states plots.

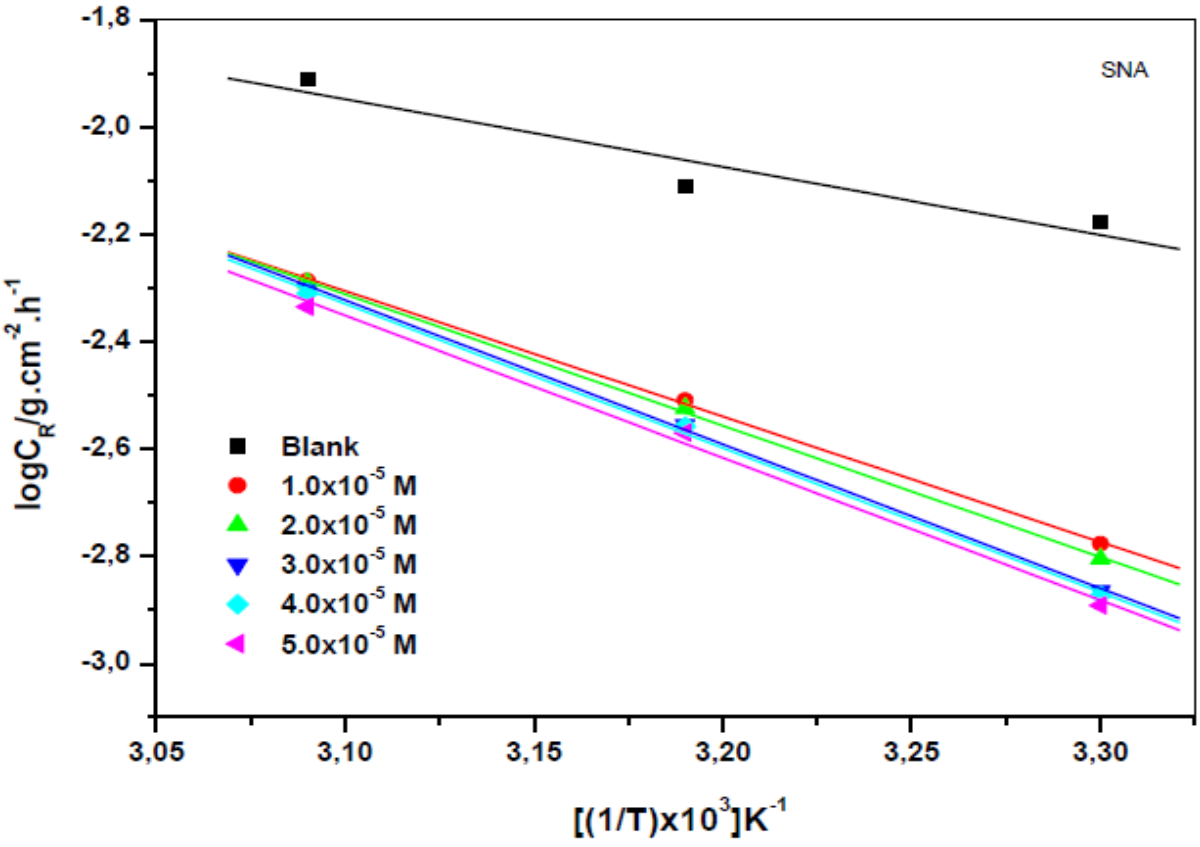

Figure 4.206: Arrhenius plots for the corrosion of mild steel in 1.0 M HCl in the absence and presence of various concentrations of SNA corrosion inhibitor.

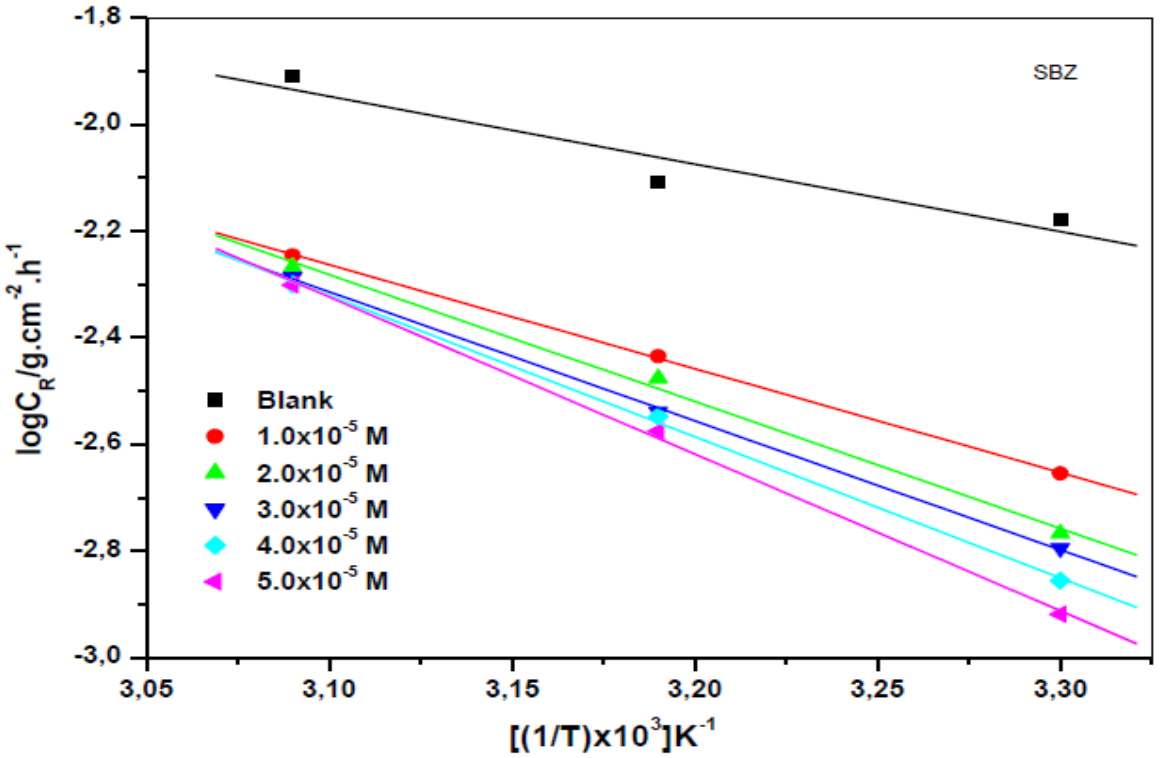

Figure 4.207: Arrhenius plots for the corrosion of mild steel in 1.0 M HCl in the absence and presence of various concentrations of SBZ corrosion inhibitor.

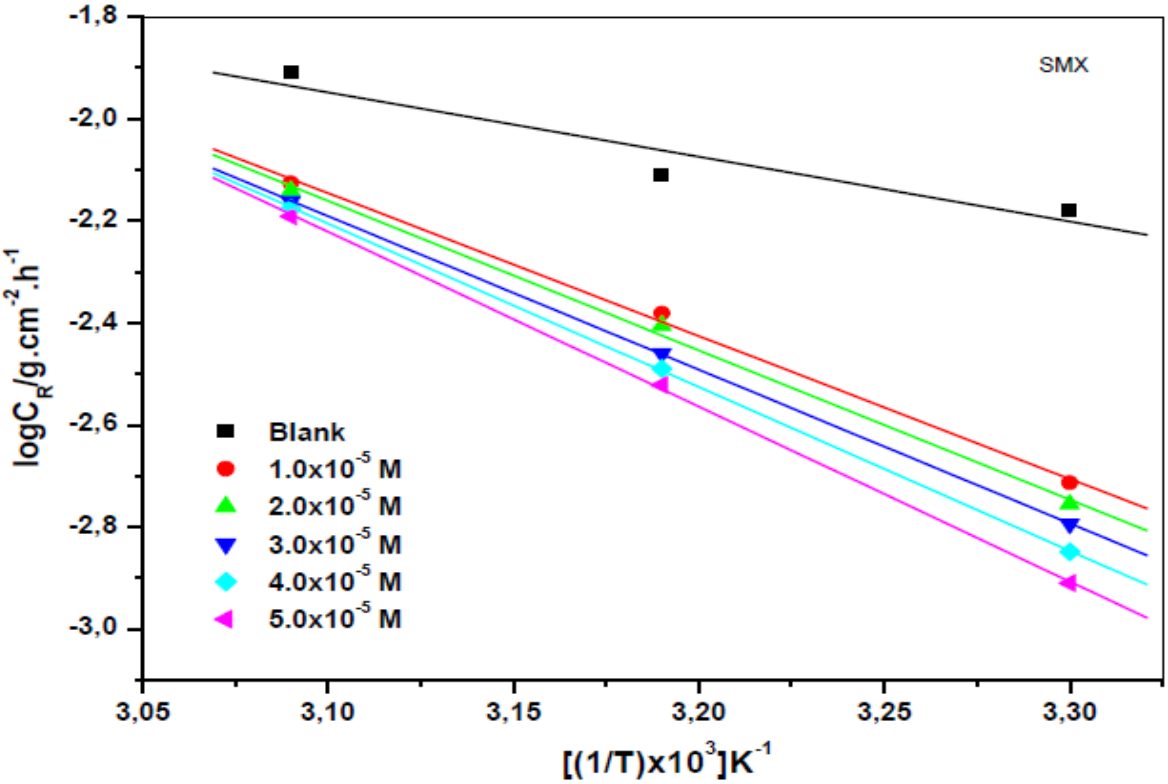

Figure 4.208: Arrhenius plots for the corrosion of mild steel in 1.0 M HCl in the absence and presence of various concentrations of SMX corrosion inhibitor.

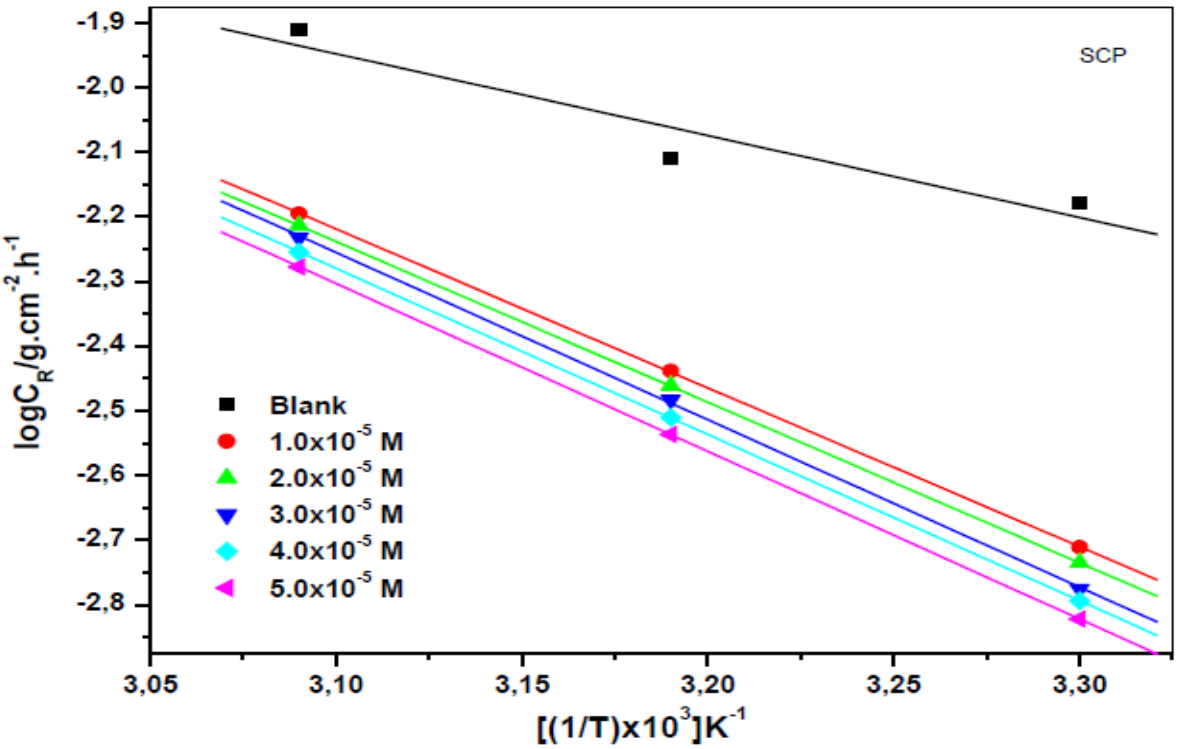

Figure 4.209: Arrhenius plots for the corrosion of mild steel in 1.0 M HCl in the absence and presence of various concentrations of SCP corrosion inhibitor.

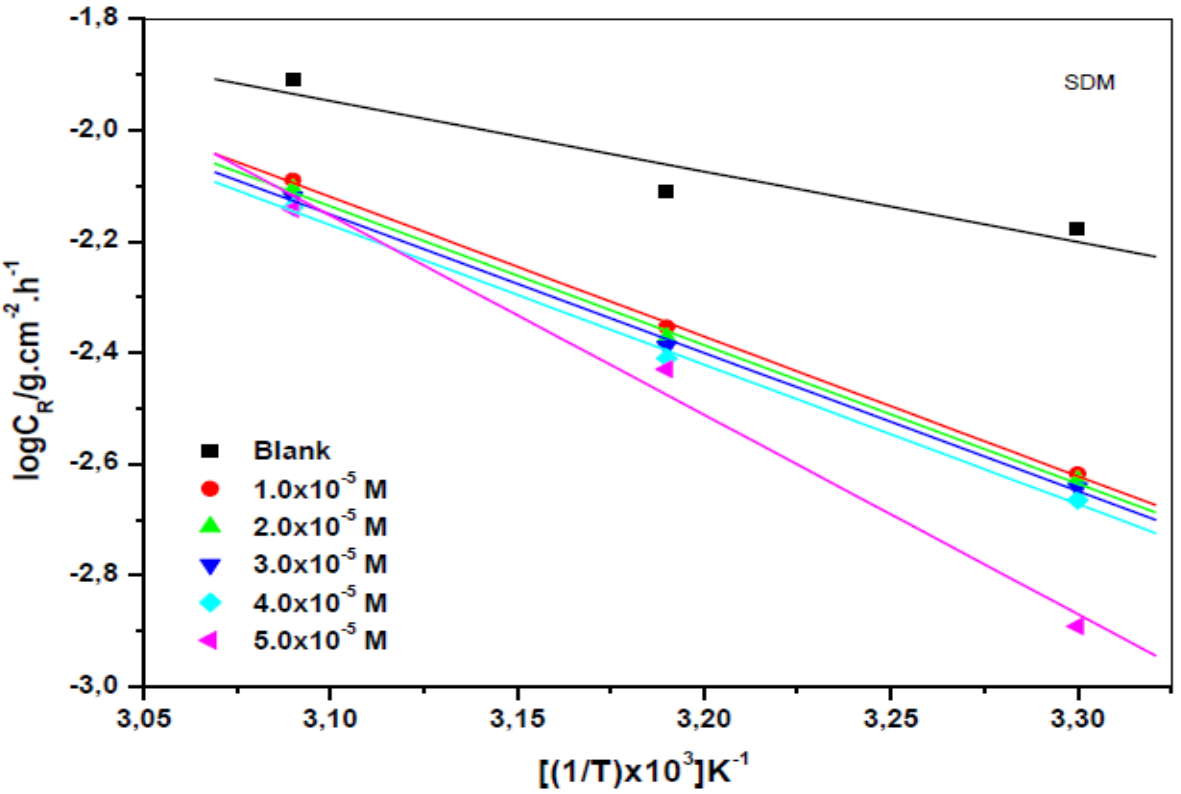

Figure 4.210: Arrhenius plots for the corrosion of mild steel in 1.0 M HCl in the absence and presence of various concentrations of SDM corrosion inhibitor.

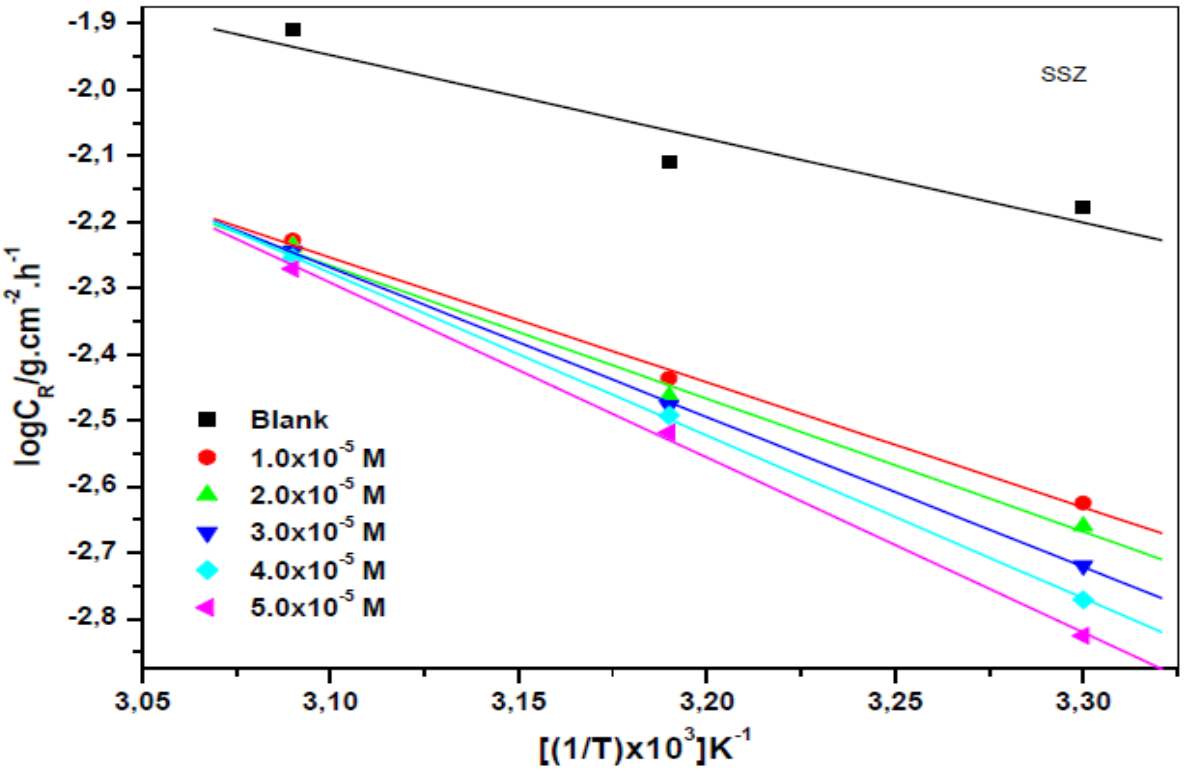

Figure 4.211: Arrhenius plots for the corrosion of mild steel in 1.0 M HCl in the absence and presence of various concentrations of SSZ corrosion inhibitor.

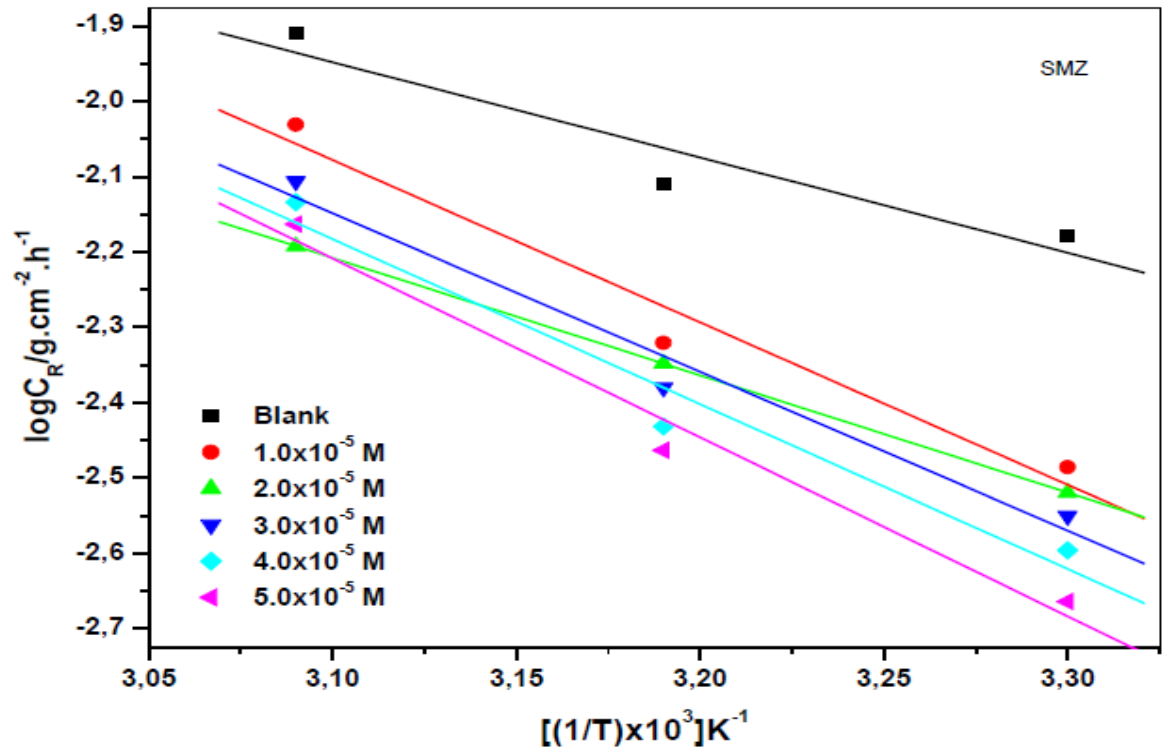

Figure 4.212: Arrhenius plots for the corrosion of mild steel in 1.0 M HCl in the absence and presence of various concentrations of SMZ corrosion inhibitor.

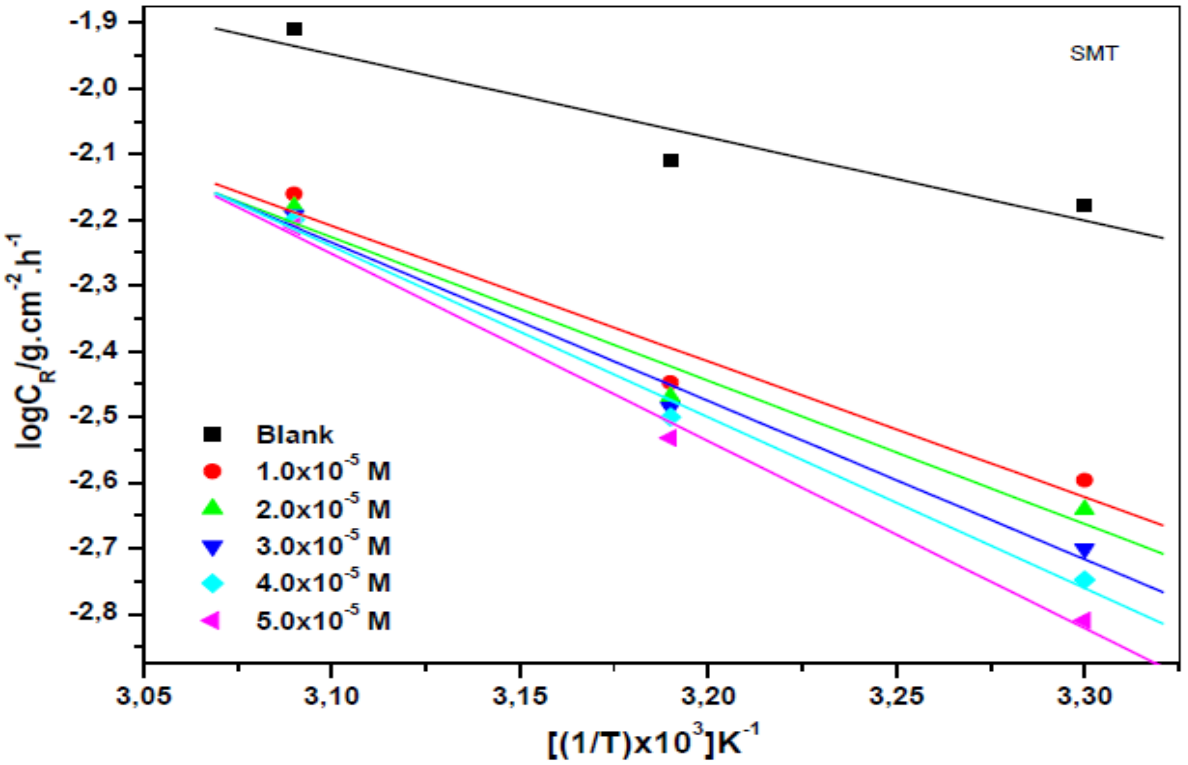

Figure 4.213: Arrhenius plots for the corrosion of mild steel in 1.0 M HCl in the absence and presence of various concentrations of SMT corrosion inhibitor.

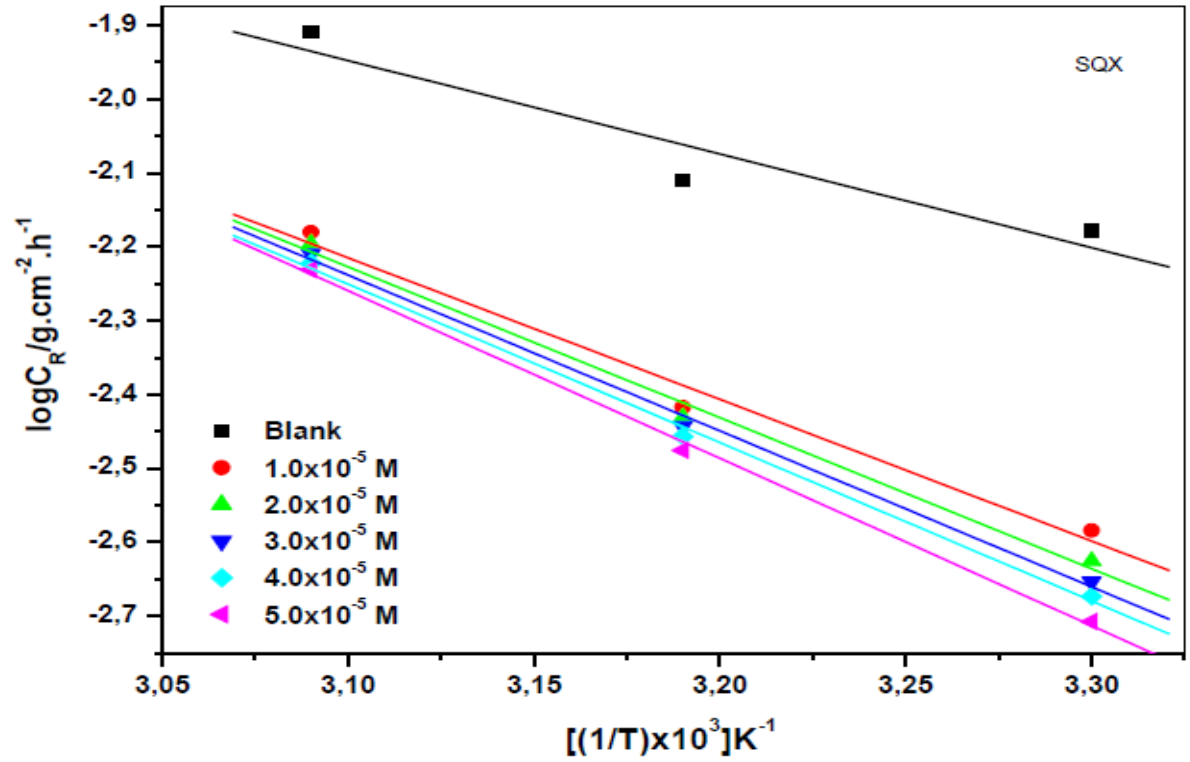

Figure 4.214: Arrhenius plots for the corrosion of mild steel in 1.0 M HCl in the absence and presence of various concentrations of SQX corrosion inhibitor.

The process of adsorption between the metal surface and the inhibitor can sometimes be an exothermic process where the heat is given off, although in some cases, endothermic process is encountered. The apparent activation energy at different concentrations of sulphonamides were calculated from the plots of log C_R versus $1/T$ as shown in Figures 4.206 − 4.214 and the results are shown in Table 4.18.

The activation energy value of 24.28 kJ.mol^{-1} was attained when there was no inhibitor added. When 1.0×10^{-5} M of SNA was added the activation energy increased to 44.90 kJ.mol^{-1} indicating that the reaction between the chlorine ions and the metal surface was lowered. At 2.0×10^{-5} M, 3.0×10^{-5} M, 4.0×10^{-5} M and 5.0×10^{-5} M, the activation energy values increased to 47.00 kJ.mol^{-1}, 51.56 kJ.mol^{-1},51.54 kJ.mol^{-1} and 50.94 kJ.mol^{-1}, respectively. The increasing activation energy values indicate that the rate at which the metal dissolute has been lowered. Similar trend of increasing activation energy values is obtained when SBZ, SMX, SCP, SDM, SSZ, SMZ, SMT and SQX were used. At 1.0×10^{-5} M of SBZ the value obtained was 37.35 kJ.mol^{-1}. When the concentration of SBZ sulphonamide is increased to 2.0×10^{-5} M, 3.0×10^{-5} M, 4.0×10^{-5} M and 5.0×10^{-5} M, the activation energy values increased to 45.65 kJ.mol^{-1}, 46.39 kJ.mol^{-1}, 50.76 kJ.mol^{-1} and 56.43 kJ.mol^{-1}, respectively. The results as far as the activation energies are concerned are at their highest with regard to SMX. At 1.0×10^{-5} M of SMX the value obtained was 53.78 kJ.mol^{-1}. When the concentration of SMX sulphonamide is increased to 2.0×10^{-5} M, 3.0×10^{-5} M, 4.0×10^{-5} M and 5.0×10^{-5} M, the activation energy values increased to 56.18 kJ.mol^{-1}, 57.83 kJ.mol^{-1}, 61.51 kJ.mol^{-1} and 65.80 kJ.mol^{-1}, respectively. The values are high and present a good inhibition process on zinc surface. The increasing concentration of the sulphonamides is observed to increase the activation energy values which indicate the fact that the inhibitors used under the study reduce the rate of metal dissolution. In the mild steel and aluminum sections of this report, it was stated that the values of activation energy above 80 kJ.mol^{-1} are in accordance with the sharing or transfer of an electron from the adsorbate molecules to the substrate substances resulting into a coordinate type of bond (chemisorption). The activation energy values of corrosion process of zinc are well below 80 kJ.mol^{-1} therefore physisorption is the type of adsorption taking place on the surface of zinc under this study. Figure 4.215 shows a typical representation plot of the variation of activation energy with the different concentrations of the corrosion inhibitors.

Table 4.18: Kinetic and activation parameters (derived from the Arrhenius and transition-states plots) for zinc in 1.0 M HCl in the absence and presence of various concentrations of inhibitors.

Inhibitor	Inhibitor Conc. (M)	Activation Energy (E_a/kJ.mol^{-1})	Enthalpy of Activation (ΔH^*/ kJ.mol^{-1})	Entropy of Activation (ΔS^*/ J.mol^{-1}.K^{-1})
Blank	0.0	24.28	21.74	–216.14
SNA	1.0×10^{-5}	44.90	42.39	–159.29
	2.0×10^{-5}	47.00	44.44	–152.74
	3.0×10^{-5}	51.56	49.04	–138.70
	4.0×10^{-5}	51.54	48.27	–141.21
	5.0×10^{-5}	50.94	48.42	–141.16
SBZ	1.0×10^{-5}	37.35	33.92	–184.57
	2.0×10^{-5}	45.65	43.11	–156.28
	3.0×10^{-5}	46.39	44.00	–154.15
	4.0×10^{-5}	50.76	46.23	–141.17
	5.0×10^{-5}	56.43	53.38	–125.28
SMX	1.0×10^{-5}	53.78	51.25	–128.44
	2.0×10^{-5}	56.18	54.88	–117.29
	3.0×10^{-5}	57.83	57.80	–108.59
	4.0×10^{-5}	61.51	61.47	–97.490
	5.0×10^{-5}	65.80	65.77	–84.470
SCP	1.0×10^{-5}	47.14	44.61	–150.44
	2.0×10^{-5}	47.66	45.25	–148.81
	3.0×10^{-5}	49.66	47.14	–143.27
	4.0×10^{-5}	49.31	46.70	–145.11
	5.0×10^{-5}	49.78	47.23	–143.93
SDM	1.0×10^{-5}	48.15	45.62	–145.40
	2.0×10^{-5}	47.82	45.29	–146.75
	3.0×10^{-5}	47.64	45.11	–147.66
	4.0×10^{-5}	48.09	45.55	–146.59
	5.0×10^{-5}	49.54	49.10	–135.67
SSZ	1.0×10^{-5}	36.21	33.68	–184.98
	2.0×10^{-5}	38.55	36.00	–178.03
	3.0×10^{-5}	50.49	40.88	–162.94
	4.0×10^{-5}	47.17	44.66	–151.39
	5.0×10^{-5}	50.74	48.21	–140.66
SMZ	1.0×10^{-5}	41.37	38.90	–165.58
	2.0×10^{-5}	29.91	27.37	–203.65
	3.0×10^{-5}	40.43	37.91	–169.84
	4.0×10^{-5}	42.03	39.54	–165.45
	5.0×10^{-5}	45.60	43.16	–154.52
SMT	1.0×10^{-5}	39.64	37.09	–173.54
	2.0×10^{-5}	41.85	39.32	–166.95
	3.0×10^{-5}	46.25	43.63	–153.76
	4.0×10^{-5}	49.92	47.39	–142.21
	5.0×10^{-5}	54.65	52.12	–127.76
SQX	1.0×10^{-5}	36.78	34.28	–182.46
	2.0×10^{-5}	39.18	36.75	–174.95
	3.0×10^{-5}	40.47	37.97	–171.38
	4.0×10^{-5}	41.15	38.38	–169.72
	5.0×10^{-5}	42.35	40.94	–162.60

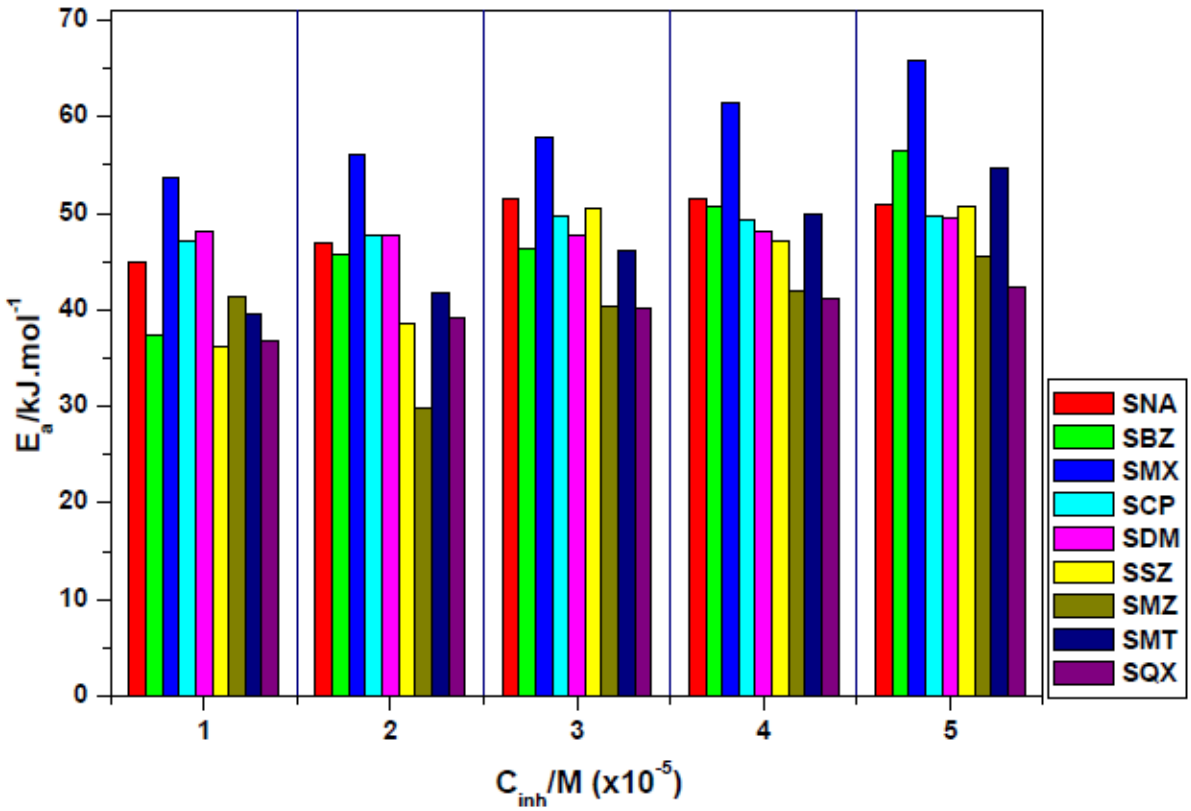

Figure 4.215: Variation of the activation energy with the concentration of the utilized corrosion inhibitors.

Investigation of inhibition efficiency on the zinc surface can be determined by the values of entropy and enthalpy of activation. The negative values of entropy show that the destruction on the metal surface has been lowered and the positive once shows that the disordering of the system has increased. Enthalpy values can present both the endothermic or exothermic reaction depending on the sign of the value. Transition state plots shown in Figures 4.216−4.224 are constructed from the equation (57).

From this equation, enthalpy of activation can be obtained from the slope while entropy of activation can be obtained from the intercept as indicated by equations (62) and (63):

$$Slope = \frac{-\Delta H^*}{R} \tag{62}$$

$$c = \ln\left(\frac{k_b}{h}\right) + \frac{\Delta S^*}{R} \tag{63}$$

where, c is the intercept and other symbols have been explained in the mild steel section.

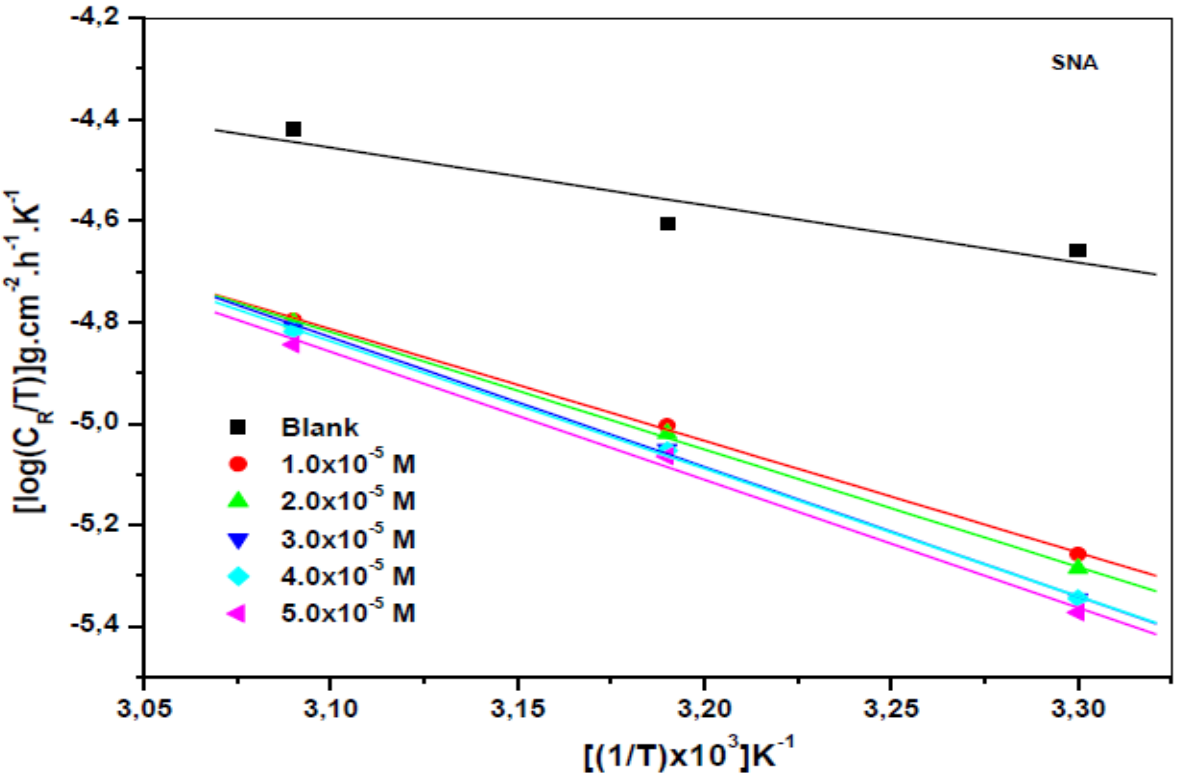

Figure 4.216: Transition state plots for the corrosion of zinc in 1.0 M HCl in the absence and presence of various concentrations of SNA corrosion inhibitor.

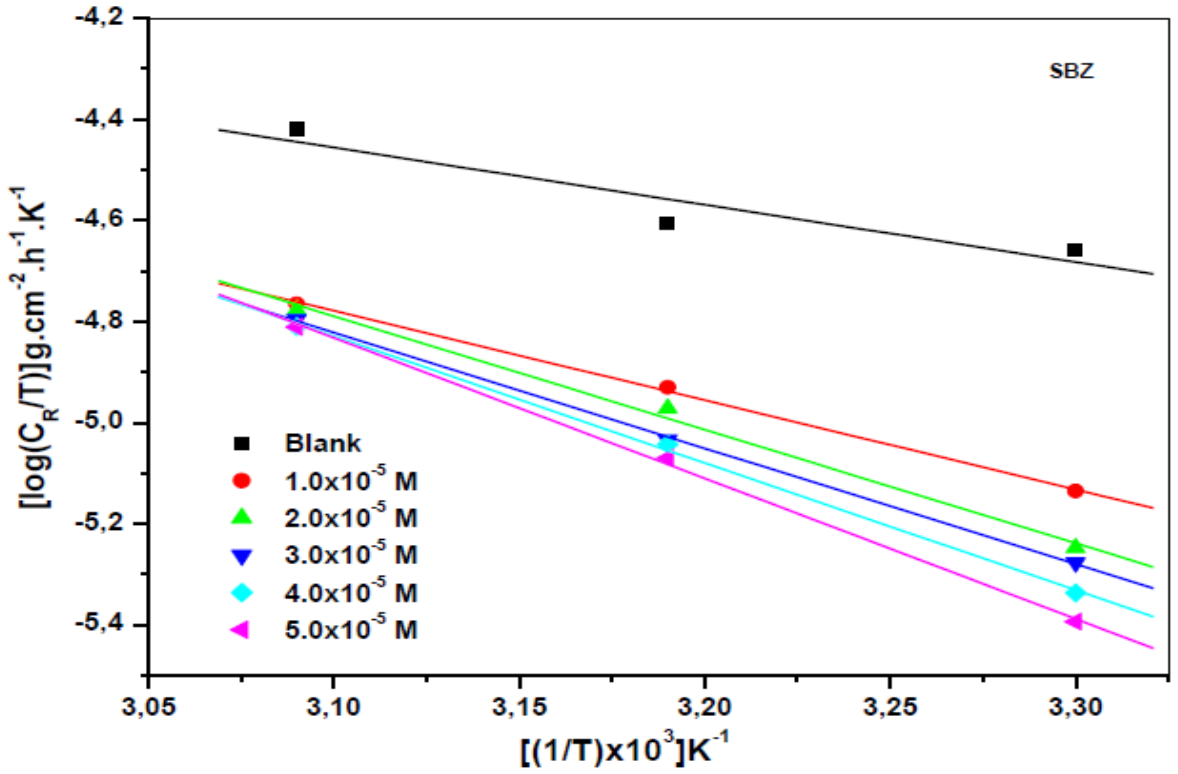

Figure 4.217: Transition state plots for the corrosion of zinc in 1.0 M HCl in the absence and presence of various concentrations of SBZ corrosion inhibitor.

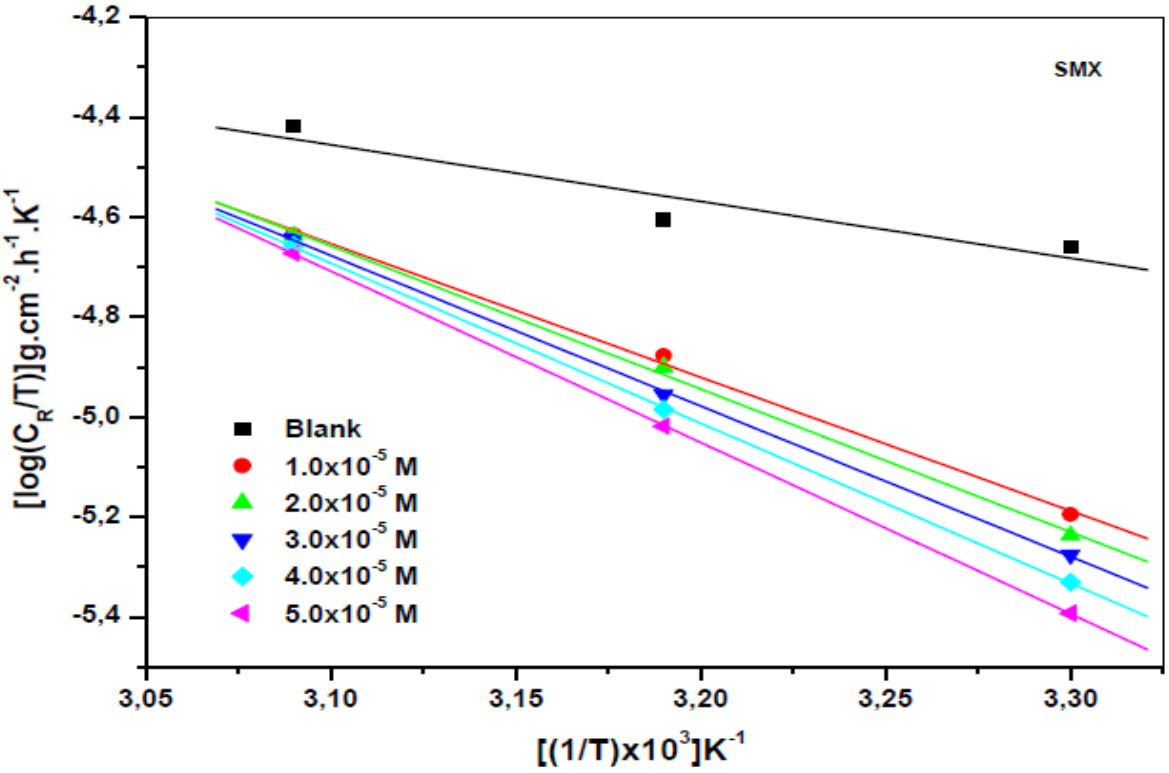

Figure 4.218: Transition state plots for the corrosion of zinc in 1.0 M HCl in the absence and presence of various concentrations of SMX corrosion inhibitor.

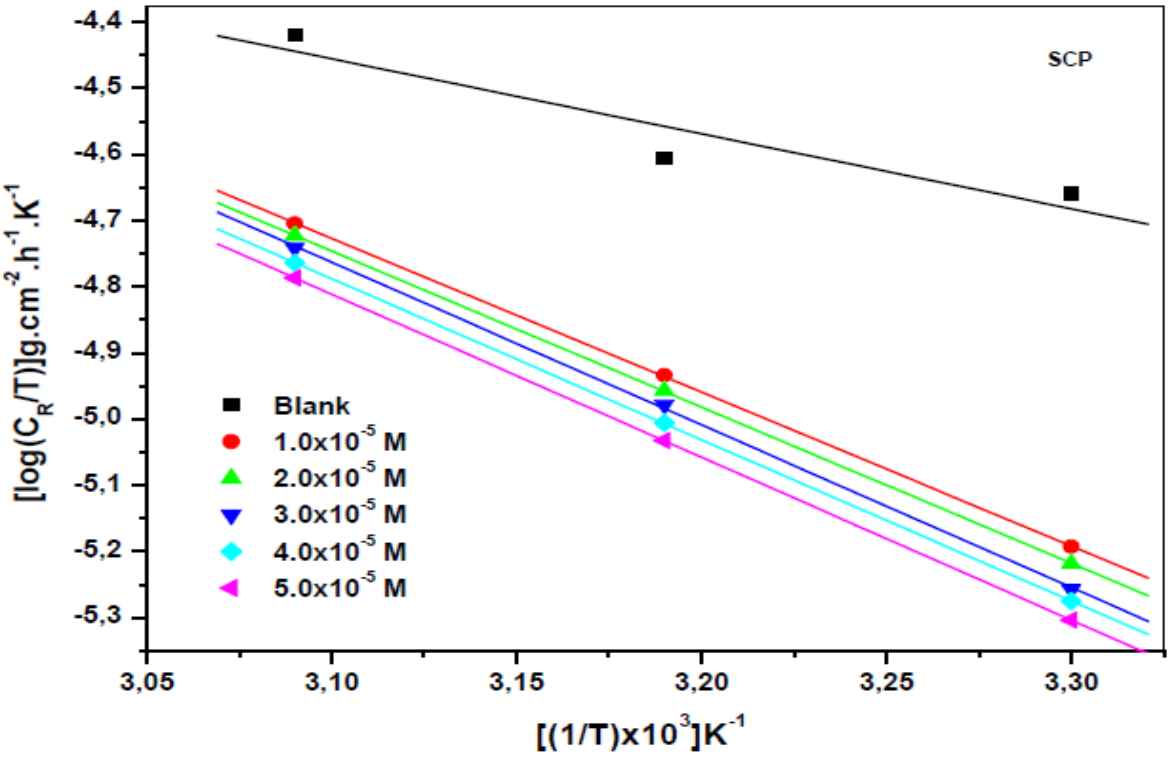

Figure 4.219: Transition state plots for the corrosion of zinc in 1.0 M HCl in the absence and presence of various concentrations of SCP corrosion inhibitor.

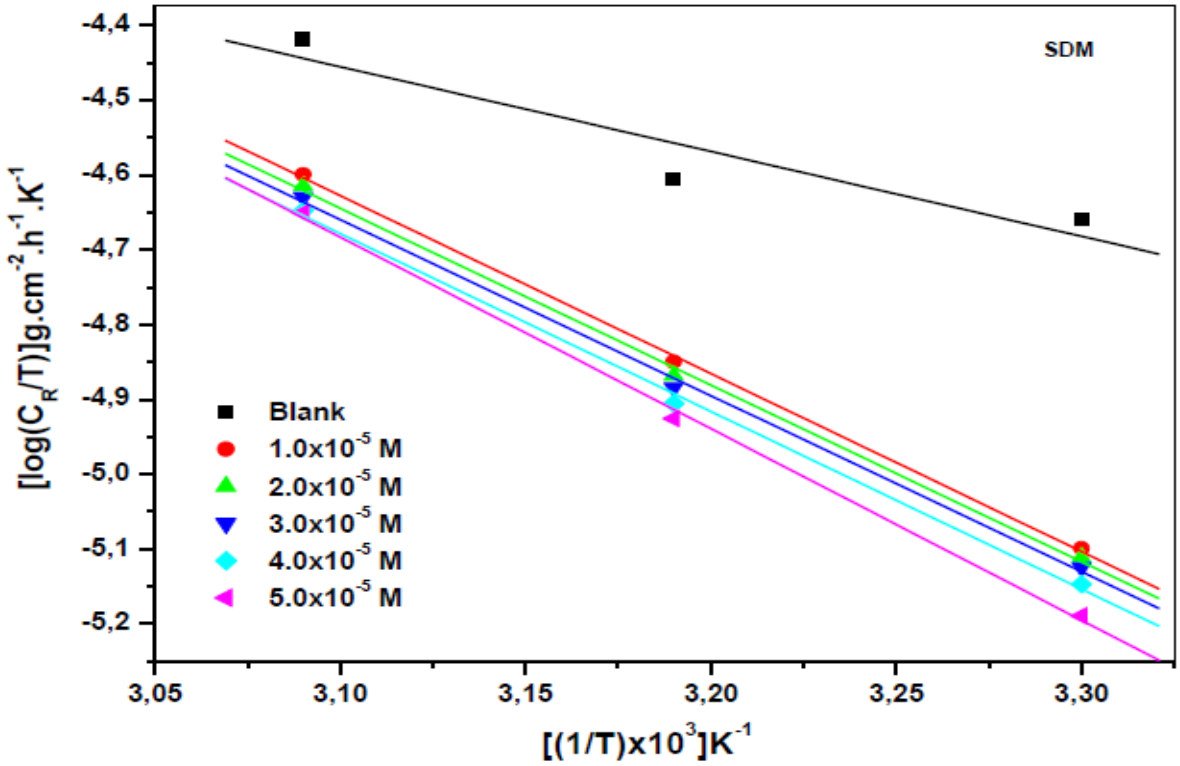

Figure 4.220: Transition state plots for the corrosion of zinc in 1.0 M HCl in the absence and presence of various concentrations of SDM corrosion inhibitor.

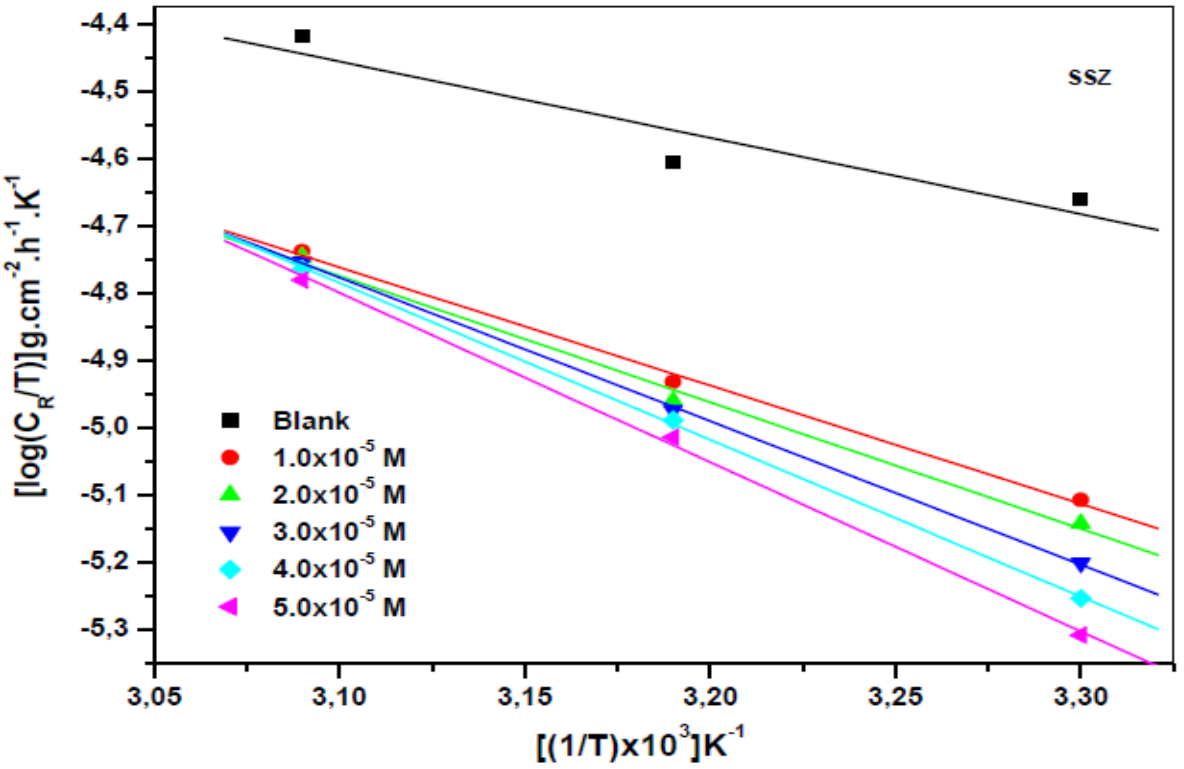

Figure 4.221: Transition state plots for the corrosion of zinc in 1.0 M HCl in the absence and presence of various concentrations of SSZ corrosion inhibitor.

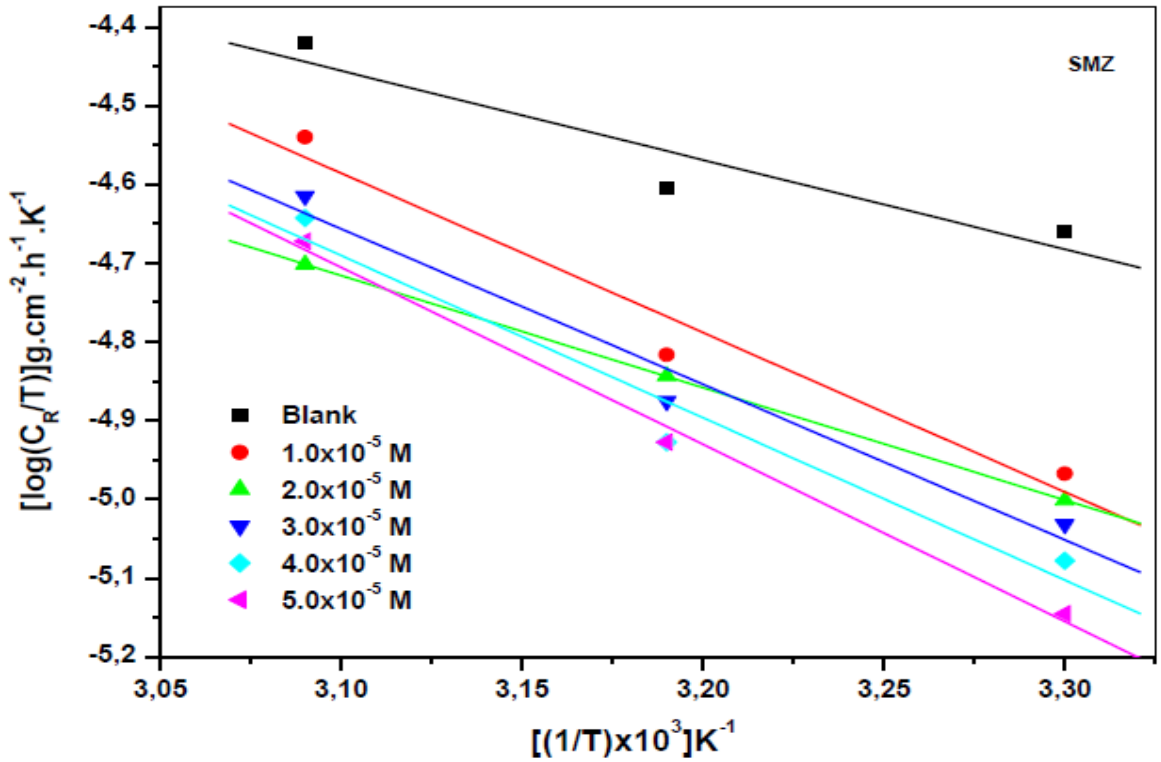

Figure 4.222: Transition state plots for the corrosion of zinc in 1.0 M HCl in the absence and presence of various concentrations of SMZ corrosion inhibitor.

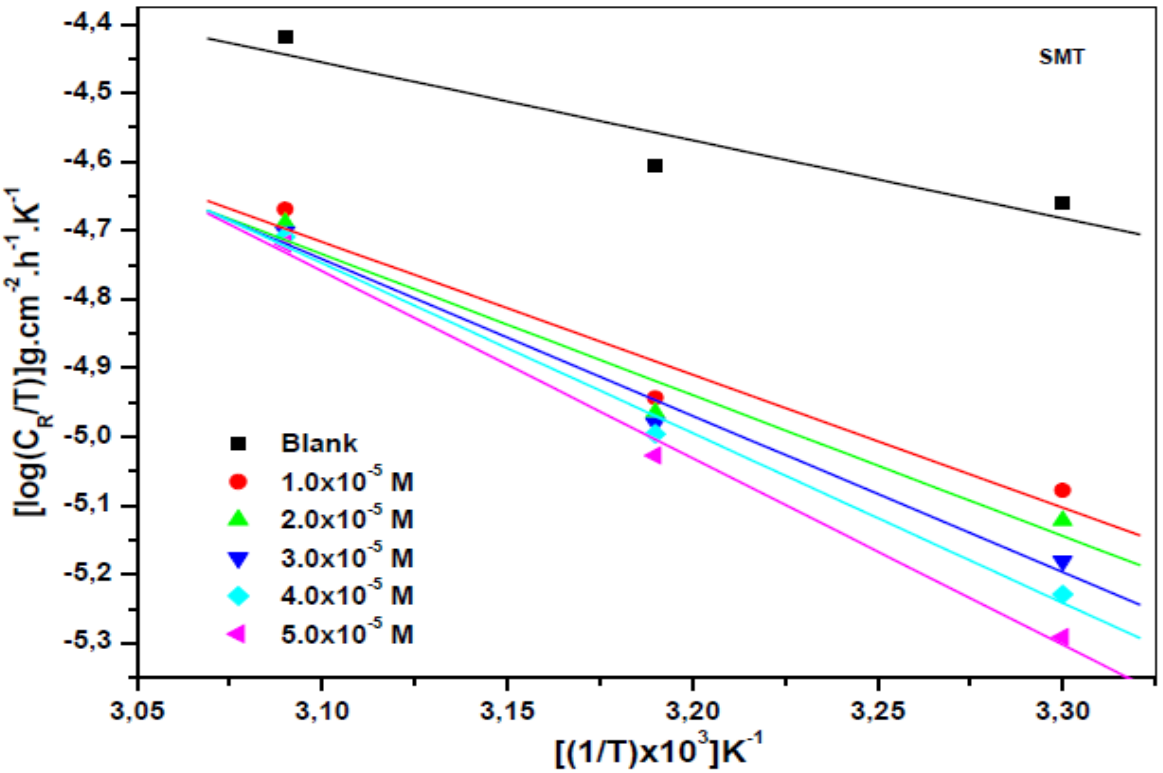

Figure 4.223: Transition state plots for the corrosion of zinc in 1.0 M HCl in the absence and presence of various concentrations of SMT corrosion inhibitor.

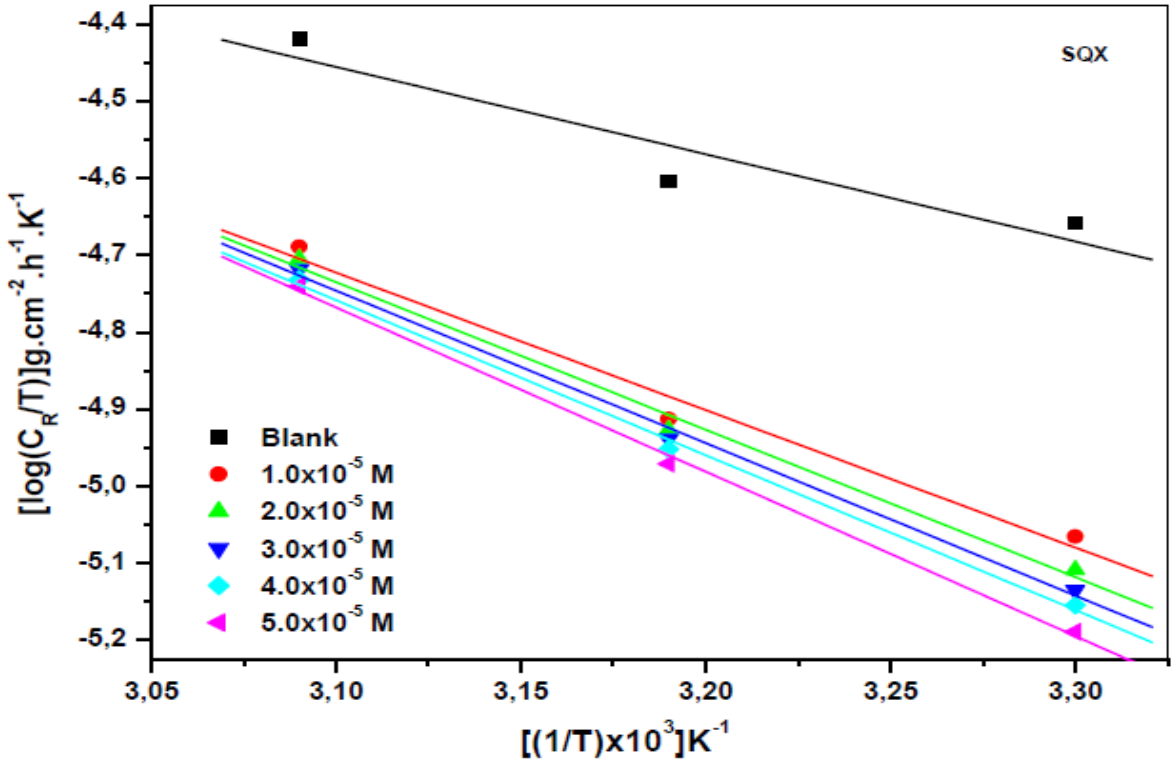

Figure 4.224: Transition state plots for the corrosion of zinc in 1.0 M HCl in the absence and presence of various concentrations of SQX corrosion inhibitor.

The positive signs of the ΔH^* values signifies that the adsorption of the nine inhibitor molecules SNA, SBZ, SMX, SCP, SDM, SSZ, SMZ, SMT and SQX is an endothermic reaction. Table 4.18 presents the values of enthalpy of activation that are close to the threshold value of 41.86 kJ.mol^{-1} which is the range of physisorption therefore this indicates that the inhibition process is an electrostatic interaction between the charged adsorbate and charged surfaces of the substrate [174]. It is observed that the values of enthalpy for SMX range between 51.25 kJ.mol^{-1} and 65.77 kJ.mol^{-1}. The type of adsorption between zinc surface and SMX inhibitor is the associated with chemisorptions. It is observed that in the absence of the inhibitor the value of enthalpy is 21.74 kJ.mol^{-1}. This value is increased to 51.25 kJ.mol^{-1} after the addition of 1.0×10^{-5} M of SMX inhibitor. It shows that addition of the inhibitor to the system reduced the rate of corrosion. Reduction of metal dissolution is further observed as the concentration of the inhibitor is increased. At 2.0×10^{-5} M, 3.0×10^{-5} M, 4.0×10^{-5} M and 5.0×10^{-5} M of SMX, the obtained values of enthalpy are 54.88, 57.80, 61.47 and 65.77 kJ.mol^{-1}, respectively. Similar trend of increasing enthalpy values with concentration is observed after the addition of all other inhibitors utilized. The values are relatively high with the highest concentration of 5.0×10^{-5} M with regard to all inhibitors.

Formation of a coordinate bond between zinc surface and the inhibitor forms a permanent layer of adsorption on the zinc surface. This layer results in higher inhibition efficiency and decreases the rate of corrosion significantly. The high values of enthalpy and activation energy are reinforcing the obtained values of inhibition efficiency. Therefore, based on activation energy and enthalpy values the adsorption processes of the nine sulphonamides are efficient towards the minimization of zinc corrosion.

The other contributing factor is the entropy of activation which is the measure of how disordered the metal surface can be after exposure to a corrosive environment. Equation 50 gives the values of entropy at different concentration for the inhibitors used under the study. Kairi *et al* reported that the negative values of ΔS^* imply that the disordering of the system on going from the reactants to the products has increased [175]. A list of entropy values obtained is presented by Table 4.18. It is observed that the value of -216.14 $kJ.mol^{-1}$ is obtained for the uninhibited system. The high negative value of entropy implies that the disordering of the zinc surface is increased on going to the activated complex. After addition of 4.0×10^{-5} M SMX, the decreased in the entropy was observed. That is, ΔS^* decreased to a value of -128.44 $kJ.mol^{-1}$. Increasing the concentration of this sulphonamide to 2.0×10^{-5} M, 3.0×10^{-5} M, 4.0×10^{-5} M and 5.0×10^{-5} M of SMX, yielded the entropy values of -117.29, -108.59, -97.490 and -84.470 $kJ.mol^{-1}$, respectively. As the concentration is increased the entropy values are observed to decrease which indicates that the rate of metal dissolution has decreased hence an increased efficiency of the inhibitor. In summary, addition of all these inhibitors give the entropy values that are moving towards the positive as the concentration is increased.

The positive values obtained after the addition of the inhibitor indicates the driving force that can overcome the barriers for the adsorption of the inhibitor on the zinc surface. The increasing ordering effect on the zinc surface is observed when all nine inhibitors are introduced. The positive values of entropy can be related to the inhibition efficiency of the sulphonamides since the disordering of the metal surface has decreased and the efficiency has increased. The results show that the order of inhibition efficiency by the sulphonamides follows the order: SBZ > SMX > SNA > SSZ > SCP > SMT > SDM > SQX > SMZ

4.3.7 ADSORPTION ISOTHERMS AND THERMODYNAMIC PARAMETERS

Adsorption isotherms can be utilized to describe the mechanisms followed during the adsorption process between the metal surface and the inhibitor [176, 177]. The adsorption of the inhibitor depends on the charge of the metal, the nature of the chemical structure of the organic product and the type of electrolyte [178].In order to obtain the adsorption isotherm corresponding to the studied compounds, several isotherms were applied and they include the Frumkin, Flory-Huggins, Freundlich, Temkin, Bockris-Swinkles and Langmuir adsorption isotherms. The best linear relationship was attained by plotting the concentration of the inhibitor/ surface coverage against the concentration of the inhibitor. This is also known as the Langmuir adsorption isotherm. With regard to the Langmuir adsorption isotherm, the surface coverage (θ) of the inhibitor on the mild steel surface is related to the concentration (C_{inh}) of the inhibitor in the bulk of the solution according to equation (60). The Langmuir adsorption isotherm plots for the adsorption of sulphonamides on zinc surfaces are shown in Figures 4.225−4.233. The values of R^2 and slopes for the sulphonamide inhibitors are recorded in Table 4.19.

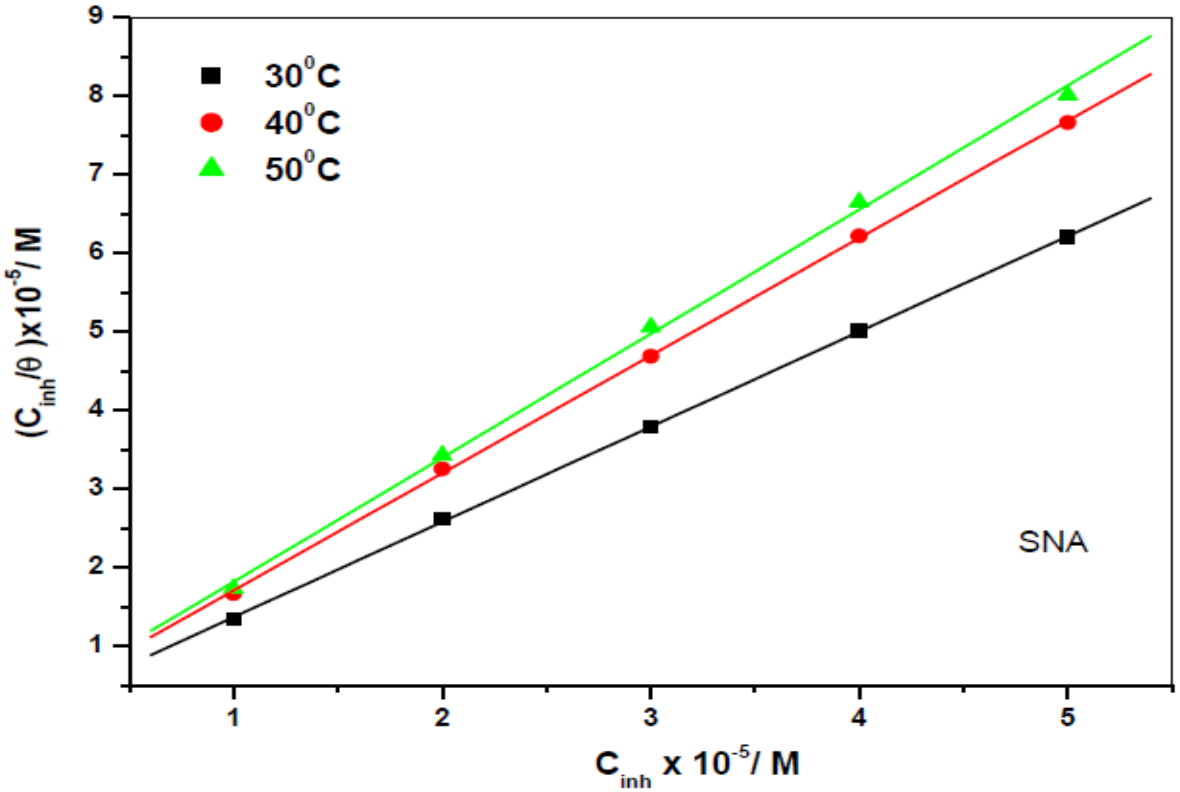

Figure 4.225: Langmuir adsorption isotherms for the corrosion of zinc in 1.0 M HCl at various temperatures for SNA corrosion inhibitor.

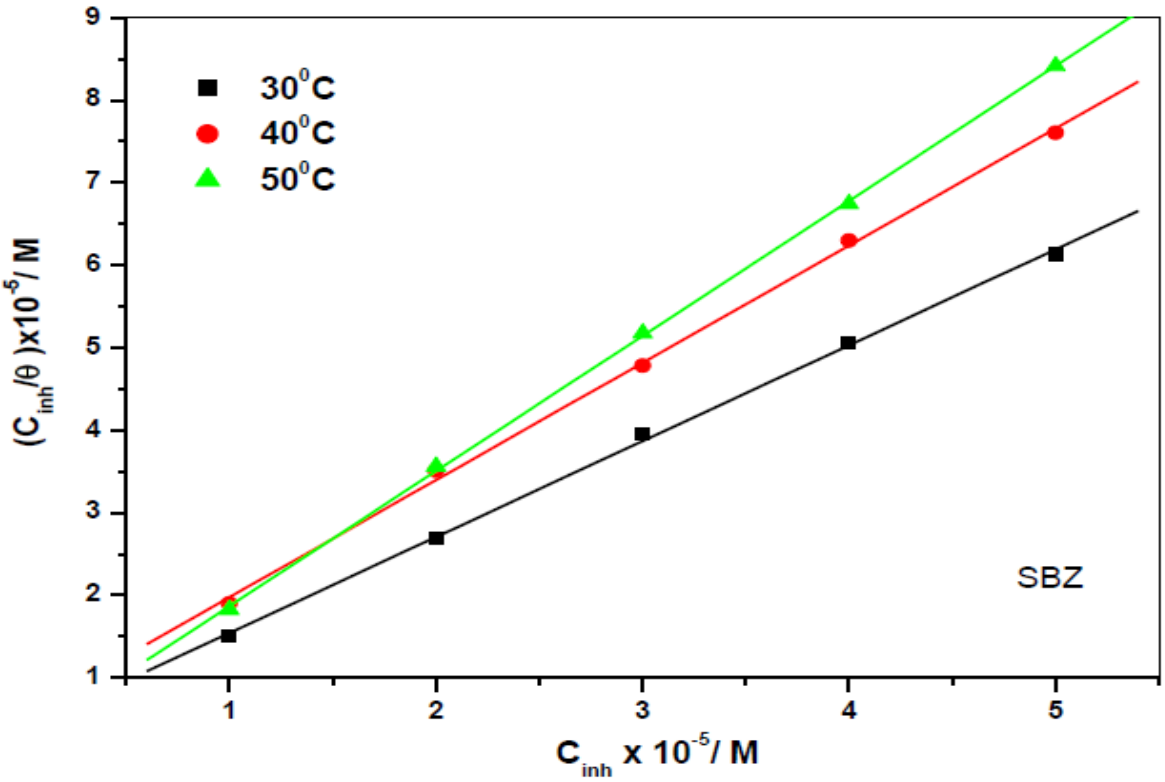

Figure 4.226: Langmuir adsorption isotherms for the corrosion of zinc in 1.0 M HCl at various temperatures for SBZ corrosion inhibitor.

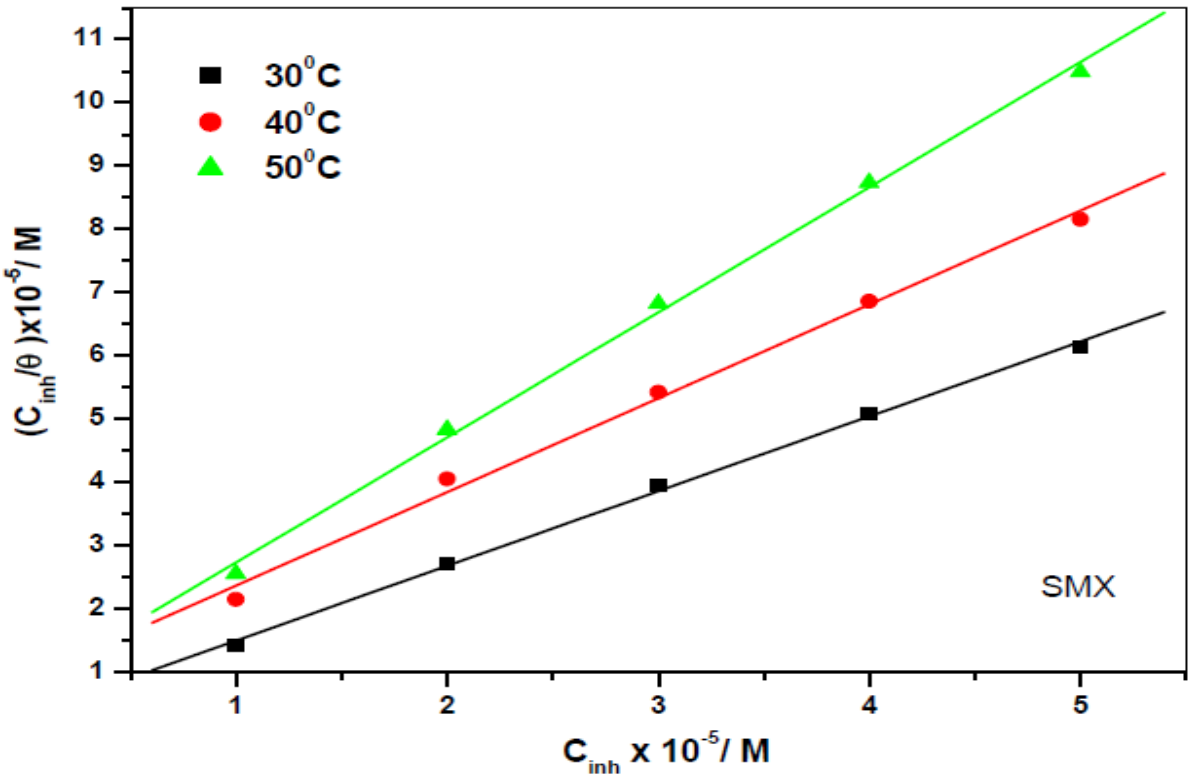

Figure 4.227: Langmuir adsorption isotherms for the corrosion of zinc in 1.0 M HCl at various temperatures for SMX corrosion inhibitor.

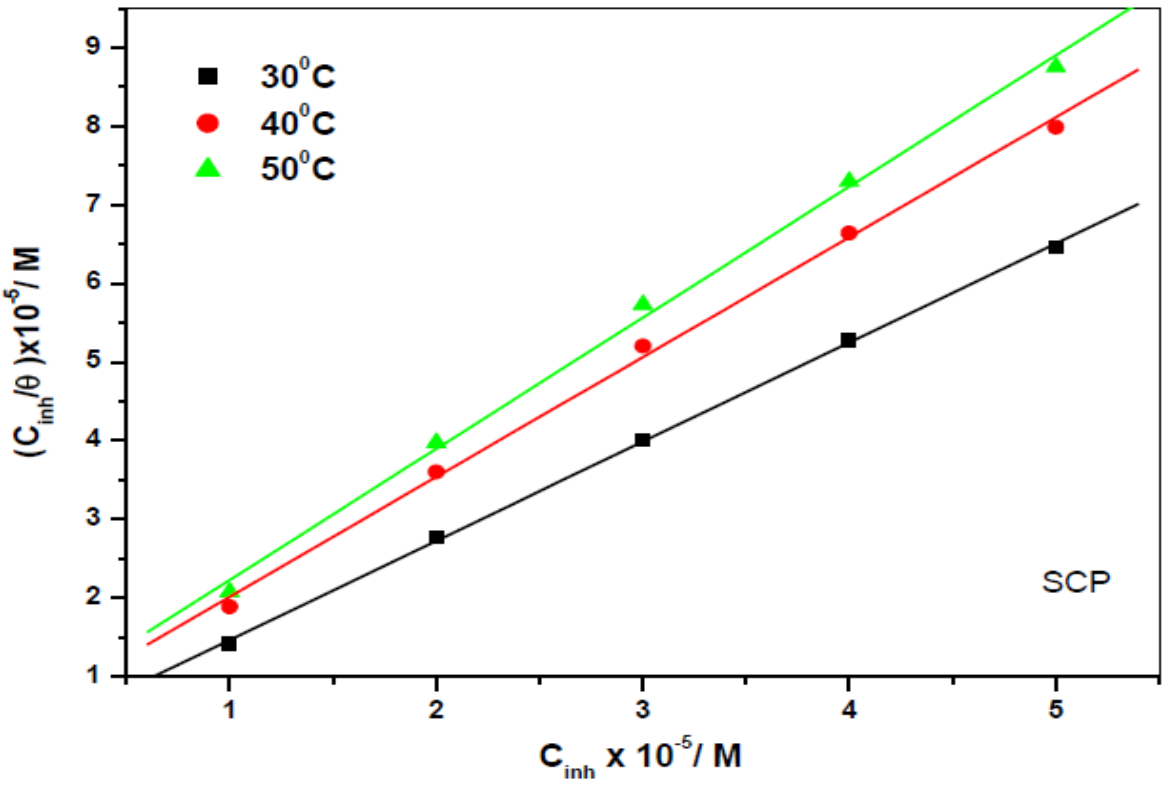

Figure 4.228: Langmuir adsorption isotherms for the corrosion of zinc in 1.0 M HCl at various temperatures for SCP corrosion inhibitor.

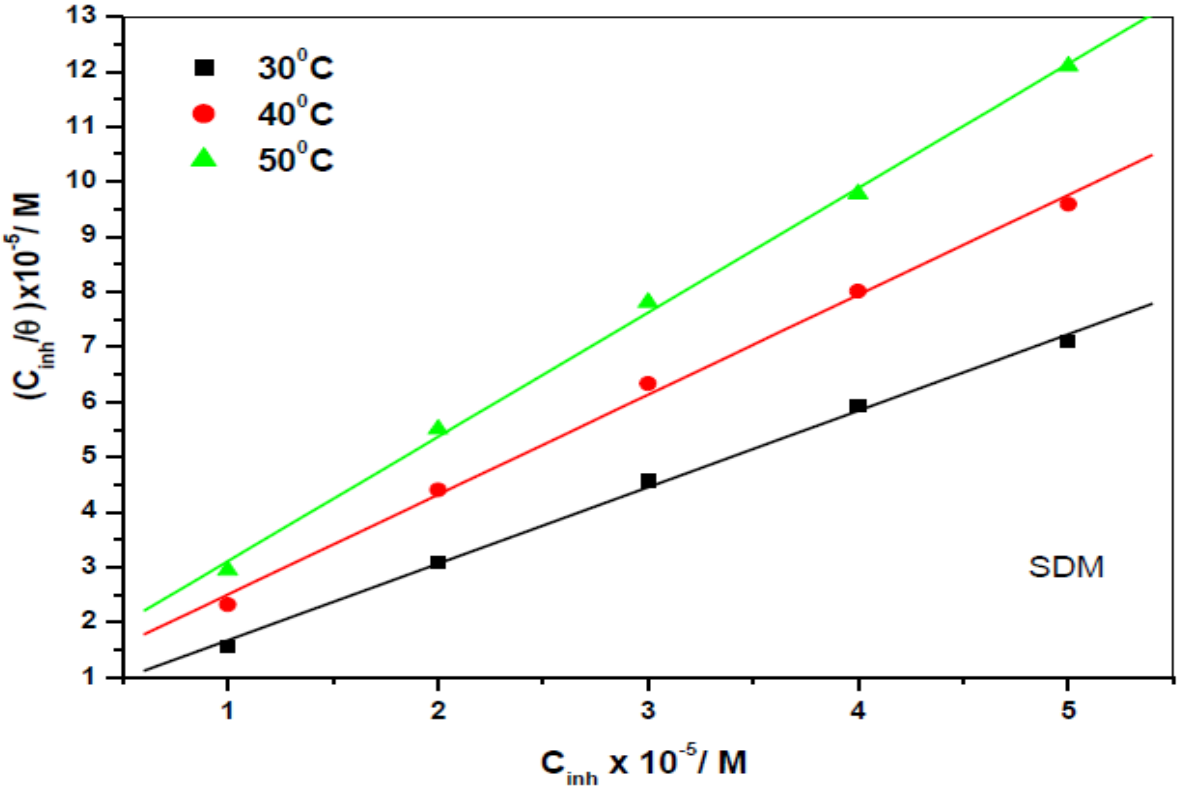

Figure 4.229: Langmuir adsorption isotherms for the corrosion of zinc in 1.0 M HCl at various temperatures for SDM corrosion inhibitor.

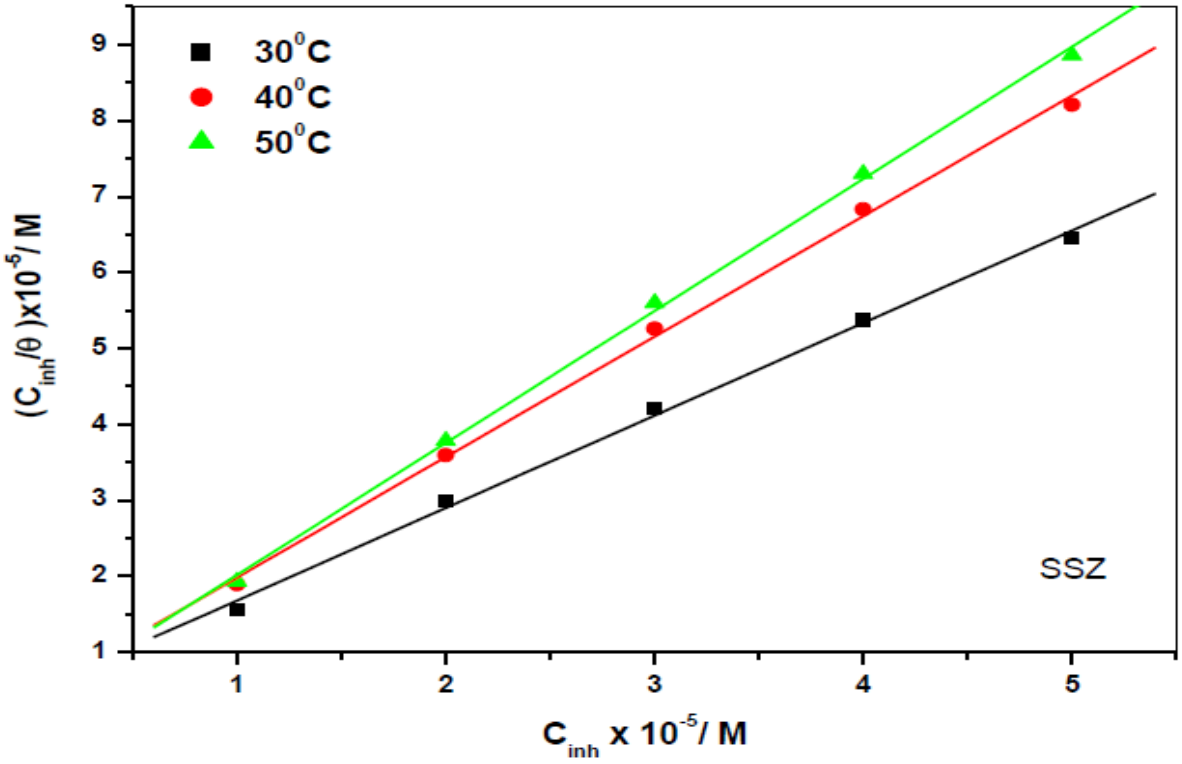

Figure 4.230: Langmuir adsorption isotherms for the corrosion of zinc in 1.0 M HCl at various temperatures for SSZ corrosion inhibitor.

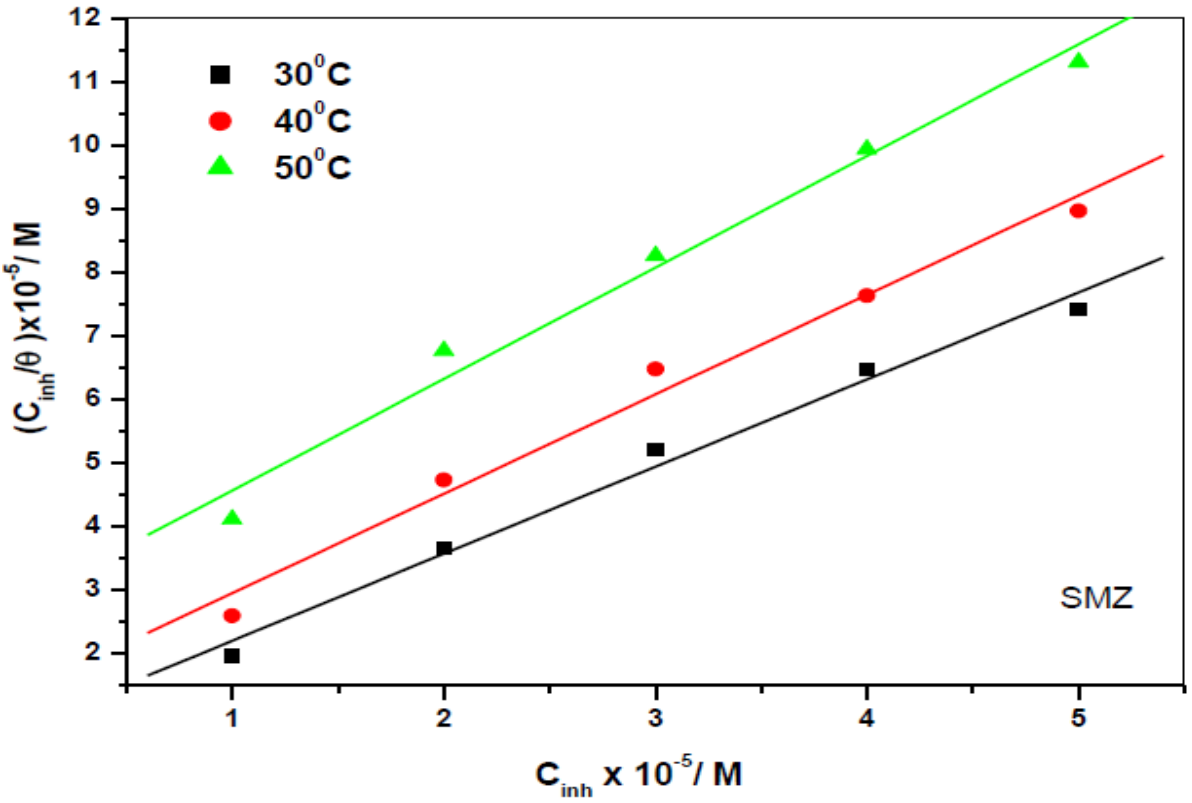

Figure 4.231: Langmuir adsorption isotherms for the corrosion of zinc in 1.0 M HCl at various temperatures for SMZ corrosion inhibitor.

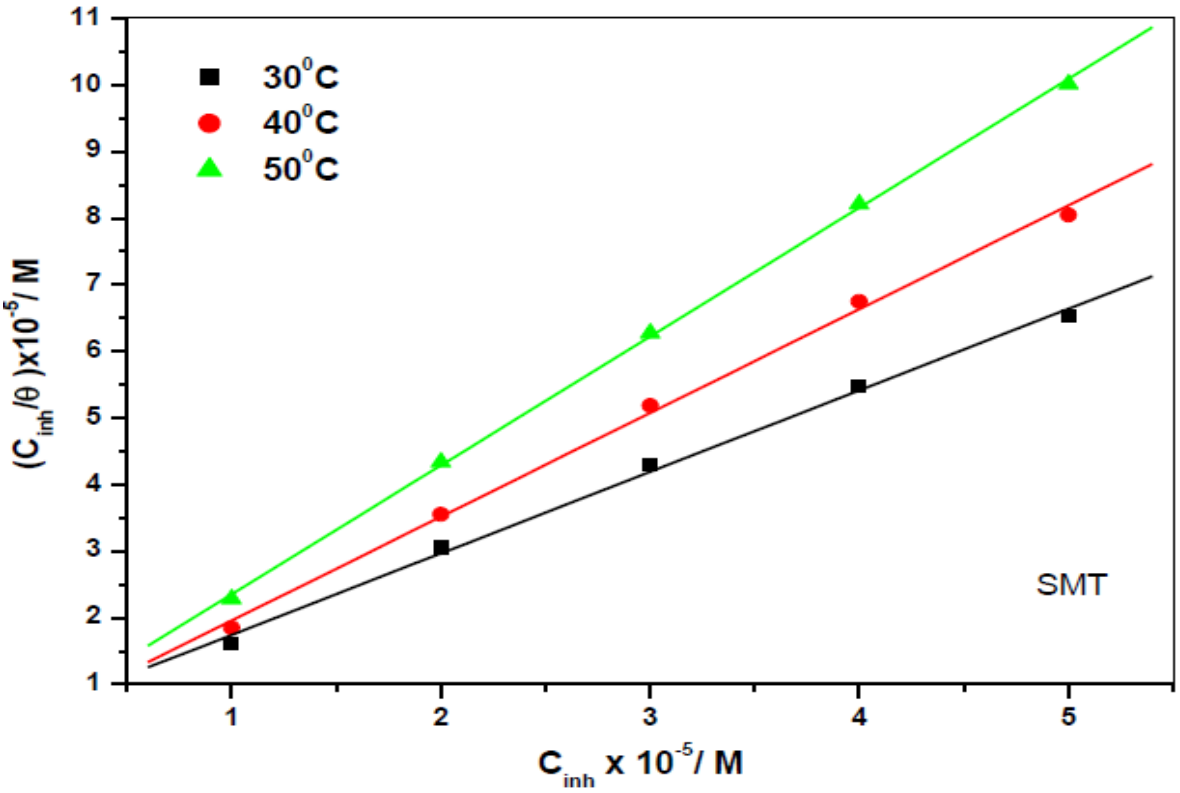

Figure 4.232: Langmuir adsorption isotherms for the corrosion of zinc in 1.0 M HCl at various temperatures for SMT corrosion inhibitor.

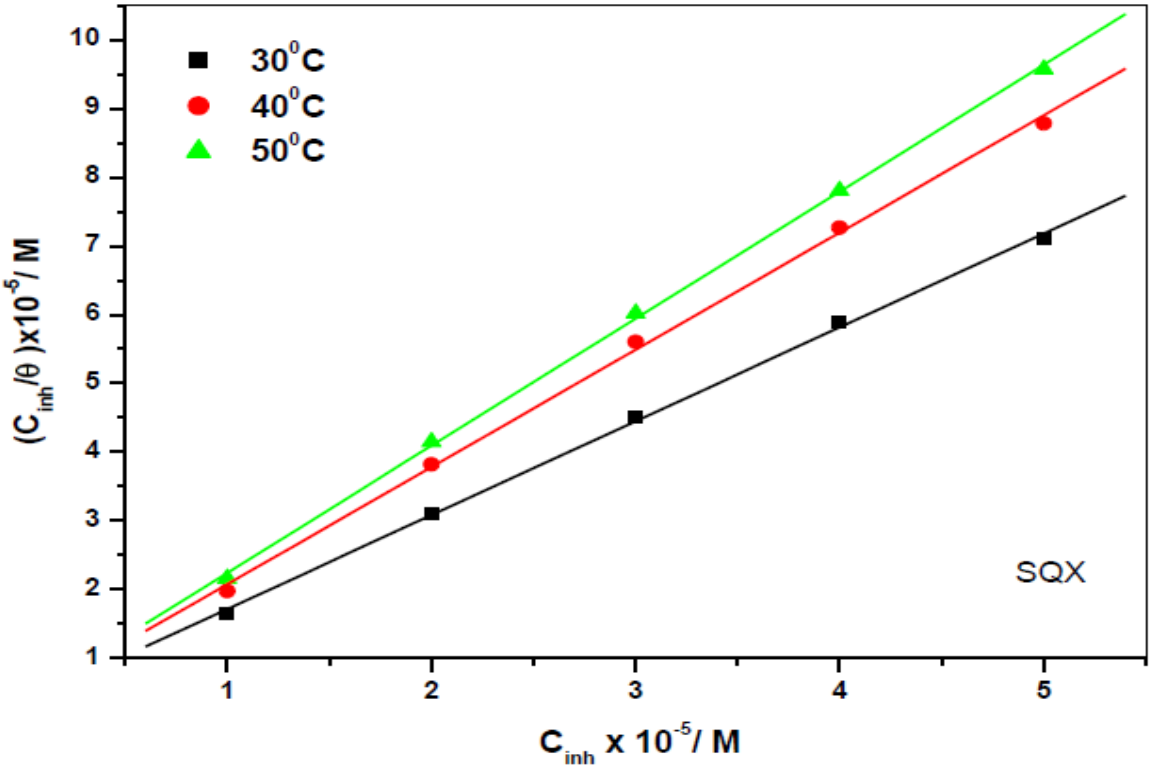

Figure 4.233: Langmuir adsorption isotherms for the corrosion of zinc in 1.0 M HCl at various temperatures for SQX corrosion inhibitor.

The values of the slope obtained from the Langmuir regression line in Table 4.19 indicate the type of layer formed on the zinc surface by the adsorbed inhibitor. The closeness of the slope to unity signifies that type of the layer is monolayer [179, 180]. The SNA has slopes of 1.211, 1.444 and 1.578.

Table 4.19: Thermodynamic and adsorption parameters (Langmuir adsorption isotherms) for zinc in 1.0 M HCl at various temperatures for the utilized corrosion inhibitors.

Inhibitor	Temperature (°C)	r^2	Slope	K_{ads} (M^{-1})	ΔG^0_{ads} ($kJ.mol^{-1}$)
SNA	30	0.999	1.211	6.513	–14.83
	40	0.999	1.444	4.773	–14.51
	50	0.999	1.578	4.220	–14.65
SBZ	30	0.999	1.162	2.621	–12.54
	40	0.999	1.420	1.798	–11.97
	50	0.999	1.637	4.301	–14.70
SMX	30	0.998	1.181	3.152	–13.01
	40	0.997	1.482	1.132	–10.77
	50	0.998	1.977	1.324	–11.53
SCP	30	0.999	1.261	4.922	–14.59
	40	0.998	1.524	2.043	–26.30
	50	0.998	1.668	1.782	–12.33
SDM	30	0.998	1.389	3.518	–13.28
	40	0.998	1.813	1.448	–11.41
	50	0.999	2.257	1.173	–11.21
SSZ	30	0.998	1.218	2.169	–12.06
	40	0.999	1.586	0.605	–09.43
	50	0.999	1.738	3.617	–14.23
SMZ	30	0.993	1.370	1.194	–10.56
	40	0.992	1.564	0.718	–09.59
	50	0.991	1.755	0.355	–08.05
SMT	30	0.998	1.223	1.920	–11.76
	40	0.998	1.558	2.494	–13.24
	50	0.999	1.933	2.370	–13.10
SQX	30	0.999	1.211	6.513	–14.83
	40	0.999	1.494	4.773	–14.51
	50	0.999	1.578	4.220	–14.65

The values of K_{ads} obtained can be further used to determine the free energy of adsorption (ΔG^{o}_{ads}) as follows:

$$k = \frac{1}{55.5}\exp\left[\frac{-\Delta G^{o}_{ads}}{RT}\right] \quad (64)$$

Where, ΔG^{o}_{ads} is the Gibbs free energy of adsorption, the value 55.5 is the molar concentration of water in solution, T is the absolute temperature and K_{ads} is the equilibrium constant for the adsorption process. It has been reported by many authors that the values of ΔG^{o}_{ads} varying between –40 kJ.mol^{-1}and above are associated with the sharing or transfer of an electron from the adsorbate to the surface of the substrate to form a coordinate type of bond (chemical adsorption mechanism) while those that are –20 kJ.mol^{-1} and lower indicated physisorption (physical adsorption mechanism) [179, 180]. Physical adsorption occurs by weak Van Der Waals type of forces, no bond formed between adsorbate and substrate surface.

The negative values of ΔG^{o}_{ads} indicate the stability of the adsorbed layer on the metal surface and spontaneity of the adsorption process while positive values symbolize a non-spontaneous adsorption process. Table 5.21 has the values of ΔG^{o}_{ads} which are all negative which means that the adsorption process of the inhibitors on the zinc surface was spontaneous. All of the values of ΔG^{o}_{ads} fall between –20 kJ.mol^{-1}and –40 kJ.mol^{-1} range, except one value recorded for SSZ at 40°C and two values recorded for SMZ at 40°C and 50°C. Values of ΔG^{o}_{ads} as shown in Table 4.19 suggest both physisorption and chemisorption processes took place but predominantly physisorption.

4.3.8 COMPARISON OF THE EFFECTS OF THE SULPHONAMIDES INHIBITORS ON THE METALS SELECTED

This study focused on the use of nine (9) sulphonamide compounds as corrosion inhibitors for three different metals namely mild steel, aluminium and zinc in 1.0 M HCl solutions at 30-50 °C. The results obtained indicated that aluminium and zinc were more durable than mild steel at all temperatures studied. In comparison to zinc and mild steel, aluminium showed the optimum protection and the order of resistance to corrosion by all three metals is such that aluminium > zinc > mild steel. This may be attributed to the fact that aluminium produces an active adsorption protective film during acid corrosion. A detailed comparison of

the effects of these sulphonamides as corrosion inhibitors on these metals is shown in Table 4.20.

Table 4.20: Comparison of the effects of the selected sulphonamides as corrosion inhibitors on mild steel, aluminium and zinc in 1.0 M HCl.

Technique/Study	Metal		
	Mild Steel	**Aluminium**	**Zinc**
EIS	• Pseudo-capacitive behaviour from n values. • Circuit for data fitting: $R_s(R_{ct}Q)$ • Nyquist plots: Imperfect semicircles.	• More capacitive behaviour than MS and Zn from n values. • Circuit for data fitting: $R_s[(R_{ct1}Q_1)(R_{ct2}Q_1)]$ • Nyquist plots: Imperfect semicircles showing more pronounced passive region	• More capacitive behaviour than MS but less Al from n values. • Circuit for data fitting: $R_s(R_{ct}Q)$ • Imperfect semicircles on the Nyquist plots.
PDP	• Consistent E_{corr} values. • b_a (02–50 $mV.dec^{-1}$) and b_c (11–58 $mV.dec^{-1}$). • Mixed-type inhibition.	• Consistent E_{corr} values. • b_a (0.09–37 $mV.dec^{-1}$) and b_c (0.05–69 $mV.dec^{-1}$). • Mixed-type inhibition.	• Consistent E_{corr} values. • b_a (07–53 $mV.dec^{-1}$) and b_c (04–26 $mV.dec^{-1}$). • Mixed-type inhibition.
FTIR	• Fe^{3+}–inhibitor complexes and SO_2 functional group from the sulphonamide compounds was the most preferred site for interaction with the mild steel surface.	• Al – inhibitor complexes and aromatic ring (though C=C) and SO_2 (through O atom) were the most preferred site for interaction with the aluminium surface.	• Zn – inhibitor complexes and aromatic rings (though C=C) and SO_2 (through O atom) and C–N (through N atom) were the most preferred site for interaction with the zinc surface.
SEM	• SEM/EDS showed the presence of Fe, traces of sulphonamides and Cl^- ions.	• SEM/EDS showed the presence of Al, traces of sulphonamides and Cl- ions.	• SEM/EDS showed the presence of Zn, traces of sulphonamides and Cl- ions.
Adsorption and Adsorption Isotherms	• Obeys Langmuir model • ΔG values (-07.83 to -14.67 $kJ.mol^{-1}$) show mixed-type inhibition with predominant physisorption. • Spontaneous adsorption.	• Obeys Langmuir model • ΔG values (-07.15 to -17.86 $kJ.mol^{-1}$) show mixed-type inhibition. • More spontaneous adsorption than in MS.	• Obeys Langmuir model • ΔG values (-09.43 to -26.30 $kJ.mol^{-1}$) show mixed-type inhibition with predominant physisorption. • More spontaneous than in MS and Al.

4.4 QUANTUM CHEMICAL CALCULATIONS

4.4.1 Results of the calculations in vacuo

The results that are obtained from the gravimetric analysis and electrochemical methods are further strengthened by the quantum chemical calculations which are very important since they provide crucial information regarding the reactivity and selectivity parameters of the inhibitor molecules [181].

Inhibitor molecules possess a variety of regions within themselves; this means that these regions have different tendencies of interactions with the surface of the metal. The reactivity and selectivity parameters can be utilized to determine and identify the molecular regions that have the tendency to react with the surface of the metal [182]. The reactivity of inhibitor compounds depends on the electronic properties such as electron density, partial charges on the atoms and dipole moment, among others. These electronic properties have their influence from the type and nature of the functional groups that are within the inhibitor molecules [182]. In this section, detailed information regarding the reactivity and selectivity parameters for the nine different sulphonamides compounds utilized in this study will be presented.

The schematic representations of these compounds and the atom numbering that is utilized in the discussion of the results are shown in Figure 3.1. Figure 4.234 shows the optimised geometries for the nine different sulphonamides compounds utilized in this study. The geometry of the molecules is of crucial importance during the selection of the inhibitor compounds due to the fact that the inhibition efficiency of these compounds also depends on the geometry of the compound. Compounds with planar geometry show better inhibition efficiency than those of less planar geometry [183]. This is due to the fact that planar geometry inhibitor compounds have better chances of covering a wide area of the surface of the metal than the less planar geometry ones. Moreover, compounds with more planar geometry have most of their atoms in contact with the surface of the metal, while the ones with less planar geometry have a limited number of their atoms in contact with the surface of the metal during the inhibitor-metal inhibition process.

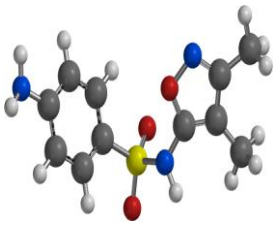

Sulphisoxazole (SSZ)

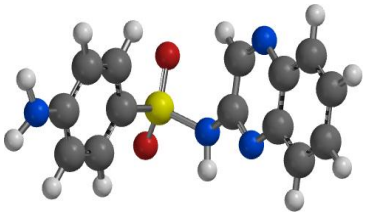

Sulphaquinoxaline (SQX)

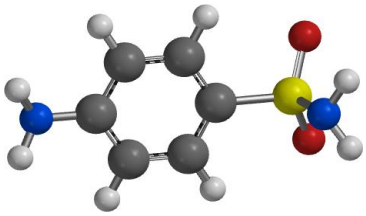

Sulphanilamide (SNA)

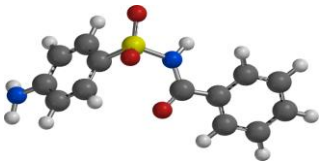

Sulphabenzamide (SBZ)

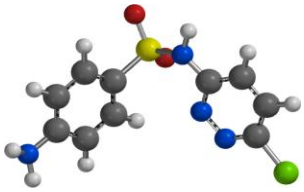

Sulphachloropyridazine (SCP)

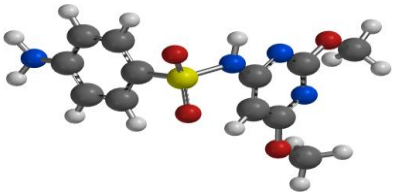

Sulphadimethoxine (SDM)

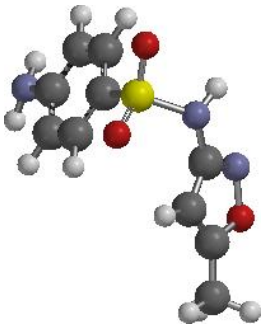

Sulphamethoxazole (SMX)

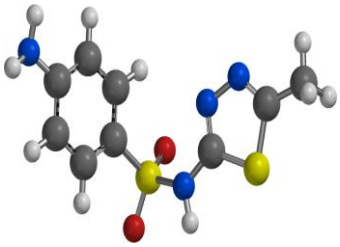

Sulphamethizole (SMZ)

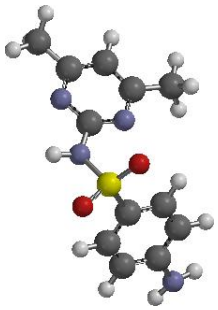

Sulphamethazine (SMT)

Figure 4.234: The optimized geometries of the studied sulphonamides compounds.

The reactive sites of the molecules can be better studied by analysing the Highest Occupied Molecular Orbital (HOMO) and the Lowest Unoccupied Molecular Orbital (LUMO) while the reactivity trend can be identified by studying the reactivity parameters such as the energy of the HOMO (E_{HOMO}), energy of the LUMO (E_{LUMO}), global softness, global hardness, Electron Affinity (EA), ionisation potential (IP)) and electronegativity (χ). The HOMO and LUMO of each of the studied sulphonamides are shown in Figures 4.235 and 4.236, respectively.

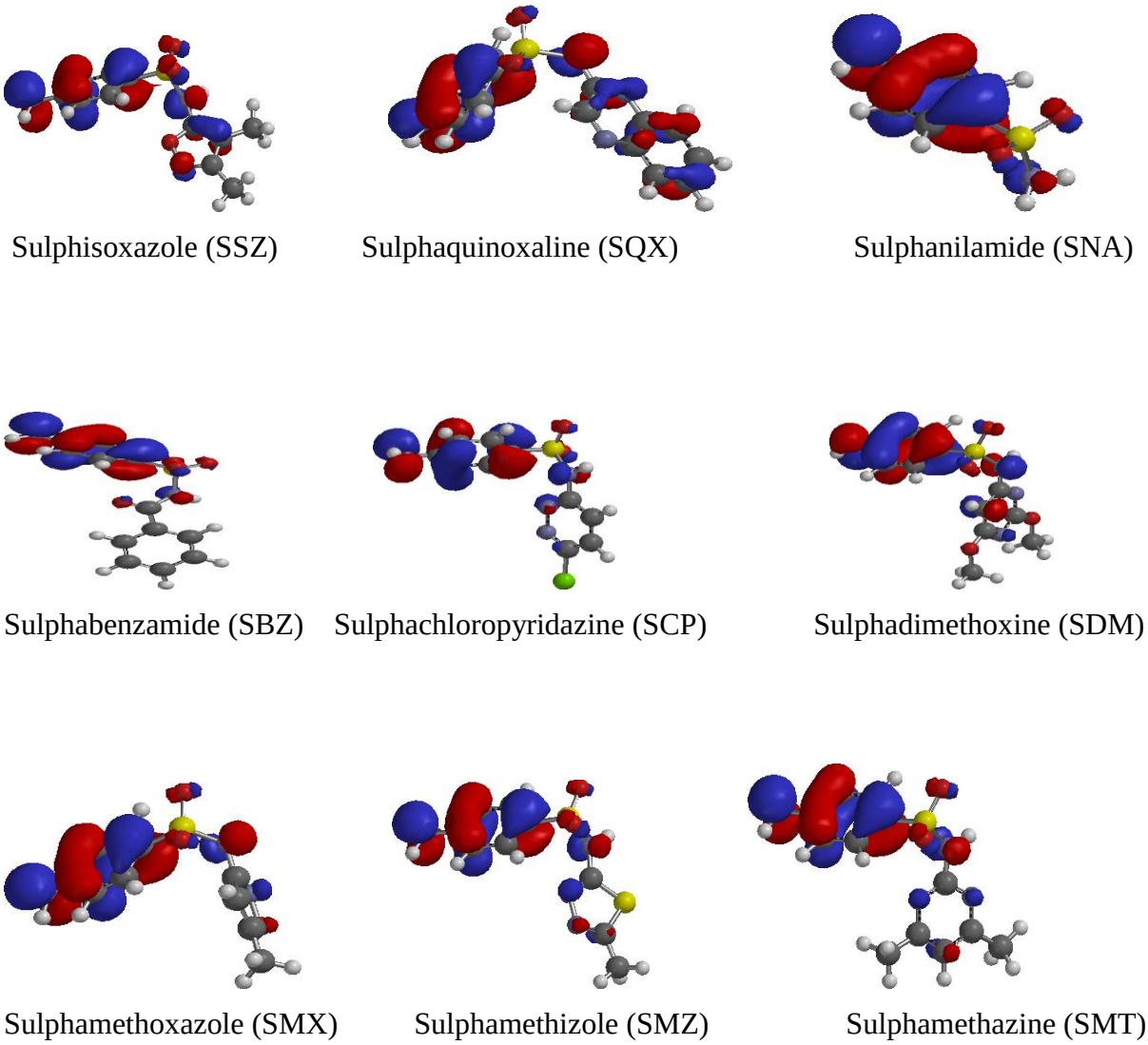

Sulphisoxazole (SSZ) Sulphaquinoxaline (SQX) Sulphanilamide (SNA)

Sulphabenzamide (SBZ) Sulphachloropyridazine (SCP) Sulphadimethoxine (SDM)

Sulphamethoxazole (SMX) Sulphamethizole (SMZ) Sulphamethazine (SMT)

Figure 4.235: The HOMO for the studied sulphonamides obtained from (B3LYP/6-31G(d,p) results *in vacuo*)

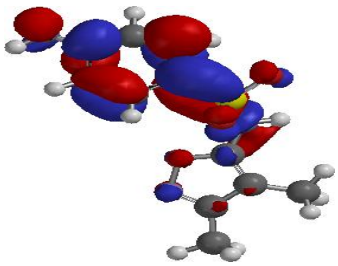

Sulphisoxazole (SSZ)

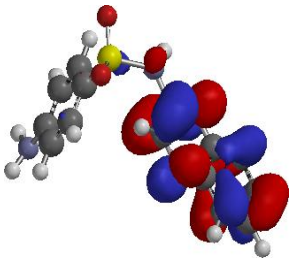

Sulphaquinoxaline (SQX)

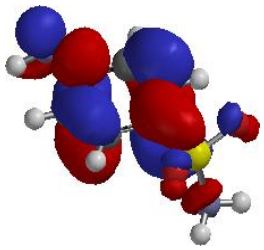

Sulphanilamide (SNA)

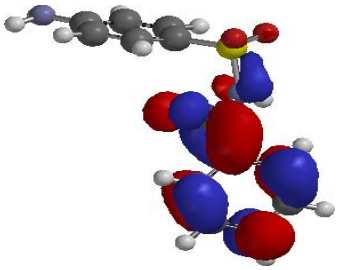

Sulphabenzamide (SBZ)

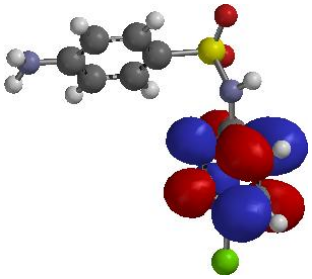

Sulphachloropyridazine (SCP)

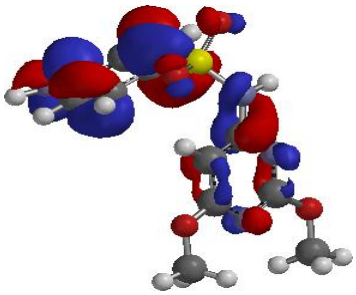

Sulphadimethoxine (SDM)

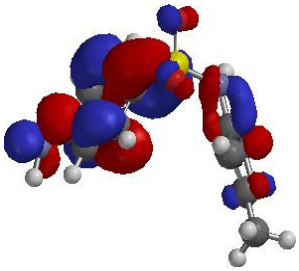

Sulphamethoxazole (SMX)

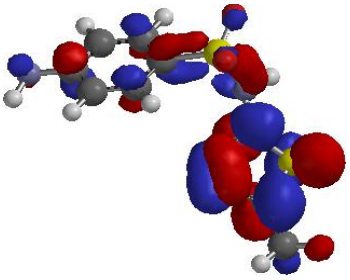

Sulphamethizole (SMZ)

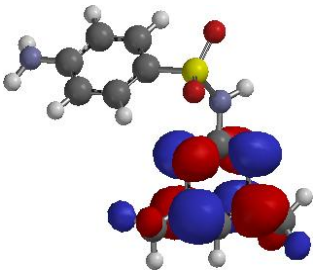

Sulphamethazine (SMT)

Figure 4.236: The LUMO for the studied sulphonamides obtained from (B3LYP/6-31G(d,p) results *in vacuo*)

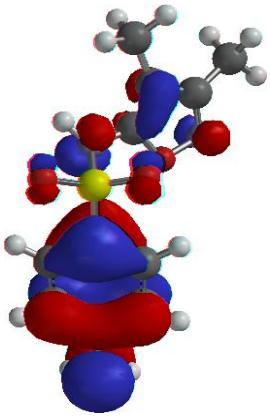

Sulphisoxazole (SSZ)

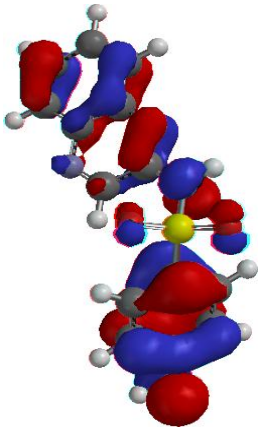

Sulphaquinoxaline (SQX)

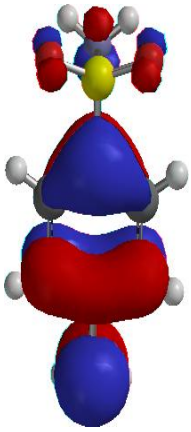

Sulphanilamide (SNA)

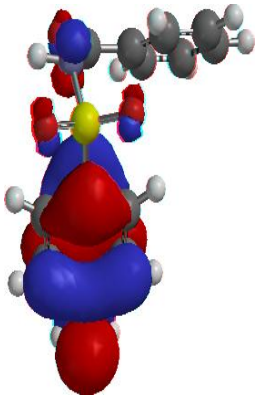

Sulphabenzamide (SBZ)

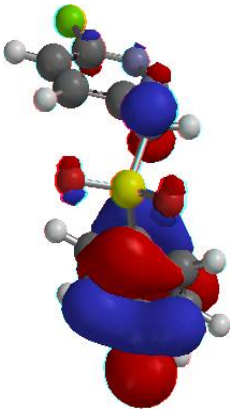

Sulphachloropyridazine (SCP)

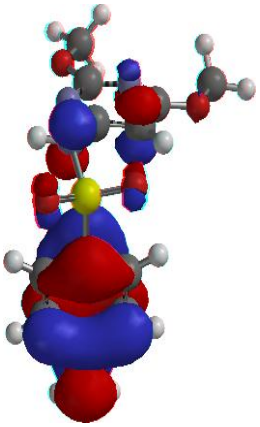

Sulphadimethoxine (SDM)

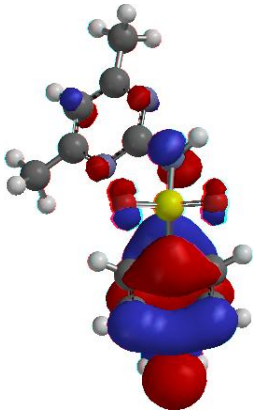

Sulphamethoxazole (SMX)

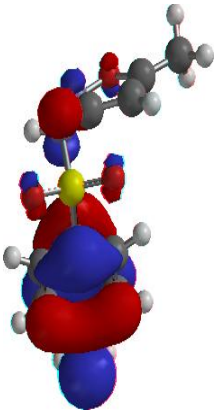

Sulphamethizole (SMZ)

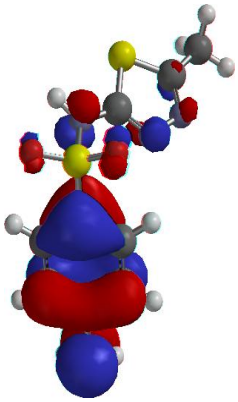

Sulphamethazine (SMT)

Figure 4.237: The HOMO densities for the studied sulphonamides obtained for neutral species.

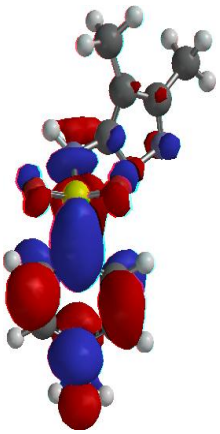

Sulphisoxazole (SSZ)

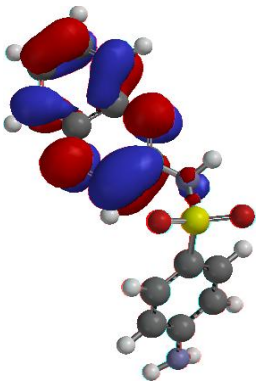

Sulphaquinoxaline (SQX)

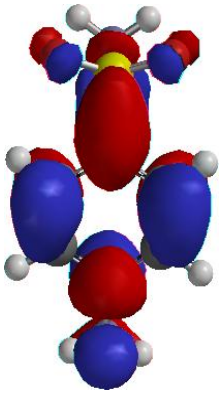

Sulphanilamide (SNA)

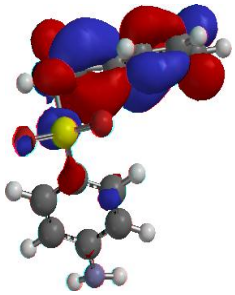

Sulphabenzamide (SBZ)

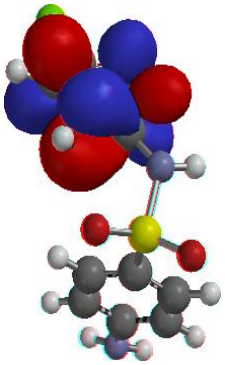

Sulphachloropyridazine (SCP)

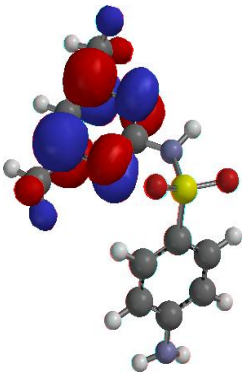

Sulphadimethoxine (SDM)

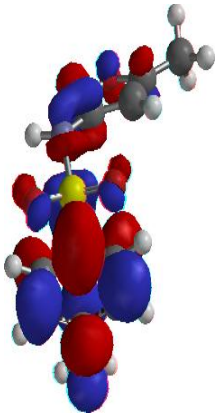

Sulphamethoxazole (SMX)

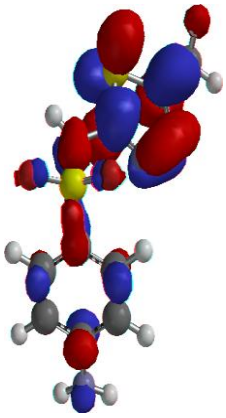

Sulphamethizole (SMZ)

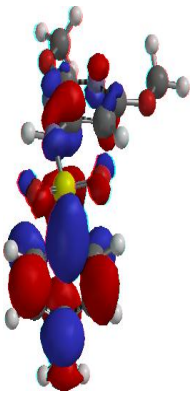

Sulphamethazine (SMT)

Figure 4.238: The LUMO densities for the studied sulphonamides obtained for neutral species.

The HOMO is considered to indicate the site on which electrophilic attach is likely to occur while the LUMO indicates the sites on which the nucleophilic attack is likely to occur. Analysis of the HOMO densities for the neutral species shows that the highest HOMO densities occurs on C2, C4, C5 and C6), the amino N1, O9 and O10 atoms for all the sulphonamides investigated. This result indicates that these are the preferred sites for electrophilic attack. The preference for the atoms in the aromatic ring to donate electrons to the metal atoms is related to the fact that the aromatic ring has π electrons which are available for donation to the metal atoms. The HOMO density on the N1, O9 and O10 atoms correspond to the lone pair of electrons in the non-bonding p orbital. The amino N1 atom has a higher HOMO density than either O9 or O10 due to the fact that O atom has higher electronegativity than the N atom and therefore it has greater tendency to hold onto its lone pair of electrons than the N atom. It is therefore expected that the amino group would have greater tendency to donate electrons to the metal surface than the O=S=O group. The HOMO is also delocalised on N11 in sulphadimethoxine, sulphamethoxazole, sulphamethizole and sulphisoxazole, C17 in sulphadimethoxine.

The LUMO density provides information on the nucleophilic attack sites. In terms of corrosion mechanism, this possibility is only applicable when the metal surface has the ability to back-donate electrons to the inhibitor molecule. Analysis of the LUMO density for the studied neutral sulphonamides shows that it is delocalized throughout the molecule in SNA, SDM, SMX, SBZ, SCP and SMT. In SQX, it is localized only in aromatic ring attached to S8 and in SMZ in aromatic ring attached to N11.

Table 4.21 reports the molecular quantum chemical parameters that are related to the reactivity of the sulphonamides that are utilized in this study. These parameters include E_{HOMO}, E_{LUMO}, the energy gap ($\Delta E = E_{HOMO} - E_{LUMO}$), molecular polarizability and dipole moment.

Molecular orbital theories of chemical reactivity such Frontier Molecular Orbital Theory (FMO) informs that the interactions between the HOMO and LUMO of reacting species is responsible for the transition of electron during the adsorption process between the metal surface and the inhibitor compound [181]. The tendency regarding the donation of an electron by a molecule is normally measured by the E_{HOMO}. This means that higher values of E_{HOMO} are associated with a higher tendency to donate electrons by the molecule to the electron deficient species [181, 182]. Thus, compounds possessing higher values of E_{HOMO} exhibit a

better inhibition efficiency of the corrosion of metals due to the fact that the adsorption of the inhibitor molecule on the metal surface is enhanced.

Table 4.21: The molecular properties for studied sulphonamides obtained from (B3LYP/6-31G(d,p) results *in vacuo*).

Molecular Property	**Inhibitor Compound**								
	SBZ	**SCP**	**SDM**	**SMX**	**SMZ**	**SNA**	**SQX**	**SMT**	**SSZ**
E_{HOMO} (eV)	-6.25	-6.24	-6.31	-6.33	-6.23	-6.19	-6.34	-6.28	-6.23
E_{LUMO} (eV)	-1.57	-2.03	-1.04	-1.06	-0.96	-0.72	-2.09	-1.28	-0.95
ΔE (eV)	4.68	4.21	5.27	5.27	5.27	5.47	4.25	4.96	5.23
μ	7.30	6.36	7.88	6.94	6.23	6.12	7.61	7.59	4.48
logP	1.58	1.52	1.39	0.14	1.42	-0.26	1.41	0.62	1.27
MP	61.35	59.82	62.91	58.69	58.93	52.49	62.91	61.53	60.19
η	2.340	2.105	2.635	2.635	2.635	2.735	2.125	2.500	2.640
σ	0.427	0.475	0.379	0.379	0.379	0.367	0.471	0.400	0.379
I (eV)	6.25	6.24	6.31	6.23	6.25	6.19	6.34	6.28	6.23
A (eV)	1.57	2.03	1.04	0.96	1.57	0.72	2.09	1.28	0.95
ω	3.267	4.061	2.563	2.452	2.452	2.182	4.174	2.858	2.411
χ	3.910	4.135	3.675	3.595	3.595	3.455	4.212	3.780	3.590

Table 4.21 suggests that the inhibitor compound possessing the highest E_{HOMO} value is SNA while the one with the lowest is SQX. SNA has a value of -6.19 eV while SQX has -6.34 eV. It is also very imperative to mention that the values of E_{HOMO} alone are not sufficient for us to draw final conclusions with regard to the adsorbability of the compound on the surface of the metal, thus the inhibition efficiency. When this is the case, a comparative study of the combination of several quantum chemical parameters is conducted, known as the Quantitative Structure Activity Relationship (QSAR).

The extent to which the molecule can accept electrons is indicated by E_{LUMO} values. Literature reveals that molecules that possess lower values of E_{LUMO} have a greater tendency to accept electrons from the species that are electron rich [184, 185]. From table 4.21, it can be observed that SNA has the highest value of -0.72 eV while SQX is the lowest at -2.09 eV. Further details regarding the reactivity of these compounds towards the metal surfaces can be obtained through a thorough investigation of the energy gap ΔE. The energy gap of the molecule can be directly related to its stability and consequently its tendency to react. Higher values of energy gap are associated with high stability of the compound and therefore a low tendency to react while lower values are associated with low stability of the compound and therefore a high tendency to react with other chemical species [186]. From the nine

compounds studied as reported in Table 4.21, SNA and SCP have the highest and lowest values of 5.47 eV and 4.21 eV, respectively.

The information regarding the polarity and reactivity of the studied compounds towards the metal surfaces can be obtained by studying their dipole moments (μ). As far as the corrosion studies are concerned, some researchers have reported that as the dipole moment increases the inhibition efficiencies of compounds also increases [183]. Other researchers observed that as the dipole moment increases the inhibition efficiencies of the compounds decreases [187]. Some literature indicates the fact that the dipole moment does not possess a good correlation with inhibition efficiencies of the studied compounds [188]. Table 4.21 also shows values obtained for the dipole moment related to the studied compounds. Nevertheless, a direct correlation to their inhibition efficiencies is not indicated by their trends.

One other imperative chemical reactivity parameter is the electronegativity (χ) of these compounds. This parameter gives information regarding the electron density within the molecule. In other words, electronegativity provides a measure of the power of an electron or a group of atoms to attract electrons towards itself [189]. This means that the compound with the highest electronegativity value possess the highest power to attract electrons or a group of atoms towards its direction. Table 4.21 indicates that SQX has the highest value of electronegativity while the lowest one is corresponding to SNA. Furthermore, the information that is provided by the electronegativity can be complemented by another reactivity parameter called global electrophilicity index (ω). Inhibitor molecules possessing higher values of global electrophilicity index are associated with good electrophiles where those with lower values are associated with good nucleophiles [189]. Nucleophiles are chemical species that donates a pair of electrons to electron-deficient specie to form a chemical bond during a chemical reaction. Electrophiles are those chemical species that accept a pair of electrons from the electron-rich specie to form a chemical bond during a chemical reaction. From the result reported in Table 4.21, the highest electrophilicity index value is corresponding to SQX while the lowest is corresponding to SNA. This would mean that SNA is a better nucleophile than SQX. Subsequently, SNA would have a higher tendency to donate electrons to the empty d orbitals of metals than SQX.

Global hardness (η) of the inhibitor compounds provides more insight regarding the resistance of an atom to a charge transfer. This implies that compounds with high values of global hardness have a higher resistance of their atoms to charge transfers. The inhibitor-

metal adsorption process would be easier with the inhibitor compound that possesses lower values of global hardness. The other molecular property that compliments global hardness is known as global softness (σ). Together these molecular properties assist in the reactivity and selectivity of the inhibitor compounds. Global softness is related to the softness of the molecule as far the reactivity is concerned. The inhibitor-metal adsorption process could take place easily at the region of the inhibitor compound where global softness possesses the highest value [190]. From our results in this investigation, global hardness values are in such a way that SNA correspond to the highest value of 2.735 and SCP to the lowest value of 2.105 as reported in Table 4.21. The values of global softness are in such a way that SCP ≈ SQX with the highest value of an average 0.47 while the lowest value of 0.367 is corresponding to SNA.

The ionization potential (I) is a molecular reactivity parameter which is very useful in the understanding of the reactivity and selectivity of inhibitor compounds. It gives information on the amount of energy that is required in order to remove an electron from the molecule [189]. In other words, the amount of energy that is released by a molecule during the inhibitor-metal adsorption process when an electron is lost can be predicted through an investigation of the ionization potential.

Beside molecular reactivity parameters, quantum chemical studies can also provide information on the molecular selectivity parameters, which include the charges on the atoms and the Fukui functions. Studies indicate that the partial atomic charges and the condensed Fukui functions are very useful parameters that provide information regarding the selectivity of the molecules [190], with some researchers having successfully managed to show that the partial atomic charges on the atoms crucial quantum chemical parameters associated with the studies of corrosion inhibitors and the corrosion inhibition process [191, 192]. Table 4.22 reports the partial atomic charges for the studied sulphonamides. It is observed from this table that the more negative charges are found on the heteroatoms N1, N11, O9 and O10. This observation is accounted for by the fact that the atoms caring the most negative charges are the ones that donate their electrons more easily [193]. It is therefore reasonable to say that during the corrosion inhibition process between a metal and the corrosion inhibitor, sulphanilamide would interact with the metal surface through the heteroatoms such as N and O. This trend in partial atomic charges is seen repeating itself even in cases of other

sulphonamides, what implies that all the sulphonamides utilised in the study do interact with the metal surface through their heteroatoms.

Table 4.22: Mulliken atomic charges and Fukui functions on the heavy atoms of the Sulphonamides used as corrosion inhibitors.

Number of the atom	Atomic charge q_N	$q_{(N+1)}$	$q_{(N-1)}$	$f^+ = q_{(N+1)} - q_N$	$f^- = q_N - q_{(N-1)}$
Sulphanilamide					
N1	-0.830	-0.848	-0.699	-0.018	-0.131
C2	0.324	0.331	0.330	0.007	-0.006
C3	-0.217	-0.317	-0.151	-0.100	-0.066
C4	-0.167	-0.258	-0.145	-0.091	-0.022
C5	-0.242	-0.229	-0.186	0.013	-0.056
C6	-0.167	-0.257	-0.144	-0.090	-0.023
C7	-0.217	-0.317	-0.151	-0.100	-0.066
S8	1.103	1.062	1.137	-0.041	-0.034
O9	-0.511	-0.544	-0.456	-0.033	-0.055
O10	-0.511	-0.544	-0.457	-0.033	-0.054
N11	-0.849	-0.839	-0.825	0.010	-0.024
Sulphachloropyridazine					
N1	-0.832	-0.851	-0.734	-0.019	-0.098
C2	0.335	0.322	0.338	-0.013	-0.003
C3	-0.224	-0.244	-0.176	-0.020	-0.048
C4	-0.122	-0.108	-0.112	0.014	-0.010
C5	-0.268	-0.261	-0.228	0.007	-0.040
C6	-0.166	-0.188	-0.152	-0.022	-0.014
C7	-0.221	-0.231	-0.169	-0.010	-0.052
S8	1.131	1.098	1.156	-0.033	-0.025
O9	-0.464	-0.482	-0.422	-0.018	-0.042
O10	-0.510	-0.545	-0.467	-0.035	-0.043
N11	-0.804	-0.799	-0.781	0.005	-0.023
C12	0.504	0.484	0.517	-0.020	-0.013
N13	-0.251	-0.334	-0.245	-0.083	-0.006
N14	-0.162	-0.260	-0.135	-0.098	-0.027
C15	0.049	0.051	0.061	0.002	-0.012
C16	-0.144	-0.234	-0.125	-0.090	-0.019
C17	-0.218	-0.313	-0.196	-0.095	-0.022
Cl18	-0.048	-0.176	0.049	-0.128	-0.097
Sulphadimethoxine					
N1	-0.831	-0.857	-0.756	-0.026	-0.075
C2	0.331	0.283	0.333	-0.048	-0.002
C3	-0.216	-0.231	-0.180	-0.015	-0.036
C4	-0.152	-0.211	-0.157	-0.059	0.005
C5	-0.266	-0.286	-0.244	-0.020	-0.022
C6	-0.168	-0.188	-0.159	-0.020	-0.009
C7	-0.216	-0.238	-0.172	-0.022	-0.044
S8	1.135	1.074	1.156	-0.061	-0.021
O9	-0.491	-0.533	-0.448	-0.042	-0.043
O10	-0.494	-0.537	-0.464	-0.043	-0.030
N11	-0.770	-0.774	-0.731	-0.004	-0.039
C12	0.474	0.443	0.473	-0.031	0.001
N13	-0.369	-0.390	-0.343	-0.021	-0.026
C14	0.434	0.402	0.458	-0.032	-0.024
N15	-0.429	-0.476	-0.393	-0.047	-0.036
C16	0.427	0.396	0.443	-0.031	-0.016
C17	-0.390	-0.393	-0.323	-0.003	-0.067
O18	-0.288	-0.302	-0.252	-0.014	-0.036
O19	-0.322	-0.334	-0.293	-0.012	-0.029
C20	-0.439	-0.423	-0.458	0.016	0.019
C21	-0.439	-0.424	-0.455	0.015	0.016

Sulphamethoxazole					
N1	-0.833	-0.863	-0.730	-0.030	-0.103
C2	0.336	0.286	0.337	-0.050	-0.001
C3	-0.215	-0.246	-0.164	-0.031	-0.051
C4	-0.175	-0.202	-0.141	-0.027	-0.034
C5	-0.269	-0.292	-0.233	-0.023	-0.036
C6	-0.152	-0.207	-0.159	-0.055	0.007
C7	-0.217	-0.229	-0.165	-0.012	-0.052
S8	1.112	1.053	1.138	-0.059	-0.026
O9	-0.488	-0.537	-0.443	-0.049	-0.045
O10	-0.499	-0.538	-0.459	-0.039	-0.040
N11	-0.762	-0.774	-0.707	-0.016	-0.055
C12	0.440	0.428	0.438	-0.012	0.002
N13	-0.176	-0.238	-0.116	-0.062	-0.060
O14	-0.230	-0.274	-0.191	-0.044	-0.039
C15	0.342	0.321	0.347	-0.021	-0.005
C16	-0.419	-0.424	-0.408	-0.005	-0.011
C17	-0.672	-0.675	-0.667	-0.003	-0.005
Sulphamethizole					
N1	-0.832	-0.859	-0.738	-0.027	-0.094
C2	0.336	0.296	0.338	-0.040	-0.002
C3	-0.224	-0.244	-0.176	-0.020	-0.048
C4	-0.121	-0.144	-0.112	-0.023	-0.009
C5	-0.267	-0.287	-0.234	-0.020	-0.033
C6	-0.167	-0.199	-0.153	-0.032	-0.014
C7	-0.220	-0.236	-0.172	-0.016	-0.048
S8	1.119	1.069	1.144	-0.050	-0.025
O9	-0.506	-0.546	-0.415	-0.040	-0.091
O10	-0.461	-0.495	-0.461	-0.034	0.000
N11	-0.776	-0.766	-0.740	0.100	-0.036
C12	0.298	0.261	0.301	-0.037	-0.003
N13	-0.228	-0.243	-0.208	-0.015	-0.020
N14	-0.169	-0.215	-0.136	-0.046	-0.033
C15	0.038	-0.001	0.059	-0.039	-0.021
S16	0.175	0.007	0.287	-0.168	-0.112
C17	-0.668	-0.661	-0.671	0.007	0.003
Sulphabenzamide					
N1	-0.832	-0.853	-0.721	-0.021	-0.111
C2	0.335	0.313	0.337	-0.022	-0.002
C3	-0.225	-0.230	-0.161	-0.005	-0.064
C4	-0.123	-0.202	-0.161	-0.079	-0.054
C5	-0.281	-0.279	-0.227	0.002	-0.054
C6	-0.175	-0.118	-0.109	0.057	-0.066
C7	-0.220	-0.247	-0.173	-0.027	-0.047
S8	1.139	1.099	1.165	-0.040	-0.026
O9	-0.462	-0.489	-0.473	-0.027	0.011
O10	-0.511	-0.545	-0.417	-0.034	-0.094
N11	-0.759	-0.759	-0.750	0.000	-0.009
C12	0.502	0.429	0.504	-0.073	0.002
O13	-0.339	-0.415	-0.321	-0.076	-0.018
C14	-0.094	-0.105	-0.087	-0.011	-0.007
C15	-0.167	-0.246	-0.192	-0.079	0.025
C16	-0.192	-0.206	-0.184	-0.014	-0.008
C17	-0.176	-0.238	-0.152	-0.062	-0.024
C18	-0.198	-0.206	-0.185	-0.008	-0.013
C19	-0.201	-0.201	-0.153	0.000	-0.048
Sulphaquinoxaline					
N1	-0.833	-0.844	-0.762	-0.011	-0.071
C2	0.337	0.325	0.339	-0.012	-0.002
C3	-0.216	-0.237	-0.180	-0.021	-0.036

C4	-0.173	-0.173	-0.163	0.000	-0.010
C5	-0.272	-0.262	-0.251	0.010	-0.021
C6	-0.160	-0.171	-0.155	-0.011	-0.005
C7	-0.216	-0.224	-0.177	-0.008	-0.039
S8	1.125	1.099	1.146	-0.026	-0.021
O9	-0.489	-0.525	-0.449	-0.036	-0.040
O10	-0.495	-0.509	-0.463	-0.014	-0.032
N11	-0.756	-0.756	-0.705	0.000	-0.051
C12	0.383	0.336	0.391	-0.047	-0.008
N13	-0.345	-0.416	-0.317	-0.071	-0.028
C14	0.155	0.150	0.164	-0.005	-0.009
C15	-0.200	-0.245	-0.163	-0.045	-0.037
C16	-0.191	-0.215	-0.182	-0.024	-0.009
C17	-0.197	-0.217	-0.159	-0.02	-0.038
C18	-0.187	-0.235	-0.160	-0.048	-0.027
C19	0.115	0.117	0.125	0.002	-0.010
N20	-0.102	-0.359	-0.256	-0.257	0.154
C21	0.383	-0.159	-0.086	-0.542	0.469
Sulphamethazine					
N1	-0.831	-0.853	-0.739	-0.022	-0.092
C2	0.329	0.301	0.332	-0.028	-0003
C3	-0.227	-0.256	-0.180	-0.029	-0.047
C4	-0.132	-0.127	-0.121	0.005	-0.011
C5	-0.260	-0.271	-0.230	-0.011	-0.030
C6	-0.162	-0.202	-0.147	-0.040	-0.015
C7	-0.220	-0.229	-0.175	-0.009	-0.045
S8	1.128	1.089	1.154	-0.039	-0.026
O9	-0.478	-0.500	-0.429	-0.022	-0.049
O10	-0.509	-0.545	-0.463	-0.036	-0.046
N11	-0.787	-0.779	-0.746	0.008	-0.041
C12	0.583	0.549	0.599	-0.034	-0.016
N13	-0.365	-0.415	-0.365	-0.050	0.000
C14	0.236	0.206	0.238	-0.030	-0.002
C15	-0.321	-0.335	-0.264	-0.014	-0.057
C16	0.238	0.184	0.236	-0.054	0.002
N17	-0.370	-0.417	-0.343	-0.047	-0.027
C18	-0.663	-0.659	-0.666	0.004	0.003
C19	-0.684	-0.680	-0.683	0.004	-0.001
Sulphisoxazole					
N1	-0.831	-0.860	-0.746	-0.029	-0.085
C2	0.332	0.283	0.333	-0.049	-0.001
C3	-0.218	-0.231	-0.175	-0.013	-0.043
C4	-0.161	-0.218	-0.149	-0.057	-0.012
C5	-0.246	-0.264	-0.221	0.000	-0.025
C6	-0.137	-0.164	-0.130	-0.027	-0.007
C7	-0.219	-0.248	-0.174	-0.029	-0.045
S8	1.089	1.021	1.116	-0.068	-0.027
O9	-0.504	-0.554	-0.453	-0.050	-0.051
O10	-0.477	-0.527	-0.431	-0.050	-0.046
N11	-0.812	-0.808	-0.776	0.004	-0.036
C12	0.593	0.556	0.623	-0.037	-0.030
C13	-0.204	-0.210	-0.174	-0.006	-0.030
C14	0.259	0.235	0.273	-0.024	-0.014
N15	-0.166	-0.215	-0.103	-0.049	-0.063
O16	-0.239	-0.243	-0.236	-0.004	-0.003
C17	-0.690	-0.693	-0.685	-0.003	-0.005
C18	-0.674	-0.678	-0.668	-0.004	-0.006

However, it should also be remembered that beside the heteroatoms, as also confirmed by the study of the HOMO orbitals, the π electrons of the aromatic ring are also involved in the interaction of the metal with the inhibitor molecules.

In terms of selectivity, the Fukui functions provide information on the site with the highest tendency to be involved in electrophilic and nucleophilic reactions. When an atom in a molecule possesses a tendency to donate an electron or a pair of electrons, that molecule is said to have a nucleophilic character while the one that has the tendency to accept electrons is said to have an electrophilic character. The nucleophilic and electrophilic Fukui functions can be estimated by using the finite difference approximations [192], as shown by equations 58 and 59, respectively.

$$f^{+} = q_{(N+1)} - q_N \quad (65)$$

$$f^{-} = q_N - q_{(N-1)} \quad (66)$$

where $q_{(N+1)}$ is the charge of the atoms on the systems with N+1 electrons, q is the charge of the atoms on the systems with N electrons and $q_{(N-1)}$ is the charge of the atoms on the systems N–1 electrons. The nucleophilic attack is normally preferred on the atoms or region in the molecule where the value of f^{+} is the highest while the electrophilic attack is preferred on the atom or region in a molecule where the value of f^{-} is the highest. The calculated Fukui functions for the non-hydrogen atoms in the studied sulphonamides are reported in Table 4.22 and also shown in Figure 4.239 for the f^{-} function. In the sulfanilamide structure, most positive part of f^{-} function is delocalized on the π system of aromatic ring attached to S8 (the ortho and para positions) and on the lone pair of electrons on the N1; in sulphadimethoxine, the most positive part of f^{-} function is delocalized on C3, C7, C5 (the ortho and para C atoms of aromatic ring A), on the lone pair of electrons on N1 and N11 atoms and on C17 atom; in sulphamethoxazole, most positive part of f^{-} function is delocalized on the π system of the aromatic ring attached to S8, on the lone pair of electrons on N1 atom and N11 (in the aliphatic chain), on the lone pair of electrons on N13 and O14 atoms; in sulphamethizole, the most positive part of f^{-} function is delocalized on the π system of the aromatic ring attached to S8,

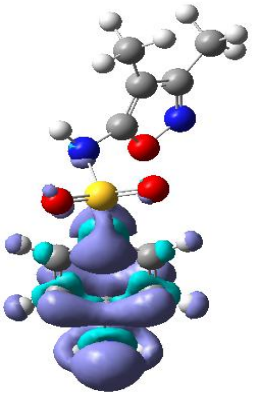

Sulphisoxazole (SSZ)

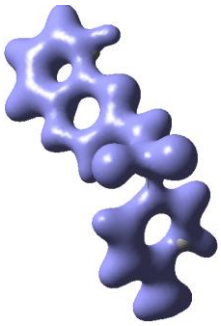

Sulphaquinoxaline (SQX)

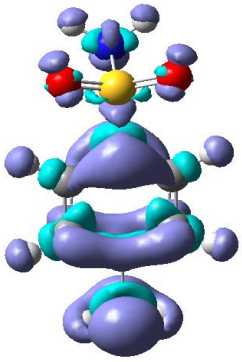

Sulphanilamide (SNA)

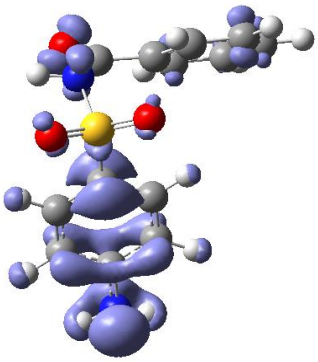

Sulphabenzamide (SBZ)

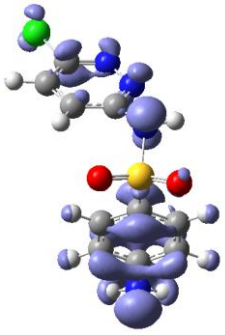

Sulphachloropyridazine (SCP)

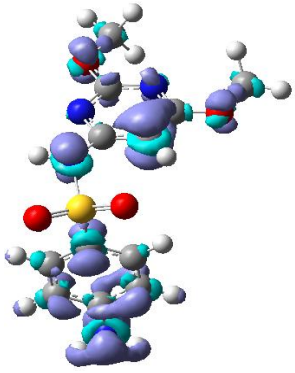

Sulphadimethoxine (SDM)

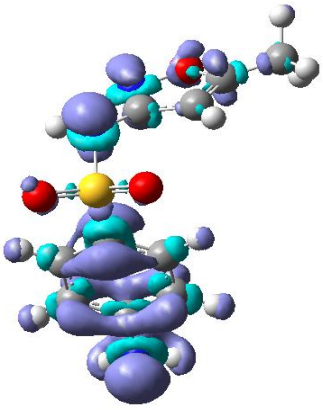

Sulphamethoxazole (SMX)

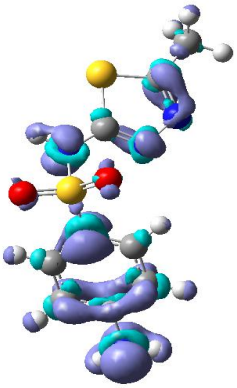

Sulphamethizole (SMZ)

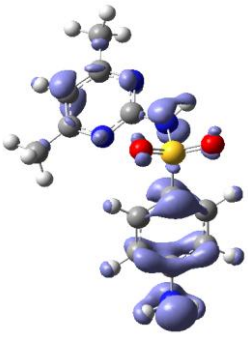

Sulphamethazine (SMT)

Figure 4.239: Illustration of the Fukui f^- function isodensity. For all the sulphonamides, the isovalue utilized to obtain the f^- function has a value of 0.0025 except the sulphur quinoxaline for which the isovalue of 0.05 value was utilized.

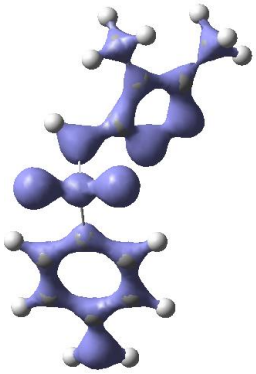

Sulphisoxazole (SSZ)

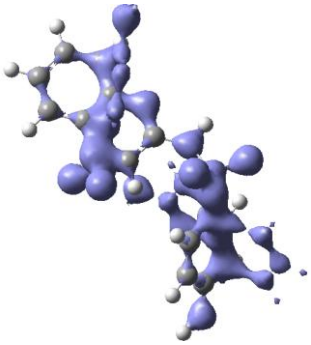

Sulphaquinoxaline (SQX)

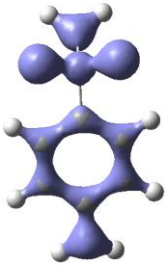

Sulphanilamide (SNA)

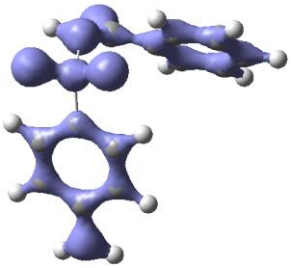

Sulphabenzamide (SBZ)

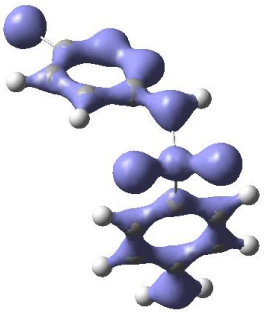

Sulphachloropyridazine (SCP)

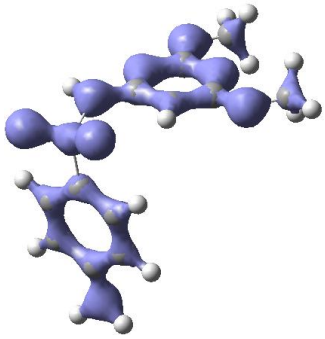

Sulphadimethoxine (SDM)

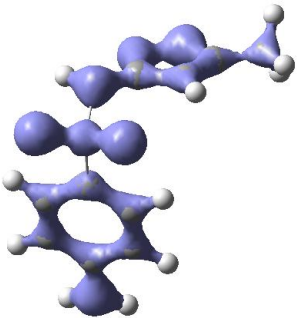

Sulphamethoxazole (SMX)

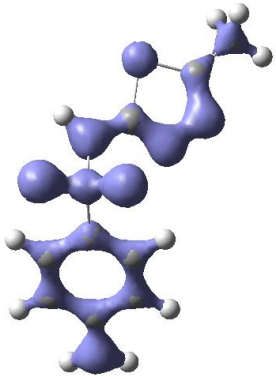

Sulphamethizole (SMZ)

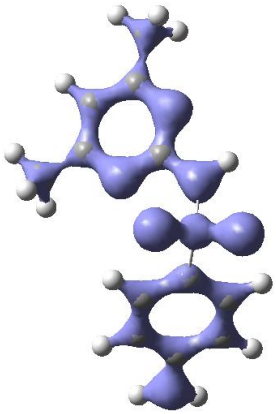

Sulphamethazine (SMT)

Figure 4.240: Illustration of the Fukui f^+ function isodensity. For all the sulphonamides, the isovalue utilized to obtain the f^+ function has a value of 0.5 except the sulfur quinoxaline for which the isovalue of 0.3 value was utilized.

In sulphisoxazole, most positive part of f^- function is delocalized entirely on the π system of aromatic ring attached to S8 and on the lone pair of electrons on the N1 atom; in sulphamethazine, the most positive part of f^- function is delocalized on the π system of the aromatic ring attached to S8, the lone pair of electrons on N1 and N11 and the C15; In sulphachloropyridazine and sulphabenzamide, most positive part of f^- function is delocalized entirely on the π system of aromatic ring attached to S8 and on the lone pair of electrons on the N1 atom. These results suggest that for sulphonamides, the preferred sites of interaction with an electrophilic species, such as a metal surface that has atoms with vacant or partially filled *d* orbitals, the preferred site of interaction with the metal surface is through the π system of aromatic ring A and the lone pair of electrons on available N atoms of the amino groups. The electrophilic attack centres identified here are similar to those identified through the discussion of the HOMO orbitals for these compounds. The only exception to the trend is the distribution of the f^- function in sulphaquinoxaline, where all the atoms in the molecule can be considered to be electron rich.

The nucleophilic attack centres shown in Figure 4. 240. In all nine sulphonamide compounds, the most of f^+ function is delocalized throughout the molecule. The nucleophilic attack centres identified here are similar to those identified through the discussion of the LUMO orbitals for these compounds.

4.4.2 Results of the calculations for the protonated inhibitors in vacuo

Once the inhibitor compound such as a sulphonamide is introduced to the aqueous hydrochloric acid solution, the process of protonation is most likely to occur. Consequently, both protonated and non-protonated species may co-exist in solution. Due to this reason, it is necessary to study the preferred species (protonated or non-protonated) of the sulphonamides to interact with the metal surface during the corrosion inhibition process. The position of protonation on sulphonamides generally favours the sites occupied by heteroatoms. This is reasonable due to the fact that a proton, which is electron deficient specie, would preferentially interact with these atoms which are electron rich. Even so, certain heteroatoms are preferred than others because protonation on certain heteroatoms may result in destabilizing the whole molecule. For instance, a protonation on oxygen that already carries two bonds will cause that oxygen to carry three bonds and change its state from neutral to being charged. Once charged, the molecule becomes unstable. Nevertheless, nitrogen atom with three bonds can still be stable, as the nitrogen which is similar to the one that is found in

NH_3. The optimized geometries of the protonated species for the studied sulphonamides are shown in Figure 4.241 and the corresponding HOMO and LUMO densities are shown in Figures 4.242 and 4.243, respectively. For sulphabenzamide, there are specifically two possible protonated geometries, SBZ-p1 and SBZ-p2; SBZ-p2 is the most preferred geometry due to its stability over SBZ-p1 (as shown by the relative energy values). The formation of the hydrogen bond that results after protonation in SBZ-p2 could account for the stability of SBZ-p2 with respect to SBZ-p1. For sulphachloropyridazine, four geometries are possible, namely SCP-p1, SCP-p2, SCP-p3 and SCP-p4; SCP-p1 is more preferred than the other three geometries. The hydrogen bond formation is very clear in this case as well and its effect brings about stability. Three possible protonated geometries were obtained for sulphadimethoxine, namely SDM-p1, SDM-p2 and SDM-p3; analysis of the geometries reveals that the presence of the neighbouring lone pairs of electrons and the formation of the hydrogen bond in SDM-p2 makes it the most preferred protonated specie. There are five possible protonation sites for sulphamethizole, namely SMZ-p1, SMZ-p2, SMZ-p3, SMZ-p4 and SMZ-p5. A comparison of the relative energies for all five geometries shows that SMZ-p1 and SMZ-p2 possesses the lowest values that are very comparable with each other. The fact that these two geometries possess the lowest energies suggests that they are the most preferable species. This lower trend in energy maybe attributed to the formation of the hydrogen bond which results in the formation of a five membered ring which in turn brings about some stability as far as the molecule is concerned. Sulphanilamide has only one possible protonation site (SNA-p1). Sulphaquinoxaline has three protonated geometries, namely SQX-p1, SQX-p2 and SQX-p3; analysis of the relative energies suggests that, although the energy difference is not very large among the possible conformers, SQX-p3 has the lowest value. For the analysis of the HOMO and LUMO orbitals and for the comparison of the other molecular reactivity parameters, only the lowest energy conformer was utilised for each protonated sulphonamide.

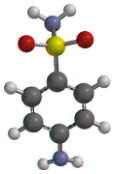

SNA

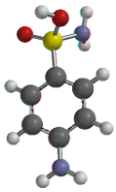

SNA-p1

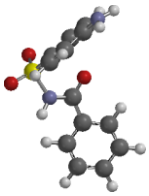

SBZ

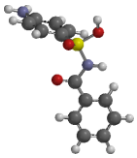

15.568
SBZ-p1

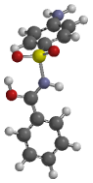

0.000
SBZ-p2

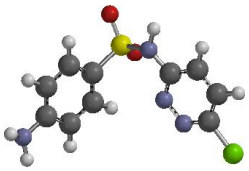

SCP

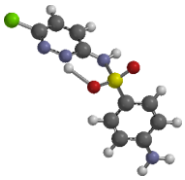

0.000
SCP-p1

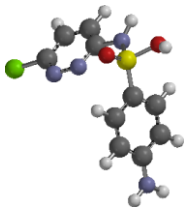

28.181
SCP-p2

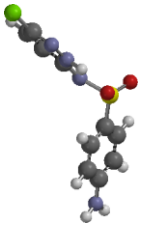

0.000
SCP-p3

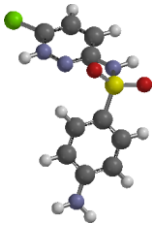

9.049
SCP-p4

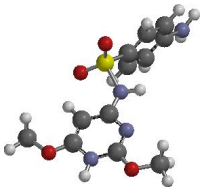

SDM

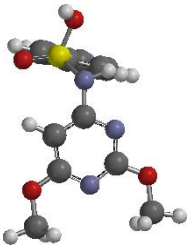

33.300
SDM-p1

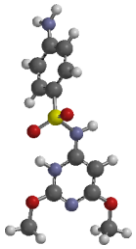

0.000
SDM-p2

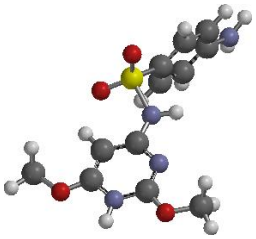

2.498
SDM-p3

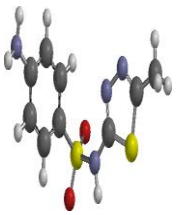

SMZ

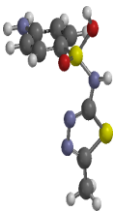

31.156
SMZ-p1

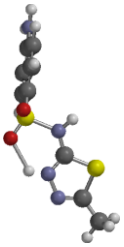

0.000
SMZ-p2

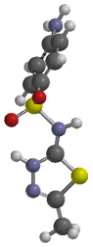

11.182
SMZ-p3

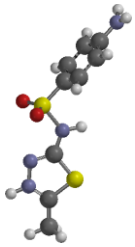

62.500
SMZ-p4

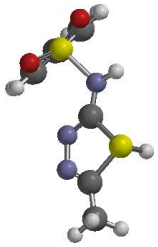

12.183
SMZ-p5

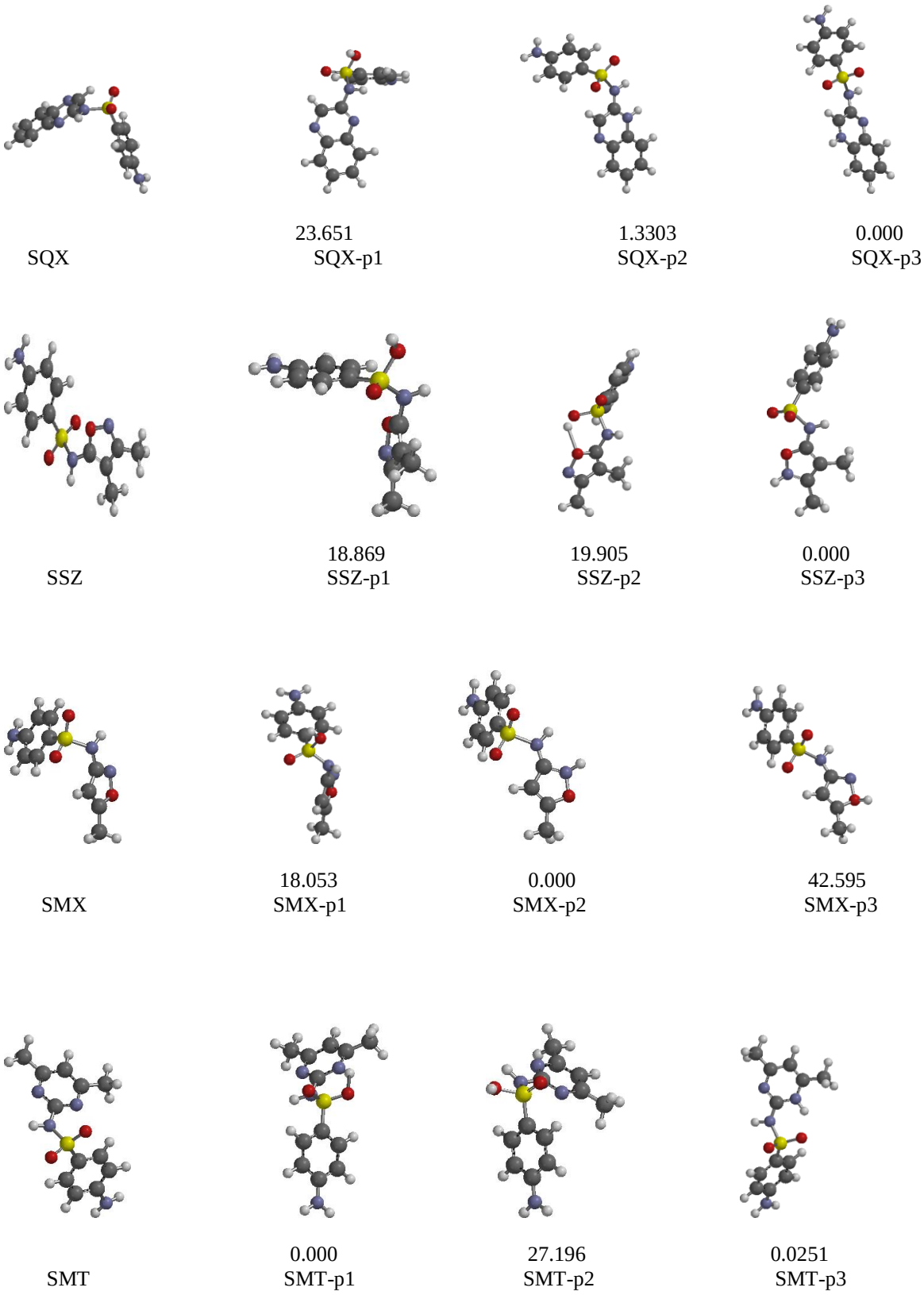

Figure 4.241**:** The optimized conformers of the neutral and the protonated species of the studied sulphonamide compounds. The relative energies (kcal/mol) for the protonated species are shown below each conformer.

In the protonated species, the HOMO is only spread on ring A, N1, O6 and O6′. The LUMO density provides information on the nucleophilic attach sites, in terms of corrosion mechanism, this possibility is only applicable when the metal surface has the ability to back-donate electrons to the inhibition molecule. Analysis of the LUMO density for the studied neutral sulphonamides shows that it is delocalised throughout the molecule in sulphanilamide and sulphadimethoxine; it is localized only in ring B in sulphamethizole and in ring A in sulphisoxazole. An analysis of the LUMO density in the protonated species for the studied sulphonamides shows that the LUMO is entirely on ring B for all the compounds except sulphanilamide.

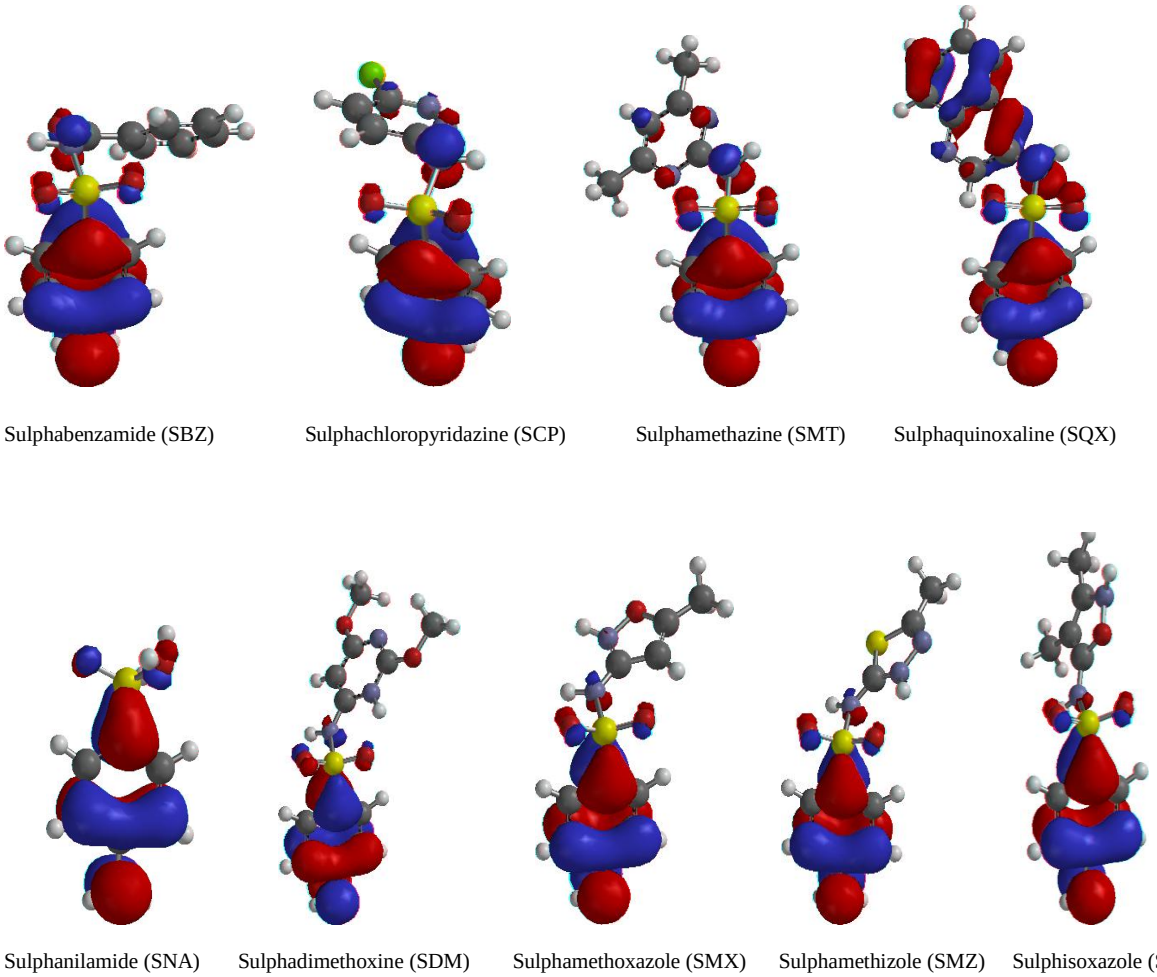

Figure 4.242: The HOMO densities for the studied sulphonamide compounds for the protonated species.

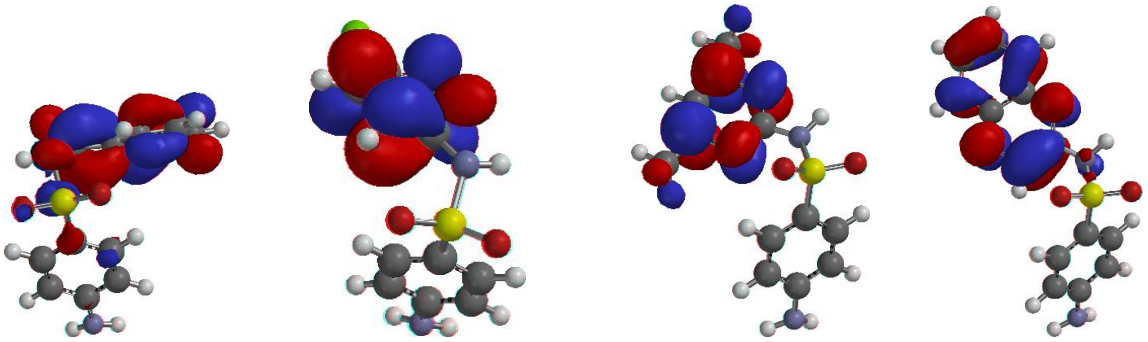

Sulphabenzamide (SBZ) Sulphachloropyridazine (SCP) Sulphamethazine (SMT) Sulphaquinoxaline (SQX)

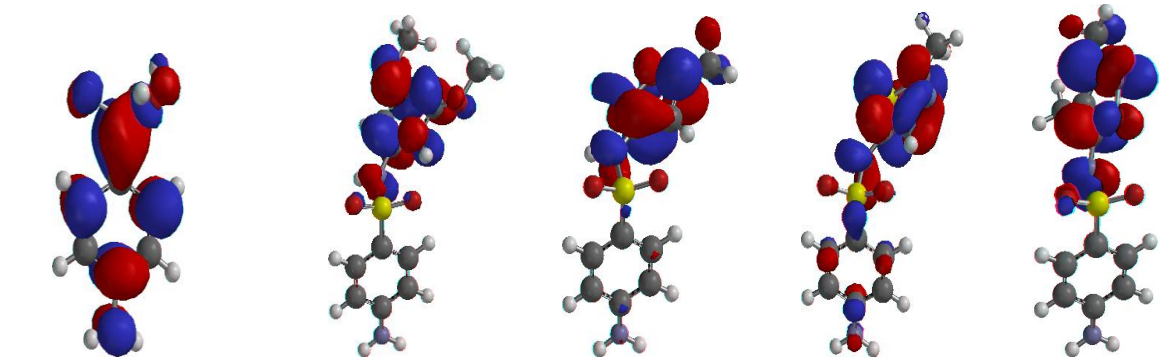

Sulphanilamide (SNA) Sulphadimethoxine (SDM) Sulphamethoxazole (SMX) Sulphamethizole (SMZ) Sulphisoxazole (SSZ)

Figure 4.243: The LUMO densities for the studied sulphonamide compounds for the protonated species.

A comparison of the calculated molecular descriptors across structures of the protonated species and across structures of the non-protonated species provides information on the variation of the trends in the molecular properties due to protonation effect. The results, reported in Table 4.23, show that with the exception of the molecular polarization, the trends in the E_{HOMO}, E_{LUMO}, ΔE, μ, logP, η, σ, I, A, ω and χ are different between the non-protonated and the protonated inhibitors. The results show that E_{HOMO} is much lower in the protonated species than in the non-protonated species, which implies that the non-protonated species are better electron donors than the protonated species; E_{LUMO} is much lower in the protonated species than in the non-protonated species. Electrophilicity index is highest for the protonated species than for the non-protonated species. All these factors indicate that the protonated species have the least tendency to donate electrons to the metal surface. Therefore,

interaction with the metal surface would preferentially involve electrostatic interaction rather than chemical bond formation.

Table 4.23: The molecular properties for protonated studied sulphonamides obtained from (B3LYP/6-31G (d,p) results *in vacuo*).

Molecular Property	**Inhibitor Compound**								
	SBZ	**SCP**	**SDM**	**SMX**	**SMZ**	**SNA**	**SQX**	**SMT**	**SSZ**
E_{HOMO} (eV)	-9.61	-9.46	-9.06	-9.87	-9.45	-10.02	-8.78	-9.12	-9.96
E_{LUMO} (eV)	-6.02	-6.53	-4.85	-5.40	-5.25	-5.61	-6.86	-5.74	-5.50
ΔE (eV)	3.59	2.93	4.21	4.47	4.20	4.41	1.92	3.38	4.46
μ	4.53	5.98	4.19	4.04	5.38	1.24	6.24	3.93	6.28
logP	-	1.70	1.57	-	1.05	-	1.04	-	-
MP	61.71	60.27	63.35	59.10	59.33	52.91	63.66	62.04	60.58
η	1.79	1.72	2.11	2.24	2.10	2.21	0.96	1.69	2.23
σ	0.56	0.58	0.48	0.45	0.48	0.44	1.04	0.59	0.45
I (eV)	9.61	9.46	9.06	9.87	9.45	10.02	8.78	9.12	9.96
A (eV)	6.02	6.53	4.85	5.40	5.25	5.61	6.86	5.74	5.50
ω	17.01	17.42	11.49	13.04	12.86	13.85	31.85	16.33	13.40
χ	7.82	7.74	6.96	7.64	7.35	7.82	7.82	7.43	7.73

4.4.3 Quantitative Structure Activity Relationship (QSAR)

The results so far is based on the attempt to correlate a given quantum chemical parameter to the observed inhibition efficiencies of the inhibitors. Nevertheless, some more conclusive remarks can be achieved through simultaneous correlation of several quantum chemical parameters to the observed inhibition efficiencies of corrosion inhibitors. The approach in which several quantum chemical parameters form a composite index which is then correlated to the experimentally determined inhibition efficiency is called quantitative structure activity relationship (QSAR). Several quantitative structure activity relationship equations were utilized to correlate the quantum chemical index with the experimental inhibition efficiencies. The selection of the appropriate model equation depends strongly on the type of adsorption mechanism. Among the equations utilized to develop quantitative structure activity relationship when the adsorption obeys Langmuir isotherms (as is the case with the sulphonamides studied in this work), is the linear and the non-linear multiple regression equations developed by Lukovits [194, 195].

The linear multiple regression equation is of the form;

$$IE_{theor} = Ax_i C_i + B \tag{67}$$

where A and B are the regression coefficients determined through regression analysis, x_i is a quantum chemical index characteristic of the molecule i, C_i is the experimental concentration of the inhibitor.

The non-linear multiple regression equation is of the form:

$$IE_{theor} = \frac{(AX_i + B) * C_i}{1 + (AX_i + B) * C_i} * 100 \tag{68}$$

where A and B are constants obtained by regression analysis; X_i is a quantum chemical index characteristic for the molecule; C_i is the inhibitor concentration in μM.

Both equations were used to correlate the composite index of quantum chemical parameters with the experimental inhibition efficiency of the studied sulphonamides. The results show that the linear multiple regressions were not successful since a poor correlation was produced

between quantum chemical parameters and experimental inhibition efficiency. The non-linear multiple regression equations were more successful as they provided a good correlation between quantum chemical parameters and experimental inhibition efficiency. An optimum of five quantum chemical parameters was sufficient to produce good correlation with experimentally determined inhibition efficiency. Table 4.24 shows a combination of the quantum chemical parameters that provided the best correlation. Included in this table are the equations for the prediction of theoretical inhibition efficiency and the corresponding sum of squared errors (SSE) and R^2 values. The best QSAR equation correlating theoretical inhibition efficiency with the experimental inhibition efficiency corresponds to the combination of ω, E_{LUMO}, μ, η and logP quantum chemical parameters. This equation informs that the increase in ω, E_{LUMO} and η accompanied by a decrease in μ and logP leads to a high inhibition efficiency. Overall, the R^2 and SSE values are within the range of 0.951 - 1.000 and 0.000-2.313, respectively. The values of R^2 are very close to unity and those of SSE are reasonably small. It is therefore reasonable to conclude that the combination of five quantum chemical parameters provided a better correlation between quantum chemical parameters and the experimentally determined inhibition efficiencies of the sulphonamides studied.

$$\%IE_{WL} = (2.47*\omega + 8.56 \times 10^{-2}*E_{LUMO} - 5.27 \times 10^{-2}*\mu + 6.20*\eta - 4.11 \times 10^{-2}*logP - 21.81)*5000/ (1 + (2.47*\omega + 8.56 \times 10^{-2}*E_{LUMO} - 5.27 \times 10^{-2}*\mu + 6.20*\eta - 4.11 \times 10^{-2}*logP - 21.81)*50) \quad (69)$$

Table 4.24: Quantum chemical parameters utilized to derive the non-linear multiple regression equation that correlates the theoretically estimated and the experimentally determined inhibition efficiencies.

Quantum chemical parameters[a]	Derived QSAR equation	$R^{2,b}$	SSE[c]
ω, E_{LUMO}, μ, η, logP	$\%IE_{WL} = (2.47*\omega + 8.56 \times 10^{-2}*E_{LUMO} - 5.27 \times 10^{-2}*\mu + 6.20*\eta - 4.11 \times 10^{-2}*logP - 21.81)*5000/(1 + (2.47*\omega + 8.56 \times 10^{-2}*E_{LUMO} - 5.27 \times 10^{-2}*\mu + 6.20*\eta - 4.11 \times 10^{-2}*logP - 21.81)*50)$	1.000	0.000
ΔE, E_{LUMO}, E_{HOMO}, η, ω,	$\%IE_{WL} = (-1.44*\Delta E + 3.48*E_{LUMO} - 3.50*E_{HOMO} + 1.07*\eta + 1.75*\omega + -17.85)*5000/(1 - 1.44*\Delta E + 3.48*E_{LUMO} - 3.50*E_{HOMO} + 1.07*\eta + 1.75*\omega + -17.85)*50)$	0.994	0.303
ΔE, E_{LUMO}, σ, η, ω	$\%IE_{WL} = (-1.85*\Delta E - 0.10*E_{LUMO} - 21.48*\sigma + 4.36*\eta + 1.50*\omega + 2.72)*5000/(1 + (-1.85*\Delta E - 0.10*E_{LUMO} - 21.48*\sigma + 4.36*\eta + 1.50*\omega + 2.72)*50)$	0.990	0.469
ΔE, E_{LUMO}, μ, η, logP,	$\%IE_{WL} = (-0.08*\Delta E + 0.32*E_{LUMO} - 7.77x10^{-3}*\mu - 0.72*\eta - 3.18 \times 10^{-2}*logP + 2.85)*5000/(1 + (-0.08*\Delta E + 0.32*E_{LUMO} - 7.77x10^{-3}*\mu - 0.72*\eta - 3.18 \times 10^{-2}*logP + 2.85)*50)$	0.954	1.193
ΔE, E_{LUMO}, MP, η, ω	$\%IE_{WL} = (0.40*\Delta E - 5.24x10^{-2}*E_{LUMO} + 0.03*MP - 0.08*\eta + 0.23*\omega - 4.28)*5000/(1+(0.40*\Delta E - 5.24x10^{-2}*E_{LUMO} + 0.03*MP - 0.08*\eta + 0.23*\omega - 4.28)*50)$	0.951	2.313

[a] The quantum chemical parameters were obtained from the in vacuo results calculated using the B3LYP/6-31G(d) method.
[b] R^2 is the coefficient of determination,
[c] SSE is defined as:

$$SSE = \sqrt{\sum_{i=1}^{n} \left(IE_{pred} - IE_{exp}\right)^2} \quad (70)$$

where IE_{pred} is the predicted inhibition efficiency, IE_{exp} is the experimental determined inhibition efficiency, and *n* is the number of observations (compounds) considered.

CHAPTER 5

CONCLUSIONS

5.1 CONCLUSIONS

In this study, nine (9) sulphonamide derivatives, namely; Sulphaquinoxaline (SQX), Sulphamethoxazole (SMX), Sulphamethazine (SMT), Sulphisoxazole (SSZ), Sulphanilamide (SNA), Sulphamethizole (SMZ), Sulphachloropyridazine (SCP), Sulphabenzamide (SBZ) and Sulphadimethoxine (SDM) were used as corrosion inhibitors for the protection of three different metals, namely; mild steel, aluminium and zinc surfaces in 1.0 M hydrochloric acid solutions at 30-50 °C. The investigation was carried out using electrochemical [Potentiodynamic polarization (PDP), electrochemical impendence spectroscopy (EIS)], Fourier Transform Infrared spectrometry (FTIR), Scanning Electron Microscopy (SEM) and gravimetric techniques. Quantitative structure activity relationship (QSAR) studies using some quantum chemical/theoretical techniques e.g. density functional theory (DFT) was also utilized to calculate quantum chemical parameters of the selected inhibitors and correlate them with the experimentally obtained inhibition efficiency and to derive equations for computation of theoretical inhibition efficiencies.

The imperfect semicircles on the Nyquist plots indicated an efficient inhibition of mild steel, aluminium and zinc by all nine sulphonamide compounds used as inhibitors. The aluminium electrochemical impedance spectroscopy curves showed a more pronounced passive region. This behaviour is due to the fact that aluminium has a higher tendency to form oxide films than both mild steel and zinc. The values of constant phase element exponent (n) were almost approaching unity, which is symbolic for a pseudo-capacitive behaviour of the electrode. The results also showed that all nine sulphonamides protect the surfaces of mild steel through a mixed-type adsorption at the mild steel/hydrochloric acid interface.

PDP results showed that the introduction of all nine sulphonamide compounds altered the corrosion current densities for both anodic and cathodic half-reactions. This signified that both anodic dissolution of mild steel, aluminium and zinc and cathodic reduction of the hydrogen ions were inhibited thereby improving the inhibition efficiencies as the inhibitor concentration was increased. The values of E_{corr} for mild steel, aluminum and zinc inhibition did not show significant change, thus a mixed-type inhibition was proposed for the adsorption of all nine sulphonamides compounds on mild steel surfaces.

FTIR spectra confirmed the formation of Fe^{3+}-inhibitor, Al-inhibitor and Zn-inhibitor complexes. Analysis of the functional groups showed that the O atom from SO_2 functional group from all nine sulphonamide compounds was the most preferred site for interaction with the mild steel surfaces. The passivating iron oxide layers (γ-Fe_2O_3) were confirmed by the corresponding characteristic absorption bands. In cases of aluminum, analysis of the functional groups showed that the partially filled orbitals in aluminium metal accepted electrons from the aromatic ring (through C=C) and SO_2 (through O atom), thus the covalent bond was formed which resulted in aluminium surfaces being protected from aggressive Cl^- ions in the HCl solutions. In cases of zinc, analysis of the functional groups showed that the most preferred sites of interaction during the formation of these complexes were the aromatic ring (through C=C), SO_2 (through O atom) and C-N (through N atom) thus the covalent bond was formed which resulted in zinc surfaces being protected from further corrosion.

SEM micrographs and their respective EDS spectra showed the rough surfaces of mild steel, aluminum and zinc in the absence of inhibitor compounds. The introduction of all nine sulphonamides improved the surfaces of these metals through the formation of the adsorption layer onto the surfaces of mild steel. EDS spectra showed the presence of Fe, Al and Zn traces of sulphonamides and Cl^- ions. Results from the adsorption isotherms showed that the Langmuir adsorption model was adopted for these metals. The values of ΔG indicated that the inhibition of the three metals by all nine sulphonamide compounds was spontaneous and followed a mixed-type mechanism with a predominant physisorption.

Density Functional Theory method was employed in the quantum chemical studies. Calculations were done both in vacuo and in solution and by taking into consideration the protonated and the non-protonated species. The outcome of the study suggests that the trends in the quantum chemical parameters, across inhibitors, correlates well with the trends in the experimental inhibition efficiency of the inhibitors. Both the HOMO density and the f^- function point to the fact that the sites with the highest tendency to donate electrons to the metal ions are the aromatic ring attached to attached to S8 (due to the high electron density arising from the π electrons on the aromatic ring) and the lone pair of electrons on several heteroatoms present in each of the studied sulphonamide compounds. The quantitative structure activity relationship (QSAR) approach has provided a good indication that an optimum of five quantum chemical parameters is required for a good correlation with experimentally determined inhibition efficiency of the inhibitors. The information provided

could be utilized in the search for other sulphonamides (that have similar characteristics like the sulphonamides studied in this work) that could be better corrosion inhibitors. Moreover, this information may be used to determine better corrosion inhibitors.

RECOMMENDATIONS FOR FURTHER STUDIES

The present study focused on the inhibition characteristics of selected sulphonamides compounds on mild steel, aluminum and zinc in acidic medium. Future studies will also focus on the effect of different corrosive media including alkaline solutions.

Further aspects of quantum chemical studies such as molecular dynamics simulations will also be explored.

REFERENCES

1. Z. Ahmad, Principles of corrosion engineering and corrosion control. Butterworth Heinemann, Oxford, UK, 2006, pp. 1-8.
2. F. Walsh, Faraday and his laws of electrolysis, ***Bullet. Electrochem*.** 11 (1991) 481-489.
3. J.J. McEwan, Corrosion control in Southern Africa, Corrosion Institute of Southern Africa, Kelvin, RSA, 2004, pp. 1-135.
4. A.M. Badiea, K.N. Mohana, Corrosion mechanism of low-carbon steel in industrial water and adsorption thermodynamics in the presence of some plant extracts, ***J. Mater. Engr. Perform*.** 18 (2008) 1264-1271.
5. N.O. Obi-Egbedi, I.B. Obot, Adsorption behavior and corrosion inhibitive potential of xanthenes on mild steel/sulphuric acid interface, ***Arab. J. Chem*.** 5 (2012) 121-133.
6. A.N. Senthilkumar, K. Tharini, M.G. Sethuraman, Studies on a few substituted piperidi-4-one oximes as corrosion inhibitor for mild steel in HCl, ***J. Mater. Engr. Perform*.** 20 (2011) 969-977.
7. A. Kamis, Cost of corrosion, ***Bullet.*** *FKKKSA*, 6 (1992) 12-15.
8. V.S. Saji, Contemporary developments in corrosion inhibitors-Review of patents, ***Rec. Pat. Corros. Sci*.** 1 (2011) 63-71.
9. S.A. Umoren, I.B. Obot, E.E. Ebenso, P.C. Okafor, O. Ogbobe, E.E. Oguzie, Gum arabic as a potential corrosion inhibitor for aluminium in alkaline medium and its adsorption characteristic, ***Anti-Corros. Methods Mater*.** 53 (2006) 277-282.
10. G.H. Koch, M.P.H. Brongers, N.G Thompson, Y.P Virmani, J.H. Payer, Cost of corrosion and prevention strategies in the United States, C.C. Technologies Laboratories, Inc, 2001, USA.
11. Federal Highway Administration (FHWA), Office of the infrastructure and development. 2001, Report FHWA-RD-01-156.
12. N. O. Eddy, S. R. Stoyanov, E. E. Ebenso, Fluoroquinolones as corrosion inhibitors for Mild steel in acidic medium; experimental and theoretical studies, ***Int. J. Electrochem. Sci*.** 5 (2010) 1127-1150.
13. I. Dehri, M. Ozcan, The effect of temperature on the corrosion of mild steel in acidic media in the presence of some sulphur-containing organic compounds, ***Mater. Chem. Phys.*** 98 (2006) 316 -323.
14. Z. Szklarska-Smialowska, Pitting corrosion of Aluminium, ***Corros. Sci.*** 41 (1999) 1743-1767.

15. K. Denpo, H. Ogawa, Fluid flow effects on CO_2 corrosion resistance of oil well materials, ***NACE International*.** 49 (06) (1993).
16. M. Clugston, R. Flemming, D. Vogt, Chemistry; An introduction for Southern African students, Oxford press. (2002) 254-274.
17. M. Pour-Ghaz, O. Burkan Isgor, P. Ghods, The effect of temperature on the corrosion of steel in concrete. Part 2: Model verification and parametric study, ***Corros. Sci.*** 51 (2009) 426-433.
18. E.E. Ebenso, I.B. Obot, L.C. Murulana, Quinoline and its derivatives as effective corrosion inhibitors for mild steel in acidic media, ***Int. J. Electrochem. Sci*.** 5 (2010) 1574-1586.
19. N. Mora, E. Cano, E.M. Mora, J.M. Bastidas, Influence of pH and oxygen on copper corrosion in simulated urine fluid, ***BioMater*.** 23 (2002) 667-671.
20. M.A. Quraishi, M.Z.A. Rafiguee, S. Khan, N. Saxena, Corrosion inhibition of aluminium in acidic solution by some imdazoline derivatives, ***J. Appl. Electrochem*.** 37 (2007) 1153-1162.
21. A.K. Singh, M.A. Quraishi, Piroxicam; A novel corrosion inhibitor for mild steel corrosion in HCl acid solution, ***J. Mater. Environ. Sci*.** 1 (2010) 101-110.
22. C. Arya, P.R.W. Vassie, Influence of cathode-to-anode ratio and separation distance on galvanic corrosion currents of steel in concrete containing chlorides, ***Cem. Concr. Res.*** 25 (1995) 989-998.
23. C.K. Tan, D.J. Blackwood, Corrosion protection by multilayered conducting polymer coatings, ***Corros. Sci.*** 45 (2002) 545-557.
24. H.P. Nielsen, F.J. Frandsen, K. Dam-Johansen, L.L. Baxter, The implications of chlorine-associated corrosion on the operation of biomass-fired boilers, ***Progr. Energ. Combust. Sci*.** 26 (2000) 283-298.
25. J.F. Frandsen, Utilizing biomass and waste for power production- a decade of contributing to the understanding, interpretation and analysis of deposits and corrosion products, ***Fuel*.** 84 (2005) 1277-1294.
26. P.R. Roberge, Corrosion engineering: principles and practice, McGraw-Hill, New York, 2008, pp. 1-754.
27. H. Kumar, V. Yadav, Corrosion characteristic of mild steel under different atmospheric conditions by vapour phase corrosion inhibitors, ***Am. J. Mater. Sci. Eng*.** 1 (2013) 34-39.

28. D. Thirumoolan, V.A. Katkar, G. Gunasekaran, T. Kanai, K.A. Basha, Hyperbranched poly(cyanurateamine): A new corrosion inhibitor for mild steel in hydrochloric acid medium, ***Prog. Org. Coat.*** 77 (2014) 1253-1263.
29. M. Fahlmam, S. Jasty, A.J. Epstein, Corrosion protection of iron/steel by emeraldine base polyaniline: an X-ray photoelectron spectroscopy study, ***Synth. Met.*** 85 (1997) 1323-1326.
30. K. Nisancioglu, Corrosion of aluminium alloys, ***Proceedings of ICAA3***. 3 (1992) 239-259.
31. N. Pistofidis, G. Vourlias, S. Konidaris, E. Pavlidou, A. Stergiou, G. Stergioudis, Microstructure of zinc hot-dip galvanized coatings used for corrosion protection, ***Mater. Lett.*** 60 (2006) 786-789.
32. L.S. Dake, D.R. Baer, J.M. Zachara, Auger parameter measurements of zinc compounds relevant to zinc transport in the environment, ***Surf. Interface Anal.*** 14 (1989) 71-75.
33. B.C. Cunningham, M.G. Mulkerrin, J.A. Wells, Dimerization of human growth hormone by zinc. ***Science.*** 253 (1991) 545-548.
34. B.R.W. Hinton, L. Wilson, The corrosion inhibition of zinc with cerous chloride, ***Corros. Sci***. 29 (1989) 967-985.
35. B.G. Clubley, Chemical inhibitors for corrosion control: the proceedings of an international symposium, Royal. Soc. Chem and the institution of corrosion science and technology, University of Manchester. (1998)
36. K.L. Vasanth, Corrosion inhibition in naval vessels, NACE international, 233 (1996) 96.
37. M.A. Hegazy, M. Abdallah, M.K. Awad, M. Rezk, Three novel di-quaternary ammonium salts as corrosion inhibitors for APIX65 steel pipeline in acidic solution. Part 1: Experimental results, ***Corros. Sci.*** 81 (2014) 54-64.
38. S.A. Soliman, M.S. Metwally, S.R. Selim, M.A. Bedair, M.A. Abbas, Corrosion inhibition and adsorption behavior of new Schiff base surfactant on steel in acidic environment: Experimental and theoretical studies, ***Ind. Eng. Chem***. 20 (2014) 4311-4320.
39. S. Rengamani, S. Muralidharam, M.A. Kulandainathan, V.S. Iyer, Inhibiting and accelerating effects of aminophenols on the corrosion and permeation of hydrogen through mild steel in acidic solutions, ***J. Appl. Elecrochem.*** 24 (1994) 355-260.

40. C.M. Hansson, L. Mammoliti, B.B. Hope, Corrosion inhibitors in concrete-Part 1: The principles, ***Cem. Concr. Res.*** 28 (1998) 1775-1781.
41. A. Leng, M. Stratman, The inhibition of the atmospheric corrosion of iron by vapour-phase inhibitors, ***Corros. Sci*.** 34 (1993) 1657-1683.
42. E.E. Ebenso, Synergistic effect of halide ions on the corrosion inhibition of aluminium in H_2SO_4 using 2-acetylphenothiazine, ***Mater. Chem. Phys.*** 79 (2003) 58 – 70.
43. A. Zarrouk, I. Warad, B. Hammounti, A. Dafali, S.S. Al-Deyab, N. Benchat, The effect of temperature on the corrosion of Cu/HNO_3 in the presence of organic inhibitor: Part -2. ***Int. J. Electrochem. Sc****i*. 5 (2010) 1516-1526.
44. A.I Onen, B.T, Nwufo, E.E Ebenso, R.M. Hlophe, Titanium (IV) oxide as corrosion inhibitor for aluminium and mild steel in acidic medium. ***Int. J. Electrochem. Sci.*** 5 (2010) 1563-1573.
45. E. E. Ebenso, T. Arslan, F. Kandemirli, I. Love, C. Öğretil, M. Saracoğlu, S. A. Umoren. Theoretical studies of some sulphonamides as corrosion inhibitors for mild steel in acidic medium, ***Int. J. Quantum. Chem*.** 110 (2010) 2614–2636.
46. F. Martinez, C.M Avila, A. Gomez, Thermodynamic study of the solubility of some sulphonamides in cyclohexane. ***J.Braz.Chem.Soc.*** 14 (2003) 803-808.
47. A. Husain, A. Ahmad, M. Mujeeb, M. Akhter, New amides of sulphonamides: Synthesis and biological evaluation. ***J. Chil. Chem. Soc*.** 55 (2010) 74-77.
48. N. Anand, Sulphonamides and sulphones in J.W. Corcoran and Fred E. Hahn in Mechanism of action of antimicrobial and antitumor agents, Springer-Verlag, New York, NY, 1975, pp. 742.
49. F. Shi, M.K. Tse, S. Zhou, M.M. Pohl, J. Radnik, S. Hubner, K. Jahnisch, A. Bruckner, M. Beller, Green and efficient synthesis of sulphonamides catalyzed by Nano-Ru/Fe_3O_4. **J. Am. Chem. Soc.** 131 (2009) 1775-1779.
50. S. Caddick, J.D. Wilden, D.B. Judd, Direct synthesis of sulphonamides and activated sulfonate esters from sulfonic acids, ***J. Am. Chem. Soc*.** 126 (2004) 1024-1025.
51. J. Boyle, S. Otty, V. Sarojini, A safer and convenient synthesis of sulphathiazole for undergraduate organic and medicinal chemistry classes, ***J. Chem. Educ*.** 89 (2012) 141-143.
52. X. Deng, N.S. Mani, A facile, environmentally benign sulphonamide synthesis in water. ***Green. Chem*.** 8 (2006) 835-838.

53. B. Raju, T.P. Kogan, Solid phase synthesis of sulphonamides using a carbamate linker, ***Tetrahedron Lett.*** 38 (1997) 3373-3376.
54. I.B. Obot, E.E. Ebenso, I.A. Akpan, Z.M. Gasem, A.S. Afolabi, Thermodynamic and density functional theory investigation of sulphathiazole as green corrosion inhibitor at mild steel/hydrochloric acid interface, ***Int. J. Electrochem. Sci.*** 7 (2012) 1976-1996.
55. T. Arslan, F. Kandermirli, E.E. Ebenso, I. love, H. Alemu, Quantum chemical studies on the corrosion inhibition of some sulphanoamides on mild steel in acidic medium, ***Corros. Sci.*** 51 (2009) 35-47.
56. A. Samide, B. Tutunaru, C. Negrila, I. Prunaru, Surface analysis of inhibitor film formed by 4-amino-N(1,3-thiazol-2-yl) benzene sulphonamide on carbon steel surface in acidic media, ***Spectrosc. Lett.*** 45 (2011) 55-64.
57. A. Samide, I. Bibicu, E. Turcanu, Corrosion inhibition of carbon steel in hydrochloric acid using N-acetil p-aminobenzene sulphonamide, ***Rev. Chim.*** 60 (2009) 564 – 567.
58. H.K. Sappani, S. Karthikeyan, 4-Chloro-2-((furan-2-ylmethyl)amino)-5-sulfamoylbenzoic Acid (FSM) and N-(Isopropylcarbamoyl)-4-(*m*-tolylamino) Pyridine-3-sulphonamide (TSM) as Potential Inhibitors for Mild Steel Corrosion in 1 N H_2SO_4 Medium. Part I, ***Ind. Eng. Chem. Res.*** 53 (2014) 3415 – 3425.
59. S. Zor, S. Sağdinç, Experimental and theoretical study of sulphathiazole as environmentally friendly inhibitor on aluminum corrosion in NaCl, *Prot. Met. Physc. Chem. Surf.* 50 (2014) 244–253.
60. R.A Leach, Molecular Modelling: Principle and Applications, Pearson Prentice Hall, (2001) ISBN-10: 0582382106.
61. J. Mcmurry, Fundamentals of Organic Chemistry, Brooks/Cole, (2003) ISBN: 9780534395735.
62. N. Khalis, Quantum Chemical Approach to Corrosion Inhibition, ***Electrochim. Acta.*** 48 (2003) 2635 – 2640.
63. M. Karelson, V.S Labanov, A.R Katritzky, Quantum Chemical Descriptors in QSAR/QSPR Studies, ***Chem. Rev.*** 96 (1996) 1027 – 1043.
64. J.B. Foresman, E. Frisch, Exploring Chemistry with Electronic Structure Methods, 2nd Ed., Gaussian, Inc, (1996) ISBN: 0-9636769-3-8.
65. U. Burkert, N.L Allinger, Molecular Mechanics, ACS Monograph, ***Am. Chem. Soc.*** Washington DC, (1982).

66. N.L Allinger, Conformational Analysis III. Approaches to Some Medium Ring Compounds, ***J. Am. Chem. Soc.*** 81, (1959) 5727 – 5733.
67. H. Yoshida, MOLDA for Protein Modelling: A Molecular Modelling Program for Biological Systems, ***J. Comput. Chem. Japan.*** 2 (2003) 143 – 148.
68. P.W. Atkins, R.S. Friedman, Molecular Quantum Mechanics, Oxford University Press Inc, New York, (1997) ISBN: 9780199274987
69. K. Schulten, Notes on Quantum Mechanics, University of Illinois at Urbana-Champaign, (2000).
70. P.W. Atkins, J. De Paula, Atkins Physical Chemistry ninth edition, Oxford University Press Inc, New York, (1997) ISBN: 9780199543373
71. A. Hellman, Nonadiabaticity in the initial oxidation of Mg(0001): First-principles density-functional calculations, ***Phys. Rev.*** *B* 72 (2005) 179 – 227.
72. V. Balachandran, V. Karpagam, A. Lakshmi, Conformational stability, theoretical and experimental vibrational spectral analysis of 2,4,6-trihydroxybenzaldehyde, ***J. Mol. Struct.*** 1021 (2012) 13 – 21.
73. M. Persico, Ab Initio Methods in Computational Chemistry, in Bolis G, Martinelli A (Eds.), Approaches to Structure-Property Relationship, Tipografia Senese, Siena (1995) 99 –122.
74. G. Hall, Applications of Quantum Mechanics in Theoretical Chemistry, ***Rep. Prog. Phys.*** 22 (1959) 1– 32.
75. B.A. Mamedov, Evaluation of Two-Centre Overlap Integrals in Molecular Coordinate System Over Slater-type Orbitals, ***Chin. J. Phys.*** 42 (2004) 176 – 226.
76. M.A. Abdulsatter, K.H. Al-Bayati, Corrections and Parametization of Semi-empirical Large Unit Cell Method of Covalent Semi-conductors, ***Phys. Rev. B.*** 75 (2007) 201–245.
77. M. Ben-Nun, T.J. Martinez, Ab Initio Quantum Molecular Dynamics, ***Adv. Chem. Phys.*** 121, (2002) 439 – 512.
78. L.C. Allen, A.M. Karo, Basis Function for Ab Initio Calculations, *Rev. Mod. Phys.* 32, (1960) 275 – 285.
79. M. Lashkari, M.R. Arshadi, DFT Studies of Pyridine Corrosion Inhibitors in Electrical Double Layer: Solvent, Substrate and Electric Fields Effects, ***Chem. Phys.*** 299, (2004) 131 – 137.

80. V.F. Lotrich, R.J. Bartlett, I. Grabowski, Intermolecular Potential Energy Surfaces of Weakly Bound Dimers Computed from Ab Initio Density Functional Theory: The Right Answers for the right Reason, ***Chem. Phys. Lett.*** 405, (2005) 43 – 48.
81. R.G. Parr, Density Functional Theory, ***Annu. Rev. Phys. Chem.*** 34, (1983) 361 – 356.
82. B. Hammer, M. Scheffer, K.W. Jacobsen, J.K. Norskok, Multidimensional Potential Energy Surface for H_2 Dissociation over Cu (III), ***Phys. Rev. Lett.*** 73, (1994) 1400 – 1403.
83. Y. Yafet, J. Kwo, E.M. Gyorgy, Dipole-dipole Interactions and Two-dimensional Magnetism, ***Phys. Rev. B.*** 33 (1986) 6519 - 6522.
84. G.A. Jeffrey, in An Introduction to Hydrogen Bonding, Oxford University Press Inc, New York, (1997) ISBN: 978019095947.
85. G.A. Jeffrey, W. Saenger, in Hydrogen Bonding in Biological Structures, Springer-Verlag, Berlin and New York, (1994), ISBN: 3540579036.
86. I. Langmuir, The Arrangement of Electrons in Atoms and Molecules, ***J. Am. Chem. Soc.*** 41 (1919) 868 – 934.
87. G.N. Lewis, The Atom and the Molecule, ***J. Am. Chem. Soc.*** 38, (1916) 762 – 785.
88. L. Pauling, The Nature of the Chemical Bond (Coruell University Press, Ithaca, New York, 1960)
89. R.G. Parr, R.G. Pearson, Absolute hardness: companion parameter to absolute electronegativity, ***J. Am. Chem. Soc.*** 105, (1983) 7512 – 7516.
90. K.M. Manamela, L.C. Murulana, M.M. Kabanda, E.E. Ebenso, Adsorptive and DFT Studies of Some Imidazolium Based Ionic Liquids as Corrosion Inhibitors for Zinc in Acidic Medium, ***Int. J. Electrochem. Sci.*** 9 (2014) 3029 – 3046.
91. H. Ashassi-Sorkhabi, M. Es`haghi, Corrosion inhibition of mild steel in acidic media by [BMIm]Br Ionic liquid, ***Mater. Chem. Phys.*** 114 **(**2009) 267 – 271.
92. I. Belfilali, A. Chetouani, B. Hammouti, S. Louhibi, A. Aouniti, S.S. Al-Deyab, Quantum chemical study of inhibition of the corrosion of mild steel in 1 M hydrochloric acid solution by newly synthesized benzamide derivatives, ***Res. Chem. Intermed.*** 40 (2014) 1069 –1088.
93. H.M. Hassan, A.M. Eldesoky, R.M. Younis, W. A. Zordok, Density Functional Theory (DFT) Studies on sulfa dimedine azo derivatives as green inhibitors for C-steel in 0.5 M H_3PO_4 Solutions, *Int. J. Adv. Res*, 2 (2014) 550 –568.

94. A.D. Becke, Density-functional thermochemistry. III. The role of exact exchange, ***J. Chem. Phys.*** 98 (1993) 5648 – 5652.
95. E. E. Ebenso, T. Arslan, F. Kandemirli, N. Caner, I. Love, Quantum chemical studies of some rhodanine azosulpha drugs as corrosion inhibitors for mild steel in acidic medium, ***Int. J. Quantum. Chem.*** 110, (2010) 1003 – 1018.
96. W. Yang, R.G. Parr, Hardness, softness and the Fukui function in the electronic theory of metals and catalysis, ***Proc. Natl. Acad. Sci.*** 82 (1985) 6723 – 6726.
97. M. J. Frisch, G. W. Trucks, H. B. Schlegel, G. E. Scuseria, M. A. Robb, J. R. Cheeseman, G. Scalmani, V. Barone, B. Mennucci, G. A. Petersson, H. Nakatsuji, M. Caricato, X. Li, H. P. Hratchian, A. F. Izmaylov, J. Bloino, G. Zheng, J. L. Sonnenberg, M. Hada, M. Ehara, K. Toyota, R. Fukuda, J. Hasegawa, M. Ishida, T. Nakajima, Y. Honda, O. Kitao, H. Nakai, T. Vreven, J. A. Montgomery, Jr., J. E. Peralta, F. Ogliaro, M. Bearpark, J. J. Heyd, E. Brothers, K. N. Kudin, V. N. Staroverov, R. Kobayashi, J. Normand, K. Raghavachari, A. Rendell, J. C. Burant, S. S. Iyengar, J. Tomasi, M. Cossi, N. Rega, J. M. Millam, M. Klene, J. E. Knox, J. B. Cross, V. Bakken, C. Adamo, J. Jaramillo, R. Gomperts, R. E. Stratmann, O. Yazyev, A. J. Austin, R. Cammi, C. Pomelli, J. W. Ochterski, R. L. Martin, K. Morokuma, V. G. Zakrzewski, G. A. Voth, P. Salvador, J. J. Dannenberg, S. Dapprich, A. D. Daniels, O. Farkas, J. B. Foresman, J. V. Ortiz, J. Cioslowski, and D. J. Fox, Gaussian, Inc., Wallingford CT, Gaussian 09, Revision *C.01* (2009).
98. M.A. Abu-Dalo, N.A.F. Al-Rawashde, A. Ababneh, Evaluating the performance of sulfonated Kraft lignin agent as corrosion inhibitor for iron-based materials in water distribution systems, ***Desalination.*** 313 (2013) 105 – 114.
99. A.K. Singh, M.A. Quraishi, Adsorption properties and inhibition of mild steel corrosion in hydrochloric acid solution by ceftobiprole, ***J. Appl. Electrochem.*** 41 (2011) 7–18.
100. S.K. Shukla, M.A. Quraishi, Cefotaxime sodium: A new and efficient corrosion inhibitor for mild steel in hydrochloric acid solution, ***Corros. Sci.*** 51 (2009) 1007–1011.
101. K.S. Jacob, G. Parameswaran, Corrosion inhibition of mild steel in hydrochloric acid solution by Schiff base furoin thiosemicarbazone, ***Corros. Sci.*** 52 (2010) 224 – 228.

102. H.H. Hassan, E. Abdelghani, M.A. Amin, Inhibition of mild steel corrosion in hydrochloric acid solution by triazole derivatives: Part I. Polarization and EIS studies ***Electrochim. Acta.*** 52 (2007) 6359 – 6366.
103. H.H. Hassan, Inhibition of mild steel corrosion in hydrochloric acid solution by triazole derivatives: Part II: Time and temperature effects and thermodynamic treatments, ***Electrochim. Acta.*** 53, (2007) 1722 – 1730.
104. M. El Azhar, B. Mernari, M. Traisnel, F. Bentiss, M. Lagrenee, Corrosion inhibition of mild steel by the new class of inhibitors [2,5-bis(*n*-pyridyl)-1,3,4-thiadiazoles] in acidic media, ***Corros. Sci.*** 43 (2001) 2229 – 2238.
105. Yurt, A. Balaban, S.U. Kandermir, G. Bereket, B. Erk, Investigation on some Schiff bases as HCl corrosion inhibitors for carbon steel, ***Mater. Chem. Phys.*** 85 (2004) 420 – 426.
106. D.B. Hmamou, R. Salghi, A. Zarrouk, H. Zarrok, S.S. Al-Deyab, O. Benali, B. Hammouti, The Inhibited effect of Phenolphthalein towards the corrosion of C38 Steel in Hydrochloric Acid, ***Int. J. Electrochem. Sci.*** 7 (2012) 8988–9003.
107. D.K. Yadav, M.A. Quraishi, B. Maiti, Inhibition effect of some benzylidenes on mild steel in 1 M HCl: An experimental and theoretical correlation, ***Corros. Sci.*** 55 (2012) 254 – 266.
108. M. Yadav, D. Behera, S. Kumar, R. Sinha, Experimental and Quantum Chemical Studies on the Corrosion Inhibition Performance of Benzimidazole Derivatives for Mild Steel in HCl, ***Ind. Eng. Chem. Res.*** 52 (2013) 6318– 6328.
109. M.M. Hassan, H. Baker, S. Collie, Enhanced corrosion inhibition of mild steel by cross-linked lanolin-coatings, ***Prog. Org. Coat.*** 78, (2015) 249 – 255.
110. J. Coates, Interpretation of Infrared Spectra, A Practical Approach, in: R.A. Meyers (Ed.), Encyclopaedia of Analytical Chemistry, John Wiley and Sons Ltd, Chichester, 2000, pp. 10815 – 10837.
111. L.R. Chauhan, G. Gunasekaran, Corrosion inhibition of mild steel by plant extract in dilute HCl medium, ***Corros. Sci.*** 49 (2007) 1143 – 1161.
112. M.A. Abu-Dalo, A.A. Othman, N.A.F. Al-Rawashde, Exudate gum from Acacia trees as green corrosion inhibitor for mild steel in acidic media, ***Int. J. Electrochem. Sci.*** 7 (2012) 9303–9324.

113. M.A. Chidiebere, C.E. Ogukwe, K.L. Oguzie, C.N. Eneh, E.E. Oguzie, Corrosion inhibition and adsorption behavior of punica granatum extract on mild steel in acidic environments: experimental and theoretical studies, *Ind. Eng. Chem. Res*, 51 (2012) 668– 677.
114. W.K. Lu, R.L. Elsebaumer, B. Wessling, Corrosion protection of mild steel by coatings containing polyaniline, ***Syn. Met.*** 71 (1995) 2163– 2166.
115. P.B. Raja, M.G. Sethuraman, Atropine sulphate as corrosion inhibitor for mild steel in sulphuric acid medium, ***Mater. Lett.*** 62 (2008) 1602– 1604.
116. A.M. Abdel-Gaber, B.A. Abd-El-Nabey, M. Saadawy, The role of acid anion on the inhibition of the acidic corrosion of steel by lupine extract, ***Corros. Sci.*** 51 (2009) 1038 – 1042.
117. T. Poornima, J. Nayak, A.N. Shetty, Effect of 4-(*N*,*N*-diethylamino)benzaldehyde thiosemicarbazone on the corrosion of aged 18 Ni 250 grade maraging steel in phosphoric acid solution, ***Corros. Sci.*** 53 (2011) 3688 – 3696.
118. Y. Tang, F. Zhang, S. Hu, Z. Cao, W. Jing, Novel benzimidazole derivatives as corrosion inhibitors of mild steel in the acidic media. Part I: Gravimetric, electrochemical, SEM and XPS studies, ***Corros. Sci.*** 74 (2013) 271 – 282.
119. P. Thiraviyam, K. Kannan, Inhibition of Aminocyclohexane derivative on mild steel corrosion in 1 N HCl, ***Arab. J. Sci. Eng.*** 38 (2013) 1757– 1767.
120. R. Korde, C.B. Verma, E.E. Ebenso, M.A. Quraishi, Electrochemical and thermodynamical investigation of 5-ethyl-4-(4-methoxyphenyl)-6-methyl-2-thioxo-1,2,3,4-tetrahydropyrimidine-5-carboxylate on corrosion inhibition behavior of aluminium in 1M hydrochloric acid, ***Int. J. Electrochem. Sci.*** 10 (2015) 1081–1093.
121. M. Yadav, S. Kumar, R.R. Sinha, I. Bahadur. E.E. Ebenso, New pyrimidine derivatives as efficient organic inhibitors on mild steel corrosion in acidic medium: electrochemical, SEM, EDX, AFM and DFT studies, ***J. Mol. Liq.*** 211 (2015) 135–145.
122. M. Abouchane, M. El Bakri, R. Touir, A. Rochdi, O. Elkhattabi, M. Ebn Touhami, I. Forssal, B. Mernari, Corrosion inhibition and adsorption behavior of triazoles derivatives on mild steel in 1 M H_3PO_4 and synergistic effect of iodide ions, ***Res. Chem. Intermed.*** 41 (2015) 1907–1923.

123. A. Zarrouk, B. Hammouti, T. Lakhlifi, M. Traisnel, H. Vezin, F. Bentiss, New 1*H*-pyrrole-2,5-dione derivatives as efficient organic inhibitors of carbon steel corrosion in hydrochloric acid medium: Electrochemical, XPS and DFT studies, ***Corros. Sci.*** 90 (2015) 572 – 584.
124. A. Popova, M. Christov, A. Vasilev, Mono- and dicationic benzothiazolic quaternary ammonium bromides as mild steel corrosion inhibitors. Part III: Influence of the temperature on the inhibition process, ***Corros. Sci.*** 94 (2015) 70 – 78.
125. K.R. Ansari, M.A. Quraishi, A. Singh, Isatin derivatives as a non-toxic corrosion inhibitor for mild steel in 20% H_2SO_4, ***Corros. Sci.*** 95 (2015) 62 – 70.
126. S.A. Umoren, I.B. Obot, Z.M. Gasem, Adsorption and corrosion inhibition characteristics of strawberry fruit extract at steel/acids interfaces: experimental and theoretical approaches, ***Ionics.*** 21 (2015) 1171 – 1186.
127. F.E. Awe, S.O. Idris, M. Abdulwahab, E.E. Oguzie, Inhibitive and adsorptive effect of parinari polyandra on mild steel corrosion in aqueous sulphuric acid, ***Afr. J. Pure. Appl. Chem.*** 9 (2015) 125 – 134.
128. Y. Zhu, M.L. Free, G. Yi, Electrochemical measurement, modeling, and prediction of corrosion inhibition efficiency of ternary mixtures of homologous surfactants in salt solution, ***Corros. Sci.*** 98 (2015) 417 – 429.
129. M.A. Hegazy, S.S. Abd El Rehim, A.M. Badawi, M.Y. Ahmed, Studying the corrosion inhibition of carbon steel in hydrochloric acid solution by 1-dodecyl-methyl-1*H*-benzo[*d*][1,2,3]triazole-1-ium bromide, ***RSC. Adv.*** 5 (2015) 49070 – 49079.
130. E.E. Oguzie, Corrosion inhibition of aluminium in acidic and alkaline media by Sansevieria trifasciata extract, ***Corros. Sci.*** 49 (2007) 1527 – 1539.
131. A.M. Abdel-Gaber, E. Khamis, H. Abo-ElDahab, sh.Adeel, Inhibition of aluminium corrosion in alkaline solutions using natural compound, ***Mater. Chem. Phys.*** 109 **(**2008) 297 – 305.
132. A.K. Satpati, P.V. Ravindran, Electrochemical study of the inhibition of corrosion of stainless steel by 1,2,3-benzotriazole in acidic media, ***Mater. Chem. Phys.*** 109 **(**2008) 352 – 359.
133. A. Singh, E.E. Ebenso, M.A. Quraishi, Stem extract of brahmi *(Bocopa Monnieri*) as green corrosion inhibitor for aluminium in NaOH solution, ***Int. J. Electrochem. Sci.*** 7 (2012) 3409 –3419.

134. A.M. Neccaria, L. Chiaruttini, The inhibitive action of metacryloxypropylmethoxysilane (MAOS) on aluminium corrosion in NaCl solutions, ***Corros. Sci.*** 41 (1999) 885 – 899.
135. I.B. Obot, N.O. Obi-Egbedi, S.A. Umoren, The synergistic inhibitive effect and some quantum chemical parameters of 2,3-diaminonaphthalene and iodide ions on the hydrochloric acid corrosion of aluminium, ***Corros. Sci.*** 51 (2009) 276 – 282.
136. S.A. Umoren, I.B. Obot, E.E. Ebenso, N.O. Obi-Egbedi, The inhibition of aluminium corrosion in hydrochloric acid solution by exudate gum from *Rahia Hookeri*, ***Desalination.*** 247 (2009) 561– 572.
137. A. Yurt, S. Ulutas, H. Dal, Electrochemical and theoretical investigation on the corrosion of aluminium in acidic solution containing some Schiff bases, ***Appl. Surf. Sci.*** 253 (2006) 919 – 925.
138. V. Branzoi, F. Golgovici, F. Branzoi, Aluminium corrosion in hydrochloric acid solutions and the effect of some organic inhibitors, ***Mater. Chem. Phys.*** 78 **(**2003) 122 – 131.
139. M. Metikos-Hukovic, R. Babic, Z. Grubac, The study of aluminium corrosion in acidic solution with nontoxic inhibitors, ***J. Appl. Electrochem.*** 32 (2002) 35 – 41.
140. D. Özkır, K. Kayakırılmaz, E. Bayol, A.A. Gürten, F. Kandemirli, The Inhibition Effect of Azure A on Mild Steel in 1 M HCl. A Complete Study: Adsorption, Temperature, Duration and Quantum Chemical Aspects, ***Corros. Sci.*** 56 (2012) 143 – 152.
141. S.A. Umoren, M.M. Solomon, U.M. Eduok, I.B. Obot, A.U. Israel, Inhibition of mild steel corrosion in H_2SO_4 solution by coconut coir dust extract obtained from different solvent systems and synergistic effect of iodide ions: Ethanol and acetone extracts, ***J. Env. Chem. Eng.*** 2 (2014) 1048 – 1060.
142. I.B. Obot, N.O. Obi-Egbedi, Fluconazole as an inhibitor for aluminium corrosion in 0.1 M HCl, ***Colloids. Surf. A.*** 330 (2008) 207 – 212.
143. N.A Negm, M.F. Zaki, Corrosion inhibition efficiency of nonionic Schiff base amphiphiles of p-aminobenzoic acid for aluminium in 4N HCl, ***Colloids. Surf. A.*** 322 (2008) 97 – 102.
144. D.Q. Zhang, Q.R. Cao, X.M. He, L.X. Gao, G.D. Zhou, Inhibition effect of some amino acids on copper corrosion in HCl solution, ***Mater. Chem. Phys.*** 112 **(**2008) 352 – 358.

145. M. Finsgar, A. Lesar, A. Kokalj, I. Milosev, A comparative electrochemical and quantum chemical calculation study of BTAH and BTAOH as copper corrosion inhibitors in near neutral chloride solution, ***Electrochim. Acta.*** 53, (2008) 8287 – 8297.
146. T. Zhao, G. Mu, The adsorption and corrosion inhibition of anion surfactants on aluminium surface in hydrochloric acid, ***Corros. Sci.*** 41 (1999) 1937 – 1944.
147. A.K. Maayta, N.A.F. Al-Rawashdeh, Inhibition of acidic corrosion of pure aluminium by some organic compounds, ***Corros. Sci.*** 46 (2004) 1129 – 1140.
148. L. Tang, G. Mu, G. Liu, The effect of neutral red on the corrosion inhibition of cold rolled steel in 1.0 M hydrochloric acid, ***Corros. Sci.*** 45 (2003) 2251 – 2262.
149. A.Y. El-Etre, Inhibition of acid corrosion of aluminium using vanillin, ***Corros. Sci.*** 43 (2001) 1031 – 1039.
150. S.A. Umoren, I.B. Obot, E.E. Ebenso, Corrosion inhibition of aluminium using exudate gum from pachylobus edulis in the presence of halide ions in HCl, *E.* ***J. Chem.*** 5 **(**2008) 355 – 364.
151. H. Ashassi-Sorkhabi, Z. Ghasemi, D. Seifzadeh, The inhibition effect of some amino acids towards the corrosion of aluminium in 1 M HCl + 1 M H_2SO_4 solution, ***Appl. Surf. Sci.*** 249 (2005) 408 – 418.
152. M.A. Quraishi, A. Singh, V.K. Singh, D.K. Yadav, A.K. Singh, Green approach to corrosion inhibition of mild steel in hydrochloric acid and sulphuric acid solutions by the extract of Murraya koenigii leaves, ***Mater. Chem. Phys.*** 122 (2010) 114 – 1212.
153. A.K. Satapathy, G. Gunasekaran, S.C. Sahoo, K. Amit, P.V. Rodrigues, Corrosion inhibition by Justicia gendarussa plant extract in hydrochloric acid solution, ***Corros. Sci.*** 51 (2009) 2848 –2856.
154. S.S. Abd El-Rehim, M.A.M. Ibrahim, K.F. Khaled, 4-Aminoantipyrine as an inhibitor of mild steel corrosion in HCl solution, ***J. Appl. Electrochem.*** 29 (1999) 593 –599.
155. M. Abouchane, M. El Bakri, R. Touir, A. Rochdi, O. Elkhattabi, M. Ebn Touhami, I. Forssal, B. Mernari, Corrosion inhibition and adsorption behavior of triazoles derivatives on mild steel in 1 M H_3PO_4 and synergistic effect of iodide ions, ***Res. Chem. Intermed.*** 41 (2015) 1907 –1923.
156. M. Yadav, S. Kumar, N. Kumari1, I. Bahadur, E. E. Ebenso, Experimental and Theoretical Studies on Corrosion Inhibition Effect of Synthesized Benzothiazole Derivatives on Mild Steel in 15% HCl Solution, ***Int. J. Electrochem. Sci.*** 10 (2015) 602 – 624.

157. H.H. Hassan, E. Abdelghani, M.A. Amin, Inhibition of Mild Steel Corrosion in Hydrochloric Acid by Triazole Derivatives Part I. Polarization and EIS Studies. ***Electrochim. Acta*.** 52 (2007) 6359 – 6366.
158. H.H. Hassan, Inhibition of Mild Steel Corrosion in Hydrochloric Acid Solution by Triazole Derivatives Part II: Time and Temperature Effects and Thermodynamic Treatments. ***Electrochim. Acta.*** 53 (2007) 1722 – 1730.
159. M. El Azhar, B. Mernari, M. Traisnel, F. Bentiss, M. Lagrenee, Corrosion Inhibition of Mild Steel by the New Class of Inhibitors [2,5-bis(n-pyridyl)-1,3, 4-thiadiazoles] in Acidic Media, ***Corros. Sci.*** 43 (2001) 2229 –2238.
160. A. Yurt, A. Balaban, S.U. Kandermir, G. Bereket, B. Erk, Investigation on some Schiff bases as HCl corrosion inhibitors for carbon steel, ***Mater. Chem. Phys*.** 85 (2004) 420 – 426.
161. D.K. Yadav, M.A. Quraishi, B. Maiti, Inhibition effect of some benzylidenes on mild steel in 1 M HCl: An experimental and theoretical correlation, ***Corros. Sci*.** 55 (2012) 254 – 266.
162. K.S. Jacob, G. Parameswaran, Corrosion Inhibition of Mild Steel in Hydrochloric Acid Solution by Schiff Base Furoin Thiosemicarbazone, ***Corros. Sci*.** 52 (2010) 224 – 228.
163. M. Yadav1,D. Sharma, S. Kumar, S. Kumar, I. Bahadur, E.E. Ebenso, Electrochemical and Theoretical Studies on Amino Phosphonates as Efficient Corrosion Inhibitor for N80 Steel in Hydrochloric Acid Solution, ***Int. J. Electrochem. Sci*.** 9 (2014) 6580 – 6593.
164. S.A. Umoren, M.M. Solomon, U.M. Eduok, I.B. Obot, A.U. Israel, Inhibition of mild steel corrosion in H_2SO_4 solution by coconut coir dust extract obtained from different solvent systems and synergistic effect of iodide ions: Ethanol and acetone extracts, ***J. Env. Chem. Eng*.** 2 (2014) 1048– 1060.
165. T. Zhao, G. Mu, The adsorption and corrosion inhibition of anion surfactants on aluminium surface in hydrochloric acid, ***Corros. Sci*.** 41 (1999) 1937 – 1944.
166. W.A. Badawy, F.M. Al-Kharafi, A.S. El-Azab, Electrochemical behaviour and corrosion inhibition of Al, Al-6061 and Al–Cu in neutral aqueous solutions, ***Corros. Sci*.** 41 (1999) 709 – 727.
167. E.E. Ebenso, U.J. Ekpe, B.I. Ita, O.E. Offiong, U.J. Ibok, Effect of molecular structure on the efficiency of amides and thiosemicarbazones used for corrosion inhibition of mild steel in hydrochloric acid, ***Mater. Chem. Phys*.** 60 (1999) 79 – 90.

168. M.A. Elmorsi, A.M. Hassanein, Corrosion inhibition of copper by heterocyclic compounds, ***Corros. Sci.*** 41 (1999) 2337 – 2362.
169. A. Shaban, E. Kálmán, J. Telegdi, An investigation of copper corrosion inhibition in chloride solutions by benzo-hydroxamic acids, ***Electrochim. Acta.*** 43, (1998) 159 – 163.
170. D. Wanga, , S. Lia, Y. Yinga, M. Wanga, H. Xiaob, Z. Chen, Theoretical and experimental studies of structure and inhibition efficiency of imidazoline derivatives, ***Corros. Sci.*** 41 (1999) 1911 – 1916.
171. M. Fonsati, F. Zucchi, G. Trabanelli, Study of corrosion inhibition of copper in 0.1 M NaCl using the EQCM technique, ***Electrochim. Acta.*** 44, (1998) 311 – 322.
172. G.K. Gomma, Corrosion inhibition of steel by benzotriazole in sulphuric acid, ***Mater. Chem. Phys.*** 55 (1998) 235 – 240.
173. A.M. Al-Mayout, A.A. Al-Suhybani, A.K. Al-Ameery, Corrosion inhibition of 304SS in sulfuric acid solutions by 2-methyl benzoazole derivatives, ***Desalination.*** 116 (1998) 25 – 33.
174. M. A. Amin, S.S. Abd El-Rehim, E.E.F. El-Sherbini, R.S. Bayoumi, The inhibition of low carbon steel corrosion in hydrochloric acid solutions by succinic acid: Part I. Weight loss, polarization, EIS, PZC, EDX and SEM studies, ***Electrochim. Acta.*** 52, (2007) 3588 – 3600.
175. X. Li, G. Mu, Tween-40 as corrosion inhibitor for cold rolled steel in sulphuric acid: Weight loss study, electrochemical characterization, and AFM, ***Appl. Surf. Sci.*** 252 (2005) 1254 – 1265.
176. M. A. Amin, Weight loss, polarization, electrochemical impedance spectroscopy, SEM and EDX studies of the corrosion inhibition of copper in aerated NaCl solutions, ***J. Appl. Electrochem.*** 36 (2006) 215 – 226.
177. H. Keles, D.M. Emir, M. Keles, A comparative study of the corrosion inhibition of low carbon steel in HCl by imine compound and its cobalt complex, ***Corros. Sci.*** 101 (2015) 19 – 31.
178. H. Ashassi-Sorkhabi, B. Shaabani, D. Seifzadeh, Corrosion inhibition of mild steel by some Schiff base compounds in hydrochloric acid, ***Appl. Surf. Sci.*** 239 (2005) 154 – 164.
179. A.Y. El-Etre, M. Abdallah, Z.E. El-Tantawy, Corrosion inhibition of some metals using lawsonia extract, ***Corros. Sci.*** 47 (2005) 385 – 395.

180. F. Bentiss, M. Traisnel, M. Lagrenee, The substituted 1,3,4-oxadiazoles: a new class of corrosion inhibitors of mild steel in acidic media, ***Corros. Sci.*** 42 (2000) 127 – 146.
181. P. Udhayakala, A. Samuel, T.V. Rajendiran, S. Gunasekaran, DFT study on the adsorption mechanism of some phenyltetrazole substituted compounds as effective corrosion inhibitors for mild steel, ***Der. Pharma. Chemica.*** 5 (2013), 111–124.
182. N.O. Eddy, F.E. Awe, C.E. Gimba, N.O. Ibisi, E.E. Ebenso, QSAR, experimental and computational chemistry simulation studies on the inhibition potentials of some amino acids for the corrosion of mild steel in 0.1 M HCl, ***Int. J. Electrochem. Sci.*** 6 (2011) 931 – 957.
183. Z. Cao, Y. Tang, H. Cang, J. Xu, G. Lu, W. Jing, Novel benzimidazole derivatives as corrosion inhibitors of mild steel in the acidic media. Part II: Theoretical studies, ***Corros. Sci.*** 83 (2014) 292 – 298.
184. A.K. Singh, S. Khan, A. Singh, S.M. Quraishi, M.A. Quraishi, E.E. Ebenso, Inhibitive effect of chloroquine towards corrosion of mild steel in hydrochloric acid solution, ***Res. Chem. Intermed.*** 39 (2013) 1191 – 1208.
185. H. Wang, X. Wang, H. Wang, L. Wang, A. Liu, DFT study of new bipyrazole derivatives and their potential activity as corrosion inhibitors, ***J. Mol. Model.*** 13 (2007) 147 – 153.
186. N.O. Eddy, S.R. Stoyanov, E.E. Ebenso, Flouroquinolones as corrosion inhibitors for mild steel in acidic medium; experimental and theoretical studies, ***Int. J. Electrochem. Sci.*** 5 (2010) 1127-1150.
187. N.O. Obi-Egbedi, I.B. Obot, M.I. El-Khaiary, S.A. Umoren, E.E. Ebenso, Computational simulation and statistical analysis on the relationship between corrosion inhibition efficiency and molecular structure of some phenanthroline derivatives on mild steel surface, ***Int. J. Electrochem. Sci.*** 6 (2011) 5649 – 5675.
188. G.N. Lewis, The Atom and the Molecule, ***J. Am. Chem. Soc.*** 38 (1916) 762 – 785.
189. S. Martinez. Inhibitory mechanism of mimosa tannin using molecular modelling and substitutional adsorption isotherms. ***Mater. Chem. Phys.*** 77 (2002) 97 – 102.
190. G. Gece. The use of quantum chemical methods in corrosion inhibitor studies, ***Corros. Sci.*** 50 (2008) 2981 – 2992.
191. G. Gao, C. Liang. Electrochemical and DFT studies of β-amino-alcohols as corrosion inhibitors for brass, ***Electrochimica. Acta.*** 52 (2007) 4554 – 4559.
192. A. K. Chandra, M. T. Nguyen. Use of Local Softness for the Interpretation of Reaction Mechanisms, ***Int. J. Mol. Sci.*** 3 (2002) 310 – 323.

193. N. Khalil, Quantum chemical approach of corrosion inhibition, ***Electrochimica. Acta.*** 48 (2003) 2635 – 2640.
194. I. Lukovits, I. Bako, A. Shaban, E. Kalman, Polynomial model of the inhibition mechanism of thiourea derivatives, ***Electrochimica Acta.*** 43 (1998) 131 – 136.
195. I. Lukovits, A. Shaban, E. Kalman, Corrosion Inhibitors: Quantitative structure-Activity Relationship, ***Russian J. Electrochem.*** 39 (2003) 177 – 181.

APPENDIX

PRESENTATION AT CONFERENCES

1. Lutendo C. Murulana, Mwadham M. Kabanda, Eno E. Ebenso, Sulphonamides as Green Corrosion Inhibitors for Aluminum and Zinc in Acidic Medium. 5th International IUPAC conference on Green Chemistry. Durban, 17–21 August 2014.
2. Lutendo C. Murulana, Mwadham. M. Kabanda, Eno E. Ebenso, Corrosion Inhibition Potential of some Sulphonamide Compounds on Mild Steel and Zinc in Acidic Environments. SACI National 2013 convention. East London, 1– 6 December 2013.

PUBLICATIONS FROM THE STUDY

1. Lutendo. C. Murulana, Mwadham. M. Kabanda and Eno. E. Ebenso, Experimental and theoretical studies on the corrosion inhibition of mild steel by some sulphonamides in aqueous HCl. ***RSC Advances***. 5 (2015) 28743-28761.
2. Lutendo. C. Murulana, Mwadham. M. Kabanda and Eno. E. Ebenso, Investigation of the adsorption characteristics of selected sulphonamide derivatives as corrosion inhibitors at mild steel/hydrochloric acid interface surfaces: Experimental, quantum chemical and QSAR studies. ***Journal of Molecular Liquids***. 215 (2016) 763-779.